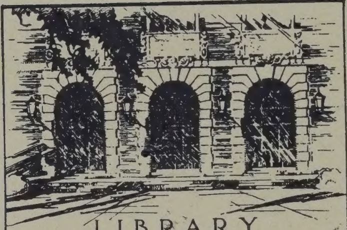

LIBRARY
OF THE
UNIVERSITY
OF ILLINOIS

624.1
P192p
1963
v.1

ENGINEERING

The person charging this material is responsible for its return to the library from which it was withdrawn on or before the **Latest Date** stamped below.

Theft, mutilation, and underlining of books are reasons for disciplinary action and may result in dismissal from the University.

To renew call Telephone Center, 333-8400

UNIVERSITY OF ILLINOIS LIBRARY AT URBANA-CHAMPAIGN

ENGINEERING

MAR 27 1998

July 8

JUN 15 REC'D

PHOTO REPRODUCTION

JAN 31 1995

FEB 13 REC'D

JUN 07 1998

JUN 07 1998

JUN 16 REC'D

L161—O-1096

L161—O-1096

ERRATA — VOL. I

Página *Page*	*Linha* *Linea* *Line*	*Onde se lê* *Error*	*Leia-se* *Corrección* *Correction*
30	9	to item 3.1	to in item 3.1
30	19	of compacted	of recompacted
30	35	of employing	of the control. Our experience has shown the advantage of employing
35	33	disturb-process seems to be under statistical control;	disturbing cause other than purely chance variation;
132	1	$\frac{V_m}{d \pi f}$	$\frac{V_m}{2 \pi f}$
132	5	peak-to-pek	peak-to-peak
137	Fig. 6	f = 1000 c p s	f= 100 c p s
143	35	E. Vay	E. Vey
162	27	seletion	selection
359	equation (6)	$R = \frac{4\,EI}{k}$	$R = \sqrt[4]{\frac{EI}{k}}$
363	equation (12)	$T = \frac{5\,EI}{n_h}$	$T = \sqrt[5]{\frac{EI}{n_h}}$
400	1	batter	better
401	25	trough	through
411	21	$R\Phi$	R_{Φ}
411	26	Δ_{x}	Δ^{x}
416	35-36	ensaios	dados
420	36	hidrálicos	hidráulicos
421	40	em tôrno de célula	em tôrno da célula
431	29	mencionados	selecionados
437	11	tinha	tinha,
437	16	circundava,	circundava
438	11	ultrapassam	ultrapassem
438	17	outros	outras
445	10	frequency of	frequency of vibration of
447	18	or	of
448	7	flap	flat
449	35	Model T-100 S	Model RT-100 S
452	25	3 percent	5 percent
453	18	to appearance	of appearance
454	3	had	has
479	22	os ensaios de cisalhamento triaxial com medidas de po-	os ensaios de adensamento com drenagem livre permiti-
482	13	figura 2	figura 3
482	18	figura 2	figura 3
503	Fig. 1 — CP 924	780.000 0,38	763.300 0,19
508	Tabela I	$\left(\frac{\sigma_x}{P}\right)_B = -1$	$\left(\frac{\sigma_y}{P}\right)_B = -1{,}0$

Segundo Congresso Panamericano de Mecânica dos Solos e Engenharia de Fundações

Segundo Congreso Panamericano de Mecánica de Suelos y Cimentaciones

Second Panamerican Conference on Soil Mechanics and Foundation Engineering

Símbolo do Congresso — Símbolo del Congreso — Symbol of the Conference

Sôbre o Hemisfério, um perfil marcante de Brasília — O Congresso Federal
Sobre el Hemisferio, un perfil remarcable de Brasilia — El Congreso Federal
Backed by the Hemisphere, a Brasilia land-mark — The Federal Congress

Anais do Segundo Congresso Panamericano de Mecânica dos Solos e Engenharia de Fundações

Memoria del Segundo Congreso Panamericano de Mecánica de Suelos y Cimentaciones

Proceedings of the Second Panamerican Conference on Soil Mechanics and Foundation Engineering

São Paulo, SP — Rio de Janeiro, GB — Belo Horizonte, MG
14 - 24 — Julho - Julio - July — 1963

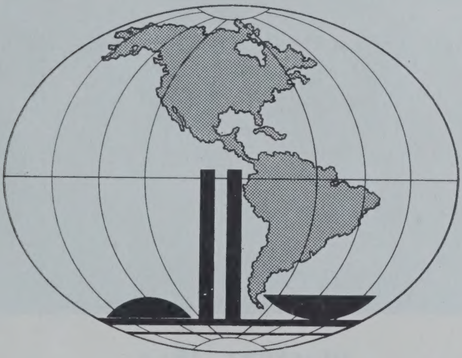

Vol. I

Associação Brasileira de Mecânica dos Solos
Caixa Postal 7141 — São Paulo 1, SP
Brasil
1963

Publicado com a colaboração das Centrais Elétricas Brasileiras S.A.

— ELETROBRÁS —

Sob a presidência do Eng. Paulo Richer

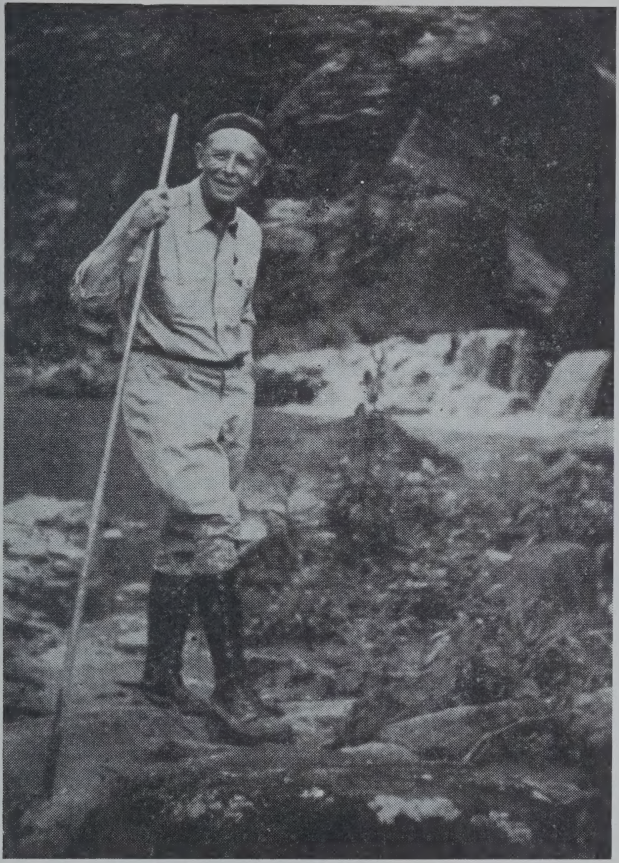

KARL TERZAGHI

A Associação Brasileira de Mecânica dos Solos respeitosamente dedica êstes Anais ao Fundador da Mecânica dos Solos, no ano de seu 80.º aniversário.

La Asociación Brasileña de Mecánica de Suelos respetuosamente dedica esta Memoria al Fundador de la Mecánica de Suelos, en el año de su 80.º natalicio.

The Brazilian Association of Soil Mechanics respectfully dedicates these Proceedings to the Founder of Soil Mechanics, in the year of his 80th birthday.

Professor Terzaghi em uma de suas viagens ao Brasil como Consultor

Profesor Terzaghi en un de sus viajes al Brasil como Consultor

Professor Terzaghi in one of his travels to Brazil as a Consultant

Foto de — Photo by — F. Pacheco Silva

624.1
P1935
1963
v.1

ENGINEERING LIBRARY

APRESENTAÇÃO

O Primeiro Congresso Panamericano de Mecânica dos Solos e Engenharia de Fundações, reunido no México em 1959, definiu como propósito fundamental daquela e das futuras reuniões, a promoção do intercâmbio de conhecimentos e experiências dos técnicos do Continente Americano neste ramo da Engenharia Civil.

A relevância dêsse objetivo, o sucesso daquele Primeiro Congresso e a honrosa escolha do Brasil para sede da reunião seguinte, levou a Associação Brasileira de Mecânica dos Solos a aceitar a incumbência de organizar o Segundo Congresso, com a intenção primeira de assegurar continuidade a essas reuniões, auspiciosamente inauguradas em 1959. Por outro lado, para melhor aproveitar o intercâmbio de conhecimentos e experiências, o temário do Congresso foi estendido a todo o campo da Mecânica dos Solos Aplicada.

Era propósito do Comitê Organizador preparar a impressão de todos os trabalhos apresentados, em número superior a meia centena, até a abertura do Segundo Congresso. Entretanto, a inesperada extensão dada à maioria dêsses trabalhos pelos seus autores, do que dá uma idéia o presente volume, e o pequeno espaço de tempo entre a data limite para recebimento dessas contribuições e a instalação do Congresso, impediu a concretização total daquele propósito. Foram assim incluídos no primeiro volume, ora apresentado, os trinta primeiros trabalhos recebidos. Os demais, juntamente com os relatórios, discussões e outras atividades do Congresso, serão incluídos no segundo volume a ser impresso ainda êste ano.

O Comitê de Organização

PRESENTACIÓN

El Primero Congreso Panamericano de Mecánica de Suelos e Ingeniería de Fundaciones, reunido en México en 1959, definió como propósito fundamental de aquella reunión, así como de las futuras, el promover intercambio de conocimientos y experiencias de los técnicos del Continente Americano en esta rama de la Ingeniería Civil.

La relevancia de este objetivo, el éxito de aquel Primero Congreso y la honrosa distinción del Brasil para sede de la reunión siguiente, llevó a la Asociación Brasileña de Mecánica de Suelos a acceptar la incumbencia de organizar el Segundo Congreso, con la intención primordial de asegurar continuidad a esas reuniones, auspiciosamente inauguradas en 1959. Por otro lado, para mejor aprovechar el intercambio de conocimientos y experiencias, el temario del Congreso fué extendido a todo el campo de la Mecánica de Suelos Aplicada.

Era propósito del Comité Organizador preparar la impresión de todos los trabajos presentados, en número superior a la media centena, hasta la abertura del Segundo Congreso. Entretanto, la inesperada extensión dada a la mayoría de los trabajos por sus autores, de lo que dá una idea el presente volumen, y el pequeño lapso de tiempo entre la fecha limite para recepción de estas contribuciones y la instalación del Congreso, impidió la concretización de aquello propósito. Así pues, fueran incluídos en este primero volumen, que ahora presentamos, los treinta primeros trabajos recibidos. Los demás, juntamente con los relatorios, discusiones y otras actividades del Congreso, serán incluídos en el segundo volumen a ser impreso en este año.

El Comité de Organización

FOREWORD

The First Panamerican Conference on Soil Mechanics and Foundation Engineering, held in Mexico in 1959, defined as a fundamental purpose of that and future meetings, the promotion of the exchange of knowledge and experience of the specialists of the American Continent in this branch of Civil Engineering.

Because of the importance of this objective, the success of that First Conference and the honoring choice of Brazil for the next meeting place, the Brazilian Association of Soil Mechanics accepted the task of organizing the Second Conference, with the primary intention of assuring continuity for these meetings, so auspiciously inaugurated in 1959. On the other hand, to take advantage of the exchange of knowledge and experience, the themes of the Conference were extended to the whole field of Applied Soil Mechanics.

It was the purpose of the Organizing Committee to prepare a printing of all of the more than fifty papers presented, before the opening of the Second Conference. However, the unexpected length of a great number of these papers, of which the present volume gives some idea, and the short period of time between the last date for receiving these contributions and the beginning of the Conference, made it impossible to realize that purpose completely. Therefore, only the first thirty papers received were included in this volume. The remaining papers will be printed later this year, along with the Reports, discussions and other activities of the Conference.

The Organizing Committee

ÍNDICE — CONTENTS

Divisão I — Propriedades dos Solos
División I — Propiedades de los Suelos
Division I — Soil Properties

Ia — Investigações de Campo — Investigaciones de Campo — Field Investigations 1

Ia/1 — Evaluation of Pressuremeter Tests in Granular Soils — *B. Ladanyi* — Canada 3

Ia/2 — Considerations about Quality Control on Compaction Process — *Evelyna B. S. Silveira and A. Silveira* — Brasil 21

✓Ia/3 — Engineering Properties of Residual Soils Derived from Igneous and Metamorphic Rocks — *G. F. Sowers* — U.S.A. 39

Ia/4 — Clay Mineral Composition and Properties of Deep Residual Soils from São Paulo, Brazil — *R. E. Grim and W. F. Bradley* — U.S.A. 63

Ib — Investigações de Laboratório — Investigaciones de Laboratorio — Laboratory Investigations 73

Ib/1 — Shear Strength Characteristics of Some Residual Compacted Clays — *P. T. da Cruz* — Brasil 73

Ib/2 — The Effect of Strain Rate on the Undrained Shear Strength of Cohesive Soils — *W. H. Perloff Jr. and J. O. Osterberg* — U.S.A. 103

Ib/3 — Effect of Vibration on Density of Sand — *E. T. Selig* — U.S.A. 129

Ib/4 — Effect of Vibration Amplitude on Wave Velocities in Granular Materials — *J. R. Hall and F. E. Richart Jr.* — U.S.A. 145

Ib/5 — Equipamento e Técnica Referentes aos Ensaios Triaxiais. Conjunto de Resultados Obtidos com Amostras de Solos Residuais — *H. U. Scherrer e P. A. Britto* — Brasil 163

Ib/6 — Large-Scale Triaxial Tests on Gravelly Soils — *D. D. Leslie* — U.S.A. 181

Ib/7 — Shearing Properties of Remolded Sodium Illite — *R. E. Olson and J. Hardin* — U.S.A. 203

Ib/8 — Subpressure Measurement in a Freezing Soil System — *A. R. Jumikis* — U.S.A. 219

Ib/9 — Correlación de Indices del Suelo con la Resistencia al Corte — *G. P. Guerra y H. P. La Salvia* — VENEZUELA 233

Ib/10 — Notas sobre Permeabilidad y Resistencia al Corte de Gravas Arcillosas — *H. P. La Salvia y G. P. Guerra* — VENEZUELA 243

Ib/11 — Shear Strength of Clays Shales Found in the Southwestern — U.S.A. — *F. M. Van Auken* — U.S.A. 255

Ib/12 — A Hyperbolic Stress — Strain Formulation for Sands — *R. L. Kondner and J. S. Zelasko* — U.S.A. 289

Divisão II — Fundações

División II — Fundaciones

Division II — Foundations

IIa — Fundações Diretas e Profundas sem Emprêgo de Estacas — Fundaciones Directas y Profundas sin el Uso de Pilotes — Foundations other than Piled Foundations 325

IIa/1 — Low Costs Shallow Foundation — *A. Silveira and Evelyna B. S. Silveira* — BRASIL 327

IIa/2 — Model Bearing Tests on a Remoulded Clay — *R. Yong, O. M. Peck and H. C. Leitch* — CANADA 337

IIb — Fundações por Estacas — Fundaciones por Medio de Pilotes — Piled Foundations 351

✓IIb/1 — Estimating Buckling Loads for Piles — *M. T. Davisson* — U.S.A. 351

IIb/2 — Bending and Buckling of Soil-Supported Structural Elements — *H. Matlock and W. B. Ingram* — U.S.A. 373

Divisão III — Obras de Terra e Rocha

División III — Obras de Tierra y Roca

Division III — Earth and Rock Structures

IIIa — Barragens de Terra e Enrocamento — Presas de Tierra y de Enrocamiento — Earth and Rock-Fill Dams 389

IIIa/1 — Thoughts Concerning the Mechanics of Slope Stability Analysis — *R. V. Whitman and P. J. Moore* — U.S.A. 391

IIIa/2 — Piezômetros em Três Marias — *O. M. Arêas* — BRASIL 413

IIIa/3 — Rockfill Compaction by Vibratory Rollers — *G. E. Bertram* — U.S.A. 441

IIIa/4 — Aspectos do Contrôle de Construção da Barragem de Furnas — *L. A. Queiroz* — Brasil 457

IIIa/5 — Cálculo de Estabilidade de Barragens de Terra pelo Computador Eletrônico Univac-1105 — *O. Pfafstetter* — Brasil 475

IIIa/6 — The Effect of Underdrain Carpet on Seepage Quantities Through Earth Dams — *A. R. Jumikis and W. J. Weber Jr.* — U.S.A. 485

IIIb — Obras de Terra e Rocha Diversas de Barragens. Geologia Aplicada — Obras de Tierra y Roca Diferentes de Presas. Geología Aplicada — Earth and Rock Structures Other than Dams. Engineering Geology 501

IIIb/1 — A Anisotropia de Maciços Rochosos e a Concentração de Tensões em Tôrno de Obras Subterrâneas — *M. D. Ruiz* — Brasil 501

√IIIb/2 — Merits and Mistakes of Geophysics in Civil Engineering — *H. Q. Golder and L. G. Soderman* — Canada 513

IIIb/3 — Mecanismo de Desagregação de Rochas Basálticas Semi-Alteradas — *M. D. Ruiz* — Brasil 533

Divisão IV — Mecânica dos Solos para Estradas e Aeroportos
División IV — Mecánica de Suelos para Carreteras y Aeropuertos
Division IV — Soil Mechanics for Roads and Airports

IV/1 — Effects of Chemical Additives on the Strength of Soil-Cement Mixtures — *M. Mateos, R. H. Tawes and D. T. Davidson* — U.S.A. 547

DIVISÃO I — *Propriedades dos Solos*

DIVISIÓN I — *Propiedades de los Suelos*

DIVISION I — *Soil Properties*

Ia. *Investigações de campo*
Investigaciones de campo
Field investigations

Ib. *Investigações de laboratório*
Investigaciones de laboratorio
Laboratory investigations

EVALUATION OF PRESSUREMETER TESTS IN GRANULAR SOILS

B. LADANYI

D.Sc., Professor of Foundation Eng., Laval University, Québec, Canada.

SUMMARY

In the methods of interpretation of pressuremeter tests proposed until now it is assumed that the volume change of the soil during the test is zero. However, when a pressuremeter test is carried out in a granular soil under drained conditions, it is shown in this paper that this assumption may result in obtaining an incorrect shape and position of the failure envelope of the soil. A new method of interpretation is proposed in the paper which takes into account the volume change of the soil during the test and makes it possible to determine the correct failure envelope also for a granular soil undergoing during the test volume changes due to compression and dilatancy.

SUMARIO

En los métodos de interpretación de experiencias por medio de presiómetro empleados hasta ahora, se ha supuesto que el cambio de volumen del suelo durante la experiencia es cero. Sin embargo, efectuando dicha experiencia en un suelo granular drenado, este documento demuestra que con esta suposición se obtiene un resultado erroneo en cuanto se refiere a la forma y posición de la curva de ruptura del suelo.

En este documento se propone un nuevo método de interpretación en el cual se tiene en cuenta la variación de volumen durante la experiencia y hace posible la determinación correcta de la curva de ruptura incluso para un suelo granular que sufre durante la experiencia cambios de volumen debidos a los esfuerzos normales y tangenciales.

1. INTRODUCTION

Two methods have been proposed until now for estimating the shear strength characteristics of soil from the results of pressuremeter tests. The first one, proposed by Ménard, 1957, is valid for a general case of a c, Φ — soil. The second one, introduced by Gibson and Anderson, 1961, concerns respectively an ideal clay ($\Phi = 0$, $c \neq 0$) and an ideal sand ($\Phi \neq 0$, $c = 0$).

The both above methods are based on the theories assuming that the soil is an ideal elastic-plastic material, whose volume change is only elastic and can be produced uniquely by changing the spherical stress.

It is known, however, that a pressuremeter test produces in the soil surrounding the borehole, a modification in both, the spherical and the deviatoric components of the stress tensor.

If the soil is a satured clay or silt, under the rate of pressure increase used in a standard pressuremeter test, this modification of stress will produce only a negligible volume change in the soil mass. If, however, the pressuremeter test is made in a granular soil, the same stress change will result in a considerable volume change of the soil, due to compression and dilatancy.

In this paper an attempt is made to evaluate the influence of the volume change of the soil during a pressuremeter test on the obtained failure envelope, and a method is proposed which makes it possible to determine the correct failure envelope also in the case when during the test the soil is undergoing volume changes due to compression and dilatancy.

2. THEORETICAL CONSIDERATIONS

RELATIONSHIP BETWEEN THE CASES OF THE EXPANSION OF A CYLINDRICAL CAVITY RESPECTIVELY FROM A FINITE RADIUS ($r_o \neq 0$) AND FROM ZERO RADIUS ($r_o = 0$)

If a cylindrical cavity is expanded in an infinite medium from a finite radius r_o, so that r_o is increased by $\triangle r$, the resulting distribution of stress and strain will be geometrically similar to that occurring in a problem of the expansion of a cavity from $r_o = 0$, outside a cylindrical surface whose relative radial displacement $\frac{u_\rho}{\rho'}$ is equal to $\frac{\triangle r}{r_o}$

The condition of similarity is therefore

$$\frac{u_\rho}{\rho'} = \frac{\triangle r}{r_o} \qquad (1)$$

where ρ' is the distance of a cylindrical surface from the center-line of the cavity before expansion, and u_ρ is the radial displacement of the same surface during the expansion of the cavity from $r_o = 0$ to r.

Hence, after the expansion from 0 to r, the distance of the considered surface from the center line of the cavity will be

$$\rho = \rho' + u_\rho \qquad (2)$$

A solution valid for the expansion of a cavity from $r_o = 0$ contains an infinite number of the values of the ratio $\frac{u_\rho}{\rho'}$ varying from $\frac{u_\rho}{\rho'} = 0$ at $\rho' = \infty$, to $\frac{u_\rho}{\rho'} = \infty$ at $\rho' = r_o = 0$. Hence, for any given value of $0 \leqq \frac{\Delta r}{r_o} \leqq \infty$, the solution of the first mentioned problem corresponding to $r_o \neq 0$ can readily be found within the solution of the second problem corresponding to $r_o = 0$.

All we need to this end, is the answer to the question: at what relative distance $\frac{\rho}{r}$ in the problem $r_o = 0$, the value of the ratio $\frac{u_\rho}{\rho'}$ is equal to a given value of $\frac{\Delta r}{r_o}$ in the problem $r_o \neq 0$.

The relationship between $\frac{\rho}{r}$ and $\frac{u_\rho}{\rho'}$, and hence also between $\frac{\rho}{r}$ and $\frac{\Delta r}{r_o}$, by taking into account the volume change of the soil, has been derived elsewhere (Ladanyi, 1961), and will be discussed later in the text.

The above mentioned similarity makes it possible to consider, instead of the problem of the expansion of a cylindrical cavity from a finite radius ($r_o \neq 0$), corresponding to a normal pressuremeter test, the analogous problem of the expansion of a cylindrical cavity from zero radius ($r_o = 0$), which is usually a simpler one.

An approximate solution for the later case is presented in the following.

EXPANSION OF A CYLINDRICAL CAVITY FROM ZERO RADIUS

The proposed approximate method for determining the state of stress in the case of the expansion of a cylindrical cavity from zero radius is based on the following assumptions:

- The medium in which the expansion of the cavity is occurring is infinite, and originally homogeneous and isotropic;
- the length of the cavity is infinite;
- the expansion is occurring in drained conditions, so that all the considered stresses are effective;
- the mass forces are neglected.

Under the above assumptions, the differential equation of equilibrium at a point at a distance ρ from the center-line of the cavity, may be written in the form:

$$\frac{d\sigma_\rho}{d\rho} + \frac{\sigma_\rho - \sigma_t}{\rho} = 0 \qquad (3)$$

where σ_ρ and σ_t are the principal normal stresses in the radial and circumferential directions respectively.

Since from the above assumptions it follows that the expansion is occurring under plane strain condition, the third principal normal stress σ_z, perpendicular to the ρ, t-plane, is a function of σ_ρ , σ_t and of the Poisson's ratio ν, and will not be considered in this paper.

Dividing Eq. (3) by σ_ρ and putting

$$\frac{\sigma_t}{\sigma_\rho} = N \qquad (4)$$

it becomes

$$\frac{d\sigma_\rho}{\sigma_\rho} = -(1 - N)\frac{d\rho}{\rho} \qquad (5)$$

This equation of equilibrium can be integrated provided the value of the ratio N between the principal stresses is known at every point of the medium.

In a previous paper [2] it was shown that the necessary relationship

$$N = f\left(\frac{\rho}{r}\right)$$

can be obtained by combining together the relationships: $N = f(\gamma)$, representing the stress-strain curve of the soil obtained in a drained triaxial test, and $\gamma = f\left(\frac{\rho}{r}, e\right)$, showing the distribution of the shear strain γ around a cylindrical cavity expanded from zero radius, where the actual volume change of the soil is taken into account. Here, e denotes the unit volume strain of the soil, positive for a volume decrease, and negative for a volume increase.

A typical shape of the curve $N = f\left(\frac{\rho}{r}\right)$ obtained by this procedure for a granular soil is shown in Fig. 1.

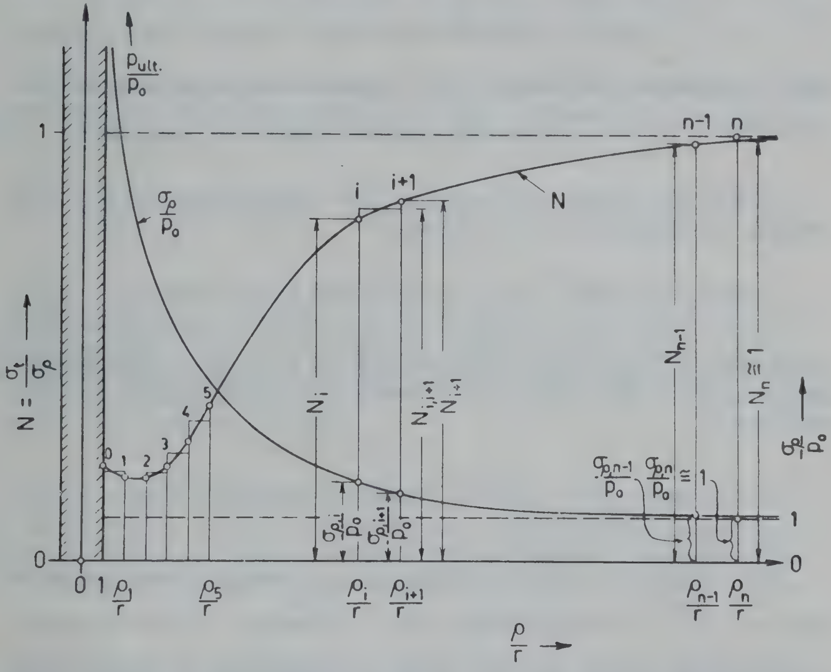
$\frac{p_{ult.}}{p_o}$
1
0
$\frac{\sigma_\rho}{p_o}$
N
i
i+1
n-1
n
$N = \frac{\sigma_t}{\sigma_\rho}$
0 1 2 3 4 5
N_i
$N_{i,i+1}$
N_{i+1}
N_{n-1}
$N_n \cong 1$
$\frac{\sigma_{\rho i}}{p_o}$
$\frac{\sigma_{\rho i+1}}{p_o}$
$\frac{\sigma_{\rho n-1}}{p_o}$
$\frac{\sigma_{\rho n}}{p_o} \cong 1$
$\frac{\sigma_\rho}{p_o}$
1
0
0 1
$\frac{\rho_1}{r}$
$\frac{\rho_5}{r}$
$\frac{\rho_i}{r}$
$\frac{\rho_{i+1}}{r}$
$\frac{\rho_{n-1}}{r}$
$\frac{\rho_n}{r}$
$\frac{\rho}{r}$

Fig. 1 — Expansion of a cylindrical cavity from zero radius. Scheme for the calculation.

Fig. 1 — Dilatación de una cavidad cilíndrica a partir de un radio igual a cero. Esquema para el cálculo.

In the above mentioned paper, Eq. 5 has been integrated approximately by replacing the actual curve $N = f\left(\frac{\rho}{r}\right)$ by a broken line, having its intersection points on the actual curve.

A simpler and for the purpose of this paper sufficiently accurate solution can be obtained by replacing the curve

$N = \left(\frac{\rho}{r}\right)$ by a diagram in steps (Fig. 1). In this latter solution, it is assumed that, within any considered interval i, i + 1, limited by the relative distances $\frac{\rho_i + 1}{r}$ and $\frac{\rho_i}{r}$, the value of N is constant and equal to

$$N_{i,\,i+1} = \tfrac{1}{2}\,(N_i + N_{i+1}) \qquad (6)$$

where N_i and N_{i+1} are the ordinates of the actual curve $N = f\left(\frac{\rho}{r}\right)$ at the boundaries of the interval. By increasing the number of steps, it is possible to approximate the curve $N = f\left(\frac{\rho}{r}\right)$ to any desired degree of accuracy.

With the above assumption, the integration of Eq. (5) within the interval i, i+1 gives

$$\ln \sigma_\rho = \ln C_{i,\,i+1} - (1 - N_{i,\,i+1}) \ln \rho \qquad (7)$$

From Eq. (7) it follows that the radial stresses at the boundaries of the interval are related with each other by the expression

$$\ln \frac{\sigma_{\rho,\,i}}{\sigma_{\rho,\,i+1}} = (1 - N_{i,\,i+1}) \ln \frac{\rho_{i+1}}{\rho_i} \qquad (8)$$

By using Eq. (8) the value of σ_ρ can be found at any distance $\frac{\rho k}{r}$, corresponding to a boundary of an interval, provided the value of this stress is known at a single point in the medium.

In fact, the value of σ_ρ is known only at infinity where σ_ρ becomes equal to the original pressure in the medium, p_o, perpendicular to the center line of the cavity.

In the proposed approximate method, however, this boundary condition cannot be taken into account. Instead, it is necessary to introduce an approximate boundary condition obtained by assuming that, at a sufficiently large but finite distance $\frac{\rho_n}{r}$, $\sigma_{\rho,n} = p_o$. At the same point, if the original isotropy of stress is assumed, N_n will be equal to unity, and

p_o will be equal to the original effective spherical stress in the soil.

Substituting this boundary condition into Eq. (8) and proceeding from step to step from the outside towards the center line of the cavity, the calculation leads to the following general expression for the radial stress $\sigma_{\rho,k}$ at the distance $\frac{\rho k}{r}$

$$\ln \frac{\sigma_{\rho,k}}{p_o} = \sum_{i=k}^{i=n-1} (1 - N_{i,i+1}) \ln \frac{\rho_{i+1}}{\rho_i} \qquad (9)$$

The internal pressure $p_{ult.}$ in the cavity necessary for expanding it from zero radius is then obtained by putting in Eq. (9) $k = 0$, $\sigma_{\rho,n} = p_{ult.}$ and $N = N_o$.

$$\ln \frac{p_{ult.}}{p_o} = \sum_{i=0}^{i=n-1} (1 - N_{i,i+1}) \ln \frac{\rho_{i+1}}{\rho_i} \qquad (10)$$

It should be noted that in the case of the expansion of a cylindrical cavity from a finite radius r_o, the value of $p_{ult.}$ given by Eq. (10) represents the limiting internal pressure to which the pressure in the cavity must tend when the ratio $\frac{\triangle r}{r_o}$ tends to infinity.

The above proposed method for integrating the equation of equilibrium (5) is approximate, but has advantage that no assumption is needed concerning the elastic properties and the shape of the failure envelope of the soil.

PRINCIPLE OF THE PROPOSED METHOD OF INTERPRETATION OF A PRESSUREMETER CURVE

From a theoretical point of view, a pressuremeter curve represents a relationship between the internal pressure p in a cylindrical cavity with original radius r_o and the corresponding increase in radius $\triangle r$. Its general form is

$$\frac{p}{p_o} = f\left(\frac{\triangle r}{r_o}\right) \qquad (11)$$

and its range is from $\triangle r = 0$ at $p = p_o$ to $\triangle r = \infty$ at $p = p_{ult}$ (Fig. 2). Owing to the above mentioned similarity between the cases of the expansion of cavities from $r_o = 0$

and $r_o \neq 0$ respectively, the relationship given by Eq. (11), and valid for the case $r_o \neq 0$, is identical with the relationship

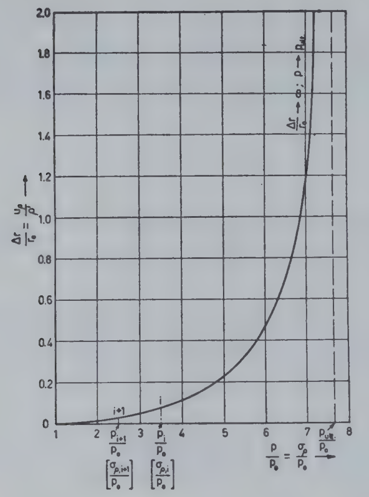

Fig. 2 — Theoretical pressure meter curve.

Fig. 2 — Curva teórica de presiones.

$$\frac{\sigma_\rho}{p_o} = f\left(\frac{u_\rho}{\rho'}\right) \qquad (12)$$

valid for the case $r_o = 0$.

Its range is from $\frac{u_\rho}{\rho'} = \infty$ at $\rho' = 0$, where $\rho = u_\rho = r$, and $\sigma_\rho = p_{ult.}$, to $\frac{u_\rho}{\rho'} = 0$ at $\rho = \rho' = \infty$, where $\sigma_\rho = p_o$.

From the same considerations, it follows that to any two successive points on a pressuremeter curve, having coordinates, say,

$$\left[\left(\frac{p_{i+1}}{p_o}\right), \left(\frac{\Delta r}{r_o}\right)_{i+1}\right] \text{ and } \left[\left(\frac{p_i}{p_o}\right), \left(\frac{\Delta r}{r_o}\right)_i\right]$$

where $p_i > p_{i+1}$, correspond in the $r_o = 0$ case the stresses $\frac{\sigma_{\rho,i+1}}{p_o}$ and $\frac{\sigma_{\rho,i}}{p_o}$ occurring at the distances $\frac{\rho_{i+1}}{p_o}$ and $\frac{\rho_i}{r}$.

Therefore, in Eq. (8) the radial stresses $\sigma_{\rho,}$ and $\sigma_{\rho,i+1}$ may be replaced by p_i and p_{i+1}, and the equation can be used for determining from the coordinates of a given pressuremeter curve the values of the corresponding ratio of the principal stresses $N_{i,i+1}$. From Eq. (8) it is obtained

$$1 - N_{i,i+1} = \frac{\log \frac{p_i}{p_{i+1}}}{\log \frac{\rho_{i+1}}{\rho_i}} \qquad (13)$$

If i and i+1 are two not very distant points of a pressuremeter curve, the value of $N_{i,i+1}$ may be considered approximately exact at the middle of the interval $i, i+1$, and will correspond to the pressure

$$p_{i,i+1} = \tfrac{1}{2}\,(p_i + p_{i+1}) \tag{14}$$

The minor circumferential principal stress $p_{t,i,i+1}$ corresponding to the radial stress $p_{i,i+1}$ is equal to

$$p_{t,i,i+1} = N_{i,i+1} \cdot p_{i,i+1} \tag{15}$$

In this manner, by putting $p_{i,i+1} = \sigma_1$ and $p_{t,i,i+1} = \sigma_3$ a Mohr stress circle is obtained for every considered interval $i, i+1$, and a failure envelope tangential to the circles can be drawn.

CONSIDERATION OF THE VOLUME CHANGE

However, in order that Eq. (13) might be used, it will be necessary to find the relationship between the term log $\frac{\rho_{i+1}}{\rho_i}$ and the deformations measured in a pressuremeter test. Moreover, since the processus is occurring in granular soil under drained conditions, volume changes of the soil should be taken into account.

In the case of the expansion of a cylindrical cavity from zero radius it was shown elsewhere [2] that the value of the distortion γ at a relative distance $\frac{\rho}{r}$ is given by

$$\gamma = \omega \left(\frac{r}{\rho}\right)^2 \tag{16}$$

where $\omega = 1 + \frac{\triangle E_{r,\rho}}{E_0}$. Herein, $\triangle E_{r,\rho}$ denotes the total volume change of the soil which during the expansion is located between the cylinders with radii r and ρ, and $E_0 = \pi r^2$.

located between the cylinders with radii r and ρ, and $E_0 = = \pi r^2 \,.\, 1$ is the current volume of the cavity.

On the other hand, in the above mentioned paper, the following relationship between γ and the ratio $\frac{u_\rho}{\rho'}$ was developed:

$$\frac{u_\rho}{\rho'} = \frac{1}{\sqrt{1-\gamma}} - 1 \tag{18}$$

Substituting (16) into (18) and solving for $\frac{\rho}{r}$ it is obtained

$$\frac{\rho}{r} = \sqrt{\frac{\omega\left(\frac{u_\rho}{\rho'} + 1\right)^2}{\left(\frac{u_\rho}{\rho'} + 1\right)^2 - 1}} \tag{19}$$

Since $\frac{u_\rho}{\rho'}$ in a $r_0 \neq 0$ — case corresponds to $\frac{\Delta r}{r_0}$ in a $r_0 = 0$ case, Eq. (19) can be written as

$$\frac{\rho}{r} = \sqrt{\frac{\omega\left(1 + \frac{\Delta r}{r_0}\right)^2}{\left(1 + \frac{\Delta r}{r_0}\right)^2 - 1}} \tag{20}$$

The deformations measured in a pressuremeter test are usually plotted in terms of the volume change of the borehole ΔV rather than in terms of the change in its radius Δr. Then, if V_0 denotes the original volume of the borehole in the zone of the test corresponding to r_0, we have

$$\left(1 + \frac{\Delta r}{r_0}\right)^2 = 1 + \frac{\Delta V}{V_0} = \frac{V}{V_0} = \frac{1}{1 - \frac{\Delta V}{V}} \tag{21}$$

Substituting (21) into (20), it becomes

$$\frac{\rho}{r} = \sqrt{\omega \frac{V}{\Delta V}} \tag{22}$$

The coefficient ω expresses the influence on the value of γ, and according to (20), also on the value of $\frac{\Delta r}{r_0}$, of the volume change of the soil due to its compressibility and dilatancy characteristics.

However, the relationship between the total volume strain e of the soil and the distortion γ, necessary for the evaluation of ω is not known, but must be found by a trial and error procedure, as explained in [2].

Two typical curves $e = f(\gamma)$ obtained for a natural sand, in tests where the spherical pressure is increasing during the shear, are shown dashed in Fig. 3. Considering the shape of the curves, it is evident that the calculations would be complicated considerably if the exact shape of the curves were taken into account.

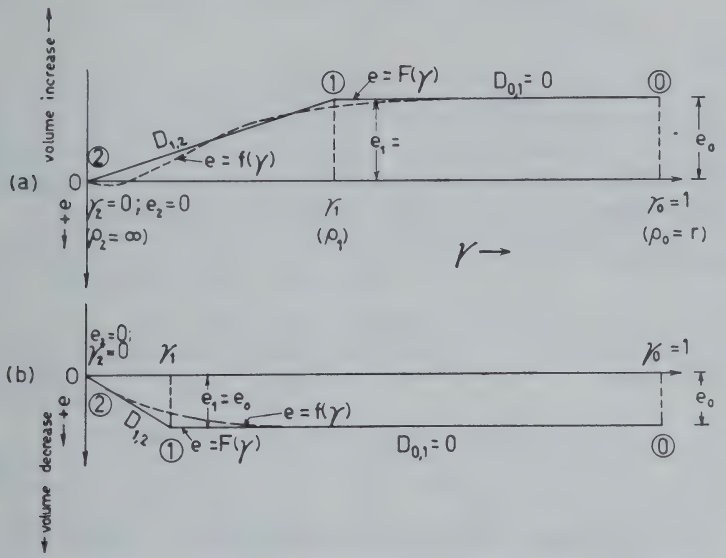
volume increase
(a)
0
②
$D_{1,2}$
$e = f(\gamma)$
① $e = F(\gamma)$
$D_{0,1} = 0$
⓪
$e_1 =$
e_0
+e
$\gamma_2 = 0; e_2 = 0$
$(\rho_2 = \infty)$
γ_1
(ρ_1)
$\gamma \rightarrow$
$\gamma_0 = 1$
$(\rho_0 = r)$
(b)
0
$e_2 = 0;$
$\gamma_2 = 0$
γ_1
$\gamma_0 = 1$
$e_1 = e_0$
$e = f(\gamma)$
e_0
②
$D_{1,2}$
① $e = F(\gamma)$
$D_{0,1} = 0$
⓪
+e
volume decrease

Fig. 3 — Typical curves volume strain e versus distortion γ obtained in drained shear with granular soils.

Fig. 3 — Curvas-tipo de una deformación volumétrica e respecto a una distorsión γ obtenidas en suelos granulares.

In the considered problem, having in mind other sources of error, such a complication would not be justifiable.

In fact, the numerical calculations show that, for taking into account in the interpretation of pressuremeter tests, the volume change of the soil, it is necessary to know only some characteristic points of the curve $e = f(\gamma)$.

Therefore, it was decided to replace the actual curve $e = f(\gamma)$ by a simpler relationship $e = F(\gamma)$, composed of two straight lines, (Fig. 3,0-1 and 1-2).

In a previous paper [2] the following expression was developed

$$\omega = \left(\frac{\rho}{r}\right)^2 \left[\left(\frac{\rho_i}{\rho}\right)^{2\,(1+D_{i,i+1})} \frac{e_i + \gamma_i}{1 + D_{i,i+1}} + \frac{D_{i,i+1} \cdot \gamma_{i+1} - e_{i+1}}{1 + D_{i,i+1}} \right] \qquad (23)$$

giving the value of ω, if, in an interval $i, i+1$, the curve $e = f(\gamma)$ is approximated by a straight line, whose equation is

$$e = D_{i,i+1} (\gamma - \gamma_{i+1}) + e_{i+1} \tag{24}$$

where

$$D_{i,i+1} = \frac{e_i - e_{i+1}}{\gamma_i - \gamma_{i+1}} \tag{25}$$

Applying Eq. (23) successively to the intervals 0-1 and 1-2 of the broken line $e = F(\gamma)$, Fig. 3, it is obtained:

interval 0-1:

$$\omega = 1 + e_o - e_o \left(\frac{\rho}{r}\right)^2 \tag{26}$$

interval 1-2:

$$\omega = \gamma_1 \left[\frac{1 + e_o}{\gamma_1 + e_o}\right]^{\left(1 + \frac{e_o}{\gamma_1}\right)} \left(\frac{r}{\rho}\right)^{2 \frac{e_o}{\gamma_1}} \tag{27}$$

Substituting ω defined by equations (26) and (27) in Eq. (22) gives:

interval 0-1:

$$\frac{\rho}{r} = \sqrt{\frac{1 + e_o}{\frac{\Delta V}{V} + e_o}} \tag{28}$$

interval 1-2:

$$\frac{\rho}{r} = \left\{\left[\gamma_1 \left(\frac{V}{\Delta V}\right)\right]^{\frac{\gamma_1}{\gamma_1 + e_o}} \cdot \frac{1 + e_o}{\gamma_1 + e_o}\right\}^{\frac{1}{2}} \tag{29}$$

From equations (28) and (29), the value of the term $\log \frac{\rho_{i+1}}{\rho_i}$, can now be determined.

Interval 0-1:

$$\log \frac{\rho_{i+1}}{\rho_i} = \tfrac{1}{2} \log \frac{\left(\frac{\Delta V}{V}\right)_i + e_o}{\left(\frac{\Delta V}{V}\right)_{i+1} + e_o} \tag{30}$$

Interval 1-2:

$$\log \frac{p_{i+1}}{p_i} = \frac{1}{2} \frac{\gamma_1}{\gamma_1 + e_o} \log \frac{\left(\frac{\Delta V}{V}\right)_i}{\left(\frac{\Delta V}{V}\right)_{i+1}} \tag{31}$$

The expressions (13), (14), (15), (30), (31) can be used for determining from the results of a pressuremeter test the shape of the failure envelope for a granular soil by considering also the volume change of the soil during the test.

However, before going further, some remarks should be made concerning the practical range of the utilization of the above formulas (30) and (31).

It is seen that the equations (30) and (31) are valid in the region where the distortion γ is respectively greater and smaller than γ_1 (Fig. 3).

The results of drained triaxial tests with granular soils show that the slope of the curve $e = f(\gamma)$ is steepest at relatively small distortions. For higher values of γ, the curve becomes nearly parallel to the γ axis. If the actual curve $e = f(\gamma)$ is replaced by two straight lines, as in Fig. 3, it is found that the intersection point 1 between the two straight lines corresponds approximately to $\gamma_1 \simeq 0.30$ for soils showing a volume increase with increasing distortion (p. ex. medium dense sands under a low spherical pressure or dense sands). On the other hand, for soils showing a volume decrease with increasing distortion (p. ex. medium dense sands under a high spherical pressure or loose sands), the value of γ_1 is located approximately at $\gamma_1 \simeq 0.1$.

From equations (18) and (21) it follows

$$\frac{V}{V_o} = \frac{1}{1 - \frac{\Delta V}{V}} = \frac{1}{1 - \gamma} \tag{32}$$

According to Eq. (32), a value $\gamma_1 = 0.1$ corresponds in a pressuremeter test to $\left(\frac{V}{V_o}\right)_1 = 1.11$ or $\left(\frac{\Delta V}{V}\right)_1 = 0.1$, while a value $\gamma_1 = 0.30$ corresponds to $\left(\frac{V}{V_o}\right)_1 = 1.43$ or $\left(\frac{\Delta V}{V}\right)_1 = 0.30$.

Since in a pressuremeter test made in a borehole, the spherical pressures in the soil in the vicinity of the borehole are relatively high, the soil is likely to undergo a volume decrease during the test so that the limits: $\gamma_1 \simeq 0.10$ and $\left(\frac{V}{V_o}\right)_1 = 1.11$ will be valid in the majority of cases.

Therefore, from the practical point of view, it will generally be sufficiently accurate using the simpler Eq. (30) for the portion of the pressuremeter curve for which $\left(\frac{V}{V_o}\right) \geqq 1.11$ or $\frac{\triangle V}{V} \geqq 0.1$ (Fig. 4).

3. PRACTICAL CALCULATION PROCEDURE

In evaluating from a pressuremeter curve the shear strength characteristics of a granular soil on the basis of the above theory, either of the two methods described in the following can be utilized.

In the first method a number of points is chosen on the portion of the pressuremeter curve where $\frac{V}{V_o} \geqq 1.11$.

From any two successive and not very distant points i, i+1 on the curve, the Mohr circles of failure can be calculated by using equations 13, 14, 15 and 30. However, the value of e_o in Eq. 30 is not known in the beginning, and must be determined by trial and error. In the first trial it is assumed that $e_o = 0$, and a first failure envelope is obtained. If the envelope is a straight line passing through the origin, as supposed for a granular soil with no cohesion, the assumption $e_o = 0$ is correct. If, on the contrary, a curved envelope passing above or below the origin is obtained, it means that the assumption $e_o = 0$ is incorrect and other po-

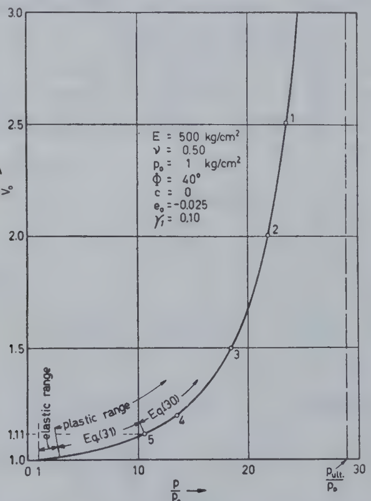

Fig. 4 — A calculated pressuremeter curve.

Fig. 4 — Curva presiométrica calculada.

sitive or negative values of e_0 must be tried until finally for a given value of e_0 a straight line envelope through the origin is obtained.

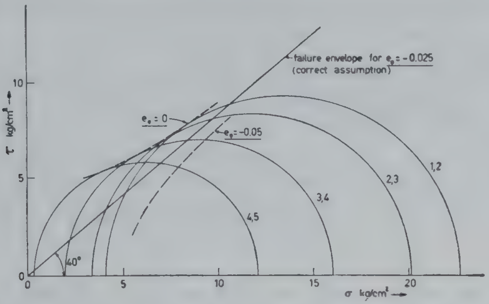

Fig. 5 — Failure envelopes corresponding to the pressuremeter curve, Fig. 4, and to various assumptions concerning the volume strain e_0 of the soil.

Fig. 5 — Curvas de rupturas correspondientes a la curva presiométrica de la figura 4 y a varias condiciones de la deformación volumétrica e_0 del suelo.

An application of this method is shown in Fig. 4 and 5. The points on the pressuremeter curve used in the calculation are 1 to 5, Fig. 4. In Fig. 5 the Mohr circles corresponding to these points are shown only for the assumption $e_0 = 0$. It should be noted that the pressuremeter curve in Fig. 4 is not measured in a test but obtained by calculation, assuming that the soil is a sand with the following properties:

$$\Phi = 40^\circ,\ c = 0,\ E = 500\ \text{kg/cm}^2,\ \nu = \tfrac{1}{2},$$

$$\gamma_1 = 0.10,\ e_0 = -\ 0.025\ \text{(volume increase)},\ p_0 = 1\ \text{kg/cm}^2.$$

In Fig. 5 it will be seen that only the correct assumption that $e_0 = -\ 0.025$ furnished the correct failure envelope corresponding to $\Phi = 40^\circ$ and $c = 0$.

At the same time, it is seen that the assumption that $e_0 = 0$ made in the two methods of interpretation mentioned in the beginning of this paper may result in finding an incorrect position and shape of the failure envelope, even if the actual volume changes in the soil are relatively small.

Another method for finding the value of Φ from a pressuremeter curve obtained in a granular soil is based on a proposition made by Gibson and Anderson, 1961. These two authors have shown that, if for a granular soil, characterized by constant values of E, ν and Φ, and no volume change in the plastic range, the results of a pressuremeter test are plotted in the form of a curve of p (log scale) against $\frac{\Delta V}{V}$ (log scale) it is found that the test points lie on a straight line.

According to the theory developed by the same authors, the slope of this line between any two points i, i+1 is equal to

$$\tfrac{1}{2}\,(1 - N_{i,i+1}) = \frac{\log p_i - \log p_{i+1}}{\log\left(\frac{\Delta V}{V}\right)_i - \log\left(\frac{\Delta V}{V}\right)_{i+1}} \qquad (33)$$

It will be seen that an expression identical to (33) is obtained by substituting Eq. (30) into Eq. (13) and by putting $e_o = 0$.

However, when $e_o \neq 0$, equations (30) and (13) give

$$\tfrac{1}{2}\,(1 - N_{i,i+1}) = \frac{\log p_i - \log p_{i+1}}{\log\left[\left(\frac{\Delta V}{V}\right)_i + e_o\right] - \log\left[\left(\frac{\Delta V}{V}\right)_{i+1} + e_o\right]} \qquad (34)$$

Eq. (34) shows that for a soil with $e_o \neq 0$ the correct value of $\tfrac{1}{2}\,(1 - N_{i,i+1})$ can be obtained only by assuming a correct value for e_o and by plotting the curve $\left[\frac{\Delta V}{V} + e_o\right]$ against p in the above diagram (Fig. 6). In practice, the correct result is obtained by trial and error, beginning with the assumption that $e_o = 0$, and ending when a straight line is obtained for a given value of e_o.

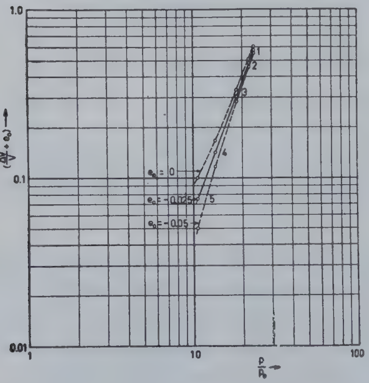

Fig. 6 — Determination of the angle Φ by the method adapted from Gibson and Anderson 1961.

Fig. 6 — Determinación del ángulo Φ por el método adaptado de Gibson y Anderson 1961.

The results obtained when the second method is applied to the points 1 to 5 of the pressuremeter curve Fig. 4 are shown in Fig. 6. For $e_o = -0.025$ a straight line is obtained whose shape corresponds to $\Phi = 40°$.

4. INFLUENCE OF COHESION

It is important to note that the method proposed in this paper will give a correct failure envelope also when it is applied to a pressuremeter curve obtained in a c′, Φ′-soil, provided the volume changes in the soil during the test are negligible. If, however, the volume changes are considerable, the shape of the failure envelope will be influenced simultaneously by the cohesion and by the volume change. In this latter case, for the proposed method to be applicable, one of the two unknown magnitudes (c′ or e) must be previously estimated by another method.

5. CONCLUSIONS

If, in the interpretation of pressuremeter tests made under drained conditions in compressible and dilatant granular soils, it is assumed that the volume change of the soil in the plastic range is zero, a failure envelope is obtained which may differ in its shape and position from the actual one. In particular it is found that, for a soil whose volume is increasing during the test ($e_o < 0$), the assumption $e_o = 0$ leads to a failure envelope located above the actual one. On the contrary, for a soil whose volume is decreasing during the test ($e_o > 0$), the assumption $e_o = 0$ results in a failure envelope located below the actual one.

The method of interpretation proposed in this paper enables taking into account the volume changes of the soil during the pressuremeter test and is therefore particularly useful in evaluating pressuremeter curves obtained in dilatant and compressible granular soils, where it can furnish correct values both of the angle of shearing resistance Φ and the volume strain at failure e_o.

REFERENCES

1. Gibson, R. E. and Anderson, W. F. (1961)
In situ measurement of soil properties with the pressuremeter. Civil Engineering and Public Works Review, London, May 1961.

2. Ladanyi, B. (1961)
Étude théorique et expérimentale de l'expansion dans un sol pulvérulent d'une cavité présentant une symétrie sphérique ou cylindrique.
Annales des Travaux Publics de Belgique, Bruxelles, Nos. 2 and 4, 1961.

3. Ladanyi, B. (1963)
Interprétation des essais pressiométriques dans les sols pulvérulents.
Les Presses de l'Université Laval, 1963.

4. Ménard, L. (1957)
Mesures in situ des propriétés physiques des sols.
Annales des Ponts et Chaussées, Paris, 127, 3, 1957.

CONSIDERATIONS ABOUT QUALITY CONTROL ON COMPACTION PROCESSES

EVELYNA BLOEM SOUTO SILVEIRA and ARAKEN SILVEIRA
Assistant Professors at the School of Engineering of São Carlos, U.S.P., São Paulo, Brazil.

SUMMARY

This paper presents some considerations about specification problems in soil compaction and their correlation with design, construction and control phases, and describes the application of statistical control chart methods. These keep in mind a better statistical control of the job as a whole and more coherent specifications with variability of construction methods and with the development of construction and measurement techniques.

RESUMO

Êste trabalho apresenta considerações sôbre os problemas da especificação na compactação do solo e sua correlação com as fases de projeto, de construção e de contrôle, e descreve a aplicação de gráficos estatísticos de contrôle, tendentes à obtenção de melhor contrôle estatístico da obra em seu todo e visando estruturar especificações mais coerentes com a variabilidade dos processos de construção e o desenvolvimento das técnicas de trabalho e de medida.

1. INTRODUCTION

The rational and economic construction of compacted embankments is employing, more and more, on the one hand more complex and improved equipments and techniques for field construction, and on the other hand more precise and rapid supplies and methods for measurement of the results obtained by compaction; furthermore, the great dimensions of works performed, as well as the increasing demand of a large number of works, requires more and more that civil engineering employ factors of safety that correspond to minimum economic criteria, that is, to minimum factors of safety compatible with risk conditions economically acceptable in each case.

At the same time, one must consider that a statistical quality control of compacted embankments should be attempted, coherentely with the development of the new construction and measurement techniques, and similarly to what is largely employed in industrial production.

Actually, the assumed statistical criteria must equally interfere with the three following phases:

a) establishment of a minimum factor of safety with which one intends do work;

b) setting-up the embankment construction specifications;

c) construction, use and interpretation of control charts, so that the desired factor of safety is guaranteed, under a certain degree of assurance.

We do not intend to examine the first phase, which will be left to a more suitable occasion. We shall herein attempt to analyse the second and more particularly the third phase.

2. SPECIFICATION

The "specification" notion in general, which has always existed, has been largely changed throughout the time: from merely qualitative statements, it became defined by exact measurements, and should nowadays be expressed by a statistical conception of deviations and tolerances.

Inasfar as concerns the construction of compacted embankments — where specification should describe the characteristics to be attained by compaction — general and indefinite expressions such as "compacted fill" were substituted by the statement of boundary allowable values, commonly minimum percent compaction and maximum range of variation of water-content, defined as related to optimum.

Nowadays, specification is developing so as to set-up the averages and allowable standard deviations, within criteria in which the variability of the compacted embankment, existing in every process that is function of a large number of variable factors, is envolved.

Among these, the thickness of the compacted layers, that varies around the average desired value, the number of passes and the load of the roller, subjected to a changeable criterion of operator and inspector, the overlapping and the number of passes, the speed of the roller and the heterogeneity of irrigation or dryness, functions of the operator technique, and the type of soil itself, that varies enormously from point to point, as shown long enough by specialized literature, are the most important factors.

Furthermore, another factor must be considered, that interferes in the variability of the results defining the characteristics attained by compaction: the variability inherent to the measurement itself, which depends upon equipment, reading operations and operator technique.

There is a real vicious circle is specification problems: for carrying out the design, one must assume some hypotheses which will govern construction specifications; the assumptions which will be considered as a basis of the design should themselves be established with the assumption of what one is going to require from the construction; the specification, as a binding element between design and construction during the construction phase, is still the same binding element construction-design in the designe phase. How, then, to specify, if one thing depends upon the other? In other words, what could break this circle?

In our opinion, mostly in what concerns compactions, two elements tied together have been determining the establishment of a specification, acting subjectively on the practical equationement of the question. These elements are: first, the limitation of our knowledge, mostly in what concerns the variations of the properties that interfere with the soil strength in function of the compaction received by the same soil; secondly, economic factors connected to the problem, which are directly related to our knowledge of the phenomenon, which, to a certain point, has been a function of the economic pressure.

Specification problems will not be solved, until we have secure elements indicating the variation of the properties of the compacted soil with the amount of compaction furnished to the same soil; with such an element, we shall be able to proceed to an economical analysis aiming at the optimum point, for which the design should be made.

The establishment of averages and standard deviations or tolerances * of the specifications defining the characteris-

---

* The second is a function of the first, for a particular frequency distribution curve and for a given acceptable probability.

tics to be attained by compaction processes should be therefore an agreement between compaction and construction costs, that is, it must be done in such a way that, theoretically, any addition in quality required from that point will not result any more in a reduction that economically makes up for the earth volume resulting from the respective increase of the soil strength owing to that compaction addition.

Let us assume that an embankment is to be constructed with a certain initial percent compaction P.C.%, and therefore slopes 1:m and 1:n and volume V.

Starting from this initial percent compaction PC%, let us assume that C_g is what will be called "general cost" of the work, corresponding to the product of the number of compacted cubic meters (V) by the cost per cubic meter compacted according to the initial percent compaction PC%; let C_c be the control cost, which, in the last measure, is a function of V (the number of cubic feet compacted), generally through compaction time; let C_a be the cost corresponding to amortization of the capital, interests, etc., and a factor refering to the faster or slower availability of the finished work. We shall call $\triangle C_g$, $\triangle C_c$ and $\triangle C_a$ the variation of any of these costs when a specification change brings us to the new slopes $1{:}m - \triangle m$ and $1{:}n - \triangle n$ (volume V′), owing to the increase of soil strength resulting from compaction addition.

Let us assume that $\triangle C_e$ is the cost of any addition of compaction itself, that is, the corresponding addition of energy furnished to the material in order to pass from the initial percent compaction PC to one grater, for which the compacted volume will be V′.

Theoretically, the ideal specification will be given by the minimization of the function:

$$F = \triangle C_e + C_g + C_c + C_a$$

This means that, starting from a certain initial percent compaction, such as 95%, of maximum dry density, refered to the Standard Proctor Test, which will result in a volume V of compacted cubic meters, if one wants to study the advantages brought by working within 100% of the same test, for instance, one should study the variation of the soil strength owing to this change in percent compaction and consequently the new slopes and the new volume V′ of compacted soil; as a result, there will be an addition of $\triangle C_e$, corresponding to the additional energy to be furnished to the volume V′ of the compacted soil; simultaneously, there will probably be a reduction of C_g, because $V' < V$; a reduction of C_c, owing to time reduction as a consequence of $V' < V$; and a reduction of C_a due to a shorter time of amortization, interests, etc., and a faster availability of the finished work.

Since C_g, C_c and C_a mostly and finally depend on the compacted volume, decision will be reached by a duely balanced comparison between the variation of the soil strength with the energy addition, and the cost of this energy addition.

Since the desired working value is settled, the standard deviations or tolerances to be required by field compaction control must be determined, taking into account the variability of the compacted embankment.

In order to determine the standard deviation for specification, we suggest that previous experience in similar conditions of soil and equipment should be taken into account, or else that the following procedure is carried out: an initial piece of embankment be constructed, in carefully established conditions that should be considered a pattern for the whole job construction; samples can be taken from this test fill, in order to have its geotechnical characteristics compared to those of design. During the construction of the test fill, five control tests are carried out, in the same lot, compacted under uniform and carefully patterned conditions of equipment and personnel: they will constitute what is called a "rational subgroup"; this operation is repeated for five rational subgroups (therefore five lots, with five tests each). A range is calculated for each subgroup (the difference between the largest and the smallest observation in the subgroup), and its average m is found. The standard deviation of the universe is given by

$$\sigma = \frac{m}{2{,}326}$$

Inasfar as concerns the tolerance, its range must be larger than 6σ, because, in normal curve, 99.7% of elements are in the range $\mu - 3\sigma$ and $\mu + 3\sigma$ (μ being the universe average); usually, the range of a 9σ (therefore $\mu \pm 4.5\,\sigma$) is adopted as a practical value[2]. Since chance variability * exceeds 6σ only in proportion of 1:300, 3σ is kept by this process for assignalable variability *, which has proved to be rather reasonable in industrial practice.

Therefore, one can estimate standard deviation or tolerance by the expression:

---

* See item 3.2.

$\sigma = \frac{1}{9}$. the range allowed by tolerance.

It should be pointed out herein that, no matter how accurate field control may be, there is always a certain amount of points of the fill with percent compaction lower than the minimum required by specifications[4]: this is the reason why specification should restrain itself to the establishment of the required average, and the acceptable percentage below a certain value, or, which is the same, the average and the standard deviation.

Coherentely, a statistical control should be carried out.

3. CONTROL CHARTS OF COMPACTION QUALITY

3.1. QUALITY CONTROL.

The following phases are executed in any process of quality control:

a) consider what was designed;

b) consider what was produced;

c) compare the designed with the produced;

d) interfere, in case both do not coincide.

As far as embankment compaction is concerned, the "designed" is given by the specification. We shall herein consider separately two cases:

i) the specification is given under the usual form of a minimum percent compaction and a maximum range of water content;

ii) the specification is given by the proposed system, of averages and standard deviations or tolerances.

Quality control charts will be developed for both cases.

3.2. VARIABILITY OF THE FILL.

The variability resulting from factors pointed out in item 2 can be separated into two classes, as all manufacturing variables:

a) the so called "chance variability", which includes all variables inherent in any manufacturing process, such as, rollers, operators, heterogeneity conditions of material, distribution of water-content within the soil, thickness of the layer, number of passes of the roller, number of tests per layer, etc.; this variability, even if located, cannot be corrected except by a significant change in the compaction or control process itself, so that the considered parameter varies within a distribution of probabilities inherent in the process, keeping its average and standard deviation.

As an example, this variability can only be reduced by an increase of the general control, a reduction of the borrow areas, a change in the mixture watering, etc.; besides, this chance variability is affected by climatic conditions.

b) The so called "assignalable variability", which is not inherent in the compaction process, altering its average or standard deviation, and is unstable in time. It generally results from some extraneous causes as improper operation of the equipments, incorrect compaction operations, equipment or inspection instruments worn out and in need of repair [1]. This variability can be assigned and controlled, without altering the compaction process, by quality control.

The chance variability generates what is known, in industry, as the "process capability": that range or variation in part or product quality that is created by the compaction process. Obviously, then, the quality tolerance or zone of acceptability must be set at least wide enough to include within its limits all the variations that are caused by the chance variables in the process. Where the tolerance is broad enough to embrace the process capability, variation beyond the limits can be assumed to result from assignalable variables [1, 3, 5]. These may be detected and located by statistical techniques and corrective measures can be applied.

Therefore, if σ is the standard deviation corresponding to chance variability, any specification must allow at least this standard deviation σ. The tolerance range is also a function of this value, as already seen.

The frequency distribution curves of percent compaction and water-content of a compacted embankment can, within a certain degree of approximation, be assumed as normal curves, which, when plotted and connected with a line, give the familiar bell-shaped curve. This is a logical result from the fact that it is produced by some system of many independent chance acting causes *, and has already been largely observed in literature and in our own experience [4].

Therefore, since the fill is kept in state of statistical control, that is, in such a control that assignalable variable is eliminated, and only chance variables stay, then the average and the standard deviation will be kept.

Control charts are a form of inspection records that guarantee that the state of statistical control is kept.

3.3. INSPECTION PLAN.

Generally, the so called "simple sampling type" is employed in compaction control of embankments: that means that the decision about acceptance or correction (recompaction or water-content correction) of the lot is taken exclusively according to the result of a test carried out on one simple sample [5]. Figure 1 shows schematically the employed system. We do not intend to discuss herein the natural variability within each lot [4], since the adopted inspection plan results from the natural need of concluding as fast as possible the final solution, so that the valuable equipment in case will not be stopped, and compaction work will go on. With the development of the new control techniques, which are faster and cheaper per additional test, as with the use of nuclear test methods — although this process is only destinated to the determination of the in situ soil characteristics, the standard characteristics still having to be properly defined — one can think of progressing to a plan of double or sequential sampling process.

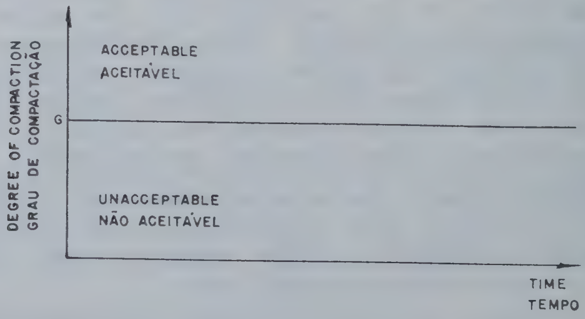

Fig. 1 — Simple sampling method.

Fig. 1 — Método de amostragem simples.

---

* Central Limit Theorem.

Figures 2 and 3 schematically summarize the two systems: in double sampling, a lot is accepted when the test result falls above a certain value G_1; the lot is corrected, when the test result falls below a certain value G_2; the inspection goes ahead with a new test, when the test result falls within a range between G_1 and G_2: the lot is accepted or corrected, depending upon the new test result falls respectively above or below a third value G_3, which lies between G_1 and G_2.

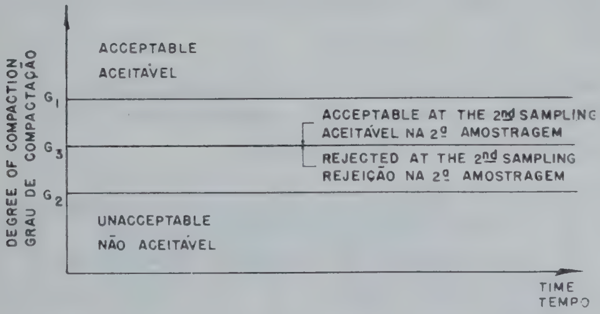
DEGREE OF COMPACTION
GRAU DE COMPACTAÇÃO
ACCEPTABLE
ACEITÁVEL
G1
ACCEPTABLE AT THE 2nd SAMPLING
ACEITÁVEL NA 2ª AMOSTRAGEM
G3
REJECTED AT THE 2nd SAMPLING
REJEIÇÃO NA 2ª AMOSTRAGEM
G2
UNACCEPTABLE
NÃO ACEITÁVEL
TIME
TEMPO

Fig. 2 — Double sampling method.

Fig. 2 — Método de amostragem dupla.

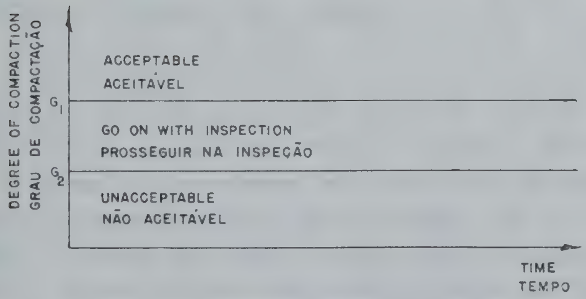
DEGREE OF COMPACTION
GRAU DE COMPACTAÇÃO
ACCEPTABLE
ACEITÁVEL
G1
GO ON WITH INSPECTION
PROSSEGUIR NA INSPEÇÃO
G2
UNACCEPTABLE
NÃO ACEITÁVEL
TIME
TEMPO

Fig. 3 — Sequential sampling method.

Fig. 3 — Método de amostragem seqüencial.

In sequential sampling, a lot is accepted if the test result lies above a value G_1; it is corrected if the result is below a value G_2; if the test result lies within the range G_1 G_2, inspection goes on, with tests successively carried out, until one of them is outside the two limits G_1 and G_2, which decides whether the lot is accepted or corrected.

3.4. CONSTRUCTION AND EMPLOYMENT OF CONTROL CHARTS

We shall analyse herein the construction of control charts, having in mind that averages and standard deviations of samples (lots) of the compacted fill have a normal frequency distribution with averages μ and σ and standard deviations $\sqrt{\frac{\sigma^2}{n}}$ and $\sqrt{\frac{\sigma^2}{2n}}$, n being the number of samples.

We shall consider separately the two cases i and ii refered to item 3.1.

3.4.1. CONTROL CHARTS FOR SPECIFICATIONS GIVEN BY MINIMUM OF PERCENT COMPACTION AND MAXIMUM RANGE OF WATER-CONTENT.

The process of control of the percent compaction in this case may be called "Acceptance-Recompaction", that is, acceptance or recompaction is decided, depending on whether the test result is respectively $\geq$ or $<$ a certain value G given by specification.

In this case, a "fraction defective" with average p can be defined as the relation of the number of compacted lots to the total number of lots considered.

It must be pointed out that, according to this criterion of setting out the specification, the system of control itself suffers some inconvenience, since the construction of the respective charts can only be carried out within a certain confidence degree for more than 10/p samples (according to the American criterion [2]); with a certain confidence level, for the aim of the charts, the number of 30 samples can be considered as the minimum to give each control point. In order to keep the time range from one point to the other from being too large to serve as a control means, a criterion can always be assumed to take the last 30 lots, the control being effected every 10 lots and employing every time the new 10 and the last 20 results that have already been plotted in the last control. This procedure, of course, somehow restricts the efficiency of employing three different marks for the points that are plotted on the charts, so that points with the same mark always correspond to all different measures.

The charts of quality control, in this case, shown in Fig. 4, can be construted as follows: similarly to what is done with standard deviation, that is, on the basis of estimated field compaction data observed in previous experience with other embankments, or of initial compaction under recommendable full-scale construction operations, and careful field control, the value p is estimated: as an example, 10 to 20% can be assumed, depending upon the case. Control charts are then constructed, with time as abcissa and fraction defective as ordenates; the control limits can be assumed as

$$p \pm 0.4 \sqrt{p\,(1-p)} \qquad \text{and} \qquad p \pm 0.6 \sqrt{p\,(1-p)}$$

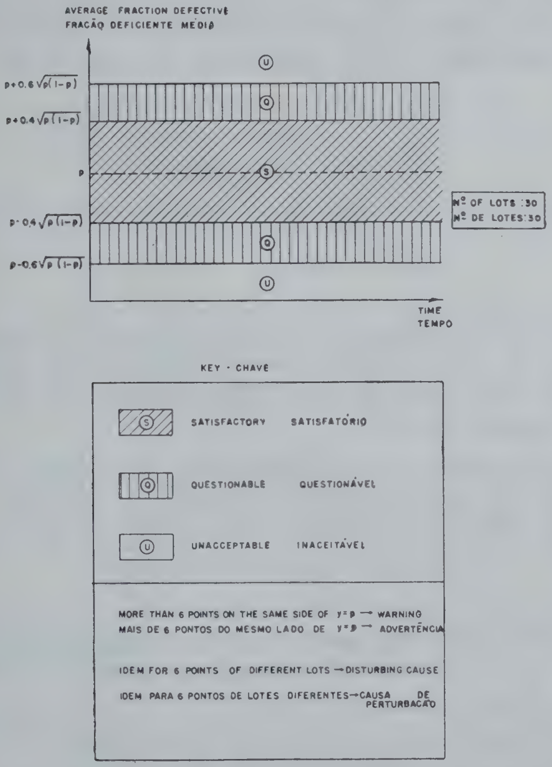

Fig. 4 — Quality control chart of percent compaction — basis: minimum value.

Fig. 4 — Gráfico de contrôle de qualidade de grau de compactação — critério: valor mínimo.

The employment of the chart control can be done as follows: for every 30 lots, the fraction defective p is computed (the number of recompacted lots to the 30 lots considered), and a point given by the pair (p, time) is plotted on control charts.

The interpretation of the results will be given in item 3.4.3.

Inasfar as concerns the water-content control, the process can be called "Acceptance-Correction", that is, if the water-content falls inside a given range, the lot is accepted; otherwise, it is rejected and its water-content must be corrected.

Let us assume that the acceptable range of water-content is given by its limits a and b, as generally occurs in practice, with a and b usually defined as a function of the optimum water-content; in this case, the values of

$$h = \frac{b + a}{2} \qquad \text{and} \qquad v = \frac{b - a}{2}$$

can be considered, and the range will be defined by

$$h \pm v$$

In order to be coherent with the accuracy of the previous method, let us assume that the control is also carried out for each 30 lots, with 10 new and the last 20 already employed in former control.

A control chart can be constructed, with time as abcissa and the average of 30 results obtained as ordenate. Fig. 5 presents the chart, in which control limits are given by

$$h \pm v \qquad \text{and} \qquad h \pm 0.2\,v$$

In keeping with the former case, the chart is employed, by plotting on it the points given by the pair (average of 30 results, time).

Interpretation will be given in item 3.4.3.

3.4.2. CONTROL CHARTS FOR PERCENT COMPACTION AND WATER-CONTENT DEFINED BY AVERAGES AND STANDARD DEVIATIONS.

We shall call variable E of control, not only the percent compaction, but also the water-content, since the construction of the charts is similar for both cases. Let μ, σ and t be respectively the average, the standard deviation and the tolerance of both parameters.

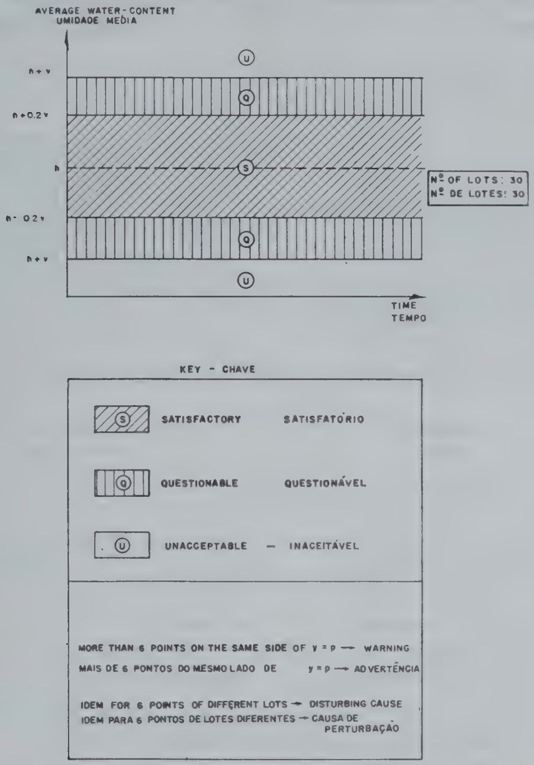

Fig. 5 — Quality control chart of water content — basis: range of variation.

Fig. 5 — Gráfico de contrôle de qualidade da umidade — critério: intervalo de variação.

In this case, the two charts (average and standard deviation, or tolerance) must be employed, for each parameter (percent compaction and water-content).

Depending upon the magnitude of the embankment and its rate of construction, and having in mind the statistical procedure employed in specifications, we assume that 10 samples can be adopted for each point of control. However, if the fill has a slow rate of construction, so that the time range between two control points is excessive as compared with the general conditions, control points of 5 lots can be carried out; although 10 sample points are preferable, from the statistical point of view, we shall herein give the construction of control charts for both cases.

a) *Chart control, for standard deviation specified* — Fig. 6A presents a model of such a chart, for 10 samples points; it can be constructed, plotting as abcissa the time, and as ordenade the average of E for the considered points.

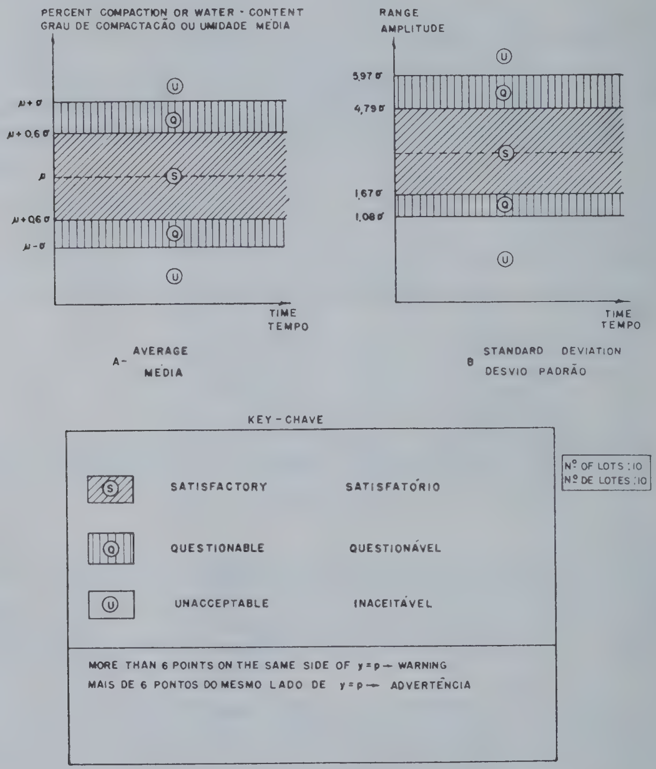

Fig. 6 — Quality control chart of percent compaction and water-content — basis: average and standard deviation.

Fig. 6 — Gráfico de contrôle de qualidade de grau de compactação e umidade — critério: média e desvio padrão.

Control limits are given by

$\mu \pm 0.6\,\sigma$ and $\mu \pm \sigma$ for 10 samples points, and

$\mu \pm 0.9\,\sigma$ and $\mu \pm 1.4\,\sigma$ for 5 samples points.

The use of the charts is very simple, plotting on the graph the points given by the pair (average, time).

Interpretation will be given in item 3.4.3.

The average chart control, however, is not enough for controlling the process, since very high and very low results can be obtained simultaneously, the average being kept approximately the same.

On account of that, the control chart for standard deviations must be employed simultaneously.

The best way of employing it has been the construction of a range chart, which, for 5 or 10 samples, as happens in our case, offers practically the same information given by standard deviation charts, and have a much simpler use [2].

The chart can be constructed, plotting as abcissa the time and as ordinate the range of the results, that is, the difference between the largest and the lowest values. Control limits (according to Pearsons, apud Leme [2]) are given by

1.08 σ, 1.67 σ, 4.79 σ and 5.97 σ for 10 samples points, and

0.37 σ, 0.85 σ, 4.20 σ and 5.48 σ for 5 samples points.

Fig. 6B shows the charts, for 10 samples points.

Interpretation will be given in item 3.4.3.

b) *Control charts, for specified tolerance* — When the specification states the average μ and the tolerance t, a chart can be computed directly for these values, with time as abcissa and the average of the values as ordinate, the control limits being given by

$\mu \pm 0.3\ t$ and $\mu \pm t$ for 10 samples points, and

$\mu \pm 0.45\ t$ and $\mu \pm t$ for 5 samples points.

Fig. 7 presents the respective scheme. Interpretation will be given in item 3.4.3.

3.4.3. INTERPRETATION OF CONTROL CHARTS.

The interpretation of the control charts is the following:

a) For points inside the zone S (Satisfactory), compaction process seems to be under statistical control; if a point lies inside the zones Q (Questionable), it is regarded as a warning of the possibility of the presence of a disturb-process seems to be under statistical control; if a point lies at the zone U (Unacceptable), it indicates that, with

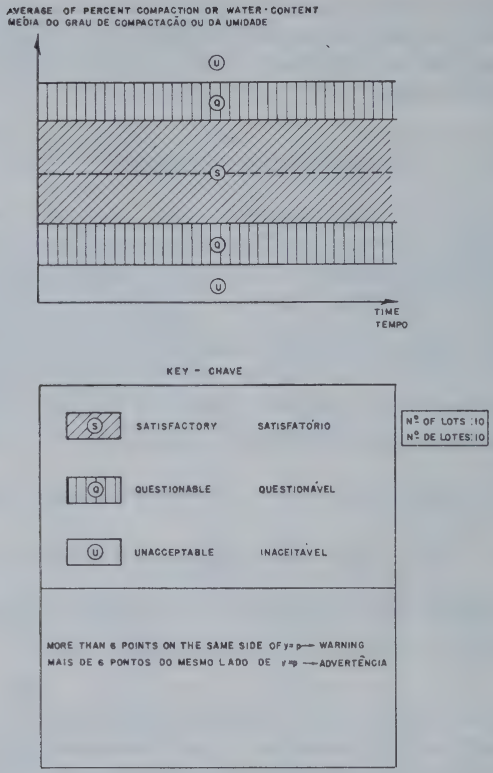
AVERAGE OF PERCENT COMPACTION OR WATER-CONTENT
MÉDIA DO GRAU DE COMPACTAÇÃO OU DA UMIDADE
U
Q
S
Q
U
TIME
TEMPO
KEY - CHAVE
S SATISFACTORY SATISFATÓRIO
Q QUESTIONABLE QUESTIONÁVEL
U UNACCEPTABLE INACEITÁVEL
Nº OF LOTS : 10
Nº DE LOTES: 10
MORE THAN 6 POINTS ON THE SAME SIDE OF y=p → WARNING
MAIS DE 6 PONTOS DO MESMO LADO DE y=p → ADVERTÊNCIA

Fig. 7 — Quality control chart of percent compaction and water-content — basis: tolerance.

Fig. 7 — Gráfico de contrôle de qualidade do grau de compactação e umidade — critério: tolerância.

98% of probability, there is a strong evidence that the out-of-control lot was not produced under the same conditions as the others, or was not tested under the same rules.

b) The presence of 5 successive points * (or 4, for 5 samples points) below or above the average value of the S zone, is also regarded as a strong evidence of the presence of any assignalable cause of variation.

---

* Where 20 previous and 10 new values are employed (item 3.4.1), the warning number is 7, and of different samples; if the mentioned marks are used, the control is easier.

3.5. ADVANTAGES OF THE PROPOSED METHOD.

The advantages of the employment of the quality control charts on compaction processes, either for roads or for earthdams, or else for pavements for industrial buildings, are numerous and easily understandable.

The most important advantages that have been observed in practice are the following: control charts give a simple and fast way of control; they allow the detection of any irregularities, either of compaction equipment (loads, speed), either of layers (thickness, overlapping), or of the measurement equipment (tare, wearing out); they give an indication of improper operational technique, either of compaction (watering, drying, spraying, compaction), or of measurement (test performance, readings, computation); they give an evidence of deficiency of operators, not only in compaction (number of passes of the roller, overlapping of layers, space between layers without sufficient compaction), but also in measurement tests; they warn for undue acceptance of inconvenient soil or at least material that is not specified for the considered place (with organic matter, or excessively sandy or clayey soil, etc.); since the charts are constructed, procedure may be carried out easily by medium level technicians, provided that immediate action is taken by the engineer in order to identify, and if possible eliminate, the disturbing cause.

Furthermore, they constitute a preventive measure intending to prevent, instead of only correcting, the production of lots that must be recompacted, that is, errors of equipment or operators can be rapidly detected and consequently corrected, so that further layers are compacted in such a way that the desired quality is naturally attained.

Last, but not least, measurement faults can be detected, either on equipment or on operators; these faults may systematically lead to errors against security; the natural wearing out and need of repair of instruments, mostly those of compaction tests, can be given as an example; this wearing out alters the volume and weight of the equipment which, if not detected in due time, may result in systematically larger or smaller parameters; consequentely, either insufficientely compacted lots, in which a correct control would demand recompaction, are accepted, or additional anti-economic expenses of energy are unnecessarily required.

These are the chief advantages observed by the use of the proposed method.

It should be mentioned that the control chart is a means, not the end itself. Thus, the quality control engineer must determine not only whether there is control, but whether the control is sufficient and at the best level to meet the specification [1].

4. CONCLUSIONS

The proposed method provides a more rational statistical specification based on previous experience or on the initial placement and compaction under careful full-scale construction and control operations; it also furnishes, with the same basis, a system of quality control charts, in order to secure adequate conformance of the compacted embankment to the design specifications and to the degree of assurance assumed in its establishment. The quality control charts are simple, fast and accessible, and provide a means to the rapid detection of any disturbing causes of defective compaction construction and control beyond those caused by chance variables.

REFERENCES

1. Carson, Gordon B. — "Production Handbook" — The Ronald Press Co., 1958.

2. Leme, Ruy Aguiar da Silva — "Curso de Estatística" — Escola Politécnica da U.S.P. — São Paulo, Brasil, 1958.

3. McGraw-Hill Industrial Organization — "Industrial Organization and Management" — 1956.

4. Mello, V. F. B.; Souto Silveira, E. B.; Silveira, A. — "The representation of the quality of a compacted embankment" — Proceedings of the I Pan-American Conference on Soil Mechanics and Foundation Engineering — México, 1959.

5. Mello, V. F. B.; Souto Silveira, E. B.; Silveira, A. — "Geotecnica's experience in compaction control of earth dams" — Proc. I Pan-American Conf. on Soil Mechanics and Foundation Engineering — México, 1959.

6. Willsmore, A. W. — "Modern Production Control" — 2nd edition — Pitman Press, Bath — 1958.

ENGINEERING PROPERTIES OF RESIDUAL SOILS DERIVED FROM IGNEOUS AND METAMORPHIC ROCKS

GEORGE F. SOWERS

Professor of Civil Engineering, Georgia Institute of Technology
Vice-President, Law Engineering Testing Co., Atlanta, Georgia, U.S.A.

SUMMARY

Residual soils derived from the in-place weathering of crystalline rocks are found in many parts of the world. The physical structure and engineering properties of these materials are unique. The texture and mineralogy still reflect the structure of the original rock, with the added complication of decreased weathering with increasing depth below the ground surface. When sheared the soils exhibit both internal friction and true permanent cohesion, both of which depend on the void ratio and the degree of saturation. Most are strongly anisotropic. They consolidate under load, with compression indexes as high as those of clays but related to void ratio rather than the liquid limit. However, their time rate of hydrodynamic consolidation is fast and secondary compression is a significant part of the total settlement. All exhibit preconsolidation, from 0 to 14 kg per sq cm, with a median of about 3 kg per sq cm. Their densities when compacted are extremely variable and likely to be low, with the median dry density between 1.5 and 1.6 g per cu cm.

SUMARIO

Suelos residuales que provienen de rocas cristalinas intemperizadas en su lugar de orígen se encuentran en muchas partes del mundo. La estructura física y las propiedades de interés al ingeniero de estos materiales son únicas. La textura y mineralogía del residuo todavía refleja la estructura original de la roca, con la complicación de que la intemperización disminuye a medida que aumenta la profundidad. Cizallados los suelos muestran rozamiento interno y verdadera cohesión permanente, ambas cosas que dependen del coeficiente de porosidad y el grado de saturación. La mayoría de estos suelos son muy ani-

sotrópicos. Este suelo se consolida bajo peso con índices de compresión tan altos como los de la arcilla. No obstante su rata de consolidación hidrodinámica es rápida y la compresión secundaria es una parte significante del asentamiento total. Todos estos suelos muestran preconsolidación de 0 a 14 kg. por centimetro cuadrado, con una media aproximada de 3 kg. por centimetro cuadrado. Cuando compactados sus densidades varían extremadamente y tienden a ser bajas.

INTRODUCTION

Residual soils derived from the in-place weathering of igneous and metamorphic rocks are found on every continent, including the subcontinents Australia and Greenland. They are particularly distributed in Southern Asia, Africa, southeastern North America, Central America, the islands of the Caribbean, and South America. Residual soils are relatively more abundant in humid, warm regions that are favorable to rapid rock decomposition. By way of contrast they are not plentiful in northern North America and Europe because continental glaciation removed them from the uplands and blanketed them in the lowlands with glacio or glacio-fluvial deposits.

The physical structure and engineering properties of these soils are different from those of the sedimentary materials on which most attention in soil mechanics has been concentrated. Texturally they are soils, and they include the full range of grain sizes found in sediments. Mineralogically, they include the principal rock forming minerals, the clay minerals and quartz that make up most sediments, plus some unique products of the alteration of both groups. Structurally, they retain much of the internal configuration of their parent rock including its bedding and its defects. As a result, much of the knowledge gained in the study of sediments does not apply to these residual soils.

Only limited study has been given to residual soils because they are most abundant in regions of slower economic and industrial development. However, many of these regions have great potential for future growth because of climate, water, mineral wealth, and surplus manpower. It is the purpose of this paper to summarize the author's experiences with these soils, largely in the southeastern United States but also in the Caribbean and in India and to point out some of the similarities and differences with the more familiar sediments.

SOIL FORMATION

The parent rocks have one feature in common. At one time they were subjected to such intense heat or pressure that they were more or less fluid. On cooling they crystallized, forming a complex fabric of tightly interbedded or interlocked mineral grains. Their structure is similar to that of an alloy, but with far more complex and variable composition. They are bound together by molecular forces on the crystal interfaces, which, because of the small spacing between crystals, are very high. The most abundant of these are the metamorphic rocks, gneiss and schist, and the igneous rocks, granite and diorite; however, basalts and similar basic rocks predominate in some regions such as South India. Also included are metamorphic rocks of lower order such as quartzite and some slates, and the many forms of intrusive and extrusive igneous rocks. Volcanic ash, when indurated, may also be grouped with these parent rocks.

Many of the rocks exhibit evidence of their formation under heat and pressure by the segregation of their minerals into parallel bands or sheets. These bands, which are often mistaken for stratification, range in thickness from several inches in the gneisses to a fraction of an inch in the schists. They are often swirled and contorted in much the same manner as hot taffy candy is formed into parallel but twisted stripes. They are rarely level; instead they are crumpled and twisted with a general tendency to dip in one direction in any one locality.

INTRUSIONS, FAULTING AND JOINTING

Most of the older crystalline rocks have been invaded by younger intrusions of igneous rocks and basalts. Some take the shape of massive domes, others dikes, while some form broad sheets, as thin as cardboard, or irregular networks of pencil-like bodies that pierce the rock like roots of a tree. All break the structure of the original rock, altering the minerals and changing the pattern of its banding or bedding.

Many of these formations have been broken by faulting. While the importance of the major faults has long been recognized, that of the minor faults is often ignored. They form surfaces of weakness that are usually not related to the major rock structure and along which weathering advances.

Nearly all crystalline rocks are broken by jointing. Some, like basalt, exhibit a regular pattern while others exhibit no pattern at all. Like the faults these are surfaces of weakness and channels for deep weathering.

WEATHERING, SOIL FORMATION

Residual soils accumulate in regions where the rate of rock decomposition exceeds the rate at which the products of weathering can be removed by mass wasting or erosion. Any of the environmental conditions that are favorable to rock decomposition, including warm climate, well-distributed rainfall, thick vegetation whose decay contributes organic acids, and gentle slopes are conducive to residual soil accumulation. Steep slopes, dry climate, or highly seasonal rainfall contribute to mechanical weathering or rapid erosion and are unfavorable.

The length of time the formation has been exposed to weathering is a major factor in residual soil development. Most of the rocks, with the exception of volcanic ash deposits and some schists, decompose slowly. Therefore the greatest deposits of residual soils are in areas of old rocks which have been exposed for long periods, such as the Piedmont region of the eastern United States, of Pre-Cambrian age, which has probably been exposed since the Triassic era or at the latest, the Cretaceous.

Rock composition influences the weathering rate. The quartzites decompose so slowly that they often remain as knobs of solid rock surrounded by residual soils from rocks of equal age but different compositions. Some schists, particularly those high in chlorite, appear to weather rapidly.

It has been the author's observation that the most important factor in the rate of rock weathering is the presence of cracks and fissures through which air and water can penetrate the formation. Massive rocks weather slowly while formations that have been badly broken by shear or jointing weather rapidly and deeply.

The depth of weathering and the thickness of the residual soil blanket is extremely variable because of these factors. At one level site for an office building in Atlanta the footings in one corner were supported by sound gneiss that required blasting for removal. At the opposite corner 200 ft. (65 M) away caissons were excavated 85 ft. (25 M) through residual soil derived from the same rock until the sound rock was reached. This irregularity in the soil thickness is particularly severe in formations that are strongly banded, (with the minerals segregated in layers), where dikes are present, or in areas that exhibit closely spaced and irregular faults.

Typical depths of residual soils are as follows:

Piedmont Region[1], Southeastern U.S.A.	20 to 75 ft (6 to 24M)
Angola, Africa[2]	25 ft (8M)
South India[3]	25 to 50 ft (8 to 15M)
South Africa[4]	30 to 60 ft (9 to 18M)
West Africa[5]	33 to 66 ft (10 to 20M)
Brazil[6]	33 to 83 ft (10 to 25M)

In very old regions the greatest thickness of residual soil is often on the hill tops while the least is in the valleys that have been eroded in the soils. In young, mountainous regions the greatest thickness is usually on the flanks of the slopes.

The boundary between soil and rock is seldom sharp. The degree of weathering becomes less with increasing depth until eventually the rock becomes sound and hard.

SOIL PROFILE

The residual soil profite ordinarily can be divided into three zones:

1. The Upper Zone — A crust of stiff red sandy clays.
2. The Intermediate Zone — A thick bed of loose to firm micaceous sandy silts and silty sands.
3. The Partially Weathered Zone — The transition to unweathered rock consisting of gravelly silty sands with lenses of relatively sound rock.

UPPER ZONE

The upper zone has undergone the most advanced weathering. The soil minerals include quartz, micas, clay minerals, and iron oxides. The quartz is angular and is often stained red or yellow from the iron oxides. The clay minerals are largely members of the kaolinite group (including halloysite), and illites. Residual soils derived from basic rocks tend to contain montmorillonites. Both biotite and muscovite mica are present in widely varying amounts, with some vermiculite and similar hydrous micas [7, 8]. Iron oxides, usually highly oxidized, give the soils the deep red colors which are so characteristic.

The typical grain size curve, Fig. 2, reflects the high degree of weathering in the smooth gradation and the large percentage of fines. The liquid limits range from 30 to 80 with the plastic indexes from 12 to 45. According to the Revised Public Roads System (Highway Research Board System) the soils are classified A-6 and A-7; according to the Unifed System (Corps of Engineers and Bureau of Reclamation) they are CL or CL-ML, with an occasional CH in soils derived from basic rocks.

The soils of this zone are homogenous, with little evidence of macrostructure or of the structure of the rock from which they were derived. Occasionally zones of scattered boulders or seams of angular quartz may be observed which mark the path of weathered, resistant dikes but between these the soil appears structureless.

The upper zone is usually stiff. There are at least two causes. First, the soils are desiccated, particularly in the tropical and subtropical regions where they bake in the hot sun. Since the clays are largely of the kaolinite family, they do not tend to absorb water during wet seasons and swell. Second, the leaching of the soluble minerals from the surface tends to cause the accumulation of these materials in the deeper parts of the upper zone where they harden into weak cements.

The less soluble iron and aluminum compounds remain above and become highly oxidized, and harden. This process, termed laterization, appears to have been operative to some extent in the upper zone of all residual soils derived from crystalline rocks. Laterization occurs most rapidly in hot humid regions where the surface soils develop concretions or nodules of aluminum and iron oxide that are rich enough to be used as ores, and where the process may extend as deep as 100 ft. [9]. True laterites have the nodular structure while lateritic soils exhibit only the cementing and deep coloring. The term semilaterite has been applied to soils of the subtropical and warmer temperate regions that are partially cemented but have only a limited amount of iron-aluminum accumulation.

The thickness of the crust is usually from 3 to 8 ft. (1 to 2.5 M). In the steep mountains it may be less, while in the flat hilltops it may exceed 10 ft. (3 M).

INTERMEDIATE ZONE

The intermediate zone is the most important from the foundation engineering point of view. Most structures are founded on it, the design of excavation bracing and the slopes of open cuts depend on its properties, and it is an important source of borrow materials.

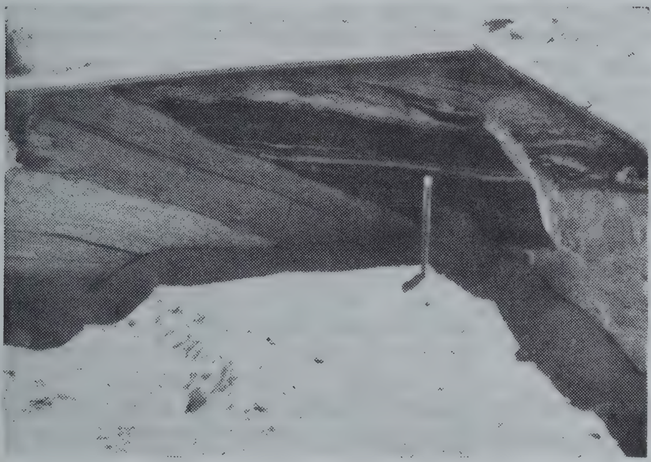

Fig. 1 — Structure of residual soil derived from biotite gneiss showing flow banding and discontinuities of the original rock.

Fig. 1 — Estructuras de suelos residuales provenientes de gneis biotita con bandas de movimiento y discontinuedades de la roca original.

This zone is formed by the incomplete weathering of the rocks. Since the break-down is not complete, the soils still reflect many of the characteristics of the original rock. The most striking feature of most of the soils of the intermediate zone is their banding, as shown in Fig. 1. This is the segregation of the soil minerals in the same parallel stripes or bands as the original rock. While this banding resembles stratification, it is different in that the bands are erratic, twisted and contorted, and often steeply tilted. Figure 1 shows the corner of a footing excavation 3 ft. deep. The soil bands dip downward to the right but they are interrupted, at the center of the picture by fault and numerous small intrusions. The soil bands are brilliant red, brown, orange, and white, like stick candy. The term "saprolite" has been given to these materials which are soil in texture but which still retain the appearance and structure of the parent rock.

The soil minerals are predominately quartz, clay minerals and partially weathered feldspars, and mica. The quartz consists of irregular fragments which formed from the interlocking crystals of the rock. While the grains appear angular, they ordinarily do not have the broken-glass-like sharp edges that are produced by fracture. The sizes range from gravel to silt, depending on the original rock texture, but in any one band they tend to be uniform. The clay minerals are largely of the kaolinite family, including kaolinite, halloysite, and gibbsite [7, 8, 10]. Large zones of partially kaolinized feldspar often are present. Occasionally thin seams of illite and montmorilonite clays are found which are the weathering products of some of the basic dikes. These dikes are particularly troublesome since they are often so small and widely spaced that they are not detected by borings. In spite of their small size, their ability to absorb water, swell, and soften sometimes makes them the slip surface for landslides and cave-ins.

An important characteristic of the soils of the intermediate zone is their content of various types of mica. Most of the original crystalline rocks contain large amounts of mica. Since these minerals do not decompose as readily as the feldspars, the soils contain large quantities of unweathered or slightly weathered mica, including muscovite, biotite, and vermiculite. Some soil bands may be all mica while others may contain none. Typical mica percentages vary from 5 to 25 percent. The micas are usually oriented, with their planes of cleavage parallel to the banding. This creates planes of weakness in the soil which are very hazardous in deep excavations and cuts. Most of the mica flakes are small, in the sizes of silts and fine sands, but larger particles are not uncommon.

Depending on the original rock, the soils contain iron oxides as well as very small amounts of oxides of other metals such as manganese. These are found in varying stages of oxidation which gives the soils wide varieties of coloration, from deep red and purple, through yellow, white, brown, and orange, to green and even blue.

The grain size curves for the soils of the intermediate zone, Fig. 2, usually include a uniform to well-graded curve of sand sizes plus a long flat curve in the silt and clay sizes. The coarser fraction consists of unweathered quartz and mica while the finer is composed of the clay minerals. The liquid limits are moderately high, from 25 to 60, but the plasticity indexes are low, from 0 to 20. (Unfortunately it is very difficult to make accurate determinations of the Atterberg limits in these soils because they tend to slide instead of flow in the liquid limit cup, and the plastic limit threads are so spongy that they cannot be easily rolled.) According to the Revised Public Roads System the soils are classified A-4 and A-5. According to the Unified System, they are ML and MH. All may be described as micaceous silty sands and sandy silts.

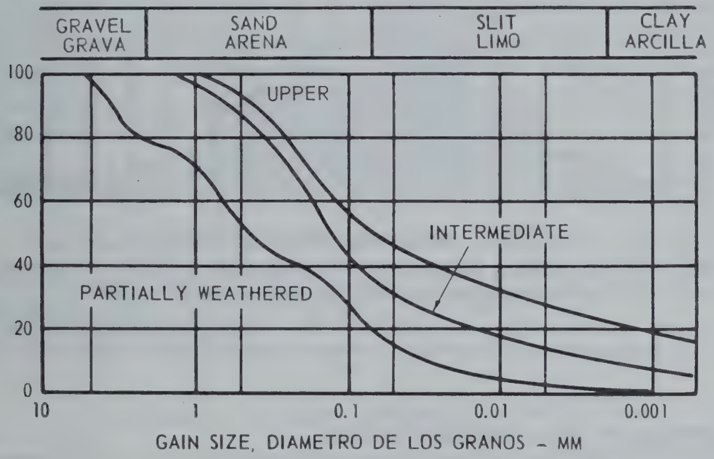

ZONE ZONA	LIQUID LIMIT LIMITE LIQUIDO	PLASTIC INDEX INDICE DE PL.	CLASSIFICATION-CLASIFICACION UNIFIED	 USBPR
UPPER	30-80	12-45	CL, CH	A-6, A-7
INTERMEDIATE	30-65	0-25	ML, MH	A-4, A-5
PART. WEATH	NON PLASTIC	NON PLASTIC	SM, GM	A-1, A-2

Fig. 2 — Typical grain size and plasticity data.

Fig. 2 — Data típica de tamaño de grano y plasticidad.

The micro structure of the soils is very interesting. In the parent rock the crystals were intertwined and interlocked. During weathering the feldspars and similar minerals alter, but the quartz and most of the micas remain unchanged. The basic framework of the soil consists of a quartz-mica skeleton with kaolins and similar minerals in between. The quartz and micas are still interlocked and retain some of their original bonding. The kaolins, which tend to occupy a larger volume than the feldspar which formed them, are slightly compressed within the quartz-mica framework.

The void ratios of the intermediate zone are often high. A frequency distribution curve of void ratios, based on over 1,000 undisturbed samples is shown in Fig. 3. This indicates that the average void ratio is about 1, but void ratios as high as 2 occur. The amount of mica is a major factor in determining the void ratio — the greater the mica percentage, the higher the void ratio usually will be.

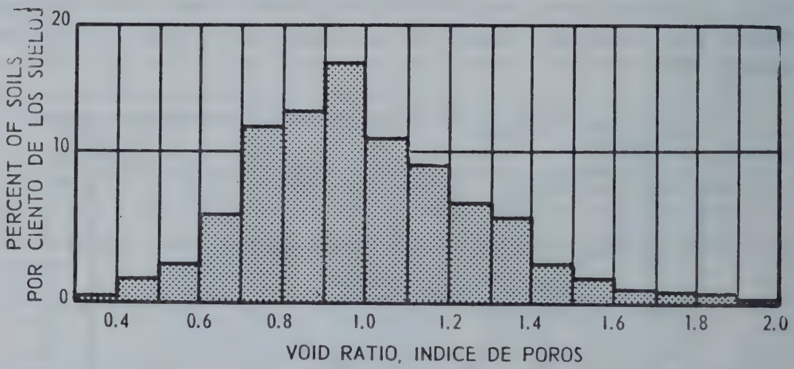

Fig. 3 — Frequency distribution of void ratios of undisturbed soils of the intermediate and partially weathered zones.

Fig. 3 — Distribución de frequencia del índice de porosidad de suelos no perturbados de la zona de intemperización intermedia y parcial.

PARTIALLY WEATHERED ZONE

There is no well-defined lower limit to the intermediate zone. Instead, the degree of weathering becomes less with increasing depth until unaltered rock is reached. The transition between soil and rock is the third zone — the Partially Weathered Zone. This zone is characterized by lenses or bands of relatively sound rock separated by seams of the same sandy silts and silty sands that are found in the intermediate zone.

The typical grain size curve, Fig. 2, reflects the lesser weathering. Gravel sizes and even boulder sizes are encountered, with only small percentages of fines. The grain size curves are irregular and they vary considerably from point to point in the soil mass. The soils are usually non-plastic or slightly plastic. According to the Revised Public Roads System, they are A-1 and A-2; according to the Unified System, SM and GM with some GW, GP, SW, and SP. The void ratios of this zone are extremely variable, they may be as high as the typical values for the intermediate soils and as low as 0.10 in the rock.

ENGINEERING PROPERTIES OF THE SOILS

The engineering properties of strength, compressibility, permeability, and compacted density reflect the degree of weathering and the structures of the soils. The properties of the upper zone are similar to those of other inorganic homogenous clays of low to medium plasticity. These soils are insensitive, strong, and heavily preconsolidated by desiccation. They seldom present serious or unusual problems in soil engineering. By contrast, the soils of the intermediate and partially weathered zone are anything but homogeneous. Numerous tests of these latter soils have been performed under the author's direction at Georgia Institute of Technology, and by the Law Engineering Testing Co., Inc. The following discussion of soil properties is limited to the soils of the intermediate and partially zones where most of the unusual soil engineering problems are encountered.

PERMEABILITY

Permeability testing has been conducted on a limited number of undisturbed samples using both falling head and constant head permeameters. The typical values are given in the following table.

TABLE 1 — Typical permeability coefficients

Soil Description	Permeability coefficient in cm per sec	
	Parallel to banding	Perpendicular to banding
Micaceous silty sand	1.0×10^{-4} to 5×10^{-4}	0.5×10^{-4} to 2.0×10^{-4}
Micaceous sandy silts	0.2×10^{-4} to 2×10^{-4}	0.1×10^{-4} to 0.5×10^{-4}

These values are comparable to those of inorganic silty sands and sandy silts of other geologic origins. The permeability is higher parallel to the banding than it is perpendicular to the banding. The ratio of the parallel to the perpendicular ordinarily lies between 2 and 4.

The permeability of the soil mass may differ greatly from the above values because of dikes and similar intrusions of unweathered rock or seams which weather into true clays that obstruct seepage. On the other hand the numerous cracks, fissures, and shear zones that are present in most residual soils provide paths for rapid seepage. Most seepage problems in excavations and in dam foundations arise because of these cracks which may deliver substantial flows through otherwise impervious materials. In spite of high seepage, these soils tend to resist seepage erosion far better than the sedimentary soils of the same texture, silts and fine soils. (The author has observed fast flowing springs out of the virgin silts below several dams without any evidence of erosion or piping.) Seepage control is difficult because of the erratic pattern of the aquifers, but is usually possible by deep drainage trenches.

STRENGTH TESTS

Various types of strength tests have been employed for the micaceous sandy silts and silty sands including unconfined compression, direct shear, triaxial shear, and the rotating vane. The results show that the soils consistently exhibit strength with no confining pressure and also a significant increase in strength with increasing confinement. On this basis, it can be seen that the unconfined compression test gives strength values that are entirely too low for economical design. The soils often fail along planes of weakness which sometimes cannot be predicted by an examination of the samples before testing. Direct shear tests, which necessarily predetermine the failure plane, therefore, sometimes give unduly high figures for strength. The only satisfactory method of testing for strength of these soils is the triaxial shear test. Even with this method large samples and numerous tests may be necessary to obtain an accurate picture of the soil strength. Some experiments with the vane shear have been performed but the results have been difficult to interpret [11].

Consideration of the rate of loading compared to pore water pressure changes has been found as important in the saprolite soils as for clay. Because of the relatively high permeabilities of most of the soils, truly undrained (quick or Q) shear is difficult even in naturally saturated samples. Instead, most tests are consolidated-undrained (consolidated-quick or R) in which the soil is allowed to consolidate fully under the lateral confining pressure and then is sheared rapidly without drainage. Pore pressure measurements can be conducted during such tests in order to obtain the effective stresses, particularly the effective stresses at failure, in the same manner as such tests are conducted on clays. Drained or consolidated (slow or S) tests in which no pore pressures are developed and in which the effective stresses can be obtained directly, are seldom made because they are time consuming.

A large proportion of the undisturbed soils are not saturated. These are tested by consolidated-undrained procedures. However, even though pore pressure measurements are made they may not fully define the effective stresses in the soils because of capillary tension.

STRENGTH CHARACTERISTICS

Two sets of typical Mohr envelopes for micaceous sandy silt soils are given in Fig. 4: one set approximately 50 percent saturated, the undisturbed condition; and the other set for similar samples of the same soil but saturated. One envelope in each set represents the total or applied stresses at failure and the other the effective stresses at failure determined by the following relation:

$$\bar{\sigma} = \sigma - u$$

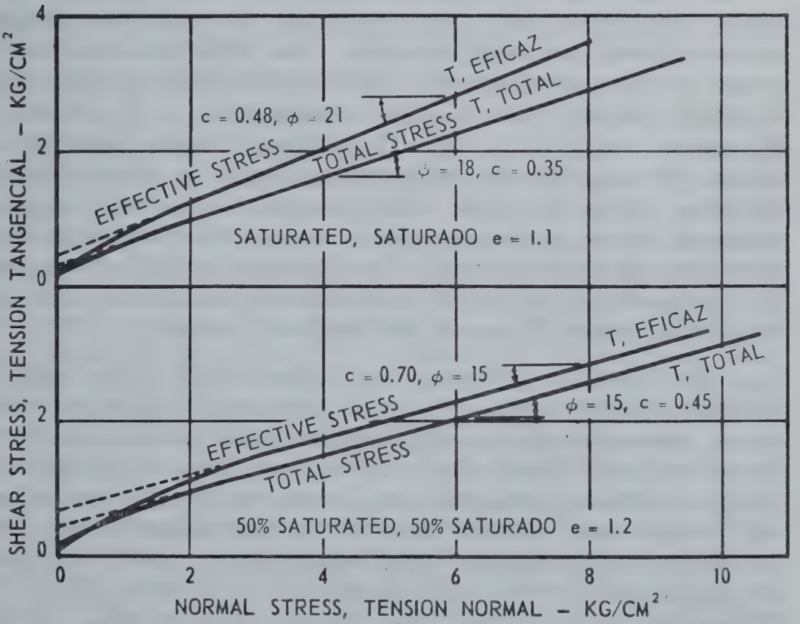

Fig. 4 — Typical Mohr envelopes of undisturbed soils of the intermediate zone in consolidated-undrained (R) shear.

Fig. 4 — Línea de envoltura Mohr típica para suelos no perturbados de la zona intermedia en consolidación-cizallamiento (R) no drenado.

UNIVERSITY OF ILLINOIS LIBRARY

In this expression σ is the total or applied stress, u is the measured pore pressure (which may not be the true or average pore pressure in a partially saturated soil) and $\bar{\sigma}$ the effective or intergranular stress.

All four envelopes consist of two parts; a straight line at confining pressures that are typically greater than 1 or 2 kg per sq cm, and a concave downward curve at lower pressures. The straigth line can be defined by the familiar Mohr-Coulomb expression:

$$s = c + p \tan \Phi$$

where c is the apparent cohesion or simply cohesion and Φ is the angle of shear resistance. Since the lower part of the envelope is curved, the intercept, c, must be found by projecting the envelope back to the shear axis. The true cohesion or actual intercept of the envelope on the shear axis is substantially less than (in many cases half or one third of) the apparent cohesion.

As might be expected the effective stress envelopes are higher than the total stress envelopes for both the partially saturated and saturated samples. The differences are not as great as for clays however. The limited pore pressure data available indicate pore pressure coefficients, A, as defined by Skempton[12] of 0.3 to 0.4. The angle of shear resistance is about the same but the apparent cohesion is greater for the effective stress envelope. This suggests that the apparent cohesion of the saturated soil is caused by something other than pore pressure effects. The apparent cohesion is greater for the partially saturated soil than the saturated. The difference is probably caused by capillary tension.

The relation between the initial void ratio and the strength parameters, c and $\varnothing$, for consolidated-undrained shear (uncorrected for pore pressures) is shown on Fig. 5. In general, the points above the average lines on both graphs are for partially saturated soils; those below are for saturated. While these are for soils of the southeastern U.S., it is interesting that limited data reported by the U.S. Bureau of Reclamation[13] for the western U.S., Puerto Rico, and Singapore (Malaya) plot close to the average lines on both graphs as do the data reported by Vargas[6] for Brazil. As can be seen, there is a considerable scatter of the points, particularly in the relation between void ratio and cohesion.

One factor responsible for the scatter appears to be the soil grain structure, which is not sufficiently described by void ratio. Another is pore pressure. However, pore pressure changes do not affect the behavior of these soils to the same extent as normally consolidated clays.

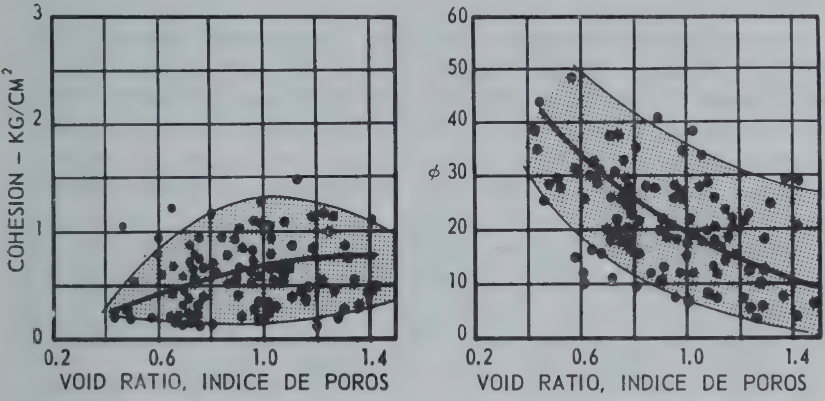

Fig. 5 — Shear strength parameters, c (cohesion) and ∅ (angle of shear resistance) for undisturbed samples of the intermediate and partially weathered zones. Upper half of each curve is partilly saturated; lower half saturated.

Fig. 5 — Parámetros de resistencia a cizallamiento, c (cohesión) y ∅ (ángulo de resistencia a cizalladura), de muestras saturadas; las de arriba de muestras parcialmente saturadas.

Of course, any discussion of the mechanics of the soil strengths must be based on effective stress data. However, the limited data available indicate that the angle of shear resistance of total stress on consolidated undrained shear is not greatly different from that of effective stress and that the apparent cohesion from total stress is in proportion to that from effective stress envelopes. Therefore, tentative hypotheses can be advanced to explain the behavior of these soils in shear. The cohesion of the soil is probably that part of the mineral bond of the original rock which remains in the quartz-mica skeleton. In the low void ratio soils with little mica, the quartz framework is so brittle that the bonds have been partially destroyed by the expansion of the feldspars upon weathering. In the very high void ratio soils, the framework is so small a part of the total mass that the cohesion is again low. At the intermediate void ratios, however, the unweathered mica-quartz skeleton can absorb some swelling and since it is a major portion of the total mass the soil retains high cohesion. Therefore, the cohesion curve of Fig. 5 is humped.

The internal friction of the soil appears to be the result of both interlocking and true friction. As might be expected, the friction increases with decreasing void ratio. The variation in the friction angle for any given void ratio appears to be caused by the presence of oriented mica and similar minerals.

The loss of strength (envelope curvature) below a confining pressure of less than 1 or 2 kg per sq cm can be attributed to the expansion of the compressed kaolin within the skeleton, which breaks the quartz-mica bonds. This is confirmed by the behavior of the moist soil when it is exposed without confinement. So long as the soil is moist, capilary tension holds the kaolin within the framework in a compressed condition and maintains the cohesive bond. If the soil becomes either dry or inundated, the capillary tension is destroyed, the kaolin expands, and the cohesive bond in the soil skeleton is obliterated. The soil "swells" and loses all its strength except that due to internal friction.

STRENGTH VARIATIONS

The saprolite soils of the intermediate and partially weathered zones are far from homogeneous. The variations in mineral content of the parent rock and in the degree weathering produce a mass with both strong and weak zones. The condition is aggravated when the rock was faulted or jointed and these cracks are retained as weaknesses in the soil.

When the variations in strength, or cracks occur at random and they are closely spaced, the mass may be macroscopically or statistically homogeneous. Limited studies indicate that the effective strength of the soil as exhibited in landslides is more then the minimum and less than the average strength found by laboratory tests of undisturbed samples. When the soils of different strengths or the cracks are widely spaced the effective strength appears to be close to the minimum measured by laboratory tests, including the shear strengths along the cracks that are oriented favorably for potential movements.

The strength of banded soils, such as those derived from gneiss and schist, may vary greatly from band to band but are relatively constant within any band. In this way they resemble stratified soils, and in some extreme cases, varved deposits. Unlike most stratified deposits, the banding is rarely level and often contorted or swirled. Macroscopically, the strength of the mass is statistically anisotropic: the strength parallel to the banding is approximately that of the weakest band while that perpendicular to the banding is somewhat less than the weighted average of the bands.

Microscopically, the saprolite soils often have anisotropic strength properties because of the parallel orientation of their flakey grains, particularly the micas and kaolinite clays. As might be expected they are weaker in shear parallel to the grain faces than perpendicular to them. More study is needed of this anisotropy, however.

COMPRESSIBILITY — CONSOLIDATION

When subjected to vertical pressure with lateral confinement the saprolite soils consolidate similar to other soils. The pressure-void ratio curves, Fig. 6, resemble those for undisturbed clays. On the semi-logarithmic coordinates the curves are relatively flat; they become rapidly steeper at pressures between 1 and 5 kg per sq cm; and they form steep straigth lines at higher pressures.

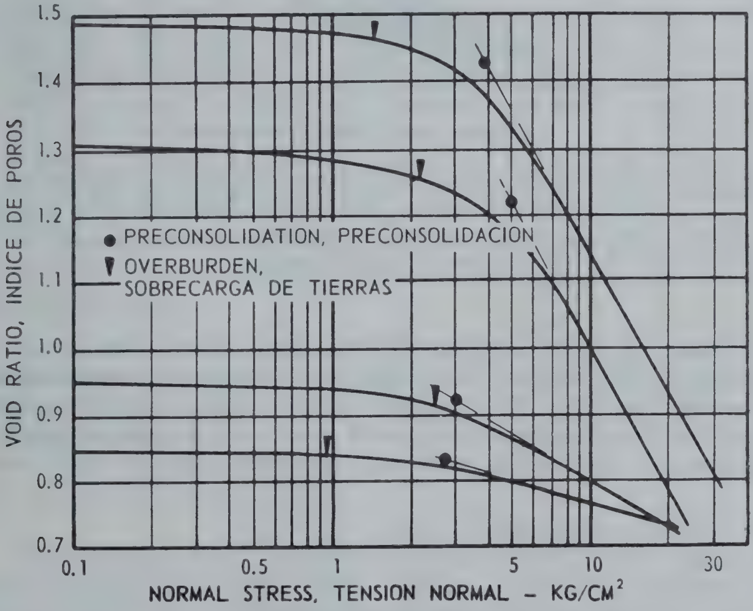

Fig. 6 — Typical pressure-void ratio curves for undisturbed samples from the intermediate zone.

Fig. 6 — Curvas típicas de presión vs. coeficiente de porosidad de muestras sin perturbar de la zona intermedia.

The compression index, C_c [*], is a measure of the relative compressibility of the soil at higher pressures (and of the relative steepness of the straight line).

Tests on undisturbed samples from 50 sites in the Southeastern U.S. show a definite relationship between the undisturbed void ratio and the compression index, Fig. 7. This is described by the equation

$$C_c = 0.75\ (e - 0.55) \qquad (1)$$

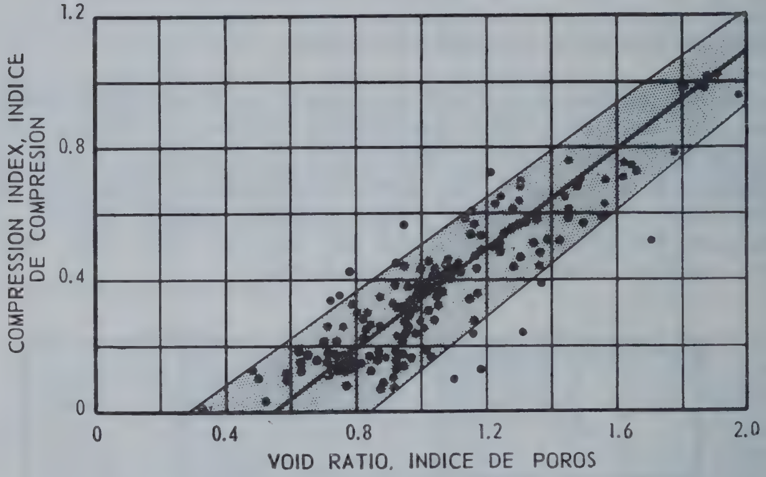

Fig. 7 — Relation of compression index to void ratio of undisturbed soils of the intermediate and partially weathered zone.

Fig. 7 — Relación entre índice de compresión e índice de porosidad de suelos no perturbados.

There is some scatter of the data about this relation. In general the points above the line, the more compressible, represent the soils having the highest mica contents; those below the line represent the soils that are higher in kaolins and quartz. Although published data for similar soils from

---

[*] The compression index is defined by,

$$C_c = \frac{-\Delta e}{\log(\overline{\sigma}_0 + \Delta\sigma) - \log \overline{\sigma}_0}$$

where $\overline{\sigma}_0$ and $(\overline{\sigma} + \Delta\sigma)$ are two pressures on the steep, straight line portion of the pressure void-ratio curve and Δe is the corresponding difference in void ratios.

other regions are scarce, tests quoted by Vargas on Brazilian soils[6] plot close to the line. Very limited tests on saprolites from Puerto Rico and Panama by the author also fall close to the line. A few points lie well below the shaded zone of limited scatter on Fig. 7. Two of these represent weathered porous volcanic soils. Data on volcanic soils from Italy[14] in some cases plot in the shaded zone below the curve and in others just below the shaded zone close to the points for the volcanic soils of the southeastern U.S.

PRECONSOLIDATION

All the soils appear to be preconsolidated to some degree as can be seen by the shapes of the pressure-void ratio curves, Fig. 6. There is no correlation between the preconsolidation load as computed by Casagrande's empirical method[15] and the present overburden load. In fact, two samples, made within a foot of each other but in different bands of a saprolite soil, can have greatly different preconsolidation loads.

The preconsolidation load is probably related to the residual mineral bonds of the parent rock. When the rock cooled, the differential contraction of the various minerals caused high stresses to develop between the grains. Some of these stresses undoubtedly remain in the quartz-mica framework even though the feldspars and some of the micas have been altered by weathering. It is possible that the volume changes associated with weathering also produced stresses which were partially retained by the soil grain structure. The fact that the least weathered soils tend to have the highest preconsolidation loads lends some support to the first hypothesis.

A statistical or frequency distribution of indicated preconsolidation loads is given in Fig. 8. The median is about 3 kg per sq cm, but values as high as 14 kg per sq cm have been observed.

TIME-RATE OF SETTLEMENT

Settlements tend to occur rather rapidly in saprolite soils, both in laboratory tests and in the actual structures. A significant part of the settlement occurs very rapidly, some because of elastic distortion, but largely because many of the soils are not saturated. Typically, as much as two thirds of the change of void ratio occurs virtually instantaneously in the typically 50 to 70 percent saturated materials.

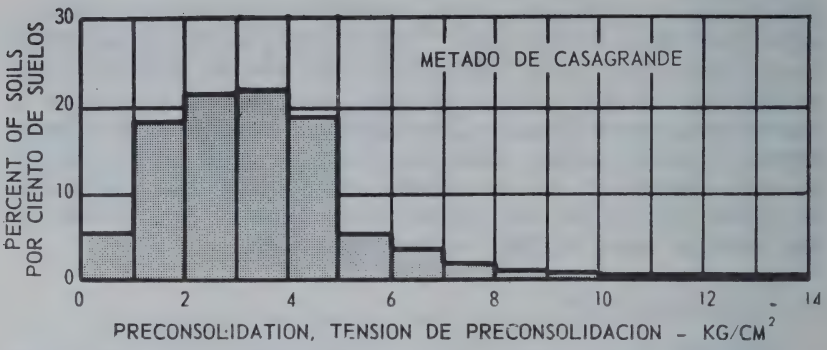

Fig. 8 — Frequency distribution of the preconsolidation load of undisturbed soils of the intermediate and partially weathered zones.

Fig. 8 — Distribución de frecuencia del peso de preconsolidación de suelos no perturbados.

Hydrodynamic or primary consolidation also develops rapidly because of the high permeability of the silty bands and because of the drainage provided by the more pervious but less compressible quartz-rich bands and by the numerous cracks. Because of these discontinuities it is seldom possible to make a realistic prediction of the time rate of primary consolidation from laboratory test results. Measurements of the settlement of full size structures show that primary consolidation seldom is significant after from 3 to 9 months.

Secondary compression is often a significant factor in structural settlement. Because the greatest part of the primary consolidation usually takes place before the tile, plastering and painting are commenced, the cracking in the finished surfaces (which is that most obvious to the eye) is for the most part the result of secondary compression. The amount of secondary settlement is relatively large, similar to that in organic soils. It appears to be directly related to the amount of mica present: the greater the mica content the greater the secondary compression. This requires further study, however.

SHRINKAGE AND EXPANSION

Like clays, the micaceous silty sands and sandy silts in both the undisturbed and compacted state shrink on drying and expand when they are allowed to absorb moisture. The magnitudes of these volume changes resemble those of highly plastic clays in spite of the very low plasticities of most of these saprolite soils.

Shrinkage appears to be a purely mechanical process in which the soil is compressed by capillary tension on the pore water. In general the soils that are finest grained, with the greatest initial void ratio (and also the greatest compressibilities, as indicated by Fig. 7, shrink the most. Unlike clays, the soils often expand appreciably when dried well beyond the shrinkage limit. This is caused by the loss of capillary tension in the dry voids which permits the resilient quartz-mica framework to spring back towards its original volume. This expansion of the soil on drying is troublesome in foundation construction. The soil, damp and firm when first exposed, becomes loose and fluffy when exposed to air and sun. This necessitates deeper excavation that exposes fresh damp firm soil which soon dries so that the sequence must be repeated. During hot dry weather it is prudent to protect the soil from drying with a thin concrete working slab if there is an appreciable time interval between excavation and pouring the footing concrete.

Expansion of the soil on wetting appears to be largely a mechanical process in the low plasticity soils in which the reduction of capillary tension permits the disturbed quartz-mica soil skeleton to regain its former void ratio. On swelling the unloaded surface of the soil slowly disintegrates. Apparently unequal expansion breaks the remaining mineral bonds of the soil.

COMPACTION

The upper and intermediate zones are important sources of borrow for earth construction. The materials are clays, micaceous silts, and micaceous silty sands which are ordinarily not adapted to good compaction. While the soils of the partially weathered zone classify as good materials for construction they are usually difficult to excavate and break up, and their gradations are often too irregular to be satisfactory.

The maximum dry densities of the compacted soils of the intermediate and partially weathered zones by the Standard Proctor test (ASTMD 698-58T) may be as low as 78 lbs per cu ft (1.25 g per cu cm) or as high as 130 lbs per cu ft (2.08 g per cu cm). A frequency distribution curve based on over 1,000 samples is shown in Fig. 10. This indicates median maximum density between 95 and 100 lb per cu ft (1.5 and 1.6 g per cu cm) which is lower than is usually considered satisfactory for the best fills. The optimum moistures usually fall between 12 and 35 percent with the higher values for the low-density, highly micaceous soils.

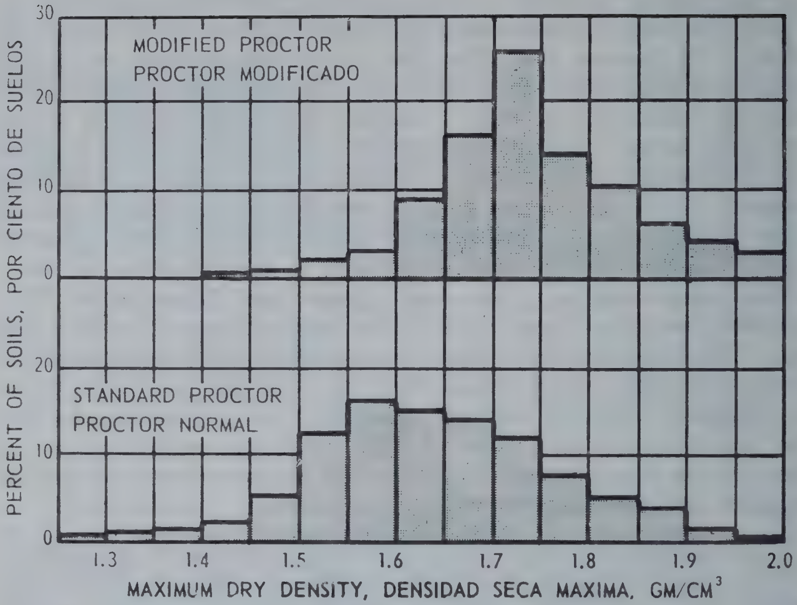

Fig. 9 — Frequency distribution of maximum compacted dry densities.

Fig. 9 — Distribución de frecuencia de densidades compactadas máximas.

Surprisingly enough, the engineering properties of the soils, particularly the strength, are not as poor as might be expected from the low maximum densities if the compaction percentages exceed about 95 percent of the Standard Proctor maximum. The angle of internal friction is relatively high, from 15 to 35 deg, and the cohesion may be as high as 3,000 lb per sq ft (1.5 kg per sq cm). The compressibility is moderate to low and there is little swelling, but there may be as much as 4 or 5 percent shrinkage upon drying from the optimum moisture. When the compaction percentage falls below 95% the quality of the compacted soils falls off rapidly.

ACKNOWLEDGEMENTS

The data on the properties of the soils and on the engineering problems involved were largely secured from two sources: Engineering reports in the files of Law Engineering Testing Company, Atlanta, and unpublished reports on research in the Soil Mechanics Laboratory of Georgia Institute of Technology. The author is particularly indebted to Mr.

G. B. Dalrymple, Mr. C. M. Kennedy and Mr. A. M. Showalter of the Law Engineering Testing Company and to C. Hedges, graduate student of Georgia Tech for helping to make the data available. Much of the data were collected as a part of the work of the Task Committee on the Products of Weathering of Bed Rock of the Joint Committee on Engineering Geology, ASCE and Geological Society of America.

REFERENCES

1. G. F. Sowers — "Soil Problems in the Southern Piedmont Region" — *Proceedings ASCE,* vol. 80. Separate 416, 1954.

2. H. N. Ferreira and L. J. Silva — "Terrenos Vermelhos das Zonas Florestais" — Luanda, Angola, vol. 1.

3. C. S. Fox — "Buchanans Laterite of Malabar and Kanara" — *Gerl Survey of India,* 1939, vol. 69.

4. A. B. A. Brink and B. A. Kanley — "Collapsible Grain Structure in Residual Granite Soils in Southern Africa" — *Proceedings, Fifth International Conference on Soil Mechanics Foundation Engineering,* Paris, 1961, vol. I, p. 611.

5. J. Florentin, G. L'Hériteau et M. Farhi — "Etude de Quelques Propriétés Physico-Mécaniques d'Echantillons de Latérites Eluviales" — *Proceedings, Fourth International Conference on Soil Mechanics and Foundation Engineering,* London, 1957, vol. 1, p. 28.

6. M. Vargas — "Some Engineering Properties of Residual Clay Soils Occurring in Southern Brazil" — *Proceedings, Third International Conference on Soil Mechanics and Foundation Engineering,* Zurich, 1953, vol. 1, p. 67.

7. T. W. Lambe and R. T. Martin — "Composition and Engineering Properties of Soil" — *Proceedings, Highway Research Board,* Washington, vol. 35, p. 674, 1956.

8. G. F. Sowers; V. Hurst; K. Kennedy et al. — Engineering Reports of the Law Engineering Testing Co., Atlanta, 1942-1963.

9. K. S. Bawa — "Laterite Soils and Their Engineering Characteristics" — *Journal of the Soil Mechanics and Foundations Division, ASCE,* vol. 83, SM4, Nov. 1957.

10. B. D. Tate and H. G. Larew — "The Effect of Structure on the Resilient Rebound of Soils in the Southern Piedmont Province of Virginia" — Paper present at Highway Research Board, Washington, Jan. 1963.

11. E. T. Miller — *Vane Tests of Soils of Southern Piedmont* (a thesis submitted in partial fulfillment of the degree of M.S. in Civil Engineering) — Georgia Institute of Technology, 1957.

12. A. W. Skempton — "The Pore Pressure Coefficients A and B" — *Géotechnique,* vol. 4, 1954.

13. J. J. Gibbs; J. W. Hilf; W. G. Holtz and F. C. Walker — "Shear Strength of Cohesive Soils" — *Proceedings, Research Conference on Cohesive Soils,* ASCE, Univ. of Colorado, Boulder, June 1960.

14. F. Penta; A. Croce; F. Esu — "Engineering Properties of Volcanic Soils" — *Proceedings, Fifth International Conference on Soil Mechanics and Foundation Engineering,* Paris, 1961, vol. 1, p. 285.

15. A. Casagrande — "Structure of Clay and its Importance in Foundation Engineering" — *Journal Boston Society of Civil Engineers,* April 1932.

CLAY MINERAL COMPOSITION AND PROPERTIES OF DEEP RESIDUAL SOILS FROM SÃO PAULO, BRAZIL

R. E. GRIM
University of Illinois, Urbana, Ill.

W. F. BRADLEY
Illinois Geological Survey, Urbana, Ill.

SUMMARY

This paper deals with the results of mineralogical analysis proceeded on samples from 2 deep borings, and the results of soil tests run on the same samples. One of the borings was made in the vicinity of the city of São Paulo in a residual soil developed on gneiss, and the other was made in the city of São Carlos in a residual soil developed on sandstone.

Test results indicated that kaolinite is predominant in the weathering of both profiles. In the lower horizons of the boring open in the sandstone, montmorillonite is also present. In both profiles there appears gibbsite in the upper layers, which is forming from kaolinite. The kaolinite which appears in the boring open in gneiss, probably results from alteration of mica. It was impossible to find out whether the feldspar was weathering directly to kaolinite or through a transient intermediate stage. In the profile of sandstone some kaolinite may be formed by way of an intermediate montmorillonite stage.

The activity (Skempton) of these soils is small when there is dominance of kaolinite as the clay mineral; is slightly higher when residual mica is also present and is notably higher as montmorillonite is encountered. When the clay fraction in a sample is low anomalous high activity values may be found.

Penetration resistance is in correlation with the degree of weathering in the soil. It is lowest in the most highly weathered levels and increases in the least weathered.

SUMÁRIO

O artigo relata os resultados de análises mineralógicas, feitas em amostras de sondagens profundas, em confronto com as respectivas características geotécnicas. Tra-

ta-se de duas sondagens: uma feita nos arredores da cidade de São Paulo, em solo residual de gneiss, e outra, na cidade de São Carlos, em solo de decomposição de arenito.

Dêsses estudos conclui-se que a caolita é o produto de decomposição dominante nos dois perfis. Nas camadas inferiores, do perfil de arenito, aparece, entretanto, também a montmorilonita. Em ambos os perfis ocorre a gipsita nas camadas superficiais; êsse universal está se desenvolvendo a partir da caolinita. No perfil de gneiss a caolinita deve ter provido diretamente da decomposição da mica. Não é possível determinar-se se os feldspatos são decompostos diretamente em caolinita ou passam por estágio intermediário. No perfil de arenito alguma caolinita deve se ter formado por meio de um estágio intermediário de montmorilonita.

A atividade (Skempton) dêsses solos é pequena quando a caolinita domina, aumenta ligeiramente com a mica e torna-se muito maior quando a montmorilonita está presente. Quando a fração argila, na amostra, é pequena, aparecem valôres anormais da atividade.

A resistência à penetração mostra-se com um índice correlativo do grau de decomposição do solo. É pequena nas camadas de alto grau de decomposição e aumenta quanto menos decomposto é o solo.

INTRODUCTION

In 1953, one of us (R.E.G.) had the opportunity to visit the State of São Paulo in Brazil, to examine the deep red residual soils which cover much of the State, and to learn something of the problems in soil mechanics encountered with these soils.

Professor Milton Vargas, of the Polytechnic School University of São Paulo, kindly offered to supply samples of cores of boring which had penetrated deeply into these soils for clay mineral analyses. He also offered to supply soil mechanics test data for these same samples. Borings and soil test were done at the I.P.T. (Instituto de Pesquisas Tecnológicas) — University of São Paulo.

The clay mineral data presented herein are the work of the authors.

The soil mechanic test data are the work of Professor Vargas and his colleagues.

The authors are responsible for the correlation and the general conclusions.

The authors wish to acknowledge their indebtedness to Professor Vargas and to express their appreciation for his kindness and very willing cooperation.

ANALYTICAL DATA

The location of the borings, the description and depths of the core samples, the Penetration Resistance, Atterberg Limits, grain-size distribution, and Activity for the core samples are given in Figures 1 and 2.

The boring section A, in Figure 1, is from a residual soil developed on gneiss at the village of Sacoman just southeast of São Paulo along the highway to Santos.

The boring section B, in Figure 2, is from a residual soil developed on Botucatu-Piramboia sandstone of Triassic age at the College of Engineering, São Carlos, State of São Paulo, Brazil.

The approximate relative abundances of crystalline phases are depicted graphically in Figures 3 and 4.

Accuracy of quantitative estimations by X-ray diffraction methods is somewhat limited in any but the most favorable cases. In the case of the present cores, the small scale inhomogeneities of the rock, the erratic presence of large quartz grains, and the unequal plastic properties of the several component minerals introduce additional sources of error. Therefore, although the graphs list percentage figures as ordinates, it should be borne in mind that actual figures may be in error by as much as 10 percent. The tendency toward internal consistency is probably somewhat better.

In the graphs the abundances of the layer minerals, those making the greatest contribution to the plasticity, are plotted from the left, and quartz, the free oxides, and feldspar from the right. The inaccuracies of estimation are thus accumulated in the middle ground, and are reflected in the imperfection of fit between the two halves.

It has not been attempted to differentiate the states of the iron oxide. High in the sections the iron exists in a rudimentary goethite crystallization commonly called limonite. In some deeper horizons it exists as hematite. The distinctive colors are as definitive as the diffraction criteria.

Of the clay minerals other than kaolinite, it is noteworthy that in section A, Figure 3, the mica is rather coarse and apparently represents residual white mica. In section B, Figure 4, both the mica and montmorillonite are presumably degradation products.

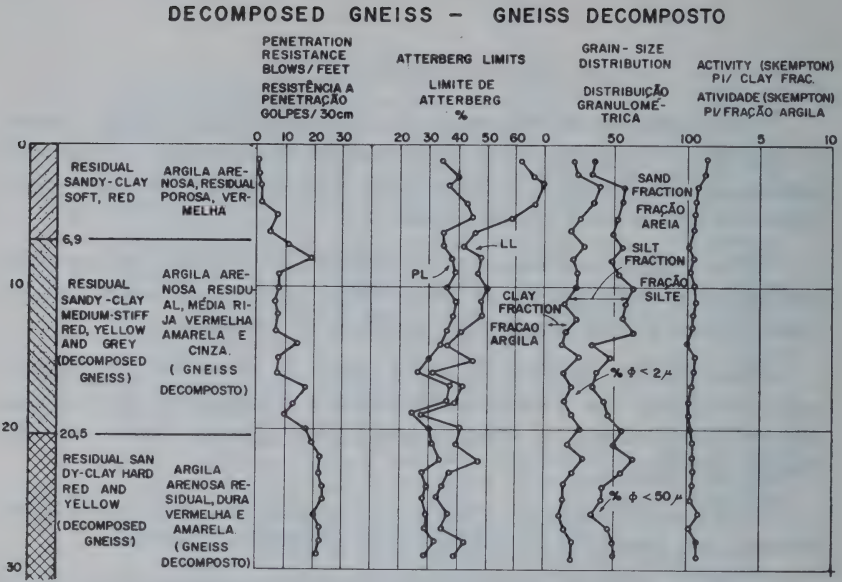

Fig. 1 — Location, description and analytical data for core from Sacoman, São Paulo, Brazil.

Fig. 1 — Locação, descrição e dados analíticos de amostras do Sacoman, São Paulo, Brasil.

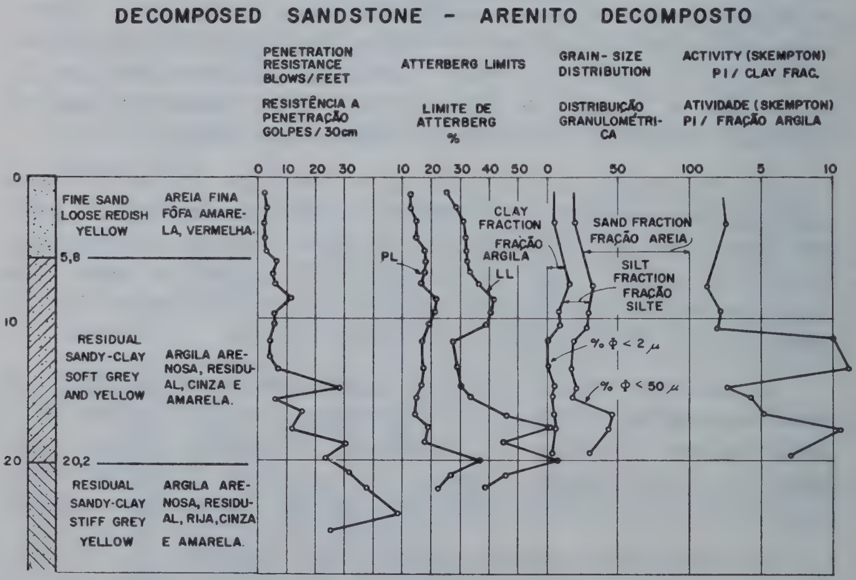

Fig. 2 — Location, description, and analytical data for core from São Carlos, São Paulo, Brazil.

Fig. 2 — Locação, descrição e dados analíticos de amostras de São Carlos, São Paulo, Brasil.

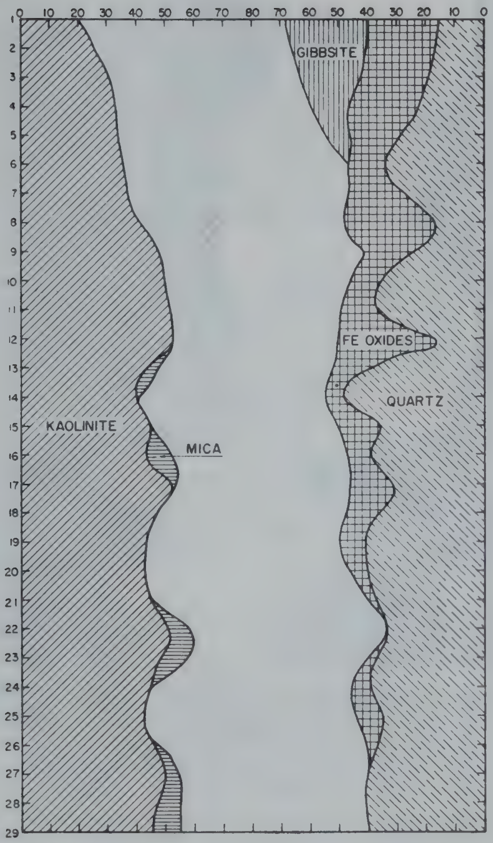

Fig. 3 — Mineral composition of core samples from Sacoman.

Fig. 3 — Composição mineralógica das amostras do Sacoman.

DISCUSSION OF RESULTS

SACOMAN BORING

Te log of the boring shows soft red sandy clay to a depth of 6.9 m., and red, yellow, and gray decomposed gneiss below that depth, Figure 1. The analytical data in Figure 3 show that the gibbsite is restricted to the zone from the surface down to the break at 6.9 m. and that the abundance of this mineral decreases from the surface downward.

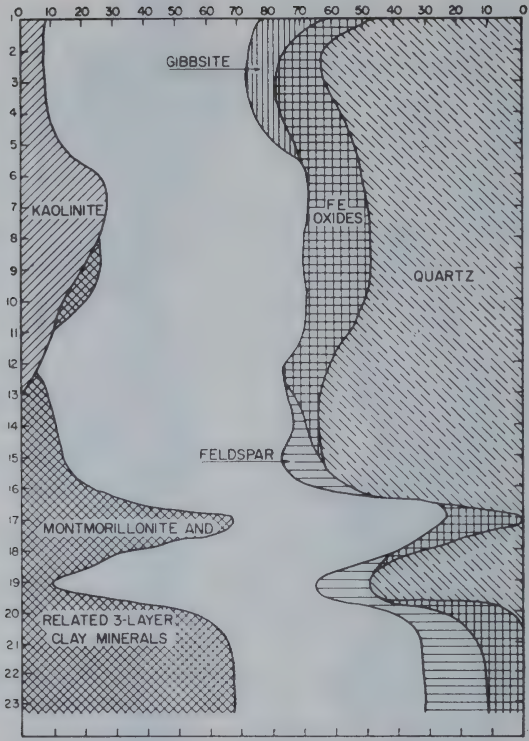

Fig. 4 — Mineral composition of core samples from São Carlos.

Fig. 4 — Composição mineralógica das amostras de São Carlos.

The clay mineral is kaolinite throughout. Below about 12 m., mica is present in small amounts but the flakes are large, and apparently are residual material from the gneiss.

The Fe oxides are most abundant in the uppermost part of the section and tend to gradually decrease in abundance downward.

It seems clear from the distribution of the mineral components that gibbsite is forming from kaolinite and that the Fe oxides in the profile are current alteration products. Also it seems quite certain that the mica is being lost in the weathering process. Further it appears that the mica is altering to kaolinite. There is no suggestion of an intermediate stage such as montmorillonite, developing between the mica and the kaolinite. Kaolinization seems to be the only process which has progressed to the deepest levels.

A comparison of the mineral composition in Figure 3 with the physical properties in Figure 1 leads to the following conclusions:

As a general statement, one would characterize Activity as uniformly low throughout the section. This is consistent with the dominance of kaolinite as the clay mineral. In the upper, highly laterized horizons, apparent slightly higher activity values are actually associated with the lowest clay mineral contents, and not with a normally active clay agent. Rather they are associated with free metal hydroxides and poorly crystallized material.

The free metal hydroxides might well be thought of as having texture like sponge fragments. They have a moderate capacity for water, but make less than a commensurate contribution to the clay size content, and to the plastic properties.

Deeper in the section the higher activities are associated with zones containing frequent residual mica flakes and typical red hematite. These zones have a "fresher", less altered appearance, Either component could make some contribution to the Activity.

Except at the top, the quartz content tends to vary as the amount of sand-sized material, and the clay mineral components with the silt and clay-fraction content. Clay mineral contents are relatively uniform. The Atterberg limits are generally small and uniform and are consistent with the uniformly dominant kaolinite component.

The entire profile gives the appearance of having been developed slowly in a grossly homogenous parent rock with low permeability. Intense weathering conditions have profoundly altered the upper levels, and alteration decreases generally with depth. The parent initially provided a basic environment into which acidic agencies of weathering permeated from the surface downward. The degree of acid diffusion into the parent has probably varied locally with small local variations in permeability. The high penetration resistances at the levels 8, 14, and 17 m. may be interpreted as remnant levels of low permeability. At or just above them are levels of iron enrichment which indicate that diffusion to lower levels was blocked there. The latter two levels of low permeability have also been able to protect some residual mica flakes. Except for the fore-going the Penetration Resistance shows a gradual progressive increase with depth as would be expected because of the general uniformity of clay mineral composition throughout the core.

SÃO CARLOS BORING

The log of the boring, Figure 2, shows a fine, loose, silty sand from the surface to 5.8 m. where some gravel is encountered. Below 5.8 m., all of the material is logged as decomposed sandstone of variegated color. The mineral analyses indicate that at depths greater than about 17 m. the character of the material changes significantly. Below about 17 m. the amount of quartz decreases, and the amount of clay mineral increases as compared to the overlying material — also there are abrupt vertical changes in composition indicating interstratification of beds of very different composition. These changes, beginning at about 17 m., are not shown in the log and indeed a cursory study of boring samples would not reveal them.

The analytical data given in Figure 4 show that gibbsite is not found at greater depths than about 5.5 m. It decreases in abundance from the top downward and is restricted to the zone above the gravel layer. It seems clearly to be a surficial weathering product.

The clay mineral composition in this section is most interesting. Kaolinite is the only clay mineral to a depth of about 7.5 m. Below 7.5 m., montmorillonite and related three-layer clay minerals appear in the section, and below about 12 m. kaolinite is absent and montmorillonite and related minerals are the only clay mineral components. Regarding the three-layer minerals, montmorillonite is typical of the large concentrations to a depth of about 19 m., whereas illitic and chloritic material is typical of greater depths. It is of great importance that the changes in clay mineral composition below 6 m. just noted are not apparent in the megascopic character of the material and are not shown in the log. It will be shown presently that this change in composition, although not revealed in the log causes a very great change in physical properties.

The relative abundance of gibbsite and kaolinite strongly suggest that gibbsite has developed from kaolinite in the present weathering cycle. The data also suggest, although much less strongly, that the kaolinite has formed from the montmorillonite. It is important that the transition of kaolinite to montmorillonite takes place above the depth interval (17 m.) at which the data indicate a large general change in the character of the parent material.

Except for a brief interval at about 18 m., feldspar is present at depths greater than about 12 m. It is of interest that feldspar persists in the section only below the kaolinite bearing levels. It seems likely that present weathering processes are eliminating feldspar.

Iron oxides occur throughout the section except for short intervals at about 17 m. and 20 m. Some of the development of iron oxides is probably due to present day weathering, but it cannot be determined from the present analytical data whether or not all of it has formed in this way.

A comparison of the mineral composition in Figure 4 with the physical properties in Figure 2 lead to the following conclusions:

Activity is low to moderate in the upper, kaolinite bearing part of the section, and becomes notably higher as montmorillonite is encountered. Actually, high in the section, the Atterberg limits are narrower than in the Sacoman section, but the low clay content leads to larger apparent Activities. The anomaly becomes acute at the level of the 12 and 13 m., where Atterberg limits are clearly narrower, but clay is virtually absent. In materials with extremely amounts of the minus-two micron fraction, the nonclay minerals can make a relatively very large contribution to Activity values. It is apparent that a very great variation in Activity values is possible without a comparable variation in Atterberg Limits or Penetration Resistance.

One may theorize that this profile developed rapidly on a stratified parent. An upper sand of relatively high permeability has permited lateritization and kaolinization which were out off abruptly by a impermeable reservoir providing a basic environment, probably first interfingering at about the 14 m. level and becoming continuous at about the 17 m. level. A further suggestion of lateral egress at about the 12 or 13 m. level is not illogical.

The upper sand host, relatively permeable and comparatively poor in basic constituents rapidly accepted the intense weathering influence and developed a profile much like the Sacoman section. The impermeable, level, rich in basic constituents, is altered to montmorillonite only at the top. The prominent nose at the 17 and 18 m. levels is mainly typical, free-swelling montmorillonite, but the abundant three-layer clays deeper in the section retain much illitic and chloritic character.

The Penetration Resistance rises at the first inferred impermeability level at about 9 m. It rises again at about 14 m. which is a second inferred impermeable level, and finally rises at the bottom of the core section in the principal impermeable parent. The montmorillonite developed in the protected areas just beneath the impermeable zones appears to produce reduced Penetration Resistance.

CONCLUSIONS

The variation in composition downward indicates that kaolinite is the clay mineral weathering product developing in both profiles. In the mica bearing profile the kaolinite that developed from mica must have done so directly. In the other profile some kaolinite may be formed by way of an intermediate montmorillonite stage from fine grained micaceous and chloritic parent material. Drainage and substrate permeability are probably both factors in determining the presence or absence of montmorillonite accumulation. It cannot be determined from the data at hand whether the feldspars and other primary silicates are weathering directly to kaolinite or through a transient three-layer intermediate stage.

In the uppermost part of the profile gibbsite is developing at the expense of kaolinite. Iron oxides are also weathering products extending downward to greater depths than does the gibbsite.

The Activity is low for samples containing kaolinite, slightly higher when mica is the clay mineral and much higher when montmorillonite is present. When the amount of clay mineral in a sample is low, anomalous high Activity values may be found.

The poorly organized materials, such as the free metal hydroxides, make a noticeable contribution to the spread of the Atterberg limits.

Penetration Resistance is inferred to derive from relative permeability of the host rock. Since relative permeability also controls intensity of weathering, Penetration Resistance is correlative with degree of weathering, and in turn with clay mineral composition. It is lowest in the most highly weather levels and increases in the least weathered.

The identities of the present clay minerals influence soil properties to unequal degrees. Kaolinite, because it has a low Activity, permits that other factors strongly influence whole properties. Montmorillonite and its related three-layer illitic and chloritic minerals are more active and largely determine the physical properties of their host soils.

SHEAR STRENGTH CHARACTERISTICS OF SOME RESIDUAL COMPACTED CLAYS

PAULO TEIXEIRA DA CRUZ

M.S., Eng. Ass. Sec. Solos I.P.T., Ass. E.P.U.S.P.

SUMMARY

From an extensive research work on the shear strength characteristics of some residual clays, done at the soils Laboratory, of the São Paulo Institute of Technological Research, in connection with earth dam projects, the author selected some of the test results to illustrate the shear strength properties of four residual clays occurrring in Brazil.

The identification properties of those four materials are:

	Clay 1	Clay 2	Clayey Sand 3	Clay 4
Liquid Limit %	61	43	—	57
Plasticity Index %	40	22	N.P.	27
Clay Fraction (finer than 2 μ)	39	42	10	42
Specific Gravity	2.94	2.70	2.69	2.73
Optimum Water Content %	23.8	19.8	11.7	28.0
Maximum Dry Density (t/m³)	1.68	1.70	1.92	1.44

Clay 1 is mostly kaolinite and is originated from decomposition of basalt. The most extensive research was done on samples of clay 2 which is also mostly kaolinite with free iron oxides (about 8%). It is supposedly originated from an "in situ" decomposition of basalt. The dry soil is light brown and the wet soil dark brown. It is commonly known as "terra roxa", in Brazil. Clayey sand 3, has 10% of clay fraction which is mainly kaolinite and secundarily montmorillonite. It is originated from the decomposition of sandstone. Clay 4 is originated from decomposition of quartzite.

Testing specimens of clay 2 were prepared with two techniques: a) kneading compaction referred in this paper as "compacted samples"; b) consolidation from a slurry — referred in this paper as "normally consolidated and over consolidated samples". Specimens were trimmed from a sample consolidated to 1 kg/cm² in a big consolidometer.

Testing specimens of clay 1 and clayey sand 3 were prepared only by kneading compaction and are called "compacted samples". Some testing specimens of clay 4, were trimmed from "undisturbed block samples" taken from the compacted clay core of a dam. Other specimens were prepared by kneading compaction or static compaction in the laboratory, using remolded material from the "undisturbed blocks". The first specimens are called "field compacted samples" in this paper.

Different modalities of triaxial compression tests were run on those four samples submited to various stress histories. Among the types of tests are drained and undrained tests run at constant chamber pressure and variable pore pressure or constant pore pressure and variable chamber pressure. Some especial undrained tests were also run, in which both axial and radial stress were increased in a constant ratio.

The stress histories are field compaction, laboratory kneading compaction, static compaction and consolidation from a slurry.

Test results indicated a fairly unique effective stress envelope for each type of soil, which is independent of the stress history. It is also shown a relation between the parameter void ratio (square root of the degree of saturation) ($e\sqrt{S}$)*, at rupture, and the shear strength of the soil, provided the original structure of the soil samples were the same.*

SUMÁRIO

De um extenso programa de pesquisas sôbre as características de resistência ao cisalhamento de argilas residuais feito no laboratório da Seção de Solos do I.P.T. de São Paulo em correlação com o projeto e a construção de barragens de terra, o autor selecionou alguns dos resultados de ensaios a fim de ilustrar as propriedades de quatro tipos de solos residuais que ocorrem no Brasil.

As características de identificação dêsses quatro solos são as seguintes:

	Solo 1	Solo 2	Solo 3	Solo 4
Limite de liquidez %	61	43	—	57
Índice de plasticidade %	40	22	N. P.	27
Fração argila ($\varnothing < 2\,\mu$)	39	42	10	42
Densidade dos grãos	2,94	2,70	2,69	2,73
Umidade ótima %	23,8	19,8	11,7	28,0
Densidade máxima (t/m^3)	1,68	1,70	1,92	1,44

A argila 1 contém principalmente caolinita e se originou da decomposição de basalto. A pesquisa mais extensa correspondeu às amostras da argila 2, que é, também, de caolinita com cêrca de 8% de hidróxidos de ferro livre.

É supostamente originada de decomposição "in situ" do basalto. O solo sêco é marrom claro e o úmido é marrom escuro. Conhece-se êsse solo localmente pelo nome de "terra roxa". O solo 3 tem 10% de fração argila, que é principalmente caolinita e secundàriamente montmorilonita. É originário da decomposição de arenito. A argila 4 originou-se da decomposição de quartzito.

Os corpos de prova da argila 2 foram preparados com duas técnicas: a) compactação por "kneading", referida neste trabalho como "amostras compactadas"; b) adensamento de uma pasta referida neste trabalho como "amostras normalmente adensadas e pré-adensadas". Os corpos de prova foram cortados de uma amostra adensada até 1 kg/cm² num grande anel de adensamento.

Os corpos de prova dos solos 1 e 3 foram preparados sòmente por compactação por pisoteamento e são chamadas "amostras compactadas". Uns dos corpos de prova da argila 4, foram cortados de amostras indeformadas em blocos retirados de um núcleo argiloso compactado de uma barragem. Outros corpos de prova foram preparados por compactação por pisoteamento ou compactação estática no laboratório, usando-se material remoldado dos blocos indeformados. Os primeiros são chamados "compactados no campo" neste trabalho.

Várias formas de ensaios de compressão triaxial foram conduzidas sôbre essas quatro amostras, submetidas a vários processos de compressão prévia. Entre os tipos de ensaios contam-se ensaios drenados e não drenados; nesses últimos a pressão de câmara foi mantida constante, observando-se as variações de pressão neutra, ou a pressão neutra foi mantida constante por contínuo ajustamento da pressão de câmara. Foram feitos também ensaios especiais do tipo não drenado, nos quais as pressões axial e radial foram aumentadas concomitantemente numa relação constante.

Os processos de compressão prévia das amostras foram: compactação de campo, compactação por pisoteamento no laboratório, compactação estática e adensamento a partir de uma pasta com teor de umidade da ordem de 100%.

Os resultados dos ensaios mostraram a existência de uma única envoltória de pressões efetivas para cada tipo de solo, independente dos processos de compressão e indicaram, outrossim, uma relação única entre o parâmetro índice de vazios (raiz quadrada do grau de saturação) ($e\sqrt{S}$), na ruptura, e a resistência ao cisalhamento do solo, para amostras que possuíam a mesma "estrutura original".

1. SHEAR STRENGTH CHARACTERISTICS OF NORMALLY CONSOLIDATED SATURATED CLAYS

Figures 1 and 2 summarize the triaxial tests performed on samples consolidated from a slurry of clay 2 from where it can be seen that the shear strength properties of that clay

are characteristic in nature of remolded normally consolidated saturated clays. The author wishes to describe in detail that behavior:

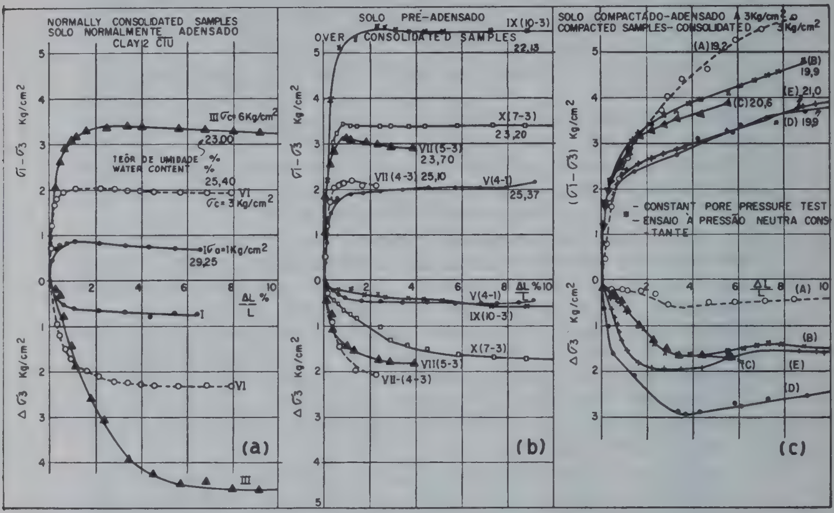

Fig. 1 — Stress-strain curves.

Fig. 1 — Curvas tensão-deformação.

Samples were let to consolidate under an hydrostatic chamber pressure. So, at the beginning of the test the pressure in all planes were the same, and the pore pressure was equal to zero.

The axial stress was increased continuously until the sample started to deform plastically at a constant or even decreasing axial load. Drainage was not permitted at any time during the shear process and a continuous measurement of the pore pressure was made.

Test results are presented in three ways: stress-strain curves (figure 1a); effective stress paths (figure 2a) and water content-strength relations (figure 3).

1.1 — Looking at figure 1a we can observe the variations of the deviator stress and the variations of the minor effective principal stress (in the case equal to the pore pressure) with the specific deformation of the samples.

We can observe that the peak strength occurs at about 1% strain, but that the peak pore pressure occurs only at about 2 to 5% strain. A schematic figure presented by Bishop and Bjerrum[1] confirms these observations. Computing the values of A (ratio of the pore pressure to the deviator stress) versus the specific deformation, we observe an increase on the values of A when strain increases from 1 to 3 and 4%.

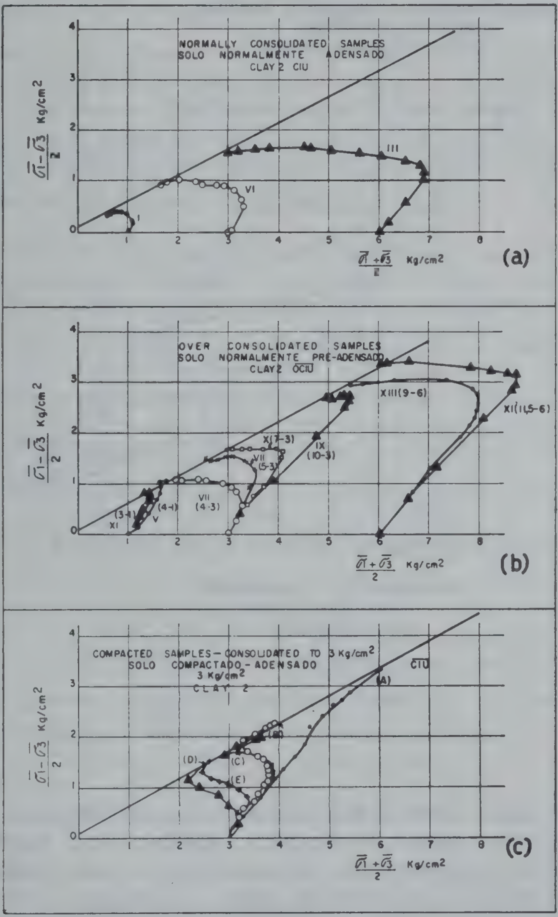

Fig. 2 — Effective stress paths.

Fig. 2 — Trajetórias de pressões efetivas.

Bjerrum[4] mentioned that the pore pressure build up is a direct function of the amount of deformation, which is indirectly a measurement of the tendencies to volume change of the sample. At the beginning of the shear process the soil structure is able to hold the full load almost without any deformation. If we maintain the peak load, the sample starts to deform gradually. The pore pressure will increase, reducing the effective normal stress on the failure plane until failure takes place (remember that $s = f\ [\bar{\sigma}\ \text{tg}\ \varphi]$).

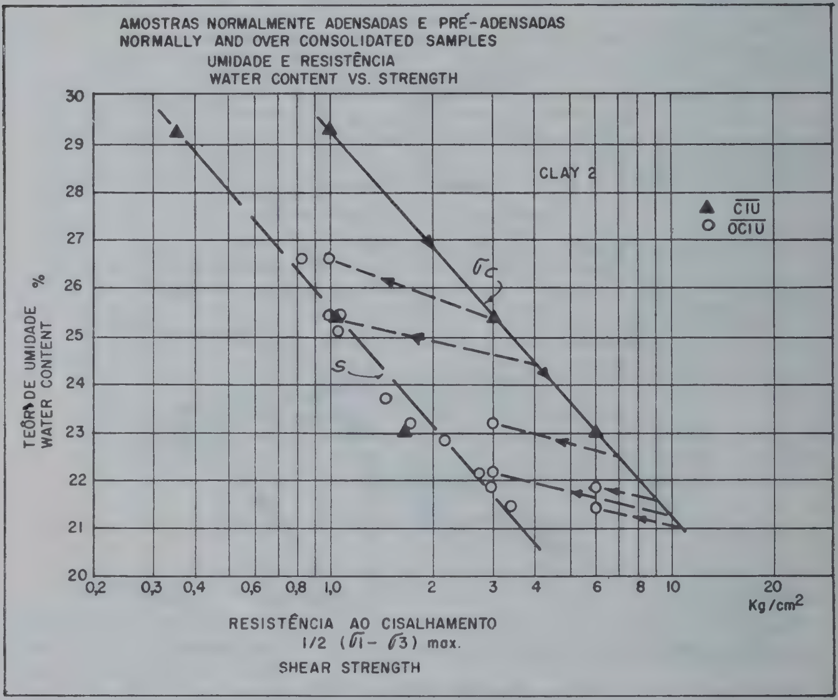

Fig. 3 — Normally and over consolidated samples.

Fig. 3 — Amostras normalmente adensadas e pré-adensadas.

There have been some attempts to distinguish two components of the shear strength: cohesion and friction. The first would develop almost instantaneously and decrease afterwards and the second would show a gradual increase with the deformation[12]. This separation might be helpfull to explain the time lag that is observed between the peak strength and the maximum pore pressure. The author, however, desagrees with that explanation because he believes that a soil structure is always in equilibrium due to the double action of internal and external forces, the nature of which are somehow different than the physical nature of cohesion and friction.

The internal forces will oppose resistance to the external forces as much as they can stand, but once the initial state of equilibrium is broken, a new position of equilibrium must be encountered. It is possible that the initial structure were the most resistent, and once it was broken the soil samples were not able to support any higher load. The stress-strain curves of figure 1a seem to indicate that once the structure has deformed 1%, it becomes weaker until failure. Sensitive clays can collapse at a specific deformation.

The ratio of the deviator stress to the consolidation pressure, for normally consolidated clays, slightly decreases for higher pressures. In the case of figure 1a we have 0.83, 0.68, and 0.57 for consolidation pressures of 1, 3 and 6 kg/cm^2, respectively. This ratio can be much more constant for other clays as for example Vicksburg clay[14].

1.2 — An undrained test on saturated specimens is by definition a constant water content test. Water content and void ratio are linear functions one of the other for saturated samples. It is well-known from the theory of consolidation that there is a linear variation of the void ratio to the consolidation pressure (in log scale) in the range of virgin compression. So, if we start with a soil at a certain water content and we let it to consolidate in a triaxial cell, at the end of consolidation we will have a well defined water content for each consolidation pressure. The water content versus consolidation pressure is a unique relation (see figure 3).

It is, important, however, to remember that the initial water content prior to the consolidation at the triaxial cell, plays a very important role. If we have two different water contents at the initial state of equilibrium that is the original structure, and we submit each sample to a consolidation process, we may arrive at two parallel lines in the water content-pressure graph. So the uniqueness of the water content-consolidation pressure relation will hold only if the original water contents of the samples were always the same. This fact was observed by Nasim[9] and by the author in a series of tests run on marine clay samples from Japan. See figure 4, for a schematic picture of the phenomenon.

Now if we remember that there is a relation between strength and consolidation pressure, and also a relation between water content and consolidation pressure we could expect a relation between water content and shear strength. This has been observed by Henkel[5] and by the author (figure 3).

The importance of this finding is of practical interest, once the determination of the water content of a clay sample is a very simple task. If we can stablish relations between water content and strength of a specific saturated clay, then the simple determination of its water content can be a good information about its shear strength. At this point the author wishes to recall that samples reconsolidated in the laboratory may define a different water content-shear strength relationship. This relation, however, may be very close to a parallel to the natural water content-shear strength relation. See figure 4.

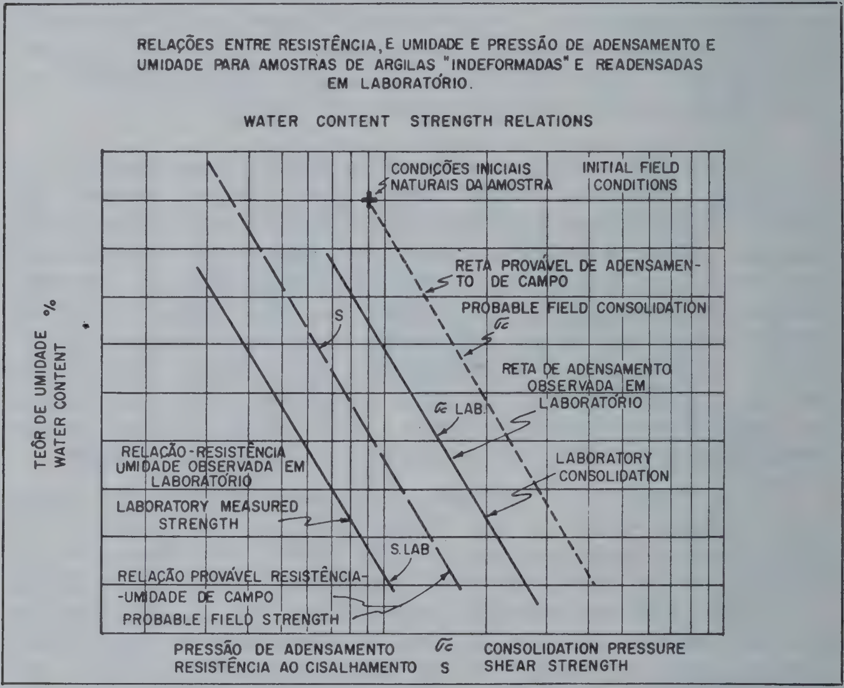

Fig. 4 — Strength-water content-consolidation pressure.

Fig. 4 — Resistência-umidade-pressão de adensamento.

1.3 — A third way of analysing test results is to look at the shear process in terms of effective stresses developed in definite planes. The best plane to be studied should be the failure plane but there are two difficulties: it is unknown before failure and the computations of the normal and tangential stresses in this plane are somewhat complicated. Two other effective stress diagrams have been proposed: a) to plot the effective stresses in the plane that has two equal principal stresses (that is the case of common triaxial tests). The coordinates are the major principal effective stress, or the axial stress and the radial effective stress multiplied by the square root of 2; b) to plot the effective stresses in a plane inclined 45°, which coordinates are the semi-sum and the semi-difference of the principal effective stresses (see figure 2a).

In this figure we can observe a similar shape of the curves. Each curve is more or less an ampliation or a reduction of the two adjacent curves.

The effective stress paths shown in figure 2a are very characteristics of normally consolidated saturated clays. The mean effective principal stress increases slightly until 60% to 70% of the soil strength is mobilized, then there is a reversion of the curves caused by a marked built up of the pore pressure; this continues until failure.

We can observe that once the paths get to the failure envelope the tendency, if any, is to follow the envelope in downward direction. This behavior can only be observed in strain controlled tests, because in stress controlled tests the maximum deviator stress will produce a continuous slide in the soil samples, and we loose the information beyond that point.

We can at this point transcribe the first conclusion on the basic shear strength behavior of remolded saturated clays, according to Henkel[5]:

"(i) There was a unique relationship between the shear strength (or maximum deviator stress) measured in the test and the water content at failure for all types of tests on normally consolidated samples, provided compression and extension tests were considered separately."

2. SHEAR STRENGTH CHARACTERISTICS OF OVER CONSOLIDATED SATURATED CLAYS

If we take a sample of soil and consolidate it to a certain pressure, and then let it equilibrate (swell) under a lower pressure, we are submitting that sample to a stress history commonly known as over consolidation. Natural overconsolidation is common in nature, due to different processes among which are: rising of the natural water table, suction of ground-water, removal of existing loads as old buildings, natural erosion of hills, surface drying of the soil.

In figure 1b the values of the deviator stress as well as the variation of the minor principal effective stress (in the case equal to the pore pressure) were plotted versus the specific axial deformation for a series of triaxial tests run on over consolidated saturated samples of the clay 2.

Samples consolidated from a slurry to 1 kg/cm² were consolidated to hydrostatic pressures ranging from 3 to 11.5 kg/cm² and, then rebounded to 1, 3 and 6 kg/cm². For each of the equilibrium pressures were run 2, 4 and 2 tests respectively. Special attention was given to the rebound pressure of 3 kg/cm² because compacted samples seem to have an equivalent consolidation pressure in the range of 3 to 5 kg/cm² (Standard Proctor compaction energy).

Deviator stress-strain curves are similar to those of normally consolidated samples with the exception of samples equilibrated to 6 kg/cm². In these samples the peak deviator stress occurs at about 6% strain. Curves corresponding to tests VII and X (figure 1b), show a small peak followed by a strength decrease.

Pore pressure-strain curves are quite different for over-consolidated clay samples. Let us consider, for example, the curves of figure 1b — we may observe that the magnitude of the pore pressure depends on the maximum consolidation pressure. The pore pressure parameter A (at failure) is plotted versus the over consolidation ratio in figure 5; in the same figure are indicated the values of the maximum deviator stress for all samples rebounded to 3 kg/cm². This behavior is very characteristic in nature of over consolidated saturated clays; a similar graph was presented by Skempton[13] in 1954, when he introduced the pore pressure parameters A and B.

Returning to figure 1b we observe that the pore pressure remains fairly constant during a wide range of deformations, for over consolidation ratios above 3. It seems to indicate a kind of flow failure considering that the deviator stress remains also constant.

An observation of the shape of the specimens during failure indicates the tendency to a barrel shape of the samples resulting in a family of planes of failure. This might be due to the tendency to expand during failure which results in decreasing pore pressures at the failure planes. Consequently the effective stress increases, and a weaker plane starts to fail. So, what happens is a continuous change of failure plane until a complete disarrangement of the structure takes place and the specimen fails.

2.1 — The over consolidation process results in the formation of an equilibrium soil structure for each specimen — this structure is doubtless different from that resulting of a normal consolidation of a similar specimen to the same rebound pressure. Test results indicate that the over-consolidated samples are always stronger.

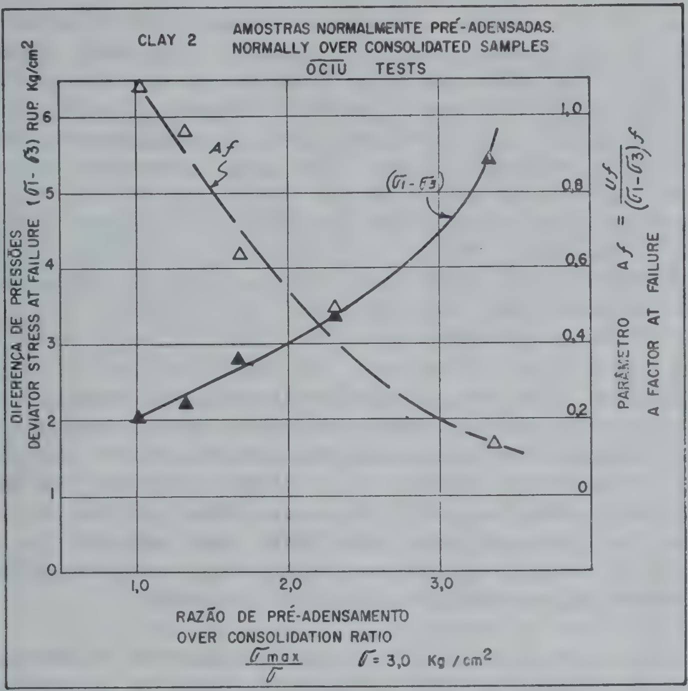

Fig. 5 — Over consolidated samples.

Fig. 5 — Amostras pré-adensadas.

From the theory of consolidation, we know that if we submit a sample of soil to a consolidation process, and at any pressure we let the sample rebound to a lower pressure, the final void ratio is smaller than the void ratio at the same pressure in the virgin compression (figure 3). The same occurs with the water content. As we saw the strength of a sample is in direct dependence of its water content for normally consolidated clays. Henkel[5] has shown that there is also an unique relation between water content and strength for samples consolidated to the same maximum pressure.

In figure 3 the author plotted his test results in terms of water content at failure versus shear strength (log scale) for all over-consolidated samples; and also the straight line relationship for normally consolidated samples. According to this figure there is practically no difference for the two stress histories. This behavior seems to be a particularity of the clay 2. According to this figure for a specific water content, no matter the stress history, the strength is very much the same. The question is whether at failure the soil structure is also the same. We can compare for example tests V and VI, or another pair: III and X. For both cases we have about the same average effective pressures at failure and consequently the same deviator stresses (figures 2a and 2b). This stands for the final state of equilibrium between internal and external forces. The pore pressures are quite different and in all cases at the beginning of the test the pore pressure were zero and the effective stresses were different. The initial water content was the same for each pair of tests; so we have two samples that for different external pressures can hold the same proportional amount of water, what is possible only for two different structures. During shear these structures will suffer successive changes until failure. For the normally consolidated samples there was a decrease in the mean effective stress during shear; for the normally over consolidated samples there was an increase of the same stress. So it is possible that at failure both samples ended up with the same structure, but it is also possible that two different structures can support the same load. It is enough to compare compacted samples strengths with normally consolidated samples strengths.

2.2 — Let us consider now the effective stress paths. Figure 2b summarizes test results on the clay 2 specimens.

We observe in figure 2b, that at the beginning of the failure process there is a remarkable increase in the mean principal effective stress, that continues until 90 to 100% of the maximum deviator stress is developed, when there is a reversion of the curve. The pore pressure will continue to rise and the deviator stress will remain practically constant or even decrease until failure. At the failure envelope in some cases we can observe a second point of failure that has a lower deviator stress. In no case we have observed a series of points following the failure envelope in the upward direction.

All paths are somehow similar and again we can say that each effective stress path is an ampliation or reduction of the two adjacent paths.

At this point we can transcribe the completion of the first conclusion of Henkel[5]:

"....a similar behavior was obtained for over consolidated specimens having a common maximum consolidation pressure."

We can observe from figures 2a and 2b that there are common effective stress envelopes for each series of tests. This confirms the second conclusion of Henkel[5]. The author transcribes the part of the conclusion that is applicable to the tests run on samples of clay 2:

"(ii) Common effective stress Mohr failure envelopes were obtained for all types of tests on normally consolidated samples. Common effective stress Mohr failure envelopes were also obtained for all types of tests on overconsolidated samples having the same maximum consolidation pressure."

Henkel, however, does not make any comparison between the common effective stress Mohr failure envelope of normally consolidated and overconsolidated samples. For clay 2 it is interesting to mention that both envelopes are very much the same, and that for engineering purposes it can be considered unique.

Analysing Henkel test results, we observe a small deviation of the unique envelope at the low range of pressures, specially for the overconsolidated samples. For heavily overconsolidated samples there is a tendency to expand during the shear process, which results in the development of negative pore pressures. The correct measurement of these negative pressures is sometimes difficult and it is possible that those deviations of the unique effective stress envelope could be explained by possible differences in the pore pressure measurements at the base of the specimen and the real pore pressure at the failure zone. In the other hand the heavy over consolidation process can result in a proportionally stronger structure.

For practical applications the question is whether we can count with those higher strengths (due, eventually to high negative pore pressures) or not.

3. SHEAR STRENGTH CHARACTERISTICS OF COMPACTED CLAY SAMPLES

If we find in the current literature a relatively large number of test results expressed in terms of effective stresses for saturated soils, the amount of information of the same nature for compacted non-saturated soils is considerably smaller.

The main difficulty is the presence of two fluids in the pores of the soil, which result in two pore pressures: the air and the water pressures. The pore pressure is a combination of both.

To illustrate this point the author prepared figure 6, which represents test results of a test presented by Bishop[2]. In this test both air and water pressures were measured. The author drawn three effective stress paths; one considering the pore pressure as the air pressure, the second considering the water pressure as the pore pressure and the third considering the combined pore pressure. So, we can define three effective stress envelopes, from which only one is the real effective stress envelope of the soil. It is interesting to observe that the real envelope and the envelope assuming the pore water pressure as the pore pressure for samples of high degree of saturation are very much the same.

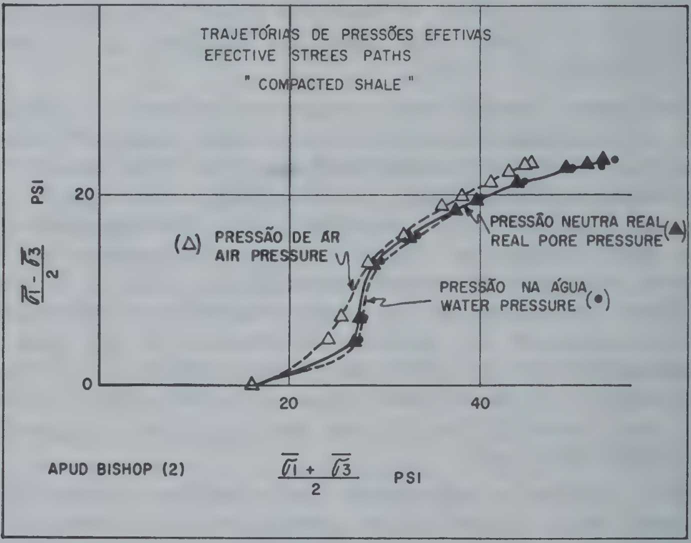

Fig. 6 — Effective stress paths.

Fig. 6 — Trajetórias de pressões efetivas.

So it is necessary to measure at least the pore water pressure during the tests, and take it as the pore pressure. The envelope that we obtain through this procedure will define a slightly higher friction angle and a slightly lower cohesion intersept. This means that in the low pressure range the envelope is in the safe side, but the reverse is valid for the high pressure range.

The use of back pressure to increase the degree of saturation of soil sample has been widely used, but the author believes that this procedure may introduce some changes in the soil structure prior to shear. We will come back to this point later on.

In all tests presented in this paper, the measurements of the pore pressure were made at the base of the specimens through pore stones of high bubbling pressures. We assumed that the measured pore pressures are pore water pressures, and we drawn all the effective stress paths based on those pore pressure.

The author wishes to examine in detail the results of the tests proceeded on samples of the clay 2. Other test results of the same nature are also presented, which will serve as additional data on the shear strength behavior of compacted clays.

Test results of axial compression tests will be analysed in terms of both total and effective stresses.

We will start with the series of tests of the type:

Consolidated Isotropically Undrained, with Pore Pressure Measurements.

Samples were prepared by kneading compaction with equivalent Standard Proctor Energy at various water contents.

3.1 — Stress-strain relations: typical test results are presented in figure 1c, respectively to consolidation pressure of 3 kg/cm^2. The deviator stress and the variations of the minor principal effective stress were plotted versus the axial specific deformation of the samples. We observed that at 1% strain 50% or more of the shear strength was mobilized, but that failure of the specimens occurred solely at 10%, 15% or even 20% strain. Between one percent strain and failure we observed a continuous rise of the deviator stress. Some of the curves are practically composed of two straight lines, as for example test number B (figure 1c) in which the slopes of the lines are roughly 6:1 and 0.3:1. This behavior is definitely different from the behavior of normally consolidated and over consolidated samples of the same soil.

The curves of the pore pressure or variations of the minor effective stress show, in general, a continuous rise up to 3 to 4% strain, followed by a stationary value, or a small decrease of the order of 10% to 20% of the maximum observed value. The behavior is not too different from that of over consolidated samples, with the difference that for those samples there was no reduction of the pore pressure before failure.

The three samples that were consolidated (equilibrated) to a chamber pressure of 1 kg/cm^2, presented a rather confusing behavior characterized by a somewhat erratic variation of the pore pressure.

Figure 1c seems to indicate that the compacted samples are able to gain in strength with the deformation. This gain in strength could be explained by the reduction of the pore pressure for increasing strains. Anyhow, between 1 and 3% strain the pore pressure continued to increase, what might be due to an eventual time lag in the measurements of the pore pressure. The same fact was observed for normally consolidated and overconsolidated samples, as we mentioned before.

It is interesting to mention that each sample of each series were consolidated to the same chamber pressure, but in spite of that we observed different values of strength and pore pressure in tests of the same type. So we can say that the strength of compacted samples (same compaction energy) depends on something else than the consolidation pressure. To analyse this point the author prepared figure 7b, where the values of the shear strength (one half of the maximum deviator stress) were plotted versus the failure water content. In the same figure are also indicated the results of Unconsolidated Undrained Tests proceeded on compacted samples of the same soil.

3.2 — This graph is similar to those of normally consolidated and overconsolidated test series. The straight line relationship appears in a new form:

i) it is composed of two parts, with a breaking point at a water content slightly below the optimum water content;

ii) it is dependent on the chamber pressure at failure.

The water content at failure is a function of the molding water content plus the effects of the consolidation and shear processes. The structure of the soil samples prior to shear is primarily a function of the molding water content because the variation in structure due to the consolidation process are of secondary influence. The chamber pressure during the failure process plays also an important role in the magnitude of the shear strength of the sample. This could be explained considering that compacted soil samples have a tendency to expand during shear and that the expansive forces would be opposed by higher chamber pressures.

The combined effect of molding water content plus consolidation, can be seen considering tests number 2, C and c, that have approximately the same molding water content and which define a straight line relationship between failure water content and strength (see figure 7b). This fact is of the same nature of what happens to normally consolidated and overconsolidated samples that have the same water content prior to consolidation.

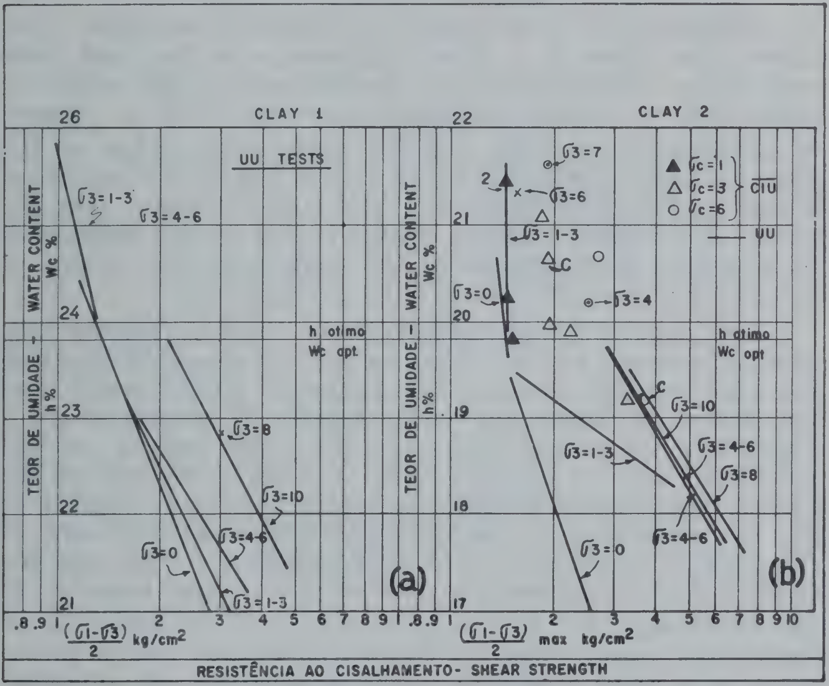

Fig. 7 — Strength vs. water-content.

Fig. 7 — Resistência-teor de umidade.

The original structure has a definite influence on the future shear strength of compacted soils.

It would be desirable to eliminate the influence of the chamber pressure in strength relations. This seems possible by introducing a new parameter that takes into account not only the water content of the soil, but also the relative magnitude of the air-water relation in the voids.

We have already seen that for low chamber pressures the water content — strength relations show a breaking point a little below the optimum water content. For these samples the degree of saturation is usually lower than for samples submitted to higher chamber pressures. We observe a remarkable increase in strength for a relatively small change in the water content, what is due to the increasing proportion of air in the voids. So, in compacted soil structures there are two important factors: a) the volume of the voids to the volume of the soil particles — that is the void ratio — e; b) the relative amount of air and water in the voids that is measured through the degree of saturation — S.

Experimental data, based on failure conditions, has shown that there is a direct dependence of the void ratio and degree of saturation on the strength of the soil: the relationship is between the parameter void ratio $\times$ (degree of saturation)$^{1/2}$ ($e\sqrt{S}$) and the decimal logarithm of the shear strength of the soil, taken as one half of the maximum deviator stress (see figure 8). The author believes that the scatter that appears in the figure is due to the difficulties of a precise measurement of the void ratio and degree of saturation of the samples at failure conditions.

This type of graph eliminates the third parameter (the chamber pressure) of the previous one. It also indicates that the void ratio is a controlling factor of higher order than the degree of saturation. The degree of saturation is a function of the proper void ratio, the water content and the specific gravity of the soil. The void ratio depends on the equilibrium between internal and external forces applied to the soil structure; the water content is a measurement of the capacity of the soil to retain water in the voids and the specific gravity depends on the nature of the minerals of the soils particles. So the parameter $e\sqrt{S}$ is doubtless an interesting measurement of the soil structure, and it is expected that the strength of a soil be related to its structure at failure.

3.3 — Effective stress paths — Figure 2c shows typical effective stress paths for compacted samples of the clay 2 at various water contents, consolidated to 3 kg/cm^2.

We observed that for all samples consolidated to 1 and 3 kg/cm^2, and for 2 tests ($\sigma_c = 6$ kg/cm^2), the mean effective principal stress at failure is larger than the consolidation pressure, what means an increase of the normal effective stress at a plane of 45° during the shear process. This is also true for the normal effective stress on the failure plane in almost all cases.

The second observation is that there is a series of points that follow the effective stress envelope (in the upward direction), before the samples dismantles or shows a continuous deformation at a constant load.

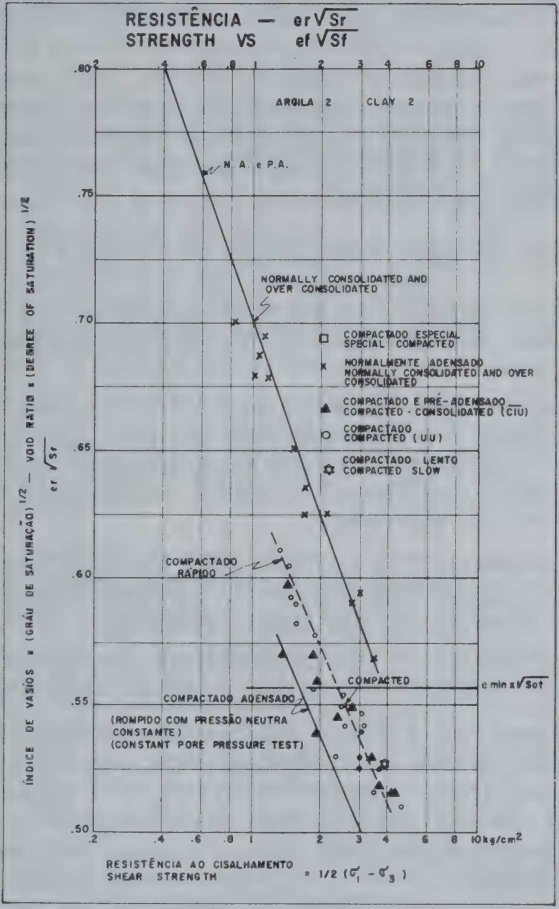

Fig. 8 — Strength — $e_f \sqrt{S_f}$.

Fig. 8 — Resistência — $e_r \sqrt{S_r}$.

The third thing to observe is the characteristic S shape of the stress paths. These curves are no more ampliations or reductions of the neighboring curves as is the case of normally and over consolidated samples. This may be due to the constancy of the water content.

The shape of these curves is different from those of normally consolidated and overconsolidated specimens, even for the cases of saturation of the specimens.

The relative position of the stress paths depends on the value of the parameter void ratio $\times$ (degree of saturation)$^{1/2}$; lowering the parameter the curves tend to the right, which implies in higher strengths and lower pore pressure.

For one sample of each group the test was run with constant pore pressure and variable chamber pressure. This test procedure resulted in the measurements of shear strength characteristics that differ from the other technique (constant cell pressure) in two ways:

a) the effective stress paths fell to the left of all tests;

b) the samples with the same parameter $e\sqrt{S}$ at failure were weaker. See figure 8 — we have two parallel straight lines.

So, we see that the mode of failure can also influenciate the strength of a compacted clay sample. The reduction of the chamber pressure may induce a different volume change of the sample (facilitates the lateral expansion), that results in a weaker soil structure.

It is important to mention that the effective stress envelopes are practically the same, independently of the consolidation pressure or the failure process.

Some conclusions can be drawn on the behavior of compacted clay samples, when submitted to undrained failure:

i) There was a unique relationship between the strength (or one half of the maximum deviator stress) measured in the tests and the parameter void ratio $\times$ (degree of saturation)$^{1/2}$ at failure, for all tests on compacted consolidated samples, provided constant pore pressure test and constant chamber pressure tests are considered separately. The relationship is of parallel straight lines for the two modalities of tests.

ii) Common effective stress failure envelopes were obtained for both types of compression tests on all consolidated compacted samples, independently of the molding water content of the specimens and the consolidation pressure."

4. TEST RESULTS IN TERMS OF TOTAL STRESSES

The Unconsolidated Undrained Test has been advocated as a good measurement of the shear strength of a compacted soil mass at the condition characterized as "the end of the construction period". This is the case of clay soil masses of low permeability, where there is no time to dissipate the construction pore pressures. At least that test is used as a lower limit of the shear strength to be used in earth dam projects.

Test results of a series of unconsolidated undrained triaxial compression tests on compacted samples of clay 2 are presented in figure 9a. In the same figure are shown also the test results of a series of unconfined compression tests rum on samples of the same clay.

From figure 9, we may observe that:

a) a change of only half percent on the value of the water content is enough to change the total strength parameters c and φ;

b) the change in the water content (reduction) implies in an increase on the friction angle. The cohesion remains relatively constant.

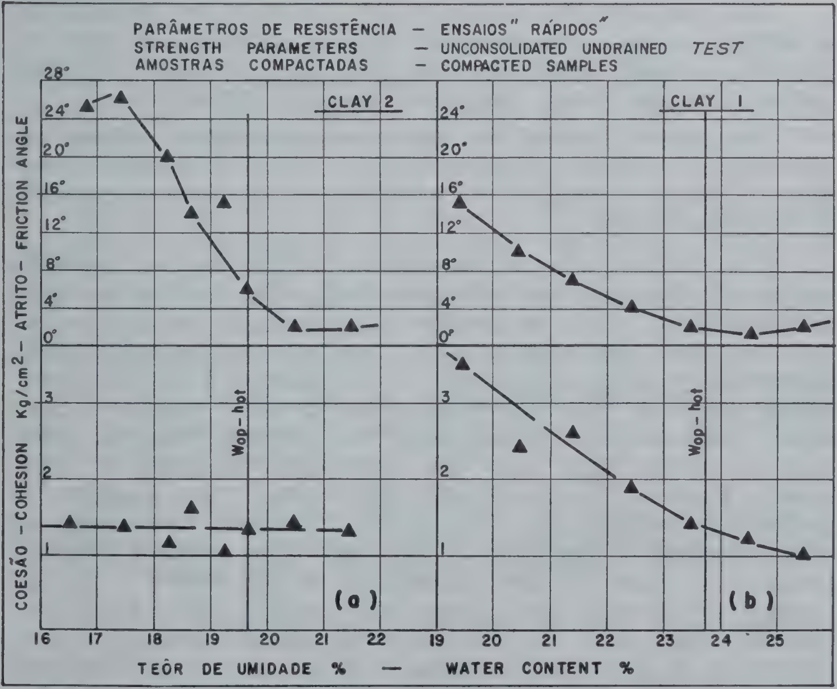

Fig. 9 — Strength parameters.

Fig. 9 — Parâmetros de resistência.

Conclusion b is not necessarily a characteristic of compacted clay soils. Compare for example with the test results of figure 9b, where the tendency is to increase both cohesion and friction angle for decreasing water contents. The clay 1 is mainly kaolinite.

The values of the water content shown in figure 9 are molding water contents, which are also failure water contents. For field conditions they would be the placement water contents.

Figure 9 serves also to illustrate that the strength parameters in terms of total stresses are far from being constant. This fact is fairly important to designers. Any soil structure design based on total stresses, will require laboratory tests that should represent the best approach to field conditions.

The test results of figure 9 were also plotted in figure 7. This type of graph has been already commented previously.

5. SPECIAL TESTS (E)

The measurement of the proper value of the strength of a sample of soil, requires not only a molding as close as possible to field conditions, but also the application of load increments that would approach the field situation.

The second part of the above requirement is not so important for saturated specimens, but it is a necessary refinement of triaxial tests, if we want to get as close as possible to field strengths.

The difficulty is in the determination of the probable values of the principal stresses that will develop in each field condition. Let us consider, for example, an element of soil that has been compacted in one layer of an earth dam. Immediately after compaction it is submitted to the pressures resulting from the compaction process (negative pore water pressures are developed); the vertical external pressure is atmospheric and the horizontal pressure is very small. Further layers of soil, will submit the element to increasing vertical and horizontal pressures, the value of which depend on the type of the soil. The vertical external pressure is close to the summation of γz, where γ is the density of the soil and z the layer depth. The horizontal pressure may vary for the different planes between a maximum of $K_a \gamma z$ and a minimum of $K_p \gamma z$ (K_a in the direction parallel to the axis, and K_p in the direction perpendicular to the transverse axis of the dam). The difference between K_a and K_p are due to possible different deformations in both directions. If we assume that there are no horizontal deformations then $K_a = K_p = K_o$.

The values of K_a and K_p are unknown for a wide range of soil types, at least for the author's knownledge.

The next difficulty is that the principal stresses at a point on an insipient earth mass failure surface do not coincide with the vertical and horizontal pressures at the same point. Bishop[3] has shown that the major principal stress for an earth mass at a slope of 3 (hor.) to 1 (vert.) varies from 0.8 to 1.2 times the vertical stress, taken as γz, from point to point.

In the other hand the values of K_a and K_p may vary with the magnitude of the vertical pressure and the relative position into the earth mass.

All these difficulties seem to be enough to discourage the execution of any tests. These tests are still limited to a few types:

a) to run tests with the same radial pressure in all directions;

b) to run tests with an additional confinement of the sample — as for example to use cylindrical samples semiconfined with a "half metalic can" or to use prismatic samples confined in two planes with vertical metal plates fixed one to the other.

The testing technique a results in a constant value for K, and the technique b implies in a variable K value. In the case of prismatic samples there are two K values in the two horizontal axis, and in the case of cylindrical samples the value of K is variable. The value of K in the planes that have additional confinement is unknown.

The author run triaxial compression tests of the three types above on samples (compacted) of clay 2. Some findings can be mentioned:

a) for the same failure water content, additionally confined samples are stronger than normally confined samples — the stronger being the prismatic sample;

b) the effective stress envelope is the same for the three tests;

c) the pore pressure is higher for the additionally confined samples at the same water content.

These tests, though they do not represent precise field conditions, are a much better approximation, than the common unconsolidated undrained tests.

Results of two of these tests are shown in figure 10a and 10c. The first gives stress strain curves and the second effective stress paths.

It is interesting to compare stress strain curves with those from unconsolidated undrained (UU) tests proceeded upon compacted samples of the same clay (see figure 10a). We can observe that for samples compacted at about optimum water content, the deviator stress for the E tests is smaller than the deviator stress for the UU tests at the same specific deformation, but that for samples compacted at 2% or more (T2) above optimum both types of tests give about the same stress-strain curve.

As earth dams are in general compacted at or around the optimum water content, this difference in strain is significant for possible informations on the deformations of the earth mass.

The second important information concerns the pore pressure predictions. The pore pressures are usually compared with the total major principal stress (observed in the tests), which in field conditions is similar to the vertical pressure. The curves on figure 10b give some relations between the pore pressure and the major principal stress.

We may observe that the ratio pore pressure-total major principal stress remains very constant for a wide range of the principal stress (T1). In the proximity of failure it increases rapidly. This behavior is more an intrinsic characteristic of each soil at a specific water content, than a general behavior of compacted clays.

Let us consider now the effective stress paths (figure 10c). We may observe an effective stress path that is completely different from any other that we have mentioned before. It is more similar to a normally consolidated effective stress path of a saturated sample. It is important to recall that the total stress path is also different, what might invalidate any comparisons.

6. DRAINED TESTS

Drained tests were run on compacted samples of the clay 2 by the author and at the Norges Geotekniske Institut [10]. Tests results are presented in figure 11, as Mohr circles.

This type of tests has been advocated for some years as the best way to measure the real friction angle of the soil as well as the cohesion intersept.

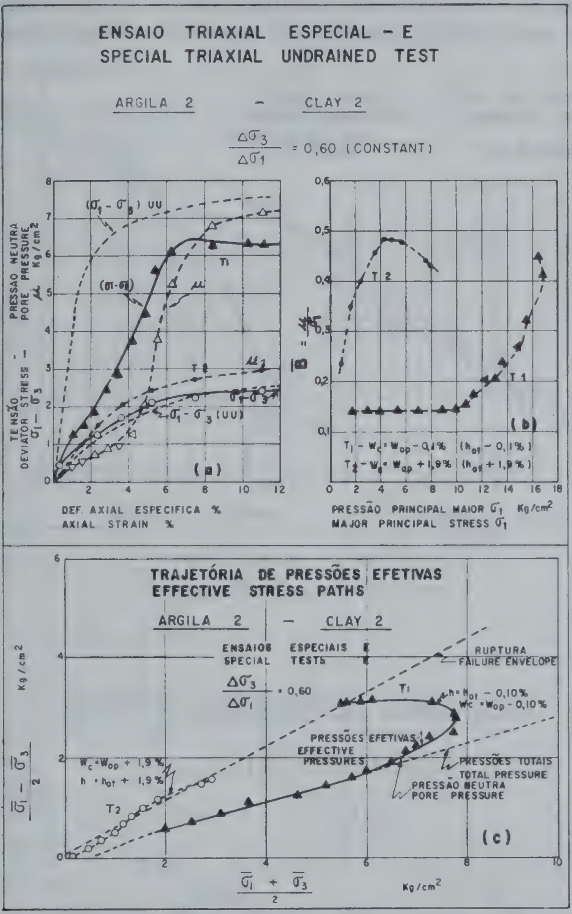

Fig. 10 — Special triaxial test.

Fig. 10 — Ensaio triaxial especial.

In these tests the difficulties of measurement of the pore pressures are eliminated, once at every moment the pressure should be effective. This, however, is possible only if the test is run so slowly, and with so small stress increments, that at every moment the pore pressures were dissipated by drainage, what from a theorectical point of view is impossible. In the usual test procedure, an axial load is applied to the sample at intervals of n hours (n is a function of the permeability of the soil: 12, 24 and 48 hours intervals are common in tests on clay samples). At the moment of application of the load, a pore pressure is developed within the sample; a consolidation process starts immediately, which should be completed before the next load increment is ap-

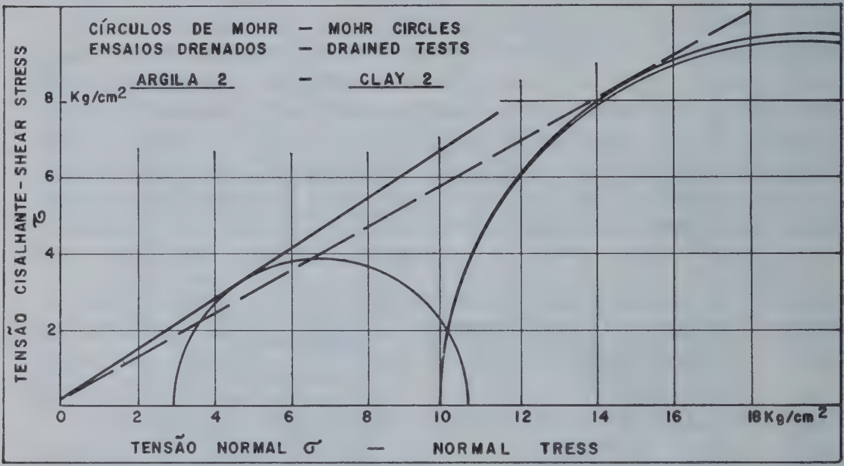

Fig. 11 — Drained tests.

Fig. 11 — Ensaios drenados.

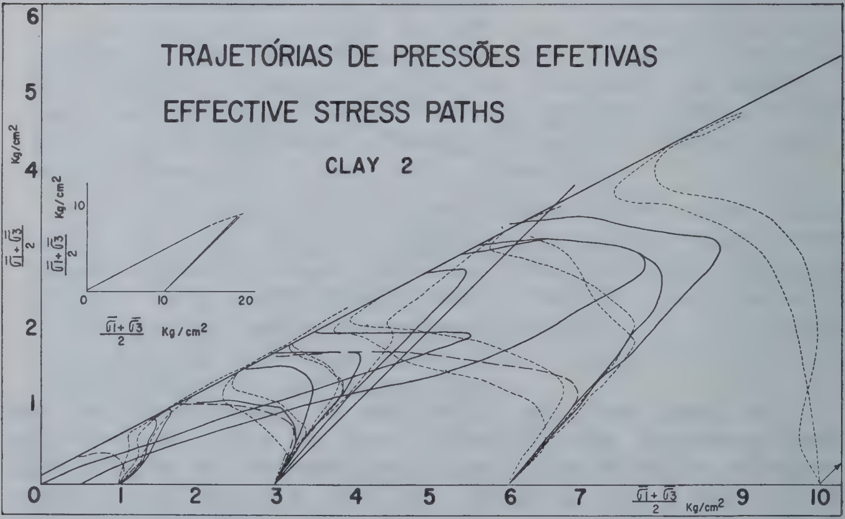

Fig. 12 — Effective stress paths.

Fig. 12 — Trajetórias de pressões efetivas.

plied. When failure is incipient, the load increments are usually reduced, but even so failure of the specimen can occur at the moment of application of the last load increment, when the resulting pore pressure was not completely dissipated. Of course, some refinements can be introduced to improve the test procedure and reduce the error to nonsignificant values.

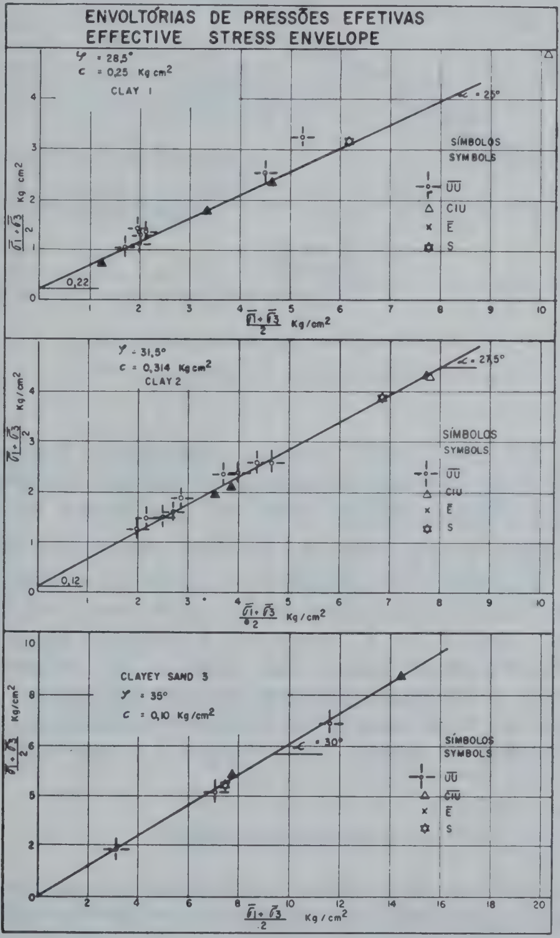

Fig. 13 — Effective stress envelope.

Fig. 13 — Envoltórias de pressões efetivas.

In strain controlled tests the velocity of deformation can be adjusted in order to dissipate practically all the developed pore pressures.

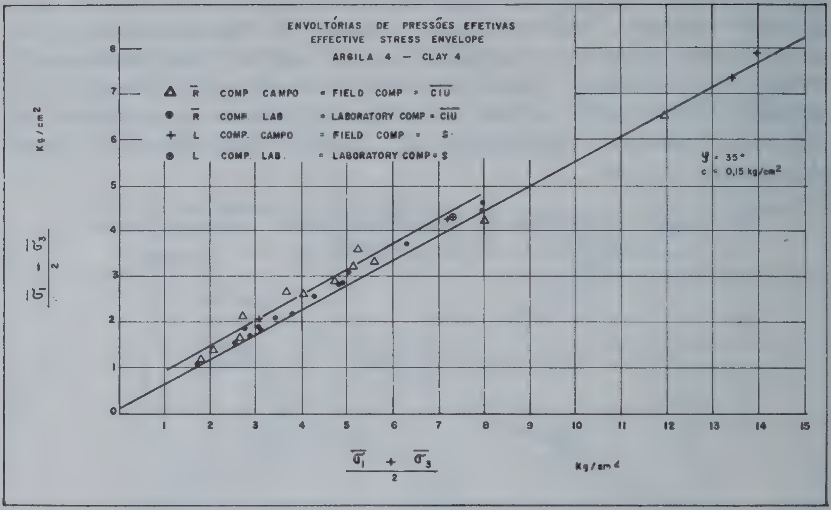

Fig. 14 — Effective stress envelope.

Fig. 14 — Envoltórias de pressões efetivas.

There are two more points concerning the quality of drained tests as a good measurement of soil properties: a) the relative time to failure and b) the range of pressures.

In relation to the time to failure, creep and thixotropic effects are concern. As far as the range of pressure, due to the concomitant consolidation of the specimens, in some cases the test is carried to a range of pressures that might be above the field conditions, and where the effective stress envelope may eventually change slightly its slope. Compare for example the test results on samples consolidated to 3 and 10 kg/cm² prior to failure (see figure 11 and 12).

CONCLUSIONS

Test results permit some conclusions about the behavior of residual clayey soils in connection with the shearing resistance.

i) The effective stress Mohr failure envelope for a residual clayey soil is an intrinsic property of the type of clay. It is a constant which independs on the stress history the soil structure and the failure process, provided the mineralogical composition remains the same. It can be expressed by the equation of a straight line, of the type

$s = c + \bar{\sigma} \operatorname{tg} \varphi$, in a certain range of pressure, c is the cohesion intersept and φ the internal friction angle of the soil. Deviations of the straight line relationship may occur for very low or very high pressures. See figures 12, 13, 14.

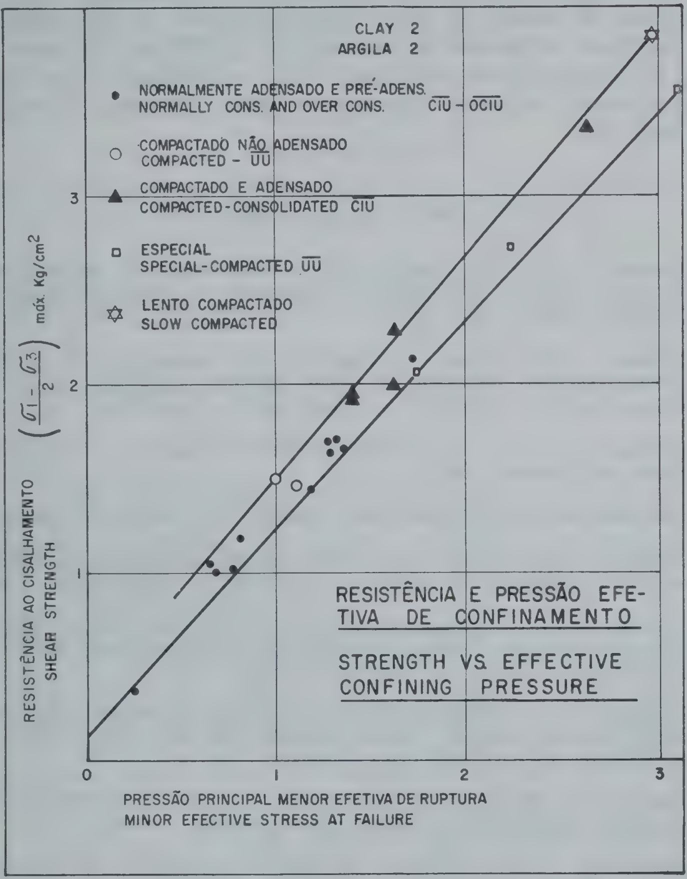

Fig. 15 — Strength vs. effective confining pressure.

Fig. 15 — Resistência e pressão efetiva de confinamento.

ii) There is a unique relationship between the strength of a residual clayey soil (one half of the maximum deviator stress) and the parameter void ratio . (degree of saturation)$^{1/2}$ — $e\sqrt{S}$ —, provided the original structure, as well as the type of failure are considered separately. The relationship is a straight line in a semi-log plot. Different types of failure, and or different original structures may define parallel straight lines in the semi-log plot. See figure 8.

iii) The shear strength of a residual clayey soil is dependent on the minor principal effective stress at failure. See figure 15.

iv) The behavior of a compacted residual clay, when submitted to shear is very characteristic in its nature. It is a peculiar behavior of the clay that differs in many ways from the behavior of the same clay submitted to a different stress history prior to the same shear process. See figures 1, 2 and 12.

REFERENCES

1. Bishop, A. W.; Bjerrum, L. — The relevance of the triaxial test to the solution of stability problems — Shear strength Conf. A.S.C.E. 1960 — pg. 437.

2. Bishop, A. W.; Alpan, I.; Bligh, G. E.; Donald, I. B. — Factors controlling the strength of partly saturated cohesive soils. Shear Strength Conf. A.S.C.E. — June 1960 — pg. 503.

3. Bishop, A. W. — The stability of earth dams — Sc. D. Thesis Univ. of London, 1952.

4. Bjerrum, L. — Soil Mechanics Lectures — M.I.T. — 1961.

5. Henkel, D. J. — The shear strength of saturated remolded clays — Shear Strength Conference — A.S.CE — June 1960 — pg. 533.

6. Henkel, D. J. — The correlation between deformation, pore pressure and volume change characteristics of saturated clays — Ph. D. Thesis — Univ. of London — 1958.

7. Henkel, D. J. — The relationship between strength, pore pressure and volume change characteristics of saturated clays. Geotechnique, IX — 1959, pg. 119-135.

8. Instituto de Pesquisas Tecnológicas — Ensaios Geotécnicos. Barragem de Chavantes — C.O. 213.044, 1962.

9. Nasin, N. — The influence of rate of strain on the strength of saturated clay — M.I.T. — M.S. Thesis 1961.

10. Norges Geotekniske Institutt — Report 61-606 May 1962 — Oslo, Norway.

11. Rodio S/A. — Rio de Janeiro — Relatório 26-41, maio 1962.

12. Schmertman, J.; Osterberg, J. — An experimental study of the development of cohesion and friction with axial strain in saturated cohesive soils — Shear Strength Conf. 1960.

13. Skempton, A. W. — The pore pressure coefficients A and B — Geotechnique, vol. 4, nº 4, pg. 143-147 — 1954.

14. Whitman, R.; Ladd, C. C.; Cruz, P. — Discussion on anisotropic consolidation of clays — Shear Strength Conf. A.S.C.E. — 1960, pg. 1049.

THE EFFECT OF STRAIN RATE ON THE UNDRAINED SHEAR STRENGTH OF COHESIVE SOILS

W. H. PERLOFF, JR.

Assistant Professor, Civil Engineering and Engineering Experiment Station,
The Ohio State University, Columbus, Ohio

J. O. OSTERBERG

Professor of Civil Engineering, Northwestern University, Evanston, Illinois

ABSTRACT

In a previous paper, the writers have shown that the undrained strength of cohesive soils, as measured by the triaxial compression test, can be expressed as an explicit function of the stress history for a constant rate of strain. In the present paper, test data are presented which indicate the interrelated effects of strain rate and stress history. It is shown that undrained shear strength can be expressed explicitly in terms of the stress history and the strain rate. This can be done because the Skempton pore pressure parameter at failure (and therefore the pore pressure) is also an explicit function of the two variables. The results are shown to be consistent with those of previous investigations. In addition it is seen that consideration of the interrelationship between stress history and strain rate effects permits more rational interpretation of results of tests performed at varying strain rates.

RESUMEN

En un escrito anterior, los mismos autores demostraron que el esfuerzo cortante sin drenaje de los suelos cohesivos, — como es medido actualmente por el ensayo a la compresión triaxial — puede ser expresado como una función explicita de los esfuerzos previos en el suelo (historia de esfuerzos) para una rata constante de deformación. En el presente escrito, se presentan datos de ensayos que indican la relación de los efectos de la rata de deformación y los esfuerzos previos en el suelo. Se demuestra que el esfuerzo cortante sin drenaje puede expresarse en función de los esfuerzos previos en el suelo y la rata de deformación. Esto es posible debido a que el parámetro de Skempton para la presión de los poros en *el momento de falla (y por lo tanto la presión de los poros) és también función explicita de esas dos variables. Los actuales resultados han demostrado ser consistentes con los de investigaciones previas. Es también visto, que las relaciones entre los esfuerzos previos en el suelo y el efecto de la rata de deformación permite una interpretación más racional de los resultados obtenidos en ensayos verificados a distintas ratas de deformación.*

INTRODUCTION

As early as the nineteenth century, Vicat (1833) and Collin (1846) recognized that the strength of clay soils could not properly be discussed without considering the effect of time. One of the most important effects of time on strength is that of strain rate on the undrained shear strength of cohesive soils. This problem has been investigated by many authors in relation to undisturbed, remolded, and compacted clays [1]. In spite of the large number of investigations performed, only one general conclusion can be drawn from all of the results presented: namely, that in general, the strength of a cohesive soil tends to decrease as the rate of strain decreases. In only three of these investigations (Bjerrum et al., 1958; Crawford, 1959; Seed et al., 1960) were pore water pressures measured. Even these analyses have not shed much more light on the effect of strain rate on strength parameters in terms of effective stresses. It will be shown below that this confusion has been due, at least in part, to the fact that previous investigations have not considered that the effect of strain rate on strength is a function of the stress history of the soil. That is, strain rate effects are influenced by the stress history.

The writers have previously shown (Perloff and Osterberg, 1962) that the undrained shear strength of a cohesive soil, when tested at a constant strain rate, can be expressed as an explicit function of the over-consolidation ratio. This can be done without the use of effective stresses because the effective stresses themselves are a function of the over-consolidation ratio. The investigation described below is an attempt to determine the interrelationship between the effects of stress history and strain rate on the undrained shear strength of clays.

---

[1] See, for example: Hvorslev (1938), Macey (1941), Rutledge (1947), Casagrande and Wilson (1951), Seed and Chan (1957), Bjerrum et al. (1958), Crawford (1959), Osterberg and Perloff (1960), Seed et al. (1960), and many others.

EXPERIMENTAL ANALYSIS

Description of soil used. The soil used in this investigation has, as its chief constituent, the clay mineral illite. It is found in the Goose Lake area of Grundy County, Illinois, and is sold under the trade name of "Grundite" by the Illinois Clay Products Company. The origin and properties of this soil have been discussed in some detail by Grim and Bradley (1939). The clay is upper Pennsylvanian in age and has been exposed, at the site where it is mined, by erosion of the sediments immediately overlying it. "The source of this clay, like that of the other underclays of the Pennsylvanian, is believed to be somewhat weathered surface material from the area enclosing the region of accumulation." (Grim and Bradley, 1939, p. 162). The classification properties are shown in Table 1.

TABLE 1 — Classification Properties of Grundite

w_L (%)	w_P (%)	I_p (%)	G	Clay Fraction (%)
54.5	26.0	28.5	2.74	85

Specimen preparation. The Grundite was received from the Illinois Clay Products Company in dry powdered form. It was mixed, as received, with distilled water to a water content of approximately 43 per cent, which was as close to the liquid limit as the soil could be molded. The moist clay was thoroughly mixed by hand and by a mechanical mixer. It was then passed through a "Vac-Aire" sample extruder several times to ensure uniform moisture distribution. This equipment, designed for the extrusion of clay specimens, has been described by Matlock et al. (1951). On the third time through the extruder, specimens approximately four inches long were cut and immediately covered with six coats of a flexible wax. Waxed specimens were placed on a shelf inside a sealed jar, which had water in the bottom to maintain 100 per cent humidity. The jar was then placed in a humid room. The specimens were cured for approximately six weeks. During that time, at periodic intervals, specimens were removed and tested in unconfined compression to determine if thixotropic hardening was taking place. No evidence of thixotropic hardening was apparent, since the unconfined strengths of all the specimens tested during the six week period after extrusion were the same within ±1.5 per cent.

Testing procedure. Preparation of specimens for triaxial testing is described in detail by Perloff and Osterberg (1962). Specimen dimensions and properties are given in Table 2.

TABLE 2 — Specimen Dimensions and Properties

Length (cm)	Diameter (cm)	Initial Wt. (gm)	Water Content (%)	Void Ratio
7.60	3.54	134.29 ± 0.57	43.2 ± 0.4	1.183 ± 0.012

A specific over-consolidation ratio, σ_p/σ_c, was obtained by consolidating a specimen in a triaxial chamber under an hydrostatic pressure, σ_p, higher than the pre-consolidation pressure induced by the extrusion process (approximately 0.6 kilograms per square centimeter), and then rebounding the specimen under an hydrostatic pressure, σ_c, which gave the desidered σ_p/σ_c. Results of these consolidation tests are shown in Figure 1. These data represent tests on 23 specimens. Some of the tests consisted of a single load increment, some of several increments. There were too many tests to indicate each with a separate symbol. To avoid confusion, only two of the rebound curves are shown.

When consolidation was completed, the drainage line was closed, pressure removed from the triaxial chamber, and the glycerine drained. The specimen was then taken out of the chamber and the rubber membranes and filter strips were removed. The specimen was immediately recovered by either one or two membranes, with a layer of silicone fluid between them, depending upon the duration of test to be performed. A solid base and cap were placed on the ends of the specimen. A small hole, approximately ¼ inch in diameter, was cut in the membrane at mid-height of the specimen and a pore pressure measuring needle, filled with distilled water, was inserted into the specimen. The design of the pore pressure needle is described in Perloff and Osterberg (1962). Pore pressures were measured by a null-balance device designed at the Norwegian Geotechnical Institute and constructed by Geonor A/S, Oslo, Norway. The design and operation of this device are described in detail by Andresen et al. (1957).

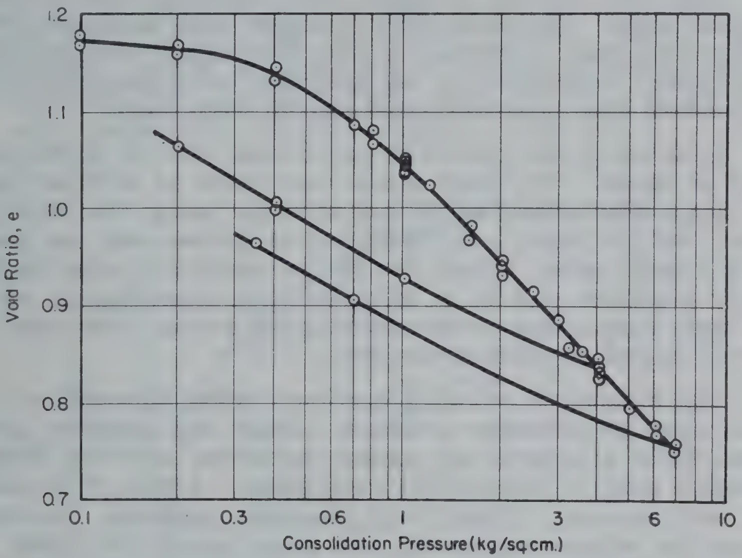

Fig. 1 — Triaxial consolidation results for grundite.

Fig. 1 — Resultados de la consolidación triaxial en la grundita.

After insertion of the pore pressure needle, the specimen was mounted on the testing frame and the hole in the membrane around the needle was sealed with a liquid rubber compound. The triaxial chamber was placed over the specimen, glycerine introduced to fill the chamber, and the desired chamber pressure applied. The solid lucite cap and base of the specimen permitted no drainage. In general, a chamber pressure of 2 kilograms per square centimeter higher than the consolidation pressure for the specimen was used, to induce a back pressure in the pore water and ensure that there were no air bubbles in the soil or measuring system. When pore pressure equilibrium had been reached, the test was begun.

The loading set-up consisted of a variable speed motor connected to a series of interchangeable gears, so that the testing speed could be varied to provide strain rates from 100 per cent per hour to less than 0.1 per cent per hour. The range of strain rates used in this series of tests was from 100 per cent per hour to 0.4 per cent per hour. Thus, the time to failure varied from about ten minutes to thirty hours.

The load on the specimen was measured with a steel proving ring. The pore water pressure was measured with a Bourdon gage connected to the Norwegian pore pressure apparatus. Deflections of the specimen were measured with a standard dial gage with divisions of 0.001 inch.

Four series of tests were performed, each at a different rate of strain. The first series was tested at 100 per cent per hour, the second at 16 per cent per hour, the third at 2 per cent per hour, and the fourth at 0.4 per cent per hour. Within each series, either five or six specimens were tested. Each specimen was at a different over-consolidation ratio, so that there were over-consolidation ratios from one to twenty tested at each strain rate.

The manner in which a specimen failed appeared to depend upon the chamber pressure. Under low chamber pressures, three kilograms per square centimeter and less, failure occurred along a well-defined shear plane. Little, or no bulging was apparent. Under high chamber pressures, five kilograms per square centimeter and more, specimens failed by bulging. There was no shear plane evident, although the load on the specimen decreased after reaching a maximum. Between three and five kilograms per square centimeter chamber pressure, the failure appeared to be a combination of both types, although the shear plane was not always very distinct. Sometimes, in this intermediate chamber pressure zone, there were many parallel shear planes apparent. When a shear plane occurred, it was generally parallel to the pore pressure needle and tangent to it. This was very likely due to the fact that the pore pressure needle created stress concentration in the specimen. All of the shear planes were inclined at an angle of approximately 52 degrees to the horizontal. The test results did not appear to be influenced by the mode of failure.

RESULTS

A summary of the data obtained from the tests described above is given in Appendix I. Typical stress-strain and pore pressure-strain curves are shown in Figure A-1. The results of these tests are plotted in Figures 2 to 5. These figures show the ratio of the principal stress difference at failure to the consolidation pressure immediately prior to testing, $(\sigma_1 - \sigma_3)/\sigma_c$, and the pore pressure parameter at failure, A_f, as a function of the over-consolidation ratio, σ_p/σ_c. The choice of these dimensionless parameters as the variables to study is justified by the semi-theoretical analysis presented by Perloff and Osterberg (1962). Each figure represents a series of tests run at the same rate of strain. In the following discussion, the quantities $(\sigma_1 - \sigma_3)/\sigma_c$ and A_f will always refer to the conditions at failure.

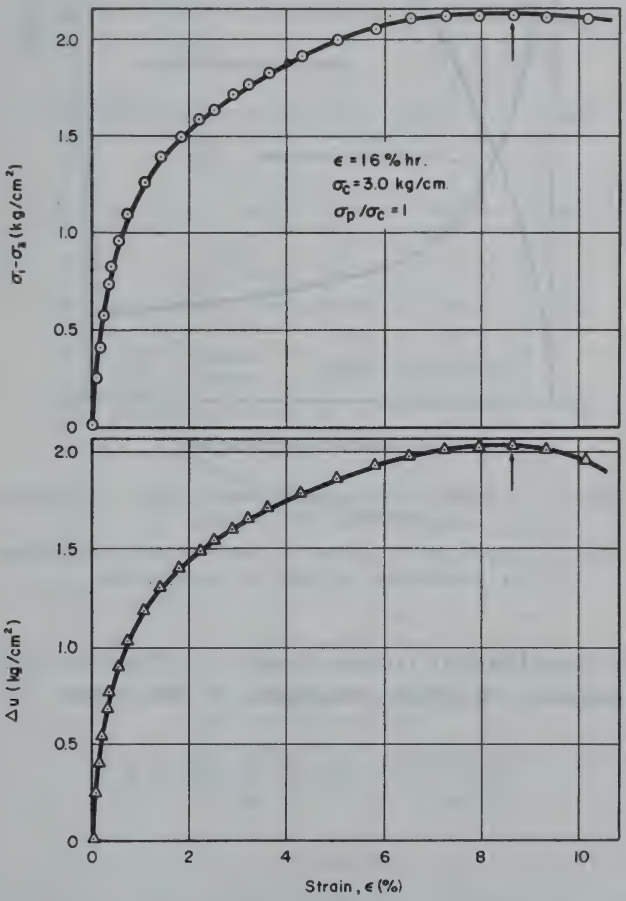

Fig. A.1 — Typical curves of $\sigma_1 - \sigma_3$ and Δu plotted vs. strain.

Fig. A.1 — Curvas típicas de $\sigma_1 - \sigma_3$ y Δu vs. deformación.

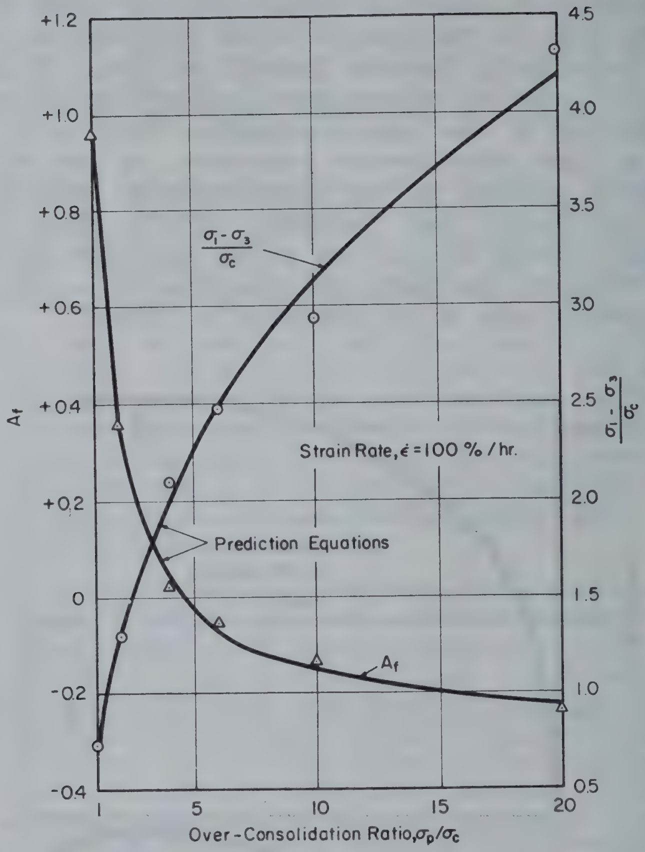

Fig. 2 — Effect of over-consolidation ratio on failure conditions for grundite.

Fig. 2 — Efecto de la relación de sobre-consolidación sobre las condiciones de falla en la grundita.

The experimental curves shown in Figures 2 to 5 have the appearance of power functions of the form:

$$\frac{\sigma_1 - \sigma_3}{\sigma_c} = r \left(\frac{\sigma_p}{\sigma_c} \right)^s + t \tag{1a}$$

and

$$A_f = m \left(\frac{\sigma_p}{\sigma_c} \right)^{-n} + p \tag{1b}$$

where r, s, t, and m, n, p are constants for a constant strain rate. Perloff and Osterberg (1962) have shown that equations 1a and 1b do, in fact, describe the observed data in Figure 2 as well as similar results published by other investigators.

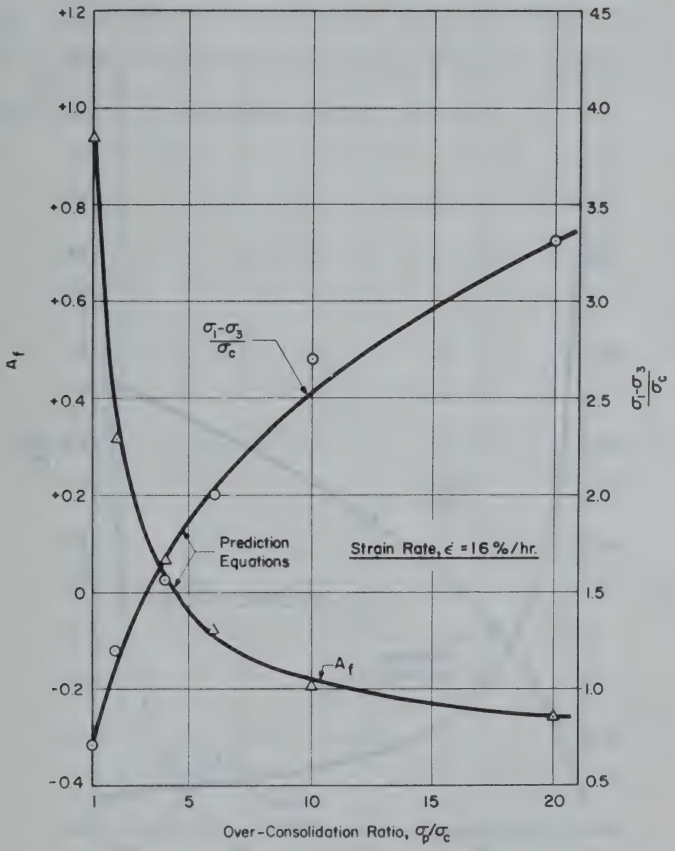

Fig. 3 — Effect of over-consolidation ratio on failure conditions for grundite.

Fig. 3 — Efecto de la relación de sobre-consolidación sobre las condiciones de falla en la grundita.

The method of fitting equations 1a and 1b to the experimental results is given in detail in Perloff and Osterberg (1962) and will be discussed only briefly here. If experimental curves are of the form of equations 2a and 2b then:

$$\log\left(\frac{\sigma_1 - \sigma_3}{\sigma_c} - t\right) = \log r + s \log\left(\frac{\sigma_p}{\sigma_c}\right) \qquad (2a)$$

and

$$\log (A_f - p) = \log m - n \log \left(\frac{\sigma_p}{\sigma_c}\right) \qquad (2b)$$

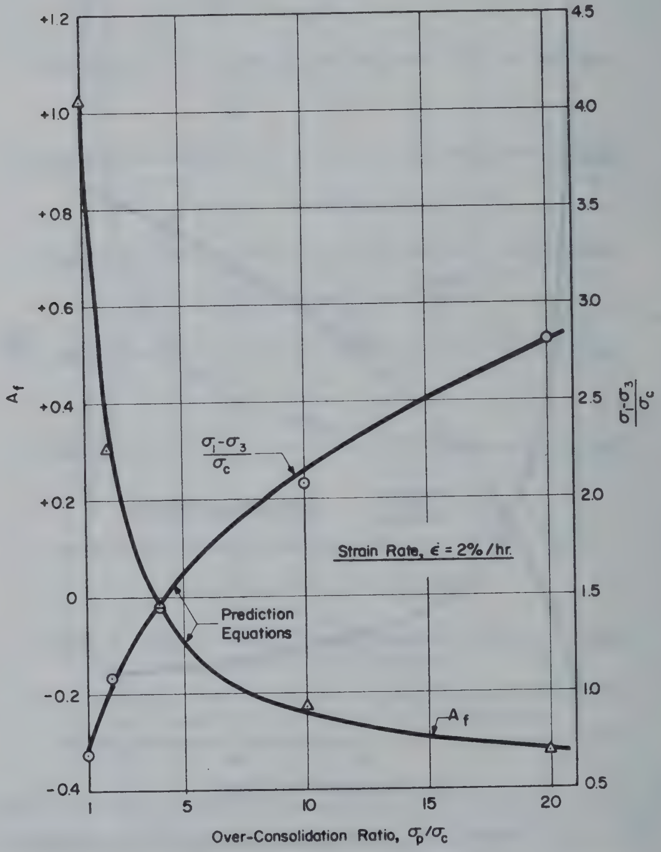

Fig. 4 — Effect of over-consolidation ratio on failure conditions for grundite.

Fig. 4 — Efecto de la relación de sobre-consolidación sobre las condiciones de falla en la grundita.

Note that equations 2a and 2b are equations of straight lines. Thus, if the experimental data can be described by equations 1a and 1b, they must appear as straight lines when plotted in the form of equations 2a and 2b, i.e., on log-log paper. Equations 2a and 2b are, therefore, test plots of the validity of representing the experimental results by equations 1a and 1b. Evaluation of the constants t and p can be done mathematically, as suggested by Johnson (1952, p. 117) or, more simply, by trial and error, as described by Perloff and Osterberg (1962). The constants r, m, and s, n can be found by substitution into equations 2a and 2b. When $\sigma_p/\sigma_c = 1$, $\log(\sigma_p/\sigma_c) = 0$ and $r = (\sigma_1 - \sigma_3)/\sigma_c - t$, $m = A_f - p$. The constants s and n are the slopes of the straight lines on the logarithmic plots.

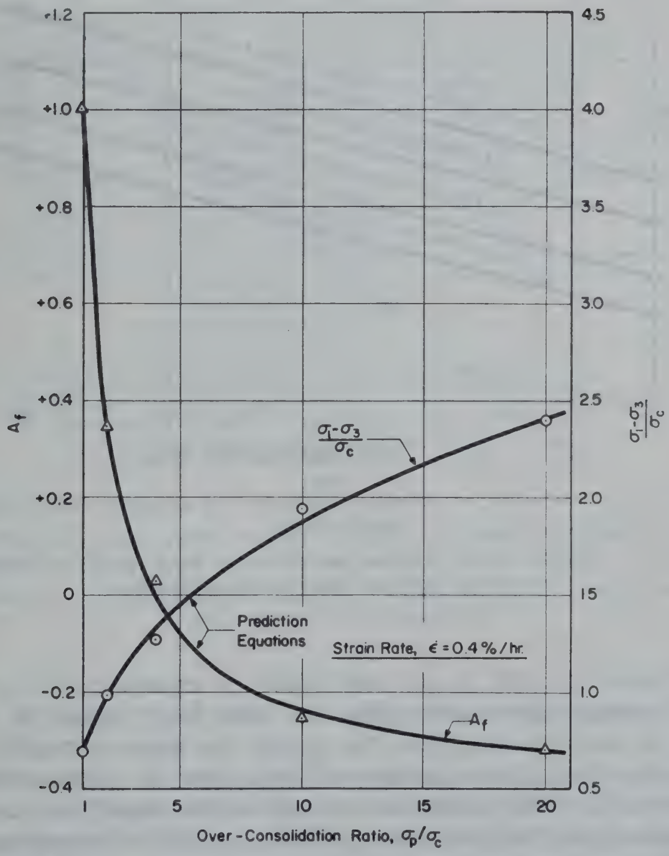

Fig. 5 — Effect of over-consolidation ratio on failure conditions for grundite.

Fig. 5 — Efecto de la relación de sobre-consolidación sobre las condiciones de falla en la grundita.

Figure 6 shows the test plots for the four series of experiments, each at a different rate of strain. It can be seen that straight lines are obtained on the test plots, indicating that the experimental data can be represented by equation 1a. The best straight lines were calculated by the method of least squares. Numerical values of r, s, t are shown on the curves to which they correspond.

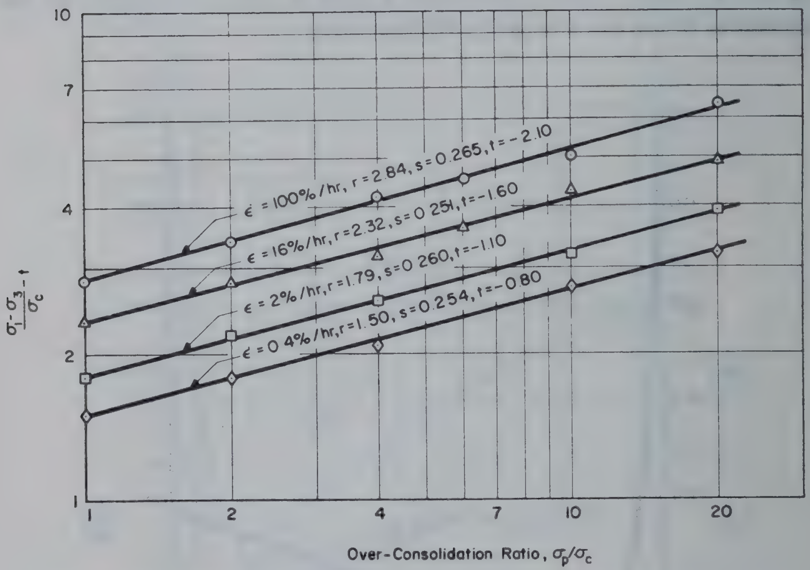

Fig. 6 — Test plots of strength equation for grundite clay at four strain rates.

Fig. 6 — Trazado de la ecuación de esfuerzos para arcilla (grundita) a cuatro distintas ratas de deformación.

Figures 7 and 8 are test plots of equation 1b for the pore pressure parameter data for the four series of tests. Again it can be seen that the points lie along straight lines indicating that the experimental data can be represented by equation 1b. The numerical values of the constants m, n, p are shown on the test plots. The close fit of equations 1a and 1b to the experimental data can be seen in Figures 2 to 5. The "experimental" curves for $(\sigma_1 - \sigma_3)/\sigma_c$ and A_f vs. σ_p/σ_c are, in fact, plots of equations 1a and 1b with the appropriate constants found in Figures 6 to 8.

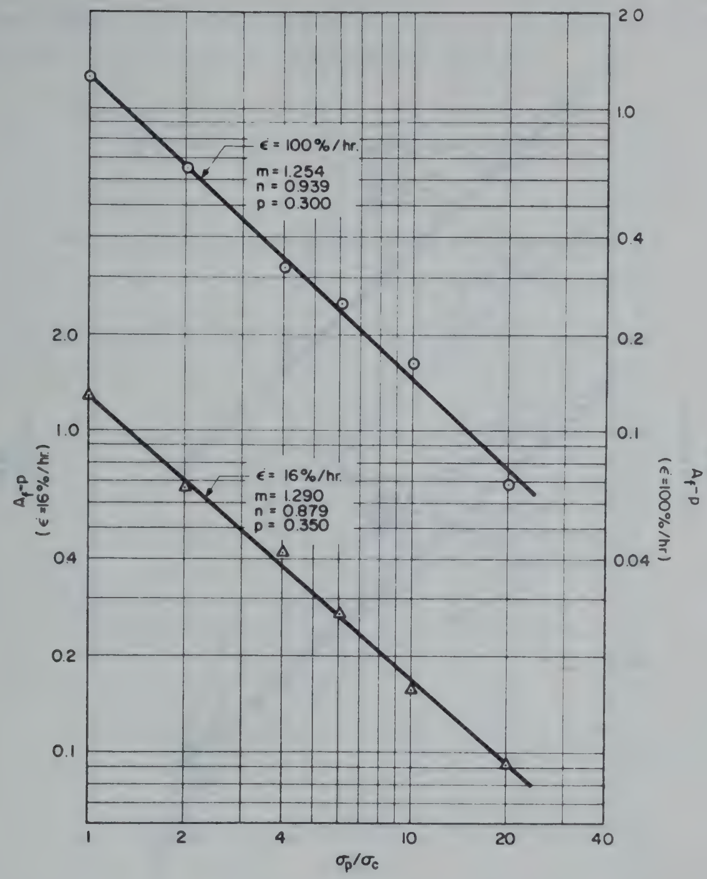

Fig. 7 — Test plots of pore pressure parameter equation for grundite.

Fig. 7 — Trazado de la ecuación paramétrica de la presión de los poros para la grundita.

EFFECT OF STRAIN RATE ON RESULTS

The effect of strain rate on the strength parameter can be seen in Figure 9, which is a plot of equation 1a for the four strain rates tested, with the experimental points omitted. It can be seen that the value of $(\sigma_1 - \sigma_3)/\sigma_c$ decreases as the strain rate decreases, and that this effect becomes more pronounced as the over-consolidation ratio increases. In fact, the strain rate appears to have very little effect on the

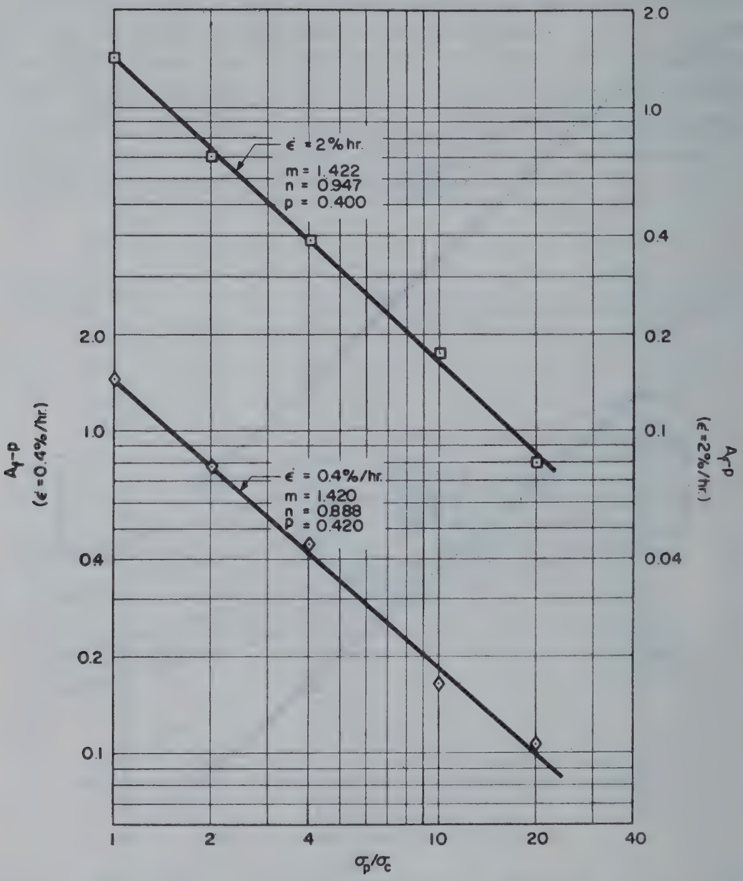

Fig. 8 — Test plots of pore pressure parameter equation for grundite.

Fig. 8 — Trazado de la ecuación paramétrica de la presión de los poros para la grundita.

strength parameter for this soil when it is normally consolidated ($\sigma_p/\sigma_c = 1$). In order to express this relationship in explicit terms, the stress history constants r, s, t, which are determined in Figure 6, are plotted as functions of the relative strain rate in Figure 10. The relative strain rate is defined as $\dot{\varepsilon}/\dot{\varepsilon}_0$ where $\dot{\varepsilon}$ is the strain rate and $\dot{\varepsilon}_0$ is an arbitrary base value of strain rate (in this case, $\dot{\varepsilon}_0$ was chosen as *one per cent per hour,* for convenience). The relative strain rate is used rather than the absolute strain rate in order to keep the relationship in dimensionless form. Reiner (1960, p. 246) discusses the advantages of keeping such power functions in dimensionless form.

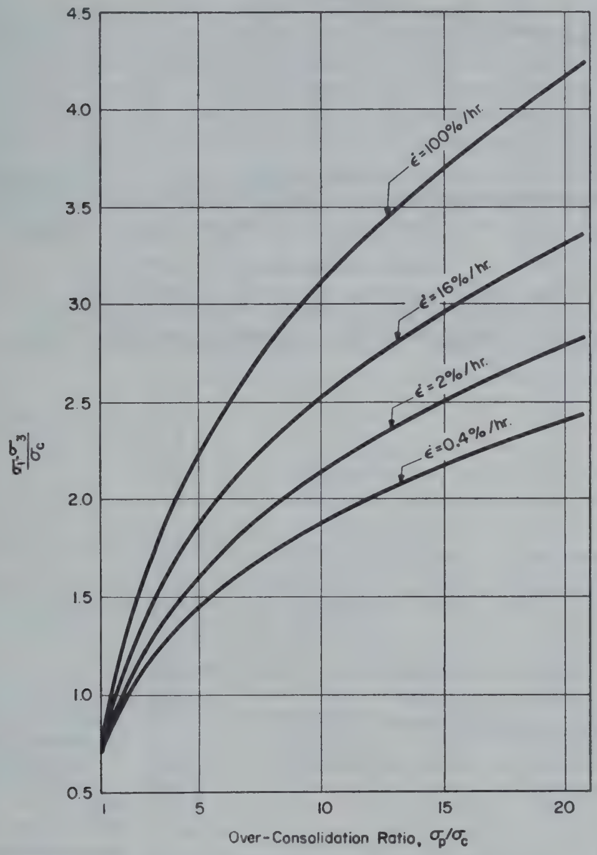

Fig. 9 — Plot of equation 1a for four strain rates.

Fig. 9 — Trazado de la ecuación 1a para cuatro diferentes ratas de deformación.

Referring to Figure 10, it can be seen that the plots of r, s, and t versus the relative strain rate, on logarithmic scales, form straight lines. Therefore, a power law equation can be written for each. These equations are shown in the figure. Note that r and t are affected by the rate of strain, while s appears to be independent of strain rate.

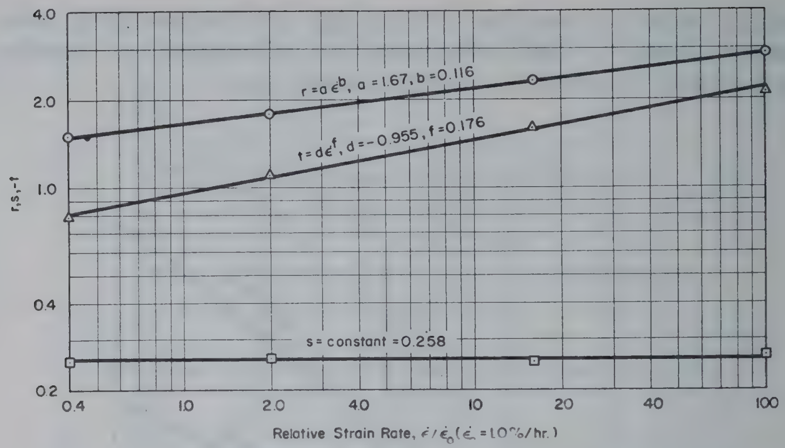

Fig. 10 — Effect of strain rate on r, s, and t.

Fig. 10 — Efecto de la rata de deformación sobre r, s, y t.

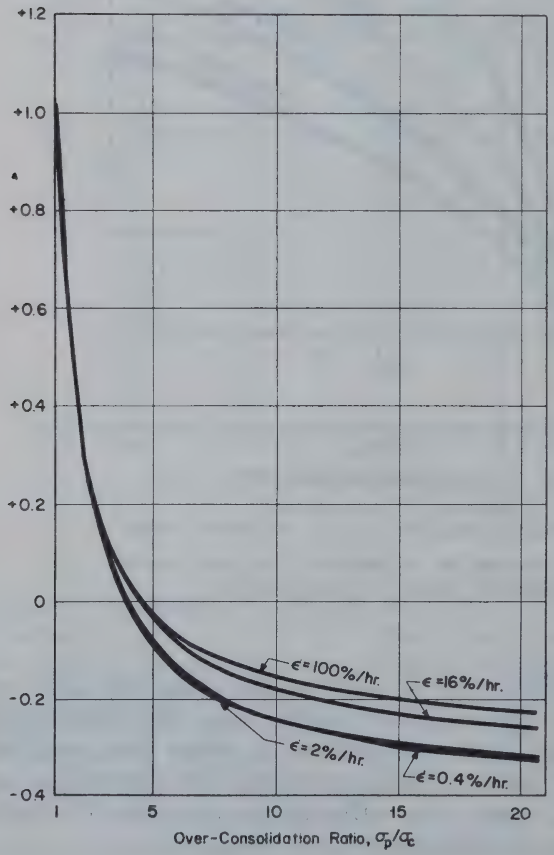

Fig. 11 — Plot of equation 1b for four strain rates.

Fig. 11 — Trazado de la ecuación 1b para cuatro diferentes ratas de deformación.

Figure 11 is a plot of equation 1b for the four strain rates tested. This figure indicates that the effect of strain rate on A_f is not nearly so great as on $(\sigma_1 - \sigma_3)/\sigma_c$. Though it is difficult to see in the figure, for $\sigma_p/\sigma_c = 1$, A_f decreases as the strain rate increases; whereas, for $\sigma_p/\sigma_c = 20$, A_f increases as the strain rate increases. In the intermediate range, the curves cross and it is not apparent from this figure what effect the strain rate has. Figure 12 illustrates this effect more clearly. It is a plot, on logarithmic scales, of the values of m, -n, p versus the relative strain rate. Again the plotted points indicate straight line relationships on the logarithmic plot. This suggests the power law relationships between m, n, p and the relative strain rate which are shown on the figure. Note that the value of m decreases as the strain rate increases, though only sligthly. The value of p is negative, and moves closer to zero as the strain rate increases. The value of n, the exponent in equation 1b, appears to be a constant for the strain rates investigated.

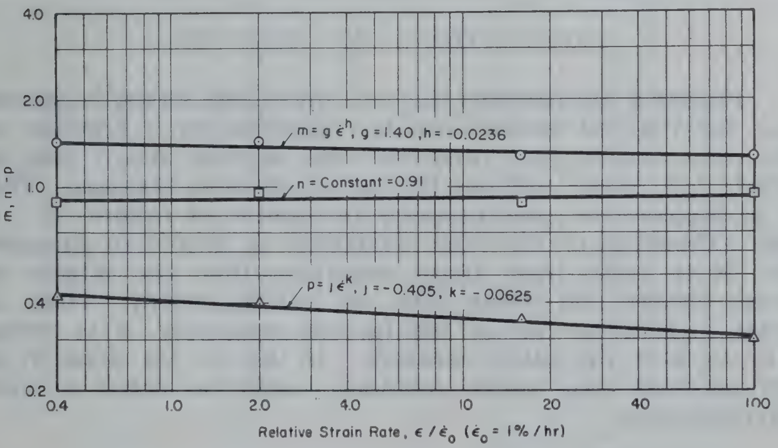

Fig. 12 — Effect of strain rate on m, n, and p.

Fig. 12 — Efecto de la rata de deformación sobre m, n, y p.

The fact that r, s, t, and m, n, p can be expressed explicitly in terms of the relative strain rate, $\dot{\varepsilon}/\dot{\varepsilon}_0$, makes it possible to rewrite equations 1a and 1b to include the effect of strain rate as well as stress history:

$$\frac{\sigma_1 - \sigma_3}{\sigma_c} = a\left(\frac{\dot{\varepsilon}}{\dot{\varepsilon}_0}\right)^b \left(\frac{\sigma_p}{\sigma_c}\right)^s + d\left(\frac{\dot{\varepsilon}}{\dot{\varepsilon}_0}\right)^f \qquad (3a)$$

and

$$A_f = g\left(\frac{\dot{\varepsilon}}{\dot{\varepsilon}_0}\right)^h\left(\frac{\sigma_p}{\sigma_c}\right)^{-n} + j\left(\frac{\dot{\varepsilon}}{\dot{\varepsilon}_0}\right)^k \tag{3b}$$

where $\dot{\varepsilon}_0$ is the base value of strain rate equal to one per cent per hour, a, b, s, f, and g, h, n, k are dimensionless constants of the equation. The numerical values of these constants for Grundite Clay and the range of strain rates tested are given in Table 2.

TABLE 2 — Numerical Values of Constants in Equations 3a and 3b

a	b	s	d	f	g	h	n	j	k
1.67	0.116	0.258	—0.955	0.176	1.40	—0.0236	0.91	—0.405	—0.0625

IMPLICATIONS OF RESULTS

Equation 3a indicates that the undrained strength parameter for the soil studied can be expressed as a function of the over-consolidation ratio and the relative strain rate at which it is tested, without the use of effective stresses. This is so because the pore pressure parameter at failure, A_f, is also a function of the same variables, as shown in equation 3b. It is clear from these equations that the effects of stress history and strain rate are interdependent. Thus, in order to consider one of the factors separately, it is necessary to hold the other constant. If this is not done, it is obvious that any results obtained would be liable to misinterpretation.

RESULTS FROM OTHER INVESTIGATIONS

Using published data from other investigators, it has been shown (Perloff and Osterberg, 1962) that equations 1a and 1b correctly describe the behavior of several other soils when tested at a constant strain rate.

Previous investigations into the relationship between stress and strain rate have been discussed in detail by Perloff (1962). Of particular interest is the suggestion made by Terzaghi (1925, 1931) and Hvorslev (1938) that there was a "yield stress" for a clay soil, below which the strain rate

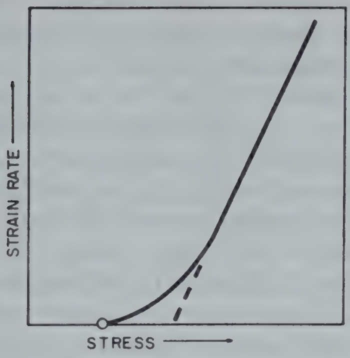

Fig. 13 — Suggested flow law for clay.

Fig. 13 — Ley de flujo sugerida para la arcilla (Terzaghi, 1931).

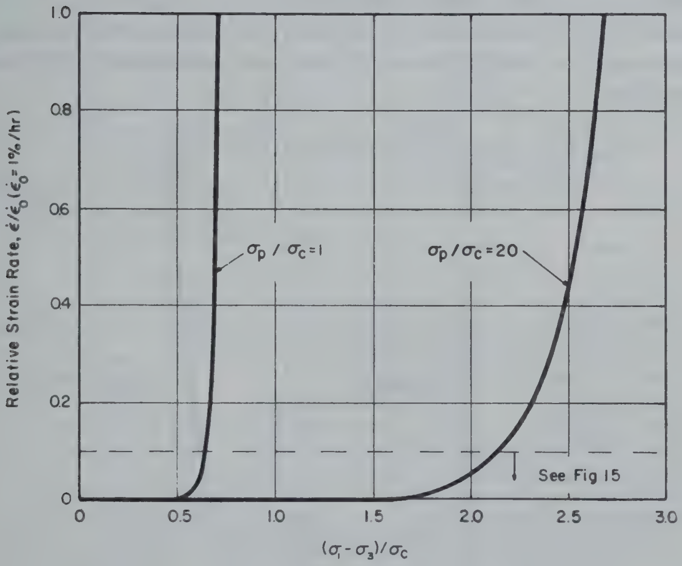

Fig. 14 — Plot of equation 1a for two values of σ_p/σ_c.

Fig. 14 — Trazado de la ecuación 1a para dos diferentes valores de σ_p/σ_c.

would be zero. Figure 13 shows the flow law suggested by Terzaghi (1931). The existence of such a "yield stress" suggests that there must be some strain rate below which the ultimate shearing resistance of the soil will not decrease and, that at zero strain rate, the soil will have a finite strength. At first glance, equation 3a appears to be a contradiction of this statement, since for $\dot{\varepsilon} = 0$, the shearing resistance is also zero. Figure 14 is a plot of equation 3a for two values of σ_p/σ_c, extrapolating from a relative strain rate of 1.0 back to zero. It can be seen that, although the equation does go through zero, it is an excellent approximation for a material with a yield stress. In order to determine if this effect was due to the wide range of strain rates considered, the portion of Figure 14 below the dotted line was plotted in Figure 15 with the $\dot{\varepsilon}/\dot{\varepsilon}_0$ axis expanded ten times. It can be seen that even at these very low strain rates, equation 3a still approximates a material with a yield stress. However, the prediction equations discussed were derived from data covering a range of strain rates from 0.4 to 100 per cent per hour. There is no reason to assume that the equation will be valid at very low strain rates. Furthermore, a base yield stress could be added to the equation if it were necessary. Thus, while equation 3a does not imply the existence of a yield stress, it can be reconciled with such a suggestion.

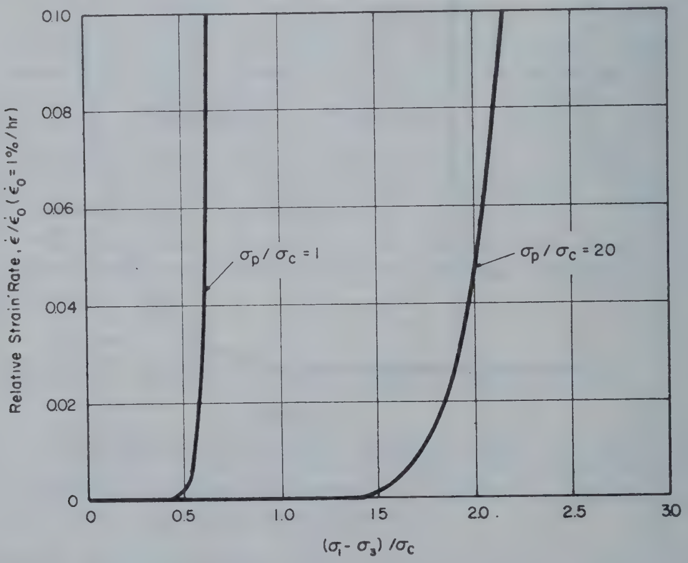

Fig. 15 — Plot of lower portion of figure 14 with $\dot{\varepsilon}/\dot{\varepsilon}_0$ axis expanded 10 times.

Fig. 15 — Trazado de la porción inferior de la figura 14 con el eje $\dot{\varepsilon}/\dot{\varepsilon}_0$ expandido diez veces.

Bjerrum et al. (1958) and Crawford (1959) performed consolidated-undrained triaxial compression tests with measured pore pressures, at varied strain rates, on two clays. Figure 16 shows the effect of strain rate on $(\sigma_1 - \sigma_3)/\sigma_c$, as calculated from their data. The upper half of this figure shows the results from Crawford (1959) for a very brittle Laurentian clay. The pre-consolidation pressure for the clay Crawford (1959) tested was in the neighborhood of 2.5 to 3.0 kilograms per square centimeter; however, he did not give the exact value. It is estimated that the upper curve, in the portion of Figure 16 relating to his data, represents an over-consolidation ratio of approximately 1.5. The lower curve for Crawford's data represents normally consolidated clay. The lower half of Figure 16 shows the results from Bjerrum et al. (1958) for a normally consolidated Norwegian clay. It can be seen that for both soils, $(\sigma_1 - \sigma_3)/\sigma_c$ increases as the strain rate increases, and that the relationship between $(\sigma_1 - \sigma_3)/\sigma_c$ and $\dot{\varepsilon}/\dot{\varepsilon}_0$ can be approximated by straight lines on the logarithmic plot. Both soils were tested in their natural states and the wide scatter in Bjerrum's data is very likely due to the wide variation in initial void ratio. Note that for Crawford's data the effect of strain rate on $(\sigma_1 - \sigma_3)/\sigma_c$ appears to be more pronounced for the over-consolidated specimens than for the normally consolidated specimens.

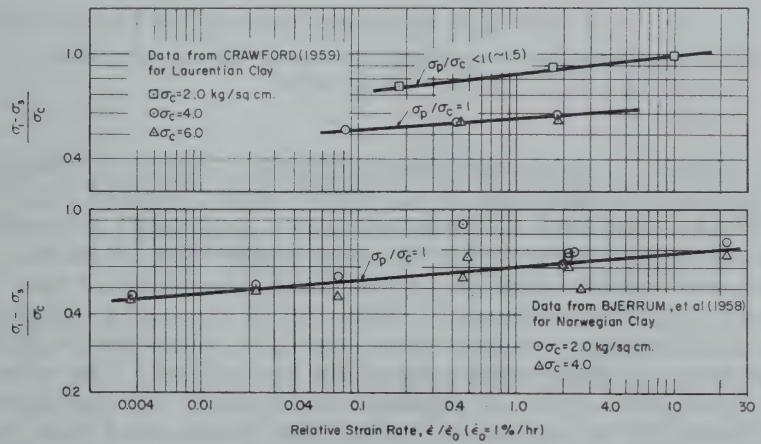

Fig. 16 — Effect of strain rate on strength (data from Bjerrum, et al., 1958, and Crawford, 1959).

Fig. 16 — Efecto de la rata de deformación sobre los esfuerzos (Bjerrum, et al., 1958, y Crawford, 1959).

Figure 17 is a logarithmic plot of equation 3a, for Grundite, at constant values of σ_p/σ_c, with the writers' experimental results superimposed on the curves. It can be seen that for $\sigma_p/\sigma_c = 20$, a plot of equation 3a is a straight line. As σ_p/σ_c decreases, the curvature of the line increases slightly. The effect of strain rate on strength, for constant overconsolidation ratios, as predicted by equation 3a and shown in Figure 17, is the same as that for the data from Bjerrum et al. (1958) and Crawford (1959) shown in Figure 16. The strength parameter, $(\sigma_1 - \sigma_3)/\sigma_c$, increases as the strain rate increases, and this effect becomes more pronounced as σ_p/σ_c increases, as it did with the data from Crawford (1959) in Figure 16.

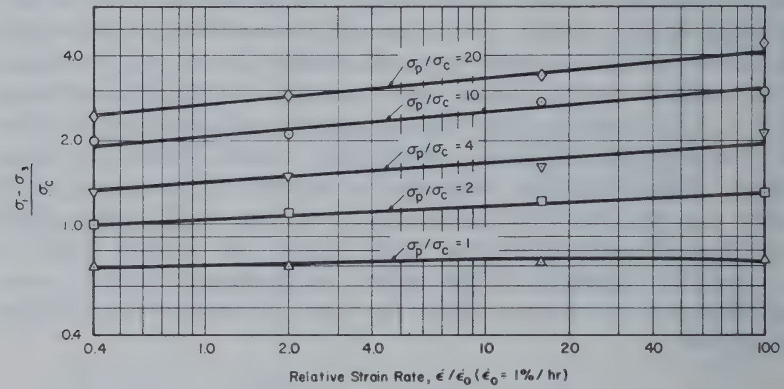

Fig. 17 — Plot of equation 1a for constant values of σ_p/σ_c for grundite.

Fig. 17 — Trazado de la ecuación 1a para valores constantes de σ_p/σ_c en la grundita.

Figure 18 shows the effect of strain rate on A_f for the soils tested by Bjerrum et al. (1958) and Crawford (1959). It can be seen that A_f decreases as the strain rate increases, approximately linearly on the logarithmic plot. Crawford's data also indicate that as $\dot{\varepsilon}/\dot{\varepsilon}_0$ increases, the slope of the A_f versus $\dot{\varepsilon}/\dot{\varepsilon}_0$ line decreases. Figure 19 is a plot of equation 3b, for Grundite, at two values of σ_p/σ_c with the writers' experimental data superimposed on the curves. The effect of strain rate on A_f, as predicted by equation 3b, and shown in Figure 19, is similar to, though less pronounced than the results from Bjerrum et al. (1958) and Crawford (1959). The fact that strain rate has less of an effect on A_f for Grundite than for the Norwegian and Laurentian clays may be due to differences in structure. The Norwegian and

Laurentian clays are both marine soils, tested in their natural states, and might be expected to exhibit a more flocculent structure than the remolded Grundite (cf. Lambe, 1958).

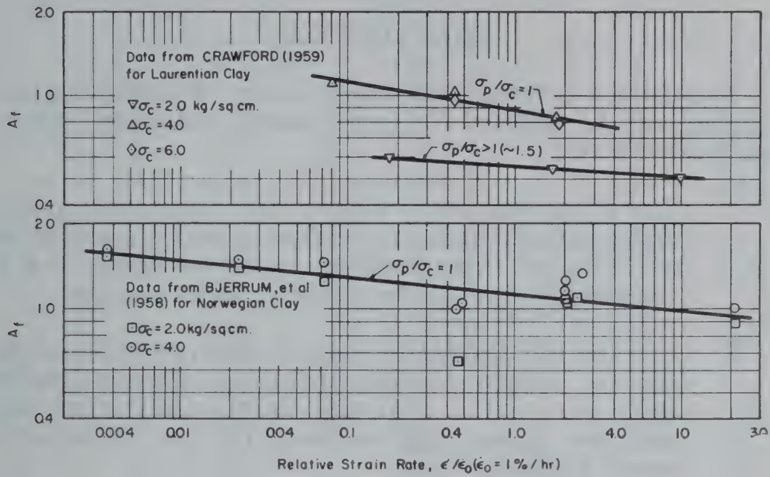

Fig. 18 — Effect of strain rate on A_f (data from Bjerrum, et al., 1958, and Crawford, 1959).

Fig. 18 — Effecto de la rata de deformación sobre A_f (Bjerrum, et al., 1958, y Crawford, 1959).

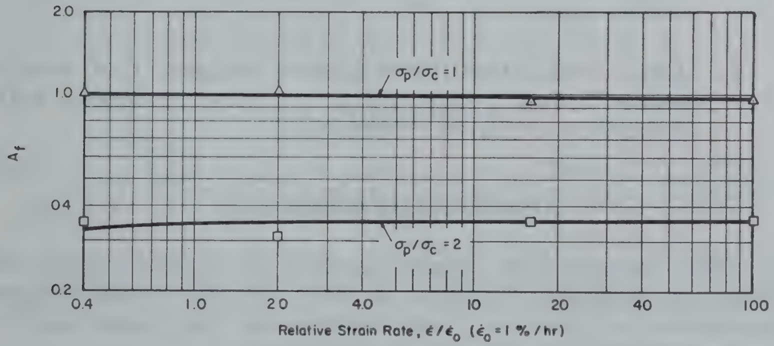

Fig. 19 — Plot of equation 3b for two values of σ_p/σ_c for grundite.

Fig. 19 — Trazado de la ecuación 3b para dos valores de σ_p/σ_c en la grundita.

Note that the results from Bjerrum et al. (1958) and Crawford (1959) exhibit a more logical pattern when the strength is expressed as $(\sigma_1 - \sigma_3)/\sigma_c$ and the interrelationship between stress history and strain rate is considered.

Thus, it can be seen that the writers' results, and the prediction equations derived from them, are consistent with the results of previous investigations.

CONCLUSIONS

Based on the results discussed above, the following conclusions can be drawn for consolidated-undrained triaxial compression tests:

1. The effects of stress history and strain rate on the undrained strength of a cohesive soil are interrelated. One of these factors cannot be considered independently unless the other is held constant.

2. For the soil tested, an explicit empirical relationship can be written relating the shear strength parameter, $(\sigma_1 - \sigma_3)/\sigma_c$, to the over-consolidation ratio and the strain rate, without the use of effective stress analysis.

3. The use of effective stress analysis is not required because the Skempton pore pressure parameter at failure, and therefore, the effective stresses, are also functions of the over-consolidation ratio and the strain rate.

4. Data from other investigators suggest that conclusions 2 and 3 are valid for other cohesive soils, natural as well as remolded.

ACKNOWLEDGEMENTS

This research was made possible by a grant from the Advanced Research Projects Agency of the United States Department of Defense, administered by the Material Research Center of Northwestern University.

The writers wish to thank Dr. Laurits Bjerrum of the Norwegian Geotechnical Institute and Mr. Carl B. Crawford of the National Research Council of Canada for the loan of their original data reported in Bjerrum et al. (1958) and Crawford (1959).

Note: This work was performed by the senior author, under the direction of the junior author, as part of a Ph. D. dissertation submitted to Northwestern University.

TABLE A.1 — Summary of Test Results for Grundite Clay

Specimen Number	$\dot{\varepsilon}$ (%/hr)	$\sigma_c = \sigma_3$ (kg/cm²)	σ_p/σ_c	$(\sigma_1, \quad \sigma_3)^f$ (kg/cm²)	u_f (kg/cm²)	ε_f (%)	e_f
3- 1	100	1.60	1	1.185	+1.13	11.0	1.023
3-13	100	0.50	2	0.650	+0.23	10.8	1.085
3-20	100	1.00	4	2.09	+0.045	10.9	0.927
3- 9	100	1.00	6	2.47	—0.13	9.7	0.897
3-26	100	0.40	10	1.17	—0.16	8.9	1.007
3- 6	100	0.35	20	1.51	—0.35	10.1	0.962
3-22	100	0	∞	0.427	—0.14	9.8	1.173
3-21	16	3.00	1	2.16	+2.03	8.6	0.885
3- 4	16	1.00	2	1.20	+0.38	10.3	0.981
3-11	16	0.25	4	0.393	+0.025	10.5	1.123
3-24	16	0.60	6	1.205	—0.095	9.0	0.977
3- 8	16	0.25	10	0.678	—0.13	8.8	1.087
3-19	16	0.10	20	0.332	—0.085	9.2	1.152
3-14	2	2.00	1	1.38	+1.41	10.0	0.930
3- 2	2	0.60	2	0.648	+0.20	11.2	0.972
3-17	2	0.25	4	0.365	—0.005	9.4	1.140
3-27	2	0.40	10	0.832	—0.19	8.6	0.998
3-23	2	0.30	20	0.845	—0.27	9.4	0.991
3-15	0.4	1.00	1	0.700	+0.70	10.8	1.050
3- 7	0.4	2.50	2	2.48	+0.86	9.7	0.848
3-25	0.4	0.80	4	1.02	+0.030	9.4	0.959
3- 5	0.4	0.70	10	1.365	—0.35	10.1	0.904
3-16	0.4	0.20	20	0.48	—0.15	9.8	1.124

REFERENCES

Andresen, A., Bjerrum, L., Di Biagio, E., and Kjaernsli, B. (1957) — "Triaxial Equipment Developed at the Norwegian Geotechnical Institute" — Norwegian Geotechnical Publication, No. 21, Oslo.

Bjerrum, L., Simons, N., and Torblaa, I. (1958) — "The Effect of Time on the Shear Strength of a Soft Marine Clay" — *Proceedings* of the Conference on Earth Pressure Problems, Brussels, Belgium, Vol. I, pp. 148-58, 1958.

Casagrande, A., and Wilson, S. D. (1951) — "Effect of Rate of Loading on Strength of Clays and Shales at Constant Water Content" — *Geotechnique,* Vol. II, No. 3, June 1951.

Crawford, C. B. (1959) — "The Influence of Rate of Strain on Effective Stresses in Sensitive Clay" — Symposium on Time Rates of Loading in Soil Testing, American Society for Testing Materials, STP-254, p. 36.

Grim, R. E., and Bradley, R. F. (1939) — "A Unique Clay from the Goose Lake, Illinois Area" — *Journal* of the American Ceramic Society, Vol. 22, No. 5, May, 1939.

Hvorslev, M. J. (1938) — "The Shearing Resistance of Remolded Cohesive Soils" — *Proceedings* of the United States Engineering Department's Soils and Foundations Conference, Boston, 1938.

Johnson, L. H. (1952) — Nomography and Empirical Equations, John Wiley, New York, 1952.

Lambe, T. W. (1958) — "The Structure of Compacted Clay" — *Journal* of the Soil Mechanics and Foundations Division, *Proceeding* of the American Society of Civil Engineers, Vol. 84, No. SM 2, May, 1958.

Macey, H. H. (1941) — "Rheology of Clay" — *Journal of Scientific Instruments,* Vol. 18, No. 8, August, 1941.

Matlock, H., Jr., Fenske, C. W., and Dawson, R. F. (1951) — "De-aired, Extruded Soil Specimens for Research and for Evaluation of Test Procedures" — American Society for Testing Materials Bulletin, No. 177, October, 1951.

Osterberg, J. O., and Perloff, W. H., Jr. (1960) — "Stress-Strain Characteristics of Compacted Clay Under Varied Rates of Strain" — *Proceedings* of the Highway Research Board, Vol. 39, p. 605.

Perloff, W. H., Jr. — "The Effect of Stress History and Strain Rate on the Undrained Shear Strength of Cohesive Soils" — Unpublished Report, June, 1962.

Perloff, W. H., Jr., and Osterberg, J. O. — "Effect of Stress History on Strength of Cohesive Soils" — October, 1962. Submitted for publication.

Reiner, M. (1960) — *Deformation, Strain and Flow,* Second Edition, Interscience Publishers, New York, 1960.

Rutledge, P. C. (1947) — "Cooperative Triaxial Shear Research Program of the Corps of Engineers" — Soil Mechanics Fact Finding Survey, Progress Report, Waterways Experiment Station, Vicksburg, Mississippi, April, 1947.

Seed, H. B., and Chan, C. K. (1957) — "Thixotropic Characteristics of Compacted Clays" — Journal of the Soil Mechanics and Foundations Division, Proceedings of the American Society of Civil Engineers, Vol. 83, No. SM4, November, 1957.

Seed, H. B., Mitchell, J. K., and Chan, C. K. (1960) — "The Strength of Compacted Cohesive Soils" — *Proceedings* of the Second International Conference on Soil Mechanics and Foundation Engineering, Vol. VII, pp. 54-6.

Terzaghi, C. (1925) — "Principles of Soil Mechanics: II — Compressive Strength of Clays" — Engineering News-Record, Vol. 95, No. 20, p. 796, 1925.

Terzaghi, K. (1931) — "The Static Rigidity of Plastic Clays" — *Journal* of Rheology, Vol. 2, No. 2, July, 1931.

Vicat (1833) — "Recherches Experimentales sur les Phenomenes Physiques qui Precedent et Accompagnent la Rupture ou l'Affaissement d'une Certaine Classe de Solides" — *Annales des Ponts et Chaussées,* pp. 201-68, 1833.

EFFECT OF VIBRATION ON DENSITY OF SAND

E. T. SELIG
Associate Research Engineer, Illinois Institute of Technology, Chicago, Illinois

ABSTRACT

A study was conducted to investigate the effect of vibration conditions and surcharge pressure on density of sand resulting from vibration. A container of sand was subjected to a wide range of frequencies and accelerations. Sand was added both before and during vibration and, in addition, surcharge pressure was varied. The effect of surcharge pressure is shown to be governed by the vibration intensity: from an initial loose state it may either assist in increasing density or restrict density increase. With all other factors constant, density increases with an increase in any one of the four parameters describing vibration (frequency, acceleration, velocity, or displacement); however there exists a value of the parameter above which density will decrease. Correlation of density with vibration requires the use of more than one of these parameters.

RESUMEN

Se investiga la influencia del vibrado y sobrecarga en la densidad de la arena. Un recipiente con arena fué sometido a vibraciones en un amplio rango de frecuencias y aceleraciones, añadiéndose arena antes y durante el vibrado y variándose, además, la presión. Se encontró que el efecto de la presión depende de la intensidad de la vibración: partiendo de arena suelta, puede sea ayudar a aumentar la densidad o restringir dicho aumento. Manteniendo los otros factores constantes, la densidad aumenta con cualquiera de los cuatro parámetros que definen la vibración (frecuencia, aceleración, velocidad o desplazamiento); sin embargo existe un valor del parámetro más allá del cual la densidad disminuye. Há correlación de la densidad con la vibración requiere el uso de más de uno de tales parámetros.

INTRODUCTION

Many studies have been made of the behavior of sand subjected to vibration. Most of these have concerned means of obtaining maximum density *, although there has also been interest in the strength reduction and in liquefaction during vibration (1) **. It has been adequately demonstrated that vibration has a significant effect on both the strength and density of cohesionless granular materials, and that maximum density is most easily achieved with some form of vibration. However, the relative importance of the various parameters describing vibration has not been clearly indicated and the influence of other conditions such as surcharge pressure and the associated intergranular pressure has not been fully recognized.

The results of studies which investigate some of these questions further are described in this paper. The specific purpose of the present investigation was to study the effect of the vibration conditions and surcharge pressure on the density of sand. Attention is confined to a single, uniformly graded, air-dry silica sand in which 95 per cent of the material lies between 20 and 40 mesh U.S. Standard Sieve (0.84 mm to 0.42 mm). Although the tests have been performed on one specific sand only, it is believed that the results apply qualitatively to other similar materials.

VIBRATION ARRANGEMENT

The arrangement selected for the vibration of the sand specimens is shown in Figure 1. The basic vibration unit was an electrodynamic vibration exciter which created a sinusoidal, unidirectional force of variable frequency and amplitude. A direct-current power supply operated the field coil mounted in the fixed housing of the device. Frequency of vibration was controlled by a sinusoidally varying current of desired frequency applied to the moving coil of the vibrator. The upper limit of frequency at which the exciter could be used in this particular application, while still maintaining sinusoidal motion and sufficient driving force, was around 250 cps. Once frequency was established, the other vibration parameters were adjusted by varying the amount of current supplied to the driver coil.

A signal generator coil attached to the moving core of the vibrator had an output voltage directly proportional to the velocity of travel of the core. This signal was fed into an oscilloscope where the shape of motion could be observed to insure that the vibration was sinusoidal at all times. The signal was also measured by an AC voltmeter giving a reading which was proportional to the maximum cycle velocity.

---

* Representative papers are given in the attached list of references.

** Numbers in parentheses refer to items in the list of references.

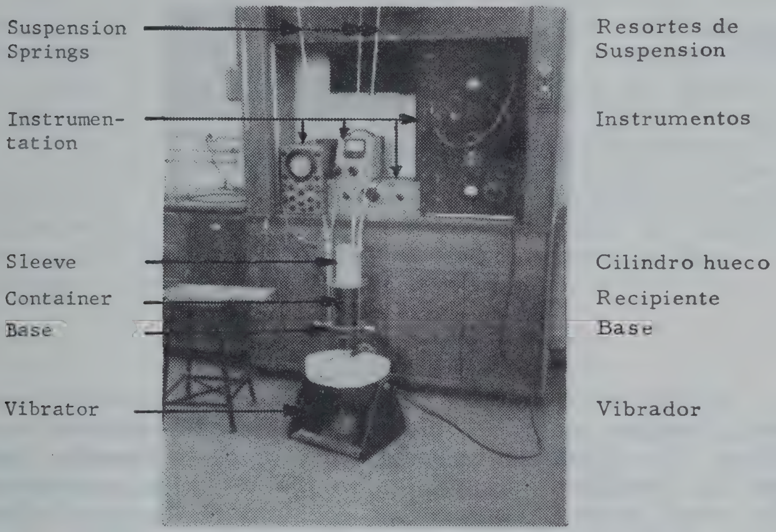

Fig. 1 — Vibration apparatus.

Fig. 1 — Aparato vibrador.

The container in which the sand was vibrated was suspended on springs to support the weight of container and sand and then rigidly coupled to the moving core of the vibrator. The assembly could vibrate in the vertical direction only. The container selected for the tests consisted of a cylindrical aluminum mold and base whose inside dimensions were 7.2 cm in diameter and 20.4 cm deep. During vibration this height was extended by attaching a sleeve to the open top of the container. Only one diameter was considered since reported results (^{2}) indicate that diameter does not significantly affect resulting density.

Since the motion of the mold during vibration was sinusoidal, the characteristics of vibration could be completely described by any two of the following four parameters: frequency, maximum velocity, maximum acceleration and peak-to-peak displacement. Frequency and maximum velocity were directly measured values for every test. The other parameters are related by the following expressions

$$d = \frac{V_m}{d\pi f}$$

and

$$A_m = 2\pi f V_m$$

where

d = peak-to-pek displacement, cm,

V_m = maximum velocity, cm/sec,

f = frequency, cps,

A_m = maximum acceleration, cm/sec^2.

TEST PROCEDURE

Several series of tests were performed to determine what sand densities could be obtained for various vibration conditions, the degree of reproducibility of these densities, and how the densities were related to the vibration parameters. The same basic procedure was followed for most of these tests. First the container and sleeve were assembled and then suspended from springs. Next the amount of sand to be vibrated was added by pouring the material slowly from a position level with the top of the sleeve (33 cm from the bottom of the mold). The rigid coupling between the base of the mold and the moving core of the vibrator was adjusted so that there would be no initial force on the core flexures due to the weight of the assembly. They were then locked in position. The combined weight of the mold assembly and the sand was thus supported entirely by the three overhead springs.

Before vibration was induced, the full rated current was applied to the field coil of the vibrator; then the desired frequency of vibration was set. The vibration was finally achieved by quickly increasing the current to the driver coil from zero until the maximum velocity was obtained corresponding to the desired conditions of vibration. For a particular test series these may have been specified in terms of any two of the four vibration parameters, but were always converted into f and V_m since these were the ones used to control the apparatus.

After the vibration had continued for the prescribed length of time, the driver coil current was quickly and smoothly reduced to zero. The container was then carefully disconnected from the vibrator and springs, the sleeve removed and the sand surface made level with the top of the container. The final density was determined from the known volume of the container and weight of sand remaining in it.

Most of the tests followed the above procedure. However, for one test series a 907-gm weight was positioned on top of the sand during vibration. In another series the sand was added during vibration rather that prior to vibration. It was in all cases poured from the same height in 227-gm increments at a rate of approximately 454 gm/min with 1 min vibration time generally elapsing between each of these increments. Since this addition of sand continually changed the amount of vibrating mass, it was necessary to readjust the current to the driver coil during the test in order to maintain constant vibration conditions.

VIBRATION EFFECTS

The effect of time of vibration on density achieved for fixed vibration conditions is illustrated in Figure 2. These results are for the case where f = 100 cps and V_m = 1.52 cm/sec approximately. Most of the change in density from the initial, loose took place immediately after vibration was begun. There was only a small further increase in density (less than 1%) achieved by vibrating the sand longer than two minutes. The same results could be expected for other vibrations conditions although the time in which most of the final density can be obtained may vary a little.

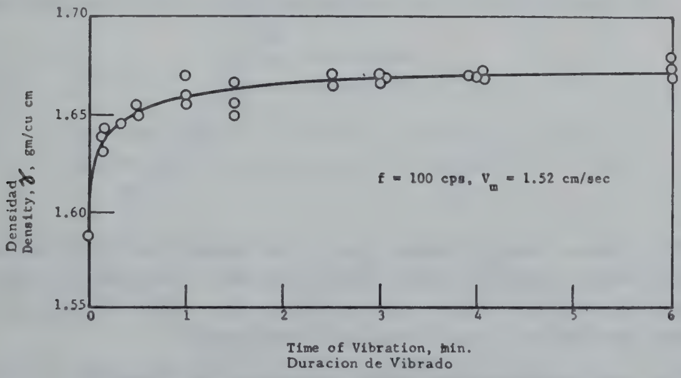

Fig. 2 — Variation of density with vibration time.

Fig. 2 — Variación de la densidad con la duración de vibrado.

The effect of variation in acceleration on the density achieved for fixed frequency, weight of sand and time of vibration is illustrated in Figure 3. Each data point shown represents an average of several trials. In general, these results indicate that as acceleration increases the density increases, but eventually reaches a maximum and then, in some cases, begins to decrease. There is no apparent unique correlation between all of the curves shown; however, there are several other relationships which should be noted. For vibration at 100 cps, increasing the weight of vibrated sand from 2,040 gm to 2,950 gm or adding a 907-gm surcharge to the 2,040 gm resulted in a decrease in final density. The reverse appears to be true for vibration at 25 cps.

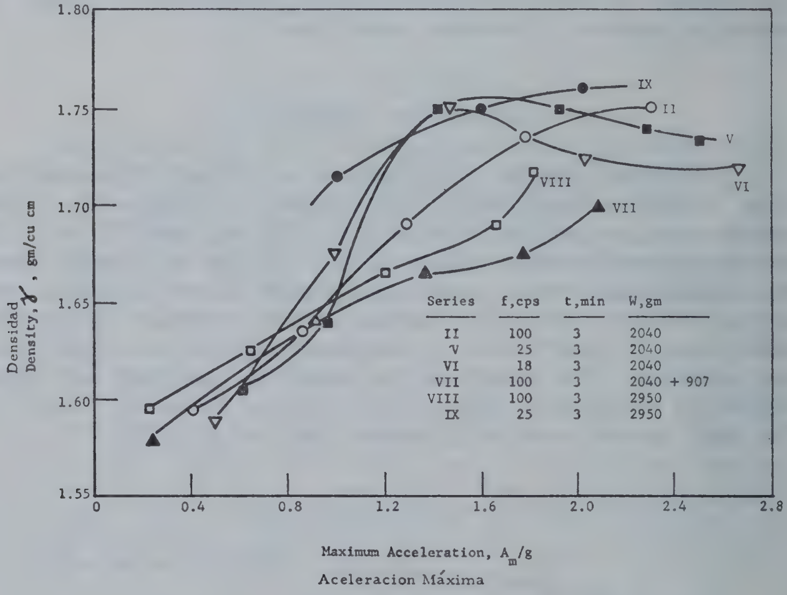

Fig. 3 — Variation of density with acceleration.

Fig. 3 — Variación de la densidad con la aceleración.

The same observations may be made for correlation of density with velocity and displacement (Figures 4 and 5); however in these latter correlations the data occur in two distinct groups on the basis of frequency.

The explanation for this behavior is thought to involve the role of intergranular pressure. Increasing the weight of sand increases the effective intergranular pressure of the

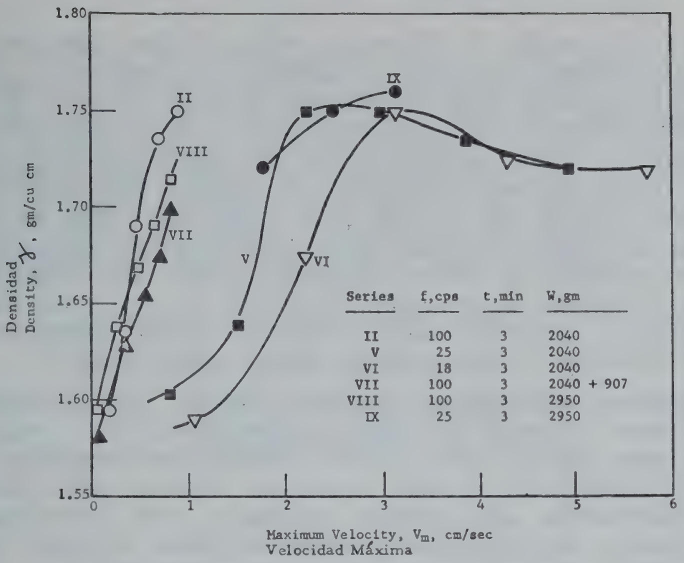

Fig. 4 — Variation of density with velocity.

Fig. 4 — Variación de la densidad con la velocidad.

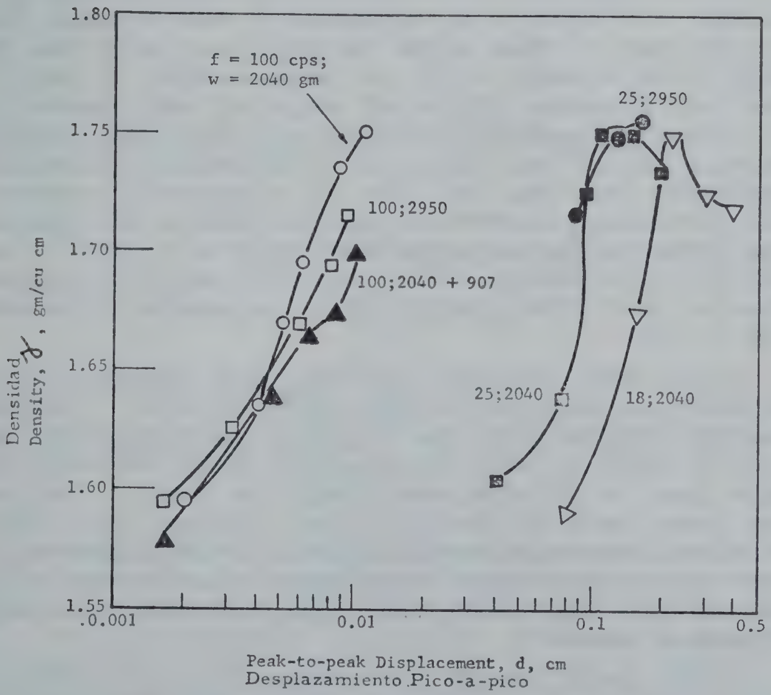

Fig. 5 — Variation of density with displacement.

Fig. 5 — Variación de la densidad con el desplazamiento.

sand in the mold. If vibration reduces these pressures sufficiently during the cycle to permit the particles to move, then the pressure helps to increase the final density. If not, the final density would be less than at lower intergranular pressures at which the particles have enough energy to overcome the intergranular friction. It appears that the former occurred during the 25 cps tests while the latter occurred during the 100 cps tests, thus explaining the opposite behavior observed at these two frequencies. The density decrease at higher accelerations is caused by too much energy so that the particles tend to separate during vibration and when vibration is halted settle into a looser state.

Similar relationships between density and acceleration have been observed by other investigators ([1, 2]). Their results have shown that: 1) the acceleration producing maximum density for a given frequency depends upon particle size distribution and particle angularity and 2) increasing acceleration also produces a decreasing shear strength which approaches some minimum value asymptotically.

In order to further examine the effect of overburden on density, tests were conducted holding vibration conditions constant and varying only the amount of sand vibrated. For the first part of these series the sand was placed into the mold before vibration as in the previous tests. It may be seen that increasing the initial weight of sand resulted in an increase in density for vibration at 25 cps, but a decrease in density at 100 cps (Figure 4). This tends to confirm the explanation involving the effect of intergranular pressure. The phenomenon observed at 100 cps confirms the reported observation ([2]) that a greater acceleration is required to obtain the same density if the height of sand is increased. However, it is evident that for other frequencies the reverse may be true.

These same vibration conditions were maintained, but the sand was added to the mold during vibration. The final densities obtained at 25 cps (Figure 6) were essentially the same as obtained when the identical weight of sand was added prior to vibration, even though the time of vibration was much longer in the latter case. However, the results at 100 cps were significantly different — the final densities were considerably higher, even higher than attained at 25 cps, and they did not decrease with an increase in weight of sand as before.

These results support the hypothesis that for 100 cps the intergranular pressure tended to prevent reorientation of the sand grains to a more dense state while for 25 cps it tended to aid in obtaining higher densities. It appears that at 25 cps the energy imparted to the particles was sufficient to cause them to separate, i.e., the acceleration was greater than that required for maximum density at 25 cps. The fact that final densities were the same when the sand was added during vibration confirms this view. The increased overpressure caused by greater depth of sand counteracts this excess energy at 25 cps resulting in higher density.

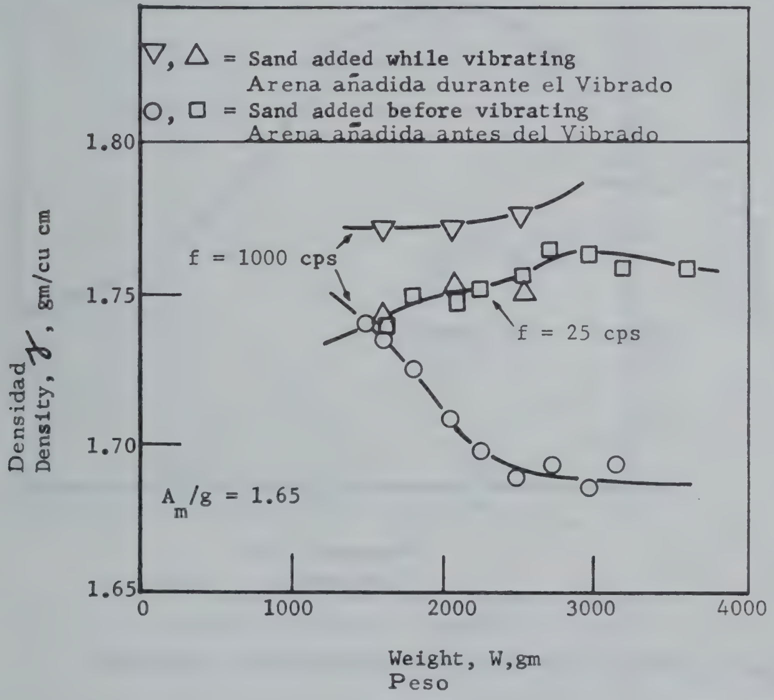

Fig. 6 — Variation of density with weight of sand for constant acceleration.

Fig. 6 — Variación de la densidad con el peso de arena para aceleración constante.

A series of tests were performed in order to compare the results in Figure 6 with other frequencies. In this test series densities were determined for 2040 gm of sand vibrated at various frequencies keeping the time and maximum acceleration the same. The results are shown in Figure 7. It may be seen that for the selected initial weight of sand the greatest density occurred at 50 cps. The densities obtained at 25 cps and 75 cps were the same. The dashed line in Figure 7, constructed from the results in Figure 6, indicates the probable curve if, for each frequency, the sand were added during vibration.

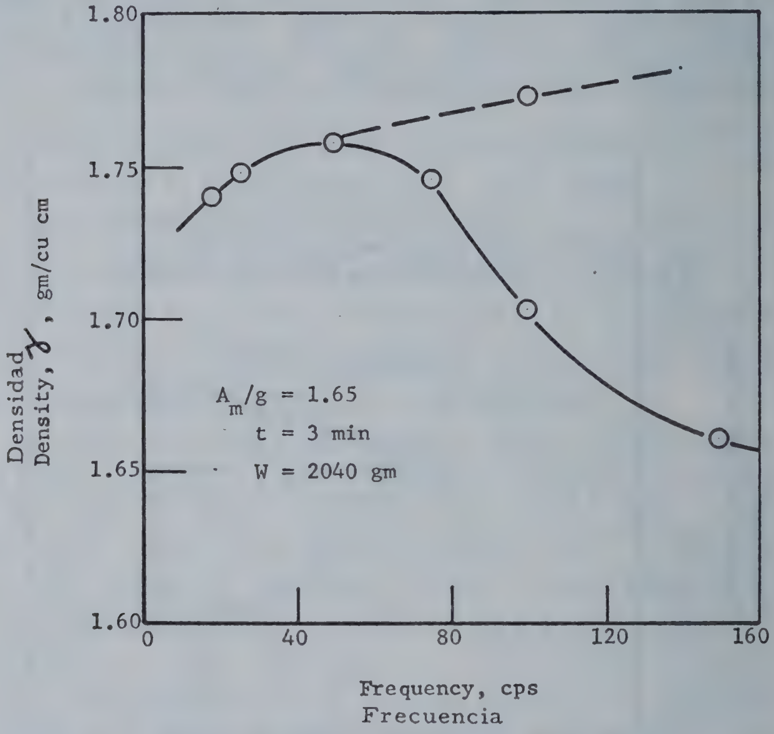

Fig. 7 — Variation of density with frequency.

Fig. 7 — Variación de la densidad con la frecuencia.

In the preceding paragraphs typical relationships between vibration conditions and the resulting density of dry sand have been discussed and illustrated. However, these examples do not provide a complete correlation between the density and the four vibration parameters. In an attempt to obtain such a correlation, density was first plotted as a function of each of the four parameters alone. No systematic pattern was achieved and no single parameter showed indications of having the principal influence on the density obtained by vibration. Since the vibration conditions are defined by any two of the four parameters, correlation was next attempted by plotting contours of constant density on graphs whose ordinate was one vibration parameter and whose abcissa was another. The data used to obtain these density contours consist of all the test results in which the initial weight of sand was 2,040 gm (all of the sand was added before vibration), and the time of vibration was 3 min. Even with such a random assortment of data this correlation was reasonably successful. The best results were achieved when A_m/g and f were chosen as the correlation parameters, although correlations using d and f have also been reported to be successful (²).

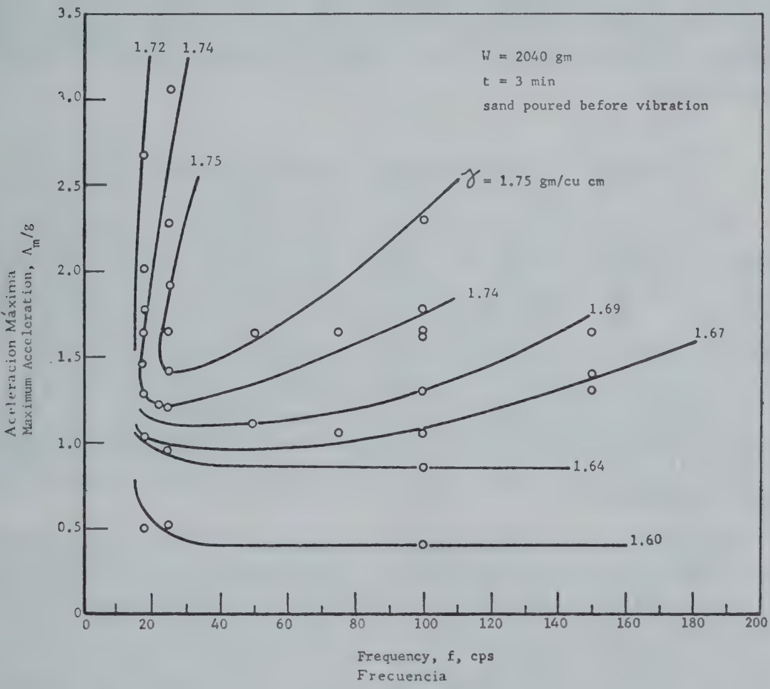

Fig. 8 — Contours of constant density as a function of frequency and maximum acceleration.

Fig. 8 — Contornos de densidad constante en función de la frecuencia y máxima aceleración.

The contours of constant density on a graph of A_m/g versus f for the above data are shown in Figure 8. The contour lines appear to be a family of nested hyperbola-shaped curves with the corresponding value of density increasing from the outermost to the innermost contour line. The innermost curve, then, apparently bounds the region designating the vibration parameters which will give the maximum density obtainable using the prescribed apparatus and procedure. It has already been shown that these contours will be different if the time of vibration or initial weight of sand is changed and if the sand is added during vibration. It is expected that these curves will also change if any of the other conditions of the test are changed such as sand grain size distribution, and angularity of the particles. Figure 8, then, serves only to indicate the type of relationship existing between the vibration conditions and the resulting density. The important conclusion which appears to have been overlooked in most investigations is that unique correlation between density and vibration requires two vibration parameters.

DENSITY VARIATION WITHIN SPECIMEN

The results of the vibration tests indicate that the final density is determined to a large degree by the energy level of vibration produced in relation to the effective intergranular pressures. These pressures tend to increase toward the bottom of the specimen because of the increasing weight of the overlying sand. Hence for constant vibration conditions it is probable that, in general, the final density of the specimen is not uniform. The densities used in the presentation of vibration results were average values for the entire 20 cm high specimen.

Several trials were made to measure the density variation throughout the specimen. The procedure involved the use of a machinist's adjustable square as a combination leveler and depth gage. The sand was carefully removed in 5 cm layers with a special scoop and vacuum extractor. The amount of sand removed per layer was carefully weighed and the density computed assuming the specimen diameter to be constant. It should be recognized that the accuracy of density measurement with this method is no better than 1 per cent because of the difficulty in accurately measuring the volume.

In Figure 9a the density variation is shown after the sand had been poured into the mold with a fixed height of fall but with no vibration. The density increased from top to bottom apparently because the overburden increased with depth. The total variation was only 2½ per cent, but this is nevertheless significant because the maximum possible density variation of this sand is only about 20 per cent.

A significant decrease in density from top to bottom was observed for intermediate densities when the sand was first poured into the container and then vibrated (Figure 9b). It is believed that the weight of overlying sand prevented the sand at the greater depths from vibrating sufficiently to increase in density as much at shallower depths where intergranular pressures were less. As the intensity of vibration was increased a higher average density was achieved with less variation (Figure 9c). In this case there was about a 2 per cent increase with depth for the top ¾ of the specimen. Hence it appears that increased overburden pressure aided vibration in achieving a higher density for the top ¾ of the specimen.

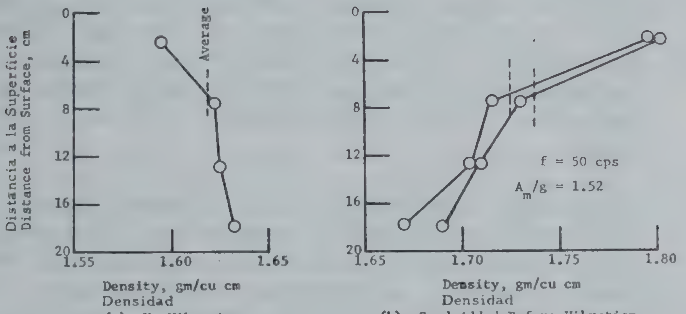

(a) No Vibration
Sin Vibrado

(b) Sand Added Before Vibration
Arena Añadida antes del Vibrado

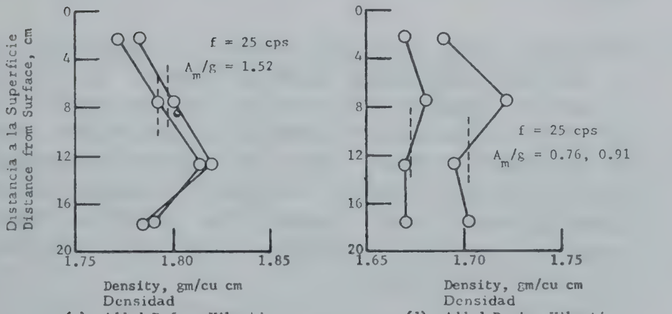

(c) Added Before Vibration
Añadida antes del Vibrado

(d) Added During Vibration
Añadida durnate el Vibrado

Fig. 9 — Variation of density within specimen.

Fig. 9 — Variación de la densidad dentro de la muestra.

Finally an examination was made of several medium density specimens which were prepared by pouring the sand during vibration (Figure 9d). Although there was a density variation of as much as 2 per cent in one case, this variation was random so that the density appears to be uniform throughout the specimen within the accuracy of measurement.

CONCLUSIONS

Specimens of dry silica sand have been subjected to a wide variety of vibration conditions to determine the relationship of the vibration parameters with the density they produce. A number of conclusions may be drawn from these tests:

1. With all other factors constant, density increases with an increase in any one of the four vibration parameters: frequency, acceleration, velocity and displacement. However there exists a value of the parameter above which density will begin to decrease.

2. No unique correlation exists between density and any one of the vibration parameters. However correlation was found between the density and two of the parameters, acceleration and frequency. This may be expected since the vibration conditions are uniquely described by any two of the four parameters.

3. Surcharge and increased depth of sand may assist or restrict increasing density caused by vibration. A certain amount of vibration is required to overcome the resistance to density change as a result of internal friction. This friction is increased by surcharge and added weight of sand. However "overvibration" will loosen the particles thus decreasing density. Surcharge and sand overburden will resist this effect.

4. A comparison of densities obtained by adding the sand slowly during vibration with that obtained when the sand is placed before vibration further illustrate the effect of intergranular pressure. Under conditions of "overvibration" both methods give the same results. When intergranular pressure has been restricting density increase, the former method gives substantially higher densities.

Methods for determining the maximum density which can be obtained with a given sand have been the subject of many vibration studies. From the present studies additional information has been obtained on this subject:

1. These results suggest that the highest densities achieved by vibrating the sand through the container are obtained with no surcharge and a minimum of overburden. Of course, the sand must not be vibrated too intensely. This approach is quite different than that of many recommended tests for maximum density ([3, 4, 5, 6, 7, 8]) in which a surcharge is prescribed.

2. Pouring the sand slowly into the container under proper vibration conditions may be the best way to achieve maximum density because the sand in all parts of the container has a chance to vibrate for a period of time with no overburden.

3. The highest density which the writer has obtained for this sand was not obtained with the methods described in this paper, that is by vibrating the container. Instead a vibrating tamper was worked around the surface of the sand as the container was slowly filled. The method is similar to previously recommended procedures in which the sand is vibrated in the air dry state ([9]) and the underwater ([10]).

ACKNOWLEDGEMENTS

The experimental work was conducted in the Soil Mechanics Laboratory of the Armour Research Foundation (now Illinois Institute of Technology Research Institute). In addition to Armour Research Foundation sponsorship, portions of the study were conducted as part of a project on "Shock Wave Propagation in Soil" supported by a grant from the National Science Foundation. The contributions of Dr. E. Vay and membres of the Soil Mechanics staff are gratefully acknowledged.

REFERENCES

1. "The Behavior of Soil During Vibration" — T. Mogami, and K. Kubo — *Proceedings,* Vol. I, 3rd Int'l. Conf. on Soil Mech. and Fdn. Eng'g., 1953, pp. 152-155.

2. "Vibration of Sands with Special Reference to the Minimum Porosity Test for Sands" — I. Alyanak — *Proceedings,* Vol. 4, Midland Soil Mechanics and Foundation Engineering Society, 1961, pp. 37-72.

3. "Soil Compaction Investigation: Report No. 5, Miscellaneous Laboratory Tests" — U.S. Army Engineers Waterways Experiment Station, Corps of Engineers, Tech. Memo 3-271, June 1950.

4. "Suggested Method of Test for Compactibility of Noncohesive Materials" — J. T. Pauls and J. F. Goode, ASTM Procedures for Testing Soils, July 1950.

5. "Laboratory Procedures for Performing the Providence Vibrated Density Test to Determine the Maximum Density of Cohesionless Soils" — New England Division, Corps of Engineers, Boston, Mass., August 1957.

6. "Suggested Method of Test for Maximum Density of Noncohesive Soils and Aggregates" — J. T. Pauls and J. F. Goode — *Procedures for Testing Soils,* ASTM, April 1958, pp. 154-158.

7. "Laboratory Methods of Compacting Granular Materials" — E. J. Felt, ASTM Spec. Tech. Pub. 239, June 1958, pp. 89-108.

8. "Tentative Procedure for Relative Density of Cohesionless Free-Draining Soils Using a Vibratory Table" — U.S. Bureau of Reclamation, Commissioner's Office, Denver, Colo., 1961.

9. "Suggested Methods of Test for Maximum and Minimum Densities of Granular Soils" — D. M. Burmister — *Procedures for Testing Soils,* ASTM, April 1958, pp. 148-150.

10. "An Experimental Study of the Maximum and Minimum Porosities of Sands" — J. Kolbuszewski — *Proceedings,* Vol. I, 2nd Int'l. Conf. on Soil Mech. and Fdn. Eng'g., 1948, pp. 158-165.

EFFECT OF VIBRATION AMPLITUDE ON WAVE VELOCITIES IN GRANULAR MATERIALS

J. R. HALL, JR.

Lecturer, Dept. of Civil Engrg., The University of Michigan, Ann Arbor, Mich.

F. E. RICHART, JR.

Prof. and Chmn., Dept. of Civil Engrg., The University of Michigan, Ann Arbor, Mich.

SYNOPSIS

Laboratory tests utilizing the resonant column method provided information concerning the effect of amplitude of vibration on the wave velocities in four granular materials. The materials were Ottawa standard sand, two sizes of glass beads, and a silt-sized crushed quartz. The effects of confining pressure, relative density, and saturation were also considered.

The results of these tests show that both the longitudinal and shear wave velocilities decrease as the amplitude of vibration is increased. For the conditions used in these tests, this decrease may be as much as 10 to 15 per cent as the double amplitude is increased from 1×10^{-5} *to* 2.5×10^{-3} *radians in the torsion tests or from* 2×10^{-6} *to* 1×10^{-3} *inches in the longitudinal tests. A comparable decrease in wave velocity of 10 to 15 per cent was found when the void ratio was changed from the minimum to the maximum value.*

The behavior of the silt-sized crushed quartz was found to depend upon the time of loading and also upon the stress history. The wave velocity increased slightly with the length of time a particular confining pressure acted. However, it was found that higher amplitude vibrations tended to destroy this time-dependent increase in velocity.

SINOPSIS

El efecto de la amplitud de vibración en la velocidad de onda de cuatro materiales granulares fué encontrado mediante ensayos de laboratorio utilizando el método de la columna resonante. Los materiales fueron arena tipo Ottawa, dos tamaños de vidrio granulado y cuarzo tritu-

rado tamaño cieno. También fueron considerados los efectos producidos por presión de confinamiento, densidad relativa y saturación.

Los resultados de estos experimentos muestran que las velocidades de onda tanto longitudinal como transversal disminuyen en sentido inverso a la amplitud de onda. De acuerdo con las condiciones de estos experimentos se encontró que la disminución puede ser hasta del 10 al 15 por ciento a medida que la amplitud doble de torsión aumenta de 1×10^{-5} *a* 2.5×10^{-3} *radianes o de* 2×10^{-6} *a* 1×10^{-3} *pulgadas en la prueba longitudinal. En la misma forma se encontró una disminución en la velocidad de onda del 10 al 15 por ciento cuando la razón de volumen de aire a volumen total de la muestra cambió desde su valor mínimo a su valor máximo.*

El comportamiento del cuarzo triturado tamaño cieno dependió del tiempo de carga y también de los distintos esfuerzos a los que se sometió la muestra. La velocidad de onda aumentó levemente al aumentar el tiempo durante el cual la presión de confinamiento actuó. Sin embargo, se descubrió que las vibraciones de mayor amplitud tendieron a destruir este aumento de velocidad dependiente de tiempo.

INTRODUCTION

The dynamic properties of a soil can be determined from measurements of the propagation of stress waves through the soil. In order to estimate these properties as they occur in the field it is necessary to know the relative importance of the variables which may exist. Some studies have been made to determine the effects of confining pressure, relative density, or per cent saturation on the velocities of wave propagation and damping in soils, for example, the papers by K. Iida[1, 2], G. Shumway[3], and B. O. Hardin and F. E. Richart[4]. However, there are several other variables which may have a significant influence on test results.

S. D. Wilson and E. A. Sibley[5] have shown comparisons between values of the constrained modulus of elasticity as determined from seismic tests, laboratory vibration tests, and static confined compression tests. The amplitudes of deformation differ by orders of magnitude in these three testing methods. The smallest deformations are associated with the seismic tests while relatively large deformations are necessary to insure accuracy of measurement in the confined compression tests. The results obtained by Wilson and Sibley show that the seismic determination gives the highest value of constrained modulus while the confined compression tests give the lowest values.

The primary object of this investigation was to determine the relative importance of the effect of amplitude of vibration on the wave velocity. The resonant column method was used to determine the velocity of the shear and longitudinal waves in a column of soil 11 in. long which was fixed at one end and free at the other. All test results are related to the amplitude at the free end of the specimen. This amplitude varied from about 2×10^{-6} to 1×10^{-3} in. double amplitude in longitudinal oscillation and from about 1×10^{-5} to 2.5×10^{-3} radians double amplitude in torsional oscillation.

THEORIES USED IN THE EXPERIMENTAL DETERMINATION OF WAVE VELOCITY

The wave velocity through a column of soil was determined from the resonant frequency of the column when excited into longitudinal or torsional oscillation. The resonant frequency is that frequency which produced the maximum amplitude of oscillation at the upper, free end of the specimen. For this type of test equipment, the resonant frequency, f, for the first mode of vibration is associated with a wave length which is four times the length of the specimen. Thus, by designating the specimen length as L′ and the wave length as L, the wave velocity may be calculated from the relationship

$$v = fL = 4\,fL' \tag{1}$$

From the computed values of shear or longitudinal wave velocities, the shear modulus and longitudinal modulus of elasticity may be evaluated from

$$v_L = \sqrt{\frac{E}{\rho}}\ , \tag{2}$$

and

$$v_S = \sqrt{\frac{G}{\rho}}\ . \tag{3}$$

In Eqs. (2) and (3), $\rho = \gamma/g$ is the mass density of the material, E is the dynamic longitudinal modulus of elasticity, G is the dynamic shear modulus, v_L is the longitudinal wave velocity, and v is the shear wave velocity.

The specimens used in this research were fixed at the base and the driver and pickup were fastened to the top free end. Therefore a correction was applied to correct for the added mass at the end of the specimen. The solution governing the natural frequency of such a system under torsional vibrations is given by

$$\omega L' \sqrt{\frac{\rho}{G}} \tan \omega L' \sqrt{\frac{\rho}{G}} = \frac{I}{I_o} \tag{4}$$

where I_o is the mass polar moment of inertia of the mass attached to the free end, I is the mass polar moment of inertia of the specimen of length L′, and ω is the circular frequency ($2\pi f$). Eq. (4) must be solved graphically or by trial and error. It is convenient to put Eq. (4) into the form

$$\beta \tan \beta = \frac{I}{I_o} . \tag{5}$$

Thus,

$$v = \frac{2\pi f L'}{\beta} . \tag{6}$$

LABORATORY TESTS OF VELOCITY IN GRANULAR MATERIALS

MATERIALS

Four different materials were used in this investigation. Each is described below and the grain size curve for each is shown in Fig. 1.

Ottawa sand. Standard Ottawa sand passing the No. 20 sieve and retained on the No. 30 sieve was used for most of the investigation. This material has a minimum void ratio of 0.50 and a maximum void ratio of 0.77. It has a specific gravity of 2.67.

Glass beads No. 2847. Glass beads, all of which lie between the No. 16 and No. 20 sieve, were obtained from the Prismo Safety Corporation, Huntingdon, Pennsylvania. These beads appear to be perfect spheres when examined under a microscope. They have a specific gravity of 2.50, a minimum void ratio of 0.57 and a maximum void ratio of 0.75.

Glass beads No. 1725. This material was also obtained from the Prismo Safety Corporation. Ninety-five per cent pass the No. 200 sieve and 96 per cent are retained on the No. 400 sieve. They have a high specific gravity of 4.31 resulting from the requirement of a high index of refraction for their commercial use. The minimum void ratio for this material is 0.57 and the maximum void ratio is 0.76.

Novaculite No. 1250. This is a very fine quartz powder obtained from the American Graded Sand Co., 189-203 East Seventh Street, Paterson 4, New Jersey. This material was considered to be a silt as shown by the grain size curve in Fig. 1.

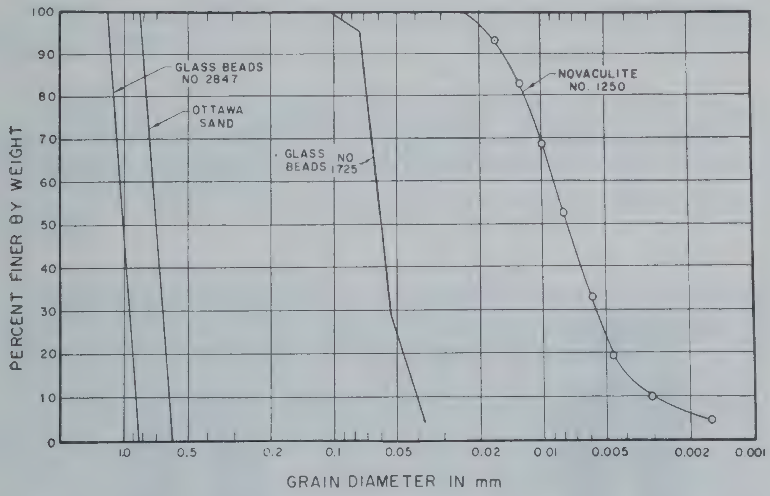

Fig. 1 — Grain size curves for the materials used in the present research.

Fig. 1 — Curvas granulométricas de los materiales usados en la presente investigación.

EQUIPMENT

Two pieces of equipment were specially designed and built to vibrate the specimen at relatively large amplitudes in the longitudinal and torsional modes. Each was constructed so that one end of the specimen was free and the other was fixed as shown in Figs. 2 and 3. Both pieces of equipment are basically the same except for the driver and the pickup as shown in Fig. 2. The frames were made from a piece of 4 in. steel pipe with lead attached for added mass to give a total weight of about 30 lbs. for each apparatus. This is necessary in order to reduce the movement of the "fixed" end to a negligible amount.

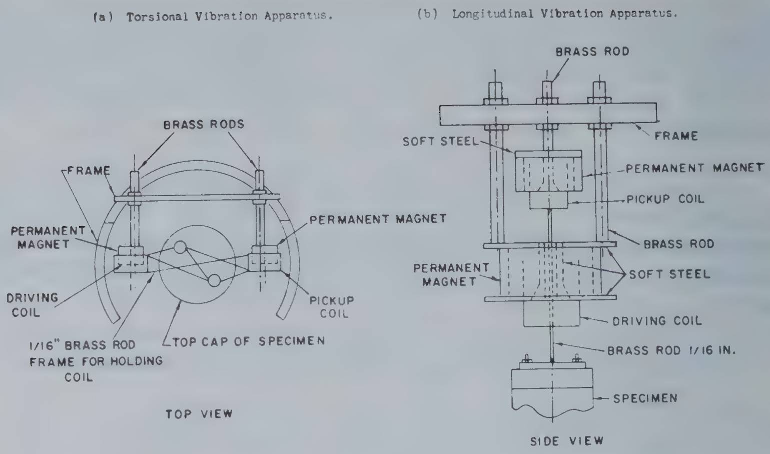
(a) Torsional Vibration Apparatus.
(b) Longitudinal Vibration Apparatus.
BRASS RODS
FRAME
PERMANENT MAGNET
PERMANENT MAGNET
DRIVING COIL
PICKUP COIL
1/16" BRASS ROD FRAME FOR HOLDING COIL
TOP CAP OF SPECIMEN
TOP VIEW
BRASS ROD
FRAME
SOFT STEEL
PERMANENT MAGNET
PICKUP COIL
BRASS ROD
PERMANENT MAGNET
SOFT STEEL
DRIVING COIL
BRASS ROD 1/16 IN.
SPECIMEN
SIDE VIEW

Fig. 2 — Vibration mechanisms used in the present research.

Fig. 2 — Vibradores mecánicos usados en la presente investigación.

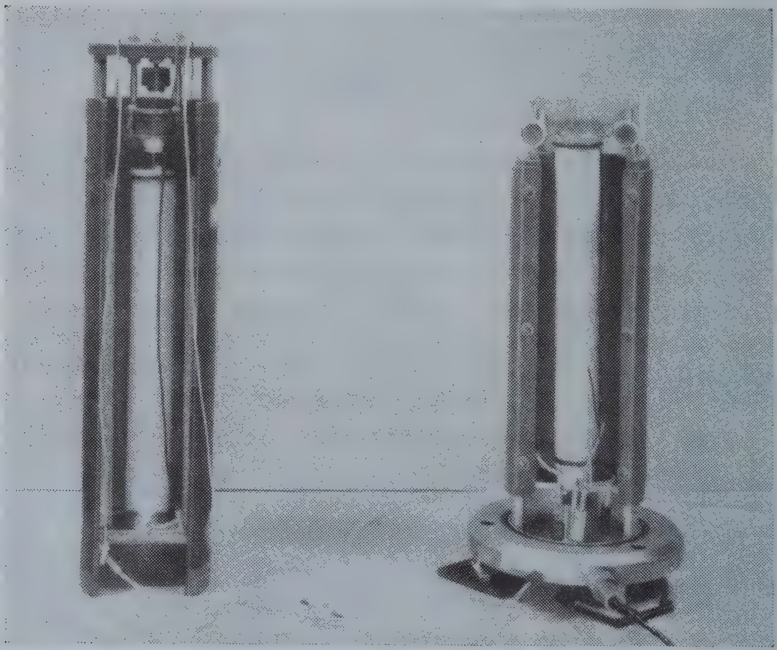

Fig. 3 — Fixed-free vibration equipment.

Fig. 3 — Equipo de vibración.

Power to the driving coil was supplied through an amplifier connected to an oscillator in the MB Electronics Type P11 power supply. Pickups were calibrated with an MB Electronics Model C31 calibrator and also with an MB Electronics Type 115 vibration pickup. A Tektronix Model 502 dual beam oscilloscope was used for the measurement of output from the pickups and also for monitoring the input to the driver. A more detailed description of the equipment and testing procedures was given by J. R. Hall[6].

SUMMARY OF TESTS

Three groups of tests were run and are summarized as follows.

Group I. These tests used specimens of Ottawa sand to obtain data on the effect of amplitude on wave velocity. The test variables included the confining pressure, pore fluid (air, water, and dilute glycerin), and the relative density of the material.

Group II. After tests of Group I were completed, tests were run on samples of each of the two sizes of glass beads in the dense condition both dry and saturated.

Group III. A torsional vibration test was run to determine the variation of velocity with amplitude for a specimen of Novaculite No. 1250 in the dry condition.

RESULTS OF VELOCITY

Group I. Figs. 4 through 6 are representative of the results for velocity in torsional and longitudinal oscillation as calculated from the tests of Group I on Ottawa sand. In these tests the variation of velocity with amplitude of vibration was determined for various confining pressures, density, and pore fluids (air, water, and dilute glycerin). The confining pressures chosen for each test were approximately 5, 10, 25, and 50 lb/in^2 and the results at each pressure are plotted in the same figure. Tests were run using the sand in both the loose and dense conditions corresponding to void ratios of approximately 0.65 and 0.51, respectively. For saturation with dilute glycerin, the mixture was 3 parts water to 1 part glycerin. Pure glycerin was not used because its viscosity is so high that an unreasonable length of time is required to saturate the specimen.

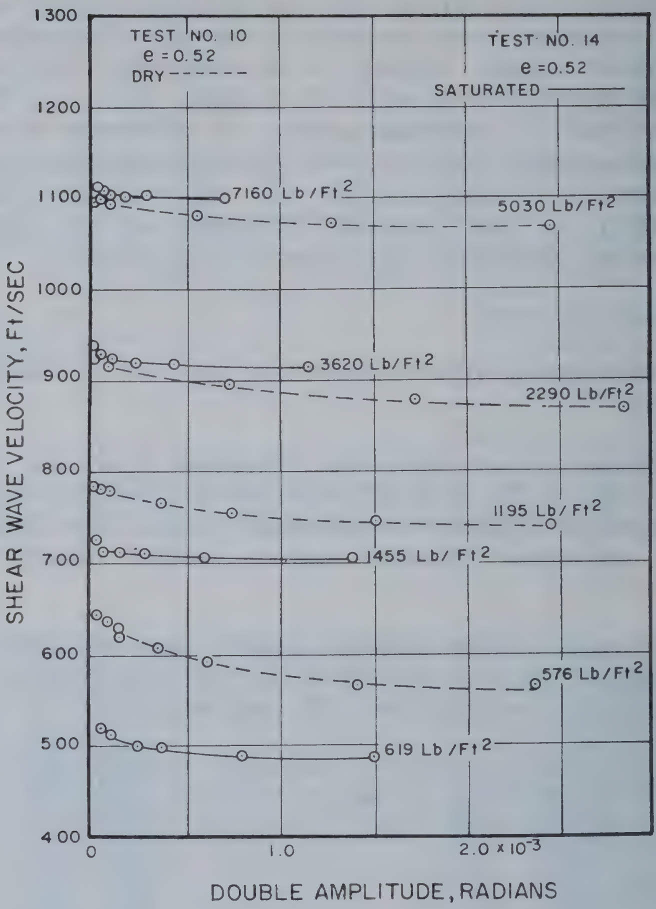

Fig. 4 — Variation of velocity with amplitude in torsional oscillation for Ottawa sand dry and saturated with water.

Fig. 4 — Variación de velocidad comparada con la amplitud en la oscilación de torsión para arena seca tipo Ottawa y para la misma saturada con agua.

Fig. 4 shows the variation of velocity with amplitude for dense Ottawa sand, dry and saturated with water, in torsional oscillation. Fig. 5 shows the variation of velocity with amplitude for loose Ottawa sand, dry and saturated with water, in longitudinal oscillation. The results for the specimen in the loose and dense conditions are essentially the same except for the change in velocity due to a change in void ratio, therefore curves for torsional oscillation of loose Ottawa sand and longitudinal oscillation of dense Ottawa sand are omitted. Fig. 6 shows the variation of velocity with amplitude for specimens of loose Ottawa sand, saturated with dilute glycerin and excited into longitudinal oscillation.

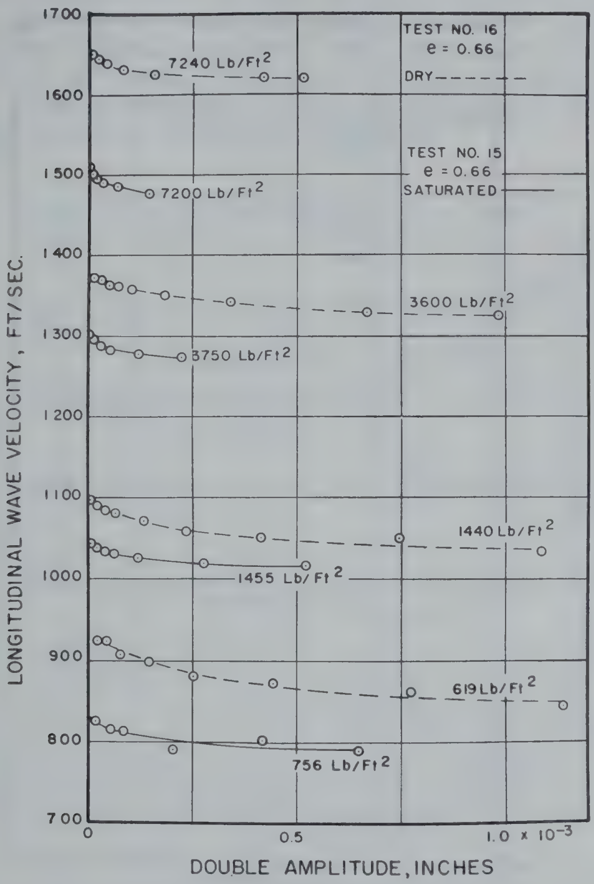

Fig. 5 — Variation of velocity with amplitude in longitudinal oscillation for Ottawa sand dry and saturated with water.

Fig. 5 — Variación de velocidad comparada con la amplitud en la oscilación longitudinal para arena seca tipo Ottawa y para la misma saturada con agua.

Group II. Typical test results for the large size glass beads are shown in Fig. 7. These curves show the results of the variation of velocity with amplitude for samples in the dense condition, both dry and saturated, in longitudinal oscillation. Fig. 8 shows results of the variation of velocity with amplitude in torsional oscillation for the small size glass beads in the dense condition. The same specimens were used for both the dry and saturated tests of the glass beads.

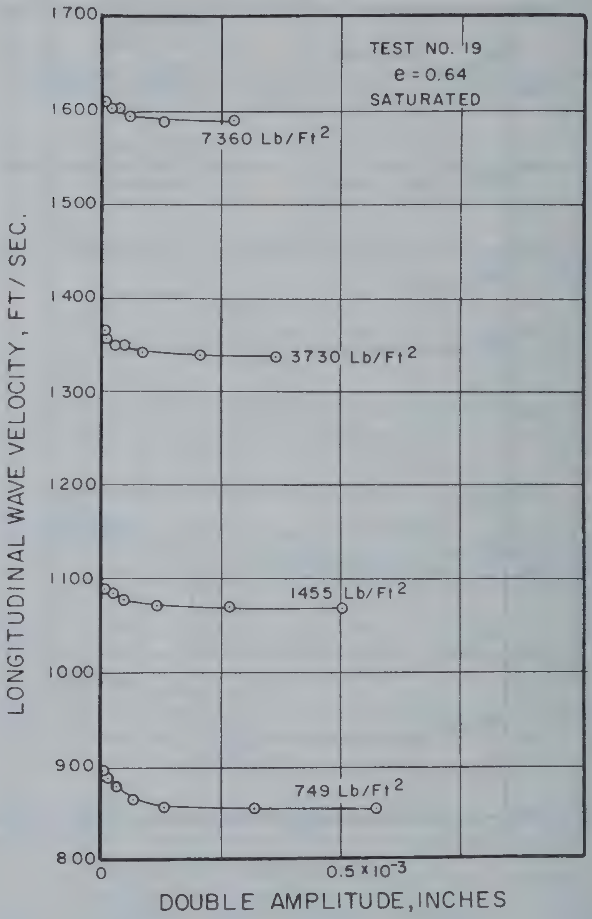

Fig. 6 — Variation of velocity with amplitude in longitudinal oscillation for Ottawa sand saturated with dilute glycerin.

Fig. 6 — Variación de velocidad comparada con la amplitud en la oscilación longitudinal para arena tipo Ottawa saturada con glicerina diluida.

Group III. Figs. 9 and 10 show the results for the variation of wave velocity with amplitude for a specimen of crushed quartz. This specimen was formed by compaction of material which had been dried for several days at a temperature of 220°C. The behavior of the crushed quartz is quite different than that of the Ottawa sand or the glass beads because of the very small grain size. The stress wave velocities depend upon the time of load application and stress history as well as upon the other variables. During test No. 28, for which the initial void ratio was 0.83 under a pressure of 14 lb/in², the specimen consolidated to a void ratio of 0.80 after having been subjected to a stress cycle confining pressures as high as 50 lb/in².

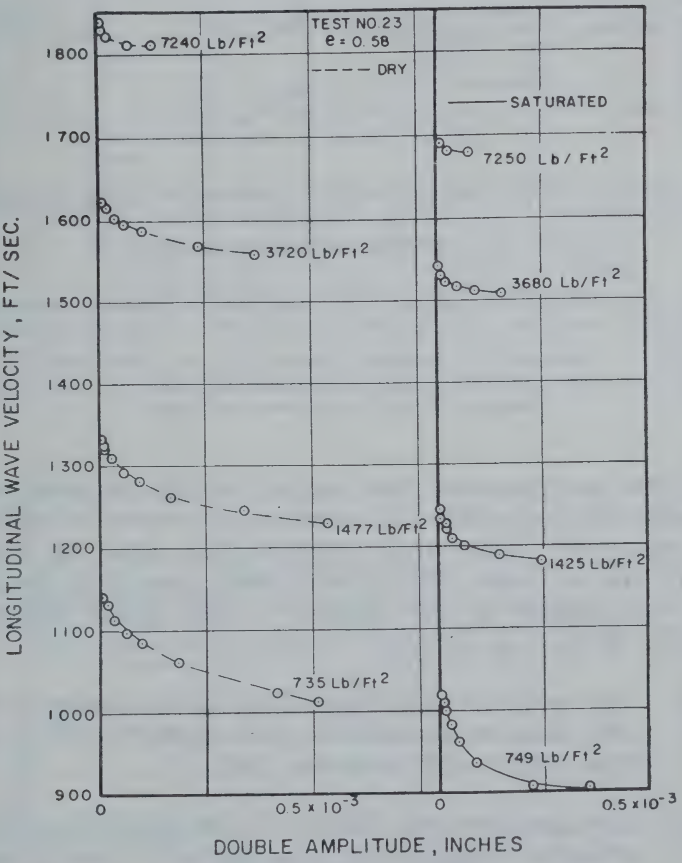

Fig. 7 — Variation of velocity with amplitude in longitudinal oscillation for glass beads No. 2847 in the dry and water saturated condition.

Fig. 7 — Variación de velocidad comparada con variaciones en la amplitud de la oscilación longitudinal para vidrio granulado No. 2847 en las condiciones seca y saturada con agua.

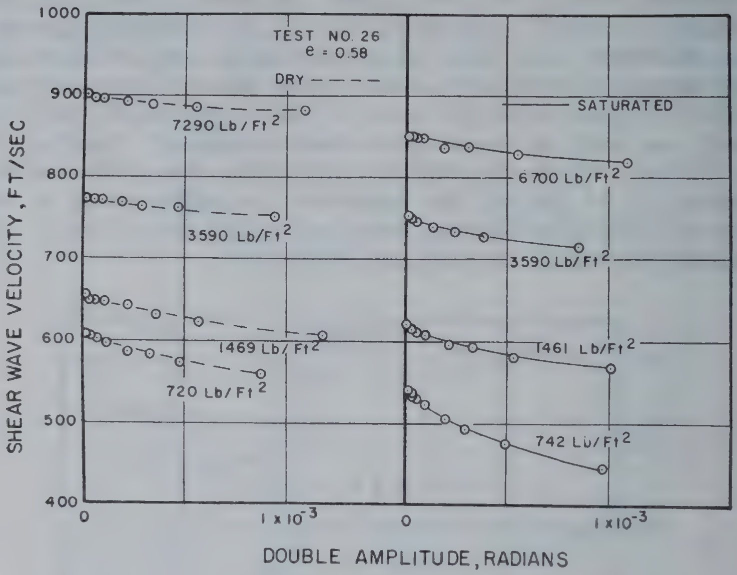

Fig. 8 — Variation of velocity with amplitude in torsional oscillation for glass beads No. 1725 in the dry and water saturated condition.

Fig. 8 — Variación de velocidad comparada con variaciones en la amplitud de oscilación de torsión para vidrio granulado No. 1725 en las condiciones seca y saturada con agua.

After each pressure was applied to the specimen, measurements of the resonant frequency were made at different time intervals. These time intervals are noted on Figs. 9 and 10 and represent the total elapsed time after the pressure was applied to the specimen. The stress history of test No. 28 was as follows:

1. The specimen was compacted, placed under a vacuum, and measurements were made for void ratio. The initial void ratio was 0.83.

2. The specimen was placed in the triaxial cell and a pressure of 2030 lb/ft² was applied. Velocity measurements were made intermittently over a period of 38 hrs.

3. The pressure was raised to 4100 lb/ft². Velocity measurements were made intermittently over a period of 140 hrs.

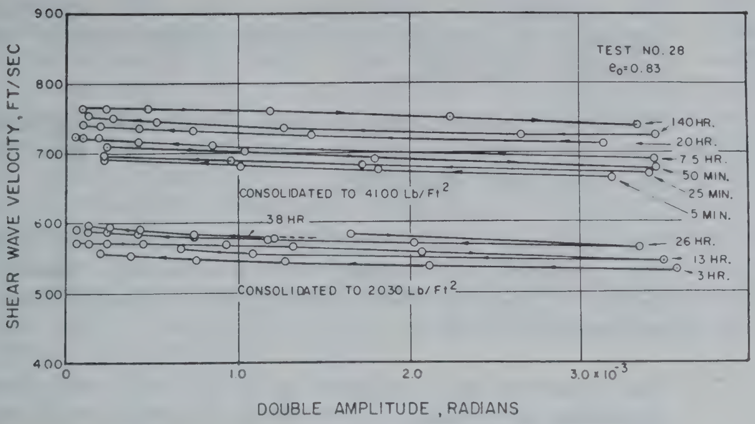

Fig. 9 — Variation of velocity with amplitude in torsional oscillation for Novaculite No. 1250 consolidated to 2030 lb/ft² and 4100 lb/ft².

Fig. 9 — Variación de velocidad comparada con variaciones en la amplitud de oscilación de torsión para Novaculite No. 1250 compactado a presiones de 2030 y 4100 lbs. por pie cuadrado.

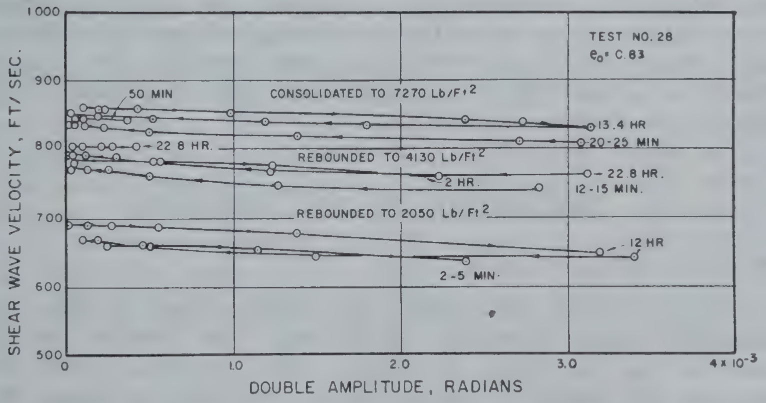

Fig. 10 — Variation of velocity with amplitude in torsional oscillation for Novaculite No. 1250 consolidated to 7270 lb/ft² and rebounded to 4130 lb/ft² and 2050 lb/ft².

Fig. 10 — Variación de velocidad comparada con variación en la amplitud de la oscilación de torsión para Novaculite No. 1250 compactado a 7270 lbs. por pie al cuadrado y depresionado a 4130 y a 2050 libras por pie al cuadrado.

4. The pressure was rebounded to 2050 lb/ft^2 and measurements of velocity were made intermittently over a period of 12 hrs.

5. The specimen was placed under a vacuum and measurements were made for void ratio. At this time the void ratio was 0.81.

6. The specimen was replaced into the triaxial cell and the pressure was raised to 7270 lb/ft^2. Measurements of velocity were made intermittently over a period of 13 hrs.

7. The pressure was reduced to 4130 lb/ft^2 and measurements of velocity were made intermittently over a period of 30 hrs.

8. Final measurements under a vacuum gave a value of void ratio equal to 0.80.

During the time intervals between measurements the specimen was not vibrated. The first measurements after each time interval were made at low amplitudes of vibration. The following measurements were made at increasing amplitudes until the maximum obtainable with the equipment was reached. Since the high amplitude vibrations affect the low amplitude measurements, a second set of measurements were usually taken after the specimen had been vibrating at high amplitudes for a period of approximately five minutes. These two methods of measurement are indicated in the figures by arrows on each curve.

DISCUSSION OF THE RESULTS

GROUP I

Fig. 4 shows the results for Ottawa sand in the dense condition under torsional oscillation. The results for this material in the loose condition were essentially the same and are not shown. The curves for the dry specimen show that the variation of velocity with amplitude is greatest at low confining pressures and low amplitudes of oscillation. The amount of velocity variation over the amplitude range measured is about 13 per cent at the low confining pressure and about 3 per cent at the high confining pressure. The results shown in Fig. 5 for the longitudinal oscillations of the specimen in the dry and loose condition are very similar to those in Fig. 4 for the torsional oscillations. The curves are similar in shape and the amount of variation of velocity is approximately the same order of magnitude. The results for specimens in the dense condition for longitudinal oscillations are not shown because they were essentially the same as for the loose condition. When the specimen was saturated with water the amount of variation of velocity with amplitude was decreased somewhat and most of it took place at small amplitudes. There was little variation of velocity with amplitude at the higher amplitudes of oscillation. Fig. 6 shows the results for Ottawa sand saturated with dilute glycerin. These curves are practically the same as those for the same material saturated with water.

GROUP II

Fig. 7 shows the results for the large size glass beads in the dense condition under longitudinal oscillation. For this material the effect of amplitude of vibration on the stress wave velocity is much more pronounced than that for the Ottawa sand. The saturated condition of the specimen gives a much greater variation of velocity in the low amplitude range than for the dry condition. The difference between the behavior of this material and that of Ottawa sand is probably due to the difference in the grain characteristics. The particles in both cases are rounded but the surface of glass beads is much smoother than that of the Ottawa sand. The small size glass beads also show a larger variation of velocity with amplitude than does the Ottawa sand. The curves for the small glass beads in the saturated condition shown on Fig. 8 do not flatten out as was indicated for the other test conditions. This difference could be due to the small grain size as well as the difference in the specific gravity of the particles. As mentioned before, the specific gravity of this material is 4.31 as compared to 2.50 for the large size glass beads. If the tests for the small beads could be carried out to higher amplitudes the results might be similar to those for the Ottawa sand and the larger size glass beads.

GROUP III

Figs. 9 and 10 show the results for the silt-size crushed quartz. As mentioned before, the dynamic properties of this material are time dependent. Consequently, the results are shown in terms of the time elapsed after the particular confining pressure had been applied. For this material there was also a variation of wave velocity with amplitude of vibration. However, the behavior is much different than for the other materials tested. The other materials showed the maximum amount of velocity variation within the small amplitude ranges while this material shows almost no variation in the same range of amplitude. It can be seen in Fig. 9 that as the material is allowed to remain under a given pressure the velocity continues to increase. However, some of this build-up can be destroyed by vibrations of larger amplitude, as shown by Fig. 9. After the specimen had remained at a confining pressure of 4100 lb/ft^2 for 140 hrs. the variation of velocity with amplitude was as shown by the top curve. After the specimen had been vibrated at high amplitudes the lower curve for 140 hrs. was obtained. Fig. 10 shows the results when the specimen had been consolidated to 7270 lb/ft^2, rebounded to 4130 lb/ft^2, and then to 2050 lb/ft^2. When the confining pressure was reduced from a high to a low pressure the velocity decreased, but when it was allowed to remain at the lower pressure the velocity increased. This increase can also be destroyed by high amplitude vibrations as shown by the lower of the three curves of Fig. 10.

CONCLUSIONS

The conclusions obtained from this study necessarily apply to granular soils which have been subjected to several load repetitions and have reached a relatively stable condition. This corresponds to construction conditions where the soil has been pre-vibrated or pre-compacted to eliminate the disastrous settlements which may accompany the first dynamic load application on loose granular soils.

The tests on Ottawa sand and glass beads gave results which should be typical for clean sands with rounded grains. The more important conclusions are listed below:

1. Both the shear and longitudinal wave velocities decrease as the amplitude of vibration is increased. This decrease may be as much as 10 to 15 per cent as the double amplitude is increased from 1×10^{-5} to 2.5×10^{-3} radians in the torsion tests or from 2×10^{-6} to 1×10^{-3} in. in the longitudinal tests.

2. Tests have shown that the effects on wave velocities produced by changes of void ratio from the maxi-

mum to the minimum value is about 10 to 15 per cent. Thus void ratio changes and changes of amplitude influence the wave velocities by comparable amounts.

Tests on the Novaculite No. 1250, a very fine-grained crushed quartz, produced results which were somewhat different from those obtained from the larger grained materials. The primary difference is that the wave velocity values obtained from laboratory tests are dependent upon stress history and upon the time the loading has been applied. The wave velocity increases slightly as a particular confining pressure continues to be applied to the specimen. However, it was also found that the higher amplitudes of vibration tended to destroy this time-dependent increase in velocity. Further investigation is required in order to evaluate the time-dependent increase in wave velocity and the vibrational energy required to destroy this gain.

ACKNOWLEDGEMENT

The studies presented in this paper represent a portion of work made possible through National Science Foundation research grant NSF-G19021. The support provided for this research is gratefully acknowledged.

This investigation was conducted as a part of the research program of the Department of Civil Engineering and the Engineering and Industrial Experiment Station of the University of Florida, Gainesville, Florida.

BIBLIOGRAPHY

1. Iida, K. (1938) — "The Velocity of Elastic Waves in Sand" — Tokyo Imperial University — *Bulletin, Earthquake Research Institute,* v. 16, pp. 131-144.

2. Iida, K. (1939) — "Velocity of Elastic Waves in a Granular Substance" — *Bulletin, Earthquake Research Institute,* v. 17, pp. 783-807.

3. Shumway, G. (1960) — "Sound Speed and Absorption Studies of Marine Sediments by a Resonance Method — Parts I and II" — *Geophysics,* v. XXV, Nos. 2 and 3, April and June, 1960, pp. 451-467 (April) and 659-682 (June).

4. Hardin, B. O. and Richart, F. E., Jr. (1963) — "Elastic Wave Velocities in Granular Soils" — To be published in the *Journal of the Soil Mechanics and Foundations Division, ASCE,* Spring, 1963.

5. Wilson, S. D. and Sibley, E. A. (1962) — "Ground Displacements from Air-Blast Loading" — *Journal of the Soil Mechanics and Foundations Division, ASCE,* December, 1962, pp. 1-31.

6. Hall, J. R., Jr. (1962) — "Effect of Amplitude on Damping and Wave Propagation in Granular Materials" — PhD Dissertation, University of Florida, August, 1962.

EQUIPAMENTO E TÉCNICA REFERENTES AOS ENSAIOS TRIAXIAIS. CONJUNTO DE RESULTADOS OBTIDOS COM AMOSTRAS DE SOLOS RESIDUAIS

HANS U. SCHERRER e PERSIVAL A. BRITTO
Engenheiros da Rodio S/A.

SUMÁRIO

Êste trabalho apresenta uma descrição do equipamento para ensaios triaxiais instalado no Laboratório de Mecânica dos Solos da Rodio S/A., do qual algumas partes foram construídas de conformidade com o equipamento usado no Instituto Geotécnico da Noruega.

Apresenta-se também uma descrição sucinta da técnica de ensaios, que, em princípio, se baseia na mesma técnica adotada naquele Instituto.

O trabalho está ilustrado com várias fotografias e com um conjunto típico de resultados de ensaios relacionando as características de diferentes tipos de solos residuais.

SUMMARY

This paper describes the triaxial equipment used at the Rodio S/A. Soil Mechanics Laboratory. Some parts were built similar to those used at the Norwegian Geotechnical Institute. A brief description of tests procedure which in general follows Norwegian technique, is also included herein.

The paper is illustrated with some photographs and a seletion of typical test results obtained from different types of residual soils.

I. INTRODUÇÃO

Extraordinário progresso vem se registrando nos últimos anos no campo da pesquisa de resistência ao cisalhamento de solos. O desenvolvimento diz respeito não só à técnica de ensaios como também à de interpretação dos resultados.

Muitos dos conceitos emitidos bem como muitos métodos de ensaios propostos são tão recentes que não estão ainda bastante difundidos. Ocorre até que a validade de algumas hipóteses mostra-se ainda na dependência de confirmação por um maior número de experiências que aquelas executadas até o presente.

Decorre não existir ainda uma padronização para os ensaios de resistência ao cisalhamento, exceto para aquêles mais simples, que seja seguida por diferentes Laboratórios de Mecânica dos Solos.

O Instituto Geotécnico da Noruega destaca-se por suas notáveis contribuições, tendo desenvolvido vários métodos de ensaios e introduzido vários aperfeiçoamentos no equipamento.

O equipamento descrito neste artigo foi construído em base dos que usam no Instituto Geotécnico da Noruega, sendo mesmo semelhantes algumas partes. Os métodos de ensaios que se vêm seguindo são também baseados nos que se adotam no citado Instituto.

Já têm sido pesquisadas as características de resistência ao cisalhamento de solos residuais, a serem utilizados na constituição do maciço de diversas barragens no Brasil. A seleção dos resultados apresentada ilustra a técnica de ensaios e relaciona estas características.

II. DESCRIÇÃO DO EQUIPAMENTO

Foi êle construído com recursos nacionais. Trata-se de um equipamento do tipo de deformação controlada ("strain-controlled"), isto é, que permite aplicar-se uma velocidade constante de deformação à amostra, enquanto é medida a resistência oferecida por ela contra essa deformação.

Está preparado para realizar ensaios com amostras de 10 até 50 cm^2 de seção transversal.

Consiste de uma prensa para compressão triaxial, 6 células ou câmaras com sistema para consolidação e saturação de 6 amostras simultâneamente e dispositivo para medição de pressões neutras. Êste conjunto revela-se com uma proporção equilibrada entre as diversas partes, permitindo um perfeito entrosamento nos trabalhos de ensaio.

CÉLULA OU CÂMARA

Por intermédio da célula pode-se aplicar uma pressão confinante à amostra e ao mesmo tempo comprimi-la axialmente. Cada célula (Fig. 1), consiste fundamentalmente de duas bases, um cilindro de "plexiglass" e hastes rosqueadas e porcas para a montagem do conjunto.

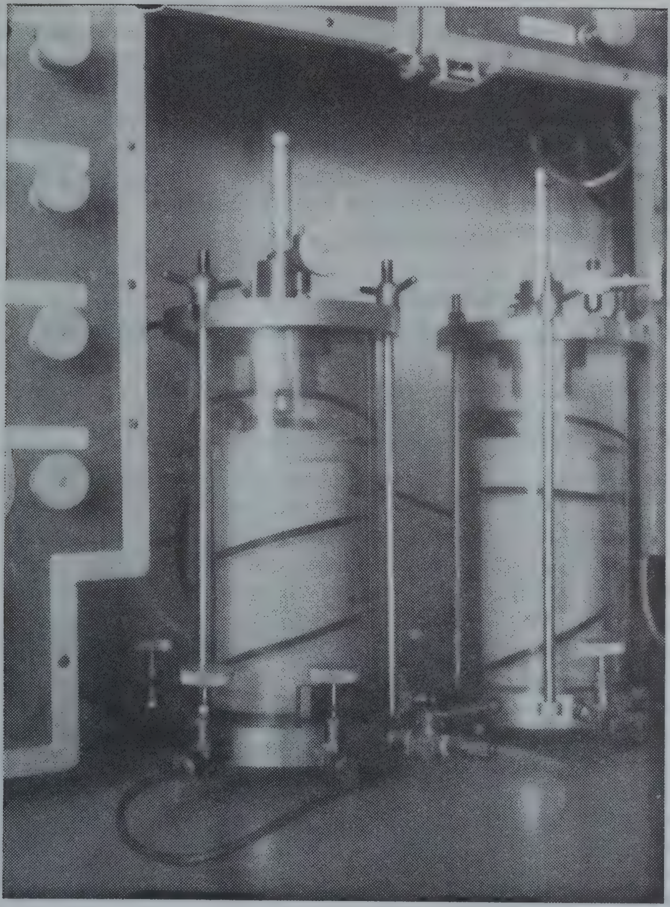

Fig. 1 — Célula triaxial para amostras de seção transversal de 10 até 50 cm².

Fig. 1 — The triaxial cell for sample cross section of 10 to 50 cm².

Na base inferior de cada célula são instaladas quatro válvulas, três delas para ligação com o interior do corpo de prova (duas pela parte inferior e uma pela superior), e a restante para ligação com o interior da câmara.

As três válvulas ligando-se com o interior do corpo de prova mostram-se em número adequado para permitir a remoção das bôlhas de ar nos tubos de ligação ou mesmo na pedra porosa, as quais iriam contribuir para medidas incorretas de pressão intersticial.

A base superior de cada célula é dotada de uma bucha de bronze e respectivo pistão e de uma válvula para comunicação com o interior da célula. As buchas contêm um pequeno reservatório destinado a receber óleo, durante o ensaio, a uma pressão ligeiramente superior àquela que se aplica no interior da câmara. Desta forma, além de se lubrificar o pistão, o que elimina quase que completamente a possibilidade de atrito, evitam-se os vazamentos, aproveitando-se da maior viscosidade do óleo.

A superfície de contacto entre bucha e pistão foi feita propositadamente bastante reduzida, para diminuir a possibilidade de atrito independentemente de lubrificação.

SISTEMA PARA SATURAÇÃO E ADENSAMENTO

O equipamento está dotado de um sistema para a consolidação (inclusive saturação) de seis amostras simultâneamente. Para cada amostra dispõe de um painel por onde se exerce o contrôle das pressões e por meio do qual se registram as variações de volume que a amostra pode apresentar. Os painéis são vistos na Fig. 2. Em essência se resume num dispositivo que permite aplicar água sob pressão no interior e em volta da amostra e registrar variações

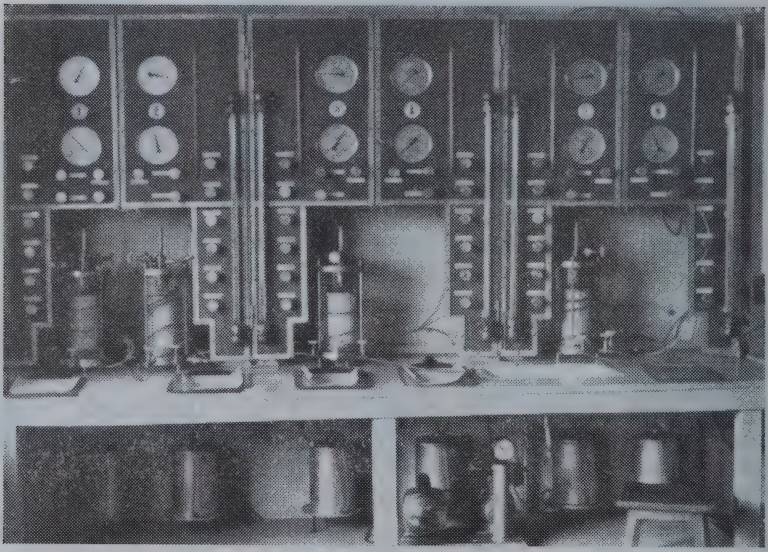

Fig. 2 — Painéis para o contrôle do adensamento e saturação dos corpos de prova.

Fig. 2 — Control panels for saturation and consolidation of the specimen.

de volume. A aplicação das pressões é feita por meio de reservatórios contendo água e ar comprimido.

No equipamento estão instaladas válvulas, manômetros, indicadores de nível, etc., em número suficiente a permitir o processamento rápido e simples das várias fases dos trabalhos tais como enchimento e esvaziamento dos reservatórios, aplicação das pressões, etc.

PRENSA PARA A COMPRESSÃO TRIAXIAL

É a parte do aparelho onde as amostras são levadas à ruptura. A caixa de engrenagem existente permite transformar-se a rotação de um motor elétrico num movimento linear uniforme do prato. Êste movimento uniforme é diretamente transmitido à amostra, cuja resistência é observada por um anel dinamômetro prêso a um sistema rígido.

A capacidade da prensa, que é vista na Fig. 3, é de 5.000 kg. São disponíveis vários anéis dinamométricos para atender a diferentes faixas de esforços conforme a pressão na câmara, tipo de material e seção do corpo de prova.

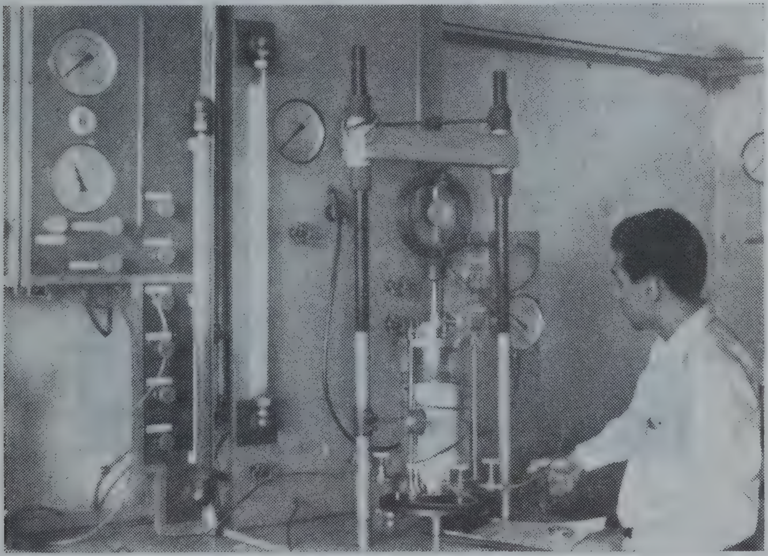

Fig. 3 — Prensa para a realização dos ensaios triaxiais.

Fig. 3 — Loading system for triaxial compression tests.

Os anéis dinamométricos são equipados com defletômetros de precisão de 0,001 mm. Para medida da deformação da amostra ou do deslocamento do prato, o defletômetro que se emprega tem precisão de 0,01 mm.

O painel da prensa se destina ao contrôle da pressão de confinamento durante o ensaio e contém também um dispositivo para medir a variação de volume da amostra, mediante a água da câmara.

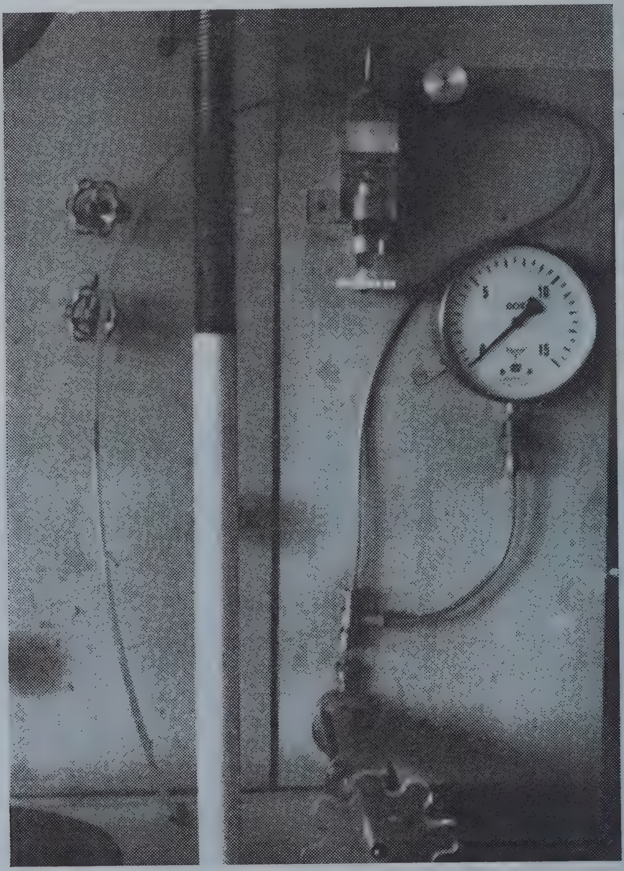

Fig. 4 — Dispositivo para a medida das pressões intersticiais.

Fig. 4 — Pore pressure measuring device.

DISPOSITIVO PARA MEDIÇÃO DAS PRESSÕES INTERSTICIAIS

O dispositivo para a medição das pressões intersticiais, visto na Fig. 4, foi construído nos moldes dos que se utilizam no Instituto Geotécnico da Noruega. Consta em princípio de um tubo em U contendo mercúrio, sendo um ramo diretamente ligado ao interior da amostra, por meio de um tubo cheio de água (tubo "Saran"), e o outro ramo, ligado a um reservatório de água de forma cilíndrica contendo um pistão com deslocabilidade controlada. Êste reservatório é ligado a um manômetro para a medida da pressão da água contida em seu interior.

As variações da pressão intersticial na amostra tendem a modificar as posições dos níveis de mercúrio nos dois ramos do tubo em U, dos quais a parte inferior é de diâmetro bastante pequeno (∾1,2 mm), de modo a permitir uma grande sensibilidade do aparelho. Esta mudança de níveis será evitada aplicando-se à água no reservatório cilíndrico, mediante um determinado deslocamento do êmbolo, uma pressão idêntica à pressão intersticial, que é observada diretamente no manômetro.

O tubo ("Saran") que se liga com o interior da amostra pràticamente não se dilata com o aumento da pressão interior e, sendo o tubo em U contido no interior de uma placa de "plexiglass", material também indeformável, as pressões neutras podem ser medidas sem que ocorra drenagem na amostra, o que é uma condição fundamental para que as pressões medidas sejam representativas.

O nível de mercúrio nos dois ramos pode ser levantado e abaixado usando-se o parafuso que regula o volume do pequeno reservatório situado imediatamente abaixo.

A parte superior de cada ramo do tubo em U, sendo de diâmetro maior que o da parte inferior, impede que o mercúrio, por qualquer motivo, saia com facilidade do seu interior.

III. PREPARAÇÃO DOS CORPOS DE PROVA

No caso de amostras indeformadas, normalmente é necessário cortá-las de tal modo a que fiquem com as dimensões adequadas para os ensaios.

Quando as amostras indeformadas são retiradas por meio do "Shelby Tube", na maioria das vêzes já têm seção transversal adequada, não sendo necessário o trabalho de preparação.

No caso de amostras compactadas, os corpos de prova são preparados (compactados) em cilindros especiais como o que é visto na Fig. 5.

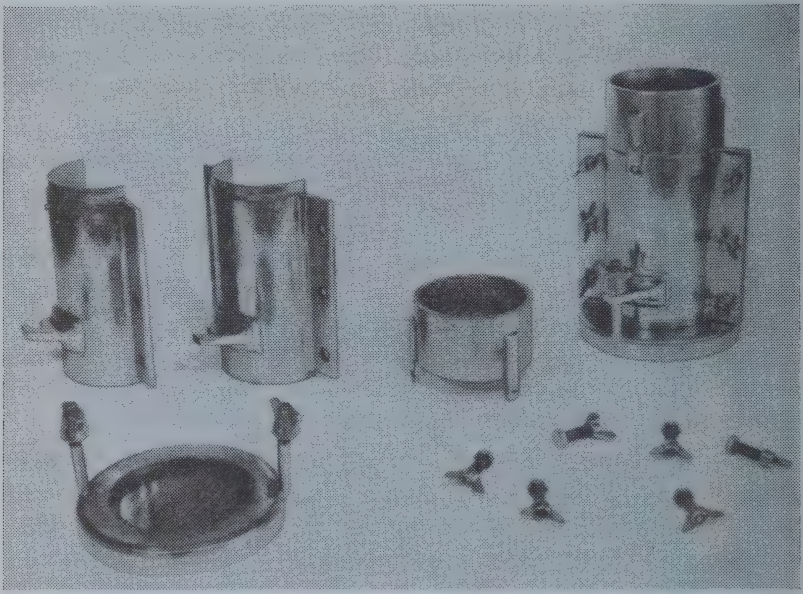

Fig. 5 — Cilindro desmontável para a preparação de amostras compactadas de 50 cm² de seção transversal.

Fig. 5 — Split mould for the preparation of 50 cm² cross section compacted samples.

O cilindro sendo desmontável facilita a remoção dos corpos de prova, que já saem com as dimensões apropriadas para os ensaios. Para a compactação usa-se aparelho semi-automático em que o pêso do martelo, a altura da queda e o número de golpes podem variar em função da energia que se quiser aplicar para permitir obter diferentes graus de compactação.

IV. TÉCNICA DOS ENSAIOS

Os ensaios a que se recorre com maior freqüência nos trabalhos de pesquisa de resistência ao cisalhamento são os ensaios rápidos, rápidos com pré-adensamento dos corpos de prova e lentos.

Os dois primeiros tipos de ensaio podem se processar com ou sem medição da pressão intersticial.

ENSAIOS RÁPIDOS

Nos ensaios rápidos sem medição de pressão neutra os corpos de prova são colocados no interior da câmara deixando-se suas extremidades em contacto com placas impermeáveis. Depois de convenientemente envolvidos pela membrana de borracha, enche-se a célula de água, sendo em seguida transportada para a prensa. A pressão no interior da câmara é elevada para o valor desejado, e, levantando-se o prato da prensa por meio de dispositivo manual, coloca-se o pistão em contacto, na extremidade inferior, com o tôpo da amostra, e, na outra extremidade, com o anel dinamométrico.

Depois de seguidos os passos acima, dá-se partida no motor. A célula passa a se deslocar para cima e em conseqüência a amostra vai se deformando. Durante os ensaios são feitas, segundo intervalos de tempo determinados, as leituras de interêsse para a avaliação dos resultados, tais como deformação da amostra, deformação do anel, variação de volume no interior da câmara, etc.

Com referência aos ensaios rápidos com medidas de pressão intersticial, em lugar de placas impermeáveis em contato com as extremidades dos corpos de prova, usam-se pedras porosas ou pedras cerâmicas que devem ser cuidadosamente saturadas. Para a saturação de tais pedras, deve-se imergi-las, por algum tempo, em água fervente e, depois de postas em contato com a amostra e de esta ter sido envolvida pela membrana de borracha, deve-se fazer percolar por elas certa quantidade de água. Usam-se pedras porosas quando se trata de amostras completamente saturadas e pedras cerâmicas no caso de parcialmente saturadas. Neste último caso recorre-se a pedras cerâmicas para impedir que o ar contido no interior do corpo de prova ocasione medidas incorretas da pressão intersticial.

É prática recomendável interpor, entre o corpo de prova e a membrana de borracha, tiras de papel filtro, para que funcionem como drenos laterais.

A seguir, enche-se a câmara de água e estabelece-se ligação com o dispositivo para medir pressão intersticial. Eleva-se a pressão confinante até o valor desejado e, sem permitir a drenagem, deixa-se a amostra sob esta condição até que a pressão intersticial atinja um valor constante. Finalmente a amostra é levada à prensa para ser comprimida axialmente, o que se deve processar da maneira já descrita, mas, desta vez fazendo-se o registro das pressões intersticiais. A duração desta fase depende do tipo de material. Em solos argilosos com baixa permeabilidade, recomenda-se um tempo mínimo de 6 a 8 horas, de tal forma a que a pressão intersticial medida represente corretamente aquela desenvolvida na zona de ruptura.

ENSAIOS RÁPIDOS COM PRÉ-ADENSAMENTO

A colocação do corpo de prova no interior da câmara se processa da mesma maneira como para os ensaios rápidos com medida de pressão intersticial.

Depois de se encher a câmara de água e de se fazer a ligação com o sistema para aplicação de pressão confinante e de contrapressão, eleva-se a primeira até um valor um pouco abaixo da pressão prevista para o pré-adensamento, e aplica-se, na extremidade inferior do corpo de prova, uma contrapressão que, por sua vez, deve ser um pouco inferior à pressão de confinamento, enquanto a outra extremidade é mantida em contato com a pressão atmosférica. Assim obtém-se a percolação de água segundo um determinado gradiente. Nesta fase o que se procura é a saturação da amostra. A pressão confinante deve ser inferior à de pré-adensamento para evitar que a extremidade superior do corpo de prova se consolide a uma pressão mais elevada que a prevista, principalmente pelo fato de que se usa aplicar vácuo a esta extremidade, repetidas vêzes, para acelerar a saturação. O aparecimento de gôtas d'água no tubo ligado à extremidade superior do corpo de prova indica ter sido atingida a saturação.

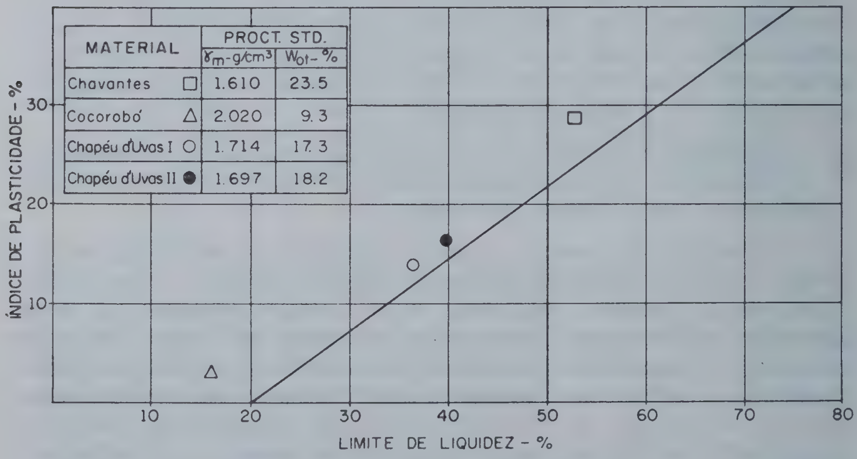

MATERIAL	PROCT. STD.	
	γ_m - g/cm³	W_{ot} - %
Chavantes □	1.610	23.5
Cocorobó △	2.020	9.3
Chapéu d'Uvas I ○	1.714	17.3
Chapéu d'Uvas II ●	1.697	18.2

Fig. 6 — Gráfico de plasticidade.

Fig. 6 — Plasticity chart.

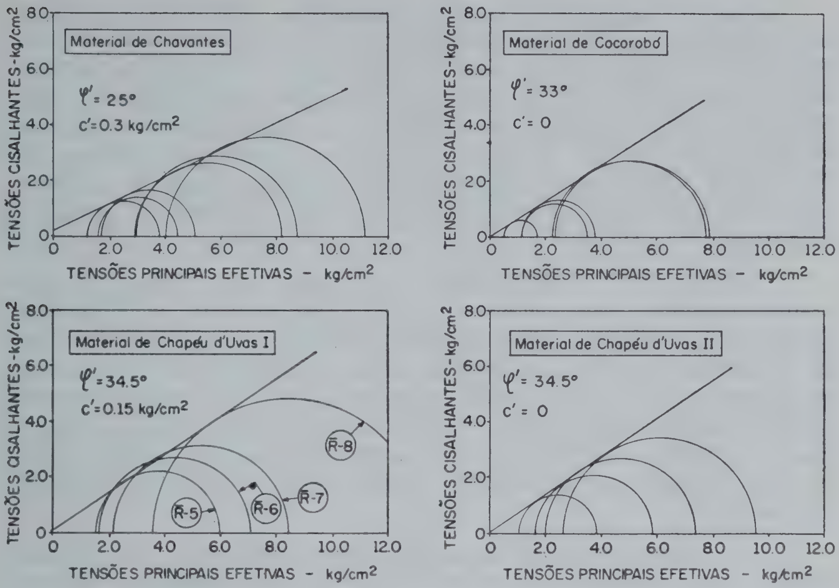

Fig. 7 — Gráficos de Mohr, em têrmos de tensões efetivas, obtidos de ensaios rápidos com pré-adensamento realizados com quatro amostras de solos residuais.

Fig. 7 — Mohr's effective stress circles. Consolidated undrained tests on four residual soil samples.

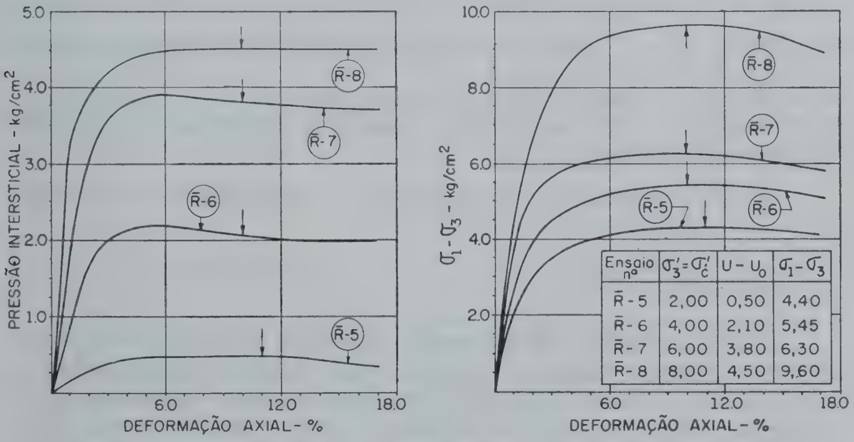

Ensaio nº	$\sigma_3' = \sigma_c'$	$U - U_o$	$\sigma_1 - \sigma_3$
R̄ - 5	2,00	0,50	4,40
R̄ - 6	4,00	2,10	5,45
R̄ - 7	6,00	3,80	6,30
R̄ - 8	8,00	4,50	9,60

Fig. 8 — Curvas tensão-deformação e de variação da pressão neutra referentes aos ensaios rápidos com pré-adensamento realizados com a amostra de Chapéu d'Uvas I.

Fig. 8 — Consolidated undrained test on the Chapéu d'Uvas I material. Deviator stress and pore pressure plotted against strain.

Uma vez saturado o corpo de prova, passa-se à fase de adensamento. Deixa-se uniformizar a pressão nos poros, que nesta altura pode assumir um valor diferente daquele adotado na saturação, e, em seguida, ajusta-se a pressão confinante a um valor tal que forneça a pressão efetiva de consolidação prevista. O corpo de prova permanece nessa situação até cessarem as variações de volume, o que se observa por meio do medidor de volume de que o painel de contrôle é dotado.

Terminado o adensamento, a célula, com tôdas as válvulas fechadas para a preservação das pressões, é transportada para a prensa. Estabelece-se, nesta altura, ligação com o respectivo painel e também com o dispositivo de medida de pressão intersticial. As pressões a que o corpo de prova estava submetido durante o adensamento continuam mantidas. A partir de então, seguem-se os mesmos passos como se se tratasse de um ensaio rápido com medida de pressão intersticial.

A duração de cada uma das fases acima depende muito do tipo de material. Quanto mais argiloso maior o tempo necessário para a saturação, adensamento e ruptura.

Às vêzes, o procedimento descrito nos parágrafos anteriores é alterado de tal modo a se submeter a amostra às mesmas condições que existirão "in situ". Por exemplo, na fase de consolidação usa-se aplicar uma pressão axial, além da de confinamento, correspondendo a um determinado valor de razão $\frac{\sigma_1}{\sigma_3}$. Isto é o que constitui o pré-adensamento anisotrópico. Também as pressões usadas nos ensaios devem se aproximar o máximo possível daquelas envolvidas no caso em estudo.

O que se procura, em princípio, é reproduzir no laboratório as condições "in situ".

ENSAIOS LENTOS

Nestes ensaios, submete-se a amostra à consolidação da mesma maneira como no ensaio rápido com pré-adensamento, não sendo costume, todavia, fazer-se uso da contrapressão. Pode-se, antes, proceder à saturação do corpo de prova, isto se se quiser saber da sua influência sôbre os parâmetros da resistência ao cisalhamento.

Concluída a consolidação a célula é levada para a prensa. A mesma pressão confinante passa então a ser aplicada por intermédio do respectivo painel, e dá-se, em seguida, início à deformação axial, deixando-se livre a drenagem da amostra. O tempo de duração desta fase deve ser suficientemente longo para permitir a dissipação contínua da pressão intersticial. Quanto mais argiloso maior o tempo necessário. A velocidade de deformação geralmente adotada é da ordem de 0,05 até 0,1% por hora, o que corresponde a um total de 6 a 12 dias para a ruptura. Durante todo êste tempo, o motor da prensa permanece em funcionamento, expondo-se a uma avaria, o que constitui, de certa forma, um inconveniente.

Altura dos corpos de prova antes do adensamento........ ....16.0 cm
Seção média dos corpos de prova antes do adensamento..........................50.0 cm^2

Nº DO ENSAIO	$\bar{R}$ - 5	$\bar{R}$ - 6	$\bar{R}$ - 7	$\bar{R}$ - 8
Altura do corpo de prova depois do adens.– cm.	15,89	15,85	15,78	15,68
Altura depois do ensaio – cm	12,05	11,94	11,98	11,92
Seção média depois do adensamento - cm^2	49,20	49,10	48,60	48,00
Seção média depois do ensaio - cm^2	65,00	65,20	64,00	63,20
Pêso esp. sêco antes do adensamento - g/cm^3	1,684	1,692	1,680	1,700
Pêso esp. sêco depois do ensaio - g/cm^3	1,720	1,740	1,750	1,807
Grau de compactação antes do ensaio - %	98,3	98,6	98,0	99,1
Umidade antes do adensamento – %	16,3	17,0	17,5	17,0
Umidade depois do ensaio – %	21,4	20,7	18,6	18,2
Índice de vazios antes do adensamento	0,614	0,610	0,620	0,600
Índice de vazios depois do ensaio	0,580	0,563	0,505	0,505
Saturação antes do adensamento – %	72,3	75,8	76,8	77,0
Saturação depois do ensaio – %	99,5	100,0	99,0	98,0
Pressão efetiva de cons. ($\sigma'_c = \sigma'_3$) - kg/cm^2	2,00	4,00	6,00	8,00
Velocidade de deformação – % hora	4,03	3,96	3,86	4,00
Deformação na rutura – %	11,0	10,0	10,0	10,0
$\sigma_1 - \sigma_3$ na rutura – kg/cm^2	4,40	5,45	6,30	9,60
Pressão neutra na rutura - kg/cm^2	0,50	2,10	3,80	4,50

Fig. 9 — Principais dados dos ensaios rápidos com pré-adensamento realizados com a amostra de Chapéu d'Uvas I.

Fig. 9 — Principal data from the consolidated undrained tests carried out on the Chapéu d'Uvas I material.

Para a realização de ensaios lentos, os autores recorrem a equipamento de tensão controlada ("stress-controlled") que não oferece êsse inconveniente. Neste tipo de equipamento, em vez de se aplicar uma determinada velocidade de deformação à amostra, a pressão axial é que assume acréscimos determinados em função do tempo. No mais é idêntico ao que vem sendo descrito. O seu funcionamento se faz sem o recurso de um motor elétrico, mas com um sistema de alavancas e pesos. Para a realização dos ensaios lentos aplicam-se acréscimos na tensão axial segundo intervalos de tempo suficientemente longos, de modo a permitir a dissipação da pressão neutra.

Os ensaios empregados na técnica de pesquisa de resistência ao cisalhamento são aquêles vistos em linhas gerais nos parágrafos anteriores. Em pesquisas mais detalhadas recorre-se a ensaios especiais, tais como: ensaios lentos (com drenagem) com σ_1 constante e σ_3 decrescente, ensaios em que a ruptura é causada pelo aumento da pressão intersticial, ensaios para determinação do coeficiente de pressão intersticial $\overline{B}$ sob várias condições, ensaios com pré-adensamento anisotrópico, etc. Êstes ensaios especiais visam a reproduzir no laboratório, mais fielmente, as condições de campo, e são realizados quando a investigação se estende a particularidades que não são consideradas nos problemas gerais.

V. RESULTADOS DE ENSAIOS COM AMOSTRAS DE SOLOS RESIDUAIS

Das investigações de laboratório levadas a efeito com solos residuais a serem empregados na construção dos maciços de algumas barragens no interior do país, foram selecionados os resultados a seguir, que se constituem em resultados típicos de uma série extensa e que ilustram a técnica de ensaios e permitem um confronto das características de resistência ao cisalhamento de solos residuais, classificados em diferentes tipos de acôrdo com o gráfico de plasticidade (Fig. 6).

Êstes resultados referem-se a amostras de zonas de empréstimo para a construção da barragem de Chavantes, que terá uma altura de 90 m, Cocorobó e Chapéu d'Uvas *, respectivamente nos Estados de São Paulo, Bahia e Minas Gerais.

Na Fig. 6 apresenta-se o gráfico de plasticidade relativo às quatro amostras escolhidas, onde figuram também os valôres do pêso específico sêco máximo e teor de umidade ótimo obtidos em ensaios de compactação Proctor Standard.

---

* Os resultados das investigações para a Barragem de Chapéu d'Uvas foram também utilizados pelo Eng. Otto Pfafstetter em seu trabalho apresentado neste Congresso.

Os gráficos de Mohr vistos na Fig. 7 definem os parâmetros de resistência ao cisalhamento das quatro amostras, em têrmos de tensões efetivas, e foram obtidos de ensaios rápidos com pré-adensamento e medida de pressão intersticial. Nas Figs. 8 e 9, apresentadas como exemplo, vêem-se respectivamente as características dos diversos corpos de prova da Amostra de Chapéu d'Uvas e as correspondentes curvas tensão-deformação e de variação da pressão neutra.

Os gráficos de Mohr da Fig. 10 dizem respeito a ensaios rápidos e lentos com uma amostra de Chapéu d'Uvas. No gráfico referente aos ensaios lentos vê-se a envoltória em têrmos de tensões efetivas, que fôra determinada também por meio de ensaios rápidos com medida de pressão intersticial (Fig. 7). No outro gráfico mostra-se a envoltória em têrmos de tensões totais, definidora da resistência ao cisalhamento para um determinado grau de saturação e teor de umidade do material.

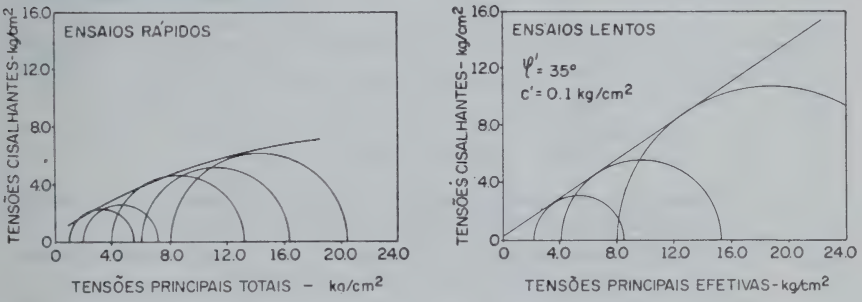

Fig. 10 — Gráficos de Mohr referentes aos ensaios rápidos e lentos com a amostra de Chapéu d'Uvas I.

Fig. 10 — Mohr's graphs obtained from undrained and drained tests on the Chapéu d'Uvas I sample.

Nas investigações para Chavantes, como um dos processos usados para a avaliação das pressões neutras desenvolvidas no caso de logo após a construção e em função do teor de umidade de colocação recorreu-se a gráficos do tipo que é visto na Fig. 11.

Neste gráfico são traçadas várias envoltórias obtidas em uma série extensa de ensaios triaxiais.

A envoltória em têrmos de tensões efetivas foi obtida em ensaios rápidos com pré-adensamento e medidas de pressões intersticiais. As outras envoltórias, aquelas em têrmos de tensões totais, foram obtidas de ensaios rápidos com corpos de prova possuindo diferentes teores de umidade de compactação. No gráfico está esquematizada a correlação entre pressão total, intersticial e efetiva.

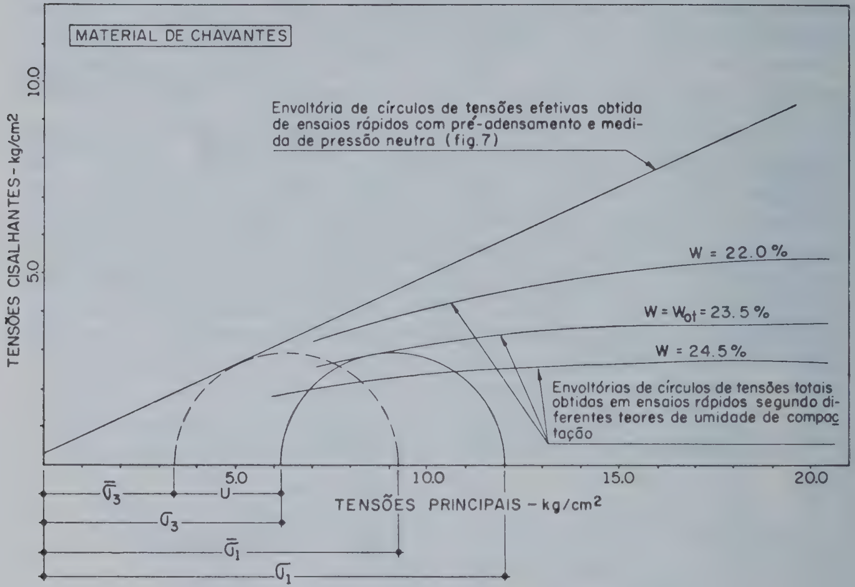

Fig. 11 — Resultados de ensaios triaxiais para a Barragem de Chavantes. Relações entre as pressões totais, neutras e efetivas.

Fig. 11 — Triaxial tests results for Chavantes Dam. Relationship between total, effective and pore pressures.

AGRADECIMENTOS

Os autores agradecem aos funcionários do Laboratório pela valiosa colaboração e, de forma especial, à Diretoria da Rodio S.A. pelo apoio e encorajamento dados.

BIBLIOGRAFIA

1. Andresen, A., Bjerrum, L., Di Biagio, E. e Kjaernsli, B. (1957) — "Triaxial Equipment developed at the Norwegian Geotechnical Institute", Norwegian Geotechnical Institute Publ. 21.

2. Andresen, A. e Simons, N. E. (1960) — "Norwegian Triaxial Equipment and Technique", Norwegian Geotechnical Institute Publ. No. 35.

3. Bishop, A. W. (1954) — "The Use of Pore Pressure Coefficients in Practice", Géotechnique, 4:148-152.

4. Bishop, A. W. e Henkel, D. J. (1962) — "The Measurement of Soil Properties in the Triaxial Test", Edward Arnold, London.

5. Lowe, J. e Johnson, T. C. (1960) — "Use of Back Pressure to increase degree of Saturation of Triaxial Test Specimens", Proc. Research Conf. on Shear Strength of Cohesive Soils, 819-836 (A.S.C.E.).

6. Skempton, A. W. (1954) — "The Pore Pressure Coefficients A and B", Géotechnique, 4:143-147.

LARGE-SCALE TRIAXIAL TESTS ON GRAVELLY SOILS

DANA D. LESLIE

Chief, Geology, Soils, and Materials Branch, Corps of Engineers, South Pacific Division, San Francisco, California, U.S.A.

SYNOPSIS

Large-scale triaxial tests were performed on a wide variety of gravelly soils with both natural and artificial gradings. The specimens were 6 and 12 inches in diameter with maximum particle sizes of 1½ and 3 inches. The tests were the consolidated drained type with lateral pressures as high as 650 psi. The results show the influence or particle size, grading, breakdown of particles, and lateral pressure on the shear strength.

SINOPSIS

Las pruebas triaxiales fueron efectuadas en gran escala en una variedad de terrenos de aluvión gravoso con ambas granulometrias naturales y artificiales. Los ejemplares eran de 1 a 12 pulgadas en diámetro con el tamaño máximo de partículas de 1½ a 3 pulgadas. Las pruebas eran de tipo consolidado drenado con presiones laterales con un máximo de 650 libras por pulgada cuadrada. Los resultados indican la influencia del tamaño de la partícula, granulometria, quebrantamiento de partículas y presión lateral en el esfuerzo cortante. Partículas de tamaño major no afectan el esfuerzo cortante tanto como originalmente se suponía. Dos diferentes terrenos con granulometria idéntica contienen diferentes características de esfuerzos cortantes, esfuerzos y deformaciones, y quebrantamiento de partículas. El quebrantamiento de partículas ocurre bajo consolidación, compatación y cortadura, aumentando con el crecimiento de presión lateral. El esfuerzo cortante disminuye con el aumento de presión lateral.

Se espera que la presentación de estos datos sean estimulo para más investigaciones.

INTRODUCTION

The shear strength of coarse-grained soils and quarried rock is becoming more important to the soils engineer now that earth and rockfill dams are being constructed to much greater heights. Of course, the strength of sands and gravels has always been important in the design of dams, but the lack of large-scale testing equipment has been a deterrent factor in limiting the amount of testing performed.

In 1947, the status of determining the shear strength of cohesionless sands and gravels was summarized in a progress report of the Corps of Engineers [1]. This report recommended values of angle of internal friction for sand varying from 30 to 35 degrees and cited a limited amount of data indicating that values from 30 to 60 degrees had been obtained for gravels. However, it concluded that the data on gravels was too limited for even tentative conclusions and that extensive triaxial research was needed.

With this progress report as a guide, equipment was developed in the Corps of Engineers' South Pacific Division laboratory and tests were performed in 1947 on 6-inch and 8-inch diameter specimens and in 1949 on 12-inch specimens. This equipment was used primarily in connection with the design of earth dams for the Corps of Engineers, but a limited amount of testing was also performed for other government agencies and foreign governments. In 1952, after nearly 200 large-scale triaxial tests had been performed, the author attempted to analyze the accumulated data into a form which would serve as a guide for estimating the strength of gravelly soils, because large-scale equipment was still not generally available. However, after an extensive study, it was concluded that the data did not lend itself to this type of study and some research was required to confirm the trends which were evident. A study of the influence of maximum particle size and the effect of changes in gradation resulting from the removal of oversize particles and their replacement with fines was considered of greatest importance.

Within the past few years, a limited amount of research has been conducted in the South Pacific Division laboratory of maximum particle size, gradation, and removal of oversize particles. Also, additional supporting data have been accumulated with respect to particle breakdown and the influence of high lateral pressures. These data have been obtained from the normal programs of investigation for earth dam projects covering a fairly wide variety of soils tested not only for the Corps of Engineers but also for government agencies and private firms. The material presented in this paper is based on these data and is limited to consolidated-drained (S) triaxial tests primarily on alluvial soils. Recognizing the importance of similar data for angular gravelly soils, research has already been started to obtain data for crushed and quarried rock. In addition, research is in progress on consolidated-undrained (R) tests on alluvial soils.

NOMENCLATURE

The shear strength of each test specimen is expressed as the angle of internal friction. It has been computed from the maximum ratio of principal stresses assuming that the rupture line is straight and passes through the origin. This is more commonly referred to as the apparent angle of internal friction. The density has been expressed as the void ratio at the beginning of the test, after consolidation under the lateral pressure. Ordinarily, it is preferable to express density for cohesionless materials in terms of relative density, but when different maximum densities were obtained for different sizes of equipment, the use of void ratio was considered to be more useful. Volume change is expressed as percent change of the total volume of the specimen at the beginning of the shear test.

MATERIAL TESTED

The gradations of the various soils tested are shown on Figures 1 through 9. All were alluvial soils with subrounded and subangular particles with the exception of Materials 1 and 3. Material 1 was rounded Ottawa sand; Material 3 was a quarried granite. All soils were nonplastic except Materials 6A, 6B, 6C, and 6D which had a plasticity index of 10.

EQUIPMENT

The test specimens were 5.9, 6, and 12 inches in diameter with corresponding heights of 13.8, 12, and 24 inches.

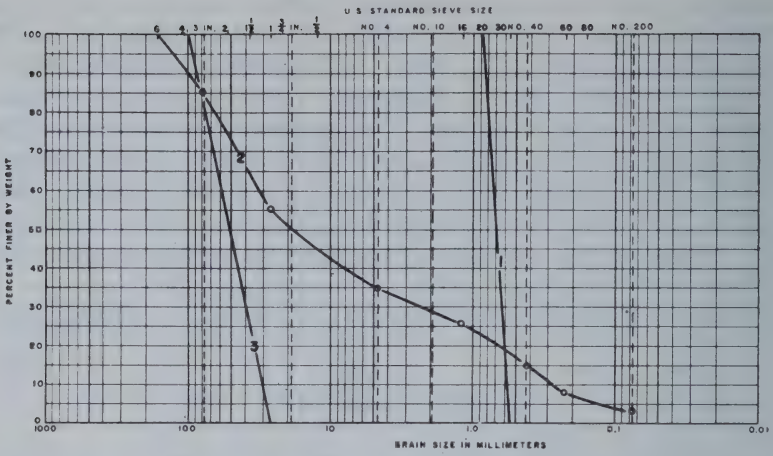

Fig. 1 — Gradation curves of Materials 1, 2, 3.

Fig. 1 — Curvas de granulometría de Materiales 1, 2, 3.

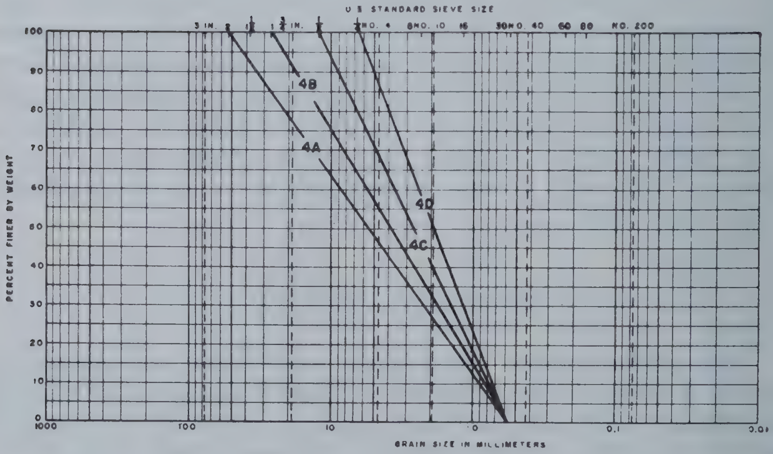

Fig. 2 — Gradation curves of Materials 4A, 4B, 4C, 4D.

Fig. 2 — Curvas de granulometría de Materiales 4A, 4B, 4C, 4D.

In 1959, the height of the 12-inch equipment was increased to 27.6 inches to avoid the influence of possible end effects. The 6-inch and 12-inch apparatus were developed by the South Pacific Division laboratory. The 5.9-inch equipment was developed by a private firm. The equipment and accessories used were essentially the same type described in the 1950 paper [2], except for many improvements added principally to increase the lateral pressure, reduce piston friction, improve piston sealing, and to control the lateral pressure.

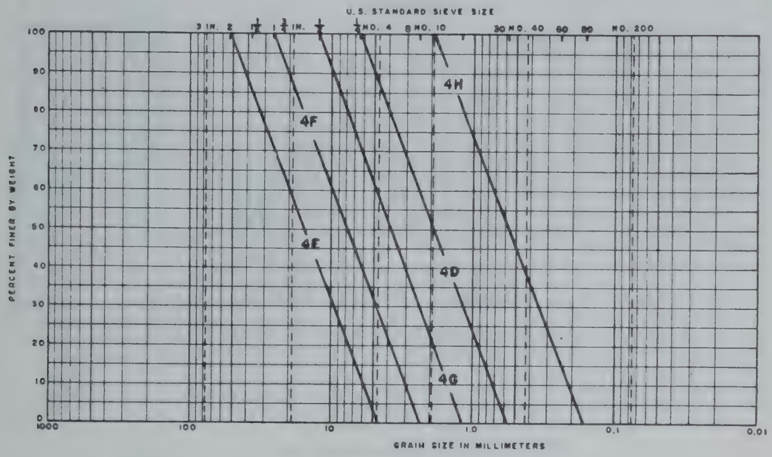

Fig. 3 — Gradation curves of Materials 4D, 4E, 4F, 4G, 4H.

Fig. 3 — Curvas de granulometria de Materiales 4D, 4E, 4F, 4G, 4H.

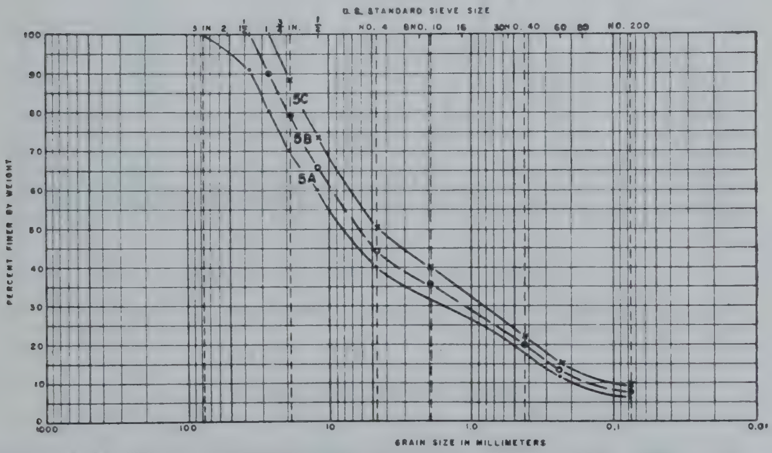

Fig. 4 — Gradation curves of Materials 5A, 5B, 5C.

Fig. 4 — Curvas de granulometria de Materiales 5A, 5B, 5C.

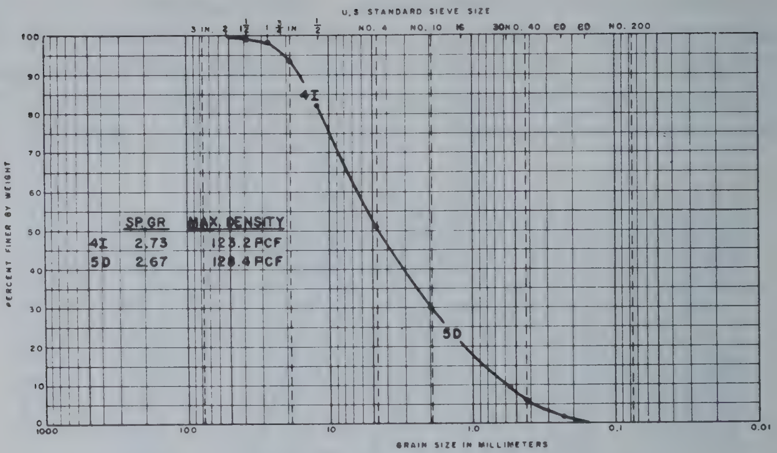

Fig. 5 — Gradation curves of Materials 4I, 5D.

Fig. 5 — Curvas de granulometría de Materiales 4I, 5D.

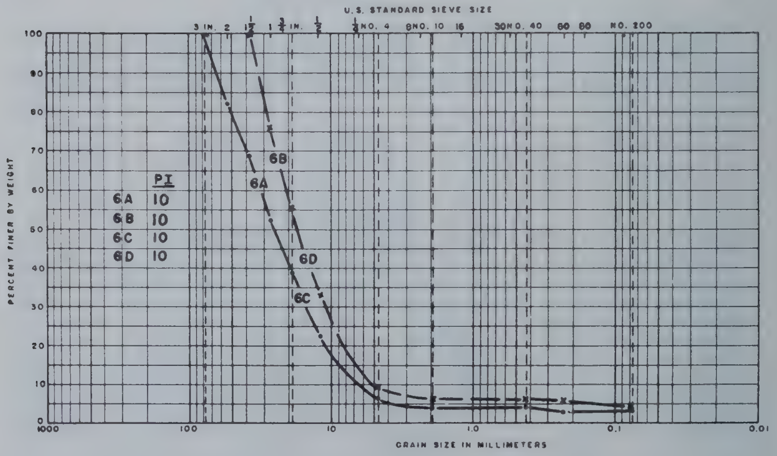

Fig. 6 — Gradation curves of Materials 6A, 6B, 6C, 6D.

Fig. 6 — Curvas de granulometría de Materiales 6A, 6B, 6C, 6D.

TEST PROCEDURE

All tests were the consolidated-drained type (S), with stress applied at a constant rate of strain. Compaction was accomplished either by impact or vibration, and, for some materials, by a combination of both methods. All specimens were saturated. For the research studies, a lateral pressure of 60 psi was used to permit direct comparisons. For other data already available, the lateral pressure varied over a wide range and was as high as 650 psi.

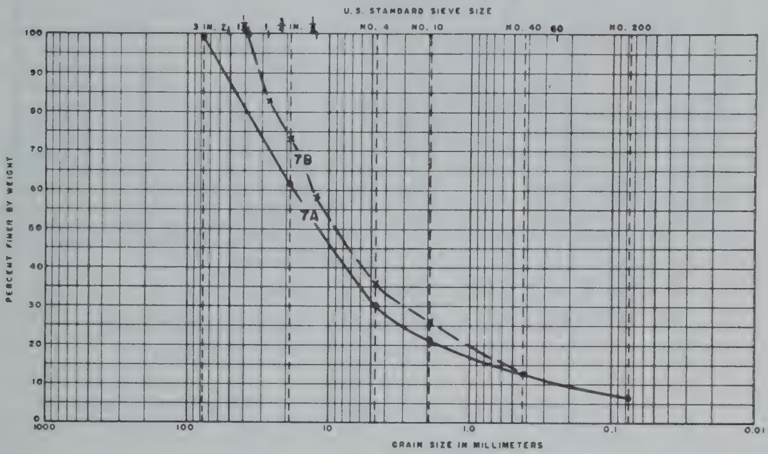

Fig. 7 — Gradation curves of Materials 7A, 7B.

Fig. 7 — Curvas de granulometría de Materiales 7A, 7B.

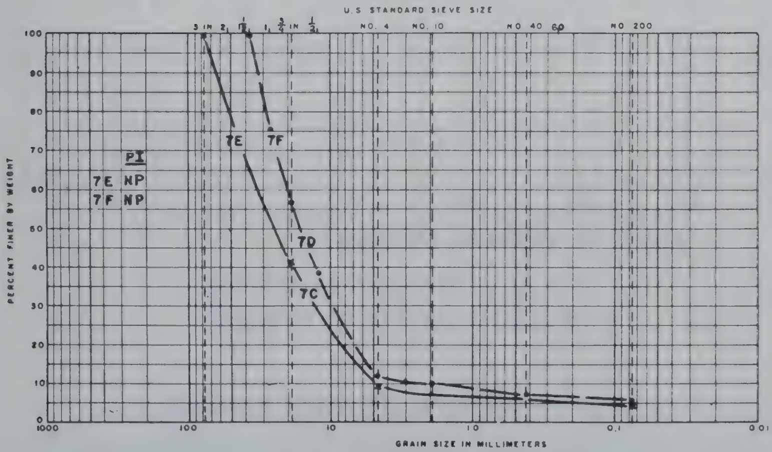

Fig. 8 — Gradation curves of Materials 7C, 7D, 7E, 7F.

Fig. 8 — Curvas de granulometría de Materiales 7C, 7D, 7E, 7F.

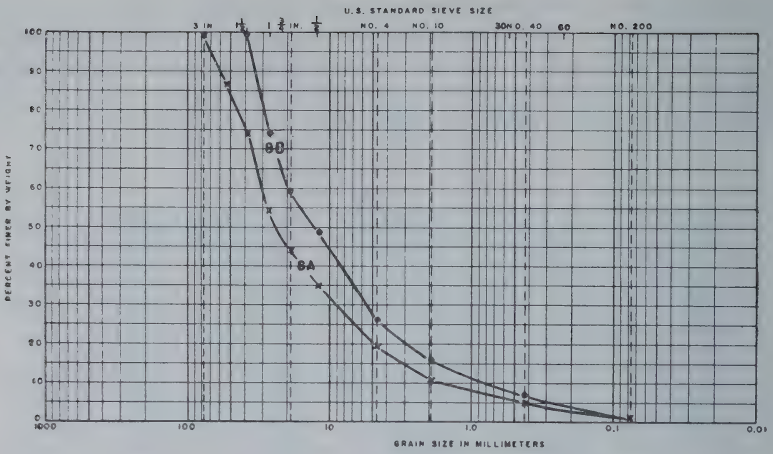

Fig. 9 — Gradation curves of Materials 8A, 8B.

Fig. 9 — Curvas de granulometria de Materiales 8A, 8B.

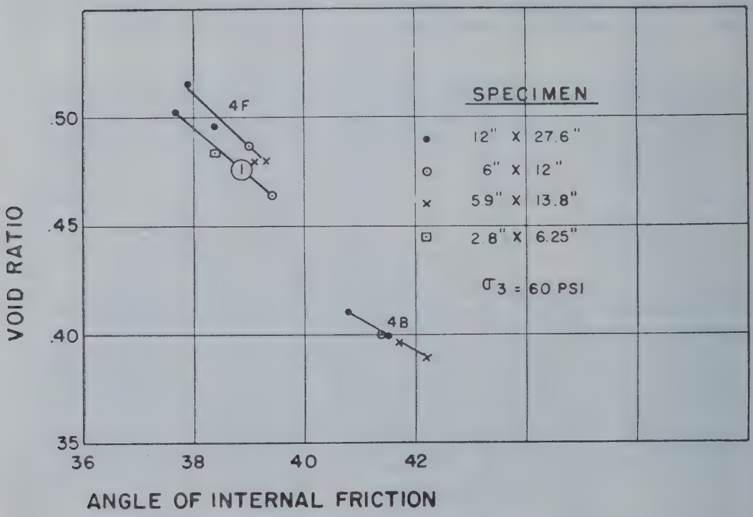

Fig. 10 — Comparison of equipment.

Fig. 10 — Comparación de equipo.

COMPARISON OF EQUIPMENT

One of the necessary steps in any study where different types of testing equipment are involved is to determine how the results compare. Material 1 (Ottawa sand) was selected for this purpose. In addition to the equipment previously described, one test was performed with a diameter of 2.8 inches and a height of 6.25 inches. Each specimen was compacted by vibration to attain the maximum density. The lateral pressure was 60 psi. The triaxial shear results are shown on Figure 10.

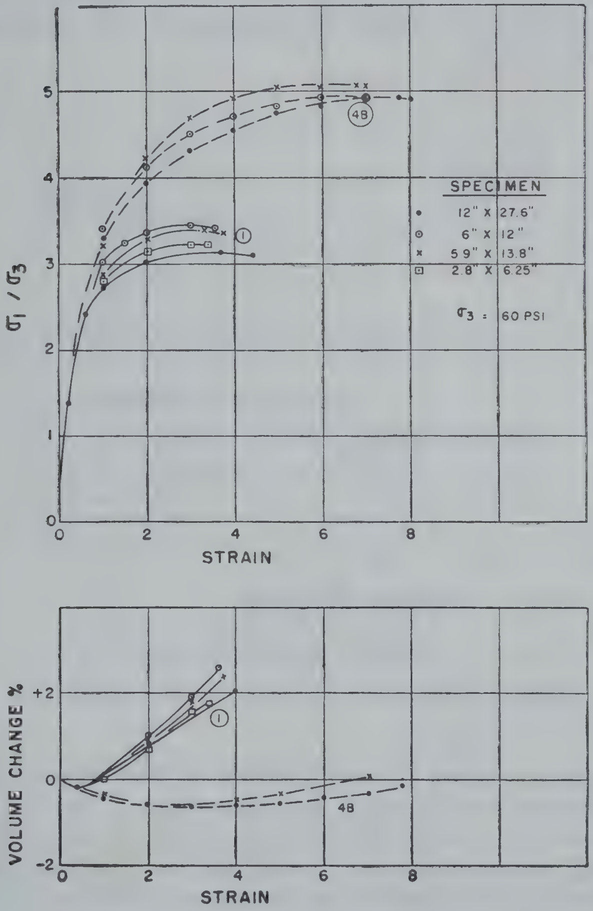

Fig. 11 — Comparison of equipment.

Fig. 11 — Comparación de equipo.

It it evident that a different maximum density was obtained for each specimen diameter, the range being 3 pcf. The highest density was obtained with the 6-inch diameter apparatus. This finding was mainly responsible for selecting the procedure of plotting void ratio, rather than relative density, versus the angle of internal friction. It will be noted that a straight-line relationship between density and the angle of internal friction is indicated, and that very consistent agreement was obtained. Results of tests on materials 4B and 4F are also shown on Figure 10, and a similar trend in consistency of results is evident. Similar consistent trends for different types of equipment are illustrated on Figures 12 and 13.

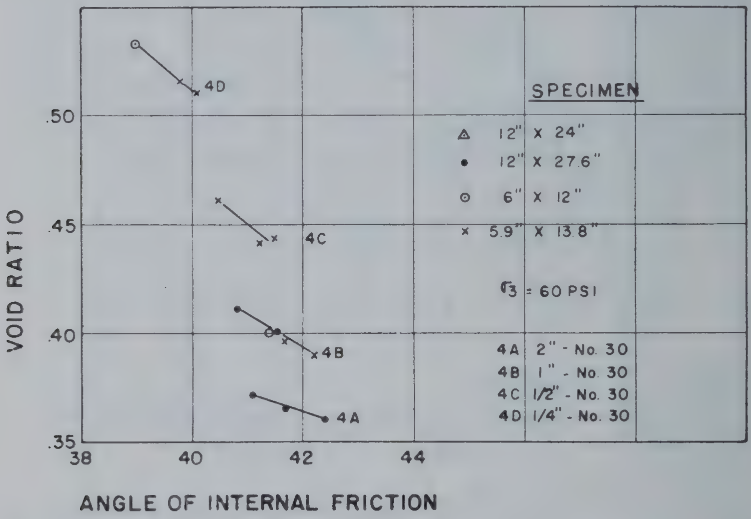

Fig. 12 — Influence of maximum particle size.

Fig. 12 — Influencia del tamaño máximo de partícula.

Figure 11 shows the comparison of the stress-strain and volume-change relationships for Materials 1 and 4B for different types of equipment. It will be noted that the stress-strain and volume-change characteristics are consistent for each material, the more dense specimens reaching their maximum strength at less strain than those less dense and showing more expansion. However, a distinct difference between Materials 1 and 4B is shown in the pattern of the volume change curves. All specimens of Material 1 behaved typically like a dense specimen consolidating slightly at the beginning of shear and then expanding appreciably greater than the original volume, whereas Material 4B consolidated to a much greater degree during the first half of the test then began to expand slowly so that the densest specimen attained its original volume at the end of the test. This difference in behavior will be discussed later.

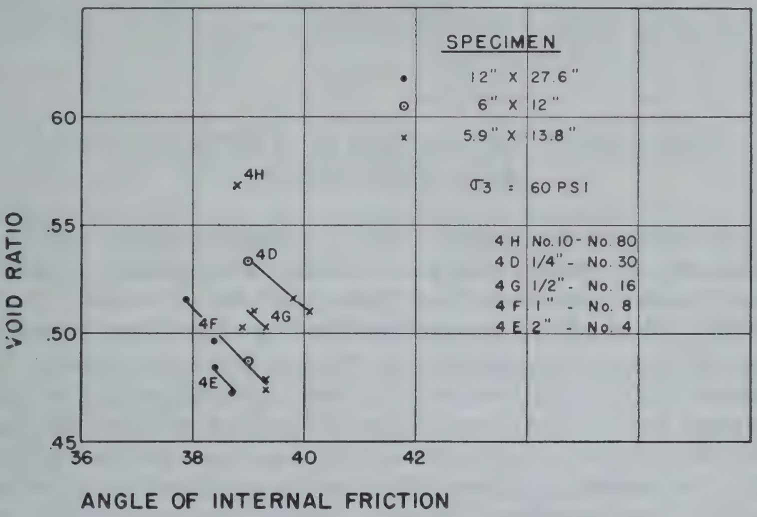

Fig. 13 — Influence of maximum particle size.

Fig. 13 — Influencia del tamaño máximo de partícula.

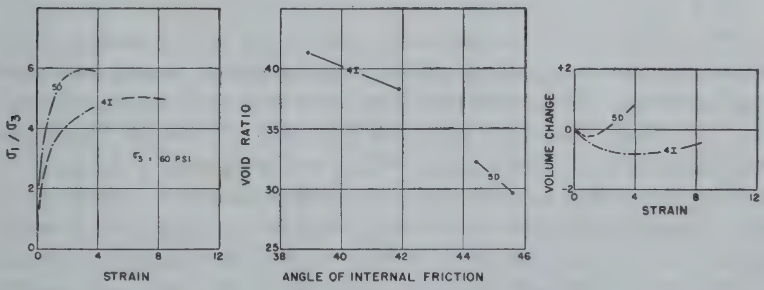

Fig. 14 — Comparison of identical gradations of different materials.

Fig. 14 — Comparación de granulometrías idénticas de diferentes materiales.

It was not the intent of this paper to present the details of the development of the equipment or the careful techniques involved in testing procedure. However, it has been possible to duplicate results with very good precision, as evidenced by the results shown for the comparison of equipment. It can be concluded that the different sizes of equipment showed a very consistent trend for all soils, and, although agreement was not obtained because of the variation in maximum density, agreement at the same density is indicated. There is a need for additional study of the compaction of specimens so as to achieve uniformity.

INFLUENCE OF MAXIMUM PARTICLE SIZE AND GRADATION

A troublesome problem always encountered by soils engineers in the design and construction of dams and embankments where coarse-grained materials are involved is the possible effect of the coarse particles on the shear strength. When it has been necessary to remove oversize particles because of the limitations of the testing equipment, the soils engineer was left to speculate on the effect produced by the removal of the coarse particles and resultant change in grading. The practice followed by various engineering organizations has varied widely. With respect to shear strength, the Corps of Engineers has followed a conservative practice of performing tests on 6-inch and 12-inch specimens containing particles up to 1½ and 3 inches but has not added any allowance for the influence of the coarser fractions omitted from the test.

Of historical interest, but still worthy of serious consideration, are two series of large-scale shear tests conducted in an attempt to determine the strength of coarse, gravelly soils. In 1940, the Los Angeles District, Corps of Engineers, made large-scale direct shear tests on Material 2 (Figure 1) but with particles larger than 3 inches removed. The equipment was the double-shear type, with specimens 12 inches square and 24 inches high. The angle of internal friction obtained from 34 tests varied from 39 to 45 degrees, averaging 42.6 degrees. In 1948, the South Pacific Division laboratory performed vacuum-type triaxial tests on Material 3 (Figure 1), a quarried granite with a maximum size of 4 inches. The specimens were 18 inches in diameter and 37 inches high. For lateral pressures of 4.4, 8.8, and 13.2 psi, angles of internal friction obtained were 47.2, 43.8, and 44.8 degrees. It is considered significant that the results of these tests fall within the same range of data presented in this paper.

As part of a research study to determine the effect of large particles, two series of triaxial tests were performed on artificially graded materials produced from the same parent soil. In the first series, four different materials were produced having straigth-line gradings with maximum sizes of ¼ inch, ½ inch, 1 inch, and 2 inches, with all materials having the identical minimum size of the 30-mesh sieve (Figure 2). The uniformity coefficients of these gradings were 3.3, 4.7, 6.7, and 9.4. The results of the triaxial tests (Figure 12) show that for each grading the angle of internal friction increased with the increase in density. At maximum density the strength increased with the increase in maximum size. It will be noted that the maximum density obtained for each gradation increased with the increase in maximum size. However, the shear strength approached a maximum value of slightly more than 42 degrees at the 1-inch top size.

In the second series of tests, materials having straight-line, parallel gradings were produced resulting in maximum particle sizes of 10-mesh sieve, ¼ inch, ½ inch, 1 inch, and 2 inches (Figure 3). All gradings had a uniformity coefficient of 3.3. The results of the triaxial tests are shown on Figure 13. As found in the first series, there is an increase in angle of internal friction with increase in density for each gradation. Similarly, the maximum density obtained for each gradation increased with maximum size, but reached a maximum value for the 1-inch and 2-inch maximum sizes. At maximum density, the highest strength was obtained for Material 4D, an intermediate gradation having a maximum sixe of ¼ inch, at about 40 degrees. For the 2-inch top size the angle of internal friction was 39 degrees. Consequently, contrary to the first series, this series of tests indicated that the intermediate sizes rather than the large particles had a greater influence on the shear strength.

Results from another series of triaxial tests obtained from data already available on a soil with a natural grading is presented in which the oversize particles were successively removed. The material was first tested with a maximum size of 3 inches, then a series with particles larger than 1½ inches removed, and finally with particles larger than 1 inch removed. This follows the normal procedure of removing oversize particles producing successive changes in grading and an increase in the percentage of fines. The gradations are shown on Figure 4. The results of the triaxial tests are summarized in Table 1, where it is apparent that Material 5B with a maximum size of 1½ inches attained a slightly higher strength than either of the materials with 3-inch and 1-inch maximum sizes.

TABLE 1 — Influence of removal of over-size particles

Material	Max size (in.)	Void ratio	Angle of Internal Friction (degrees)
5A	3	0.233	41.0
5A	3	0.232	40.8
5B	1½	0.234	41.4
5B	1½	0.233	42.2
5C	1	0.266	40.3
5C	1	0.257	41.0

Specimen size: diam. = 12 in., ht. = 24 in.

Lateral pressure: 60 psi.

On the basis of the results of these three series of tests, the findings with respect to the influence of gradation and the effect of removing oversize particles are not conclusive. The first series of tests indicate that the shear strength increased with the increase in uniformity coefficient and density but reached a maximum value at approximately the 1-inch top size. The second series show a greater strength for the ¼-inch top size. The third series show little difference as a result of removing the oversize particles. In conclusion, further studies with a variety of materials are needed to clearly separate the influence of the various factors.

DIFFERENT SOILS HAVING IDENTICAL GRADATION

When Materials 4 and 5 were originally tested, their gradations in nature and the grain shape of both their fine and coarse particles were observed to be similar. In order to study these two materials further, identical gradations were produced artificially having a maximum size of 2 inches and a minimum size of the 80-mesh sieve (Figure 5).

It will be noted that Material 5D with a lower specific gravity attained 5.2 pcf greater maximum density than 4I. Since the gradings were identical, this difference is attributed to particle shape. Gradings were determined before and after testing in order to compare the degree of particle breakdown. Petrographic analyses show that Material 4I was composed largely of graywacke sandstone with lesser quantities of serpentine and diabase and that Material 5D consisted principally of andesite, rhyolite, meta-volcanics, and minor quantities of granite, limestone, and quartzite.

The results of the triaxial tests are shown on Figure 14. There are three significant differences between the two soils: (1) Material 5D had appreciably greater strength; (2) Material 5D expanded during shear whereas 4I consolidated; and (3) Material 5D showed less breakdown of particles than 4I. For the densest condition, Material 5D had an angle of internal friction of 45.6 degrees compared to 41.9 degrees for Material 4I. Material 5D reached its maximum strength at a strain of 3 percent as compared to 7 percent for Material 4I. At maximum strength, Material 5D expanded 0.3 percent as compared to a consolidation of 0.6 percent for Material 4I. Table 2 shows that particle breakdown for Material 5D was 2 percent as compared to 4 percent for Material 4I.

In conclusion, higher density and lesser friability of the igneous rock particles of Material 5D are believed responsible for its superiority over Material 4I, which consisted principally of sedimentary particles.

PARTICLE BREAKDOWN

Undoubtedly, particle breakdown occurs to some degree in all gravelly soils during shear. It is interesting to note that J. D. Watson[3] actually observed the effect of crushing of sand grains along the shear planes of triaxial test specimens. The degree of breakdown is dependent upon such characteristics as mineral composition, structure, texture, friability, weathering, brittleness, hardness, and particle shape, to name a few. Breakdown was observed in the South Pacific Division laboratory as early as 1948, but its importance was discounted. However, as the capability of equipment was improved to apply very high lateral pressures to simulate loading conditions for very high earth and rockfill dams, particle breakdown has taken on greater importance.

A limited quantity of data relating to particle breakdown has been accumulated during the past few years. Although it is considered too meager at this stage to draw positive conclusions, there is evidence of trends which are considered worthy of attention. The results of available data on Materials 4, 5, and 6 are tabulated in Table 2 showing the breakdown under the action of compaction, consolidation, and shear.

The data for each individual sieve size have been presented in detail for each soil since this is the only way to examine how the grading is affected. It will be noted that

TABLE 2 — Particle breakdown

	4A		4B		4C		4E		4F	
Size	Before	After change	Before	After change	Before	After change	Before	After change	Before	After change
	%	%	%	%	%	%	%	%	%	%
2"-1½"	6						12	— 3		
1½"-1"	10	— 1					17	— 2		
1"-¾"	6		7	+ 1			12	— 1	12	— 5
¾"-½"	9		11				17	— 2	17	— 3
½"-No. 4	23		27	— 2	33	— 1	42	— 2	43	— 3
No. 4- 8	15	— 3	18	— 2	32	— 2	0	+ 5	28	+ 2
No. 8-10	4		5	+ 1	10	— 1		+ 1	0	+ 5
No. 10-16	11	— 2	13	— 2	12	+ 1		+ 1		+ 1
No. 16-30	16	— 4	19		23	— 2		+ 1		+ 1
No. 30-40	0	+ 1	0	+ 1	0	+ 1		+ 1		
No. 40-60		+ 1				+ 1				+ 1
No. 60-80		+ 1		+ 1		+ 1				+ 1
No. 80-200		+ 2		+ 2		+ 1				
Finer than 200		+ 5				+ 1		+ 1		
Finer than min. size		+10		+ 4		+ 5		+10		+11
Vol. change (max. σ_1/σ_3)		— 0.4		— 0.1		— 0.2		— 2.4		— 0.9
Strain (max. σ_1/σ_3)		6.1		6.7		7.7		13.7		10.5
Friction angle		41.1		42.2		41.5		38.7		39.3

$\sigma_3 = 60$ psi

TABLE 2 — Particle breakdown

Size	4G		4H		4I		5D	
	Before %	After change %	Before %	After change %	Before %	After change %	Before %	After change %
2"-1½					1		1	
1½"-1"					1		1	
1"-¾"					5		5	
¾"-½"					11	— 1	11	
½"-No. 4	42	— 5			31		31	
No. 4- 8	29	— 6			17	— 1	17	
No. 8-10	11	+ 3			5	— 2	5	— 1
No. 10-16	18	— 1	23	+ 1	10	— 1	10	
No. 16-30	0	+ 6	28	+ 4	10	+ 1	10	— 1
No. 30-40		+ 1	14	— 5	3		3	
No. 40-60			21	— 4	4		4	
No. 60-80		+ 1	14	— 4	2		2	
No. 80-200			0	+ 8	0	+ 2	0	+ 2
Finer than 200		+ 1				+ 2		
Finer than min. size		+ 9		+ 8		+ 4		+ 2
Vol. change (max. σ_1/σ_3)		— 0,7		— 1.4		— 0.6		+ 0.3
Strain (max. σ_1/σ_3)		9.6		10.0		7.4		2.8
Friction angle		38.9		38.8		41.9		45.6

$\sigma_3 = 60$ psi

TABLE 2 — Particle breakdown

Size	6A		6B			6C		6D				
	Before %	125 change %	Before %	250 change %	425 change %	Before %	125 change %	Before %	250 change %	425 change %	650 change %	650** change %
3"-2"	18	— 5				13	— 2					
2"-1½"	14	— 1				12	— 1					
1½"-1"	16	— 1	24	— 8	— 9	15	— 3	20	— 9	—18	—12	
1"-¾"	14	— 3	21	— 8	— 9	13	— 2	19	— 6	+ 2	— 6	—3
¾"-½"	16	— 3	22	— 5	— 6	19	— 3	25	— 9	—10	—13	—5
½"-No. 4	16	+ 5	24	+ 6	+ 4	20	+ 4	25	+ 6	+ 4	+ 2	+2
No. 4- 10	2	+ 4	3	+ 3	+ 6	2	+ 2	3	+ 6	+ 7	+ 9	+2
No. 10- 40	0	+ 2	0	+ 4	+ 5	1	+ 2	2	+ 4	+ 6	+ 7	+1
No. 40- 60	1	0	1	0	0	1	0	0	+ 2	+ 2	+ 2	+1
No. 60-200	0	+ 2	1	+ 2	+ 1	1	+ 1	2	+ 1	+ 2	+ 2	0
Finer than 200	3	+ 1	4	+ 6	+ 8	3	+ 2	4	+ 5	+ 5	+ 9	+2
Finer than min. size		+ 1		+ 6	+ 8		+ 2		+ 5	+ 5	+ 9	+2
Vol. change (max. σ_1/σ_3)		— 1.6		— 5.0	— 6.9		— 4.7		— 4.7	— 7.3	— 6.3	
Strain (max. σ_1/σ_3)		13.5		20	21		17.5		21	20	17.0	
Compaction *		V		V,I	V,I		V		V,I	V,I	V,I -	V,I
Friction angle		41.3		38.0	37.2		38.6		38.5	36.8	35.2	

* V — vibration

* I — impact

** compaction and consolidation

the loss of particles in the coarse fractions and the gain in the fine fractions are readily evident. In the intermediate sizes, however, the picture is not clear since there can be either a loss or a gain, or no change. When there is no change in percentage, the quantity lost by breakdown either equals the quantity gained or no breakdown has occurred. For lack of a better criterion, the change in percentage of the original minimum size has been selected to indicate the degree of breakdown.

In comparing Materials 4 and 5, it will be noted that all the various gradings of Material 4 show more breakdown than Material 5D. As previously noted, Material 5D reached its maximum strength at much less strain than any gradation of Material 4. Material 5D increased in volume during shear while all gradations of Material 4 decreased in volume.

Data pertaining to various gradations of Material 6 (Figure 6) have been included in Table 2 to illustrate what happens under various lateral pressures. The relatively large strain and reduction in volume at maximum strength for all gradings of Material 6 correspond to the relative high degree of breakdown. There is a trend of increased breakdown with increasing lateral pressure. It is significant that for Material 6D much less breakdown occurred under the combined action of compaction and consolidation than under the combined action of compaction, consolidation, and shear, indicating that a greater degree of breakdown occurred during shear.

There is a trend indicated for all soils that the angle of internal friction is reduced in proportion to the increase in particle breakdown, but this cannot be confirmed until the influence of increasing lateral pressure is known.

EFFECT OF LATERAL PRESSURE

The 1947 progress report[1] stated that the actual envelope of the stress circles for most triaxial tests on cohesionless sands is slightly curved, with the angle of internal friction decreasing slightly with increasing lateral pressure. Up to that time, the highest lateral pressure applied was 220 psi in tests on alluvial gravel having a maximum size of ½ inch. In recent testing, a limited amount of data have been accumulated for lateral pressures up to 650 psi on soils with maximum sizes of 1½ and 3 inches. The results of triaxial tests on Materials 6, 7, and 8 are shown in Table 3.

The data show that the angle of internal friction consistently decreased with increasing lateral pressure, except

TABLE 3 — Influence of lateral pressure

Material	Void ratio	Max. size (in.)	Lateral pressure (psi)	Friction angle (degrees)	Corrected friction angle (degrees)
6A	0.307	3	125	41.3	34.2
6B	0.299	1½	250	38.0	36.3
6B	0.287	1½	425	37.2	
6C	0.334	3	125	38.6	38.5
6D	0.307	1½	250	38.5	34.2
6D	0.297	1½	425	36.8	31.2
6D	0.293	1½	650	35.2	
7A	0.173	3	15	53.7	20.0
7A	0.183	3	30	49.7	47.3
7A	0.174	3	60	47.8	41.7
7A	0.175	3	125	44.8	43.2
7B	0.180	1½	250	43.1	34.7
7B	0.171	1½	425	40.2	39.0
7B	0.168	1½	650	39.9	
7C	0.296	3	15	53.4	9.6
7C	0.314	3	30	43.1	46.6
7C	0.283	3	60	44.9	38.0
7C	0.258	3	125	41.8	44.2
7D	0.231	1½	200	42.7	33.7
7D	0.233	1½	300	40.2	35.2
7D	0.219	1½	550	38.1	
7E	0.281	3	15	51.7	41.7
7E	0.277	3	30	47.5	37.3
7E	0.278	3	60	43.2	39.0
7E	0.263	3	125	41.2	39.6
7F	0.239	1½	200	40.7	34.0
7F	0.234	1½	300	38.7	29.8
7F	0.219	1½	550	35.2	
8A	0.219	3	15	50.2	44.3
8A	0.189	3	45	46.5	45.8
8A	0.185	3	90	46.0	48.1
8B	0.173	1½	100	46.4	41.6
8B	0.165	1½	300	43.1	37.7
8B	0.174	1½	500	41.2	

for some discontinuities which are evident when the size of the equipment and maximum particle size were changed. For the various gradings of Material 7, where the equipment and maximum particle size were the same, a reduction in friction angle of 9 to 12 degrees is shown for an increase in lateral pressure from 15 to 125 psi. A reduction of 3 to 5 degrees is indicated for all materials for an increase in lateral pressure from 125 to 650 psi. Except for Materials 7A and 7B, there was an appreciable increase in density with increase in lateral pressure. Since no data are available no particle breakdown for Materials 7 and 8, the influence of this factor on the reduction in shear strength is not evident.

Because of the relatively wide variation in friction angles and particularly in view of the unusually high values obtained for Materials 7 and 8 at low values of lateral pressure, the direct test values were re-computed in accordance with the procedure recommended in the 1947 report[1], using the equation $\sigma_3(\sigma_1/\sigma_3 - 1) \csc \Phi - \sigma_3(\sigma_1/\sigma_3 + 1) - 2C = 0$ for any two tests in which only σ_3 is different. This procedure was originally suggested for analyzing test results to compensate for apparatus errors, testing technique, and possible interlocking on soil particles. The corrected angles of internal friction are shown in Table 3. It will be observed that the corrected values are quite erratic, with a poorly defined trend of decreasing strength with increasing lateral pressure.

CLOSING REMARKS

It is evident that many of the relations and characteristics obtained for gravelly soils using large-scale equipment are similar to those found for cohesionless sands in the 1947 report. However, the findings to date for a fairly wide variety of gradings indicate that the shear strength of alluvial gravelly soils under high lateral pressures may not exceed a range between 35 and 40 degrees.

There is an indication that the influence of oversize particles may not be as important as was once suspected, but additional studies are still needed to confirm this conclusion. In the study of crushed and quarried rock, this factor will warrant serious attention.

With the increase in height of earth and rockfill dams, the effects of particle breakdown must be investigated further not only because of its influence on shear strength but other characteristics such as consolidation, permeability, and pore pressure. It will also be necessary to separate the effects of particle breakdown, not only under the action of compaction, consolidation, and shear, but also to determine the effects of repeated loading. Greater attention must be given to petrographic analysis so that this will be included in the normal routine for testing each soil. Eventually, data may be accumulated so that criteria may be established for classifying gravelly soils with respect to different categories such as excellent, intermediate, or poor which will be useful for determining their use for different zones of a dam.

In conclusion, it is hoped that the presentation of the data in this paper will be an incentive for more intensive investigation of all types of gravelly soils.

REFERENCES

1. Corps of Engineers, Waterways Experiment Station — *Triaxial shear research and pressure distribution studies on soils, Progress Report.* 1947.

2. Hall, Earl B. — *A triaxial apparatus for testing large soil specimens.* American Society of Testing Materials, Special Technical Publication No. 106, 1950.

3. Watson, John D. — *A triaxial compression apparatus for the determination of the stress-deformation characteristics of soils.* Proceedings, American Society of Testing Materials, Vol. 39, 1939.

SHEARING PROPERTIES OF REMOLDED SODIUM ILLITE

R. E. OLSON and J. HARDIN

Associate Professor and Research Assistant, respectively, University of Illinois, Urbana, Illinois.

SYNOPSIS

A series of consolidated-undrained triaxial compression tests was performed on samples of sodium illite which had been remolded at a liquidity index of 0.70. Normally consolidated and simply overconsolidated samples yielded the same effective stress Mohr-Coulomb failure envelope though they had significantly different void ratios. Hence, the void ratio exerted a negligible effect on the shearing strength. The effective stress angle of internal friction was very small, only 17.7 degrees. It was possible to obtain Hvorslev-Coulomb type failure envelopes with negligible scatter, provided that Bjerrum's form of the Hvorslev-Coulomb shear equation was used, but the Hvorslev cohesion was zero.

A comparison with data reported previously for sedimented samples of sodium illite demonstrated that remolding causes a reduction in void ratio, a reduction in the pore water pressures developed during shear, and a small reduction in the effective angle of internal friction.

RESUMEN

Una serie de ensayos del tipo triaxial consolidado — sin avenamiento fué llevada acabo en muestras de illita-sódica, las cuales fueron remoldeadas a un índice de liquidez igual a 0.70. Muestras normalmente e hyperconsolidadas produjeron una misma envolvente en términos de esfuerzos efectivos, aún teniendo índices de vanos completamente distintos. Por lo tanto, podemos ver que el índice de vanos ejerció un efecto despreciable a la resistencia al corte. El ángulo de rozamiento interno en términos de esfuerzos efectivos resultó bien pequeño, solamente alcanzó 17.7 grados. Fué posible obtener envolventes del tipo Hvorslev-Coulomb con una despreciable dispersión en los puntos, siempre y cuando, se usara la forma de ecuación para resistencia al corte, tipo de Bjerrum y la cohesión de Hvorslev tomándola como nula.

Comparando los resultados con otros anteriormente obtenidos en muestras sedimentadas de illita-sódica, se *encontró que la acción de remoldear las muestras ocasiona una reducción en el índice de vanos al igual que cn la presión hidrostática desarollada durante la acción de corte y además una pequeña reducción en el ángulo efectivo de rozamiento interno.*

INTRODUCTION

Investigations into the engineering properties of illite and illitic clays have been in progress at the University of Illinois since 1957[1, 2, 3]. Tests on chemically purified calcium illite[2] indicated that remolding caused a breakdown (dispersion) of the soil structure which, in turn, caused the remolded samples to have lower void ratios and lower pore water pressures during shear than sedimented samples. However, the remolded and sedimented samples had almost identical effective stress failure envelopes. Further, normally consolidated and overconsolidated samples yielded the same effective stress failure envelopes though the void ratios were materially different. The shear strength of these samples was, therefore, essentially independent of void ratio, being determined almost exclusively by the effective stresses.

However, sedimented samples of a flocculated sodium illite[3] exhibited relatively large hysteresis loops in the effective stress failure envelopes, in marked contrast to the negligible loops for calcium illite. It was demonstrated that the size of the hysteresis loops was related to the strain at failure, the largest loops occurring with the smallest strains. This implies that the added strength of the overconsolidated samples was a phenomena which was "built-in" by overconsolidation but which could be destroyed by strain.

In an attempt to investigate further the effect of soil structure on the shearing strength, a series of consolidated-undrained triaxial compression tests was performed on samples of remolded sodium illite with a pore water salt concentration of 0.1N (5.8 grams NaCl per liter of pore water).

SOIL

The illite is the finer-than-two-micron fraction of a Pennsylvanian shale from the vicinity of Fithian, Illinois. The index properties of the sodium illite include:

liquid limit	79%
plastic limit	35%
activity	0.44
specific gravity	2.85

EXPERIMENTAL PROCEDURES

The illite was made homoionic to sodium by repeated washing with 0.1N NaCl. Several one gram samples of the clay were washed with a large excess of 1N NaCl, centrifuged, and the supernatent fluid analyzed for Ca, Mg, and K. No trace of these ions was found. The clay was therefore assumed to be nominally homoionic.

The clay was prepared at a water content of 66% (liquidity index of 0.71). The testing procedure was identical to that used with the calcium illite[2] except that the slightly lower permeability of the sodium illite necessitated longer consolidation times. The final consolidation pressures were maintained for at least one week prior to shear.

EXPERIMENTAL RESULTS

CONSOLIDATION CURVES

The ambient stress consolidation curves for both the remolded and sedimented samples of sodium illite are shown in Figure 1. The water contents (void ratios) of the sedimented samples are much greater than those of the remolded samples at the same consolidation pressures. The explanation is probably that the particles in the sedimented samples flocculated into edge-to-face arrangements which could withstand high stresses and still entrap significant amounts of pore fluid. The shearing displacements during remolding cause the plate shaped particles to assume more nearly parallel positions with smaller amounts of entrapped water.

MOHR-COULOMB DIAGRAMS

Following common practice, the stresses in the soil during shear are plotted in modified Mohr-Coulomb diagrams where $\frac{1}{2}(\bar{\sigma}_1 - \bar{\sigma}_3)$ is plotted as the ordinate and $\frac{1}{2}(\bar{\sigma}_1 + \bar{\sigma}_3)$ as the abscissa. Hence, the stress conditions in the sample can be represented by a single point rather than by a circle and a considerable simplification in the shear diagrams results. The slope of the failure envelope in the modified Mohr-Coulomb diagram is Ψ and the cohesion intercept is d. These parameters are converted to the usual Mohr-Coulomb parameters through the equations:

$$\sin \varphi = \tan \Psi \qquad (1)$$

$$c = d/\cos \varphi \qquad (2)$$

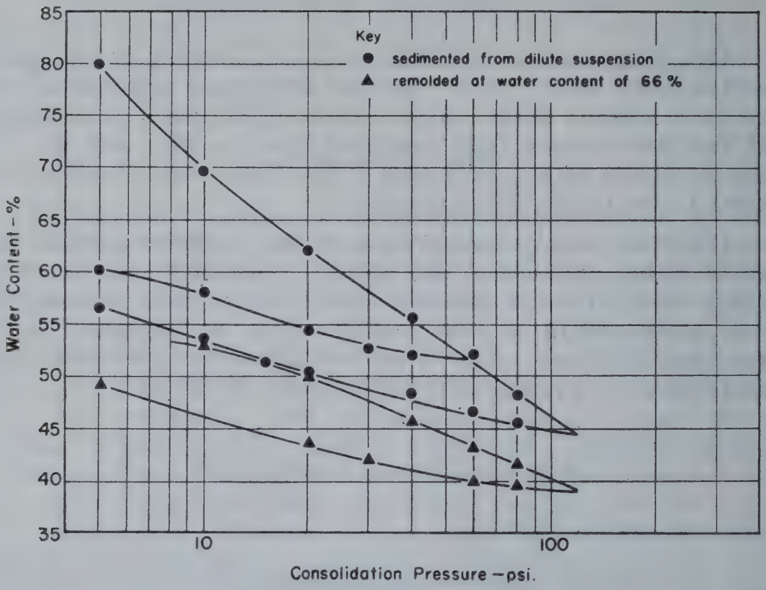

Fig. 1 — Consolidation curves for sedimented and remolded 0.1N sodium Illite.

Fig. 1 — Curvas de consolidación para 0.1N Illita sódica sedimentada y remoldeada.

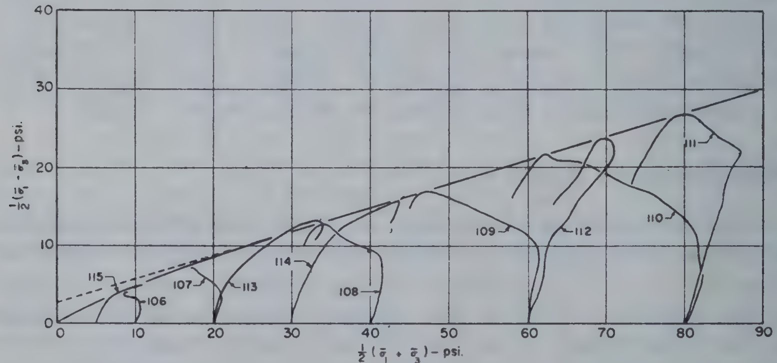

Fig. 2 — Stress path curves for remolded 0.1N sodium Illite.

Fig. 2 — Curvas de trazo de esfuerzo para 0.1 Illita sódica remoldeada.

The stress conditions in the sample during shear can be portrayed by plotting a line in a modified Mohr-Coulomb diagram representing the locus of all states of stress in the sample during shear. Such a line is called a "stress path curve." The stress path curves for all samples of remolded sodium illite are presented in Figure 2. The stress path curves in Figure 2 are labeled with the specimen number (see Appendix for further data on each specimen).

Failure may be defined as the peak stress difference, the peak effective principle stress ratio, or as the tangent point between a stress path curve and a failure envelope. The Mohr-Coulomb parameters for the three failure criteria are shown in Table 1. The differences between the three failure envelopes are quite small.

TABLE 1 — Mohr-Coulomb parameters for remolded sodium illite

Failure criterion	$\overline{\Phi}$	$\overline{C}$
$(\sigma_1 - \sigma_3)$	17.4°	3.1 psi
stress path tangency point	17.7°	2.5 psi
$(\overline{\sigma}_1/\overline{\sigma}_3)$	18.4°	2.0 psi

A remarkable aspect of the Mohr-Coulomb diagram in Figure 2 is the almost complete lack of a hysteresis loop between the normally consolidated and over consolidated failure envelopes. Since the normally consolidated and overconsolidated samples have significantly different void ratios (Figure 1) the lack of hysteresis loop implies that the void ratio exerts very little influence on the shearing strength. The lack of a hysteresis loop in the failure envelopes of the remolded sodium illite is in marked contrast to the large hysteresis loop in the failure envelopes for the sedimented sodium illite[3]. A further investigation into the effect of void ratio on shearing strength seems desirable.

EFFECT OF VOID RATIO ON SHEARING STRENGTH

The peak stress difference is plotted against the water content in the failure zone (measured at 20% strain) in Figure 3. A similar relationship was observed by Henkel[4] for remolded Weald Clay. It seems apparent that a unique relationship between water content and shearing strength, as assumed by Roscoe, Schofield and Wroth[5], does not exist.

Hvorslev[6] has presented a theory which divides the shear strength of the soil into two parts, the cohesion which is a logarithmic function of the void ratio and the internal

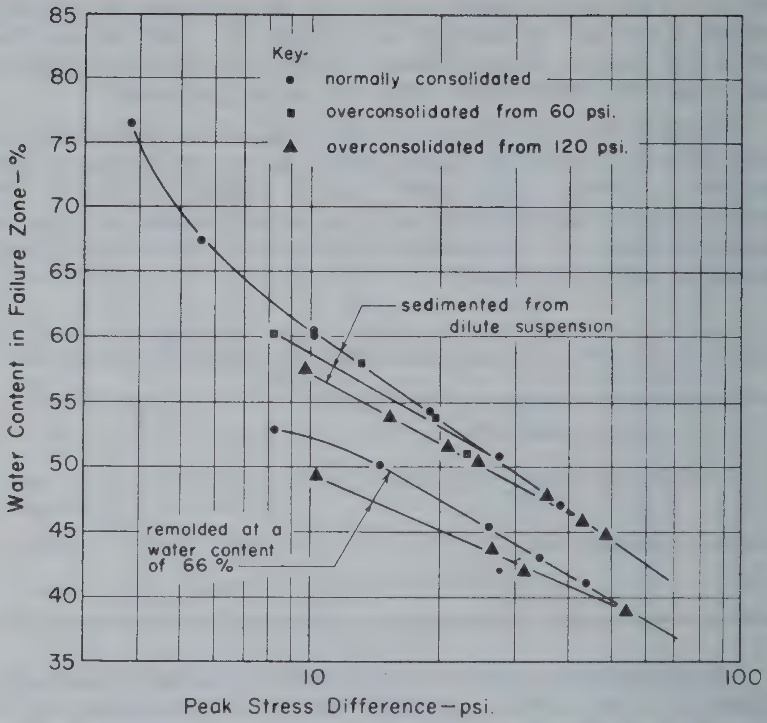

Fig. 3 — Effect of water content on the compression strength of 0.1N sodium Illite.

Fig. 3 — Efecto del contenido de humedad en la resistencia a compresión de 0.1N Illita sódica.

friction which is a linear function of the effective normal stress on the failure plane. For simplicity in plotting, the Hvorslev form of the Coulomb equation is modified to the form:

$$\frac{1}{2}\left(\bar{\sigma}_1 - \bar{\sigma}_3\right) = \bar{\sigma}_e \triangle + \frac{1}{2}\left(\bar{\sigma}_1 + \bar{\sigma}_3\right) \tan \Psi_e \qquad (3)$$

where: $\bar{\sigma}_e$ is the "equivalent consolidation pressure", i.e. the pressure on the virgin consolidation curve corresponding to the void ratio of the sample in the failure zone at the time of failure, $\triangle$ is a constant, and Ψ_e is the modified Hvorslev angle of internal friction. The parameters Ψ_e and $\triangle$ are converted to the standard Hvorslev parameters φ and κ using equations similar to equations 1 and 2.

The shearing data are plotted in a diagram of $\dfrac{\frac{1}{2}(\bar{\sigma}_1 - \bar{\sigma}_3)}{\bar{\sigma}_e}$ vs $\dfrac{\frac{1}{2}(\bar{\sigma}_1 - \bar{\sigma}_3)}{\bar{\sigma}_e}$. If the Hvorslev theory is applicable, then a straight line failure envelope should result with an intercept of $\triangle$ and a slope of Ψ_e. If the normally consolidated effective stress Mohr-Coulomb failure envelope does not pass through the origin then Equation 3 must be modified[7] to the form:

$$\frac{1}{2}(\bar{\sigma}_1 - \bar{\sigma}_3) = \bar{d}_o + \bar{\sigma}_e \triangle + \frac{1}{2}(\bar{\sigma}_1 + \bar{\sigma}_3) \tan \Psi_e \qquad (4)$$

where $\bar{d}_o$ is the cohesion intercept of the normally consolidated effective stress Mohr-Coulomb failure envelope. The shear diagram then employs $\dfrac{\frac{1}{2}(\bar{\sigma}_1 - \bar{\sigma}_3) - \bar{d}_o}{\bar{\sigma}_e}$ as the ordinate.

The Hvorslev-type calculations were performed using the stress path tangency failure criterion. The void ratio was defined as the void ratio of a thin slice of soil containing the dominant shear plane. The void ratio was determined at the completion of the test (about 20% strain) and may differ slightly from the void ratio in the same zone at failure. The equivalent consolidation pressure is obtained from the virgin consolidation curve using the void ratio just defined. However, a problem arises as to whether to use the virgin curve of the remolded samples or the sedimented samples. Hvorslev[6] remolded his samples at water contents near the liquid limit and used the virgin consolidation curve of his remolded samples to define the equivalent consolidation pressure but he assumed that his remolded curve was a reasonable approximation of the sedimented virgin curve. Thus, he considered the sedimented virgin curve to be the proper one to use.

In Figure 4a, $\bar{\sigma}_e$ was defined using the remolded virgin curve. The concave upwards nature of the curve could indicate too flat a slope of the virgin consolidation curve[6]. However, the normally consolidated Mohr-Coulomb failure envelope (Figure 2) does not pass through the origin so Bjerrum's modified Hvorslev equation should be used (Figure 4b). This failure envelope is linear and its extension passes through the origin indicating zero Hvorslev cohesion.

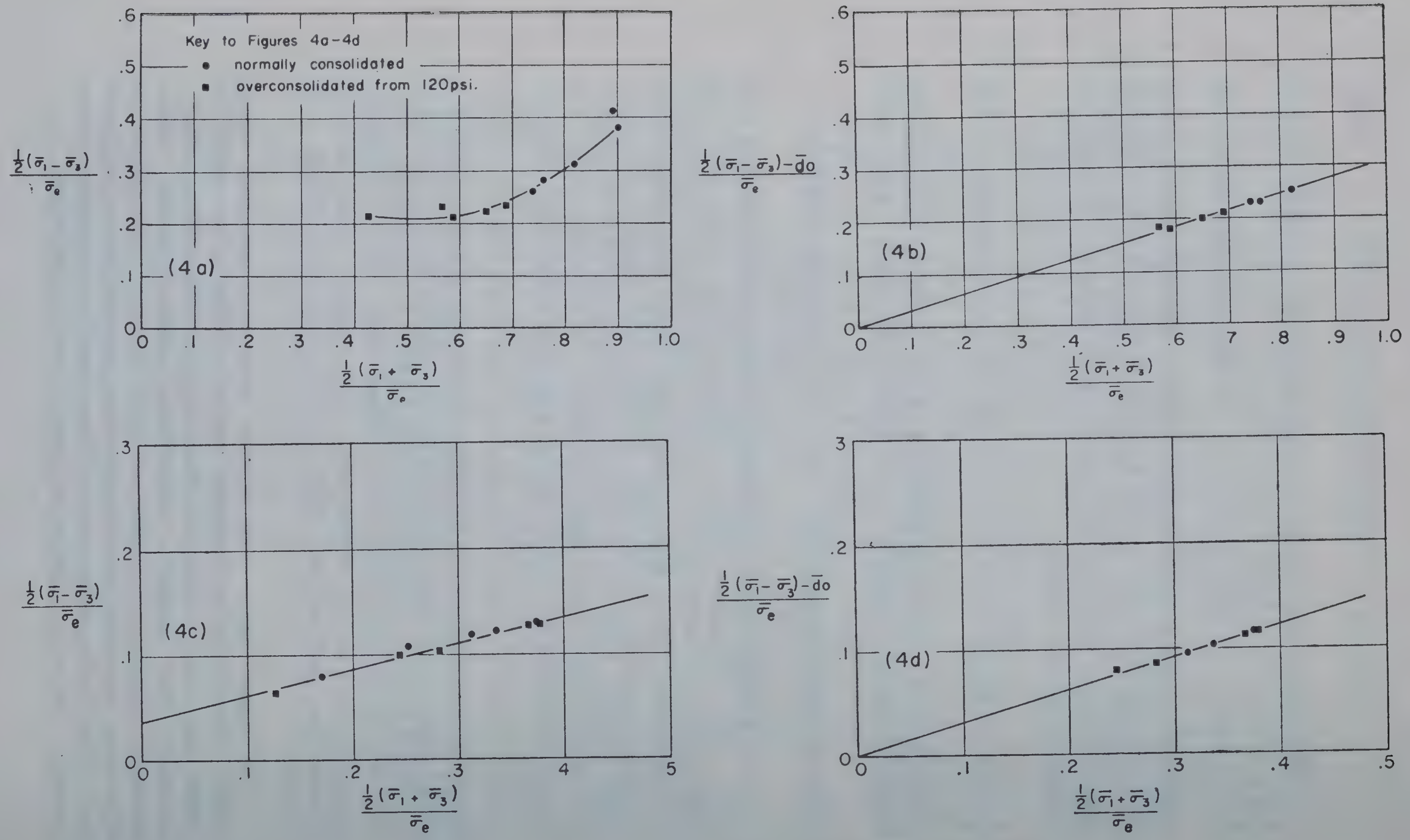

Fig. 4 — Hvorslev failure diagrams for remolded 0.1N sodium Illite.

Fig. 4 — Diagramas de rotura tipo Hvorslev para 0.1N Illita sódica remoldeada.

The sedimented virgin curve was used to define $\bar{\sigma}_e$ in Figures 4c and 4d. The failure envelope in Figure 4c exhibits a Hvorlsev-type cohesion and a rather small angle of internal friction. There is more scatter in Figure 4c than in any of the other Hvorslev diagrams. Bjerrum's modified Hvorslev equation was used to define the failure envelope in Figure 4d which exhibits a minimal amount of scatter and whose extension passes directly through the origin indicating a zero Hvorslev cohesion.

The lack of a hysteresis loop in the standard Mohr-Coulomb diagram implies a negligible Hvorslev cohesion. Figures 4b and 4d exhibit zero Hvorslev cohesion with unusual precision. Further, they yield essentially the same Hvorslev angle of internal friction, which is also the angle of internal friction obtained in the standard Mohr-Coulomb failure diagram. It is concluded that the Hvorslev theory can be applied to the shearing strength diagrams of remolded sodium illite but Bjerrum's modified equation should be used. The virgin consolidation curve of either the remolded samples or the sedimented samples can be used to define $\bar{\sigma}_e$ without affecting the Hvorslev parameters of this soil. Coupled with the data presented previously (Figures 1 through 3), the Hvorslev calculations substantiate the belief that the void ratio exerts very little, if any, influence on the shearing strength of this soil.

STRESS-STRAIN PROPERTIES

Typical stress-strain curves for remolded sodium illite are presented in Figure 5. The points corresponding to the three failure criteria are indicated on each curve. The strains at the point of tangency between the stress path curves and the failure envelope are plotted against the consolidation pressure in Figure 6. All normally consolidated samples failed at strains of 13% to 14%. For overconsolidated samples, the strain at failure decreased as the overconsolidation ratio increased.

With these stress-strain properties it is not surprising that the Mohr-Coulomb failure envelopes did not possess hysteresis loops. For sedimented samples of sodium illite it was demonstrated[3] that large hysteresis loops occurred only when the normally consolidated samples failed at small strains and overconsolidated samples failed at significantly larger strains. The effect of strain on the size of the hysteresis loops can be demonstrated in a crude way by plotting Mohr diagrams with stresses defined at *specific strains rather than*

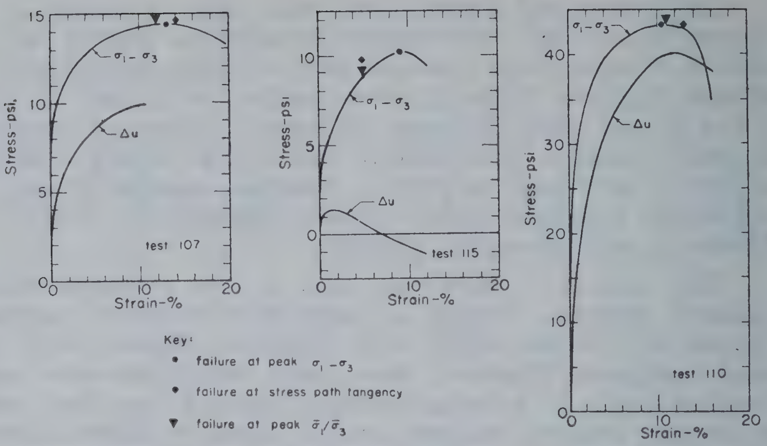

Fig. 5 — Typical stress-strain curves from triaxial compression tests on remolded samples of 0.1N sodium Illite.

Fig. 5 — Curvas típicas de esfuerzo y deformación obtenidas de ensayos triaxiales en muestras remoldeadas de 0.1N Illita sódica.

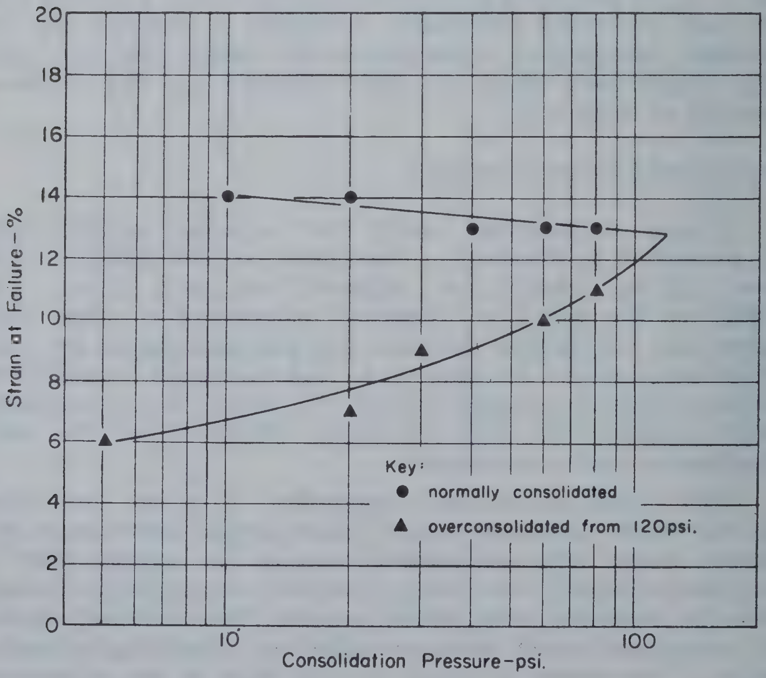

Fig. 6 — Strains at failure for remolded 0.1N sodium Illite.

Fig. 6 — Deformaciones en rotura para 0.1N Illita sódica remoldeada.

at failure. Such diagrams for remolded sodium illite at strains of 2%, 6% and 12% are shown in Figure 7. Note that these are not failure diagrams. It is apparent that the sizes of the hysteresis loops in Figure 7 are functions of strain.

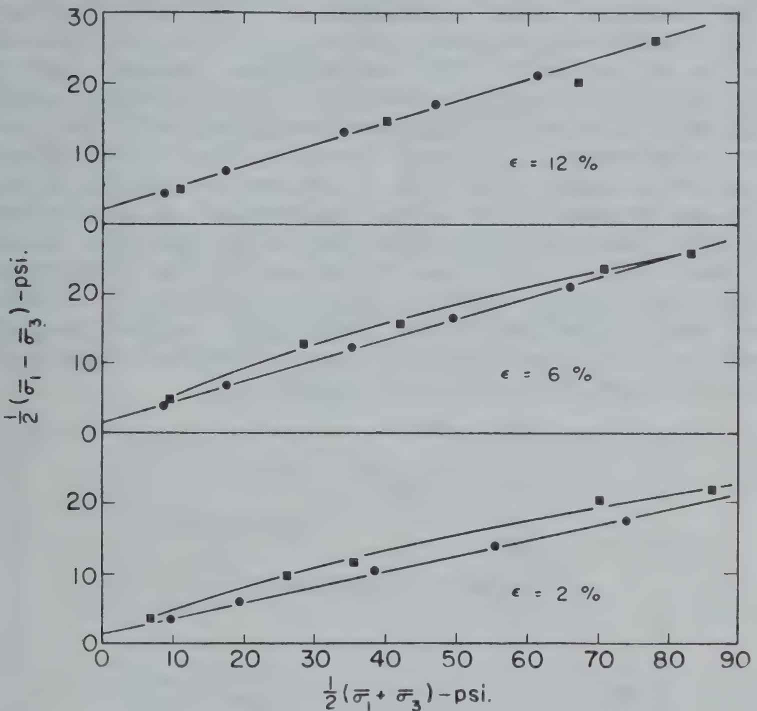

Fig. 7 — Mohr-Coulomb diagrams for remolded 0.1N sodium Illite, stresses defined at the strains indicated.

Fig. 7 — Diagramas tipo Mohr-Coulomb para 0.1N Illita sódica remoldeada, esfuerzos definidos a la indicada deformación.

PORE WATER PRESSURES

It is usually convenient to express the pore water pressures developed in a saturated soil during shear with Skempton's[8] equation:

$$\Delta u = \Delta\sigma_3 + A\ (\Delta\sigma_1 - \Delta\sigma_3) \qquad (5)$$

where A is an empirical coefficient. The symbol A_f is used to denote the A-coefficient at failure. A_f is a measure of the shear induced pore water pressures. Its value depends on the failure criterion. In this investigation A_f will be defined at the point of tangency between a stress path curve and the failure envelope.

In normally consolidated samples, A_f varies with the consolidation pressure. Typical data are shown in Figure 8 for both sedimented and remolded sodium illite. The sedimented samples[3] were consolidated to 7 psi in a onedimensional device, then extruded and set up in the triaxial cells. Because of the high initial consolidation pressure and the slight disturbance during extrusion, the sedimented samples must be considered slightly overconsolidated until they have been consolidated to at least 20 psi in the triaxial device. At pressures above 20 psi, A_f of sedimented samples is very high and appears to be almost independent of consolidation pressure. The pore water pressures in the remolded samples are much lower than those in the sedimented samples and A_f increases slightly with consolidation pressure. The higher pore water pressures in the sedimented samples probably result from the shear induced collapse of the very open structures developed during original flocculation.

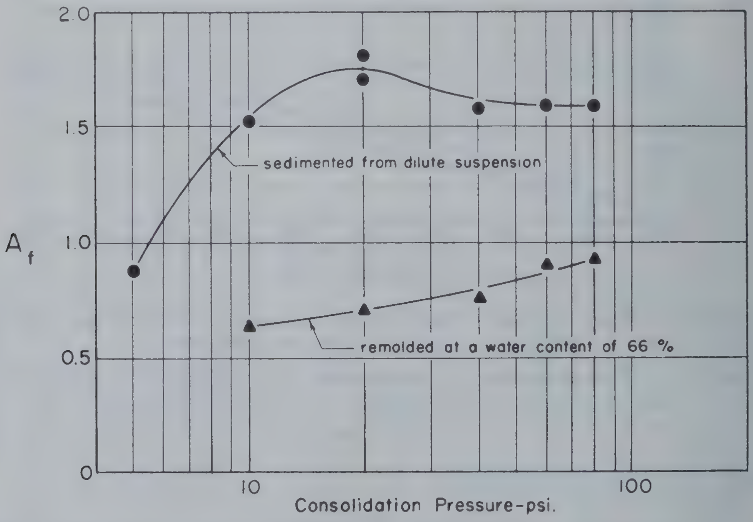

Fig. 8 — Effect of consolidation pressure on A_f for normally consolidated samples of sodium Illite, A_f at the point of stress path tangency.

Fig. 8 — Efecto de presión de consolidación en A_f para muestras normalmente consolidadas de Illita sódica, A_f definido en el punto del trazo tangencial de esfuerzos.

For overconsolidated sodium illite, A_f varies with the overconsolidation ratio[9] as shown in Figure 9. Again, smaller pore water pressures are developed in the remolded samples than in the sedimented samples. It appears that negative pore water pressures will not be developed in either the remolded or the sedimented samples of sodium illite at any overconsolidation ratio.

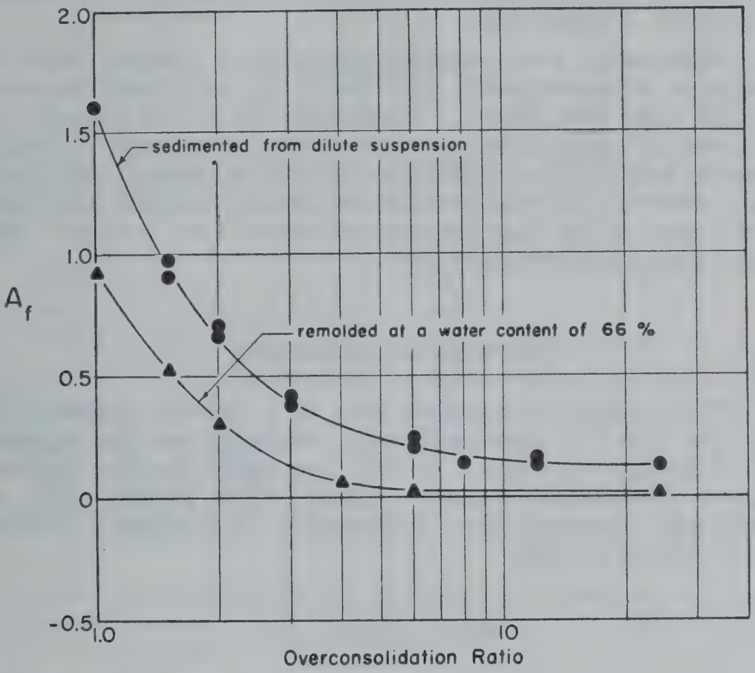

Fig. 9 — Effect of overconsolidation ratio on A_f of sodium Illite, A_f defined at the point of stress path tangency.

Fig. 9 — Effecto del factor de hyperconsolidación en A_f para Illita sódica, A_f definido en el punto del trazo tangencial de esfuerzos.

CONCLUSIONS

Normally consolidated and overconsolidated samples of remolded sodium illite yield the same Mohr-Coulomb failure envelope even though the void ratios of the normally consolidated and overconsolidated samples are quite different. Hence, the effective stress shearing strength appears to be essentially independent of the void ratio. A plot of shear strength vs the water content (void ratio) in the failure zone substantiates this interpretation. Hvorslev's theory of shear strength assumes the existence of a cohesion, which depends on void ratio, and a frictional component of strength, which depends only on the effective stress. It was demonstrated that the use of Bjerrum's modified form of the Hvorslev shear equation results in a single well defined failure envelope which is linear and whose extension passes diretly through the origin indicating zero Hvorslev cohesion. Remolded samples of sodium illite have similar properties to remolded samples of calcium illite.

Sedimented and remolded samples of sodium illite are the same mineralogically and chemically and have the same particle sizes and shapes. Hence, the difference between the engineering properties of the sedimented and remolded samples results from variations in soil structure. The more open structure of the sedimented samples results in higher void ratios at all consolidation pressures and in higher pore water pressures during shear.

ACKNOWLEDGMENT

This research represents part of a general investigation into the effect of physico-chemical variables on the engineering properties of clays. It was sponsored by the National Science Foundation (grant 13,362). The project was administered through the Engineering Experiment Station, University of Illinois.

REFERENCES

1. Olso, Roy E. and F. M. Mitronovas (1962) — "Shear Strength and Consolidation Characteristics of Calcium and Magnesium Illite", Clays and Clay Minerals, Proc. Ninth Nat. Conf., pp. 185-209, Pergamon Press, NYC.

2. Olson, Roy E. (1962a) — "Shear Strength Properties of Calcium Illite", Geotechnique, v. 12, pp. 23-43.

3. Olson, Roy E. (1962b) — "Shear Strength Properties of Sodium Illite", (in press).

4. Henkel, D. J. (1956) — "The Effect of Overconsolidation on the Behavior of Clays During Shear", Geotechnique, v. 6, pp. 139-150.

5. Roscoe, K. H. Schofield, A. N., and Wroth, C. P. (1958) — "On the Yielding of Soils", Geotechnique, v. 8, pp. 22-53.

6. Hvorslev, M. Juul (1960) — "Physical Components of the Shear Strength of Saturated Clays", Proc. A.S.C.E. Res. Conf. on the Shear Strength of Cohesive Soils, pp. 169-274.

7. Bjerrum, L. (1954) — "Theoretical and Experimental Investigations on the Shear Strength of Soils", Norwegian Geotechnical Institute Publ. No. 5, Oslo, 113 pp.

8. Skempton, A. W. (1954) — "The Pore Pressure Coefficients A and B", Geotechnique, v. 4, pp. 143-147.

9. Henkel, D. J. (1960) — "The Shear Strength of Saturated Remolded Clays", Proc. A.S.C.E. Res. Conf. on Shear Strength of Cohesive Soils, pp. 553-554.

APPENDIX

NOTATION

The following notation is used in this paper. Insofar as possible, this notation conforms to standard symbolism in soil mechanics.

English

A	Skempton's[8] pore pressure coefficient
c	cohesion intercept in a Mohr-Coulomb diagram
d	cohesion intercept in a modified Mohr-Coulomb diagram
N	normality (gram equivalent weight of solute per liter of solution)
O_r	overconsolidation ratio[4]
u	pore water pressure
w	water content — %

Greek

Δ	cohesion term in a modified Hvorslev shear diagram, or used before another symbol to indicate a change in value of the other parameter
ε	strain
σ	normal stress
τ	shear stress
φ	angle of internal friction
Ψ	slope of the failure envelope in a modified Mohr-Coulomb failure envelope

Subscripts

i	initial
a	ambient
ave	average
fz	defined in failure zone
m	maximum
f	defined at failure
c	consolidation
s	after pressure saturation

Note: A bar above a symbol designates the use of effective stresses.

TABLE 1 — Water content and consolidation data for remolded samples of 0.1N sodium illite

Test No.	w_i %	$\sigma_{3c\text{-}m}$ psi	$\sigma_{3c\text{-}s}$ psi	O_r	w_{ave} %	w_{fz} %
106	64.5	10	10	1.0	52.8	52.8
107	67.9	20	20	1.0	49.9	50.1
108	68.5	40	40	1.0	45.5	45.4
109	66.0	60	60	1.0	43.1	43.0
110	66.5	80	80	1.0	41.6	41.1
111	66.2	120	80	1.5	39.4	38.8
112	66.0	120	60	2.0	39.9	—
113	66.2	120	20	6.0	43.6	43.6
114	66.6	120	30	4.0	42.0	41.9
115	64.7	120	5	24.0	49.2	49.3

Note:

w_i — the initial water content of the sample

$\sigma_{3c\text{-}m}$ — the maximum ambient consolidation pressure during consolidation

$\sigma_{3c\text{-}s}$ — the final ambient consolidation pressure after pressure saturation

O_r — the over consolidation ratio, $O_r = \sigma_{3c\text{-}m} / \sigma_{3c\text{-}s}$

w_{ave} — the average water content of the soil after shear

w_{fz} — the water content of a thin slice of the sample containing the dominant shear plane, after 20% strain

TABLE 2 — Failure data for remolded samples of 0.1N sodium illite (*)

Test No.	Failure Criterion								
	max. $(\bar{\sigma}_1 - \bar{\sigma}_3)$			Stress Path Tan.			max. $(\bar{\sigma}_1 / \bar{\sigma}_3)$		
	$\bar{\sigma}_1 - \bar{\sigma}_3$ psi	Δu psi	ε %	$\bar{\sigma}_1 - \bar{\sigma}_3$ psi	Δu psi	ε %	$\bar{\sigma}_1 - \bar{\sigma}_3$ psi	Δu psi	ε %
106	8.2	5.2	14	8.2	5.2	14	8.2	5.2	15
107	14.4	10.1	14	14.4	10.1	14	14.3	10.0	12
108	25.9	19.1	11	25.6	19.2	13	25.8	19.2	12
109	33.8	29.9	11	33.6	30.2	13	33.8	30.0	12
110	43.2	39.8	11	43.0	39.6	13	43.2	39.8	12
111	53.5	27.2	10	53.2	27.4	11	53.5	27.2	10
112	47.6	13.7	8	47.2	14.1	10	47.2	14.3	10
113	26.3	0.1	9	25.6	0.8	7	25.8	0.7	7
114	31.2	2.0	9	31.2	2.0	9	30.8	2.7	7
115	10.2	—0.6	10	9.2	0.2	6	8.7	0.6	5

Note:

$(\bar{\sigma}_1 - \bar{\sigma}_3)$ — stress difference, no corrections applied for piston friction nor for filter drain restraint, sample area calculated assuming the sample deforms as a right cylinder,

Δu — the pore water pressure resulting from the application of the stress difference,

ε — axial strain at "failure".

(*) No corrections have been applied for the strength of the filter paper drains.

SUBPRESSURE MEASUREMENT IN A FREEZING SOIL SYSTEM

A. R. JUMIKIS
Dr. Eng. Sc., Professor of Soil Mechanics and Foundation Engineering, Rutgers — The State University, New Brunswick, New Jersey, U.S.A.

SUMMARY

This paper describes the pressure conditions in a freezing soil system associated with the upward migration of soil moisture under a freezing thermal gradient. The tensiometer theory is based on the mechanical principle of virtual work in a freezing soil system. The study of the application of the virtual work theory to a freezing soil system reveals that the tensiometer measurements do not disclose in themselves the various soil moisture transfer mechanisms resulting in the measured pressure differences (= subpressures), but indicate only the magnitude of the total pressure difference resulting from the simultaneous action of the various possible soil moisture transfer mechanisms in nature, as well as in the laboratory.

A subpressure equation for calculating the induced subpressures as a function of position and time for a given thermal gradient is presented.

SUMARIO

Esta obra detalla las condiciones de presión que se hallan en suelo durante el proceso de helamiento asociado con el movimiento de la humedad del suelo bajo un gradiente térmico helador. La teoría del tensiómetro, basada en los principios generales de trabajo virtual, en cual depende la mensuración, es tratada y el trabajo virtual en un suelo es explicado. El estudio de la aplicación de la teoría de trabajo virtual al proceso de helamiento de suelos revela que las medidas del tensiómetro no indican en si mismo (per se) los mecanismos de transportación de humedad responsables por las diferencias de presión observadas (sub-presiones), pero indican solamente la magnitud de la diferencia total causada por la acción simultanea de varios mecanismos responsables por el transporte de la humedad en suelos, igual en la naturaleza como también en el laboratorio.

Una ecuación para el cálculo de la sub-presión inducida como función de la posición y del tiempo se presenta para un dado gradiente térmico.

INTRODUCTION

The problem — In studying freezing soil systems it is interesting to know the amount of soil moisture transferred. *This amount of soil moisture transfer must be expressed by a well-defined mathematical function of the driving pressure.* The interrelationship between the amount of soil moisture transferred upon freezing and the driving pressure can most readily be established by means of the soil freezing experiment because the freezing soil systems in nature do not work with 100 percent efficiency. In these studies the problem is to measure the subpressure in a freezing soil system.

Pressure conditions in soil — The soil system prepared for the freezing experiment[1, 2] is not fully saturated; there are also air voids present. The surface of the ground-water table, the supply of water for the freezing ice lenses, is subjected to atmospheric pressure, p_a. The voids form interconnecting passages of various sizes, shapes and roughnesses for the upward flow of soil moisture and air or gas. Thus, under the influence of a temperature gradient the soil moisture flows upward from the ground-water table towards the cold front via the soil moisture films coated around the soil particles through poorly defined flow paths in a zigzag motion.

During the course of the upward migration, the flowing water loses some of its driving pressure. This means that the driving pressure in the system's flow performs some mechanical work which is lost. Thus, in doing external, over-all work the entire freezing soil system loses some of its energy. The driving pressure (soil moisture tension) of the upward flowing soil moisture in the porous medium of soil may be measured by means of so-called tensiometers[3, 4].

TENSIOMETER

Definition — A tensiometer is a device made of thin-walled micro-porous porcelain of known porosity and is used for the measurement of soil moisture tension in an unsaturated flow of soil moisture. The term "tensiometer" thus reflects literally the function of the device.

Fig. 1 illustrates some of the various types of porous elements studied by the author in his work[5, 6]. It also illustrates the type of conical tensiometer developed from these studies and now used by the author.

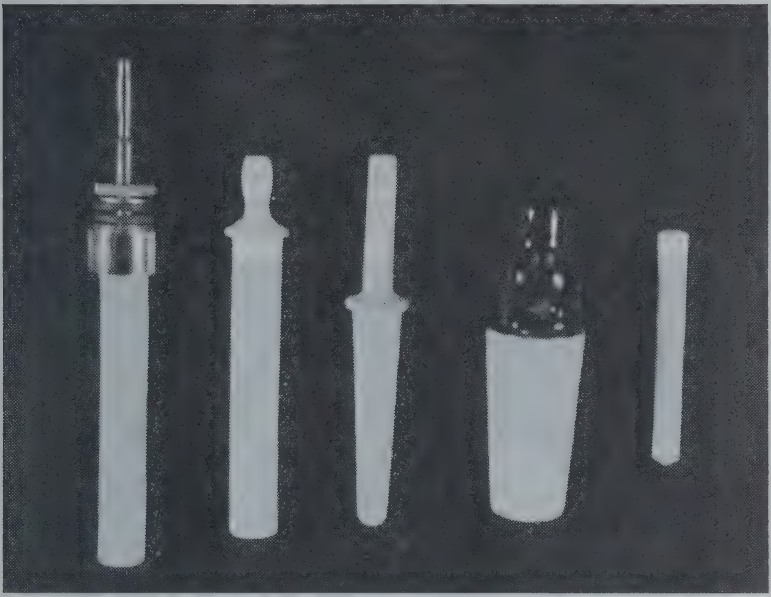

Fig. 1 — Various types of tensiometers.

Fig. 1 — Varios tipos de tensiómetros.

The properties of the porous ceramic tensiometer used in this experimental work are:

effective surface area	30.52 cm^2
number of capillaries per cm^2	2325×10^5
porosity	57%
average capillary radius	0.3
bubbling gauge pressure (= air-entry value)	2 atm.

The porous moisture-tension sensing element, or tensiometer, serves to establish contact at the external surface of the tensiometer body between the moisture films within the wall of the sensing element and those of the adjacent soil particles. The tapered, conical shape of the moisture tensiometer element affords an intimate contact between the external surface of the thin walls of the tensiometer and the soil into which this sensing element is inserted to insure a continuous water film connection. All of the tensiometers used in the soil freezing experiment are practically of the same materials, the same porosity, the same form, the same wall thickness and the same surface area, and they are nearly alike in their water-absorbing power.

The tensiometer is filled with boiled, and then chilled distilled water and connected to a mercurial two-legged manometer.

The porous ceramic moisture tensiometer may be considered to be a semi-impervious plug allowing through its porous walls only the passage of water, but not of air, gas or soil particles. Normally, the tensiometer can measure soil moisture tensions up to about one atmosphere ($\sim$ 14.7 lb/in^2).

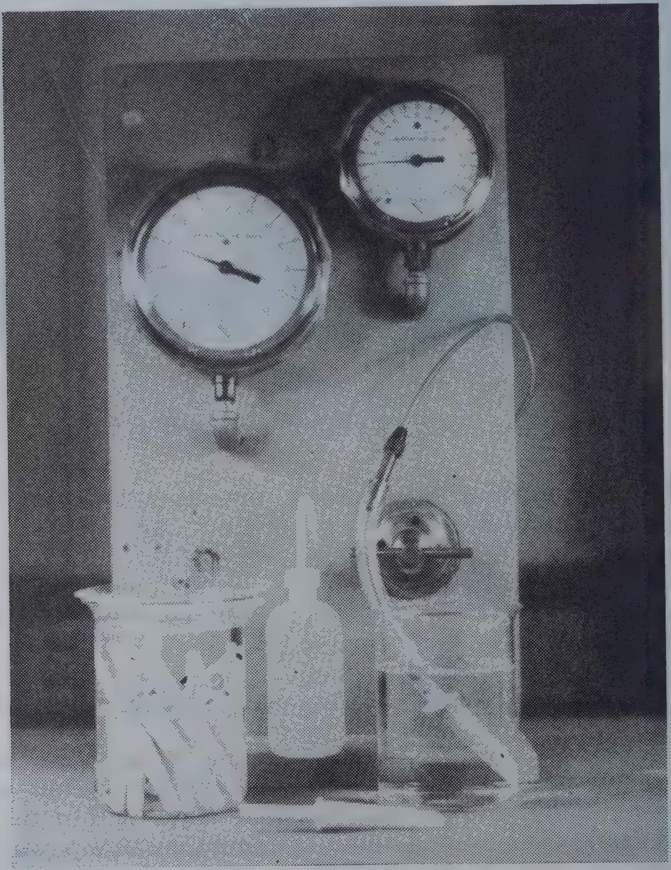

Fig. 2 — Testing of a tensiometer for its air-entry value.

Fig. 2 — Prueba del tensiómetro para establecer la presión necesaria para la entrada del aire.

The air-entry value ($=$ bubbling pressure) of the tensiometer is the pressure difference necessary to bring about an air leak through the voids of the wall of the porous ceramic element when its wall is saturated with boiled distilled water. In testing the tensiometers, their air-entry value must be greater than one atmosphere. It can thus be inferred that the air-entry value is the most critical property of the tensiometer. The air-entry values of the tensiometers used by the author are 35 psi $\backsim$ 2 atmospheres. Fig. 2 illustrates the apparatus used for testing the air-entry values (= bubbling pressures) of the tensiometers and the testing of a tensiometer for its air-entry value. The air bubbles indicate the passage of air from inside the tensiometer through its wall into water in the beaker.

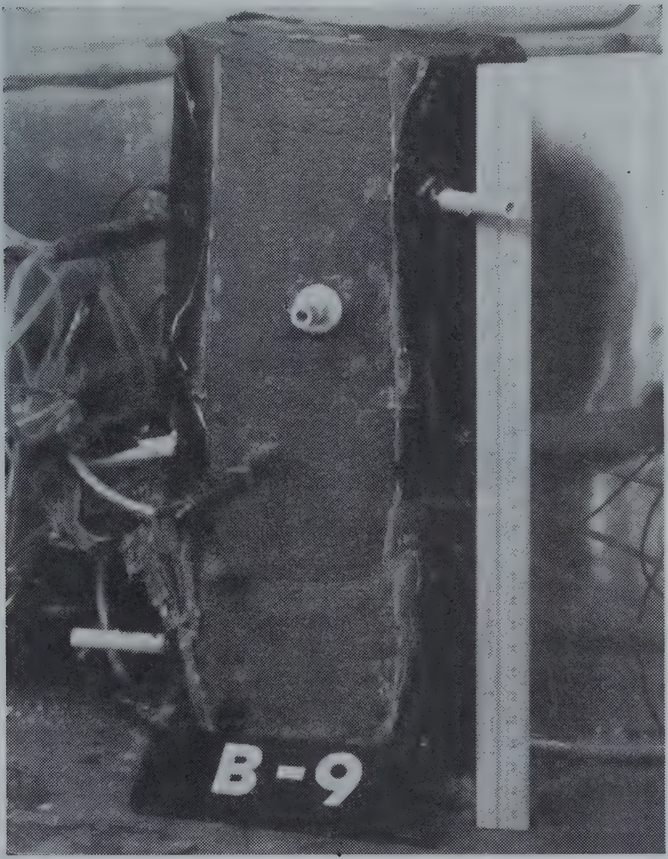

Fig. 3 — Helically spaced tensiometers and thermistors inserted in a soil system.

Fig. 3 — Colocación helicoidal de los tensiómetros y resistencias térmicas en la muestra del suelo.

After the tensiometers have passed the air-entry-value test, they are inserted in the soil system through the wall of the cylinder holding the soil sample. Fig. 3 shows a soil system after freezing studies with helically spaced tensiometers and thermistors in place. The freezing of the soil systems is performed in a specially designed freezing apparatus (Fig. 4).

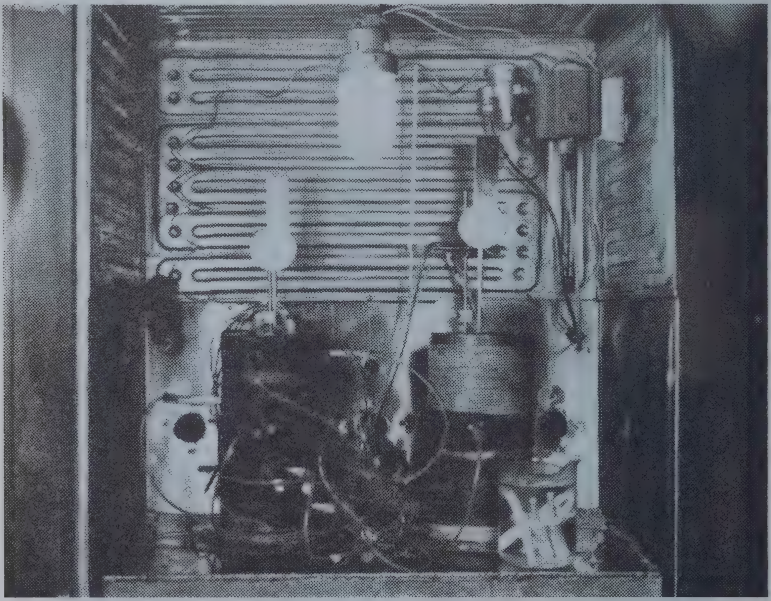

Fig. 4 — Soil freezing apparatus.

Fig. 4 — Equipo para el helamiento de suelos.

Soil moisture tension — The translocation of soil moisture through a porous soil system by the mechanism of moisture films is a special mode of flow phenomena of liquids termed the unsaturated flow of soils moisture. To measure directly the subpressure or soil moisture tension as a driving force necessary for moving the water a tensiometer can be used. *The soil moisture tension originates through the combined action of the internal forces of the soil system in a virtual displacement of the water.*

The holding of moisture in the voids of a soil at ordinary temperatures (above freezing) takes place by a complex system of forces, the combined effect of which brings about an apparent tension of the soil moisture. This moisture tension manifests itself by the amount of tension required in a contiguous liquid film phase to maintain equilibrium with the soil-water system in its given state of porosity and degree of soil moisture content. Hence the soil moisture tension is an intrinsic property of the system, a term which depends, therefore, upon the mutual affinity of the surface of the soil particles and water[1]. Therefore, *soil moisture tension represents the combined action of the internal forces in a differential or virtual translocation of soil moisture* in a soil-water system. In a freezing soil system, which because of the upward migration of soil moisture is a dynamic system, these conditions are even more complicated than at ordinary temperature. However, because of the slow process of the upward migration of soil moisture in a soil system subjected to freezing, the tensiometer is suitable for measuring soil moisture tensions (subpressures) in such dynamic soil systems.

Virtual work — The working principle of the tensiometer may be mathematically described by the mechanical principle of virtual work.

The principle of virtual work is as follows. In the case of a system of particles (soil particles and water particles, for example), this principle states that if a system of particles is in equilibrium, the total mechanical work of a set of all forces acting on the system of particles in any virtual displacement is zero. This definition of virtual work is modified to apply for a soil-water system after Timoshenko[7].

In applying the principle of virtual work the acting forces are considered to be constant during the process of a virtual displacement because of the slow process of upward flow of soil moisture under freezing conditions. A virtual displacement is here understood to be any infinitesimal or differential displacement (of water, for example) compatible with the conditions of continuity of the material.

Virtual work in a freezing soil system — Consider, in Fig. 5, an element of soil, abcd, into which a tensiometer is inserted. Note that the freezing soil system in Fig. 5 is laterally insulated (no lateral flux of heat), so that a unidirectional, upward flow of heat, soil moisture and cations in the electric diffuse double layer can take place[8].

When a differential volume of water, dV, is transferred from the tensiometer to the soil, then the draw of water out of the tensiometer brings about a decrease in pressure in the tensiometer water and the mercury rise in the closed leg of the manometer makes up the difference in volume. Thus the adjusted difference in the mercury levels in both legs of the manometer may be considered a measure of the resultant tension forces (driving pressure) prevailing in the soil-water-temperature system upon the upward flow of soil moisture.

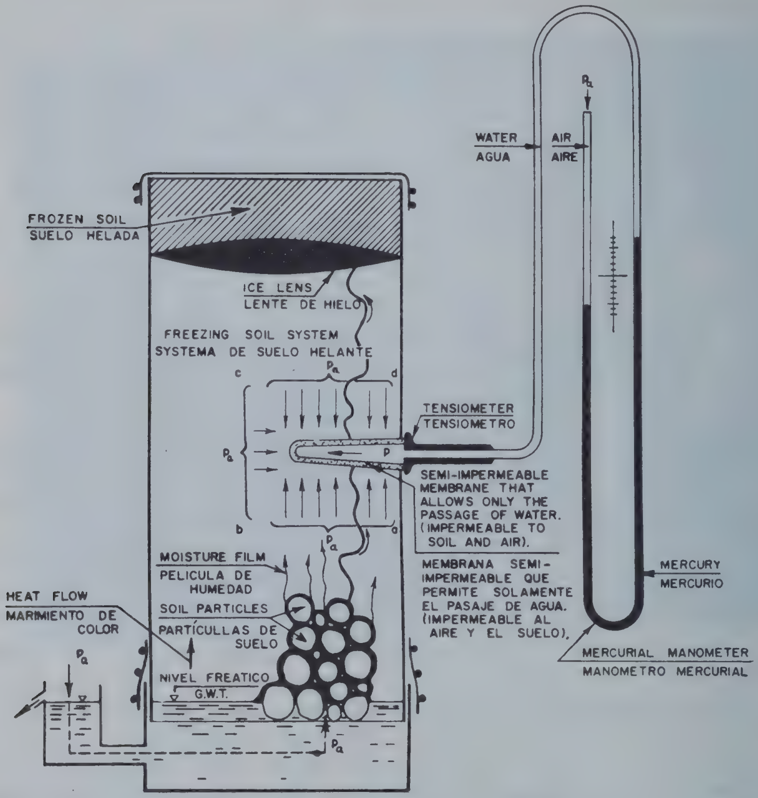
WATER
AGUA
AIR
AIRE
p_a
FROZEN SOIL
SUELO HELADA
ICE LENS
LENTE DE HIELO
FREEZING SOIL SYSTEM
SYSTEMA DE SUELO HELANTE
c
d
p_a
p_a
p
b
a
p_a
TENSIOMETER
TENSIOMETRO
SEMI-IMPERMEABLE MEMBRANE THAT ALLOWS ONLY THE PASSAGE OF WATER. (IMPERMEABLE TO SOIL AND AIR).
MEMBRANA SEMI-IMPERMEABLE QUE PERMITE SOLAMENTE EL PASAJE DE AGUA. (IMPERMEABLE AL AIRE Y EL SUELO).
MOISTURE FILM
PELICULA DE HUMEDAD
HEAT FLOW
MARIMIENTO DE COLOR
SOIL PARTICLES
PARTÍCULLAS DE SUELO
p_a
NIVEL FREATICO
G.W.T.
p_a
MERCURY
MERCURIO
MERCURIAL MANOMETER
MANOMETRO MERCURIAL

Fig. 5 — Soil-tensiometer-water system.

Fig. 5 — Relación entre el suelo, el tensiómetro y el agua.

Upon drawing out a differential volume of water, dV, from the tensiometer, water in the tensiometer is subjected to a certain pressure, p. In doing so, the resultant water absorptive forces in the soil perform a differential mechanical work, dW, and the work performed by the pressure, p, in transferring a differential volume of water, dV, from the tensiometer to the soil is (p . dV).

When this differential volume of water, dV, leaves the tensiometer and enters through its porous walls into the soil, this volume of water, dV, displaces an equal volume of air which prevailed in the partially water-saturated voids of the soil. In this case, the displacement of a volume of air, dV, against atmospheric pressure, P_a, results in a differential mechanical work, the magnitude of which is $(p_a \,.\, dV)$. Now, by the principle of virtual work, the total work done by all the forces on the system in any virtual displacement is equal to zero:

$$dW + (p \,.\, dV) - (p_a \,.\, dV) = 0. \tag{1}$$

A method based on the principle of virtual work similar to the one given here is described by Day[9] using a piston analogy, where the pressure on water, p, acts on a hypothetical plunger inserted into the candle-like tensiometer.

The work per unit volume of water taken up by the porous soil system and thereby done by the resultant water absorptive forces prevailing in the soil-water-temperature system is

$$dW/dV = p_a - p\,, \tag{2}$$

where

$p_a - p$ = pressure difference on the two sides of the porous wall of the tensiometer.

Equation (2) indicates that the mechanical work performed per absorbed unit volume of water by the soil is independent of the nature of forces which drive the water through the soil and holds for soils of all textures, such as sands, silts and clays. Hence this equation shows that the measurement of the water surface tension reveals only the magnitude of the total soil moisture driving pressure, $p_a - p$, as the resultant pressure available in the freezing dynamic soil system. The tensiometer measurements, thus, do not disclose in themselves the various soil moisture transport mechanisms resulting in the pressure difference $(p_a - p)$. As stated above, such $(p_a - p)$ measurements indicate only the magnitude of the total pressure difference resulting from the simultaneous acting of the various soil moisture transfer mechanisms, as they may be present and acting in the freezing soil system in nature as well as in the laboratory.

THE SUBPRESSURE EQUATION

The nature of the subpressure distributions in a freezing soil as a function of time and position of the tensiometers above the ground-water table is illustrated in Fig. 6. In this figure the symbols T_1, T_2, T_3, T_4 and T_5 mean the numbers of tensiometers.

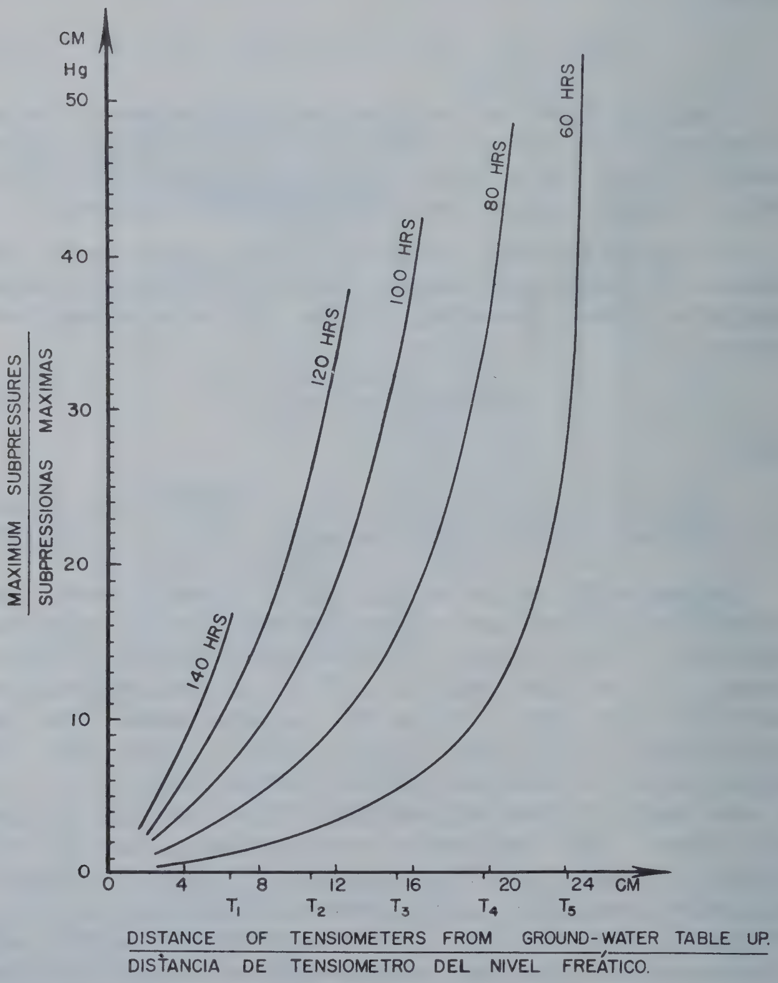

Fig. 6 — Subpressure curves.

Fig. 6 — Curvas de subpresión.

The general equation of the subpressure as a function of position of the tensiometer, h, above the ground-water table and time, t, is derived as

$$p_s = \frac{a \cdot h}{1 - b \cdot h} \qquad (3)$$

where

$$a = \frac{(t - 44.78)^{1.31373}}{241.08} \qquad (4)$$

and

$$b = (0.84674)\ (10^{0.0068469 \cdot t})\ (t^{-1}) \qquad (5)$$

are experimental coefficients.

Thus, if several soil freezing experiments with the same soil are performed under similar experimental conditions, then the subpressure, p_s, at any position and at any time can be calculated. For example, the subpressure at h = 19.8 cm (= 7.8 in) and after 67 hours of freezing (lapsed time) and at an average freezing thermal gradient of 0.62°C/cm is calculated by Eq. (3)

$p_s = 17.22$ cm pressure head of mercury or

$p_{sw} = (13.56)\ (p_s) = (13.56)\ (17.22) = 233.5$ cm pressure head of water.

The maximum subpressure recorded in the author's laboratory work on the Dunellen soil (a glacial outwash material which texturally is a silty sand) with 1.9 g/cm^3 = 120 pcf at 12% initial moisture content is $p_s = 32.0$ cm head of mercury at an average thermal gradient of 1.35°C/cm. This magnitude of subpressure was attained after 30.33 hours of intensive freezing.

CONCLUSIONS

1) The tensiometer theory is supported by the theory on virtual work.

2) Tensiometer measurements with freezing soil systems do not disclose the nature of the various possible

mechanisms by means of which soil moisture is translocated from regions at higher temperatures to regions at lower temperatures. The measurements indicate the total magnitude of subpressure, $p_a - p$, only, which is combination of all possible causes governing the moisture flow in the freezing soil system.

3) Soil moisture tension (subpressure) measurements are related to the work which the freezing soil system must perform against the action of the surface forces in order to transfer soil moisture from the ground-water table to the cold front.

4) Theoretically, tensiometer readings indicate subpressure values up to about one atmosphere. Reliable readings, however, can be obtained by tensiometers up to only about 0.85 atm = 646 cm Hg = 8760 cm of water pressure, because otherwise much or all of the water may be sucked out of the tensiometer, bringing about, among other things, the collapse of the plastic tubing which connects the tensiometer with the manometer tube. Hence the tensiometer reading become erratic.

5) A tensiometer affords continuous measurements of the subpressures, $p_a - p = p_s$, the motive force for translocating the soil moisture.

6) The moisture tensions are different for different types of soils mainly because of the different surface characteristics of the soil particles, their electrophysical properties, soil structure, texture and density.

7) The placing of thermistors, tensiometers and electrodes at different depths permits one to observe in the freezing soil system the development of temperature and subpressure gradients causing the soil moisture to flow, and the induced electromotive force between the two ends of the freezing soil system facilitating the upward flow of soil moisture.

8) The experimental results permit the establishment of a general empirical equation expressing the subpressure, p_s, as a function of the position, h, of the tensiometer from the ground-water table, and the elapsed time, t, from the beginning of freezing the soil system.

9) Examination of tensiometers after a soil freezing test reveals that those tensiometers which were intercepted

by the frost penetrating into the soil contained ice. However, in the author's soil-freezing experiments with tensiometers during the past eight years, no tensiometer was observed to be damaged because of the freezing temperatures, viz. ice in and around them.

10) The maximum developed subpressure in a freezing soil system prepared from the Dunellen soil, a silty glacial outwash material from New Jersey, has been measured in the author's laboratory experimental work as $p_s =$ $= 32.0$ cm head of mercury.

11) It is believed, though, judging from the author's soil-freezing experiments with soils packed at 90 percent porosity, and at 32.9 percent porosity, for example, that among the various possible soil moisture transfer mechanisms the upward flow in the film phase is the most effective mechanism among other simultaneously operating soil moisture transfer mechanisms, as the following figures may indicate: under simultaneous and similar freezing conditions two freezing soil systems (a silty soil) packed at $n = 90$ percent porosity and $n =$ $= 32.9$ percent, the amount of soil moisture transferred to the cold front was 62.4 cm^3 by clear vapor diffusion and 259.4 cm^3, respectively, by combined film and other possible moisture transfer mechanisms, or at ratio of about 1:4. In the cited comparative test the two soil systems were subjected to freezing for seven days at an average temperature gradient of 1.0°C/cm.

ACKNOWLEDGMENT

Grateful acknowledgment is made to the National Science Foundation for sponsoring financially by grant NSF-G 6577 the author's studies at Rutgers. The State University on "Upward Migration of Water in Soil Exposed to a Freezing Atmosphere." This paper is prepared within the scope of that project, and constitutes a part of the work.

The author also expresses his appreciation to Dr. E. C. Easton, Dean, College of Engineering, for encouragement and support of this work; to Dr. M. L. Granstrom, Chairman, Department of Civil Engineering, for advice and effective help in improving the frost action in soils research laboratory, and to Professor J. J. Slade, Jr., Director, Bureau of Engineering Research, all of Rutgers. The State University, for discussing the author's work.

The author was assisted in this work in the laboratory by two Research Assistants, Messrs. Joseph M. Casero and Warren D. Smith, Jr., both graduate students in Civil Engineering, whose assistance is likewise appreciated very much.

The author's thanks go also to Mrs. Ruth Ahrens for editing this paper.

REFERENCES

1. Jumikis, A. R. — "Some Concepts Pertaining to the Freezing Soil Systems", *Special Report No. 40. Water and Its Conduction in Soils,* (An International Symposium), 1958, pp. 178-190, Highway Research Board, National Academy of Sciences, Washington, D.C.

2. Jumikis, A. R. — "The Soil Freezing Experiment", *Bulletin No. 135,* Highway Research Board, 1956, pp. 150-156, National Academy of Sciences, Washington, D.C.

3. Baver, L. D. — *Soil Physics,* 1948, pp. 211, 212, John Wiley & Sons, Inc., New York.

4. Richards, L. A., and Gardner, W. — "Tensiometers for Measuring the Capillary Tension of Soil Water", *Journal,* American Society of Agronomy, vol. 28, pp. 352-358 (1936).

5. Jumikis, A. R., and Turner, K. A., Jr. — "Report on the Construction of an Improvised Apparatus to Measure the Suction Force in Subgrade Soils upon Freezing", April 15, 1954, submitted to the Joint Highway Research Project Committee, Rutgers. The State University, New Brunswick, New Jersey (mimeographed).

6. Jumikis, A. R. — "Suction Force in Soils upon Freezing", *Proceedings,* American Society of Civil Engineers, Vol. 80, Separate No. 445, pp. 445-1 to 445-4, New York (June, 1954).

7. Timoshenko, S. — *Theory of Elasticity,* 1934, p. 138, McGraw-Hill Book Co., Inc., New York.

8. Jumikis, A. R. — "Concerning a Mechanism for Soil Moisture Translocation in the Film Phase upon Freezing", paper presented at the 39th Annual Meeting of the Highway Research Board, January, 1960, Washington, D.C.

9. Day, P. R. — "Soil Moisture Tension Measurements: Theoretical Interpretation and Practical Application", *Clay and Clay Minerals, Proceedings,* 3d National Conference on Clays and Clay Minerals, held at the Rice Institute, Houston, Texas, October 26-29, 1954. Published by the National Academy of Science, National Research Council, *Publication No. 395,* Washington, D.C., 1955, pp. 557-566.

CORRELACION DE INDICES DEL SUELO CON LA RESISTENCIA AL CORTE

GUSTAVO PEREZ GUERRA y HUGO PEREZ LA SALVIA

Ingenieros, Miembros Principales de la firma Ingeniería de Suelos S.A.
Caracas, Venezuela.

SUMARIO

El diseño de una presa en el Occidente de Venezuela planteó un interesante problema de selección de valores de diseño de la resistencia al corte a ser usados en el análisis de estabilidad. Se usó para ello una correlación que liga la resistencia al corte con granulometría y plasticidad, resolviéndose el problema de una manera que se cree es original.

Posteriormente, se aplicó el método a otros casos con resultados satisfactorios.

Este trabajo plantea el problema, describe la correlación y muestra los resultados obtenidos.

SUMMARY

The design of a dam in Western Venezuela posed an interesting problem in the selection of design values of shear strength for stability analysis. A correlation was found which links shear strength to grain size and plasticity, thus solving the problem in what it is thought to be an original way.

The same method was later applied to other cases with satisfactory results.

The paper states the problem, describes the correlation and shows the results obtained.

CASO DE LA PRESA EL DILUVIO

Esta presa, situada a 70 kilómetros al Oeste franco de Maracaibo, en el occident de Venezuela, será una estructura de enrocamiento de 85 mts. de altura, que embalsará 380.000.000 m^3 de agua para abastecimiento de la Ciudad de Maracaibo y riego de 10.000 hectáreas de tierra. El elemento impermeable de la presa será un núcleo inclinado de tierra compactada, obtenida de un depósito cercano.

El préstamo es un cono aluvial, producto de desintegración y trasporte de rocas basálticas, calizas y graníticas de la Sierra de Perijá. El suelo es una arcilla marrón-rojiza a crema, con cantidades variables de arena y grava; varía de GC a CL en la Clasificación Unificada y tiene las características indicadas en las Figuras 1 y 2. La exploración del préstamo se hizo por meio de numerosas fosas y taladros de mano, distribuídos para cubrir bien toda el área.

La resistencia al corte del depósito se investigó por medio de ensayos de compresión triaxial del tipo $\overline{R}$ con medición de presión de poros, usando el equipo ilustrado en las Figuras 3 y 4. Todos los ensayos, con una única excepción, se hicieron con especímenes de 1.5" de diámetro y 3" de altura, compactados a la densidad deseada en un aparato Harvard de compactación en miniatura dotado de un cilindro de las dimensiones apropiadas. Los especímenes se cortaron a una rata de deformación controlada de 0.06% por minuto. El ensayo MI se hizo con especímenes de 2.8" de diámetro y 5.6" de altura, compactados por episonamiento en un cilindro especial.

Para la preparación de especímenes de 1.5" de suelos gruesos, se tamizó la muestra por un tamiz No. 4; para especímenes de 2.8" el tamizado se hizo con un tamiz de ½". En algunos ensayos se sustituyó la fracción gruesa así removida con un peso equivalente de la fracción comprendida entre tamices No. 10 y No. 4.

Los especímenes se compactaron a la densidade óptima normal, con contenidos de humedad alrededor de 2% por encima de la óptima normal. Las presiones de poro se midieron en la base de la muestra con un aparato de desplazamiento nulo de tipo Bishop. En ningún ensayo se usó contra-presión.

Las envolventes de los ensayos $\overline{R}$ reflejan la variación amplia de las diversas muestras ensayadas, como se podrá observar en la Figura 5, la cual muestra las envolventes límites obtenidas en la serie de catorce muestras ensayadas.

No se pudo encontrar ninguna tendencia de muestras de iguales características a agruparse en zonas locales del préstamo. Ante la necesidad de seleccionar un valor de resistencia al corte para usarlo en el análisis de estabilidad, se buscó alguna correlación válida, que permitiera estimar estadísticamente la resistencia del depósito a base del gran número de muestras clasificadas en el laboratorio.

Después de varios tanteos se encontró que existía una buena correlación entre el ángulo de la envolvente $\overline{R}$ y un

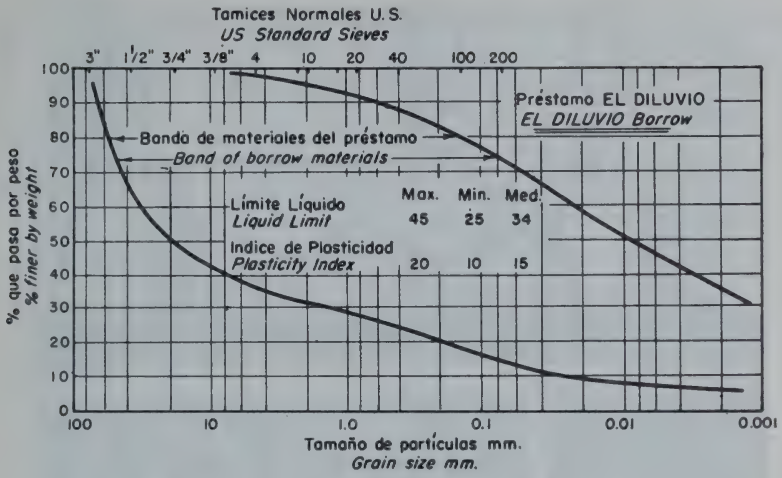

Fig. 1 — Características del Préstamo El Diluvio.

Fig. 1 — Characteristics of El Diluvio Borrow.

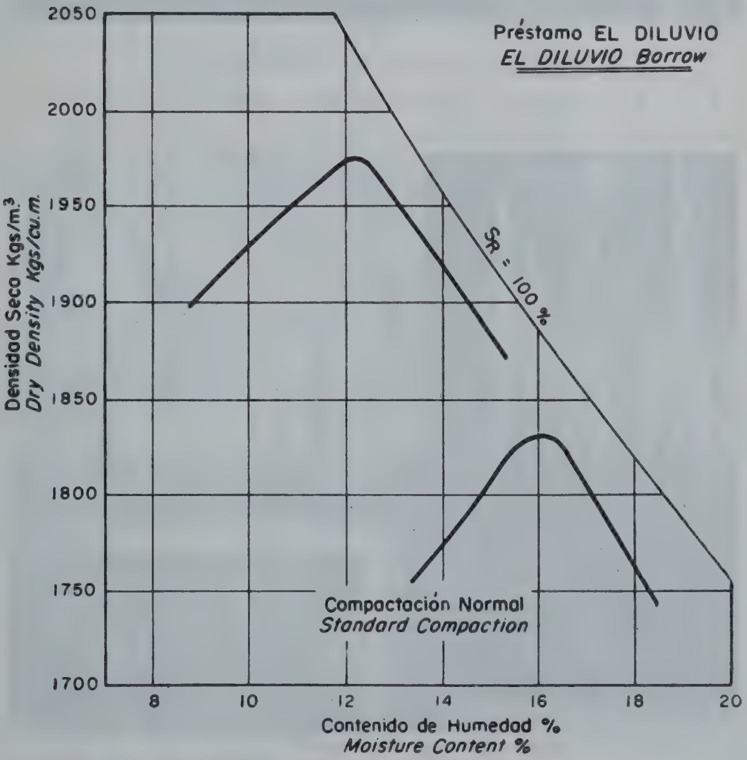

Fig. 2 — Banda de compactación del Préstamo El Diluvio.

Fig. 2 — Compaction band of El Diluvio Borrow.

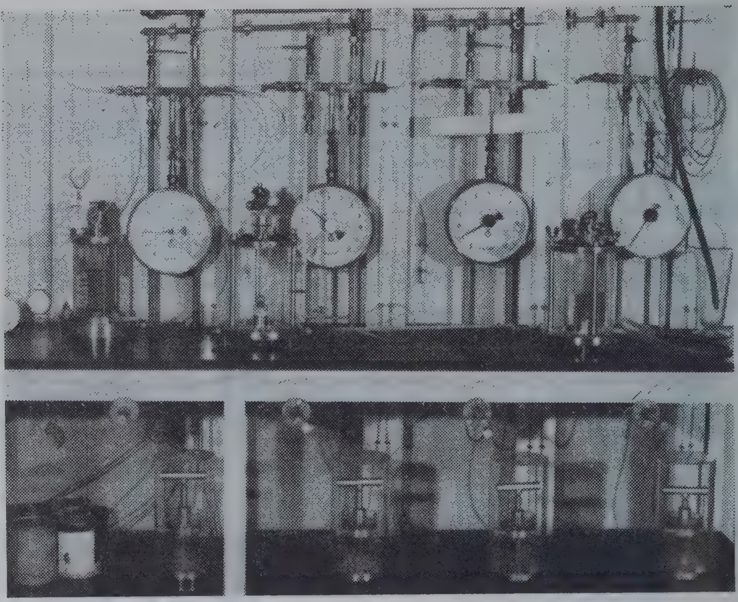

Fig. 3 — Aparatos de presión lateral.

Fig. 3 — Lateral pressure apparatus.

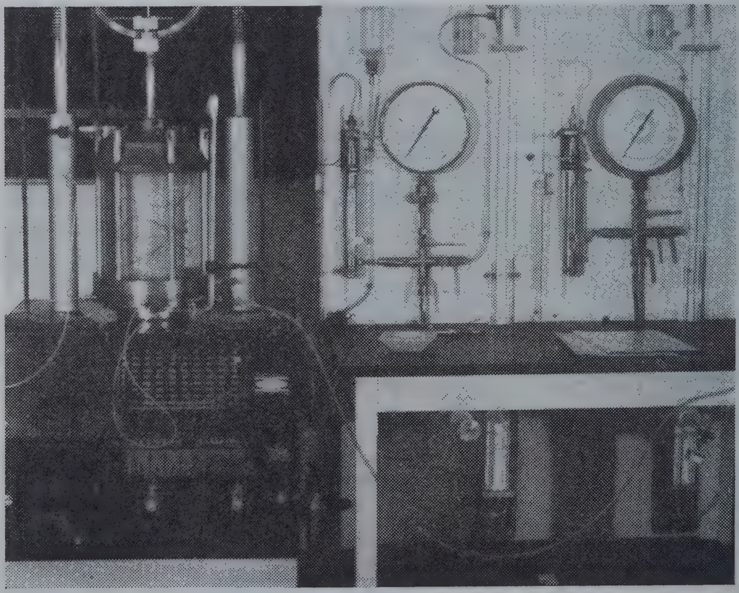

Fig. 4 — Equipo triaxial.

Fig. 4 — Triaxial equipment.

factor, "PF", obtenido multiplicando el índice de plasticidad del suelo por la fracción decimal de partículas menores de 60 micrones. La fracción de partículas menores de 60 micrones se tomó en cada caso de la curva granulométrica del material usado para el ensayo, después de tamizado por el tamiz No. 4 o de ½", con o sin sustitución de los gruesos eliminados. La Figura 6 muestra la correlación obtenida.

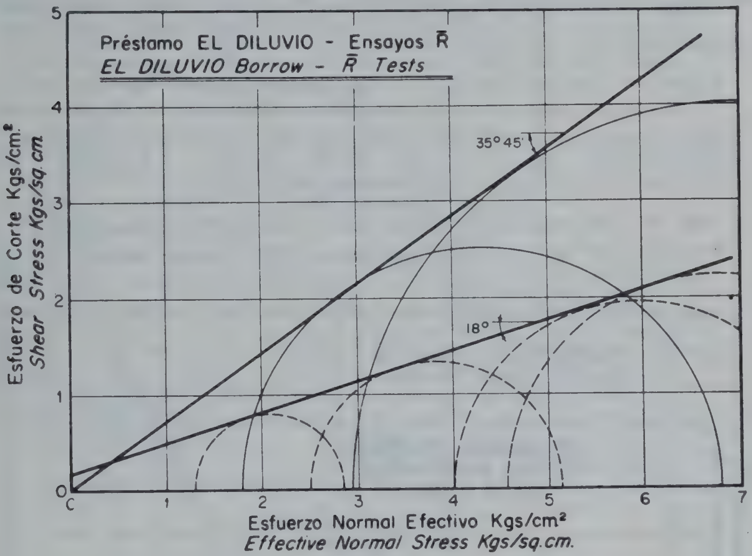

Fig. 5 — Valores límites de resistencia al corte.

Fig. 5 — Limit values of shear strength.

Los ensayos marcados M I y M II son de muestras compuestas obtenidas por mezcla a partes iguales de tres muestras del depósito. La muestra M I se ensayó quitándole la fracción mayor de ½" y la M II quitándole la fracción mayor que el tamiz No. 4. La diferencia en tamaño máximo produjo variaciones en el factor "PF" y en Tan ∅ de una muestra a otra, pero ambos puntos caen bien dentro de la zona de la curva media. Esto parece demostrar que las curvas PF vs. tan ∅ obtenidas pueden ser usadas para estimar los valores de tan ∅ de las muestras reales completas, cuyos factores PF serán menores que los de las muestras ensayadas.

Con base a la curva de la Figura 6 se estimó la resistencia al corte de las 138 muestras clasificadas y se preparó un gráfico de frecuencia acumulada que aparece en la Figura 7. Puede verse que sólo el 14% del suelo del préstamo tiene un valor de tan ∅ de menos de 0.466, que fué el valor adoptado para el análisis. Se piensa que el trabajo de explotación del préstamo y el trasporte y la colocación en la obra tendrán un efecto reductor en el porcentaje de suelo con resistencia menor que el valor de diseño.

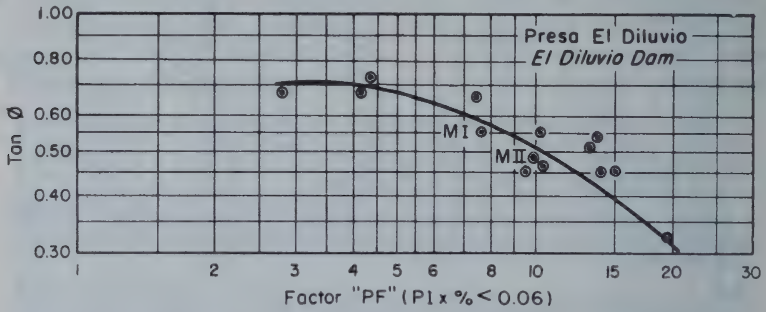

Fig. 6 — Correlación de PF vs tan Φ del Préstamo El Diluvio.

Fig. 6 — PF vs tan Φ correlation of El Diluvio Borrow.

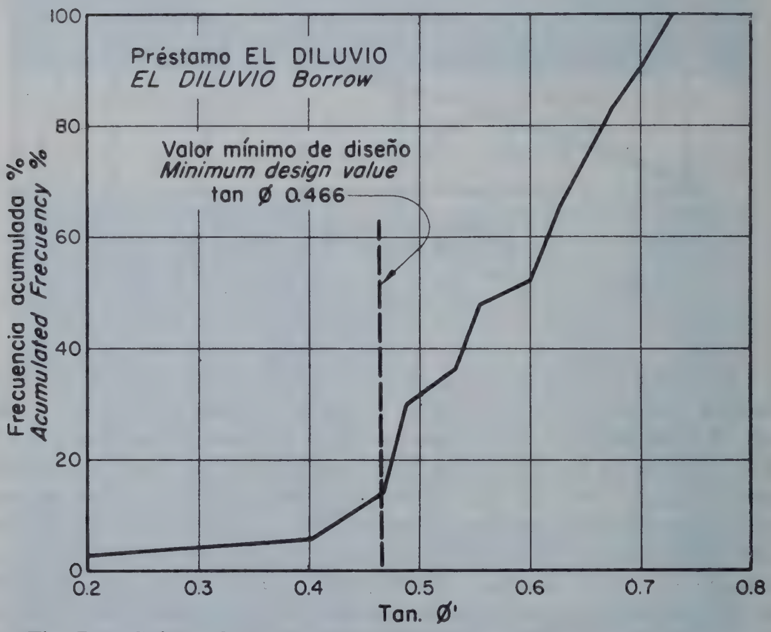

Fig. 7 — Gráfico de frecuencia acumulada del Préstamo El Diluvio.

Fig. 7 — Accumulated frecuency graph of El Diluvio Borrow.

CASO DE LA PRESA EL ISIRO

Posteriormente se encontró una situación similar en el diseño de la Presa El Isiro, 7 kms. al sur de Coro, también en el occidente de Venezuela. La presa tendrá una altura de 30 mts. y almacenará agua para el abastecimiento de la población de Coro y de la Península de Paraguaná.

La presa será de terraplén compactado, con un núcleo central de suelo fino impermeable y secciones exteriores de grava arcillosa. Ambos materiales se encuentran en una terraza de las cercanías del sitio de presa. Las Figuras 8 y 9 contienen las características de clasificación y de compactación de los suelos del préstamo. El fino impermeable es del tipo CL y la grava del GC.

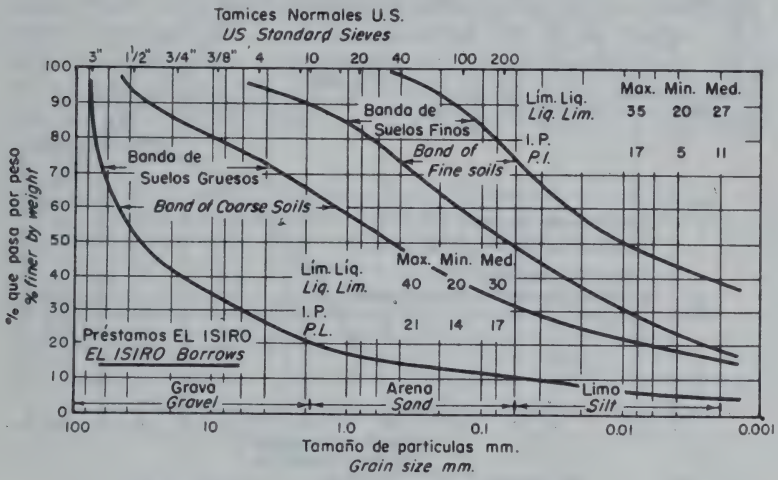

Fig. 8 — Características del Préstamo El Isiro.

Fig. 8 — Characteristics of El Isiro Borrow.

La resistencia al corte se midió, como antes, con ensayos $\bar{R}$ de especímenes de 1.5" de diámetro y 3" de altura para todos los ensayos del fino impermeable y la mayoría de los de la grava arcillosa. En estos últimos se hizo uno con especímenes de 4" de diámetro y 8" de altura y se ensayaron tres muestras en una máquina de corte directo del tipo de deformación controlada, usando especímenes de 2.5" de diámetro y de 1.9-1.3 cms. de altura. Perez La Salvia y Perez Guerra (1963) dan datos adicionales de los ensayos de esta grava arcillosa.

Las muestras triaxiales se cortaron a una rata de 0.06% por minuto; los ensayos de corte directo marcados A y C fallaron en 96 a 168 horas, mientras que el marcado B se cortó a una rata de 0.008 cms./minuto, fallando en alrededor de 2.5 horas.

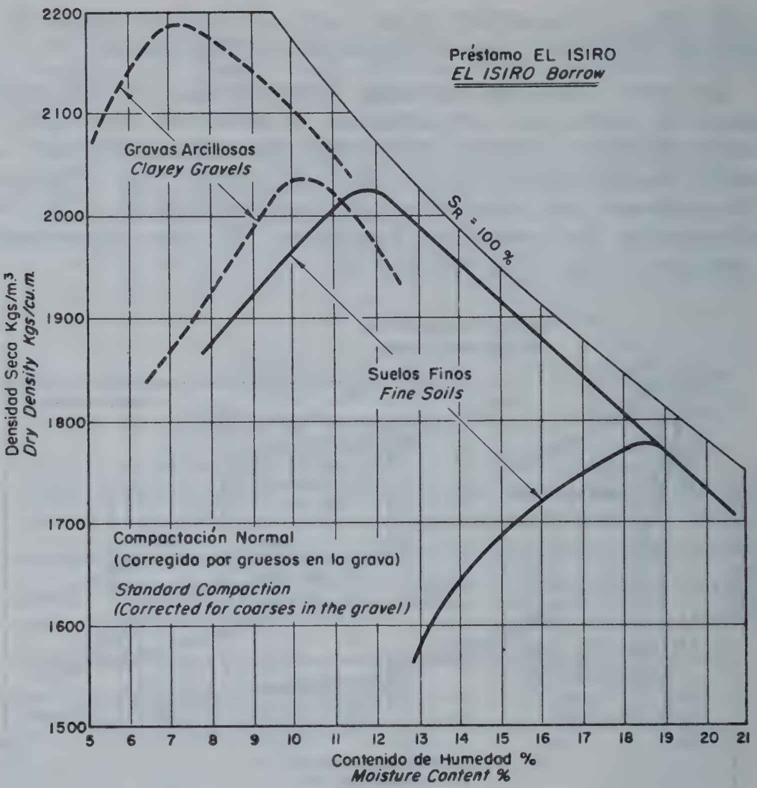

Fig. 9 — Bandas de compactación del Préstamo El Isiro.

Fig. 9 — Compaction bands of El Isiro Borrow.

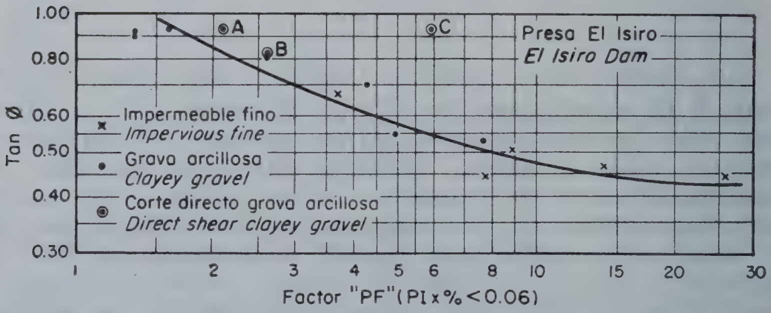

Fig. 10 — Correlación de PF vs tan Φ del Préstamo El Isiro.

Fig. 10 — PF vs tan Φ correlation of El Isiro Borrow.

La Figura 10 muestra la correlación de la resistencia al corte con el factor PF. Se notará que la correlación es especialmente buena para uma amplia variación del factor

PF y que el gráfico incluye valores tanto del impermeable fino como de la grava arcillosa. Hay un punto de la grava arcillosa, de factor PF = 6, que cae completamente fuera del márgen de los otros ensayos, sin que se pueda encontrar una explicación razonable, excepto error de clasificación.

OTROS CASOS

La Figura 11 muestra unos pocos datos de los préstamos para otros dos proyectos de presa, pero sólo con fines comparativos, ya que la homogeneidad de estos suelos no justifica la aplicación del método. La homogeneidad se refleja en la poca variación de tan ∅ y en la baja pendiente de las curvas de correlación. A pesar de esto, la correlación es satisfactoria.

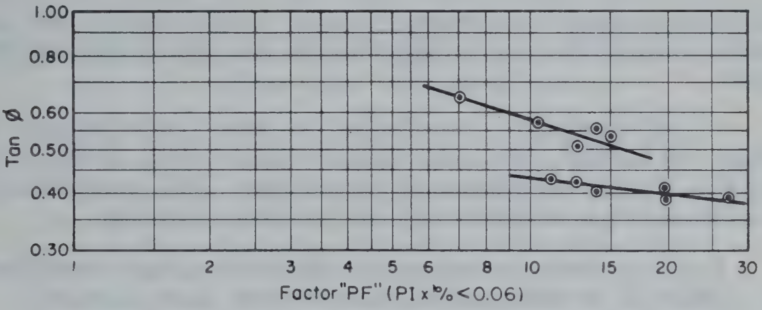

Fig. 11 — Otros dos casos de correlación.

Fig. 11 — Another two cases of correlation.

Se notará que los resultados de los últimos tres ejemplos son mejores que los del primero. Esto puede atribuirse a pequeños refinamientos de técnica. Como el porcentaje de finos (—0.006 mm.) tiene una gran influencia en el valor del factor PF, es necesario cuidar faltas de exactitud debidas a una operación rutinaria. Por ejemplo, se encontró al sustituir la fracción gruesa de una muestra con un peso equivalente de, digamos, fracción de — No. 4 a + No. 10, que esta última fracción debe ser lavada para evitar la inclusión de los finos que recubran las partículas de la fracción añadida, los cuales, de otra manera, alterarían el porcentaje de finos usados para el cálculo del factor de correlación.

Tratándose de suelos muy finos, con 90% o más menor que 0.06 mm., la correlación parece ser todavía válida, pero entonces el factor PF se convierte en el índice de plasticidad IP, ya que la fracción fina vale 1.0, o poco menos. Varios investigadores han notado la correlación entre el ángulo verdadero de fricción y el índice de plasticidad de arcillas, habiéndose publicado recientemente un buen ejemplo de correlación por Kwan Yee Lo (1962) ensayando materiales volcánicos del Valle de México. En el artículo en referencia se da también un resúmen de resultados de otros investigadores.

CONCLUSIONES

1. Parece existir una correlación definida entre el ángulo efectivo de fricción de un suelo y un factor "PF", obtenido multiplicando el índice de plasticidad del suelo por la fracción decimal del porcentaje de partículas menores de 0.06 mm.

2. Parece haver una curva de correlación para cada depósito de suelos del mismo orígen y composición, sin importar la distribución de tamaños de los suelos del depósito dado.

3. Al aplicar la correlación se debe tener cuidado de tomar en cuenta *todos* los finos incluídos en la muestra ensayada, siendo especialmente importante esta consideración cuando se haga sustituciones de fracciones gruesas.

4. Se necesita investigación sistemática para establecer la validez de la correlación para diversos tipos de suelos.

RECONOCIMIENTOS

El trabajo de laboratorio que sirve de base a este artículo se hizo en relación con diseños preparados para el Instituto Nacional de Obras Sanitarias de Venezuela. El Ingeniero Peter S. Parsonson estuvo a cargo del laboratorio y tomó parte importante en el desarrollo de la correlación; el Inginiero Fernando Trías Matheus colaboró en el trabajo de laboratorio.

REFERENCIAS

Perez La Salvia y Perez Guerra (1963) — "Notas sobre Permeabilidad y Resistencia al Corte de Gravas Arcillosas" — Memoria 2.° Congreso Pan. Am. M. de S. y Ciment. São Paulo-Rio de Janeiro-Belo Horizonte, Brasil, 1963, Vol. I.

Kwan Yee Lo (1962) — "Shear Strength Properties of a Sample of Volcanic Material of the Valley of Mexico" — Géotechnique, Vol. XII, No. 4, pag. 303.

NOTAS SOBRE PERMEABILIDAD Y RESISTENCIA AL CORTE DE GRAVAS ARCILLOSAS

HUGO PEREZ LA SALVIA y GUSTAVO PEREZ GUERRA
Ingenieros, Miembros Principales de la firma Ingeniería de Suelos S.A.
Caracas, Venezuela.

SUMARIO

En dos casos recientes, la firma de los autores hubo de diseñar presas de tierra usando gravas arcillosas de terrazas sedimentarias como material de préstamo.

Una de las presas es El Isiro, a 7 kms. al sur de Coro, al occidente de Venezuela; la otra es Santa Clara, en el oriente del país, cerca de la población de Clarines.

El depósito de grava arcillosa de El Isiro fué localizado desde los reconocimientos preliminares y se pensó en usarla para terraplén permeable y semi-permeable; el trabajo de laboratorio hecho posteriormente hizo ver, sin embargo, que la grava tiene una permeabilidad "baja" a "muy baja". Al mismo tiempo, los ensayos de corte dieron valores de tan Φ *mayores de 0.8, a pesar del alto contenido de finos.*

Posteriormente, se encontraron gravas del mismo tipo en el diseño de la Presa Santa Clara, que es una estructura menos importante, de solo 12 mts. de altura. La experiencia del caso anterior permitió diseñar la presa baja con un número limitado de ensayos.

Este trabajo muestra los resultados de ensayos de laboratorio de permeabilidad y resistencia al corte de estas gravas arcillosas.

SUMMARY

In two recent instances, the authors' firm designed rolled-earth dams using clayey gravels from sedimentary terraces as borrow material.

One of the dams is El Isiro, 7 kms. south of Coro, in western Venezuela; the other is Santa Clara, in eastern Venezuela, near the town of Clarines.

Preliminary field reconnaissance for El Isiro Dam located the gravel deposit and planned to use it for

pervious to semi-pervious fills; subsequent laboratory work showed, however, that the gravel has a "low" to "very low" permeability. Shear tests, at the same time, gave values of tan Φ higher than 0.8 in spite of the high content of fines.

Later on, material of the same kind was found in connection with the design of Santa Clara Dam, which is a structure of lesser importance, only 12 meters high. The experience of the former case permitted the design of the low dam with a limited amount of testing.

This paper shows the laboratory results of permeability and shear tests on these clayey gravels.

GRAVAS DE EL ISIRO

Las gravas del depósito están formadas por partículas redondeadas de arenisca y caliza duras, en una matriz limo-arcillosa, de alta compacidad en su estado natural. Las Figuras 1 y 2 muestran las características de clasificación y compactación de la grava.

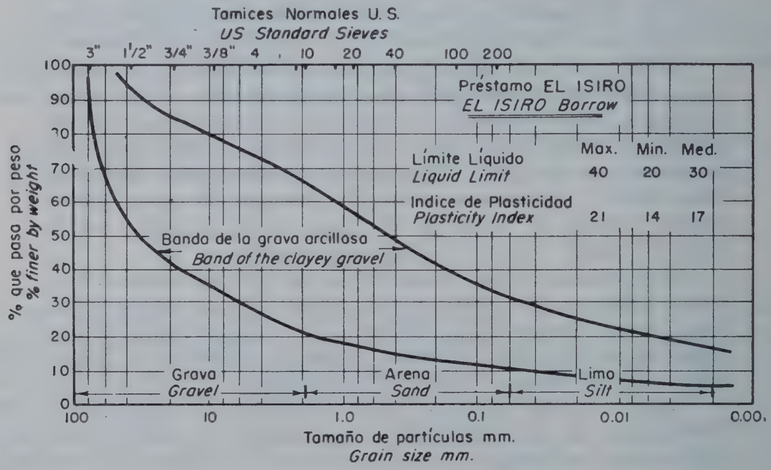

Fig. 1 — Características de la grava arcillosa de El Isiro.

Fig. 1 — Characteristics of El Isiro clayey gravel.

Ensayos de permeabilidad. Se hicieron varios ensayos de carga variable con un permeámetro vertical, usando muestras de 22.5 cms. de diámetro y alrededor de 20 cms. de altura. El tamaño máximo de grano usado para los ensayos fué de 1½"; las muestras se compactaron directamente en el permeámetro a la densidad deseada.

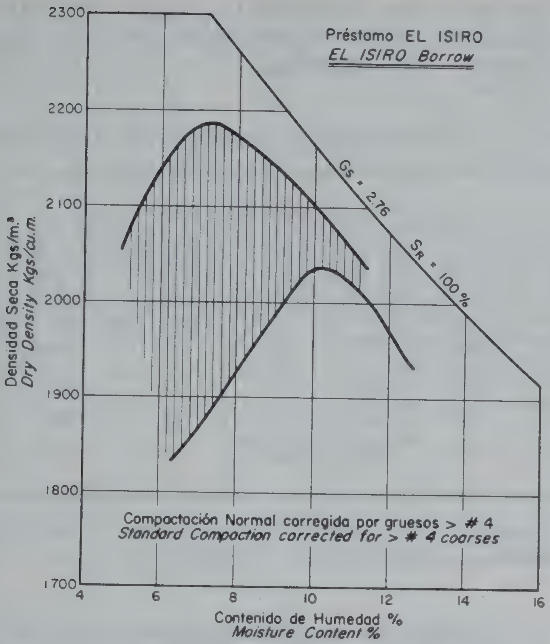

Fig. 2 — Banda de compactación de la grava arcillosa de El Isiro.

Fig. 2 — Compaction band of El Isiro clayey gravel.

Esta primera serie de ensayos fué insatisfactoria, pues hubo filtraciones entre la muestra y la superficie interior del permeámetro. Se ideó entonces una manera de colocar un sello de arcilla entre la muestra y el permeámetro, la cual permitió hacer un ensayo satisfactorio.

A continuación se hicieron ensayos comparativos con grava lavada de ¾" de tamaño máximo, a la cual se le agregaron porcentajes variables de la fracción fina pasante el tamiz No. 200 de la misma grava. Para estos ensayos se usó una cámara triaxial de 4" de diámetro, con una presión lateral efectiva de 2.15 kgs./cm^2. La carga se creó con buretas conectadas a las planchas porosas de bronce de la base y el tope de la muestra. Las muestras se colocaron secas al aire, compactándolas en un cilindro especial y sostenidas con algo de vacío hasta aplicar la presión lateral. La Tabla 1 da los datos y resultados de estos ensayos.

Los ensayos hacen ver que buena parte de la permeabilidad de esta grava proviene de su buena gradación y que los valores de permeabilidade están de acuerdo con los contenidos de grava y de finos del suelo. En general, puede suponerse que para una densidad de campo de 2.200 kgs./m^3, la permeabilidad probable del terraplén será del alrededor de 1×10^{-7} centímetros por segundo.

Tabla 1 — Permeabilidad de las gravas de El Isiro

Ensayo No.	Tamaño maximo	Diametro muestra	Altura muestra	Contenido de grava %	Contenido finos (—200) %	Densidad seca kgs./m^3	"k" cms./sec.
1	1-1/1	18.0	25.2	32	27	2017	0.5 ×10^{-7}
2	3/4	10.16	21.5	18	0	1915	3.0 ×10^{-4}
3	3/4	10.16	21.5	18	15	1940	1.2 ×10^{-5}
4	3/4	10.16	21.5	18	30	1987	0.75×10^{-6}

Nota: La humedad de la muestra del ensayo No. 1 fué de 12.1%; las demás se compactaron secas al aire.

Tabla 2 — Resistencia al corte de las gravas de El Isiro

Ensayo No.	Muestra No.	Tipo de ensayo (véase clave)	Diametro muestra	Altura muestra	Tan Φ
1	12.231	Qd cs — Nº 4	10.0	21.5	0.900
2	12.231	Qd cs — ¾"	10.16	21.5	0.933
3	12.231	$\overline{R}$ cs — Nº 4	3.57	8.0	0.900
4	12.387	CD cs — Nº 4	3.56	7.93	0.810
5	12.387	CD cs — Nº 4	6.40	1.91	0.810
6	12.386	CD cs — Nº 4	6.40	1.91	0.933
7	12.409	CD cs — Nº 4	6.40	1.30	0.933

Clave:	Qd	Ensayo Rápido, compactado y ensayado en seco
	m$\overline{R}$	Ensayo Consolidado — Drenado con medición de presión de poros
	CD	Ensayo de Corte Directo
	cs	Con sustitución de la fracción gruesa
	ss	Sin sustitución de la fracción gruesa

Resistencia al corte. Se ensayaron al corte cuatro muestras típicas de la grava. Los datos de los ensayos aparecen en la Tabla 2, y la Figura 3 da las granulometrías reales de las muestras ensayadas.

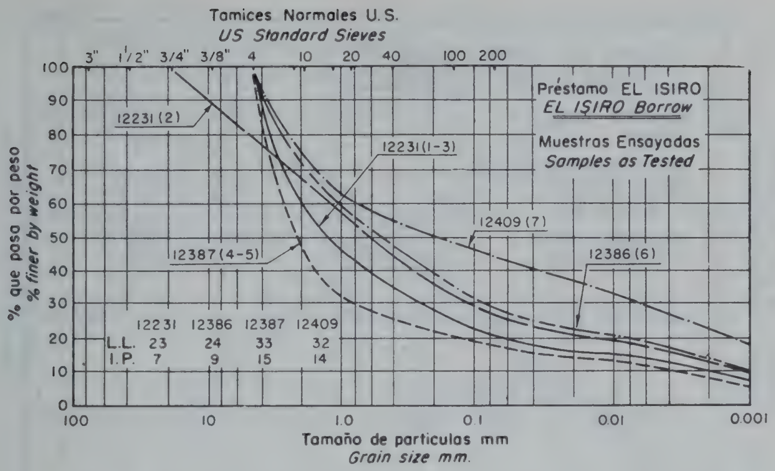

Fig. 3 — Préstamo El Isiro — Características de las muestras ensayadas.

Fig. 3 — El Isiro Borrow — Characteristics of samples tested.

Para evitar el largo tiempo requerido por ensayos de tipo $\overline{\mathrm{R}}$ en muestras de 4" de diámetro, se ensayaron las muestras 12.231 y 12.387 usando especímenes de 3.57 cms. de diámetro, con un tamaño máximo del tamiz No. 4. La influencia de la presencia de las partículas más gruesas se investigó con dos ensayos Q con especímenes de 4", compactados y ensayados en seco para evitar la influencia de presiones de poros. Uno de los ensayos Q se hizo en la fracción que pasa la malla de ¾" y el otro en la fracción que pasa el tamiz No. 4. Las Figuras 4 y 5 dan los resultados de estos ensayos. Se verá que los ensayos Q (en seco) y R de la fracción menor que el No. 4 dan resultados practicamente iguales y que hay un pequeño aumento de resistencia en el ensayo Q (en seco) de la fracción menor de ¾".

En base a estos resultados, la muestra 12.387 se ensayó con especímenes pequeños de la fracción menor que el No. 4. Además del ensayo $\overline{\mathrm{R}}$ de esta muestra, se hizo un ensayo de corte directo, cuyos resultados figuran en el diagrama de Mohr de la Figura 6.

Las muestras 12.386 y 12.409 se ensayaron al corte directo con los resultados mostrados en la Figura 7.

Los ensayos triaxiales $\overline{\mathrm{R}}$ se hicieron a una rata controlada de deformación de 0.06% por minuto y las presiones

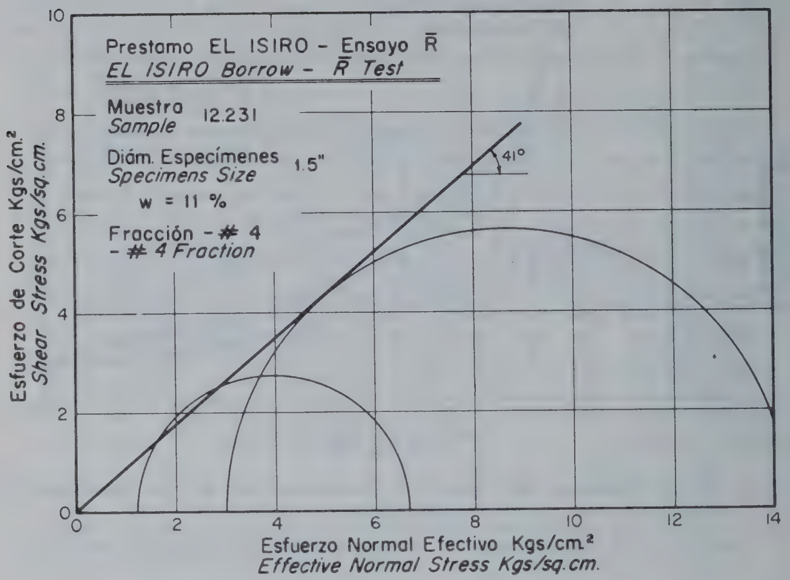

Fig. 4 — Préstamo El Isiro — Ensayo $\overline{\text{R}}$ de muestra 12231.

Fig. 4 — El Isiro Borrow — $\overline{\text{R}}$ test of sample 12231.

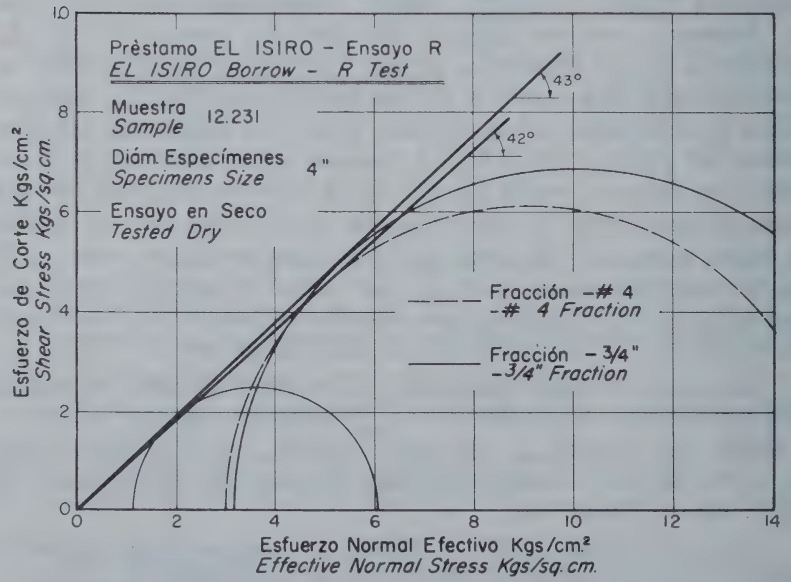

Fig. 5 — Préstamo El Isiro — Ensayo R de muestra 12231.

Fig. 5 — El Isiro Borrow — R test of sample 12231.

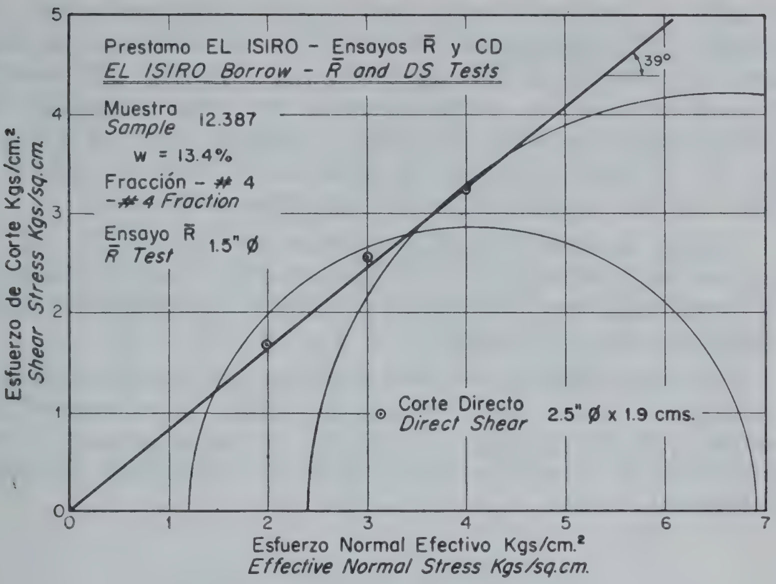

Fig. 6 — Préstamo El Isiro — Ensayos R̄ y CD de muestra 12387.

Fig. 6 — El Isiro Borrow — R̄ and DS tests of sample 12387.

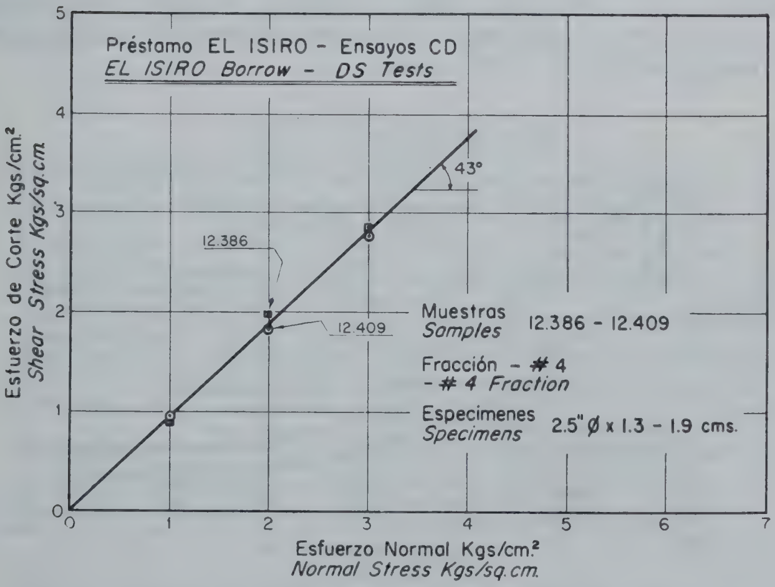

Fig. 7 — Préstamo El Isiro — Ensayos CD de muestras 12386 y 12409.

Fig. 7 — El Isiro Borrow — DS tests of samples 12386 and 12409.

de poro se midieron en la base de los especímenes con un indicador de desplazamiento nulo del tipo Bishop; la rata para los ensayos Q fué de 0.05% por minuto. El ensayo de corte directo No. 5 fué hecho a una rata controlada de deformaciones de 0.008 cms./min., mientras que los ensayos No. 6 y 7 fueron lentos, con tiempos de falla de cuatro a siete días, en una máquina de esfuerzos controlados.

Todos los ensayos, con excepción de los No. 2 y 6, se hicieron con material en el que la fracción gruesa eliminada fué sustituída por un peso equivalente de partículas comprendidas entre los tamices No. 4 y No. 16.

Se puede concluir de estos ensayos que los tamaños mayores que el tamiz No. 4 tienen un efecto relativamente secundario en la resistencia al corte de estas gravas y que para fines de diseño se puede usar con seguridad un valor de fricción de 0.9.

GRAVAS DE SANTA CLARA

Estas gravas son también de terrazas sedimentarias, con partículas redondeadas de arenisca dura, en una matriz limo-arcillosa, con alta compacidad en estado natural. Las Figuras No. 8 y 9 muestran las características de clasificación y compactación de estas gravas.

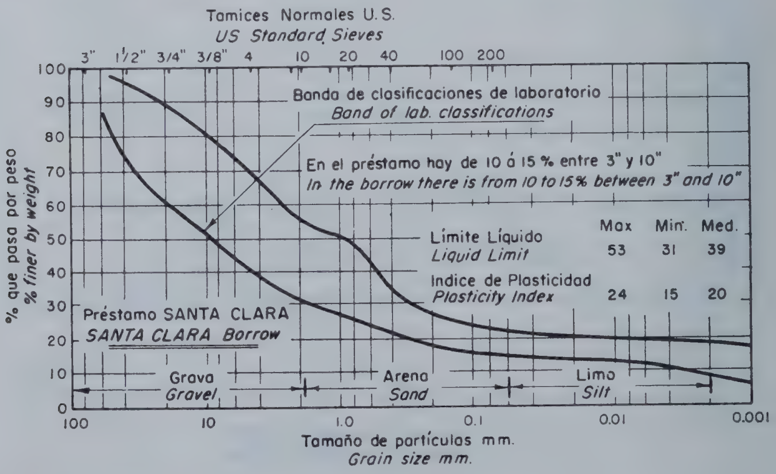

Fig. 8 — Características de la grava arcillosa de Santa Clara.

Fig. 8 — Characteristics of Santa Clara clayey gravel.

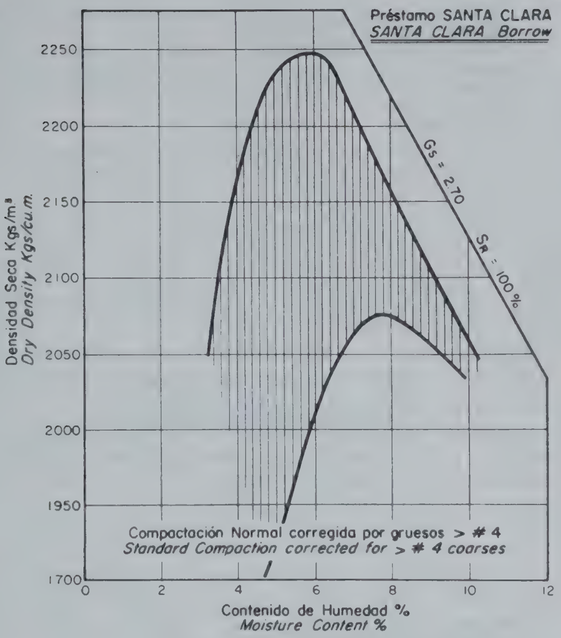

Fig. 9 — Banda de compactación de la grava arcillosa de Santa Clara.

Fig. 9 — Compaction band of Santa Clara clayey gravel.

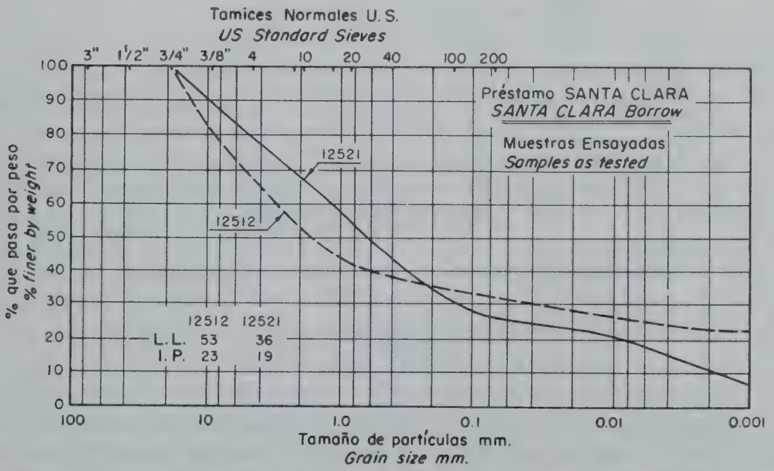

Fig. 10 — Préstamo Santa Clara — Características de las muestras ensayadas.

Fig. 10 — Santa Clara Borrow — Characteristics of samples tested.

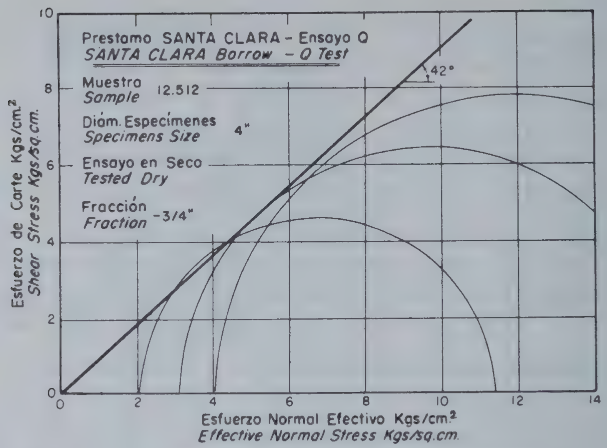

Fig. 11 — Préstamo Santa Clara — Ensayo Q de muestra 12512.

Fig. 11 — Santa Clara Borrow — Q test of sample 12512.

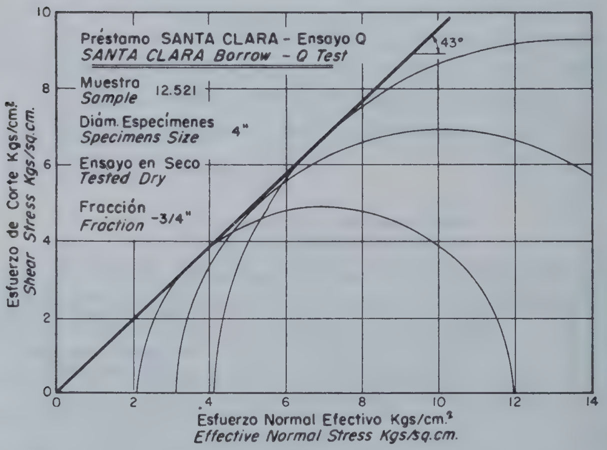

Fig. 12 — Préstamo Santa Clara — Ensayo Q de mustra 12521.

Fig. 12 — Santa Clara Borrow — Q test of sample 12521.

Resistencia al corte. Sólo dos ensayos se hicieron de esta grava, ambos del tipo Q en compresión triaxial, en especímenes de 4" de diámetro y de 215 cms. de altura, con suelo compactado seco-al-aire. Se eliminó la fracción mayor que ¾" y no se sustituyó la fracción gruesa. Los ensayos se hicieron principalmente como una comprobación, para extender a este préstamo los resultados obtenidos con la grava de El Isiro. La Figura 10 da la granulometría de las dos muestras ensayadas y las Figuras 11 y 12 los resultados de los ensayos.

COMPARACIÓN CON OTROS DATOS

Que sepamos, los únicos datos publicados son los debidos a Holtz y Ellis (1961) del Bureau of Reclamation de los Estados Unidos de América; se ensayaron cinco diferentes gradaciones de la misma grava, variando el porcentaje de grava comprendida entre los tamices No. 4 y 3", obteniéndose valores de tan ∅ variando de 0.45 a 0.68.

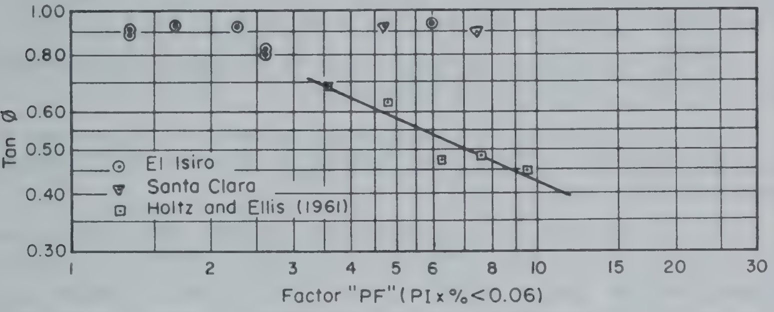

Fig. 13 — Comparición y correlación de datos.

Fig. 13 — Comparison and correlation of data.

Se puede hacer una buena comparación de los valores publicados por Holtz y Ellis y los de los ensayos de El Isiro, usando el factor de correlación "PF" desarrollado por Perez Guerra y Perez La Salvia (1963); este factor, obtenido por el producto del índice de plasticidad y el porcentaje de finos menores que 0.06 mm., parece ser determinante de la resistencia al corte de suelos compactados. Para las gravas de El Isiro el factor tiene valores de 1.3 a 2.6, mientras que la grava ensayada por el Bureau of Reclamation da valores del factor de 3.6 a 9.7. El dibujo de estos valores, que aparece en la Figura 13, muestra las diferencias y suministra, al mismo tiempo, una buena comprobación de la correlación con la grava del Bureau. Debe notarse, sin embargo, que hay un ensayo de El Isiro con un factor de 6.0 que cae lejos de los otros; los dos ensayos de Santa Clara, también mostrados en la figura, caen también fuera de la zona de los otros ensayos. No se pudo encontrar explicación a esta irregularidad de esos tres ensayos, pero se piensa que, como el trabajo de laboratorio no se hizo con fines primordiales de investigación, puede haber alguna variación entre las porciones de la muestra usada para clasificación y la usada para el ensayo de corte. Debe también notarse que mientras nuestros ensayos tienen una cohesión "cero", Holtz y Ellis encontraron una intercepción positiva en el eje de resistencias. Esto podría también relacionar-se a las diferencias en factores PF.

CONCLUSIONES

Los ensayos descritos y los resultados obtenidos permiten formular las siguientes conclusiones:

1. Las gravas arcillosas ensayadas alcanzan, cuando se las compacta con energía normal, pesos unitarios superiores a los 2.000 kgs./m^3, con textura similar a la del concreto.

2. Su gradación de partículas y su contenido de finos les confieren una baja permeabilidad.

3. Su resistencia al corte está representada por un ángulo efectivo de fricción del órden de los 40°, con cohesión practicamente nula.

4. La resistencia a la fricción parece estar determinada principalmente por el valor del factor "PF"; la fracción gruesa mayor que el tamiz No. 4 (4.76 mm.) parece tener sólo un efecto secundario en el valor del ángulo de fricción.

5. Las características de las gravas las hacen deseables para construcción de terraplenes de presa sobre fundaciones incompresibles, siempre que se drenen adecuadamente.

RECONOCIMIENTOS

El trabajo de laboratorio que sirvió de base a este artículo fué hecho en relación con diseños hechos para el Instituto Nacional de Obras Sanitarias de Venezuela, con los Ingenieros Peter S. Parsonson y Fernando Trías Matheus a cargo del laboratorio.

REFERENCIAS

Holtz y Ellis (1961) — "Triaxial Shear Characteristics of Clayey Gravel Soils" — Proc. 5ta Conf. Int. de Mec. de Suel. e Ing. de Fund., Paris, 1961, Vol. I, pag. 143.

Perez Guerra y Perez La Salvia (1963) — "Correlación de Indices del Suelo con la Resistencia al Corte" — Proc. 2.ª Conf. Pan-Am. de Mec. de Suel. y Cim., Brasil, 1963, Vol. I.

SHEAR STRENGTH OF CLAY-SHALES FOUND IN THE SOUTHWESTERN U.S.A.

F. M. VAN AUKEN
Chief of Geology, Soils and Materials Branch
U.S. Army Engineer Division, Southwestern, Dallas, Texas (USA)

SUMMARY

Three shale types (Del Rio, Eagle Ford, Pepper) and one bentonitic shale were investigated to determine their effective shearing strengths. Comparison of the effective strength of shales that have failed as a result of natural or man-made slides with strengths determined by conventional laboratory methods shows that the latter are invariably too high. Procedures have been developed in the laboratory to produce effective strength parameters by working with size and shape of specimens and variation in rate of testing. As a result of the development of new techniques in testing, more reliability can be placed in the laboratory evaluation of the strength of shales. Long duration tests on thin specimens 0.25 inches thick are required, as is a precision strain controlled direct shear device capable of sustained constant strain application for up to 10 days per test. Use of the torsion-compression test to seek out weak zones which would have to be manually pre-selected in the direct shear test provides answers to some of the gaps of information. The triaxial compression test does not generally fit a test program for development of the shear strength of brittle shales.

RESUMEN

Investigamos tres tipos de pizarra arcillosa (Del Rio, Eagle Ford y Pepper) y un pizarra arcillosa de bentonite para determinarse sus resistencias efectivas al esfuerzo cortante. Comparación de la resistencia efectiva de pizarras arcillosas que fallaron de resultas de corrimiento natural o provocado con resistencias determinadas por métodos tradicionales de laboratorio demostra que las últimas son demasiado altas. Desarrollamos unos procedimientos en el laboratorio para producir parámetros efectivos de resistencia con manipular el tamaño y forma de la muestra y también manipular la velocidad de los ensayos. De resultas de los nuevos procedimientos en los ensayos, más confianza se tenemos en el valorar de laboratorio de la resistencia de pizarras arcillosas. Ensayos de larga duración en muestras finas (0.25 pulgadas) son *necesarios y también uno aparato de precisión de corte directo de deformación controlada, competente de mantener aplicación de deformación constante hasta 10 días por ensayo. Usamos el ensayo de torsión y compresión para determinar las zonas débiles. El ensayo de compresión triaxial no sirve por lo general a un programa de estudio de la resistencia al corte de pizarras arcillosas quebrádizas.*

INTRODUCTION

Failure of slopes and/or foundations of earth structures is generally a progressive phenomenon. Failure initially commences with local overstress where shearing stresses exceed the available shearing resistance. As the mass is set in motion, the failure spreads. This occurs because the resistance of most materials decreases with an increase in deformation. Finally, a new balance of forces is achieved or a general failure occurs. Consequently, it is obvious that the initial shearing stresses represent maxima and that the average shearing resistance of the mass is much lower than the initial shearing strength of the material.

Rutledge (1941) pointed out that the shearing resistance of materials as determined by laboratory testing is generally smaller than that of the material in situ, because of disturbance in sampling and preparation of specimens for test, change of environment and in many cases due to progressive failure during test. However, testing procedures commonly used for determination of the shearing resistance of materials often fail to emphasize the importance of time effects on the change of shear strength. This is unfortunate because the latent effects of time, environment and progressive failure are often neglected in the methods currently used in analyzing the stability of slopes and foundations for earth structures. However, these effects are sometimes considered by arbitrarily reducing the strength components used in design or by reverse analysis of the strength of the materials in question based on an actual failure. Many investigators have set forth procedures for determining the shear strength of clays, especially those homogeneous soils for which there is generally found close agreement between theory and practice. This close fit is generally abetted by the ease with which these materials may be sampled, prepared for test and tested. Not so, is the case for those materials in the quasi-region between sensibly plastic and brittle states. In this area are found the shales and clay shales. Techniques for determining the strength of shales which, while exhibiting the general physical characteristics of clays, nevertheless perform like brittle materials, have not been fully exploited.

CLAY SHALES

In the southwestern area of the USA, the Corps of Engineers is constructing a group of earth dams in an area characterized by the presence of compaction shales which serve as the foundation for the dams and their ancillary structures. These shales, located in the Gulf Coastal Plain area of Texas, are generally of Upper or Lower Cretaceous Age. Typically, the shales are nonfissile to fissile, laminated to nonlaminated and at the overburden contact are soft, clayey, gray to tan in color and are variably weathered. At greater depths, these shales become fresh and unweathered and are soft to moderately hard, massive and variably calcareous with occasional limestone and bentonite streaks scattered throughout the mass. These shales slake rapidly upon exposure to air and break down rapidly with alternate wetting and drying action. The geology of the area is complex, inasmuch as the Gulf Coastal area has been alternately subjected to inundation of the land mass and repeated immergence from the sea. While these shales are overconsolidated, large volume changes associated with local changes of load as occasioned by structural excavations are not large. This suggests that near surface volume changes have become maximized by a long duration expansion cycle.

There are three major shale formations at one of the dam sites (Waco) known as Eagle Ford, Pepper and Del Rio in descending order from the surface. The Eagle Ford shale contains numerous bentonite seams. All three shale formations form the foundation for the earth fill. The general physical characteristics of these shales are:

TABLE 1 — Summary of Physical Characteristics

Mineral constituents	Eagle Ford bentonite	Eagle Ford shale	Pepper shale	Del Rio shale
Montmorilonite, %	50	20	20	10
Illite, %	15	15	20	15
Kaolinite, %	15	20	20	15
Quartz, %	5	10	15	5
Gypsum, %	—	—	5	—
Calcite, %	2	10	—	—
Other, %	13	25	20	55*
Density, lbs/cu. ft.	85	116	105	124
Water content, %	32	16	20	16
Plasticity Index	65	45	50	42
Liquid Limit, %	125	65	70	60

* Calcium.

On Figure 1 are shown plots of Plasticity Index versus Liquid Limit.

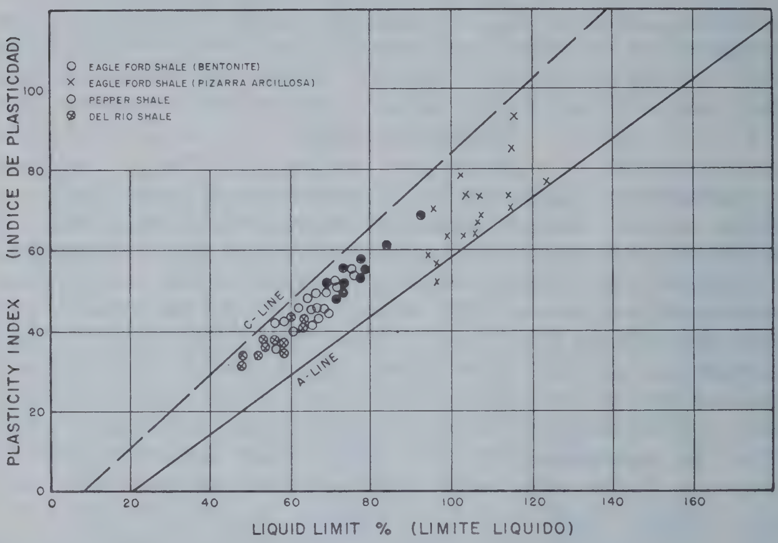

Fig. 1 — Comparison of Atterberg limits for Eagle Ford, Del Rio and Pepper shales with Eagle Ford bentonites.

Fig. 1 — Comparación de límites de Atterberg para pizarra arcillosa de Eagle Ford, Del Rio y Pepper con bentonites de Eagle Ford.

Waco Slide. During construction of a portion of the Waco Dam, a section of the embankment overlying the Pepper shale underwent movement. A slide occurred which was approximately 1500 feet wide involving the foundation (Pepper shale) for a distance of about 700 feet downstream from the centerline of the dam. The movement was generally concentrated in the mid-Pepper shale about 20 feet from the top of the member and was essentially horizontal. One of the features of this slide was the long duration of the movement — about 30 days. Studies of the movement showed that the greatest acceleration occurred during the period 10 to 14 days after commencement of the slide. This strikingly shows the progressive nature of the slide and what an important part creep played in the over-all problem. Stability analyses employing shear strength constants developed by conventional laboratory direct shear tests (Q and R) indicated satisfactory values for the design selected. Test data disclosed that the strength of the shale foundation, when tested by the same criteria used for evaluating the overburden, showed that the shale was much stronger than the overburden and that any potential slide would be concentrated in the embankment and foundation alluvium.

Conventional methods ordinarily used for evaluating brittle to quasi-brittle materials in which creep or progressive failure could occur may grossly over-evaluate the strength of such materials. In order to evaluate the actual strength of the shale involved in the slide, the data from and the configuration of the slide itself were used as the basis for reverse computations of the physical components. Conditions for these computations assumed zero cohesion and actual effect of piezometric pressures and internal forces. Studies of the slide determined that the sliding plane could best be approximated by a combination of circular arcs and a horizontal plane. For a safety factor of unity based on the weights of materials involved, pore pressures and the dimensions of the slide, a coefficient of effective internal friction of about 8 degrees was obtained. This value, when compared to the values obtained from usually acceptable test procedures for determination of the strength of brittle materials, clearly showed the need for development of a more suitable test environment.

PRINCIPLES FOR EVALUATION

Use of the effective strength principle for evaluating the strength of soils has long been advocated by many soils investigators (Skempton and Bishop, 1954, et al.). However, use of this principle in rock or other brittle to quasi-brittle pseudo rocks (shales, etc.) has not yet been fully justified. For advocates of the effective strength principle, a simple test differentiating intergranular stresses from pore water pressures is all that is generally needed for adequate design purposes. But other tests in which a time factor has been introduced and pore pressures dissipated can also be used. The usual array of Q, R and S tests represents an oversimplification of environments. An S test may be of 6 hours, 6 days or 6 weeks duration with varying degrees of consolidation and pore water pressure dissipation having occurred. The effect of cementation and/or molecular bond may or may not be included in the end result. There are also many conditions that exist in the prototype that can only be vaguely duplicated in the laboratory counterpart. A condition in which a combination of pore-water pressure development, which requires a diminution of volume for increased pressures resulting from load transfer, and artesian pressures may occur. Measurements of pore pressures due to consolidation of a saturated compressible material does not fully account for the latter condition. A test on a saturated brittle material in which excess pore pressures are induced and maintained during a test of long duration on a specimen in which failure on a horizontal plane can be controlled was needed.

One of the major problems that has plagued researchers in the study of soil mechanics principles has been the inability to produce realism in the relation of laboratory experiments to conformability in the structure. The mathematical guide lines that have been established are helpful, but one must work with materials which are to be used in a structure and here is where artificiality ceases and reality begins. It is somewhat of a paradox that most of the basic research in soil mechanics has been concentrated on what is considered to be the most troublesome material of which and on which structures are founded-clay. This anomaly, if one can call it such, is the result of a two-part problem concerned with the difficulty in designing a safe structure on clay and the comparative ease with which soft-plastic clays can be handled in the laboratory. Consequently, the efforts of most research in the study of soils is in the latter field, especially in the use of remolded test specimens (compacted clays) and not in the area of complex undisturbed foundation clays or shales. This over-simplification of the researchers' material is a necessary step to provide guidance in the study of similar undisturbed soils. The real problem is concerned with determination of the in-situ characteristics of a soil that is to serve as the foundation of the structure under consideration. The problem is a far more difficult one if the foundation is shale, a material that provides the transition of the quasi-gray region between soil and rock or between plasticity and brittleness. Immediately, one is confronted with the fact that shales and shaley clays must be tested in the undisturbed state. Depending upon their grain size characteristics, shales may be classified as clay shales, silt shales and sandy shales. Correspondingly, the nonlaminated argillaceous rocks may be classified as mudstones, siltstones and sandy siltstones. Such classifications take no account of the nature and degree of solidification. These factors are of great importance in identifying strength, resistance to weathering, deformation and rebound (Burwell, 1950). Clays and silts are changed into shales through a process of compaction or cementation or a combination of both. The degree of compaction attained depends upon size of load, duration, thickness of deposit and permeability of the mass. Under the most favorable conditions, the process of consolidation proceeds until the free water and some of the molecular water film is dissipated and the soil particles are brought into an interlocking contact. At this stage, a physio-chemical union may commence and cementation and solidification begin. Depending on the degree of density attained, the physical properties of shale may vary widely in their behavior to stress and strain. There is no sharp division between the performance of compaction and cemented shales. Those which have been produced by compaction alone revert to the original muds from which they were formed when subjected to weathering forces and the speed of disintegration is a function of the density, cyclic desiccation and the nature and degree of fineness of the constituent particles. Low grade shales of the compaction type, such as the Pepper, Del Rio, Eagle Ford and the bentonitic shales noted in this paper, will undergo complete disintegration after several cycles of wetting and drying. Notwithstanding the common use of the term shale as in an indicator of a weak material, there are many shales that, for practical design purposes, are as good as hard rock. The problem is simply one of properly evaluating the strength and durability characteristics of the material when subjected to a hostile environment. Other factors, such as stress relaxation (creep), thixotropic strength regain, effect of pore water pressure dissipation and elastic properties must be evaluated. These evaluations are made more difficult because destruction testing is required and since, obviously, a series of identical specimens cannot be made available, a difficult correlation problem is introduced. One of the most commonly used methods for evaluating the strength of shales where laboratory methods either are not available or have not provided satisfactory results consists of evaluating the stability of slopes in areas where slides have occurred (Lane, 1961). This method can produce satisfactory data for design except for the time-dimension. Usually, no data are available regarding the effect of creep (progressive shear) or, in the case of natural slopes that show historical slides, when the slide occurred in relation to the establishment of the original slope. Thus, the effect of time is generally ignored in analyses of this type. However, in the laboratory, a test program can be established for evaluating the effects of time and environment on the strength of shales.

LABORATORY TEST PROGRAM

DIRECT SHEAR TESTS

Rate of deformation. Because of the low permeability of shales, drained tests must be performed at a very low rate of strain if the condition of negligible excess pore pressure is to be satisfied. The measured shear strength is a linear function of the excess pore pressure at failure. For the direct shear test at a given normal stress, the relationship between the Q and S test at failure and the strength with partial dissipation of pore pressure may be written as

$$S = Q_f + \overline{U}_f \ (S_f - Q_f) \qquad (1)$$

Where S = strength at failure at any degree of pore pressure dissipation at failure $\overline{U}_f$

Q_f = undrained strength $\overline{U}_f = 0$

S_f = drained strength $\overline{U}_f = 1$

$\overline{U}_f$ = degree of dissipation at failure

Determination of a suitable rate of testing may be calculated for guidance in lieu of employing a trial and error procedure. Bishop and Henkel (1957) published a means of determining the theoretical degree of dissipation, U_f, by utilizing the theory of consolidation. This is expressed by

$$\overline{U}_f = 1 - \frac{h^2}{f c_v t_f} \qquad (2)$$

Where h = ½ the thickness of sample

c_v = coefficient of consolidation

t_f = time to failure

and f = 2 for a direct shear test.

Also, $$t_f = \frac{h^2}{2\ c_v\ (1 - \overline{U}_f)} \qquad (3)$$

Generally, it is assumed that a theoretical degree of dissipation of 95% will be necessary to insure the measurement of the effective strength in a test where pore pressures are not concurrently measured. For clarity in computing the time to failure for a direct shear test wherein a specimen

0.5 inch thick by 3 inches square is employed, equation (3) may be written as

$$t_f = \frac{h^2}{2\ c_v\ (0.05)} = \frac{10\ h^2}{c_v} \qquad (4)$$

Description of apparatus. A special device for performing the direct shear tests described herein was developed in the Southwestern Division Laboratory of the Corps of Engineers, USA. This apparatus required precision shear boxes in which the test specimen could be failed in direct shear without removal from the cutting device used to trim the specimen to exact dimensions. This is essential in performing tests on brittle materials exemplified by the shales evaluated and reported in this paper. Use of the conventional shear box, into which the test specimen is extruded from the trimming device, would have resulted in serious error in testing procedure. On Figure 2 is shown a view of the testing apparatus. Three multiple unit machines, consisting of 6 individual test units, were used during this investigation. Each test unit is independently actuated through an electrically powered speed reducer. Since tests were to be performed at rates of strain varying from 0.01 to 0.000001 inches per minute, a special transmission and speed reduction apparatus was developed. Basically, this unit consisted of a gear reduction box and an infinitely variable "Zero-Max" speed reducer which operates without belts, gears or cone sheaves. Horizontal stress to the specimen was applied at a predetermined rate by means of the rotary to linear motion transmission. Stress was measured by means of a proving ring. Normal stress to the specimen was applied by a dead weight system which was free to move with the specimen, thereby eliminating any eccentricity in the loading system. In order to correct for variation in rate of strain caused by fluctuation of shearing strength mobilized during a single test, several tests were performed with a pacing device. This device consisted essentially of coupled selsyn motors (master and slave) which mechanically actuated two linear transducers. One of the transducers indicated specimen movement which was measured by a linear motion recorder. The second transducer-recorder arrangement indicated the pacer motion. Theoretically, the coupled selsyn motor driving and pacing devices should have maintained a constant rate of strain. However, the differential between the linear transducers often indicated that the strain rate varied slightly during a long term test (6 to 10 days). When this occurred, manual adjustment of the "Zero-Max" speed reducer was necessary.

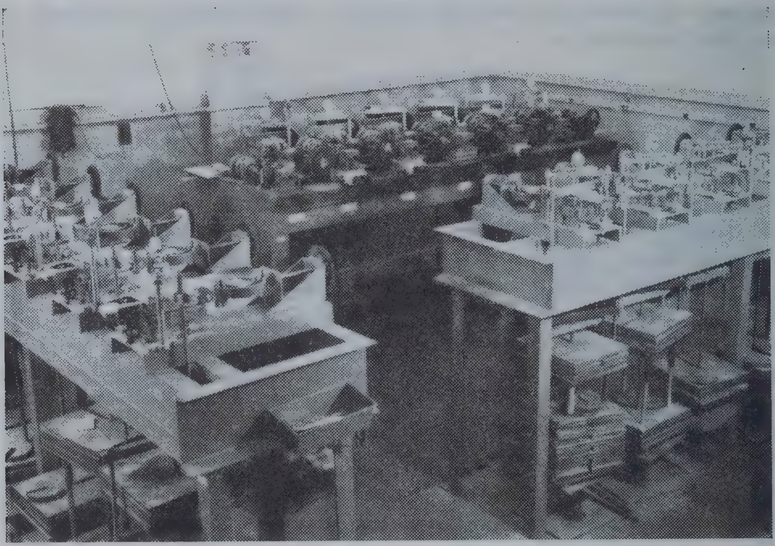

Fig. 2 — General view of direct shear testing apparatus.

Fig. 2 — Vista general de aparato de corte directo.

Hvorslev (1960) showed that the horizontal and vertical deformations during a direct shear test do not change linearly with the thickness of the specimen. While the shear deformation in a thin specimen (0.25 inch thick) is generally assumed to be more uniformly distributed than those in a thick specimen, this assumption has not been verified. In order to determine the influence of progressive failure in a quasi-brittle shale, an experimental direct shear test was performed on a specimen on the top surface of which were embedded three SR-4 strain gages placed at the edges and center of the specimen. These gages, which are sensitive to strains measured in micro-inches, were read at regular intervals during a 30 minute Q-test on the typical shale tested in this program. On Figure 3a are plotted the relation of applied shear stress to horizontal deformation, while on Figure 3b are plotted horizontal movement in inches of the total specimen versus movement in micro-inches of the areas covered by the strain gages. Strain gage 4 initially indicated tension at a low order of stress which was translated to compression as the stress was increased. Gages 5 and 6 indicated compression throughout all stages of stress. The data obtained from the stress-strain curves shown on Figure 4a were then used as a basis for computing the apparent

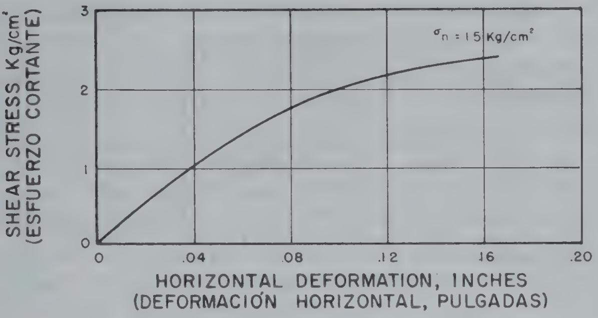

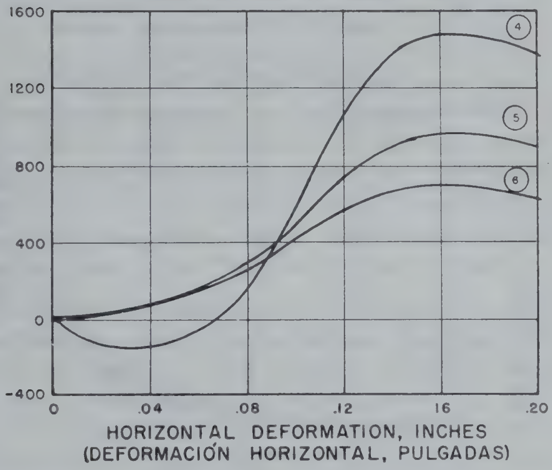

Fig. 3a — Relation of applied stress to horizontal deformation. SR-4 tests.

Fig. 3a — Relación de tensiones aplicadas a deformación horizontal. Ensayos de SR-4.

Fig. 3b — Relation of measured horizontal deformation to micro-inch movement of edges and center of specimen. SR-4 tests.

Fig. 3b — Relación de deformación horizontal medida con el movimiento en micro pulgadas de la orilla y centro de la muestra. Ensayos de SR-4.

stress distribution in the direction of the applied load as shown on Figure 4b. The stress distribution, while not exactly linear, is so nearly a straight line function that it could be termed linear. The average stress is approximately 60 percent of the maximum. Development of additional data has verified this relationship and it now appears that cognizance of progressive shear may be very significant.

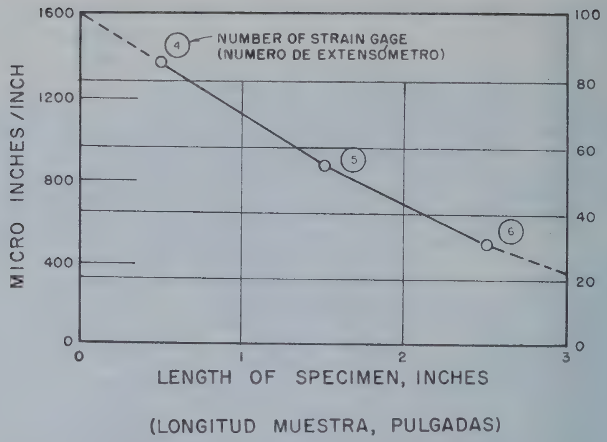

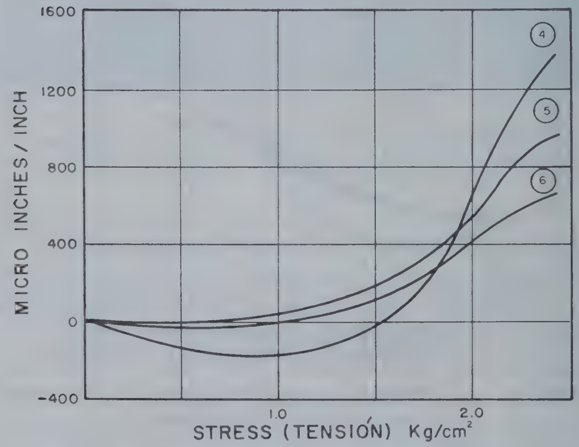

Fig. 4a — Relation of shear stress to strain gage deflections.

Fig. 4a — Relación de esfuerzo cortante a flecha extensómetro.

Fig. 4b — Variation of internal stress in specimen in direction of horizontal shear.

Fig. 4b — Variedad de tensiones internas en la muestra en la dirección horizontal de corte.

Test procedure. All shale specimens tested in this investigation were undisturbed and were obtained from 6-inch nominal diameter "Denison" (1942) cores. During storage, all cores were preserved in moisture-proof containers which, in turn, were placed in a moisture and temperature controlled "humid" room.

All specimens as prepared for test were 3 inches square and 0.25 to 0.50 inch thick. Each specimen was trimmed to exact size with the aid of the cutting device from which the test specimen was not removed. The cutting device is constructed in two parts with the line of separation coincident with the plane of induced failure as placed in the shear box. Use of this procedure eliminates the operation of extruding the specimen into the shear box and assures a very close fit. Each test specimen of a three point test series was preconsolidated to loads of 1.5, 3.0 and 6.0 kg/cm^2 until 100% consolidation had been achieved in accordance with Taylor's (1948) square-root-of-time method. All specimens were submerged in water in the shear box and the preconsolidation load was applied in one increment. Since 18 individual direct shear machines were used for this investigation, each test could be preconsolidated and tested in long-time shear without change of equipment. This eliminates an objectionable transfer operation if the test specimens are preconsolidated with one device and then transferred to the shear machine for test. With a 6-day schedule, an output of 30 three-point long-time direct shear tests per month was possible.

No correction for change of area during the test, as caused by shearing strain, was made. In performing a test, the specimen encased in the cutting device was placed in the shear box, the alignment pins removed, the specimen submerged in water and the vertical load applied. When preconsolidation was complete, as determined from a study of time-deflection curves, the shearing force was applied at a constant predetermined rate of strain. For the long duration tests, incremental readings at 6-hour intervals provided sufficient data for a 6-day test. The designations for the test conditions were as follows:

TABLE 2 — Summary of Testing Rates

Test Category	Rate of Constant Strain
Q (Quick)	0.05 inches per minute.
S (Slow)	0.001 inches per minute.
VS (Very Slow)	0.0001 inches per minute.
US (Ultra Slow)	0.000001 inches per minute.

Specimen thickness was either 0.25 or 0.50 inches. A constant rate of strain, in accordance with the above schedule, was employed in all tests performed on all shales reported herein. Since all tests were destructive in nature and were performed on undisturbed test specimens, a large number of specimens was required. Due to variations in physical characteristics of each specimen, such as density, moisture content, etc., a system as follows was developed to correlate the data. All samples were divided into four groups and at least 10 three-point shear tests were performed on each group in the Q, S, VS and US categories. Supplementary data, consisting of density, moisture content before and after test, specific gravity and Atterberg limits were determined on each specimen. Typical results of tests on the shales reported herein are shown on Tables 3 to 6.

TABLE 3 — Bentonite Seams

Test	LL%	PI	γ (1)	W_o%	S_o%	Φ	C	H (2)	Time (3)
US	103	39	83.5	36.4	93	19.9	0.0	0.25	5270
US	96	39	79.0	43.4	100	12.3	0.6	0.25	6280
Q	96	39	85.4	36.9	98	19.0	0.3	0.50	6
Q	96	39	86.1	38.5	100	18.3	0.4	0.50	6
Q	114	40	79.8	43.2	100	18.9	0.3	0.50	5
Q	107	39	82.8	41.1	100	15.6	0.6	0.50	5
Q	99	35	77.9	44.9	100	16.1	0.5	0.50	6
Q	103	24	98.5	27.2	95	18.2	0.6	0.50	5
US	103	24	99.8	27.3	100	24.0	0.1	0.25	11900
Q	96	39	82.9	41.0	100	21.0	0.0	0.50	5
US	96	39	80.0	41.3	99	12.2	0.2	0.25	4240
VS	115	45	82.7	41.0	100	17.4	0.2	0.25	430
US	115	45	86.3	38.9	100	15.7	0.3	0.25	5130
Q	115	45	80.7	43.4	100	21.0	0.0	0.50	6
US	97	44	80.9	40.3	100	16.2	0.3	0.25	7200

(1) γ = Lbs/cu. ft.
(2) H = Height of specimens in inches.
(3) Time = Time to failure in minutes.

TABLE 4 — Pepper Shale

Test	LL%	PI	γ (1)	W_o%	S_o%	Φ	C	H (2)	Time (3)
US	76	22	112	19.9	99	10.7	0.3	0.25	2105
US	66	19	114	18.0	99	12.9	0.6	0.25	4620
US	78	22	105	23.1	99	9.5	0.2	0.25	6650
S	64	22	105	21.0	94	17.1	0.3	0.50	150
S	64	22	108	21.1	99	19.3	0.2	0.25	87
US	64	22	109	20.8	100	16.5	0.2	0.25	3640
VS	75	21	104	24.1	99	15.4	0.4	0.50	244
S	75	21	104	24.5	99	15.1	0.2	0.25	71
US	75	21	105	24.5	100	13.8	0.3	0.25	2560
S	78	22	99	26.2	100	11.7	0.3	0.50	71
S	78	22	99	25.6	98	13.5	0.1	0.25	65
US	78	22	98	26.8	100	12.9	0.1	0.25	4300
S	92	23	94	30.7	100	12.2	0.4	0.50	71
S	92	23	95	29.3	100	14.3	0.1	0.25	143
US	92	23	94	30.1	100	14.4	0.2	0.25	2800

(1) γ = Lbs/cu. ft.

(2) H = Height of specimens in inches.

(3) Time = Time to failure in minutes.

TABLE 5 — Del Rio Shale

Test	LL%	PI	γ (1)	W_o%	S_o%	Φ	C	H (2)	Time (3)
S	60	19	118	17.0	100	21.0	0.8	0.50	98
US	64	19	116	17.4	100	13.7	0.2	0.25	3050
Q	64	19	118	16.5	97	23.4	0.0	0.25	9
US	63	20	114	17.5	91	13.6	0.2	0.25	3260
Q	64	19	117	16.4	100	21.1	1.0	0.25	10
Q	65	17	124	14.9	100	20.0	0.3	0.25	9
Q	55	19	122	14.8	99	22.1	0.7	0.50	9
US	55	19	119	15.6	100	24.4	1.1	0.50	6660
Q	55	19	119	16.4	100	30.1	0.5	0.25	7
US	58	16	122	16.9	100	20.8	0.3	0.25	7870
Q	58	16	114	18.8	100	31.2	0.3	0.25	9
Q	63	19	116	17.7	100	17.9	0.1	0.25	5
Q	55	15	120	15.0	97	19.7	0.2	0.25	6
US	55	15	119	15.0	95	20.0	0.0	0.25	2910
US	71	22	111	19.8	96	15.2	0.1	0.25	3350

(1) γ = Lbs/cu. ft.

(2) H = Height of specimens in inches.

(3) Time = Time to failure in minutes.

TABLE 6 — Eagle Ford Shale

Test	LL%	PI	γ (1)	W_o%	S_o%	Φ	C	H (2)	Time (3)
VS	—	—	114	16.1	85	39.2	1.9	0.50	197
VS	61	24	116	16.3	98	21.3	2.3	0.50	278
VS	61	24	117	14.4	97	24.1	1.0	0.50	1050
S	66	23	118	16.1	100	25.2	0.0	0.50	105
S	66	23	116	16.6	100	26.7	0.1	0.25	121
US	66	23	116	16.2	99	20.4	0.1	0.25	8180
VS	74	22	115	17.4	100	19.7	0.0	0.50	299
VS	74	22	116	17.3	100	18.4	0.4	0.25	269
US	74	22	115	17.8	98	18.4	0.5	0.25	7440
S	71	23	113	17.9	100	12.8	0.5	0.50	168
S	71	23	113	17.6	100	22.4	0.2	0.25	165
US	71	23	113	18.3	100	22.6	0.3	0.25	5067
S	67	23	113	16.8	100	10.3	0.9	0.50	96
S	67	23	116	17.0	100	20.6	0.5	0.25	176
US	67	23	116	17.2	100	6.6	0.8	0.25	5100

(1) γ = Lbs/cu. ft.
(2) H = Height of specimens in inches.
(3) Time = Time to failure in minutes.

INFLUENCE OF SPECIMEN SHAPE

In performing direct shear tests, use is made of specimens conforming to either flattened cubes or cylinders. Thin squares are preferable to thin cylinders for two major reasons. The stress distribution is less complex in the square specimen and the rate of area change is constant during test. However, the actual preparation of the specimen for test is slightly more difficult for the square specimen than for the circular type. Once the area function is established, only the thickness of the specimen needs to be fixed. Generally, this area ranges between 9 and 16 square inches which fits most laboratory equipment used in the U.S.A. This size range represents the maximum areas that can be carved from the standard 6-inch diameter Denison core barrel commonly used for field exploration. Generally, the thickness of specimens varies from 0.25 to 1.0 inches dependent on the type of material being tested and whether Q, R or S tests are being performed. For the Q tests, a thick specimen may be used regardless of whether the material is brittle or plastic. However, for the S, VS and US tests on clay-shales, it is convenient to utilize a thin specimen in order to enhance pore pressure dissipation and to reduce the total time of test. From equation (4) it can be seen that the time of test for any degree of pore pressure dissipation varies as the square of the specimen thickness. Thus, for a specimen 1 inch thick, for the shales reported herein, the theoretical time for U_f of 95% is 5000 minutes as compared to 1250 minutes for a specimen 0.50 inch thick and 20,000 minutes for a specimen 2.0 inches thick. The choice of specimen thickness — apart from duration of test considerations — is closely associated with material type, i. e., brittle or plastic soils. For plastic soils the lower limit of thickness is fixed only by the mechanics of specimen preparation which may limit the thickness to about 0.125 inch. Development of a normal pressure distribution and a valid shear plane has been achieved for such thin samples (Casagrande, 1960). However, for brittle materials, not only are thin samples difficult to prepare for test (precise dimensions are required), but there is a tendency for development of edge failures and/or conchoidal fractures during test. When this occurs, and the thinner the specimen the more likely it will occur, the data obtained are questionable. It is apparent that the measured strength is a combination of shear and sliding friction and does not reflect the true strength of the material. For sensibly hard materials (cemented shales, etc.) the specimen thickness should normally be not less than 1 inch and the time to test should be extended to 20,000 minutes as a minimum. On the other hand, the soft to moderately soft compaction shales described herein, in many cases, can be tested with the specimen thickness ranging from 0.25 to 0.50 inch, dependent upon the degree of density. Duration of test is adjusted to the time required for 95% dissipation of pore pressure. All the data presented herein were accumulated from tests performed on 0.25 and 0.50 inch thick specimens.

TRIAXIAL COMPRESSION TESTS ON SHALE

Conventional test procedures employing the triaxial compression test for determination of the shearing strength of shales, either in terms of total or effective stresses, do not produce the true shearing strength parallel to the bedding planes. Study of cylindrical specimens tested with bedding planes normal to the axis of the cylinder shows that the shear plane at the moment of failure generally makes an angle of 25 to 35 degrees with the vertical axis of the specimen. Thus, the measure of shear strength under this condition with the plane of failure making an angle of 55 to 75 degrees with the bedding planes represents a form of cross bed shear. On Figures 5a and 5b are shown a comparison of typical triaxial compression and direct shear tests results obtained on identical Pepper shale specimens. These tests were performed at an equivalent rate of shear strain. Data as follows were obtained:

TABLE 7 — Comparison of Triaxial and Direct Shear Tests

Test Type	LL %	PI	γ	W_o %	S_o %	Shear Strength ϕ	Shear Strength C, Kg/cm²
Triaxial	66	19	114	17.6	100	2	2.1
Direct Shear	66	19	114	17.6	100	12	0.6
Triaxial	76	22	110	19.8	100	2.5	2.1
Direct Shear	76	22	110	19.8	100	8	0.4

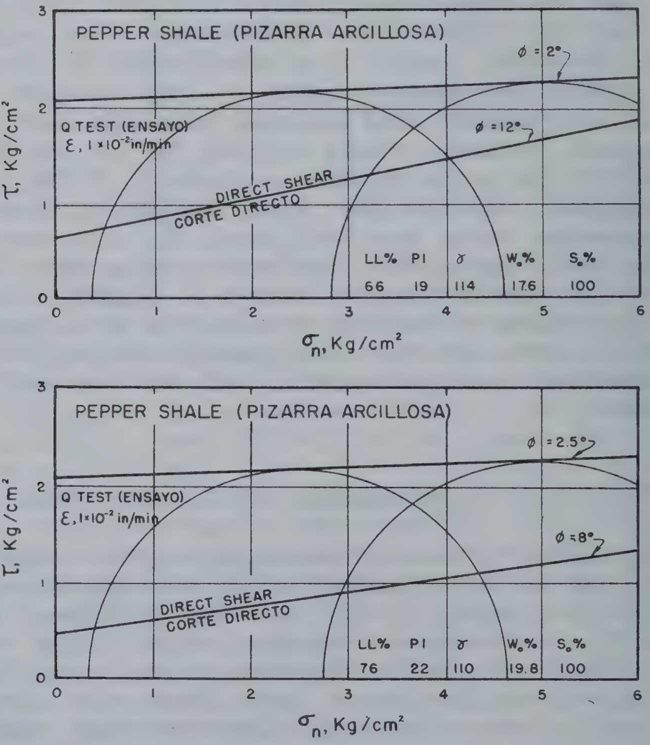

Fig. 5a,b — Comparison of triaxial and direct shear tests on identical specimens.

Fig. 5a,b — Comparación de ensayos triaxial y corte directo en muestras idénticas.

It is obvious that an equivalent strength would require a normal load in excess of the effective preconsolidation pressure for this shale. For laminated shales, the constituent particles of the mass are oriented with a pronounced parallelism with the structural laminations. For design of structures on shale in which there is a continuity of weak laminations on which failure could occur, a test should be used that can produce failure along the stratification. The direct shear will produce this result.

TORSION-COMPRESSION TESTS

Torsion shear tests are not commonly used in the USA in spite of the fact that such tests can provide valuable information on stress-strain relationships after initial failure. Also, even though a specimen may fail in pure shear, i. e., simple tension, this condition is generally encountered only in brittle to quasi-brittle materials. For a range of plastic to semi-plastic materials and with consideration to the critical height of test specimen, failure can be induced in a horizontal plane by utilization of equipment designed to produce failure along a single line of action. Tests of this type can be performed on any material which possesses cohesion. Certain capillary forces occur during application of compressive load and concurrently volume changes occur, but the advantage of maintaining a relatively constant area during test and the simplicity of equipment design and test procedure are factors that cannot be overlooked in setting up a shear test program. The principal disadvantages of the use of a solid cylindrical specimen is that the shearing stresses and strains increase from zero at the center of the specimen to a maximum at the outer surface and that progressive failure takes place during the test. Volume changes also increase from zero at the center to a maximum at the cylindrical surface. Consequent unequal changes in height of the test specimen are counteracted by radial displacements and plastic flow, but cause an unequal distribution of the compressive load. Furthermore, the variation of the rate of linear displacement from a maximum at the surface to zero at the center may affect the over-all shearing resistance. In spite of these apparent shortcomings, the torsion-compression test is suited to the determination of the strength of non-uniform material, such as compaction shales consisting of alternately variable zones of soft and hard phases. Whereas, in most direct shear testing techniques, the zone of failure is pre-selected, in a torsion-compression test in which the height to area ratio is about 2, failure occurs in the weakest zone which is selected by the test procedure per se. Also, direct use can be made of undisturbed samples without any further effort being necessary for specimen preparation.

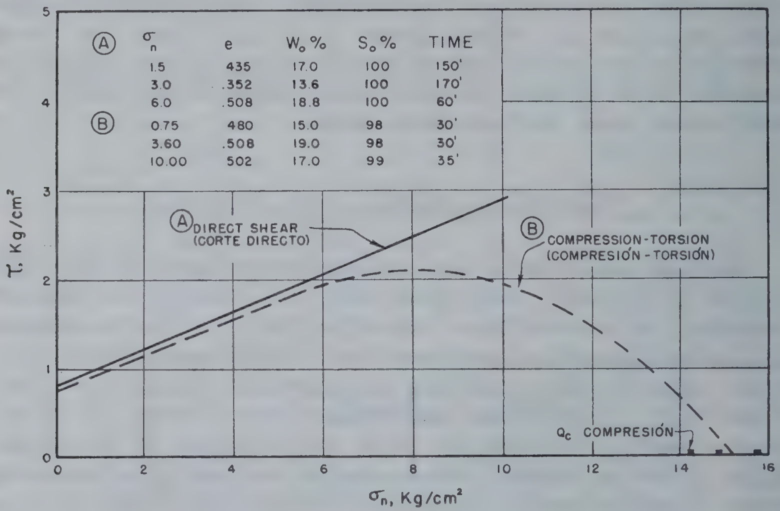

	σ_n	e	W_o %	S_o %	TIME
Ⓐ	1.5	435	17.0	100	150'
	3.0	.352	13.6	100	170'
	6.0	.508	18.8	100	60'
Ⓑ	0.75	480	15.0	98	30'
	3.60	.508	19.0	98	30'
	10.00	502	17.0	99	35'

Fig. 6 — Comparison of direct and torsional shear tests on identical specimens.

Fig. 6 — Comparación de ensayos de corte, directo y torsión, en muestras idénticas.

Application of a torsional force to a solid cylindrical specimen results in maximum shear stresses on a plane normal to the axis and normal stresses (tension and compression) on planes 45° to the axis. For specimens which fail in tension, failure occurs in a helical pattern normal to the direction of the maximum tensile stress. In these cases, it is obvious that the shear strength along bedding planes in the specimen approximately normal to the axis of the cylinder is at least as great as the measured tensile strength. Otherwise, the specimen would have failed in shear along the bedding planes. Thus, the importance of the torsion-compression test in evaluating the shear strength of laminated shales is obvious. The test automatically seeks out the weak planes, if any. It should be noted that in the torsion-compression test, like the direct shear test, failure is induced by the application of two forces, a compressive force and a shearing stress. However, in the torsion-compression test, the specimen is not restrained from failure in compression as is the case with the direct shear test. Thus, to some degree, the test involves a combination of stresses induced in unconfined compression and pure torsion. Obviously, a specimen can be failed in shear if the compressive force is twice the shear strength. Therefore, a normal stress not in excess of one-half the unconfined compressive strength provides an upper limit which cannot be exceeded in performing tests to determine the maximum torsional shear value. Generally, the maximum compressive force employed is not greater than overburden pressure plus structure load. On Figure 6 is shown a comparison of a singular direct shear test and a torsion-compression test on the Del Rio shale. It is noted that the "angle of internal friction" for the two entirely different test categories is essentially constant for compressive stress in the range of zero to slightly less than one-half of the compressive strength.

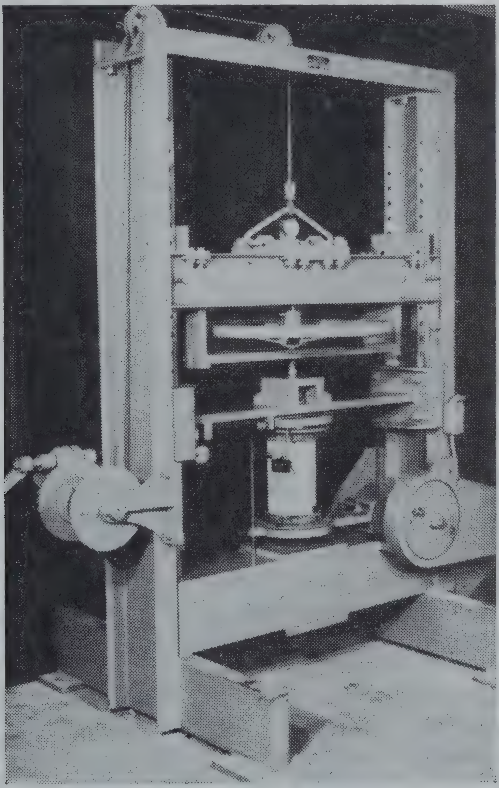

Fig. 7 — General view of torsional shear apparatus.

Fig. 7 — Vista general del aparato de corte a torsión.

The torsion-shear device shown on Figure 7 was designed for use in testing a variety of soft to hard materials. It can be used for testing solid cylinders varying from 2 to 20 inches in diameter, and in 2 to 24-inch lengths. Essentially the device consists of a rectangular framework and compression and torsion force applicators. Vertical load is applied mechanically and measured by proving bars and an electronic load capsule. Torsional stress is mechanically applied and measured by means of a proving ring. Angular strain is recorded on 0.0001 inch dial indicators. Computations for torsional shear are computed from the formula:

$$T_t = \frac{16T}{\pi D^3} \qquad (5)$$

in which T = applied Torque — inch pounds

D = diameter of specimen in inches

T_t = shear strength, psi

If the specimen fails in a horizontal plane, the shear strength is computed from the formula

$$T_t = \frac{12T}{\pi D^3} \qquad (6)$$

These formulae can easily be derived by reference to Timoshenko (1956).

RELATION OF SHEAR STRESS TO TEST DURATION FOR SHALES AND CLAY-SHALES

Determination of the effective strength of shales by rapid tests in which pore pressure measurements are attempted is difficult because of two major reasons:

(1) Shales are structural; i. e., the grain to grain contact represents a condition brought about by either compaction or chemical cementation. Thus, pressure in the free water phase cannot develop until this structure is altered.

(2) The migration of water in the void spaces of shales with lamellar stratification varies with the degree of nonhomogeneity.

As a result of these two conditions, long-term tests are required for measurement of effective strength parameters. Measurement of pore pressures in tests of long duration presents performance problems. Therefore, it is logical to use a test procedure in which the conditions (1) and (2) above can be circumvented. Use of a long duration drained test in which pore water pressures do not develop provides one solution. Constant strain tests are preferred to incremental stress tests because the stress is uniformly applied and the moment of failure can be determined with greater accuracy. For shales, a long duration, controlled-strain direct shear test fulfills these requirements.

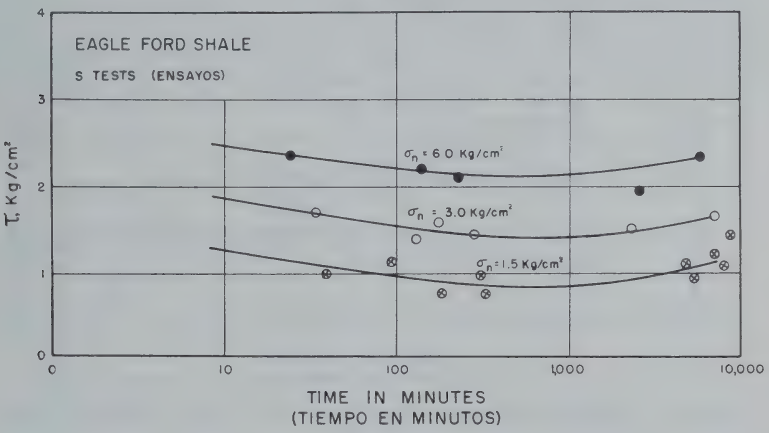

Fig. 8 — Relation of stress to log of time for typical Eagle Ford shale.

Fig. 8 — Relación de la tensión con el log. del tiempo para pizarra arcillosa típica de Eagle Ford.

On Figure 8 is shown the results of typical direct shear tests on the Eagle Ford shale. As previously described, these shales are brittle materials. Each point represents a point plot of stress versus log of time for a particular normal stress. Test duration ranged from 10 minutes to 10,000 minutes. The data indicate satisfactory trends for development of a family of curves for σ_n of 1.5, 3.0 and 6.0 kg/cm^2. Of particular significance is the fact that as the log of time increases, the shape of the curves becomes concave downward along the abscissa. A pessimum shear strength at a test time of about 1,000 minutes is indicated, as longer or shorter test times show higher strengths. Study of the shear deformation-time versus volume change curves for these brittle shales show that, in the early stages of a long duration test, the structure of the shale is gradually altered by the application of stress. As the stress is increased, the constituent grains begin to separate and rearrange themselves, resulting in a volume decrease. As the shales are 100% saturated, pore pressures develop as much from the results of the internal adjustment as from the applied external stresses. Finally, as movement continues and point contact between grains without cementation is re-established, the volume increases and pore water pressures are dissipated. As a result, there is a strength regain. This may more accurately be described as a thixotropic phenomenon.

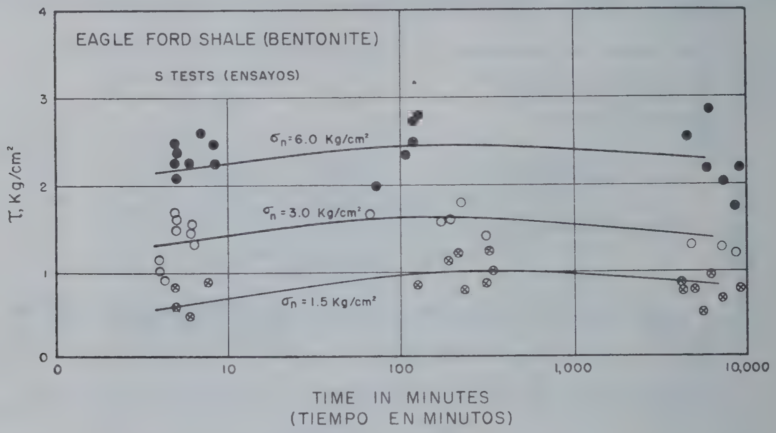

Fig. 9 — Relation of stress to log of time for typical bentonitic shale.

Fig. 9 — Relación de la tensión con el log. del tiempo para pizarra arcillosa típica de bentonite.

Conversely, the results of tests on bentonitic seams of the Eeagle Ford shale show an entirely different trend. Whereas the shales described in the above paragraphs were brittle in character, the bentonitic seams were plastic in nature. On Figure 9 is plotted a typical shear stress versus the log of time for a given series of normal stresses. As with the brittle shales, the test duration ranged from 10 to 10,000 minutes. These data also indicate satisfactory trends for development of a family of curves for σ_n of 1.5, 3.0 and 6.0 kg/cm². In this case, as with other test data on plastic clays reported by Bishop and Henkel (1957), O'Neil (1962), Casagrande (1951) and Hirschfeld (1960), normal results were obtained. The plots of shear stress versus log of time become convex upward as measured along the abscissa. A maximum strength at a test time of about 800 minutes was obtained.

INCREMENTAL STRUCTURE COLLAPSE

During the investigation of time effects on the strength of the shales and clay shales reported herein by means of controlled strain direct shear tests, it was observed that the shape of the stress-shear deformation curve indicated incremental structural collapse. This phenomenon has been reported by Trollope and Chan (1960) during a series of controlled stress tests on compacted silty clays as a "step-strain" condition. When stress is applied to a specimen of soil, the matrix originally carries the load. However, as plastic yield occurs, there is a gradual transfer of applied stress from the matrix to the coarser elements of the structure. When sufficient migration of these larger and stronger particles to the failure area obtains, a condition of structural collapse occurs. As additional stress is applied in increments,

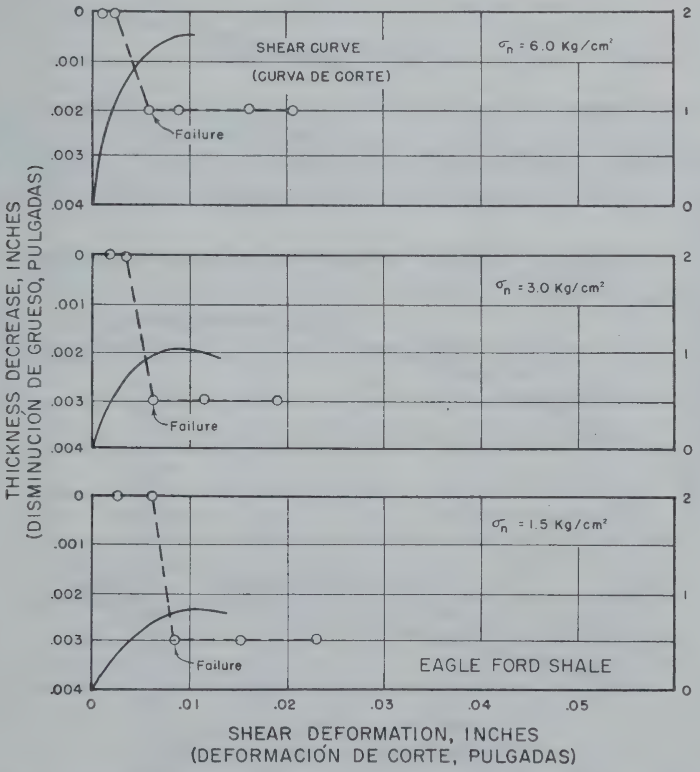

Fig. 10 — Relation of stress at failure to thickness decrease of single increment structural collapse.

Fig. 10 — Relación de tensión en rotura para disminución de espesor para una rotura estructural de uno solo incremento.

as was noted in Trollope's work, a series of events occur. For each increment of load additional shear strength is mobilized and, as strain continues, support for this new strength condition is lost and incremental collapse occurs. This mechanism is repeated until the optimum shear resistance condition is reached after which the soil fails in viscous flow.

Results obtained during the investigation of the strength of the shales considered herein disclosed a considerable variation in collapse structure depending on variation of density, moisture content and mineral composition. For the shales exhibiting a high degree of density and some cementation, such as Eagle Ford, volume change during test as reflected by thickness decrease versus shear deformation curves, internal structure collapse occurs in one increment. On Figure 10 are plotted the results of a single VS test on the Eagle

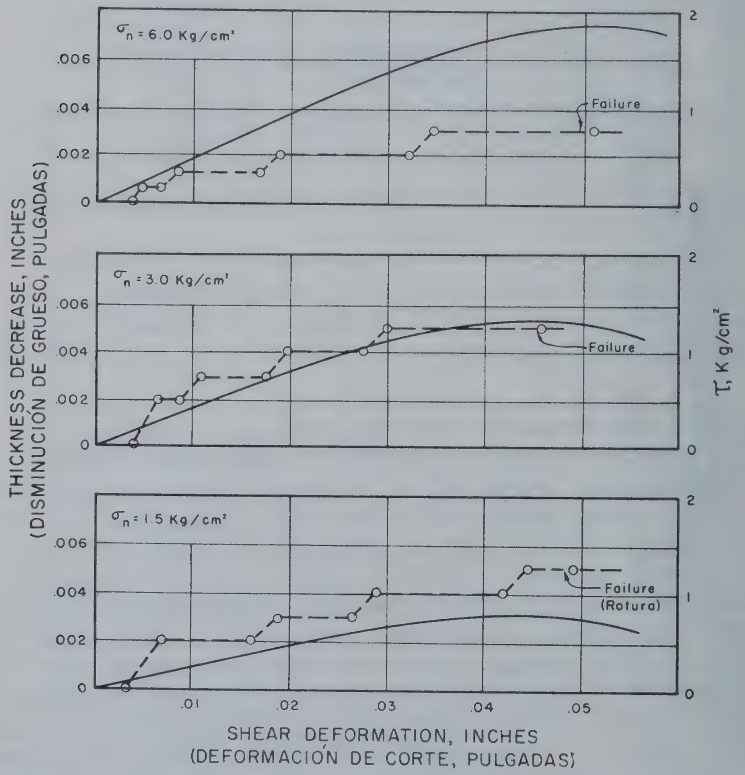

Fig. 11 — Relation of stress at failure to thickness decrease for a multiple increment structural collapse.

Fig. 11 — Relación de tensión en rotura para disminución de espesor para rotura estructural de múltiplo incremento.

Ford shale. While the thickness decrease versus horizontal movement for σ_n of 1.5, 3.0 and 6.0 kg/cm² curves show the structure of the specimen collapsed in a single increment, the stress-shear deformation curves show no interruptions or steps. Thus, the phenomenon of sudden collapse at the moment of failure can be observed only if volume changes are allowed but are defined by accurate measurements. These data suggest that failure of brittle materials in a direct shear test must occur suddenly and at a very low strain percentage.

Figure 11 shows the results of a single VS test on the moderately plastic Pepper shale. In this case, the thickness change versus shear deformation curves for σ_n of 1.5, 3.0 and 6.0 kg/cm² show a multiple interval collapse structure. This suggests a form of progressive shear as a series of minor incremental adjustment of internal structure occurs before final failure is achieved.

PRE-SPLIT TESTS

As a check on the effect of structural collapse, a series of direct shear tests were performed on the Eagle Ford and Pepper shales involving the concept of pre-splitting companion specimens. The specimens selected showed results as shown:

TABLE 8 — Summary of Tests on Pre-Split Specimens

Shale	γ (1)	W_o	LL%	PI	Φ	c (2)
Eagle Ford	115.3	15.4	49	22	22.8	0.0
	115.7	14.3	45	22	27.6	0.0
	115.0	13.9	22	20	21.7	0.0
Pepper	116.0	17.4	85	22	8.2	0.0
	116.1	16.7	82	22	10.2	0.0
	117.0	16.3	82	22	10.2	0.0
	113.1	19.3	94	25	7.7	0.0
Standard Specimens						
Eagle Ford	114.0	15.1	52	19	39.6	0.1
	115.9	16.3	50	18	38.0	1.5
	114.8	13.9	55	21	36.0	0.4
	116.1	13.8	52	20	38.1	0.5
Pepper	115.0	16.2	88	22	16.0	0.3
	117.9	17.2	88	22	20.2	0.3
	116.8	16.7	73	23	15.0	0.7
	117.0	16.9	73	23	16.7	0.4

(1) γ = Lbs/cu. ft. (2) c = Cohesion, Kg/cm².

A comparison of the total strength of the pre-split versus the non-split specimens at normal loads ranging from 1 to 10 kg/cm^2 indicates that the strength of the pre-split specimens was about 25 to 50 percent of the non-split specimens. Since these shales are fissile, it is comparatively simple to split the specimens on a plane and rejoin the separated halves for an exact fit. The separation plane is then fitted to the shear box at the exact position where normal shear would have occurred. While these data compare shear and sliding friction, the decay in strength is associated with structural collapse. The analysis is complicated by the fact that sliding friction is independent of strain whereas shear and structural collapse are strain dependent.

INFLUENCE OF VOID RATIO ON STRENGTH

Void ratio influence the frictional and cohesive components relating to the strength of brittle shales in that the volume changes are strongly influenced by the energy required to effect structural collapse and transfer that energy to sliding friction. It has been shown by Casagrande (1960), Hvorslev (1960) and Rutledge (1941) that a measure of void ratio at the moment of failure is significant. However, it is extremely difficult to ascertain the void ratio at failure (in plastic soils) due to difficulty in determining the failure plane or zone of failure and is even more difficult when evaluating the strengths of brittle shales. In direct shear tests on shales employing small thin specimens, the initial and the final void ratios for the total specimen are the only data generally available with regard to internal volume changes. The changes in void ratio on or near the induced plane of failure in a direct shear test on a specimen only 0.25 inch thick cannot be accurately determined. Therefore, in the evaluation of the effect of void ratio on shales, the initial value is used in all the data presented in this study. For tests on shale which require use of undisturbed specimens of variable void ratio, a common base for evaluation was established by plotting e versus log of stress at failure. There was generally a wide scatter of points, but the data indicate trends for establishment of a family of curves. These data can then be used to plot a series of shear curves for particular void ratios.

INFLUENCE OF SPECIMEN SIZE AND TEST TIME

In the course of this investigation during which in excess of 150 direct shear tests were performed on shales ranging from plastic to brittle characteristics, it was noted that the shear parameters not only varied with void ratio and duration of test, but also with specimen thickness. In order to eliminate the effect of variable void ratio and test duration, a series of shear envelopes were developed. Strength values for each normal stress applied were determined at a constant void ratio of 0.440 equivalent to an average value for design usage. Test duration effects were eliminated by use of the data shown on Tables 3 to 6, in which the time to failure was reduced to a common base by use of Formula (4). The resulting set of shear parameters for test categories Q, S, VS and US, corrected to an e_i of 0.440 and test duration of 1,000 minutes, are shown on Figure 12 for Del Rio shale. The effect of sample thickness on the data shows that a range of strengths for a given test procedure was dependent on specimen thickness. Thus, for a series of US tests, the strength components Φ and c range from 24 degrees and 0 kg/cm^2 for the 0.25 inch thick specimen to 22 degrees and 0.7 kg/cm^2 for the 0.5 inch thick specimens. These data show that, for design of a structure on shale, a test procedure must be adopted that will result in measuring the effective strength including the side effect of progressive shear. Similar tests and analyses on the Pepper shale shows strength components comparable to those computed as effective at the moment of the Waco slide, i. e., zero cohesion and Φ of 9 degrees. Figure 13 shows a comparison of the strength parameters developed from the S and US data for the Eagle Ford shale. The Ultra Slow tests follow the lower strength pattern. On Figure 14 is shown a comparison of the strength envelopes based on VS and US tests for a range of void ratios. In every case the Ultra Slow tests indicate lower values for the Eagle Ford bentonites. Figure 15 illustrates the strength parameters developed from the VS and US data for the Pepper shale. Again, the Ultra Slow test invariably shows the most conservative values.

CONCLUSIONS

As a result of this investigation of the shear strength of shales and clay-shales by means of triaxial compression, direct shear and torsion-shear tests, certain facts have emerged. It is concluded that, in those cases wherein the bedding planes of a shale foundation are parallel to a zone of potential shear, the strengths exhibited by the triaxial compression test are non-conservative. The direct shear and, in many cases, the torsion-shear test, provide a more realistic

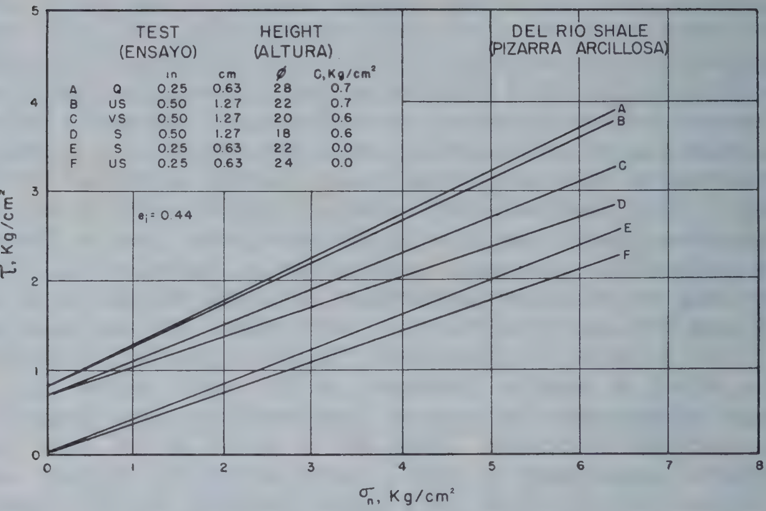

Fig. 12 — Variation of strength with specimen thickness for different rates of strain, Del Rio shale.

Fig. 12 — Variación de resistencia con espesor de muestras para diferentes velocidades de deformación, pizarra arcillosa de Del Rio.

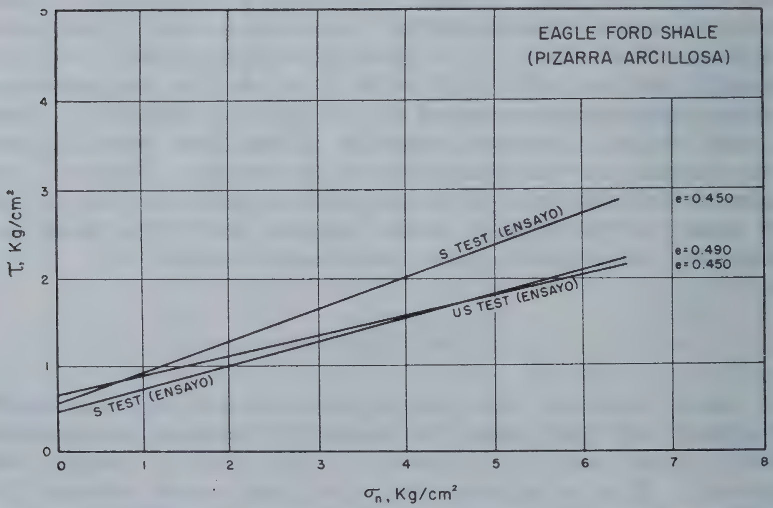

Fig. 13 — Relation of strength at variable void ratios and rates of strain, Eagle Ford shale.

Fig. 13 — Relación de resistencia a varios indices de poros y velocidades de deformación, pizarra arcillosa de Eagle Ford.

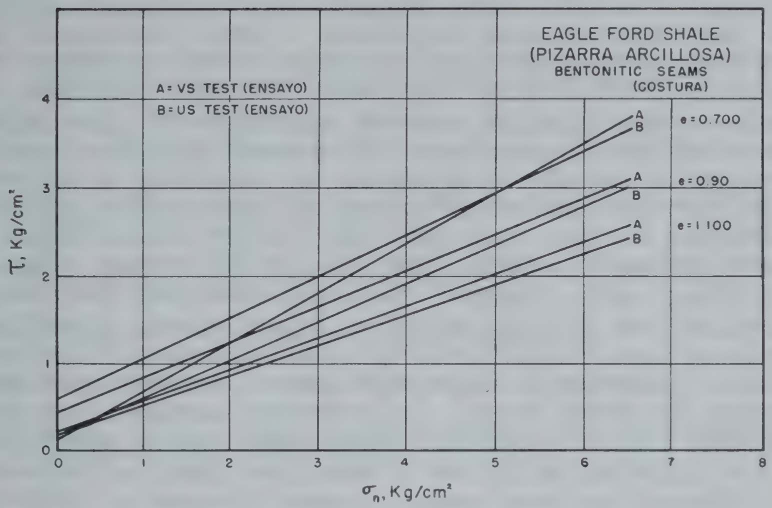

Fig. 14 — Relation of strength at variable void ratios and rates of strain, Eagle Ford bentonites.

Fig. 14 — Relación de resistencia a varios índices de poros y velocidades de deformación, bentonites de Eagle Ford.

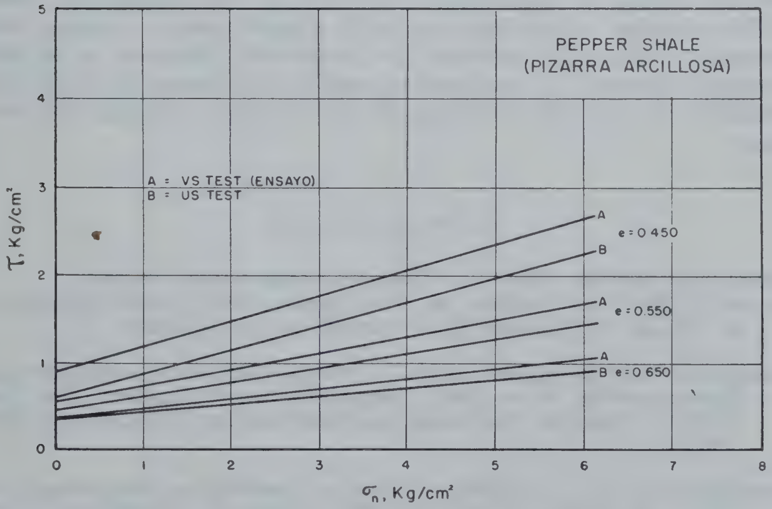

Fig. 15 — Relation of strength at variable void ratios and rates of strain, Pepper shale.

Fig. 15 — Relación de resistencia a varios índices de poros y velocidades de deformación, pizarra arcillosa de Pepper.

strength evaluation, since the external forces can be applied so that cross-bed shear is avoided. Further analysis of the data shows that the size and shape of the specimen, the duration of the test and the method of stress application all have a bearing on the strength measurements. For brittle materials the deformation at the moment of failure is independent of the size of specimen. In fact, there is evidence that, for the shales tested during this investigation and corroborated by large scale field tests, failure occurs within a total movement ranging from 0.01 to 0.03 inches. This is significant since it shows how little movement in a large structure can be tolerated before failure occurs. Associated with the fact that failure is not strain dependent is the condition of structural collapse which occurs simultaneously with failure for brittle shales. It is further concluded that progressive failure occurs in a direct shear test on brittle materials as shown by the test in which the stress was measured at different specimen areas. A stress decrease of about 75 percent from load edge to trailing edge of the direct shear specimen was recorded at the moment of failure.

A time of test for shales should be developed such that the pessimum strength can be determined. This requires equipment capable of sustaining a constant rate of strain up to 10 days. For the shales evaluated herein, the pessimum strength required at least 1 day to failure time. For semi-brittle shales a maximum strength is developed at about 1,000 minutes, as is the case with plastic clays. Again, long duration tests are required to accurately forecast a reliable strength value. A minimum sample thickness of 0.25 inch resulted in the lowest strength for a given testing environment.

REFERENCES

Bishop and Henkel (1957) — "Triaxial Compression Testing".

Burwell (1950) — "Geology in Dam Construction" from "Application of Geology to Engineering Practice", ed. by S. Paige.

Casagrande and Hirschfeld (1960) — "Stress-Deformation and Strength Characteristics of a Clay Compacted to a Constant Dry Unit Weight", Research conference on shear strength of Cohesive Soils (1960).

Casagrande (1951) — "Effect of Rate of Loading on the Strength of Clays and Shales at Constant Water Content", Geotechnique, vol. 2, pp. 251-263.

Denison (1942) — Core Barrel developed by the late H. L. Johnson for securing 6-inch undisturbed specimens by rotary drilling.

Hvorslev (1960) — "Physical Components", Research conference on shear strength of Cohesive Soils (1960).

Lane (1961) — "Field Slope Charts for Stability Studies", Proceedings of Fifth International Conference on Soil Mechanics.

O'Neil (1962) — "Direct-shear Test for Effective-Strength Parameters", vol. 88SM4, August 1962, Proceedings of ASCE.

Rutledge (1951) — "Relation of Undisturbed Sampling to Laboratory Testing", ASCE, vol. 109, 1944.

Skempton and Bishop (1954) — Soils, "Building Materials", their elasticity and inelasticity, ed. by M. Reiner.

Taylor (1948) — "Fundamentals of Soil Mechanics".

Timoshenko (1956) — Strength of Materials, 3d Edition.

Trollope and Chan (1960) — "Soil Structure and the Step-Strain Phenomenon", vol. 86, No. SM2, April 1960, Proceedings of ASCE.

A HYPERBOLIC STRESS-STRAIN FORMULATION FOR SANDS

DR. ROBERT L. KONDNER
Associate Professor of Civil Engineering

JOSEPH S. ZELASKO
Research Assistant

Civil Engineering Department
Technological Institute
Northwestern University
Evanston, Illinois

ABSTRACT

A two-constant hyperbolic stress-strain relation has been developed for sands in triaxial compression. The ultimate shear strength of the soil is contained within the general formulation and appears in the mathematical limit of the stress as the strain becomes excessive. The divergent concepts of a stability analysis as compared with a load-deformation approach to soil mechanics phenomena related to sands are shown to be compatible within the framework of the hyperbolic stress-strain relation. This has been quantitatively demonstrated for a uniform, fine dune sand tested in loose and dense conditions in triaxial compression for various constant values of the octahedral normal stress. The initial tangent modulus and ultimate shear strength of the sand are linear functions of the octahedral normal stress. The failure criterion contained in the stress-strain relation is used to compute the Mohr-Coulomb failure envelope in the two-dimensional stress-space for both dense and loose conditions of the sand. The general stress-strain formulation developed is shown to be compatible with the results reported in the literature by other investigators for a variety of sands and granular materials tested under various conditions.

RESUMEN

Una relación bi-constante hiperbólica tensión-esfuerzo se ha desarrollado para arenas en compresión tri-axial. La última resistencia al corte del suelo está en la formulación general y aparece en el límite matemático del esfuerzo *cuando la tensión es excesiva. Los conceptos diferentes de un análisis de estabilidad comparados con una deformación de carga con respecto a los fenómenos de mecánica de suelos relacionados con las arenas, demuestran ser compatibles dentro del criterio de la relación hiperbólica tensión-esfuerzo. Esto se ha demostrado cuantitativamente para una arena uniforme y fina procedente de dunas, probada en condiciones suelta y compacta en compresión tri-axial para varios valores constantes del esfuerzo normal octahédrico. El módulo tangencial inicial y la última resistencia al corte de la arena, son funciones lineales del esfuerzo normal octahédrico. El criterio de quiebre de la relación tensión-esfuerzo se ha usado para calcular el quiebre Mohr-Coulomb desarrollado en el bi-dimensional espacio-esfuerzo para ambas condiciones de la arena, densa y suelta. La formulación general tensión-esfuerzo desarrollado demuestra ser compatible con los resultados presentados en la literatura por otros investigadores para una variedad de arenas y materiales granulosos probados bajo muchas condiciones.*

INTRODUCTION

Theoretical studies of sand-foundation systems are always confronted, at one stage or another, with the requirement of specifying either a stress-strain relation or a failure criterion for the sand. Some of the questions that arise are: What form of stress-strain relation should be used?, What is its range of applicability?, What form of failure criterion should be used?, What are the significance and magnitudes of various coefficients contained within these forms?, What is the nature of the interaction between the sand and the structure?, and How do the answers to the above questions vary with: confinement due to body forces, magnitude and type of applied stress level, configuration of the foundation system, relative density of the sand, and particular type of sand? The present state of knowledge in the field of soil mechanics is quite often inadequate to satisfactorily answer such questions.

The major developments in soil mechanics with regard to response of sand-foundation systems have been accomplished with regard to the consideration of ultimate applied loads utilizing stability or limit analysis concepts. It has been well recognized for some years that many of the problems which are analyzed utilizing a limit analysis approach are in reality problems in which the load-deformation response plays the predominant and controlling role. Thus, in the rheology of soil masses and soil-foundation systems there are two distinct considerations; namely, the load-deformation-time response of the system and the ultimate load which the system can sustain and still perform within tolerable limits. In order to circumvent, in practice, the difficulty of not being able to predict and evaluate load-deformation-time response of a particular soil-foundation system, a sufficiently large factor of safety, based on a stability analysis, is applied to keep the deformation within tolerable limits. Indeed, it would certainly be better engineering and much more advantageous to develop a realistic and usable theoretical approach by load-deformation-time response could be computed. However, to obtain theoretical solutions, it is necessary to use some form of stress-strain-time relation for the soil. At present, no such relations are available. Thus, it is easy to understand why soil mechanicians have used a stability or limit analysis approach instead of a rigorous load-deformation-time approach.

Soil mechanicians have traditionally worked with a single parameter, the maximum or failure shear stress called the shear strength, for any one type of stress-strain test; that is, worked with only one point on the stress-strain curve rather than consider the overall material response as given by the entire stress-strain curve. The authors take the viewpoint that it would be much more beneficial with regard to the range and depth of analysis, from both the stability and deformation viewpoints, if the stress-strain relations for the soil could be formulated such that the failure criterion, as given by one of the conventional forms such as the Mohr-Coulomb criterion, would be contained within the general stress-strain formulation and appear in the mathematical limit of the stress as the strain becomes excessive. With such a form, the divergent concepts of a stability or limit analysis as compared with a load-deformation approach to soil mechanics can be shown to be compatible within the general framework of the formulation. Many of the concepts presented in the present discussion have been previously advanced by Kondner[1, 2, 3] and quantitatively demonstrated by Kondner[2, 3] for direct shear testing and triaxial compression testing of cohesive soils. The present work is an extension of Kondner's work to the area of triaxial compression testing of sands. Since it is anticipated that the general three dimensional formulation will be rather complex and require considerable time and effort to develop, a simplified initial phase will be considered in this paper. An unsolved problem commanding considerable interest in the field is the effect of confining stress (due to either body forces or applied stresses) on the stress-strain response and the failure criterion of sand for dense and loose states. Such a study is presented herein, in terms of triaxial compression in which the effect of confinement is given in terms of the octahedral normal stress.

The octahedral normal stress is equal to one-third of the first invariant of the stress tensor and is also equal to the mean hydrostatic stress. By definition, the octahedral normal stresses are stresses acting normal to the planes whose outer normal unit vectors make equal angles with the directions of the three principal stresses. Thus, it can be shown that

$$\sigma_{oct} = \frac{I}{3} = \frac{\sigma_1 + \sigma_2 + \sigma_3}{3} = \sigma_m \tag{1}$$

where σ_{oct} is the octahedral normal stress, I is the first invariant of the stress tensor, σ_1 is the largest principal stress, σ_2 is the intermediate principal stress, σ_3 is the smallest principal stress, and σ_m is the mean hydrostatic stress.

Note that

$$I = \sigma_x + \sigma_y + \sigma_z = \sigma_1 + \sigma_2 + \sigma_3 \tag{2}$$

where x, y and z refer to any cartesian coordinate system while 1, 2, and 3 refer to the directions of the principal stresses or the eigenvectors of the stress tensor.

For the conventional triaxial compression test, which is actually a biaxial state of stress, the two lower principal stresses are equal to the lateral or chamber pressure and

$$\sigma_2 = \sigma_3 . \tag{3}$$

Therefore, equation (1) becomes

$$\sigma_{oct} = \frac{\sigma_1 + 2\sigma_3}{3} = \sigma_m \tag{4}$$

HYPERBOLIC STRESS-STRAIN RELATION

Previous research involving uniaxial compression, triaxial compression and direct shear of cohesive soils (Kondner [2, 3, 4]) as well as the response of various soil-solid systems (Kondner et al.[5, 6, 7, 8]) indicates that the two-constant hyperbolic form of mathematical relation for stress-strain response has a number of very interesting and significant aspects.

Figure 1 is a rectangular hyperbola passing through the origin of co-ordinate in a two dimensional stress-strain space and having as asymptotes the lines

$$\begin{aligned} \varepsilon + \alpha &= 0 \\ \sigma - \beta &= 0 \end{aligned} \tag{5}$$

where σ denotes the normal stress difference $(\sigma_1 - \sigma_3)$ and ε is the axial strain.

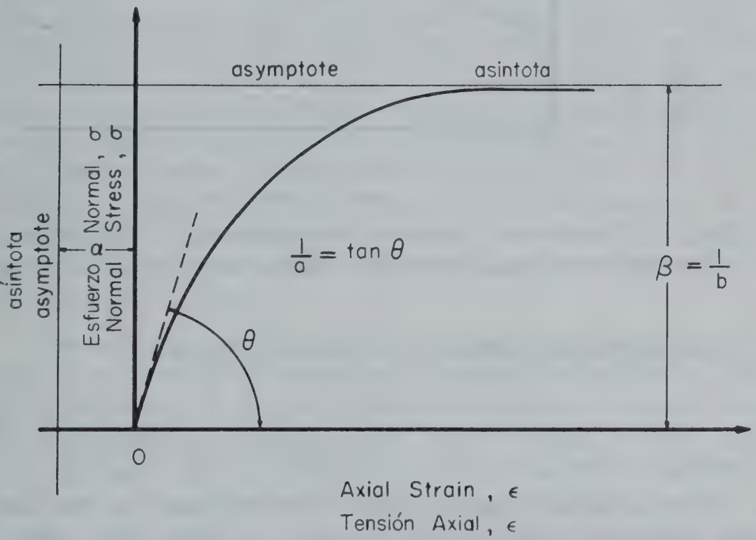
asymptote
asintota
Esfuerzo a Normal, σ
Normal Stress, σ
asintota
asymptote
1/a = tan θ
θ
β = 1/b
O
Axial Strain, ε
Tensión Axial, ε

Fig. 1 — Rectangular Hyperbolic Representation of Stress-Strain.

Fig. 1 — Representación Hiperbólica Rectangular de Tensión-Deformación.

The equation of the hyperbola can be written as:

$$\varepsilon\sigma - \beta\varepsilon + \alpha\sigma = 0. \tag{6}$$

Dividing equation (6) by σ and rearranging terms give

$$\frac{\varepsilon}{\sigma} = a + b\varepsilon \tag{7}$$

where $$a = \frac{\alpha}{\beta}$$

and $$b = \frac{1}{\beta}. \tag{8}$$

Figure 2 is a plot of the straight line form of equation (7) in terms of ε/σ and ε.

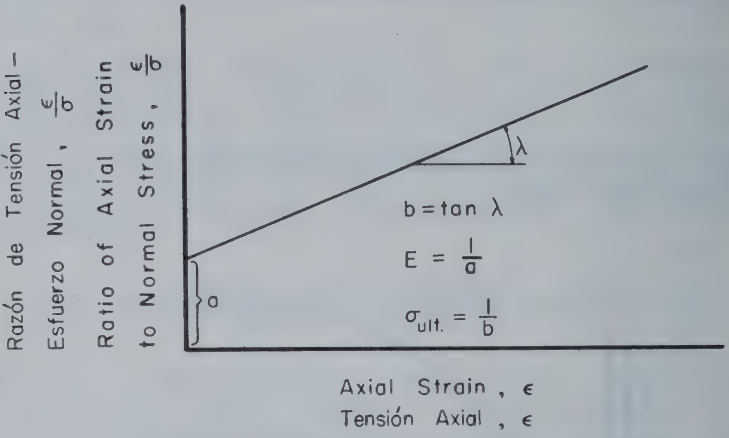
Razón de Tensión Axial – Esfuerzo Normal, $\frac{\epsilon}{\sigma}$
Ratio of Axial Strain to Normal Stress, $\frac{\epsilon}{\sigma}$
λ
$b = \tan \lambda$
$E = \frac{1}{a}$
$\sigma_{ult.} = \frac{1}{b}$
a
Axial Strain, ϵ
Tensión Axial, ϵ

Fig. 2 — Transformed Hyperbolic Representation of Stress-Strain.

Fig. 2 — Representación del Hiperbólico Tensión-Deformación, Transformado.

Solving for the stress in equation (7) gives:

$$\sigma = \frac{\varepsilon}{a + b\,\varepsilon} \qquad (9)$$

By differentiating equation (9) with respect to the axial strain and evaluating the derivative at ε equal zero gives:

$$E_i = \left(\frac{d\,\sigma}{d\,\varepsilon}\right)_{\varepsilon=0} = \frac{1}{a}\,. \qquad (10)$$

The quantity $\left(\frac{d\,\sigma}{d\,\varepsilon}\right)_{\varepsilon=0}$ is the initial tangent modulus, E_i, of the soil tested and is given by equation (10) as the inverse of the intercept, a, of the straight line form on the ε/σ axis of Figure 2.

The ultimate value of the normal stress difference can be obtained by taking the mathematical limit of equation (9) as the axial strain becomes excessive:

$$\sigma_{ult} = \lim_{\varepsilon \to \infty} \sigma = \frac{1}{b} \qquad (11)$$

Thus, the ultimate strength of the soil is measured by the inverse of the slope of the straigth line as given in Figure 2.

Present knowledge in the field clearly indicates that if equation (9) can be used to represent the sand response in triaxial compression, the intercept, a, and the slope, b, will both be functions of the relative density of the sand, first invariant of the stress tensor, and test conditions. The present study is the initial phase of an extensive study of the stress-strain response of sands and as such is restricted to the limiting cases of relative density, dense and loose states, for a range of values of the first invariant of the stress tensor given in terms of the octahedral normal stress. For the low rates of axial strain conventionally used in triaxial compression testing of sands where pore water is free to flow in or out of the soil, strain rate effects appear to be unimportant. However, such is not the case for dynamic loading. Strain rate effects are minimized by the particular test procedure utilized.

The use of the two-constant hyperbolic form of mathematical relation is certainly not the only form having desirable attributes and is not intended to be an "exact" fit of the experimental data over the entire range of the stress-strain response, but is intended to be a reasonable representation over a large range of deflection or strain.

EXPERIMENTAL APPARATUS AND PROCEDURE

The experimental apparatus consisted of a standard triaxial compression arrangement shown schematically in Figure 3. The saturated sand specimens were approximately 1.40 inches in diameter by 3.15 inches in length and were confined in a 0.012 inch thick rubber membrane. Lateral confinement was obtained using glycerine as the chamber fluid within the lucite cylinder. Chamber pressures were obtained by applying air pressure to the chamber fluid and were measured with a Bourdon pressure gauge. Axial loads were applied by direct loading with dead weights utilizing a hanger and piston rod system. Axial deformations of the specimens were measured using an indicator dial having a sensitivity of 0.001 inches. All the tests conducted were free-draining and volume changes within the specimens were measured by utilizing a pipette connected to the specimen through the base of the chamber.

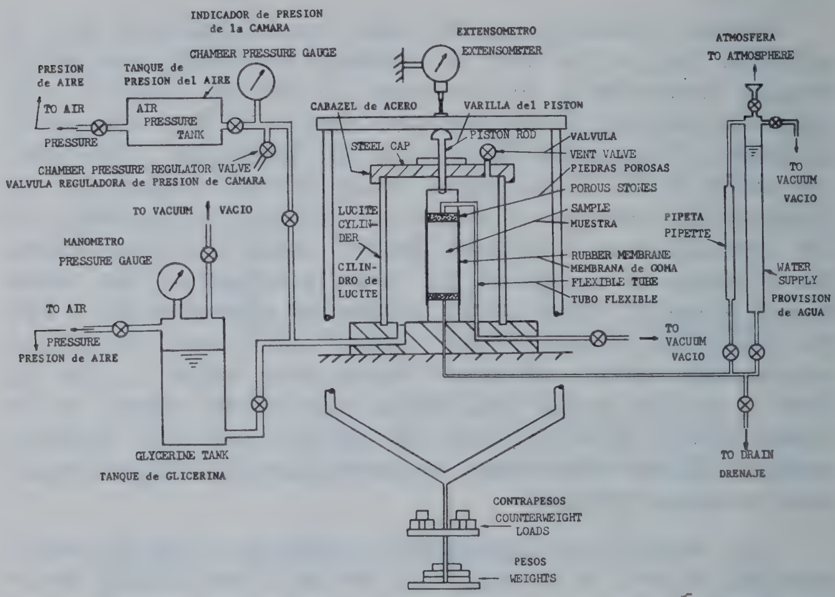
INDICADOR de PRESION de la CAMARA
CHAMBER PRESSURE GAUGE
PRESION de AIRE
TANQUE de PRESION del AIRE
TO AIR PRESSURE
AIR PRESSURE TANK
CHAMBER PRESSURE REGULATOR VALVE
VALVULA REGULADORA de PRESION de CAMARA
TO VACUUM
VACIO
MANOMETRO
PRESSURE GAUGE
TO AIR PRESSURE
PRESION de AIRE
GLYCERINE TANK
TANQUE de GLICERINA
EXTENSOMETRO
EXTENSOMETER
CABAZEL de ACERO
STEEL CAP
VARILLA del PISTON
PISTON ROD
LUCITE CYLINDER
CILINDRO de LUCITE
VALVULA
VENT VALVE
PIEDRAS POROSAS
POROUS STONES
SAMPLE
MUESTRA
RUBBER MEMBRANE
MEMBRANA de GOMA
FLEXIBLE TUBE
TUBO FLEXIBLE
TO VACUUM
VACIO
ATMOSFERA
TO ATMOSPHERE
TO VACUUM
VACIO
PIPETA
PIPETTE
WATER SUPPLY
PROVISION de AGUA
TO DRAIN
DRENAJE
CONTRAPESOS
COUNTERWEIGHT LOADS
PESOS
WEIGHTS

Fig. 3 — Schematic Diagram of Experimental Apparatus.

Fig. 3 — Diagrama Esquemático del Aparato Experimental.

The basic experimental procedure upon which the present developments are formulated consists of applying a hydrostatic (isotropic) state of stress to the specimen and then testing the specimen by applying increments of axial stress while maintaining a constant value of the octahedral normal stress equal to the value of the original hydrostatic state of stress. This was accomplished by reducing the chamber pressure with the pressure regulator valve while the increment of axial load is applied. The strains utilized were conventional engineering strains based on the initial length of the specimen. Axial stresses were computed using the standard cross sectional area correction. The axial stress, σ_1, is equal to the sum of the chamber pressure, σ_3, at any applied axial stress level plus the total increment of applied axial stress, σ_A.

A number of calibration tests were conducted with equal chamber pressure reduction increments and equal axial load increase increments to acquaint the test operator with the strain characteristics of the particular sand tested. Thus, if the increments of increased axial load are small, the increments of chamber pressure reduction are small and the respective changes in axial strain and cross-sectional area are also small and can be estimated accurately for each increment of loading. Therefore, the use of equation (4) and the results of the calibration tests allow the determination of the increment of axial load for a small increment in chamber pressure reduction and, hence, the octahedral normal stress is maintained constant throughout the test. This technique works quite well, even when the specimen is approaching failure, where even smaller increments are used.

Since the tests were conducted using finite changes of stress, a finite interval of time was needed to allow the specimen to strain and adjust to each stress increment. This "creep effect" was such that the strains increased with time but at a decreasing rate. Stress changes were not applied until the sample had ceased straining from the preceding stress increment.

When the initial hydrostatic state of stress is applied to the specimen, a weight must be applied to the hanger system to compensate for the effect of the area of the piston rod. Thus, as the chamber pressure is reduced during the test, the amount of this initial piston rod compensation weight must also be reduced. By utilizing a large number of small weights predetermined to correspond to the chamber pressure reduction increments, it was possible to make the necessary adjustments.

Tests were conducted on both loose and dense specimens at four different values of octahedral normal stress. The pressures used were 15, 30, 45, and 60 psi which correspond to 1.055, 2.110, 3.165, and 4.220 kg per sq. cm. A minimum of two loose and two dense tests for each value of octahedral normal stress were conducted.

SAND STUDIED

The particular sand studied in the experimental program was a uniform fine dune sand from Wolf Lake, Indiana. Its specific gravity is 2.68. Figure 4 gives a grain-size analysis for the sand.

ANALYSIS OF EXPERIMENTAL RESULTS

For the sake of simplicity with regard to the correlation of the present results with other work within the field of soil mechanics, the normal stress difference, $(\sigma_1 - \sigma_3)$, is denoted, as it is in conventional soil mechanics terminology, as the "deviator stress." The normal stress difference, $(\sigma_1 - \sigma_3)$, is not to be confused with the components of the deviatoric portion of the stress tensor commonly used in deformable mechanics.

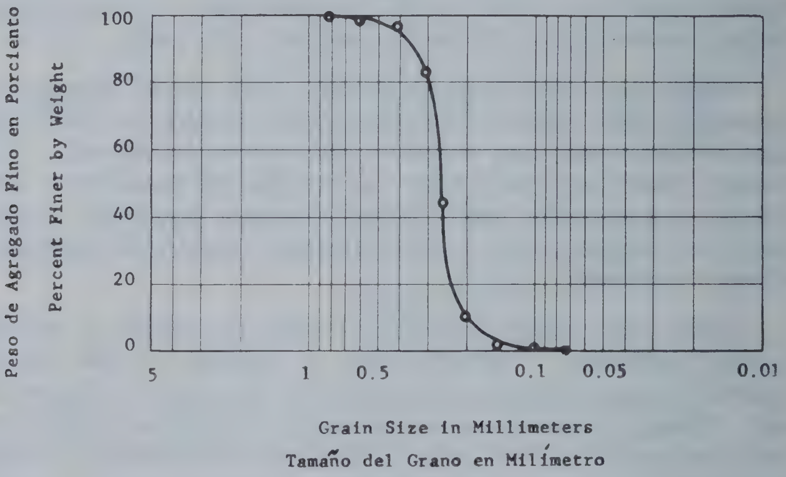

Fig. 4 — Sand Gradation Curve.

Fig. 4 — Curva del Tamaño del Grano de las Arenas.

In terms of the deviator stress, the hyperbolic stress-strain relation of equation (9) takes the form:

$$\sigma_1 - \sigma_3 = \frac{\varepsilon}{a + b\,\varepsilon}, \qquad (12)$$

and can be transformed into the linear form

$$\frac{\varepsilon}{\sigma_1 - \sigma_3} = a + b\,\varepsilon. \qquad (13)$$

Figure 5 is a plot of the deviator stress, $(\sigma_1 - \sigma_3)$, versus the axial strain, ε, with various values of the octahedral normal stress, σ_{oct}, ranging from 1.055 to 4.22 kg per sq. cm. for a dense state in which the average void ratio was 0.610.

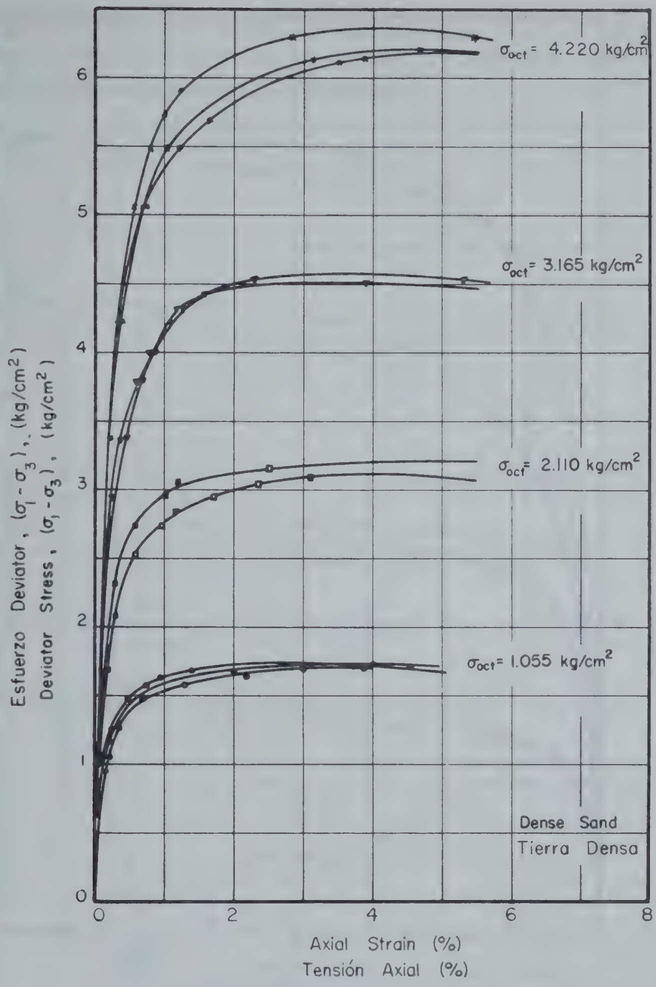

Fig. 5 — Deviator Stress versus Axial Strain for Various Values of Octahedral Normal Stress: Dense Sand.

Fig. 5 — Esfuerzo Deviator versus Tensión Axial para Varios Valores del Esfuerzo Normal Octahédrico: Tierra Densa (Compacta).

Figure 6 is a similar plot of the deviator stress versus axial strain with the same range of octahedral stresses for a loose state in which the average void ratio was 0.739. Figures 5 and 6 contain at least two tests for each value of octahedral stress. The average curve of deviator stress versus axial strain was obtained for each particular value of octahedral normal stress given in Figures 5 and 6. The resultant res-

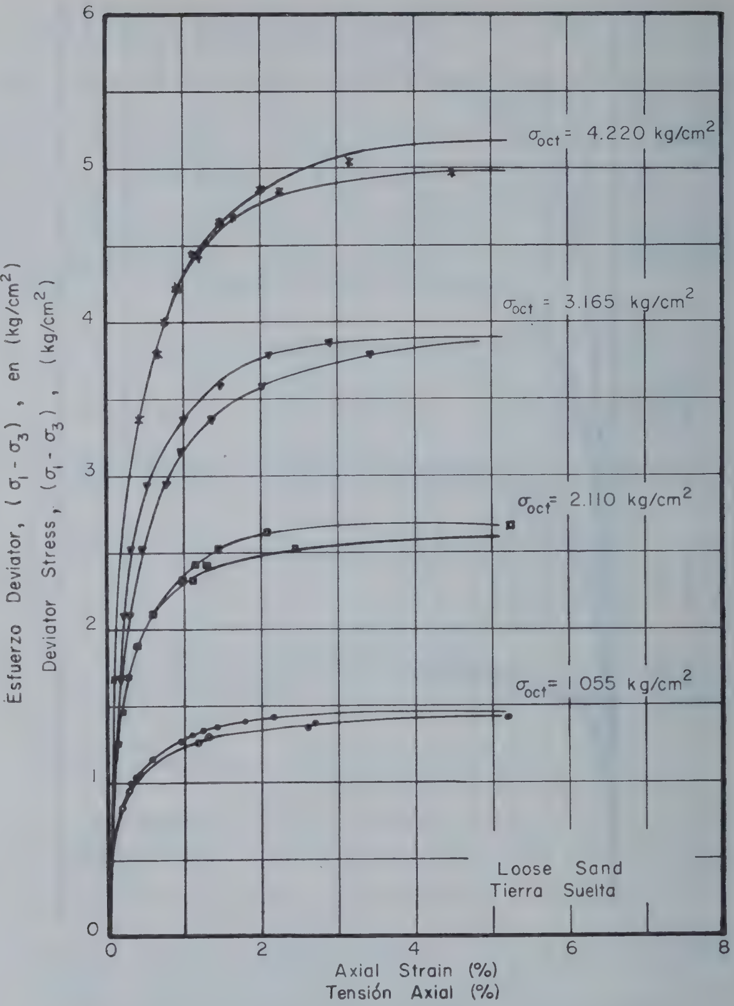

Fig. 6 — Deviator Stress versus Axial Strain for Various Values of Octahedral Normal Stress: Loose Sand.

Fig. 6 — Esfuerzo Deviator versus Tensión Axial para Vários Valores del Esfuerzo Normal Octahédrico: Tierra Suelta.

ponse was replotted in the two-constant hyperbolic form of equation (13) in terms of $\varepsilon/(\sigma_1 - \sigma_3)$ versus ε as given in Figures 7 and 8 for the dense and loose states respectively. The applicability of the hyperbolic form as a representation of the stress-strain response is indicated by the agreement between the straight lines and the average values of the experimental response. Figures 7 and 8 indicate that the hyperbolic form is a good representation of the stress-strain response from a low value of strain all the way through the failure condition of the specimens.

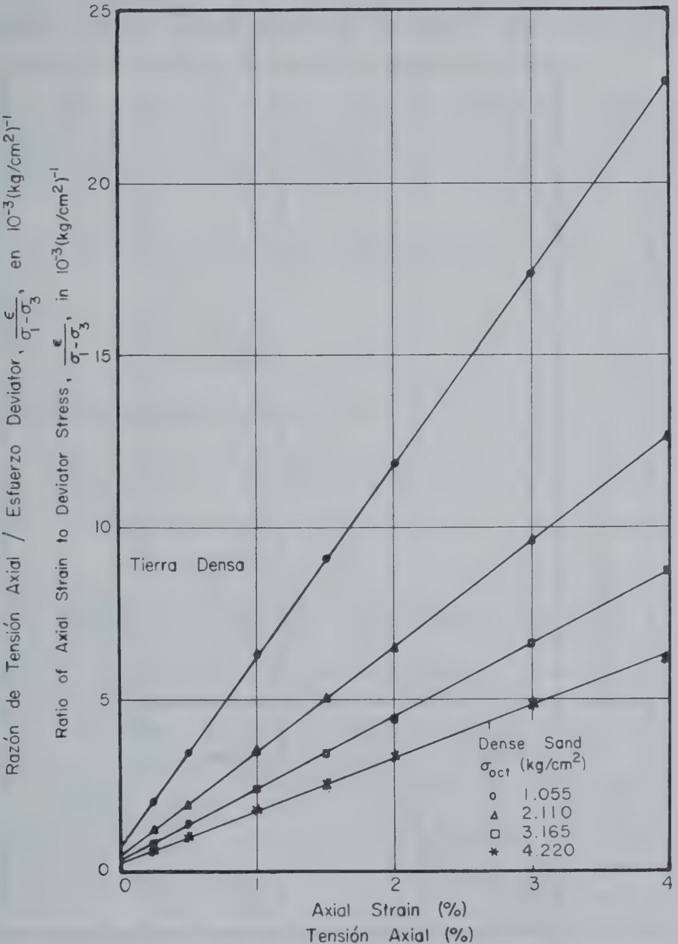

Fig. 7 — Transformed Hyperbolic Stress-Strain Response: Dense Sand.

Fig. 7 — Respuesta del Hiperbólico Tensión-Deformación, Transformado: Tierra Densa (Compacta).

In order to obtain the explicit form of the hyperbolic stress-strain relation of equation (12), it was necessary to determine the explicit forms of the parameters a and b as functions of the various test parameters. Since the present study is restricted to the limiting cases of relative density, dense and loose states, there is no point in trying to get the explicit form of the parameters a and b as functions of relative density. As clearly indicated in Figures 5 through 8, the primary factor influencing the soil response for the tests conducted was the value of the octahedral normal stress.

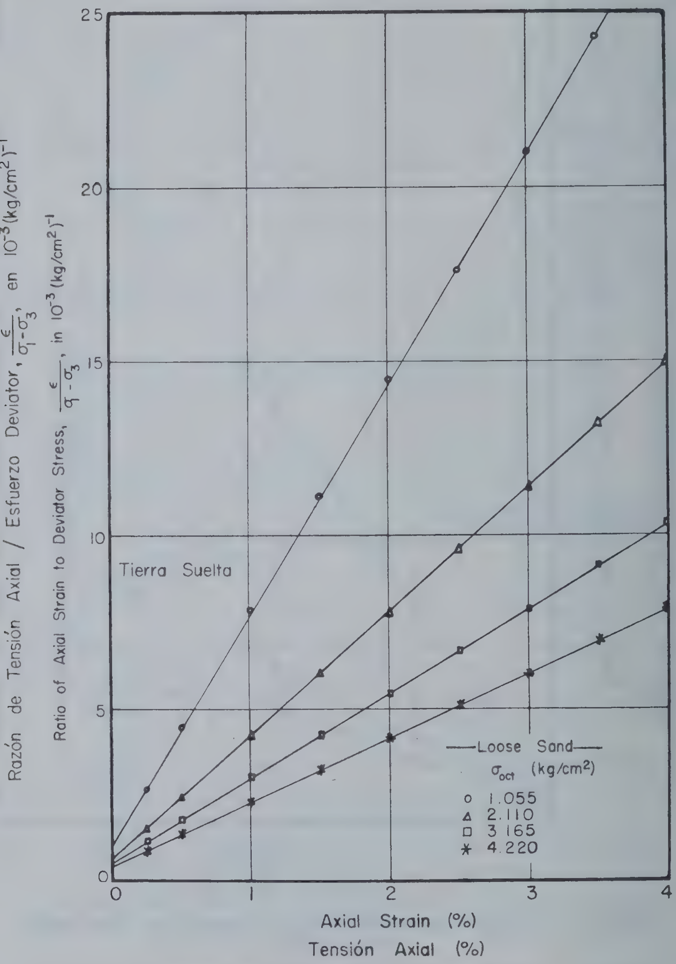

Fig. 8 — Transformed Hyperbolic Stress-Strain Response: Loose Sand.

Fig. 8 — Respuesta del Hiperbólico Tensión-Deformación, Transformado: Tierra Suelta.

Figure 9 is a plot of the inverse of the slopes of Figure 7 as a function of the octahedral normal stress, σ_{oct}, for the dense sand. A similar plot for the loose sand is given in

Figure 10. The straight lines obtained indicate that the parameter $\frac{1}{b}$ can be written in the form:

$$\frac{1}{b} = A + B\,\sigma_{oct} \tag{14}$$

where the values A and B are the intercept and slope respectively of Figures 9 and 10. The parameters A and B are functions of the relative density of the sand. For the dense sand,

$$A = 0.17 \text{ kg. per sq. cm.}$$

and (15)

$$B = 1.49,$$

while for the loose sand,

$$A = 0.23 \text{ kg per sq. cm.}$$

and (16)

$$B = 1.22.$$

It should be noted that the form of equation (14) leads to some very interesting points. The fact that the parameter A is not equal to zero for either the dense or loose conditions indicate that for a value of zero octahedral normal stress, condition of zero confinement, the sand has a small but finite shear strength which is proportional to the value of the parameter A. Such a response is not compatible with conventional concepts of classical shear strength theory of cohesionless soils. A number of possible causes for such a response come to mind. The first and foremost conclusion is that the finite value of A is simply a membrane effect since membranes were used to confine the specimens. Thus, the true soil response between $\frac{1}{b}$ and the octahedral normal stress may actually be linear through the the origin. This is conceivable considering that the response of Figures 9 and 10 could be reasonably approximated by a straight line through the origin, plus the fact that the data presented in these figures are subject to some experimental error. On the other hand, the initial portion of the response in Figures 9 and 10, for which there is no data, may be non-linear with the curve going through the origin. For such a situation,

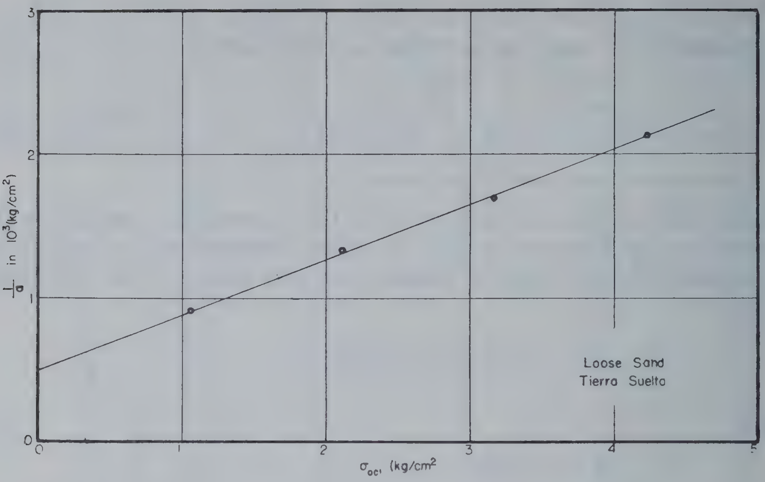

Fig. 9 — Inverse of Slope of Transformed Hyperbolic Plot versus Octahedral Normal Stress: Dense Sand.

Fig. 9 — Reversa de la Pendiente del Esfuerzo Hiperbólico Transformado versus el Esfuerzo Normal Octahédrico: Tierra Densa.

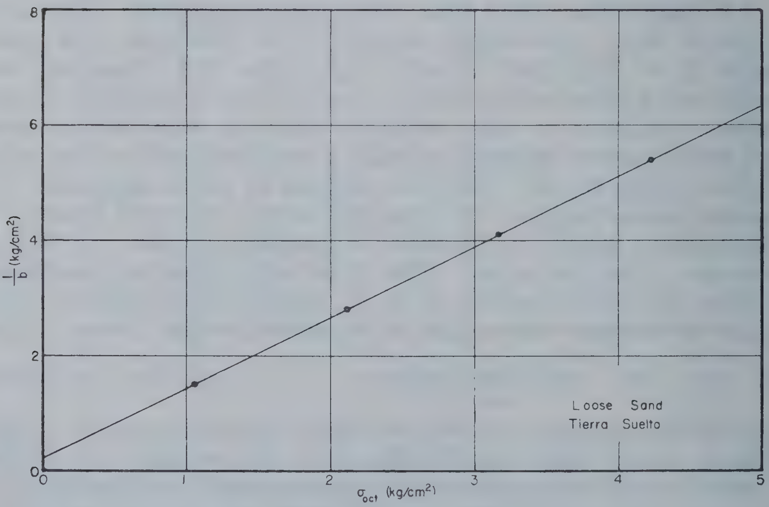

Fig. 10 — Inverse of Slope of Transformed Hyperbolic Plot vs. Octahedral Normal Stress: Loose Sand.

Fig. 10 — Reverso de la Pendiente del Esfuerzo Hiperbólico Transformado versus el Esfuerzo Normal Octahédrico: Tierra Suelta.

the response given by equation (14) would be limited to the range of values of octahedral normal stresses studied; namely, 1.055 to 4.22 kg. per sq. cm. Several other explanations might be that the finite value of A is due to a manifestation of normal stress effects of a nature related to those reported by Weissenberg[9] or that the value is due to phenomena related to incomplete saturation of the specimen. It is interesting to note that Lambe[10], when discussing the triaxial compression of a cohesionless soil, credits Chen[11] with having "showed that the plot of shear stress against normal stress had a shear strength intercept of C_1 at zero normal stress." In addition, Lambe also credits Chen with finding that the membrane has little influence on the value of the maximum stress although it may influence the shape of the stress-strain curve. Thus, one must conclude that the finite value of the parameter A has some experimental precedence in the literature, but it is certainly not clear whether such a response is a manifestation of sand behavior or experimental procedure and technique.

Although it is extremely difficult to define a failure stress for the tests conducted, it is possible to use a rather subjective criterion defining failure as that deviator stress level at which the increment of axial strain becomes excessive resulting in what is, for all practical purposes, a horizontal portion of the deviator stress-axial strain curve. The use of such an artificial criterion allows a comparison between the inverse of the hyperbolic slopes given by equation (14) and the value of $(\sigma_1 - \sigma_3)$ at failure. Figure 11 is such a comparison. The dashed line indicates a perfect correlation factor of one while the solid line gives the actual correlation factor, k, of 1.043. Thus, the measured failure value of $(\sigma_1 - \sigma_3)_f$ is 95.8 percent of $\frac{1}{b}$. Therefore, one can write

$$(\sigma_1 - \sigma_3)_f = \frac{0.958}{b} \tag{17}$$

and the failure criterion becomes

$$(\sigma_1 - \sigma_3)_f = 0.958 \; [A + B\,\sigma_{oct}] \tag{18}$$

where the values of A and B are given by equations (15) and (16).

The relation between the hyperbolic intercept and the octahedral normal stress for the dense and loose states are

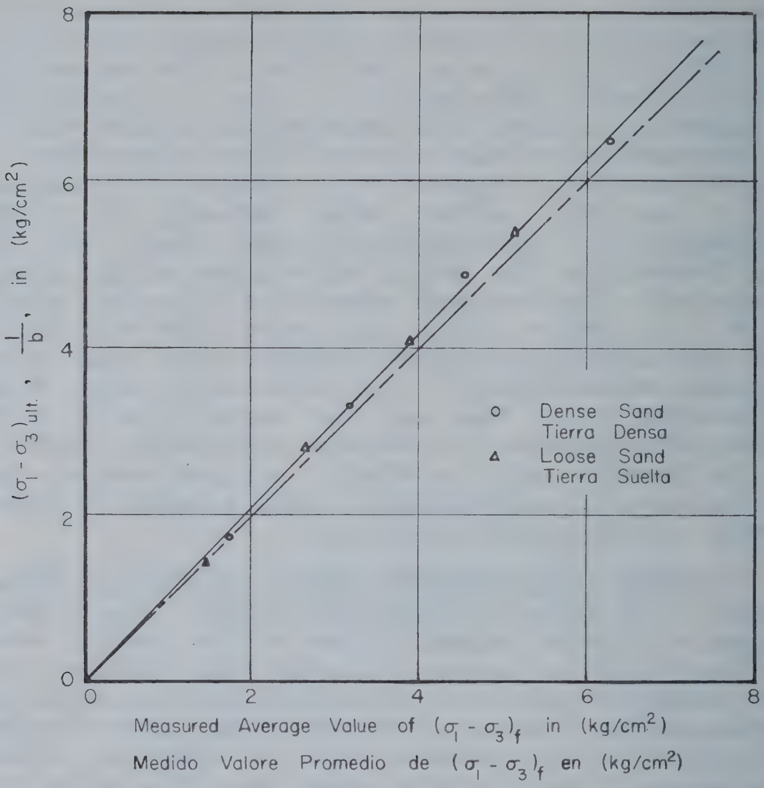

Fig. 11 — Correlation of Deviator Stress at Failure: 1/b and Measured Values.

Fig. 11 — Correlación del Esfuerzo Deviator en el Quiebre: 1/b y Valores Medidos.

given in Figures 12 and 13 in terms of $\frac{1}{a}$ versus σ_{oct}. The straight lines obtained indicate that the initial tangent modulus given by equation (10) can be written as

$$E_i = \frac{1}{a} = [C + D\,\sigma_{oct}] \tag{19}$$

where the values of C and D are the intercept and slope respectively of Figures 12 and 13 and are functions of the relative density of the sand. For the dense sand,

$$C = 700 \text{ kg. per sq. cm.} \tag{20}$$

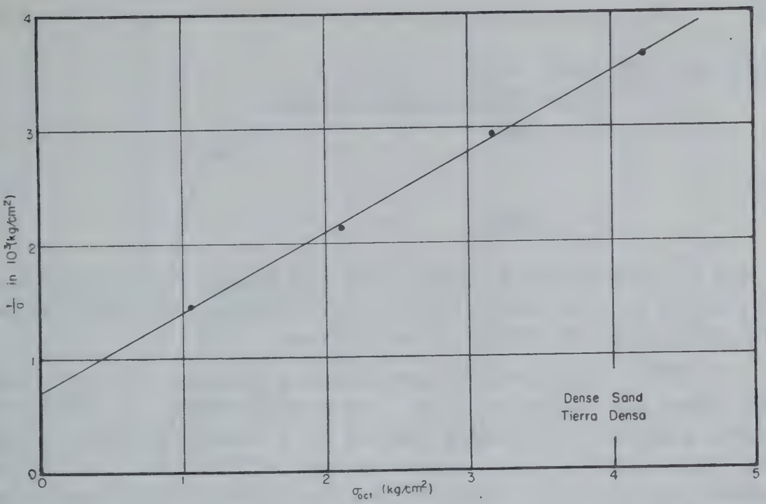

Fig. 12 — Inverse of Intercept of Transformed Hyperbolic Plot versus Octahedral Normal Stress: Dense Sand.

Fig. 12 — Reverso de la Intercepción del Esfuerzo Hiperbólico Transformado versus el Esfuerzo Normal Octahédrico: Tierra Densa.

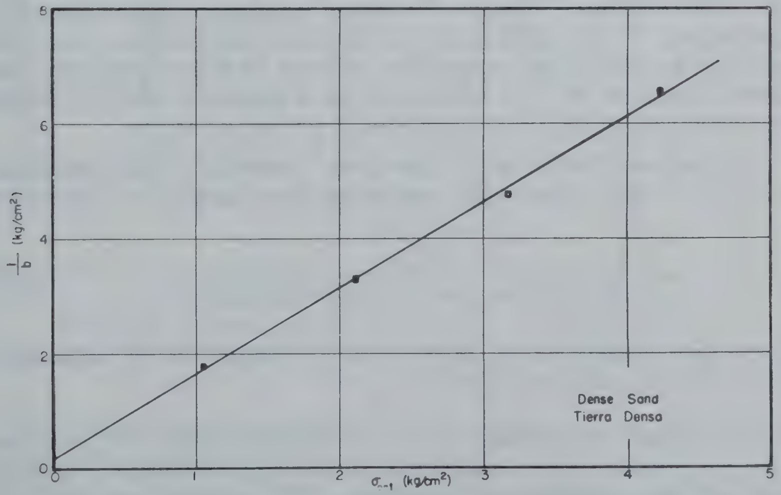

Fig. 13 — Inverse of Intercept of Tranformed Hyperbolic Plot versus Octahedral Normal Stress: Loose Sand.

Fig. 13 — Reverso de la Intercepción del Esfuerzo Hiperbólico Transformado versus el Esfuerzo Normal Octahédrico: Tierra Suelta.

and (20)

while for the loose sand,

$$C = 500 \text{ kg. per sq. cm.}$$
$$D = 695$$

and (21)

$$D = 385.$$

It is interesting to note that the linear form of Figures 12 and 13 as well as equation (19) correlate to some degree with the work of other investigators.

In 1876, Boussinesq[12] postulated a generalized hypothesis describing the behavior of a "pulverized mass" in which the secant modulus of rigidity varied as a linear function of the first invariant of the stress tensor. Since the octahedral normal stress is one-third of the first stress invariant, Boussinesq was essentially relating the rigidity modulus linearly with octahedral stress. Terzaghi and Peck[13] present a very interesting discussion of the effects of confining pressure on the initial tangent modulus and present results credited to Scheidig which indicate a linear variation of initial modulus with confining pressure for loose sand and a limited linear approximation for dense sands. Thus, the results presented in Figures 12 and 13 tend to agree with previous experiments and observations. There is some question regarding the signicance of the intercepts in Figures 12 and 13, but this question seems to be somewhat related to the previously discussed problem of the intercepts in Figures 9 and 10 which were related to the ultimate shear stress criterion.

Substitution of equations (14) and (19) into equation (12) gives the hyperbolic stress-strain relation in the form

$$\sigma_1 - \sigma_3 = \frac{\varepsilon}{[C + D\,\sigma_{oct}]^{-1} + [A + B\,\sigma_{oct}]^{-1}\,\varepsilon} \qquad (22)$$

where the values of A, B, C, and D are given by equations (15), (16), (20), and (21).

To give an indication of the applicability of equation (22) to represent the response of the experimental program, plots of the response of equation (22) versus experimental data obtained from the various tests are given in Figures 14 and 15. The solid lines are the predicted stress-strain response computed by equation (22) and the points are experimental data.

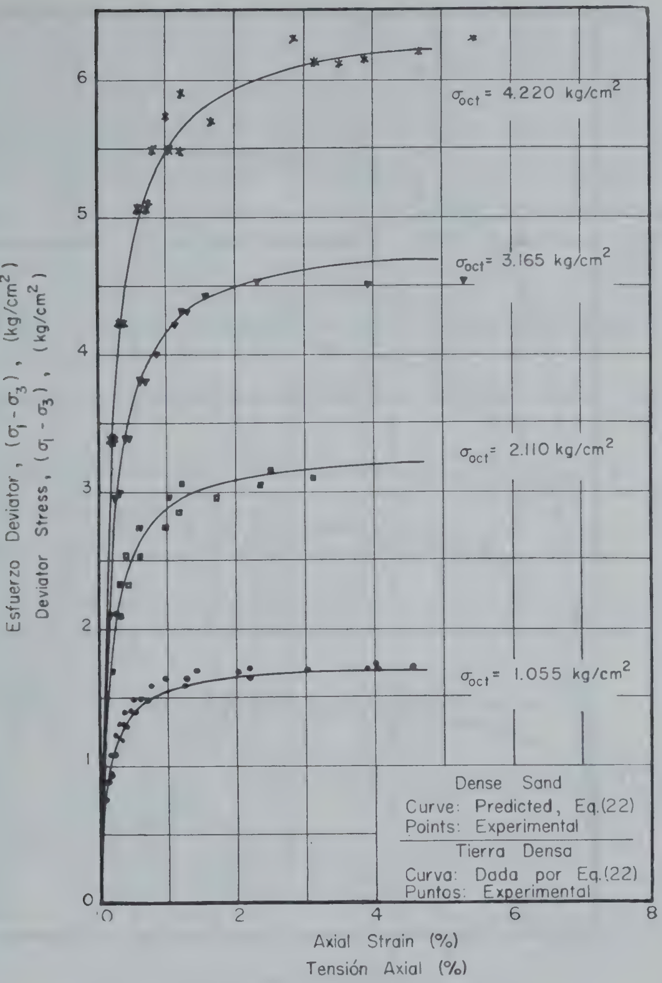

Fig. 14 — Comparison of Hyperbolic Prediction Eq. and Measured Response: Dense Sand.

Fig. 14 — Comparación de la Equación de la Predicción Hiperbólica y la Respuesta Medida: Tierra Densa.

Although the correlation of the hyperbolic stress-strain relation of equation (22) with the experimental data is quite encouraging, it makes for a more interesting comparison to use the relationship of equation (22) to predict in advance the deviator stress-axial strain response for conventional triaxial compression tests with constant values of the chamber pressure for both a dense and a loose state. Such tests were

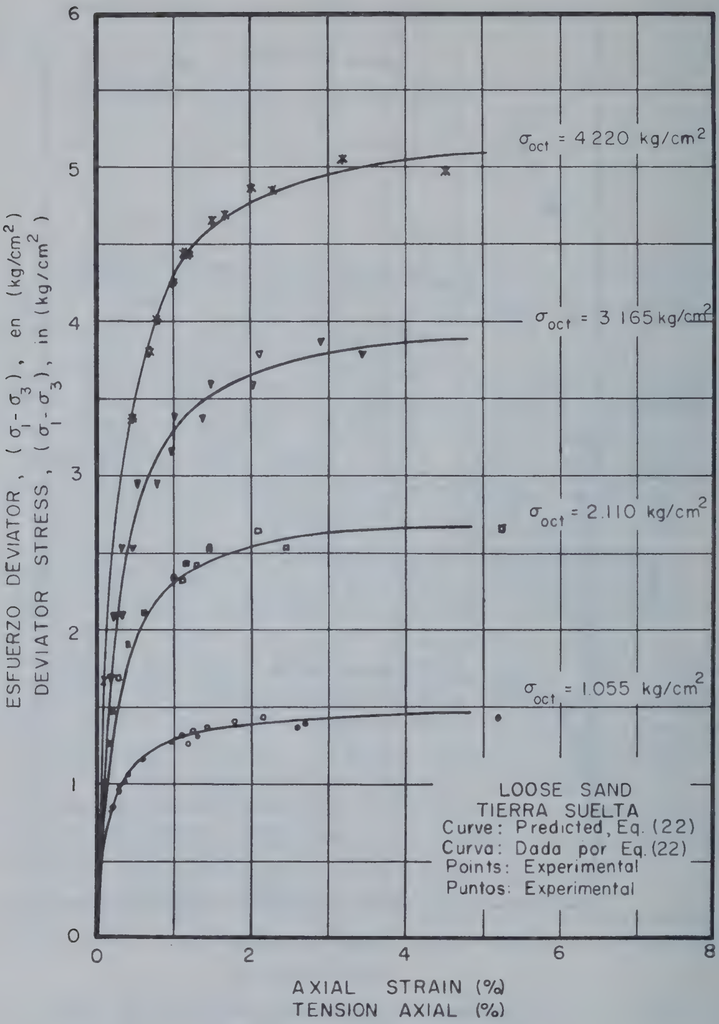

Fig. 15 — Comparison of Hyperbolic Prediction Eq. and Measured Response: Loose Sand.

Fig. 15 — Comparación de la Equación de la Predicción Hiperbólica y la Respuesta Medida: Tierra Suelta.

conducted utilizing a direct static weight procedure for constant chamber pressures of 2.11 kg. per sq. cm. Note that although the chamber pressure, σ_3, is constant for each test, the octahedral normal stress, σ_{oct}, is constantly changing during the test. The test procedure used in developing equation (22) was such that the octahedral normal stress was maintained constant for any one particular test. The results of this comparison are presented in Figures 16 and 17 where the solid curve is the response computed using equation (18) and the points are experimental. Figures 16 and 17 both indicate that the predicted stress response is lower than the measured values for the higher values of strain with differences of 7.9 and 5.3 percent at an axial strain of 4 percent. The initial values tend to be fairly representative of the response. It is interesting to note that if a straight line representation through the origin had been used in Figures 9 and 10, the coefficients in equation (22) would have changed and better correlations would have been obtained in Figures 16 and 17.

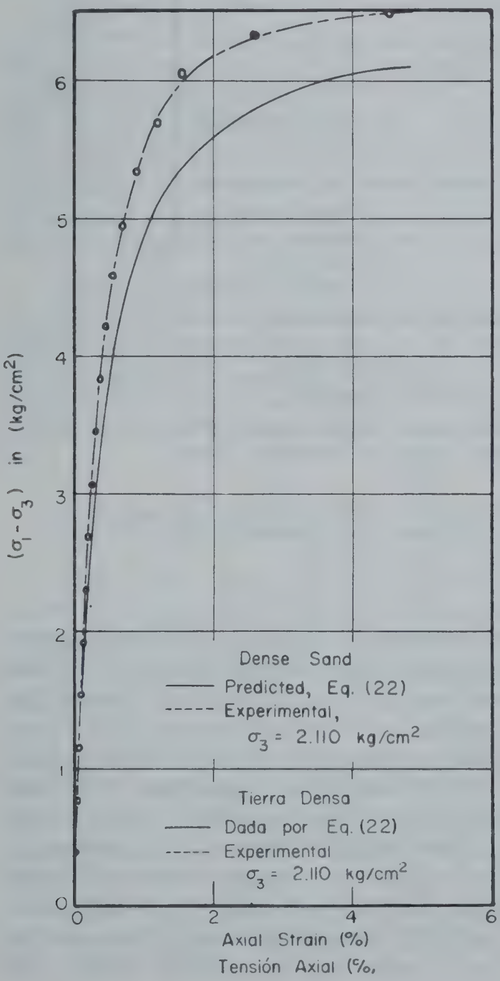

Fig. 16 — Comparison of Hyperbolic Prediction Eq. and Measured Response: Dense Sand.

Fig. 16 — Comparación de la Equación de la Predicción Hiperbólica y la Respuesta Medida: Tierra Densa.

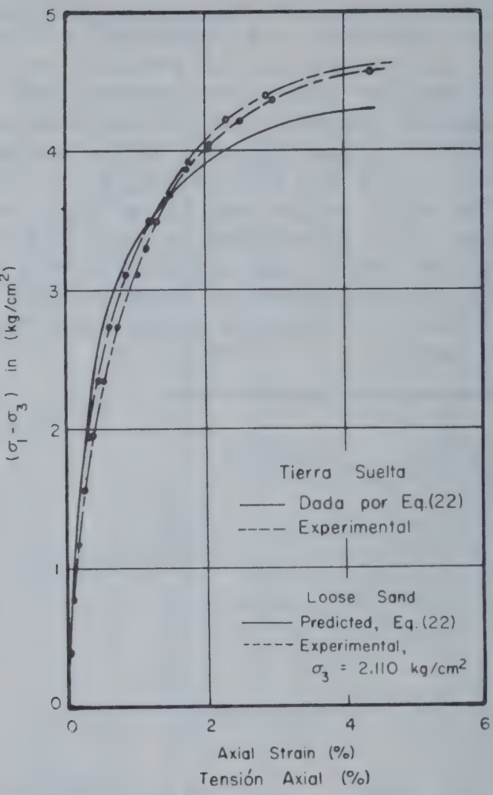

Fig. 17 — Comparison of Hyperbolic Prediction Eq. and Measured Response: Loose Sand.

Fig. 17 — Comparación de la Equación de la Predicción Hiperbólica y la Respuesta Medida: Tierra Suelta.

Although Figures 14, 15 and 11 indicate the applicability of equation (18) to represent the failure criterion of the experimental response for the sand studied, it is interesting to examine the form of equation (18) in terms of the conventional Mohr-Coulomb failure envelope in a two dimensional stress space. For the sake of illustration, equation (18) was used to compute the response for the following hypothetical situation. It is assumed, for the particular sand utilized in the experimental program, that five nearly identical specimens, each for both loose and dense states, are tested in standard, free draining, triaxial compression using a constant lateral pressure throughout any one particular test. The lateral pressures used for both dense and loose conditions are one, two, three, four and five kg. per sq. cm. Under these conditions, equation (18) gives the response indicated in Figures 18 and 19 for the loose and dense states respectively. Thus, equation (18) gives for the loose state, Figure 18, an angle of internal friction of 29°-46' while it gives for the dense state an angle of internal friction of 35°-22', Figure 19. The two values of the angle of internal friction agree well with the range of values given in the literature by numerous authors. For example, Hough[14] gives values ranging from approximately 30° for a loose condition to approximatelk 36° for a dense condition for a uniform fine sand. Thus, equation (18) does give a realistic range of friction angles.

Although it does not show too clearly, the straight lines of Figures 18 and 19 intersect the shear strength axes and have very small but finite intercept values. This is related to the previous discussion of the finite value of the parameter A in equation (18). The conclusion of that discussion was that the finite value of the parameter A has some experimental precedence in the literature (work of Chen[11]), but that it is certainly not clear whether it is a manifestation of sand behavior or experimental procedure and technique.

Thus, the use of equation (18) to predict Figures 18 and 19 indicates that the concept of a failure criterion contained within the stress-strain relation of equation (22) and appearing in the mathematical limit of the stress-strain relation, as the strain becomes excessive, is compatible with the conventional concepts of the Mohr-Coulomb failure criterion.

CORRELATIONS WITH OTHER INVESTIGATIONS

The basic developments presented in this paper have shown that it is possible to satisfactorily represent the stress-strain response over a large range of strain, for a particular sand, with a two-constant hyperbolic relation such that the ultimate shear strength of the sand is contained within the relation and appears in the mathematical limit of the stress as the strain becomes excessive. Although it is not the only applicable mathematical form having desirable attributes, the two-constant hyperbolic relation has been utilized and as such, it is desirable to determine if such a form has general applicability with regard to some of the triaxial compression test results, for sands, reported in the literature. The following results reported by various investigators have been selected at random.

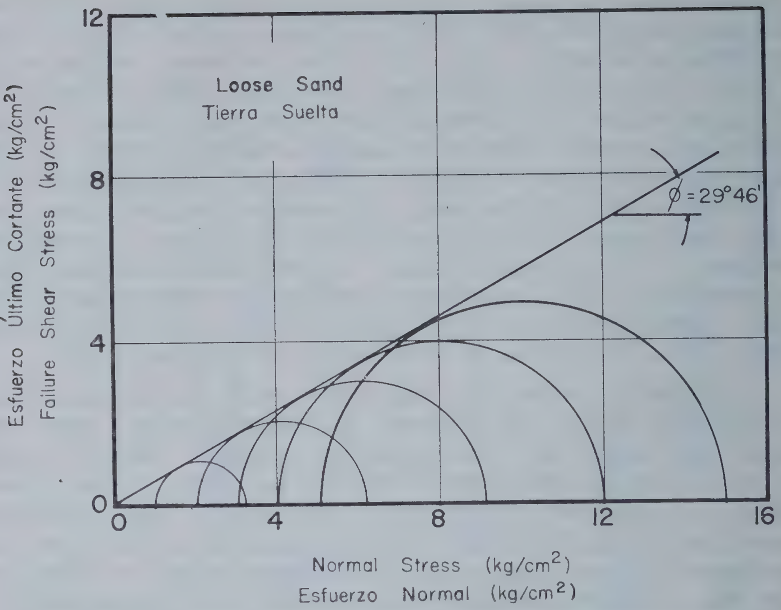

Fig. 18 — Computed Failure Surface in Two-Dimensional Stress-Space: Loose Sand.

ig. 18 — Superficie de Quiebre Calculada en Esfuerzo-Espacio Bi-Dimensional: Tierra Suelta.

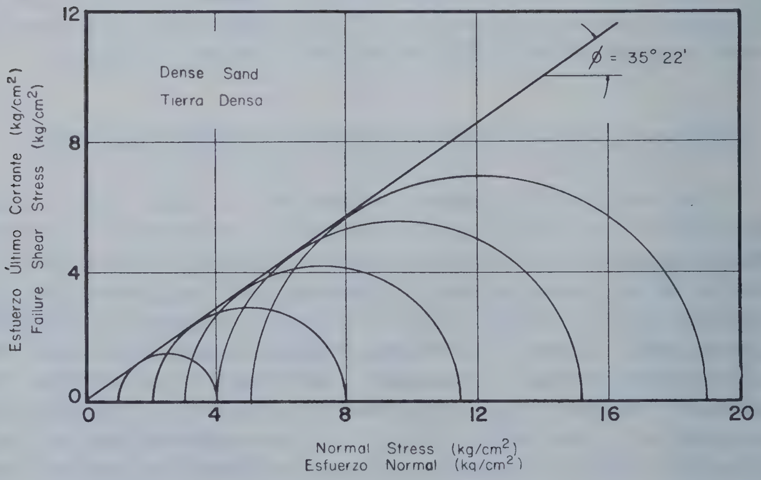

Fig. 19 — Computed Failure Surface in Two-Dimensional Stress-Space: Dense Sand.

Fig. 19 — Superficie de Quiebre Calculada en Esfuerzo-Espacio Bi-Dimensional: Tierra Densa.

No attempt has been made to use the explicit forms of the parameters a and b, as given by equations (14) and (19), in the correlations with other investigations because the numerical values of the coefficients are functions of the particular sand tested, void ratio of the sand, and test conditions. Thus, the correlations are primarily with regard to the applicability of the general hyperbolic form of equation (12) as a reasonable representation of the sand response.

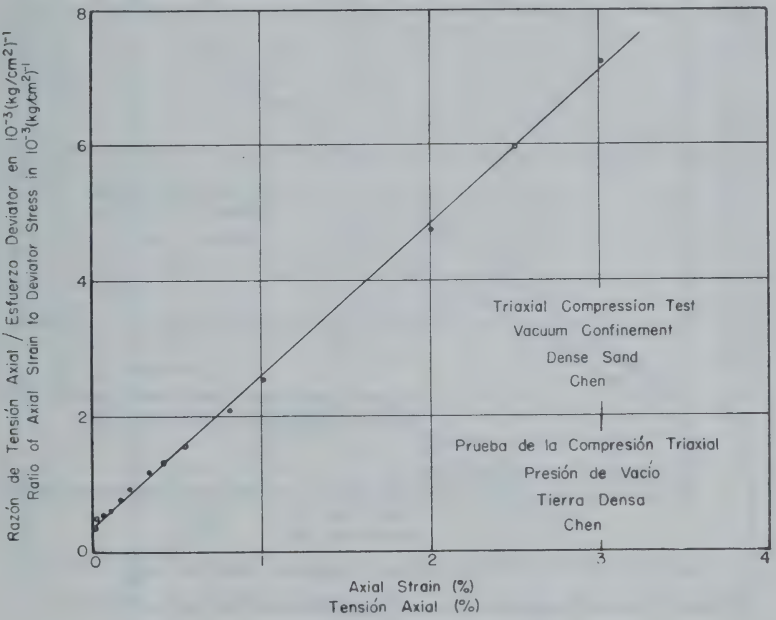

Fig. 20 — Triaxial Compression Response: Chen.

Fig. 20 — Respuesta de la Compresión Tri-axial: Chen.

The hyperbolic form of equation (12) is non-linear and as such indicates a non-linear response even at small values of strain. One of the few studies conducted in which the stress-strain response was accurately determined at very small values of strain is the work of Chen [15]. A typical set of Chen's results have been replotted in transformed hyperbolic form in terms of $\varepsilon/(\sigma_1 - \sigma_3)$ versus ε and are given in Figure 20. The test was for a dense sand using a vacuum confinement. Figure 20 indicates that the hyperbolic form of equation (12) represents the response fairly well even at very small strains. The normal stress difference at failure $(\sigma_1 - \sigma_3)_f$ obtained from the inverse of the slope of the straight line representation of Figure 20 is 63.2 psi as compared with the measured value of approximately 60 psi, a difference of approximately 5.3 percent. Thus, the correlation factor of equation (18) for this particular case would be approximately 95 percent.

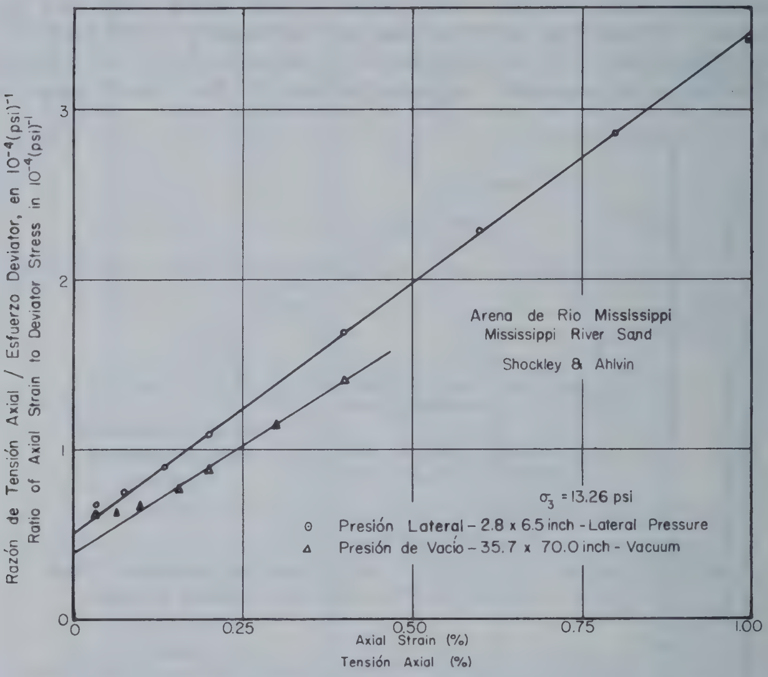

Fig. 21 — Triaxial Compression Response: Shockley and Ahlvin.

Fig. 21 — Respuesta de la Compresión Tri-axial: Shockley y Ahlvin.

Several other triaxial compression tests in which small strain values are given are those reported by Shockley and Ahlvin[16] for a Mississippi River sand. The tests were conducted using various loading cycles and only the initial cycle was utilized. Thus, failure of the specimen was not obtained. The transformed hyperbolic plots for these tests are given in Figure 21. The large specimen (36 by 70 in.) was confined by vacuum to a pressure of 13.26 psi while the small specimen (2.8 by 6.5 in.) was confined with lateral pressure to the same value. Both tests indicate a reasonable hyperbolic representation, although at very small strains the data seem to deviate with a concave curvature upward and approaching a horizontal line intersecting the $\varepsilon/(\sigma_1 - \sigma_3)$ axis above the straight line intercept. This would tend to indicate that the initial portion of the original stress-strain

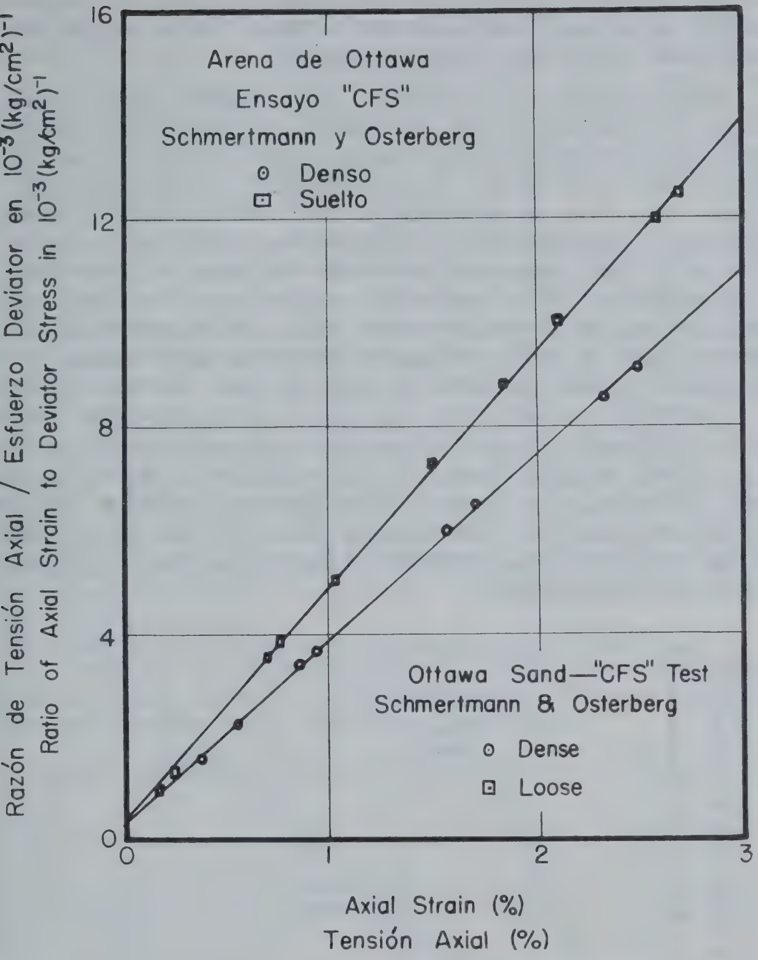

Fig. 22 — Triaxial Compression Response: Schmertmann and Osterberg.

Fig. 22 — Respuesta de la Compresión Tri-axial: Schmertmann y Osterberg.

curve was linear. It will be seen that the majority of the test results, given in the following figures, which deviate from the straight line form at low strains actually deviate with a concave curvature downward the origin. Such response indicates a greater non-linearity than that given by the hyperbolic fit. This non-linear trend was also noticed by Kondner[3] for cohesive soils tested in triaxial compression and plotted in transformed hyperbolic form. It is interesting to note that even the larger specimens reported in Figure 21 exhibit hyperbolic response for a fairly large range of the strains to which they were subjected.

Several tests on an Ottawa sand having grain sizes between Nos. 30 and 40 U.S. std. sieves are reported by Schmertmann and Osterberg [17] using the so-called "CFS"-test technique. These tests are given in transformed hyperbolic form in Figure 22. The applicability of the two-constant hyperbolic form as a representation of the stress-strain response is indicated by the agreement between the straight lines and the sand response. The inverse of the straight line slopes give ultimate values of the deviator stress at failure of 2.21 and 2.81 kg. per sq. cm. compared with measured values of approximately 2.25 and 2.90 kg. per sq. cm. In the CFS test, it is difficult to determine the exact ultimate value because of the difficulty of controlling the induced pore water pressure. Both straight lines of Figure 22 have the same intercept indicating the same initial tangent modulus for both stress-strain curves. This agrees with the idea of a common initial portion of the stress-strain curves as given by Schmertmann and Osterberg.

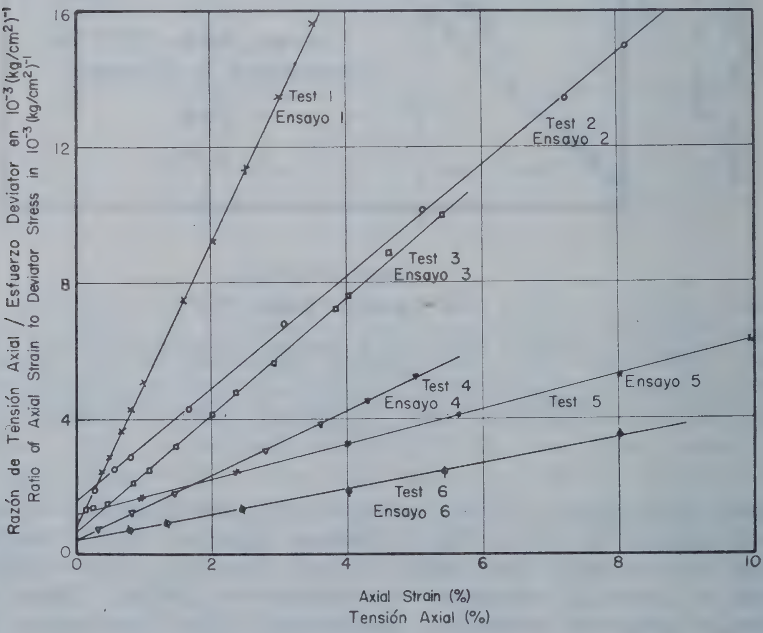

Fig. 23 — Triaxial Compression Response: Various Investigators.

Fig. 23 — Respuesta de la Compresión Tri-axial: Muchos Investigadores.

Figure 23 includes the test results reported by a number of authors replotted in transformed hyperbolic form. Test 1 is a triaxial compression test reported by Taylor and Whitman[18] for a standard 20/30 Ottawa sand with a void ratio of 0.49 and a confining pressure of 14 psi. The failure value of the deviator stress given by the inverse of the slope of Figure 23 is 33.9 psi compared to the measured value of 32 psi reported by Taylor and Whitman.

Tests 2 and 4 of Figure 23 are from results reported by Taylor[19] for a saturated Fort Peck sand in a loose condition (void ratio = 0.834) and a dense state (void ratio = = 0.605) respectively. The tests were conducted using specimens 1.40 inch in diameter and 2.99 inches in length under a lateral pressure of 30 psi and a rate of axial strain of 1.8 percent per min.

Test 3 is from data reported by Meese and Long[20] for a uniform quartz blasting sand with a lateral pressure of 1.78 tons per sq. ft. Tests 5 and 6 were plotted from the results of tests reported by Watson[21] on a medium fine sand in a loose state (void ratio = 0.737) and a dense condition (void ratio = 0.565) respectively under a lateral pressure of 6.32 kg. per sq. cm.

In general, the transformed hyperbolic representations of Figure 23 are quite good with the correct relative positions of the comparable loose and dense conditions.

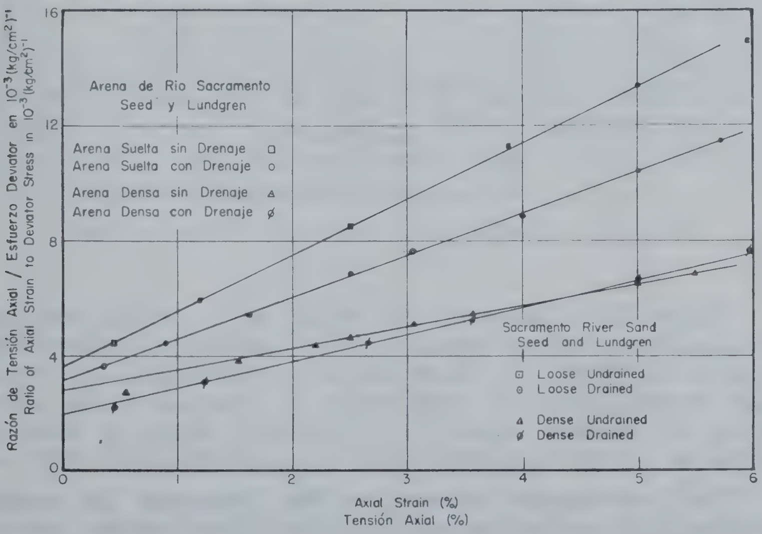

Fig. 24 — Triaxial Compression Response: Seed and Lundgren.

Fig. 24 — Respuesta de la Compresión Tri-axial: Seed y Lundgren.

Figure 24 is a transformed hyperbolic plot of data reported by Seed and Lundgren[22] for drained and undrained triaxial compression tests on a Sacramento River sand in a loose state (void ratio = 0.78) and a dense condition (void ratio = 0.59) under a lateral pressure of 2.0 kg. per sq. cm.

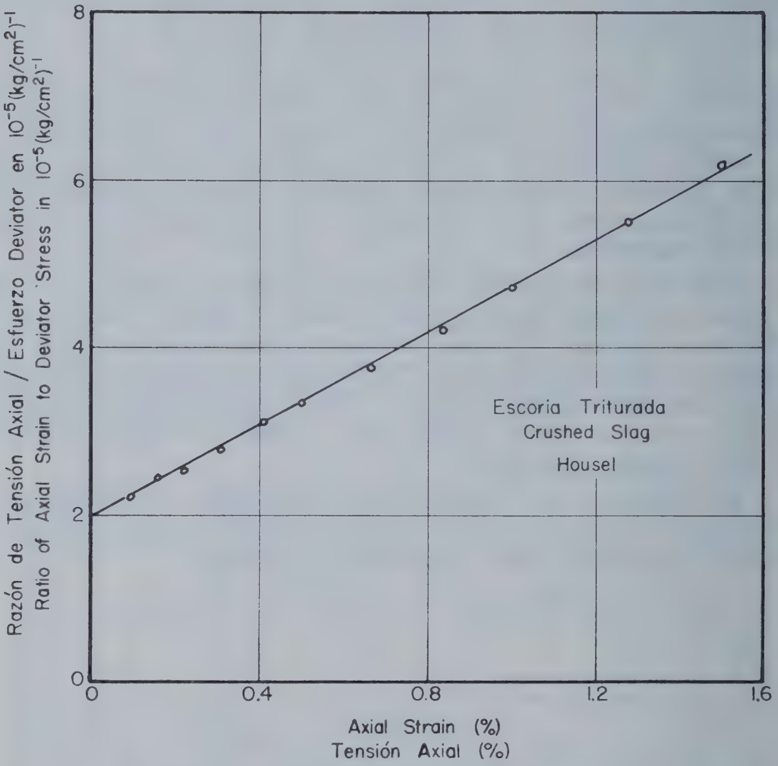

Fig. 25 — Triaxial Compression Response: Housel.

Fig. 25 — Respuesta de la Compresión Tri-axial: Housel.

Figure 25 is based on the results of a triaxial compression test at a lateral pressure of 45 psi for a crushed slag reported by Housel[23]. Even for the crushed slag, the hyperbolic representation is good with the inverse of the slope giving an ultimate value of the deviator stress of 3565 psi compared to the recorded value of approximately 3550 psi.

The test results reported in the literature by various investigators for a variety of sands tested under various conditions and presented in Figures 20 through 25 indicate that there is perhaps some generality to the applicability of the two-constant hyperbolic form as a representation of stress-strain response of sands in triaxial compression. Many more examples of stress-strain curves that can be satisfactorily represented by such a form are contained in the literature. This does not mean that all sand response can be represented by such a form but simply that it has some generality.

CONCLUSIONS

A two-constant hyperbolic stress-strain relation has been developed for sands in triaxial compression such that the ultimate shear strength of the soil is contained within the general formulation and appears in the mathematical limit of the stress as the strain becomes excessive. Thus, the divergent concepts of a stability analysis as compared with a load-deformation approach to soil mechanics phenomena related to sands are shown to be compatible within the framework of a hyperbolic stress-strain relation.

The explicit form of the stress-strain relation utilized can be written as:

$$\sigma_1 - \sigma_3 = \frac{\varepsilon}{a + b\,\varepsilon} \tag{12}$$

where $(\sigma_1 - \sigma_3)$ is the normal stress differences usually referred to in soil mechanics as the deviator stress, ε is the axial strain, and the parameters a as well as b are functions of the type and relative density of the sand tested and the octahedral normal stress acting. The explicit forms of the parameters a and b, for the particular uniform fine dune sand studied, take the forms

$$\frac{1}{b} = A + B\,\sigma_{oct} \tag{14}$$

and

$$\frac{1}{a} = C + D\,\sigma_{oct} \tag{19}$$

where σ_{oct} is the octahedral normal stress and the values of the parameters A, B, C, and D are functions of the relative density and have been determined for loose and dense conditions.

Taking the derivative of equation (12) with respect to strain and evaluating the derivative for zero strain gives

$$E_i = \left[\frac{d\ (\sigma_1 - \sigma_3)}{d\ \varepsilon} \right]_{\varepsilon=0} = \frac{1}{a} \tag{10}$$

where E_i is the initial tangent modulus of the sand.

By taking the mathematical limit of equation (12) as the strain becomes excessive one obtains:

$$\lim_{\varepsilon \to \infty} (\sigma_1 - \sigma_3) = \frac{1}{b} = k\ (\sigma_1 - \sigma_3)_f \tag{23}$$

where $(\sigma_1 - \sigma_3)_f$ is the ultimate or failure value of the deviator stress and k is a correlation coefficient of 1.043. Thus, the failure criterion for the sand tested can be written as:

$$(\sigma_1 - \sigma_3)_f = 0.958\ [A + B\,\sigma_{oct}] \tag{18}$$

The failure relation given by equation (18) has been shown to give conventional Mohr-Coulomb failure envelopes in terms of a two dimensional stress space. The angles of internal friction predicted using equation (18) in terms of the Mohr-Coulomb representation are 35°-22' for the dense state and 29°-46' for the loose condition.

Randomly selected test results reported in the literature by various investigators for a variety of sands and granular materials indicate that there is some generality to the applicability of the two-constant hyperbolic form of equation (12) as a representation of stress-strain response for sands. These correlations are presented in Figures 20 through 25.

ACKNOWLEDGMENTS

The authors are indebted to the many researchers whose published test results have been analyzed in this paper.

REFERENCES

1. Kondner, R. L. — A Non-Dimensional Approach to the Vibratory Cutting, Compaction and Penetration of Soils, *Technical Report No. 8,* Dept. of Mech., The John Hopkins Univ., Baltimore, Med., 1960.

2. Kondner, R. L. — Hyperbolic Stress-Strain Relation in Direct Shear, Submitted for Publication, 1962, 35 pp.

3. Kondner, R. L. — Hyperbolic Stress-Strain Response in Triaxial Compression, Submitted for Publication, 1962.

4. Kondner, R. L. and Vendrell, J. R. — Clay Mineral Effects on the Stress-Strain Response of Soils in Direct Shear, *Eleventh Clay Minerals Conference,* Ottawa, Canada, 1962.

5. Kondner, R. L. — Friction Pile Groups in Cohesive Soil, *Journal of the Soil Mechanics and Foundations Division,* ASCE, v. 88, 1962, pp. 117-149.

6. Kondner, R. L. and Krizek, R. J. — Correlation of Load Bearing Tests on Soils, *Preprint, H.R.B.,* 1962, 60 pp.

7. Kondner, R. L., Krizek, R. J. and Schimming, B. B. — Lateral Stability of Rigid Poles Subjected to an Applied Couple, Submitted for Publication, 1962, 36 pp.

8. Kondner, R. L. and Cunningham, J. A. — Lateral Stability of Partially Embedded Rigid Poles, Submitted for Publication, 1962.

9. Weissenberg, K. — A Continuum Theory of Rheological Phenomena, *Nature,* vol. 159, 1947, p. 310.

10. Lambe, T. W. — Soil Testing for Engineers, John Wiley and Sons, Inc., New York, N.Y., 1951, pp. 105-106.

11. Chen, L. S. — Stress-Deformation and Strength Characteristics of Cohesionless Soils, Doctor of Science Thesis, Harvard Univ., Dec., 1944.

12. Boussinesq, J. — Essai Theorique sur l'Equilibre d'Elasticité des Massifs Pulvurents Comparé à celui de Massifs Solides et sur la Poussée des Terres sans Cohésion, *Mémoires* Couronnées et Mémoires des Savants Etrangers Publiées par l'Academie de Belgique, tome XL, Bruxelles.

13. Terzaghi, K. and Peck, R. B. — Soil Mechanics in Engineering Practice, John Wiley and Sons, Inc., New York, N.Y., 1948, pp. 108-109.

14. Hough, B. K. — Basic Soil Engineering, Ronald Press Co., New York, N.Y., 1957, pp. 150-151.

15. Chen, L. S. — An Investigation of Stress-Strain and Strength Characteristics of Cohesionless Soils by Triaxial Compression Tests, *Proc.* 2nd Internatl. Conf. on Soil Mech. and Foundation Engrg., vol. 5, Rotterdam, 1948, pp. 35-43.

16. Shockley, W. G. and Ahlvin, R. G. — Nonuniform Conditions in Triaxial Test Specimens, *Proc.* ASCE Research Conf. Shear Strength of Cohesive Soils, 1960, p. 356.

17. Schertmann, J. H. and Osterberg, J. O. — An Experimental Study of the Development of Cohesion and Friction with Axial Strain in Saturated Cohesive Soils, *Proc.* ASCE Research Conf. Shear Strength of Cohesive Soils, 1960, p. 667.

18. Taylor, D. W. and Whitman, R. V. — The Behavior of Soils Under Dynamic Loadings, *M.I.T. Report,* August, 1954, p. 171.

19. Taylor, D. W. — Fundamentals of Soil Mechanics, John Wiley and Sons, Inc., New York, N.Y., 1948, p. 335.

20. Meese, R. H. and Long, R. W. — Triaxial Compression Tests on Soils Using Variable Lateral Pressure, *ASTM,* S.T.P. No. 254, 1959, p. 366.

21. Watson, J. D. — A Triaxial Compression Apparatus for the Determination of the Stress-Deformation Characteristics of Soils, *Proc.* ASTM, vol. 39, 1939, p. 1051.

22. Seed, H. B. and Lundgren, R. — Investigation of the Effect of Transient Loading on the Strength and Deformation Characteristics of Saturated Sands, *Proc.* ASTM, vol. 54, 1954, p. 1294.

23. Housel, W. S. — Interpretation of Triaxial Compression Tests on Granular Mixtures, ASTM, S.T.P. No. 106, 1950, p. 268.

DIVISÃO II — *Fundações*

DIVISIÓN II — *Fundaciones*

DIVISION II — *Foundations*

IIa. *Fundações diretas e profundas, sem o emprêgo de estacas*

Fundaciones directas y profundas, sin el uso de pilotes

Foundations other than piled foundations

IIb. *Fundações por estacas*

Fundaciones por medio de pilotes

Piled foundations

LOW COST SHALLOW FOUNDATION

ARAKEN SILVEIRA e EVELYNA BLOEM SOUTO SILVEIRA
Assistant Professors at the School of Engineering of São Carlos of the U.S.P.
São Paulo, Brazil.

SUMMARY

This paper presents the experience made on the buildings constructed at the School of Engineering of São Carlos, of the University of São Paulo, in which a new solution for its foundations was employed, based on studies carried out in 1958 and published at the 2nd Brazilian Conference on Soil Mechanics. The main data of that study are summarized and complemented herein, and a typical design of the foundations is indicated; its performance has shown to be very satisfactory, according to the three years old observations.

SUMÁRIO

O presente trabalho relata a experiência realizada nos edifícios construídos para a Escola de Engenharia de São Carlos, da Universidade de São Paulo, nos quais foi empregada uma nova solução para as suas fundações, baseada em estudos efetuados em 1958, publicados no II Congresso Brasileiro de Mecânica dos Solos. Os principais dados daquele estudo foram resumidos e complementados, indicando-se um projeto típico das fundações, cujo comportamento se tem mostrado bastante satisfatório em face das observações realizadas há já três anos.

1. INTRODUCTION

In 1958, the authors were concerned with the study of a typical soil (decomposed sandstone) of the city of São Carlos, State of São Paulo, Brazil, for the purpose of a regional study and also to furnish background data for the possible development of a building code for common light structures. A general study of shallow footing foundations was carried out by a comparison of a load test in situ with several load tests run in laboratory for investigations of size effects as well as the effect of soaking.

The paper was published in the Proceedings of the 2nd Brazilian Conference on Soil Mechanics[1]. As a conclusion, a solution was envisaged for the problem of the economic improvement of the soil at the bottom of shallow pits provided for footings of light structures.

The solution consisted in removing the soil below shallow footings up to a specified depth, and then proceeding to its reposition in layers, compacting it by means of light manual tamping.

Model and triaxial compression tests were performed upon samples taken from a test pit in which compaction was carried out in the same way that was envisaged in laboratory studies, and a solution was proposed.

Soon afterwards, new buildings of the School of Engineering of São Carlos, were to be built. The one or two-storey buildings were conceived for laboratory, class-rooms and amphytheaters, and consisted of light structures. The new envisaged solution was designed, with great economic advantage. In many other places of the São Paulo State and even in the city of São Paulo, the same solution was applied with success.

2. CHARACTERISTICS OF THE SOIL

The soil concerned is a sand which is part of the "Series Bauru", a residual soil from sedimentary rock; its grain-size distribution is given in Fig. 1; its average natural void ratio is approximately 0.8.

Freitas[2] investigated the mineralogical composition of the sand and found it to be composed mainly of quartz with some feldspar. A few heavy minerals and calcium carbonate were observed.

Atterberg limits of the material are approximately

Liquid Limit = 28%

Plastic Limit = 15%

Quick (undrained) and slow (drained) triaxial tests carried out upon undisturbed block samples lead us to strength envelopes $s = 0.05 + \sigma \tan 3.4^\circ$ and $s = \sigma \tan 27^\circ$ respectively; the stress-strain curves have indicated that local shear case is to be expected according to Terzaghi's theory for ultimate bearing capacity.

The average value of 0.4 of compression index was obtained from consolidation tests carried out on undisturbed block samples.

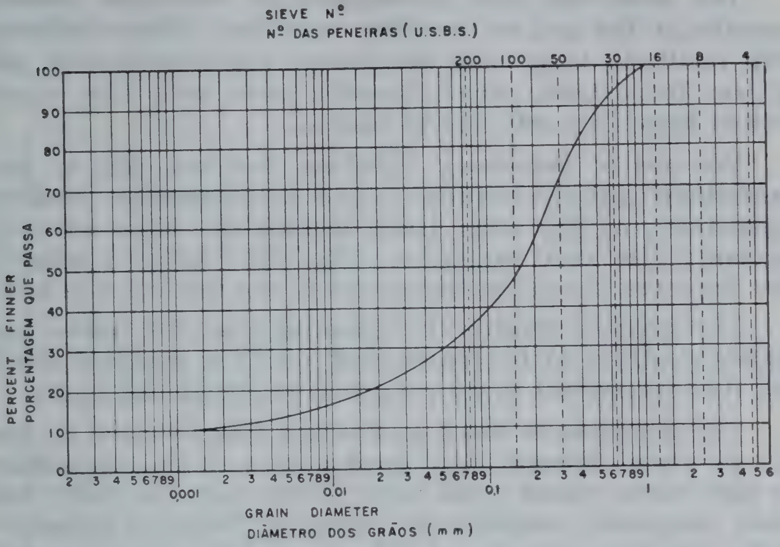

Fig. 1 — Grain curve distribution.

Fig. 1 — Curva granulométrica.

A very small bearing capacity of the soil was observed, for shallow foundations:

1. Observation of the performance of shallow foundations of small buildings at the same town, designed for 0.5 kg/cm^2 of allowable bearing capacity, has shown that this value is excessive, for a normal construction of the footings, because there is a great deal of local houses that present damages and signs of cracking.

2. Values smaller than 0.5 kg/cm^2 are generally indicated by dynamic penetration resistance in exploratory borings executed at the site.

3. The Building Code of Boston and its adapted form for Brazilian Code indicate, for load test values, an allowable bearing capacity of approximately 0.4 kg/cm^2 (with a safety factor 2).

4. A value of approximately 0.25 kg/cm^2 is found to be appropriated for the soil under consideration, taking into account the average strength envelopes $s = 0.05 + \sigma \tan 3.4^\circ$ (kg/cm^2) for undrained tests and $s = \sigma \tan 27^\circ$ for drained tests, and according to Terzaghi's theory for ultimate bearing capacity, for local shear case.

The value that can be assumed for allowable bearing capacity of the soil is therefore very low. Then, buildings with relatively high loads are always constructed with pile or pier foundations, which transfer loads onto firm strata located below the soft one in case.

For one or two-storey buildings, however, pile or pier foundations are too expensive, and anti-economic. Shallow foundations, on the other hand, become too large and consequently also very expensive. For this reason, a solution that improves the soil at the bottom of the footings was tried.

The process consists in removing the soil under the shallow footings to be constructed, up to a specified depth, and then to proceed to its reposition in compacted layers.

The procedure is based on the fact that the sand in case has its shear strength very much improved by compaction. In fact, some recent tests have shown that the same soil, when compacted according to Standard Proctor Compaction Test, presents a cohesion of 0.2 kg/cm^2 and a friction angle of 30^o, and, compacted according to Modified Proctor Compaction Tests, have 0.5 kg/cm^2 of cohesion and 40^o of friction angle (Fig. 2).

For the specific case, however, one could not expect to require a very great amount of energy to be furnished to the soil, owing to the economic conditions of the small buildings to be constructed: economic criteria suggest that compaction should be obtained by means of light manual tamping.

A 1.0 meter wide and 1.5 meters depth pit was excavated. The removed material was replaced, and was compacted in ten successive layers, up to 0.5 meters depth. Compaction was attained with natural water-content (near optimum, according to the tests), by means of a simple rammer, of reinforced concrete, with approximately 15 kg, falling through about 20 cm, according to normal field conditions for a man's work. Each layer was compacted by approximately 150 blows. We can estimate in about 4,500 kgm/m^3 the total compaction energy furnished (approximately 7% that of Proctor Standard Test).

Undisturbed block samples were taken from the site, and triaxial compression tests were carried out. Fig. 2 shows the results of the tests, leading to an average value of $s = 0.4 + \sigma \tan 6.8^o$ (kg/cm^2).

Allowable bearing capacity, according to the same Terzaghi's theory, can be estimated in 0.95 kg/cm^2. Model load tests were carried out, and their careful interpretation, with the criteria established before [1], led to a value of 0.65 kg/cm² for the allowable bearing capacity of the material.

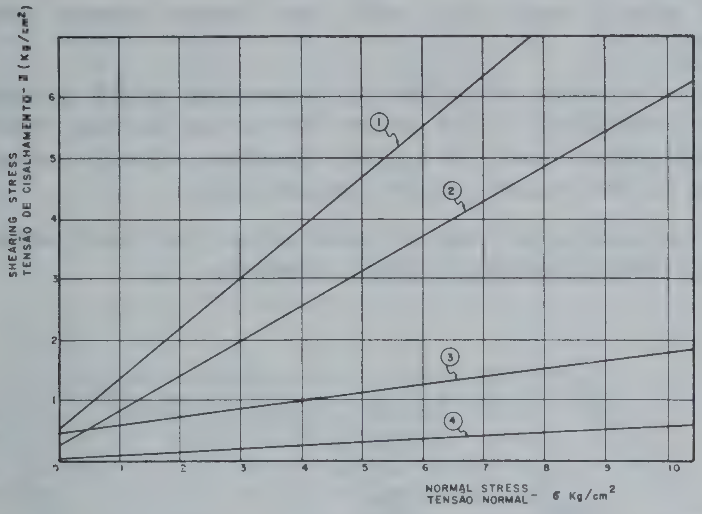

NUMBER NÚMERO	COMPACTION TYPE TIPO DE COMPACTAÇÃO	APPLIED ENERGY ENERGIA APLICADA (Kgm/m²)	STRENGTH ENVELOPES ENVOLTÓRIAS DE RESISTÊNCIA (Kg/cm²)
1	MODIFIED PROCTOR PROCTOR MODIFICADO	282.000	$0.5 + \sigma\,\mathrm{tg}\;40.0^\circ$
2	STANDARD PROCTOR PROCTOR NORMAL	56.000	$0{,}2 + \sigma\,\mathrm{tg}\;30{,}0^\circ$
3	HAND TAMPING SOCAMENTO NATURAL	4.500	$0{,}4 + \sigma\,\mathrm{tg}\;6{,}8^\circ$
4	NONE (NATURAL SOIL) NENHUMA (SOLO NATURAL)	0	$0.05 + \sigma\,\mathrm{tg}\;3.5^\circ$

Fig. 2 — Strength envelopes determined with different compaction energies.

Fig. 2 — Envoltórias de resistência determinadas com diferentes energias de compactação.

Allowable bearing capacity, therefore, is shown to have an improvement of 100 to 200%.

One could think of employing more energy, near that of Standard Proctor Test for example: although a large improvement of shear strength can be obtained by the process, we still believe that the envisaged solution — light manual tamping — is more convenient:

1. it is much cheaper, which agrees with the construction conditions of a one or two-storey building;
2. it gives, with 7% of Proctor energy, a reduction of 35% of natural void ratio, while the Proctor energy gives 58%;
3. for a 0.5 meter wide footing, a pressure of 0.3 p would be transferred to 1.0 meter below, the footing, which could be at most 0.3 kg/cm², therefore already according to the capacity of the natural soil;
4. it can always be done by easy means, and local personnel, which presents a great advantage.

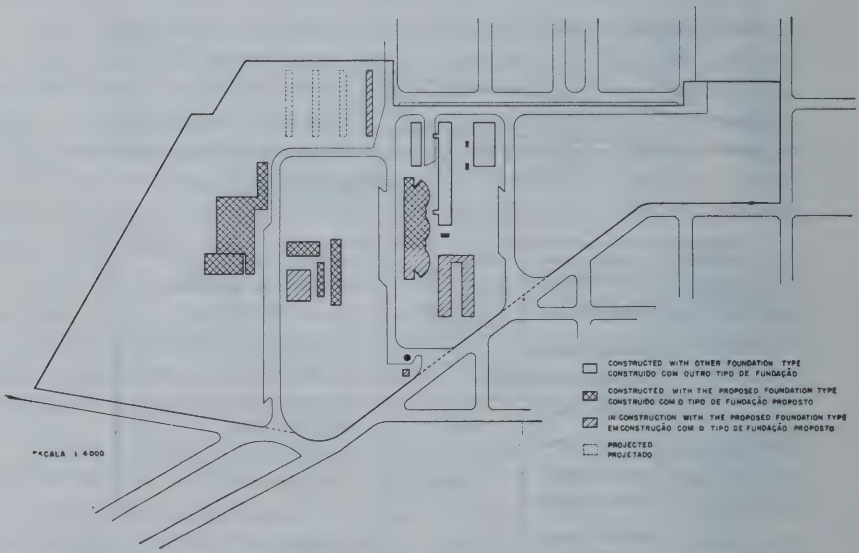
ESCALA 1:4000
CONSTRUCTED WITH OTHER FOUNDATION TYPE
CONSTRUIDO COM OUTRO TIPO DE FUNDAÇÃO
CONSTRUCTED WITH THE PROPOSED FOUNDATION TYPE
CONSTRUIDO COM O TIPO DE FUNDAÇÃO PROPOSTO
IN CONSTRUCTION WITH THE PROPOSED FOUNDATION TYPE
EM CONSTRUÇÃO COM O TIPO DE FUNDAÇÃO PROPOSTO
PROJECTED
PROJETADO

Fig. 3 — Lay-out of the present plan of the School of Engineering of São Carlos.

Fig. 3 — Disposição do planejamento atual da Escola de Engenharia de São Carlos.

3. DESIGN OF THE LOW COST SHALLOW FOUNDATIONS AT THE SCHOOL OF ENGINEERING OF SÃO CARLOS

Five one or two-storey buildings were already constructed with this method. Fig. 3 presents the layout of the buildings, and Fig. 4 shows a typical foundation design.

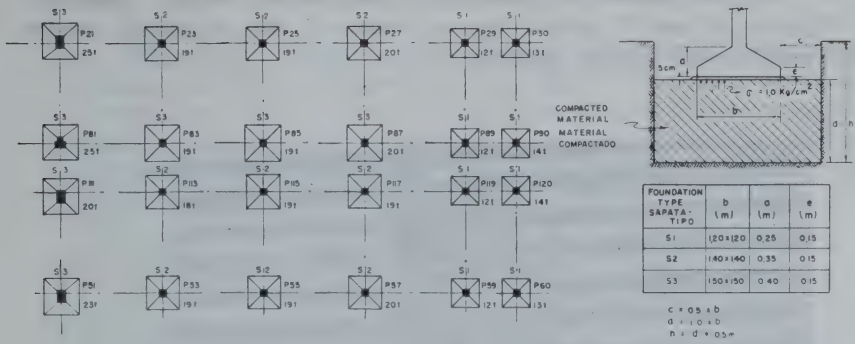
S3
P21
25t
S2
P23
19t
S2
P25
19t
S2
P27
20t
S1
P29
12t
S1
P30
13t
S3
P81
25t
S3
P83
19t
S3
P85
19t
S3
P87
20t
S1
P89
12t
S1
P90
14t
S3
P111
20t
S2
P113
18t
S2
P115
19t
S2
P117
19t
S1
P119
12t
S1
P120
14t
S3
P51
23t
S2
P53
19t
S2
P55
19t
S2
P57
20t
S1
P59
12t
S1
P60
13t
COMPACTED MATERIAL
MATERIAL COMPACTADO
5cm
a
c
e
σ = 1,0 Kg/cm²
b
d
h

FOUNDATION TYPE SAPATA-TIPO	b (m)	a (m)	e (m)
S1	1,20 x 1,20	0,25	0,15
S2	1,40 x 1,40	0,35	0,15
S3	1,50 x 1,50	0,40	0,15

c = 0,5 x b
d = 1,0 x b
h = d + 0,5m

Fig. 4 — Part of a typical foundation design.

Fig. 4 — Parte de um projeto de fundação típico.

Under every footing to be constructed, a pit of 1.0 × × b + 0.6 meters depth was opened (b being breadth), 1.0 b meters larger than every dimension of the footing, which means that 0.5 b meters were opened at each side of the footing. The removed material was replaced and compacted in layers of about 0.15 meters thickness; compaction was obtained with a reinforced concrete rammer supported by a tripod; three men worked together, so that the furnished energy would be approximately the same as of the test pit.

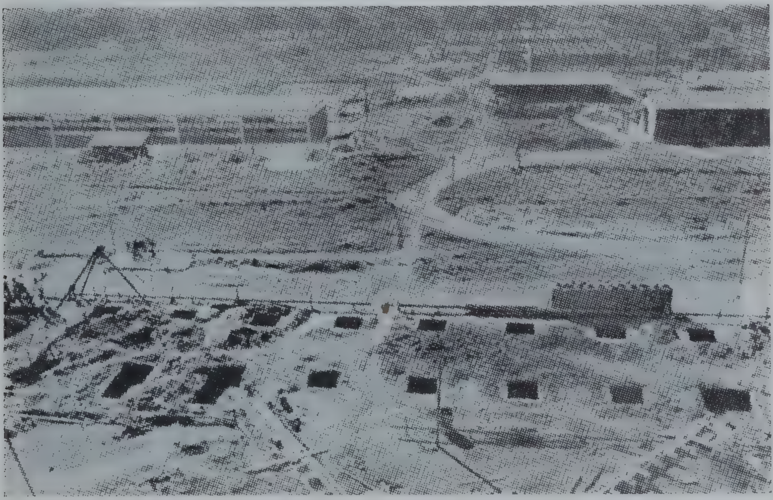

Fig. 5 — General view of foundations under construction.

Fig. 5 — Vista geral da construção das fundações.

Fig. 5 shows a photo of the works being executed. Figures 6 and 7 shows some views of the buildings under several construction phases.

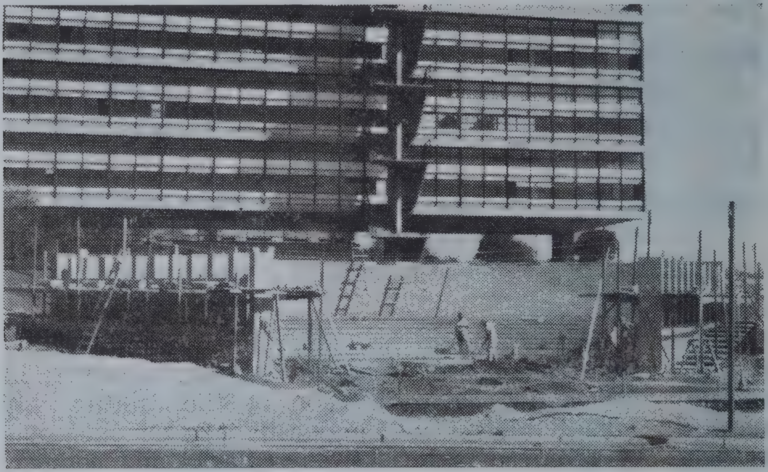

Fig. 6 — Construction phase.
Fig. 6 — Fase da construção.

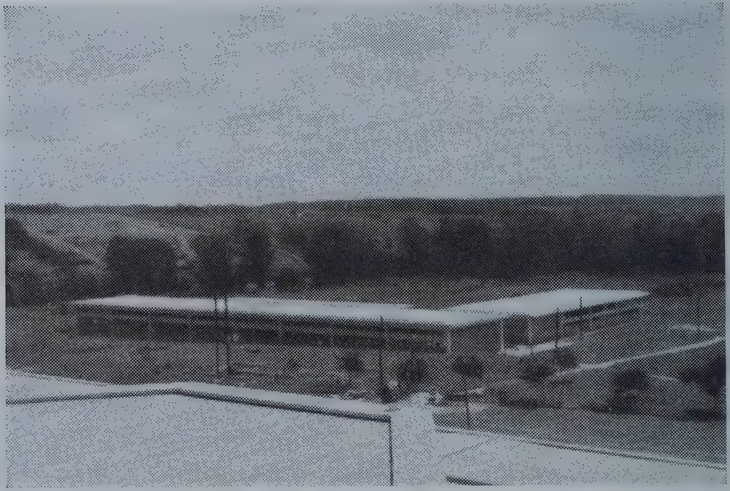

Fig. 7 — Typical building referred to in the text.
Fig. 7 — Edifício típico referido no texto.

4. ECONOMICS OF THE PROCESS

Economic studies envolving the available solutions have shown that the envisaged one was about 3 to 11 times cheaper (depending upon loads and local conditions), and the most practical, chiefly for regions far from the major and resourceful towns, and sometimes the only compatible with local supplies.

5. PERFORMANCE OF THE CONSTRUCTIONS

Careful attention was given to the performance of the constructions: after three years, no damage was observed in any building, that can be assumed to result from a bad behaviour of the foundations.

The envisaged process can be considered successful, and is now adopted as a general solution for many one or two-storey buildings constructed over analogous soils.

6. CONCLUSIONS

The removal of the natural sandy material considered, up to a certain depth below the shallow foundations, and its reposition in layers compacted by means of light manual tamping, was proved to be a successful solution as a low cost shallow foundation for several one or two-storey buildings constructed at the School of Engineering of São Carlos, Brazil. The cost of this process seems to be from 3 to 11 times cheaper than any other method compatible with the problem. The same solution should be tried for other sandy soils and the results should be pointed out for further employment of the method.

REFERENCES

1. Souto Silveira, Evelina B. & Silveira, Araken — "Investigação do arenito decomposto de São Carlos para fundação de pequenas construções" — Anais do 2.º Congresso Brasileiro de Mecânica dos Solos — Vol. I — 1958.

2. Freitas, Rui Osório de — "Sedimentação, estratigrafia e tectônica da Série Bauru" — São Paulo, 1955.

MODEL BEARING TESTS ON A REMOULDED CLAY

R. YONG
Associate Professor and Director, Soil Mechanics Laboratory, McGill University, Montreal, Canada.

G. M. PECK
Formerly, Commonwealth Scholar; now, Research Engineer, Department of Public Works, Hobart, Australia.

H. C. LEITCH
Graduate Research Assistant, Soil Mechanics Laboratory, Department of Civil Engineering and Applied Mechanics, McGill University.

ABSTRACT

In the consideration of the bearing capacity of footings, a distinction is made between local and general shear failure. Whilst it is possible to separate these in theory, in practice the boundary between local and general shear failure is very often indistinct.

This paper evaluates the bearing behaviour of model footings on a remoulded clay, the properties of which would dictate bearing characteristics in this region, and also to apply semi-rational analyses using both punching shear and quasi-elastic deformation theories. Included also are comparisons between predicted and observed bearing capacities using conventional and proposed bearing theories.

RESUMEN

Considerando la capacidad de sustentación de cimientos, se hace una distinción entre una rotura local y una rotura general. Pero, mientras que es posible separarlas en teoría, en la práctica la frontera entre la rotura local y la general es a menudo indistinta.

Este folleto evalúa el comportamiento de la sustentación de cimientos modelos en una arcilla remoldeada, cuyas propiedades deberían indicar las características de sustentación en esta región, y se aplica también a análisis semi-racionales empleando tanto la rotura hecha a punzón como las teorías de deformación casi-elástica. Las comparaciones entre las capacidades de sustentación previstas y las observadas, empleando las teorías de sustentación convencionales y propuestas, están también incluidas.

INTRODUCTION

In the design of footings, the two important criteria considered are settlement and shear. In the case of a granular subsoil, the use of rational design formulae incorporating shear strength parameters is the accepted practice, with settlement evaluation based upon empirical relationships as a secondary consideration. However, the reverse procedure has been found to be more applicable for footings founded on clay soils. In general, shear and settlement are treated as two separate design operations. A suitable theory of bearing capacity is used to establish the ultimate shear resistance in bearing of the soil, quite apart from settlement computations which are based upon a different set of parameters and boundary conditions.

Terzaghi (1943) has defined conditions leading to both local and general shear failures. Whilst it is possible to separate these conditions in theory, in practice, the boundary between local and general shear failure is very often indistinct. In view of this, it is desirable to arrive at some compromise which would accommodate this apparent discontinuity.

This study was designed with two purposes in mind: (a) to evaluate the behaviour of model footings on a remoulded clay — the properties of which would dictate bearing characteristics in this region, and (b) to apply a semi-rational analysis using both punching shear and quasi-elastic deformation theories.

EXPERIMENTAL PROCEDURES

The physical and chemical properties of the kaolinitic clay used for this study are given in Table 1.

In order to meet the scaling requirements necessary for sensible model testing, the properties of the clay had to be modified. This was achieved by the use of chemical additives which altered the performance characteristics with regard to shear and compaction. Based upon a preliminary study of various additives it was decided that the addition of 1% by weight of sodium tripolyphosphate best met the requirements. The consistency limits for the modified clay were: LL = 33.3%, PL = 29.6%.

To allow for a visual examination of the soil beneath the model footing, a rectangular glass box with removable sides of ½ inch thick plate glass was used. The internal dimensions of the box were 4 inches by 22½ inches by 23½ inches high. With the footing size of 1½ inches wide by 4 inches long, it was possible to simulate a strip footing behaviour provided that friction between the end faces of the model footing and glass was negligible. This was achieved by greasing the sides of the container totally since this procedure was also required to minimize friction between the soil and the glass sides. Observation of soil movement under loads was facilitated by previous gridding of the visible sides of the soil mass.

TABLE 1 — Physical and Chemical Properties of Kaolinitic Clay

Chemical Analysis	%	Calculated Proximate Analysis	%
Silica	47.9	Clay	87.7
Alumina	37.1	Felspathic (Micaceous) Matter	11.5
Ferric Oxide	0.41	Ferric Oxide	0.4
Titanium Dioxide	0.05	Lime	0.2
Magnesia	0.20	Magnesia	0.2
Lime	0.20		100.0
Potash	1.87		
Soda	0.05		
Loss when calcined at 950^{o}	12.22		
	100.00		

Estimated Kaolinite Content = 85%
Specific Gravity based on Mineralogical Data = 2.69

Grain Size Distribution

Particle Size (microns)	Percent Less than
30	99.99
10	94.30
2	59.0

The soil was placed in the box in layers such that when compacted (by means of a vibratory compactor) these were from ¾ inches to 1 inch thick. By scarifying the top of each layer, excessive stratification was avoided and a high degree of uniformity was achieved. To allow for a wider range in bearing behaviour, subsoil moisture contents were varied for different test series.

Load was applied to the model footing either at a constant strain rate or in equal incremental loads. It was found that both these techniques gave comparable results for this study.

The unconfined compressive strength of the subsoil was determined from samples cored directly from the soil in the container in the undisturbed portion immediately following each bearing test series. In this manner, the apparent "cohesion" of the soil could be determined. Undrained triaxial tests were conducted on companion samples prepared in the Harvard Miniature Compactor at comparable moisture contents. Whilst pore pressure measurements were made, because of the partial saturation of the samples, these proved to be relatively difficult to use in data analysis. Since also the triaxial samples were not obtained directly from the container, the use of these triaxial results can be questioned.

DISCUSSION OF RESULTS

The results of footing tests are tabulated in Table 2 and representative load settlement curves are given in Figures 1 and 2.

TABLE 2 — Model Bearing Test Results

Sample No.	Ave. Water Content %	"Cohesion" C (psi)	Observed Failure load (lbs)	q_{obs} psi	q_p psi	q_{obs}/q_p
1	30.9	5.33	110	18.3	27.4	0.668
2	29.4	5.10	103	17.2	26.2	0.653
3	32.2	5.02	95	15.9	25.7	0.620
4	31.1	6.52	180	30.0	33.5	0.895
5	29.3	7.11	170	28.3	36.5	0.776
6	34.3	8.83	190	31.7	45.4	0.698
7	31.0	7.78	190	31.7	40.0	0.793
8	29.1	8.83	210	35.0	45.4	0.772
9	27.9	9.15	210	35.0	47.1	0.743
10	28.1	5.22	145	24.2	26.9	0.90

In the tabulated values for the observed bearing capacity, comparison is made with the well-known Prandtl bearing capacity relationship, $q_p = 5.14C$. The ratio of the observed bearing capacity to the predicted Prandtl capacity varies from 0.62 to 0.90 with an average of 0.75.

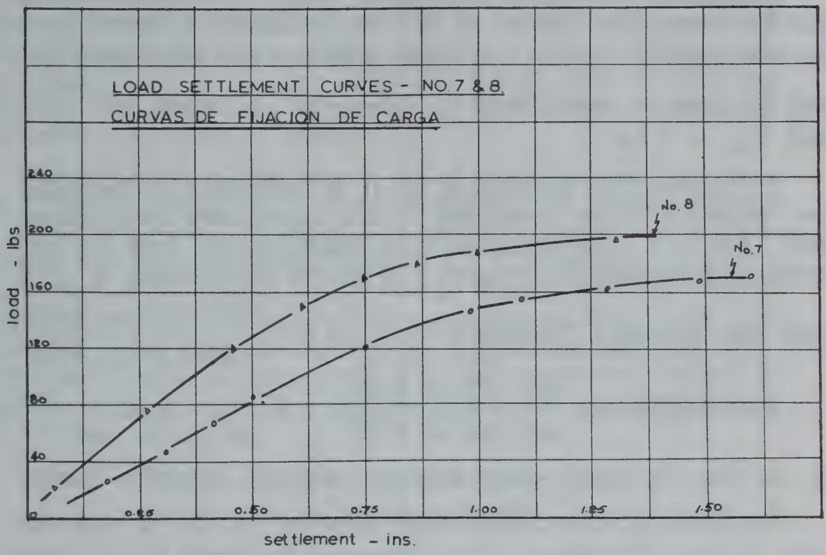

Fig. 1 — Load-settlement curves.

Fig. 1 — Curvas de cargas-asientos.

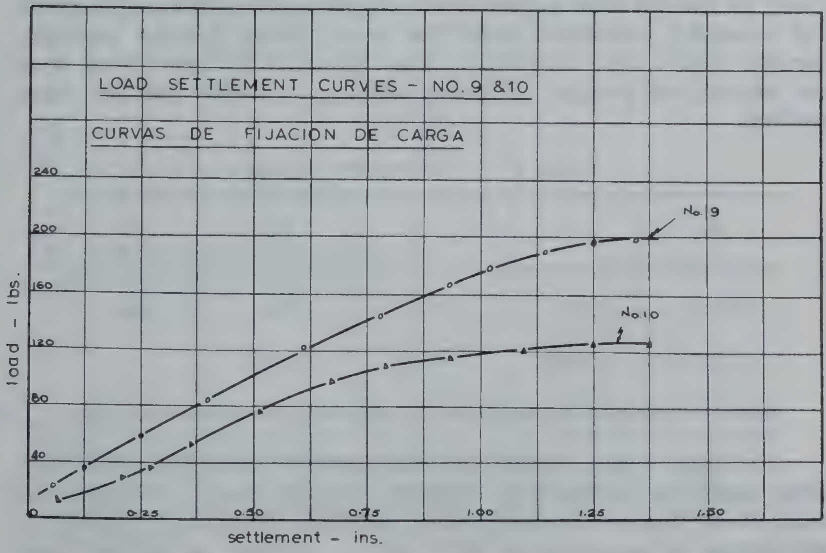

Fig. 2 — Load-settlement curves.

Fig. 2 — Curvas de cargas-asientos.

Applying Terzaghi's local shear failure criterion and using the empirical factor of 2/3 to establish a lower limit for the bearing capacity, a ratio between the parameter N_c' and N_{cp} can be established — where N_c' is equal to $\frac{2N_c}{3K}$ and $N_{cp} = 5.14$.

To define the parameter K, it is necessary to consider the "cohesion" C as measured in the unconfined compression test. For a $\Phi = 0$ analysis, C is taken as one half the unconfined compressive strength. If on the other hand, $\Phi \neq 0$, then the apparent "cohesion" $C_a = C \dfrac{\sin (45 - \Phi/2)}{\sin (45 + \Phi/2)}$

Defining K as $\dfrac{\sin (45 + \Phi/2)}{\sin (45 - \Phi/2)}$, $K \cdot C_a = C$.

N_c is the Terzaghi dimensionless bearing capacity factor.

In Table 3, the relationship between Φ, N_c/K and the ratio N_c'/N_{cp} are given. By comparing the ratio q_{obs}/q_p with the ratio N_c'/N_{cp} and reconciling one to the other, the average "friction angle" Φ is approximately 4°. This allows for an improved agreement between predicted Prandtl values and observed bearing capacity. However the strength contribution from the "friction" component must be overlooked in order to obtain this agreement. Applying the Terzaghi bearing capacity equation with the local shear failure capacity factors, and further reducing the capacity by one third does not altogether predict ultimate bearing capacity for the cases studied.

TABLE 3 — Correlation Ratios

Φ	0°	5°	10°	15°
N_c/K	5.14	6.03	7.02	8.53
N_c'/N_{cp}	0.667	0.786	0.912	1.11

In most cases, using the parameters obtained from triaxial tests on companion samples, the Terzaghi equation for local shear failure underpredicts ultimate bearing capacity — sometimes by as much as 40 to 50%. It may be argued that the triaxial test samples are not valid samples since they were not cored from the container, but as far as possible, the water contents, densities and degrees of saturation were equal to the soil compacted in the container. Because the samples were not totally saturated (degree of saturation ranging from 70 to 85%) the effective stress parameters were not used, although pore pressures were measured during the conduct of the triaxial tests.

The situation is one where if the $\Phi = 0$ analysis is used (the Prandtl equation is representative) an overprediction of ultimate bearing capacity will result. Using the general bearing capacity equation developed by Terzaghi which accounts for the friction and cohesion parameters, an underprediction results. This in no way detracts from the usefulness of these equations, since the conditions and properties of the soils used in this study were designed specifically to evaluate bearing capacity relationships not necessarily covered by these equations.

PROPOSED ANALYSES

QUASI-ELASTIC DEFORMATION THEORY

Figure 3 represents a simplified picture of the model tests conducted, showing a linearized shear deformation boundary immediately before failure (see Figures 4 and 5 for actual photographs of soil deformation under load).

From test conditions and observations:

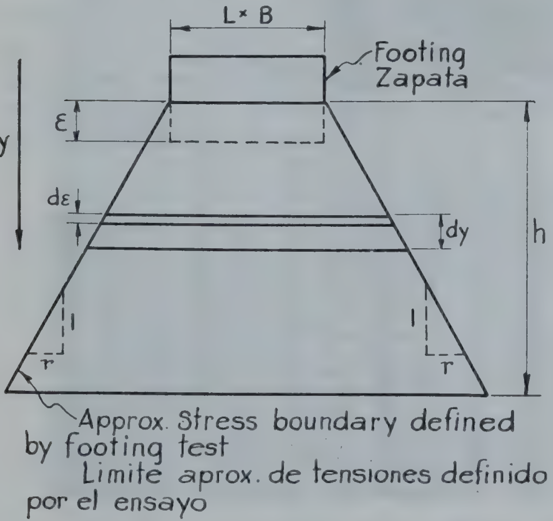
L × B
Footing
Zapata
y
ε
dε
dy
h
1
r
1
r
Approx. Stress boundary defined by footing test
Limite aprox. de tensiones definido por el ensayo

$L = 4''$

$B = 1\frac{1}{2}''$

$h = 3\frac{1}{2}''$

$r = 0.414$

Fig. 3 — Stress boundary defined by footing test.

Fig. 3 — Limite de tensiones definido por el ensayo.

Being:

L = length of footing

B = width of footing

ε = total settlement

Q = total load on footing

2L = effective perimeter

A = area of footing

$$E = \frac{Q/A}{d\varepsilon/dy} = \frac{Q/L\ (B + 2ry)}{d\varepsilon/dy}$$

Therefore:

$$d\varepsilon = \frac{Q\,dy}{LE\ (B + 2ry)}$$

Integrating and evaluating for the boundary conditions of $y = 0$, $\varepsilon = 0$, and solving for Q, when $y = h$;

$$Q = \frac{2ErL\varepsilon}{\ln\left(1 + \frac{2rh}{B}\right)}$$

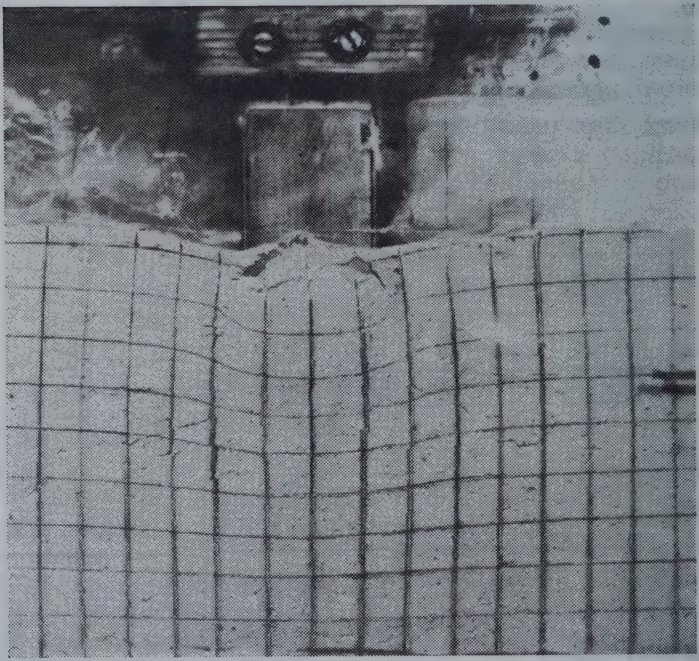

Fig. 4 — Picture of loading test.

Fig. 4 — Dibujo del ensayo de carga.

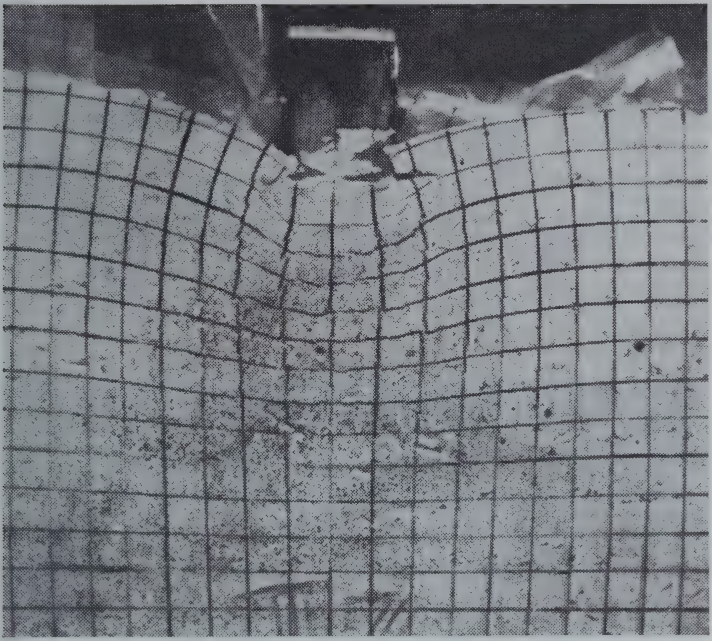

Fig. 5 — Picture of loading test.
Fig. 5 — Dibujo del ensayo de carga.

Four tests were chosen to test the derived equation. The load deformation characteristics for these tests are given in Figures 1 and 2 and from Figure 6 showing the unconfined compression test relationships, the value of E (the secant modulus — Skempton, 1951) may be determined. The results are shown in Table 4.

Table 4 — Prediction from Quasi-Elastic Deformation Theory

Test No.	(%)	E, psi.	Q, lbs. observed	Q, lbs. predicted	Q_{pred}/Q_{obs}
7	12.1	157	190	204	1.07
8	14.0	144	210	216	1.03
9	10.6	175	210	200	0.953
10	11.8	113	145	143	0.985

The ratio of predicted total load Q to observed Q varied from 0.953 to 1.07. These are further tabulated in Table 5 (in the Punching Shear Section).

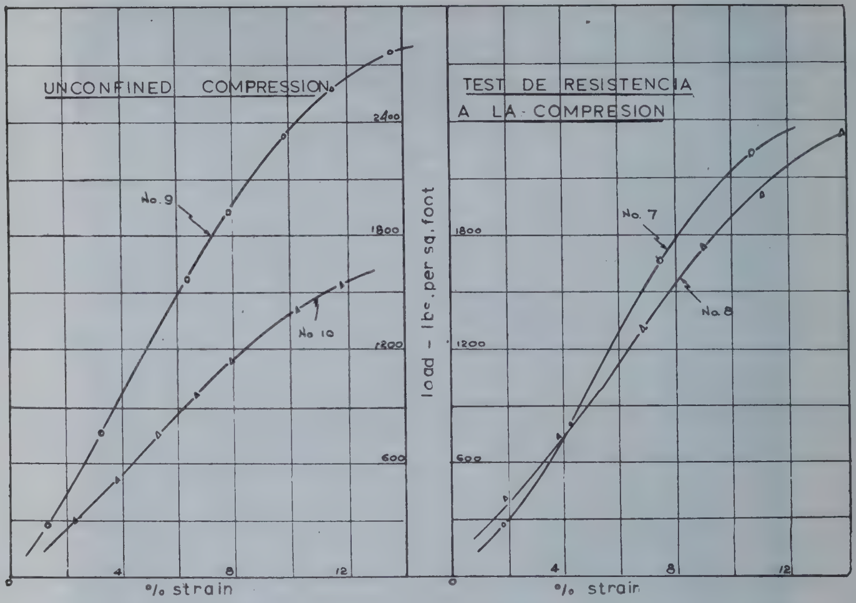

Fig. 6 — Unconfined compression test.

Fig. 6 — Ensayo de resistencia a la compresión.

PUNCHING SHEAR THEORY

Bishop, Hill and Mott (1945) have proposed an approximate theory for the indentation test for metals in which the assumption is made that penetration of a frictionless conical punch is equivalent to the expansion of a spherical hole in the material arising from plastic flow. Figure 7 shows one of the typical failure stress bulbs in the model test which is characteristic of the phenomenon described by Bishop et al. and attributed to metals. This represents the plastic flow pattern at failure, with conditions prior to failure shown representatively in Figures 4 and 5.

Since the model tests exhibit large settlements when failure loads were reached, and since the slip lines formed seemed characteristic of the type mentioned by Bishop et al., there seems to be merit in the use of the punching shear theory. The assumptions necessary for the application of the theory to metals may be reconciled to the case of soils.

Adapting the equation for use in soils and specifically for a strip loading condition:

$$q = \frac{Q}{A} = C\left[2 + \ln\frac{E}{3C}\right]$$

For a circular footing

$$q = \frac{Q}{A} = \frac{4}{3}C\left[1.75 + \ln\frac{E}{3C}\right]$$

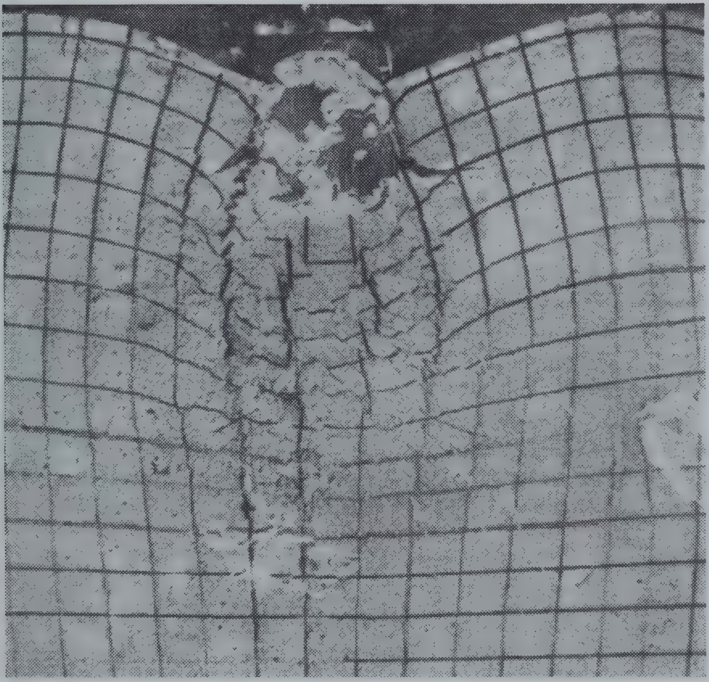

Fig. 7 — Failure stress bulb in model test.

Fig. 7 — Bulbo de tensiones en la rotura.

In Table 5, the predicted values of bearing based on this punching shear theory for a series of 10 tests together with the predicted Q from the quasi-elastic deformation theory are compared with the actual observed load bearing values.

TABLE 5 — Comparison between Theoretical and Predicted Q

Test No.	C psi	Q obs. lbs.	Q pred. lbs. (Punching Shear)	Q pred. lbs. (Quasi-Elastic)	Q pred. / Q obs. (Punching)	Q pred. / Q obs. (Quasi)
1	5.33	110	124		1.13	
2	5.10	102	118		1.16	
3	5.02	95	116		1.22	
4	6.52	180	151		0.84	
5	7.11	170	165		0.97	
6	8.33	190	205		1.08	
7	7.78	190	183	204	0.964	1.07
8	8.85	210	196	216	0.934	1.03
9	9.15	210	212	200	1.010	0.953
10	5.22	145	123	143	0.85	0.985

The application of this theory is not new or peculiar to soil mechanics and has been considered by others. Gibson (1950) applied this theory to the case of deep foundations in clay, using a large-strain theory due to Swainger (1947). The expression used for a deep circular footing in this instance was:

$$q = \frac{4}{3} c \left[1.75 + \ln \frac{E}{c} \right]$$

DISCUSSION OF PROPOSED THEORIES

The quasi-elastic deformation theory, whilst applicable in its present form to the test series, suffers from a serious set of constraints. Unless modified, the equation is valid only for small surface footings. Implicit also is the assumption that E is a constant and is independent of the lateral confinement afforded by surrounding soil at any one depth. It is possible to account for these and thus modify the equation, however this requires a precise determination of E at varying depths beneath the footing. The influence of surcharge and the estimation of lateral confinement beneath the footing must be made as a necessary condition for the evaluation of E. Theoretical predictions of Q based on values for E derived from triaxial tests at confining pressures supposedly similar to those representative of model test conditions proved unfruitful. Undoubtedly the scale model used in this study played an important part in realizing this disagreement between theory and practice. It is not suggested that this theory is of little value, but the uncertainty involved in the determination of lateral restraint in the field poses many questions that must be answered before one can proceed with the use of this theory.

Greater flexibility is achieved with the use of the punching shear theory since the sensitivity to a slight variation in E is minimized by a factor of 3 and also by the use of the logarithmic ratio of E/3C. In applying this theory to reported studies of bearing capacity (e.g. Meigh 1950, Golder 1941, Peck and Bryant 1951) reasonable agreement for bearing capacity was obtained with the reported values.

In the region where shear deformation gives rise to a plastic flow characteristic, it appears that the punching shear theory best describes behaviour of the subsoil. Undoubtedly there are limitations and constraints. The suggested use of such a theory would seem to be dictated by the case where shear failure is accompanied by excessive shear strains.

CONCLUSIONS

The results derived from this study indicate that, dependent on the assumptions used for bearing capacity analysis, i.e. $\Phi = 0$, general agreement between predicted and observed bearing capacities is poor. It is indicated that because of the local shear type of failure, which is peculiar to many highly compressible soils, an alternate method for bearing capacity analysis is needed.

The two proposed theories predict reasonably well ultimate bearing for the cases studied, however because of the greater flexibility of the punching shear theory, it would seem that this may be more appropriate for general use. The region of close agreement between predicted and observed bearing is best defined and confined to cohesive soils whose characteristic feature is high deformation under applied loads.

BIBLIOGRAPHY

Bishop, R. F., Hill, R., and Mott, N. F. (1945) — "The Theory of Indentation and Hardness Tests". Proc. Phys. Soc. of London, B.57, P.157.

Gibson, R. E. (1950) — Discussion on "The Bearing Capacity of Screw Piles and Screwcrete Cylinders". Jnl. ICE, V.34, P.382.

Golder, H. Q. (1941) — "The Ultimate Bearing Capacity of Rectangular Footings". Jnl. ICE, V.17, P.161.

Meigh, A. C. (1950) — "Model Footing Tests on Clay". M.Sc. Thesis, University of London.

Peck, R. B. and Bryant, F. G. (1952) — "The Bearing Capacity Failure of the Transcona Elevator". Geotechnique, V.3, P.201.

Prandtl, L. (1920) — "Ueber die Haerte Plastischer Koerper". Nachrichten von der Gesellschaft der Wissenschaften zu Goettingen, Mathematisch-Physikalische Klasse, P.74-85.

Swainger, K. H. (1947) — "Stress-strain Compatibility in Greatly Deformed Engineering Metals". Phil. Mag., V.38, No. 281.

Terzaghi, K. (1943) — "Theoretical Soil Mechanics". Wiley.

IIb/1

ESTIMATING BUCKLING LOADS FOR PILES

M. T. DAVISSON

Assistant Professor of Civil Engineering, 206 Talbot Laboratory,
University of Illinois, Urbana, Illinois.

SUMMARY

The theoretical elastic pile buckling loads are shown to be an upper bound to the actual buckling load. Initially deformed and dog-leg piles may fail at loads lower than the theoretical elastic buckling load because of plastic behavior in either the soil or the pile.

A discussion of the soil resistance to lateral deflection of piles reveals that the theoretical elastic pile buckling loads now available do not apply to many real soil profiles for which buckling is a possibility. New solutions are developed for a soil whose resistance to lateral movement increases directly with depth. It is shown that the pile boundary conditions exert an overwhelming influence on the behavior of the soil-pile system. Rotational restraint and translational restraint are shown to be very important.

Recommendations are made for estimating the buckling loads for piles, giving consideration to the ultimate soil resistance and the effect of pile spacing.

SUMARIO

Ha sido demostrado que las cargas elásticas de pandeo para pilotes obtenidas teóricamente, constituyen un límite superior a las cargas actuales de pandeo. Pilotes inicialmente deformados y los del tipo abruptamente pandeados (pata de perro) pueden fallar a límites de carga más bajos que la carga elasto-teórica de pandeo debido al comportamiento plástico en el suelo ó en el pilote.

Una discusión de la resistencia del suelo y la deflección lateral de pilotes, demuestra que las cargas elastoteóricas de pandeo para pilotes obtenidas actualmente, no aplican en muchos casos reales de perfiles de suelo para los cuales hay la posibilidad de pandeo. Nuevas soluciones son desarrolladas para el caso en que la resistencia del suelo a movimiento lateral aumenta directamente con la profundidad. Se demuestra que las condiciones de contorno para pilotes influyen grandemente el comportamiento del sistema suelo y pilote. Restricciones del tipo rotacional y traslacional demuestran ser muy importantes.

Recomendaciones para estimar las cargas de pandeo para pilotes son dadas tomando en consideración la resistencia máxima del suelo y el efecto del espaciamiento de pilotes.

INTRODUCTION

The presently available theoretical buckling loads for piles are based strictly on elastic soil-pile behavior. Two stiffness parameters are involved, the flexural stiffness of the pile EI and the horizontal subgrade modulus k; neither considers the limiting stress in the soil or the pile. Furthermore, the theoretical buckling loads are for perfectly straight piles. In reality a pile will have at least a slight initial curvature, and when loaded axially the curvature will increase causing both bending stresses in the pile and lateral stresses in the soil. A pile may be considered to have reached a state of incipient failure when the yield stress in either the pile or the soil has occurred, or when the elastic buckling load has been attained.

The maximum load that an initially deformed pile can carry decreases as the magnitude of the initial deformations increase. It is clear, then, that a pile may fail because of plastic behavior in either the pile or the soil, but under no conditions can the failure load exceed the elastic buckling load. The elastic buckling load, therefore, represents an upper bound to the failure load for a pile.

In the past it has been common practice to dismiss the possibility of pile buckling by comparing the proposed pile working load to the computed elastic buckling load. In general it was found that buckling was a remote possibility in all but the softest soils. Recent attempts have been made to solve the problem of an axially-loaded initially-deformed pile, recognizing that the elastic buckling load is an unconservative upper-bound to the failure load. In these more realistic approaches to the problem, the elastic buckling load becomes a special case when the initial deformations are non-existent; otherwise, the analyses generally include the elastic buckling load as a parameter.

The theoretical elastic buckling loads previously available involved a horizontal subgrade modulus that was constant with respect to depth. This condition is seldom realized in situ; granular soils and normally loaded silts and clays generally have a horizontal subgrade modulus that increases linearly with depth from a zero-value at the ground surface. Because buckling is likely to be initiated where the subgrade modulus has the lowest value, the theoretical elastic buckling loads for a subgrade modulus increasing linearly with depth are of practical importance. For the same reason, the pile boundary conditions, fixed-head, pinned-head, etc., are also important.

The following discussion examines the nature of the soil resistance to the horizontal deflection of a pile for the purpose of delineating the variation of the soil-stiffness and the ultimate soil resistance with depth. Then the theoretical elastic buckling loads are developed with various pile boundary conditions for both a constant and a linear variation of the subgrade modulus with respect to depth. Partially embedded piles are not considered because they may be treated by simple extensions of the theories used for fully embedded piles.

SOIL RESISTANCE

The resistance to the lateral deflection of a pile which is offered by the soil surrounding the pile will be considered in two stages, namely, the stiffness and the ultimate soil reaction. The stiffness k is necessary for elastic analyses whereas the ultimate soil reaction w_u represents a limit to the soil reaction w. These stages will be discussed separately.

SUBGRADE MODULUS

Figure 1 shows a typical soil reaction versus deflection curve (w-y curve) for soil surrounding a laterally loaded pile. For soil reactions less than 1/3 to 1/2 of the ultimate soil reaction, the w-y relationship can be expressed adequately by a tangent modulus. This tangent modulus is herein defined as the coefficient of subgrade reaction for a pile and is expressed by Equation 1.

$$k = w/y \tag{1}$$

Note that the soil reaction per unit of length along the pile (w) is the resultant for the width B of the loaded face of the pile.

For soil reactions exceeding approximately 1/3 to 1/2 of the ultimate soil reaction, the secant modulus shown by the dashed line on Figure 1 should be considered; in this case the modulus becomes a function of the deflection. Matlock and Reese (1961) have presented an analysis for laterally loaded piles wherein the subgrade modulus can vary with deflection. Similar techniques should be resorted to wherever the assumption of a constant value for the subgrade modulus at a given depth is not considered adequate.

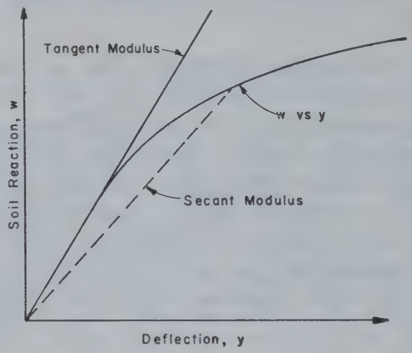

Fig. 1 — Soil reaction vs deflection.

Fig. 1 — Reacción del terreno vs deflección.

As mentioned previously, the actual variation of the subgrade modulus with depth should be considered. The dashed line in Figure 2(a) illustrates the variation of k with depth (k = constant) that has been recommended by Terzaghi (1955) and others for uniform preloaded cohesive soils. Because of the presence of the soil boundary, the soil at the ground surface is deformed in a mode similar to that for two-dimensional passive pressure. However, at depths greater than four to six pile diameters below the ground surface, the lateral deflection of the pile deforms the soil in a mode similar to that for a deep two-dimensional footing. Both the stiffness and the ultimate soil resistance are, therefore, lower near the soil boundary. This phenomenon was recognized by Wieghardt (1922) and Grandholm (1929), but was assumed to be of no significance. Davisson and Gill (1963) investigated the influence of the boundary by considering the stiffness profile of the soil to occur in layers. It was found for laterally loaded piles that errors of 100% in the deflections and moments may arise because of the assumption that k is constant with depth. Because buckling will occur where the k-values are lowest, it should be expected that the tendency to buckle will be greatest at the soil boundary. Furthermore, the axial load in a pile is likely to have its maximum value at the soil boundary because there has been no opportunity for dissipation of the load by skin friction. The pile buckling tests by Golder (1957) and Brandtzaeg and Harboe (1957) illustrate the tendency for buckling near the soil boundary.

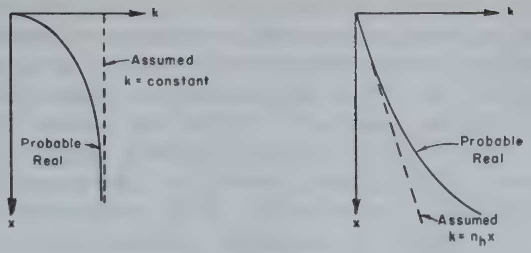

(a) Preloaded Cohesive Soils

(b) Granular Soils, Normally Loaded Silts and Clays

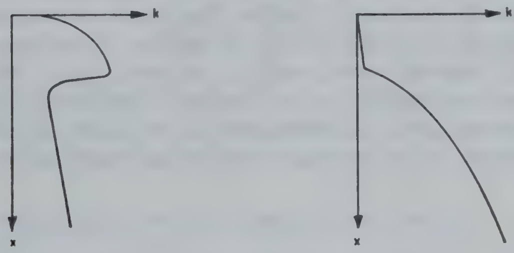

(c) Desiccated Normally Loaded Clay

(d) Soft Surface Layer

Fig. 2 — Variation of subgrade modulus with depth.

Fig. 2 — Variación del modulo de reacción del subrasante con la profundidad.

A more realistic variation of the subgrade modulus with depth for preloaded cohesive soils is shown by the solid line in Figure 2(a). At present (1963) there is insufficient data to define the real variation of k with depth, but when such information becomes available, elastic pile buckling loads can be computed by techniques that have been developed for the general case (Davisson and Gill, 1963).

For granular soils Terzaghi (1955) recommends that k be considered directly proportional to the depth x as shown on Figure 2(b). The expression for k in this case is

$$k = n_h x \tag{2}$$

where n_h is the constant of horizontal subgrade reaction expressed in lb/in.^{3}. The validity of Terzaghi's recommendation for sands has been demonstrated on a model scale by Prakash (1962). The actual variation of k with depth is indicated schematically by the solid line in Figure 2(b); Prakash's tests also indicated that this variation is realistic.

Because the zone of interest with respect to buckling is near the ground surface where the k-values are lowest, the linear approximation recommended by Terzaghi is appropriate; at greater depths the linear approximation leads to conservative analytical results. Davisson (1960) has shown that k is proportional to depth for normally loaded clays, whereas Peck and Davisson (1962) have shown that the assumption is also valid for normally loaded silts. It is convenient to note that k varies with depth in a manner similar to the variation of the ultimate soil resistance with depth.

On the basis of the foregoing discussion the probable variation of k with depth can be estimated. For example, in a desiccated normally loaded clay the variation of k with depth would be approximately as shown on Figure 2(c). For a preloaded cohesive soil with a layer of soft weak soils at the surface the variation of k with depth shown on Figure 2(d) is appropriate. Variations of k with depth for other combinations of soils and soil conditions can easily be deduced.

VALIDITY OF SUBGRADE MODULUS ASSUMPTION

In using a subgrade modulus to define the soil stiffness it is assumed that the soil may be represented by a series of independent elastic springs, whereas in reality they are interrelated in a complex fashion. The error involved may be estimated by considering the contribution of Vesic (1961) who extended Biot's (1937) work concerning a flexible beam supported on an elastic half-space. For a long relatively flexible member such as a pile the error in the computed bending moments based upon the subgrade modulus assumption is no more than a few percent when compared to the theory of elasticity solution. Therefore, the subgrade modulus concept has a reasonable theoretical foundation and is believed to be more than adequate for the problem discussed herein. Bjerrum (1957) has shown that the subgrade modulus assumption allows a reasonably accurate prediction of the elastic buckling loads for a pile.

ULTIMATE SOILS RESISTANCE

As mentioned previously, the ultimate soil resistance available at the ground surface to oppose the lateral deformation of a pile is the two-dimensional passive pressure. For preloaded cohesive soils for which the angle of internal friction φ is considered zero, the magnitude of the passive pressure is approximately 2c where c is the cohesion. By contrast, for granular soils the resistance at the ground surface is essentially zero. At depths exceeding 6 to 8 pile diameters below the ground surface, the ultimate soil resistance has transitioned to that for the bearing capacity of a fully embedded two-dimensional footing. In cohesive soils this resistance has a magnitude of approximately 8c to 11c; theoretically, values of 8.14 to 11.42 have been obtained. Model tests have shown that a value of 9c is a reasonable average. For granular soils ($c = 0$) the ultimate resistance depends on φ and the vertical effective pressure q'.

For cohesive soils the ultimate soil reaction may be expressed as

$$w_u^x = BcN_c^x \tag{3}$$

where B is the width of the pile and N_c is the appropriate bearing capacity factor at the depth x. For granular soils the ultimate soil resistance is

$$w_u^x = Bq'N_q^x \tag{4}$$

where N_q is the bearing capacity factor for the particular angle of internal friction φ and depth x. The first unified presentation of the variation of the ultimate soil resistance versus depth for a pile was presented by Brinch-Hansen (1961). The pertinent features of Brinch-Hansen's work as applied to laterally loaded poles and piles have been abstracted by Davisson and Prakash (1963). It should be noted that the ultimate soil reaction w_u is proportional to the width of the pile, whereas the subgrade modulus is nearly independent of the pile width.

EFFECT OF PILE WIDTH

Terzaghi (1955) presented an extensive discussion regarding the effect of the size of the loaded area on the subgrade modulus. For example, a loaded pile of width B produces soil reactions w and deflections y. If another pile of equal embedment in the same soil, but of width 2B, is subjected to the same loading, the soil reactions and deflections will be equal to those for the pile of width B providing the moment of inertia for the two piles is the same. Although the average unit soil pressures across the face of the pile with width 2B are ½ of those for the pile with width B, the dimensions of the stressed volume of soil are doubled because of the size of the loaded area; therefore, the deflections at the faces of the two piles must be equal. After k has been determined for a given pile, its value is unchanged if the pile width B is changed.

The foregoing discussion concerning the size of the loaded area is based on the assumption of linear elastic behavior for the soil. Actually, plastic soil behavior will most likely be initiated at the ground surface, especially for pile heads that can translate, because the soil is weakest at that point. If a pile of width B were to be widened, for example, to a width 2B for some depth below the ground surface, strictly elastic considerations would indicate no change in the load deflection behavior. However, the ultimate soil rection for the enlarged portion of the pile is approximately doubled because it depends on the pile width; this has the effect of increasing the secant modulus (Fig. 1) because the soil reaction is now a smaller percentage of the ultimate soil reaction. Therefore, the observed deflections would be somewhat reduced. It may be concluded that there is some effect of the pile width on the subgrade modulus; however, with respect to the buckling problem its effect will usually be slight.

Because the ultimate soil reaction decreases as the pile width decreases, but the subgrade modulus remains essentially the same, it should be anticipated that slender, solid, steel pile-sections would be the ones most likely to buckle because of plastic soil behavior. The test results reported by Brantzaeg and Harboe (1957) can be interpreted to support this statement. Failures of slender initially deformed piles have occurred at loads substantially below the elastic buckling load. Furthermore, piles of this type are the ones most likely to deform during the pile driving operation. Their use in soft soils should be undertaken only with care.

ELASTIC PILE BUCKLING LOADS

In order to present a clear picture of the portions of the elastic pile stability problem that have been solved, a brief review will be given of the previous work. This will be followed by a presentation of the new solutions obtained by the author. All of the results will be presented in the form of non-dimensional plots of a critical axial load coefficient versus the embedded length of the pile.

PREVIOUS WORK

All of the previous solutions for the elastic buckling loads of embedded piles were based on a subgrade modulus representation for the soil which was assumed to be constant over the length of the pile. Hetenyi (1946) presents a survey of the work by Forssell (1918, 1926), Grandholm (1929), and Cummings (1938); the governing differential equation is

$$EI \frac{d^4y}{dx^4} + P \frac{d^2y}{dx^2} + ky = 0 \qquad (5)$$

where EI is the flexural stiffness of the pile, P is the axial load, and k is the subgrade modulus, all considered to be constants. Figure 3(a) shows the positive directions of the coordinate system, with x denoting depth and y the lateral deflection.

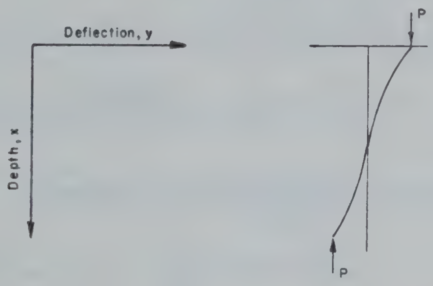

(a) (b) Free

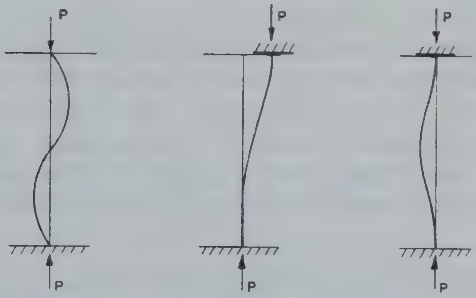

(c) Pinned (d) Fixed - Translating (e) Fixed

Fig. 3 — Pile boundary conditions.

Fig. 3 — Condiciones de contorno para pilotes.

The solutions of Equation 5 are more useful after a change of variables. Let.

$$R = \sqrt[4]{\frac{4\,EI}{k}} \qquad \text{and} \qquad l = \frac{x}{R} \qquad (6)$$

Then

$$l_{max} = \frac{L}{R} \tag{7}$$

where L is the embedded length of the pile, R is the relative stiffness factor, and l is the non-dimensional depth coefficient. By substituting these definitions into Esquation 5 and rearranging, the following equation is obtained:

$$\frac{d^4y}{dl^4} + \frac{PR^2}{EI} \cdot \frac{d^2y}{dl^2} + y = 0 \tag{8}$$

Let PR^2/EI be the axial load coefficient U; then

$$U_{cr} = \frac{P_{cr}R^2}{EI} \tag{9}$$

By substitution, Equation 10 is obtained:

$$\frac{d^4y}{dl^4} + U \frac{d^2y}{dl^2} + y = 0 \tag{10}$$

The critical values of the axial load coefficient, U_{cr}, are obtained by solving Equation 10 for U with due consideration to the pile boundary conditions and the pile length, l_{max}. The boundary conditions of greatest interest will be designated as free, pinned, fixed-translating, and fixed-non-translating, as shown on Figures 3(b)-3(e). An analog computer was used to obtain solutions for Equation 10; the techniques and the computer program have been presented by Davisson and Gill (1963).

On Figure 4, U_{cr} has been plotted versus l_{max} for a number of different conditions of restraint at the pile ends. The solution most commonly referred to is the one for pinned ends. In this case, the pile deforms into a number of sine half-waves, with the number of waves depending on the total length of the pile. U_{cr}-values are obtained for the first three modes; for all modes, the U_{cr}-values are above 2, and at certain values of l_{max} become tangent to the line $U_{cr} = 2$. The lowest values of U_{cr} for any given length l_{max} are the ones of interest; for practical purposes U_{cr} will be considered equal to 2.

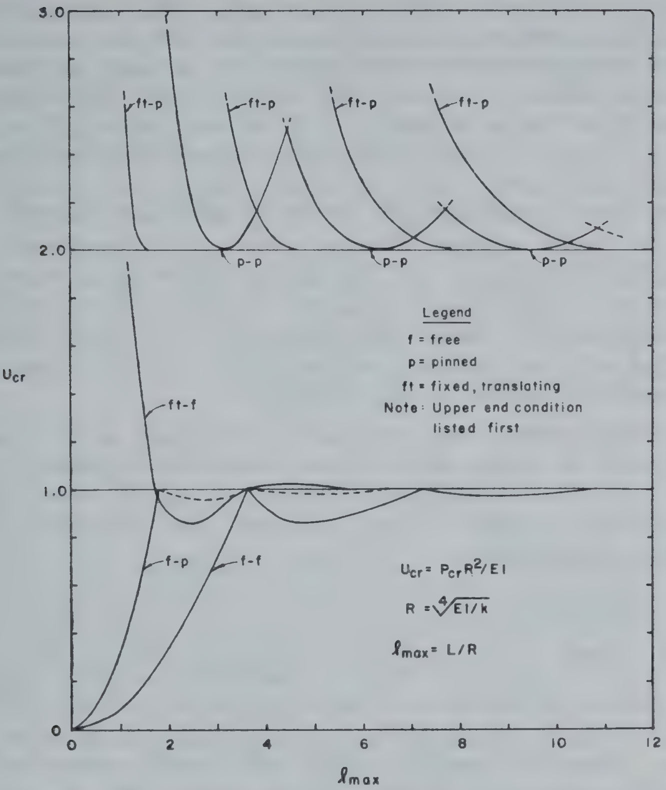

Fig. 4 — Buckling load vs length for k = constant.

Fig. 4 — Carga de pandeo vs longitud para k = constante.

Another solution commonly referred to is the one for perfectly free ends (Fig. 4). In this case U_{cr} is zero when l_{max} equals zero and increases with an increase in l_{max} until a maximum value of unity is reached. At this point, a mode change occurs and U_{cr} dips below unity, but it returns to unity when the next mode change is about to occur. With increasing pile length, the magnitude of the deviation from unity becomes negligible. Because in most practical cases l_{max} will exceed 5, U_{cr} can be considered equal to unity.

It may be concluded on the basis of the foregoing solutions that the boundary conditions exert a controlling influence on U_{cr}. On first inspection it would appear that because the U_{cr}-value for a long pile with fixed-non-translating ends is 2 (not shown in Fig. 4), there is no advantage for a fixed-head pile over a pinned pile. This occurs because the interior portions of a long embedded pile are not affected by the boundary conditions; therefore, as long as the ends of the pile do not translate, the buckling load for a fixed-end pile must be the same as for a pinned-end pile. This is not true, of course, for very short piles where the fixed boundary becomes dominant. As a practical matter, all three types of boundary conditions can occur; in addition, the pile head may be fixed against rotation but not translation. The boundary condition at the tip of the pile will in most cases behave as though it were pinned. However, Bjerrum (1957) has discussed the difficulties observed in Norway with pile tips that slip on inclined rock surfaces. In this case a free end condition would be appropriate.

Because mixed end conditions can occur, as for example in the case of a pile with a fixed head and a pinned tip, the author obtained solutions for several practical cases to help complete this study. These solutions are discussed in the following paragraphs.

NEW SOLUTIONS

For k = constant. The U_{cr}-values for a pile with a free head and a pinned tip are shown on Figure 4; U_{cr} increases rapidly with an increase in l_{max} up to the limiting value of unity. After first reaching unity, the higher modes indicated U_{cr}-values very little different from unity. The buckling appears to be controlled by the boundary offering the least restraint. It may be reasoned that a pile with a pinned head and a free tip would also have a limiting U_{cr}-value of unity.

A pile with its head fixed against rotation but not translation is a very common occurrence. When combined with a free-tip, the value of U_{cr} oscillates slightly about unity as shown on Figure 4. When combined with a pinned-tip, the value of U_{cr} becomes tangent to 2 (Fig. 4). These results could have easily been predicted on the basis of the foregoing reasoning. Because a pile with a fixed-non-translating head provides more restraint than a fixed-translating head, it may be reasoned that U_{cr} decreases to 2 when a pinned tip is considered, and to unity for a free pile-tip, but at a slower rate with respect to increasing l_{max} than for the fixed-translating case.

For $k = n_h x$. In the previous paragraphs a very ideal condition was examined, namely, k = constant. It was shown that either boundary condition may control the buckling load; however, when a soil profile is considered for which $k = n_h x$, the boundary condition at the pile head becomes extremely important compared to the boundary condition at the pile tip. Because the pile tends to buckle where the subgrade modulus is the lowest, instability will tend to occur immediately adjacent to the pile head.

When $k = n_h x$, Equation 5 becomes

$$EI \frac{d^4y}{dx^4} + P \frac{d^2y}{dx^2} + n_h xy = 0 \tag{11}$$

Let

$$T = \sqrt[5]{\frac{5\,EI}{n_h}} \text{ and } z = \frac{x}{T}, \tag{12}$$

then

$$z_{max} = \frac{L}{T} \tag{13}$$

where T is the relative stiffness factor, z is the non-dimensional depth coefficient, and z_{max} is the maximum value of the depth coefficient. By substituing the definitions into Equation 11 and rearranging, the following equation is obtained:

$$\frac{d^4y}{dz^4} + \frac{PT^2}{EI} \cdot \frac{d^2y}{dz^2} + zy = 0 \tag{14}$$

Let V denote the axial load coefficient, PT^2/EI; then,

$$V_{cr} = \frac{P_{cr}T^2}{EI} \tag{15}$$

By substitution, Equation 14 becomes

$$\frac{d^4y}{dz^4} + V \frac{d^2y}{dz^2} + zy = 0 \tag{16}$$

Equation 16 was solved for V_{cr} with the aid of an analog computer. V_{cr} versus z_{max} for a pile with a free head and a free tip is shown on Figure 5. V_{cr} starts at zero and increases with an increase in z_{max} up to a limiting value of approximately 0.71. It was not possible to obtain solution on the analog computer for values of V higher than 0.71. The author's interpretation of these results is that because the pile tends to buckle near the upper boundary, and because increasing the pile length has a rapidly diminishing influence on the behavior of the upper part of the pile, a limit is reached such that a further increase in the length of the pile will not alter the value of V_{cr}. The diminishing influence of additional increments of pile length has been adequately demonstrated by Reese and Matlock (1956).

Similar results are shown on Figure 5 for a pile with a free head and a pinned tip. Because of the increase in restraint that a pinned tip offers, compared to a free tip, V_{cr} increases more rapidly with length than for the free-tip case. The maximum V_{cr}-value that could be observed was approximately 0.78, which is only slightly higher than that for the free-tip case.

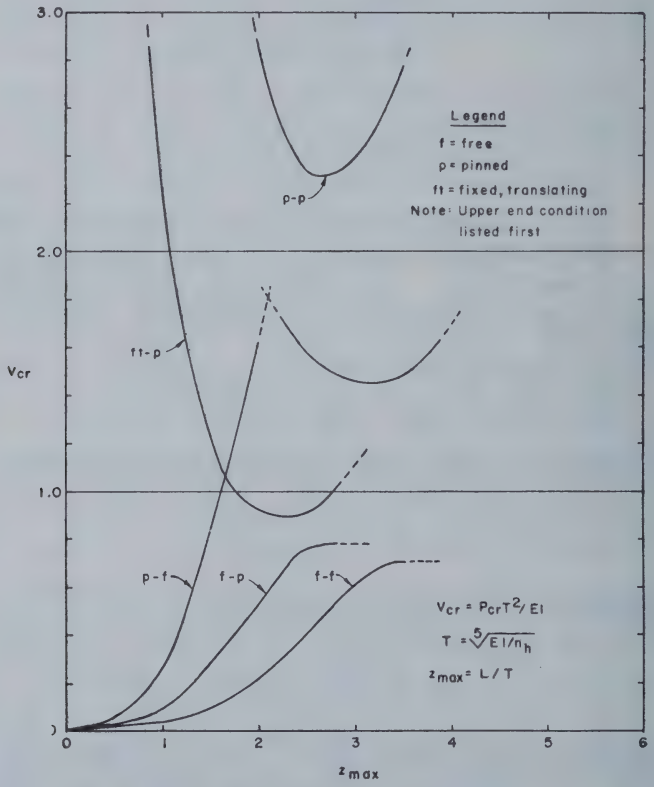

Fig. 5 — Buckling load vs length for $k = n_h x$.

Fig. 5 — Carga de pandeo vs longitud para $k = n_h x$.

The solutions for a pinned-head, free-tip pile are shown on Figure 5. A considerably higher value of V_{cr} is observed at any given length z_{max} than for the two cases previously discussed. This illustrates the effect of the restraint of a pinned-head pile when compared to a free-head pile. Two buckling modes were observed for this case, but for all practical pile lengths V_{cr} exceeds 1.44. Generally a pile will have a length exceeding a z_{max}-value of 3 to 4.

A free-tip pile with its head fixed against rotation but not translation behaves as shown on Figure 5. The minimum value of V_{cr} is approximately 0.88; it occurs at a very short pile length, namely, $z_{max} = 2.3$. V_{cr} increases rapidly for pile lengths greater than $z_{max} = 2.3$. It can be reasoned that a pile with a fixed-translating head and a pinned tip would have higher V_{cr}-values, for any given pile length, than the free-tip case. By similar reasoning it can be seen that a pile with a fixed-non-translating head and either a free tip or a pinned tip would also exhibit higher values. Finally, the results for a pile with both ends pinned was obtained (Fig. 5). The minimum observed V_{cr}-value was 2.30 at $z_{max} = 2.60$.

The foregoing analytical results conclusively demonstrate the importance of the upper boundary (fixity) of the pile. In cases where buckling is likely to be a problem, it is obvious that great benefit can be obtained by insuring that the pile head is restrained from translation; preferably, it should be fixed. The ability of the pile head to translate is a very important consideration. Note that a pinned-head condition becomes a free-head condition if translation can occur.

APPLICATION

Once the fixity of the pile ends and their tendency to translate have been evaluted, the calculation of the elastic buckling load for an initially straight pile is straightforward for soil profiles that match those assumed in the foregoing analysis. As an aid to estimating buckling loads, the range of k-values likely to be encountered for several soil-types has been tabulated. Table 1 presents typical n_h-values for sands and normally loaded silts and clays. Table 2 presents typical k-values for preloaded clays. A study of available pile-types will show that solid, slender pile-sections in very soft soils are susceptible to buckling; the utilization of high working loads on these pile-types should be approached with caution.

Where a non-uniform soil profile occurs, the elastic buckling loads will be lowest where the k-values are lowest. The buckling load may be estimated by treating the pile as though it were wholly embedded in the soil in the zone of interest; the solutions for the proper boundary conditions should be used for the variation of k with depth most nearly approximating the actual problem.

Because most real piles are initially deformed, and because the theoretical elastic buckling load is an unconservative upper bound to the actual failure load, the computed buckling loads are often no more than an aid to the judgement of the engineer faced with the task of predicting the buckling load for a pile. The use of load tests is also unconservative. Most load tests are performed in a relatively short period of time during which a large part of the axial load in the pile is dissipated by skin friction. Under service conditions the skin friction would be much less apparent and the tendency to buckle would be greater.

Analytical procedures for initially deformed piles and dog-leg piles are not sufficiently developed for use in routine engineering practice. The elastic buckling load, however, is usually one of the parameters in the analytical techniques that have been formulated. Therefore the elastic buckling loads have practical value as an initial step in the future development of analytical techniques for deformed piles. At present it requires considerable ingenuity, in addition to the aforementioned non-routine analytical techniques, to estimate the buckling load for a deformed pile. The original curvature of the pile must be known or specified in order to compute the initial pile and soil stresses. Then the pile and soil stresses due to the axial load must be estimated and combined algebraically with the initial stresses. When modified to satisfy the foregoing statements, Walter's (1951) analysis is presently the best available method for initially deformed piles, and Johnson's (1962) analysis can be made suitable for dog-leg piles.

When two or more piles in a group are subjected to lateral deflections because of vertical loads, there is the possibility that a reduction in the subgrade modulus would occur compared to the case where the piles are acting individually. Prakash (1962), in his study of group action for laterally loaded piles obtained information which can be applied to this problem. If the pile spacing exceeds 8-pile diameters in the direction of bending, there will be no interference. Further, if the pile spacing exceeds 3-pile diameters normal to the direction of bending, then no interference need be considered. Encroachment upon either of these limits will cause a reduction in the subgrade modulus. Prakash observed the change in the value of T for different pile spacings. The observed results are believed to be applicable to the case where k is a constant. The reasoning behind this is that the reduction in the subgrade modulus is primarily a geometrical consideration. A reduction in the subgrade modulus will lead to an increase in T or R, and recommendations will be given on this basis. Because of the limited nature of the information, recommendations will be given only for spacings in the direction of the deflection. At a spacing of 8-pile diameters, the increase in the values of T or R should be considered zero. At a spacing of 2.5 pile-diameters, the increase is 30%. A linear interpolation can be used between these limits.

CONCLUSIONS

The foregoing discussion leads to the conclusions listed below:

1. The effect of the pile boundary conditions is very large. Insufficient attention has been given to mixed boundary conditions and to translation of the pile head.
2. It has been shown that the assumption that k is a constant is not reasonable near the ground surface. Because k is reduced in this zone, buckling will tend to be initiated near the soil boundary.
3. For most soft soils, which are the ones of interest with respect to instability, k actually increases with depth in a nearly linear fashion. The buckling loads computed for a k-value constant with depth are unconservative for this case.
4. The elastic buckling load represents an upper bound. When the pile is initially deformed, the real buckling load is limited by the yield stress in the pile or the yield stress in the soil, whichever occurs first.
5. The failure of initially-deformed slender pile-sections is likely to be initiated by plastic behavior in the soil. Because the ultimate soil resistance is proportional to the width of the pile, slender piles represent the most serious case.
6. Approximating the soil stiffness by a subgrade modulus is a reasonable approach to the buckling problem.
7. Two or more piles in a pile group may interfere because of close spacing and cause a decreased value of the subgrade modulus to be observed; this reduces the buckling load.

ACKNOWLEDGEMENTS

The Graduate College and the Department of Electrical Engineering at the University of Illinois provided the analog computer facilities used by the author to obtain the solutions presented in this paper. Dr. M. S. McVay helped in the development of the analog computer program. Mr. H. L. Gill and Mr. K. E. Robinson aided the author in obtaining the computer solutions and drafting the figures.

REFERENCES

Biot, A. M. (1937) — "Bending of an Infinite Beam on an Elastic Foundation", *Journal of Applied Mechanics,* Vol. 4, No. 1, pp. A1-A7.

Bjerrum, Lauritz (1957) — "Norwegian Experience with Steel Piles to Rock", *Geotechnique,* Vol. 7, pp. 73-96.

Brandtzaeg, A. and Harboe, E. (1957) — "Buckling Tests of Slender Steel Piles in Soft, Quick Clay", Proc., 4th Internat. Conf. on Soil Mech. and Found. Eng., Vol. 2, pp. 19-23.

Cummings, A. E. (1937) — Discussion, "Lateral Pile Loading Tests", *Trans.* ASCE, Vol. 102, p. 255.

Davisson, M. T. (1960) — "Behavior of Flexible Vertical Piles Subjected to Moment, Shear and Axial Load", Ph.D. Thesis, University of Illinois.

Davisson, M. T., and Gill, H. L. (1963) — "Laterally Loaded Piles in a Layered Soil System", *Proc.,* ASCE, in press.

Davisson, M. T., and Prakash, Shamsher (1963) — "A Review of Soil-Pole Behavior", *Proc.,* HRB, in press.
Forsell, C. (1918) — "Berakning av palar", Stockholm.

Forsell, C. (1926) — "Knacksakerhet nos Palar och Palgrupper", Uppsats No. 10, Festskrift, Kungl., Vag-och Vattenbyggnadskarens, Stockholm.

Golder, H. Q., and Skipp, B. O. (1957) — "The Buckling of Piles in Soft Clay", *Proc.,* 4th Internat. Conf. on Soil Mech. and Found. Eng., Vol. 2, pp. 35-39.

Grandholm, Hjalmar (1929) — "On Elastic Stability of Piles Surrounded by a Supporting Medium", Ing. Vet. Akad., Hand. 89, Stockholm.

Hansen, J. B. (1961) — "The Ultimate Resistance of Rigid Piles Against Transversal Forces", The Danish Geotechnical Institute, Bull. 12.

Hetenyi, M. (1946) — "Beams on Elastic Foundations", University of Michigan Press, Ann Arbor.

Johnson, S. M. (1962) — "Determining the Capacity of Bent Piles", *Proc.,* ASCE, Vol. 88, SM6, December, pp. 65-79.

Matlock, H., and Reese, L. C. (1961) — "Foundation Analysis of Offshore Pile-Supported Structures", *Proc.,* 5th Internat. Conf. Soil Mech. and Found. Eng., Vol. 2, pp. 91-97.

Prakash, Shamsher (1962) — "Behavior of Pile Groups Subjected to Lateral Loads", Ph.D. Thesis, University of Illinois.

Peck, R. B., and Davisson, M. T. (1962) — Discussion of "Design and Stability Considerations for Unique Pier", by James Michalos and D. P. Billington, *Trans.,* ASCE, Vol. 127, Part IV, pp. 413-424.

Reese, L. C., and Matlock, H. (1956) — "Non-Dimensional Solutions for Laterally Loaded Piles with Soil Modulus Assumed Proportional to Depth", *Proc.,* Eighth Texas Conference on Soil Mechanics and Foundations Engineering, Austin.

Terzaghi, Karl (1955) — "Evaluation of Coefficients of Subgrade Reaction", *Geotechnique,* Vol. 5, pp. 297-326.

Vesic, A. B. (1961) — "Beams on Elastic Subgrade and Winkler's Hypothesis", *Proc.,* 5th Internat. Conf. Soil Mech. and Found. Eng., Vol. 1, pp. 845-850.

Walter, H. (1951) — "Das Knickproblem bei spitzenpfahlen, deren schaft ganz oder teilweise in nachgiebigem boden steht", *Bautechnik Archives,* Heft 6, pp. 40-66.

Wieghardt, K. (1922) — "Über den Balken auf nachgiebiger Unterlage", *Zeitschrift* fur Angewandte Math. und Mech., pp. 165-184.

APPENDIX

NOTATIONS

Note: The units are expressed in terms of force F and length L.

Symbol		*Units*
B	Width of pile normal to the loading	L
c	Cohesion	FL^{-2}
E	Young's modulus for the pile	FL^{-2}
I	Moment of inertia of pile cross-section	L^4
k	Horizontal subgrade modulus	FL^{-2}
L	Embedded length of pile	L
l	Depth coefficient, x/R for $k = \text{constant}$	
l_{max}	Maximum value of depth coefficient, $\frac{R}{L}$ for $k = \text{constant}$	
N_c	Bearing capacity factor for cohesion	
N_q	Bearing capacity factor for overburden pressure	
n_h	Constant of horizontal subgrade reaction	FL^{-3}
P	Axial load in the pile	F
P_{cr}	Buckling load for the pile	F
q'	Vertical effective pressure	FL^{-2}
R	Relative stiffness factor, $k = \text{constant}$	L
T	Relative stiffness factor, $k = n_h x$	L
U	Axial load coefficient, $k = \text{constant}$	
U_{cr}	Critical axial load coefficient, $k = \text{constant}$	
V	Axial load coefficient, $k = n_h x$	
V_{cr}	Critical axial load coefficient, $k = n_h x$	
w	Soil reaction	FL^{-1}
w_u	Ultimate soil reaction	FL^{-1}
x	Depth coordinate from ground surface	L
y	Horizontal deflection of pile	L
z	Depth coefficient, $\frac{x}{T}$ for $k = n_h x$	
z_{max}	Maximum value of depth coefficient, $\frac{L}{T}$ for $k = n_h x$	
φ	Angle of internal friction for the soil	

Table 1 — Typical values of n_h

Soil Type	n_h, lb/in.^{3}	
	Dry	Submerged
Sand:		
Loose	9.4	5.3
Medium	28	19
Dense	75	45
Very loose, under repeated loading		1.5
Silt:		
Very soft, organic		0.4-1.0
Clay:		
Very soft,		
static loads		2
repeated loads		1

Table 2 — Typical values of k for preloaded clays

Unconfined compression strength, q_u, tons/ft^2	Range of k lb/in.^{2}	Probable Value of k, lb/in.^{2}
0.2 — 0.4	100 — 600	110
1 — 2	463 — 926	694
2 — 4	926 — 1852	1390
>4	>1852	2780

BENDING AND BUCKLING OF SOIL-SUPPORTED STRUCTURAL ELEMENTS

HUDSON MATLOCK

Associate Professor of Civil Engineering, The University of Texas, Austin, Texas.

WAYNE B. INGRAM

Teaching Assistant, Department of Civil Engineering, The University of Texas, Austin, Texas.

ABSTRACT

Beam-columns with continuous or discontinuous transverse and angular loads and elastic restraints are represented mathematically in a manner corresponding to finite-element mechanical models. Solutions for linearly elastic cases are accomplished by direct recursion-equation elimination of unknowns.

Five practical applications are presented by which various capabilities of the general method are illustrated. The examples include a continuous footing, a flexible bulkhead, and the bending and buckling of a long pile.

RESUMEN

Las vigas-columnas con cargas continuas o discontinuas, transversales o angulares y apoyos elásticos, son representadas matemáticamente en una forma tal que corresponde a los modelos mecánicos de elementos finitos. Soluciones para casos elásticos lineales se logran eliminando incógnitas por medio de una ecuación directa de recursión.

Se presentan cinco aplicaciones prácticas por medio de las cuales se ilustran varias posibilidades del método general. Los ejemplos incluyen una fundación continua, un muro de contención flexible y la flexión y pandeo de pilotes largos.

INTRODUCTION

It is the purpose of this paper to give a brief description of an analytical method for solving a variety of problems involving a beam-column-on-foundation and to illustrate the versatility of the method by applying it to several examples. Although the data for some of the examples are artificial, the cases discussed will be recognized as being based on actual situations.

The analytical approach which is to be described stems from research on offshore foundations, in particular the study of lateral-load behavior of foundation piles. The method represents a generalization of a technique which was suggested by Gleser (Ref. 1) and extended by Focht and McClelland (Ref. 2) and Reese and Matlock (Ref. 3).

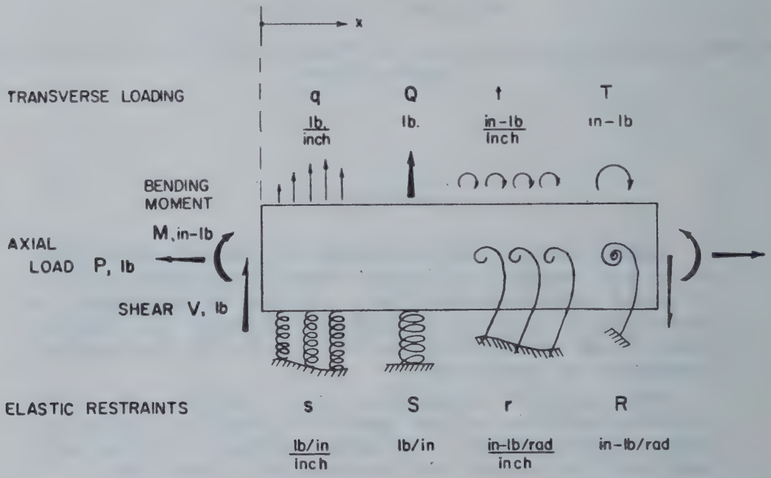
x
TRANSVERSE LOADING
q
lb./inch
Q
lb.
t
in-lb/inch
T
in-lb
BENDING MOMENT
M, in-lb
AXIAL LOAD P, lb
SHEAR V, lb
ELASTIC RESTRAINTS
s
lb/in/inch
S
lb/in
r
in-lb/rad/inch
R
in-lb/rad

Fig. 1 — Loads and restraints considered in the beam-column solution.

Fig. 1 — Cargas y apoyos considerados en la solución del sistema viga-columna.

DESCRIPTION OF METHOD

To maintain generality and therefore versatility in the method, a considerable variety of input data is considered. Figure 1 illustrates the various types of loads and restraints which might be applied to a short segment of a beam. Each of the terms illustrated in the figure is shown acting in a positive sense. Capital letters are used to designate concentrated quantities whereas the corresponding lower-case symbols indicate effects which are distributed in some way along the length of the beam.

The transverse loads and the elastic restraints may be divided into two classes: (1) loads Q and q and springs S and s, which act normal to the axis of the beam and (2) couples T and t and rotational springs R and r, which act in an angular sense. In addition, there is an axial force P which may be constant or may vary along the length of the beam.

The bending stiffness of the beam (the product EI of the modulus of elasticity and the moment of inertia) is designated by the symbol F.

The assumptions of conventional elementary beam theory provide the basis for the present method. Among these are the neglect of shearing and axial deformations and the limiting of consideration to straight beams of symmetrical cross-section. Lateral deflections are considered to be small compared to original dimensions. A deformed element of such a beam is shown in Fig. 2a. The curvature of the beam is approximated by the second derivative of the deflection y with respect to distance x along the beam. It is assumed that the material of the beam is linearly elastic and therefore the relation of Eq 1 between curvature and bending moment M is the ordinary expression from elementary beam theory.

A generalized beam element is shown in Fig 2b. The element has been deflected by an amount y and tilted through a small angle dy/dx. The various loads and elastic restraint reactions are detailed in the figure. Temporarily, only distributed effects are considered; provision for concentrated loads and restraints will be made subsequently. Equation 2 in Fig. 2b is obtained by summing the forces and moments acting on the element. This equation is similar to that of conventional beam theory except that (1) the total transverse load w includes both forces and spring reactions and (2) an additional term du/dx is added to express the rotational effects. These rotational effects include applied couples, and restraints against angular movement of the element. The two sources of angular restraint are the spiral springs and the axial load P. Although the distributed rotational effects r and t are introduced for the development of equations, it will be seen that in solving actual problems only the concentrated versions of these terms are used.

In order to apply numerical techniques for computation, Eqs. 1 and 2 are converted to the corresponding finite-difference forms given in Eqs. 3 and 4 of Fig. 2c. The beam is divided into m increments of equal length h and the subscript i designates any particular station or increment point along the beam. The finite-difference form of Eq. 1 is repeated three times as Eq. 3 to express the bending moment at three adjacent stations. The equations are then substitut-

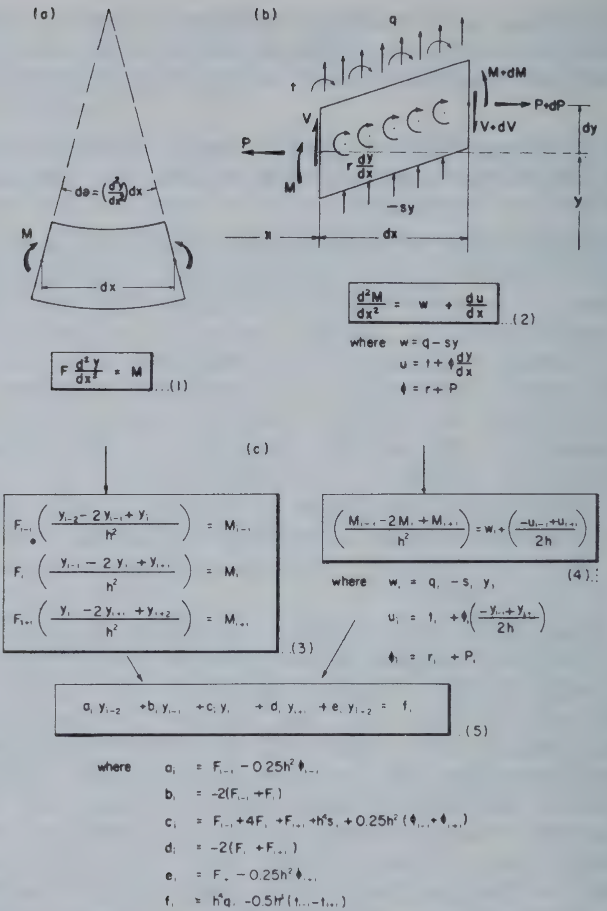
(a)
(b)
q
M+dM
P+dP
V+dV
dy
V
P
$r\frac{dy}{dx}$
M
$-sy$
y
x
dx
$d\theta = \left(\frac{d^2y}{dx^2}\right)dx$
M
dx
$\boxed{F\frac{d^2y}{dx^2} = M}$ ...(1)
$\boxed{\frac{d^2M}{dx^2} = w + \frac{du}{dx}}$ ...(2)
where $w = q - sy$
$u = t + \phi\frac{dy}{dx}$
$\phi = r + P$
(c)
$F_{i-1}\left(\frac{y_{i-2} - 2y_{i-1} + y_i}{h^2}\right) = M_{i-1}$
$F_i\left(\frac{y_{i-1} - 2y_i + y_{i+1}}{h^2}\right) = M_i$
$F_{i+1}\left(\frac{y_i - 2y_{i+1} + y_{i+2}}{h^2}\right) = M_{i+1}$ ...(3)
$\left(\frac{M_{i-1} - 2M_i + M_{i+1}}{h^2}\right) = w_i + \left(\frac{-u_{i-1} + u_{i+1}}{2h}\right)$ (4)
where $w_i = q_i - s_i y_i$
$u_i = t_i + \phi_i\left(\frac{-y_{i-1} + y_{i+1}}{2h}\right)$
$\phi_i = r_i + P_i$
$a_i y_{i-2} + b_i y_{i-1} + c_i y_i + d_i y_{i+1} + e_i y_{i+2} = f_i$ (5)
where $a_i = F_{i-1} - 0.25h^2\phi_{i-1}$
$b_i = -2(F_{i-1} + F_i)$
$c_i = F_{i-1} + 4F_i + F_{i+1} + h^4 s_i + 0.25h^2(\phi_{i-1} + \phi_{i+1})$
$d_i = -2(F_i + F_{i+1})$
$e_i = F_{i+1} - 0.25h^2\phi_{i+1}$
$f_i = h^4 q_i - 0.5h^3(t_{i-1} - t_{i+1})$

Fig. 2 — Development of fourth-order difference equation from the two second-order differential equations for the beam-column.

Fig. 2 — Desarrollo de la ecuación de diferencias de cuarto órden, derivada de dos ecuaciones diferenciales de segundo órden para las vigas-columnas.

ed into Eq. 4 to produce the fourth-order difference expression given by Eq. 5. This equation, written repetitively for each station along the beam, is the general form for a system of m + 3 simultaneous equations in which all of the deflections y_i are the unknown quantities to be solved. The expressions for the coefficients in Eq. 5 introduce all of the pertinent input data for beam stiffness, applied loads, and elastic restraints at each station.

The provide for maximum convenience and versatility it is highly desirable that provisions be made to introduce data at points along the beam in a purely random or discontinuous manner. Therefore, the key in the technique of combining two second-order equations (Eqs. 1 and 2) into a finite-difference form (Eq. 5) is that nowhere is it assumed that a derivative is continuous over an interval and nowhere is a conventional derivative of a product taken. Instead, each quantity is expressed in the most elemental finite-difference form as soon as it is introduced and all subsequent combinations are made by simple algebraic manipulation. Troublesome higher-order terms are thus avoided. If this procedure is not followed, other equally valid forms can be obtained for the coefficients in Eq. 5 but they do not provide for convenient lumping of all input-data quantities at the increment points. In all subsequent expressions the distributed quantities of load and restraint are replaced by lumped concentrated quantities at increment points. Such lumped

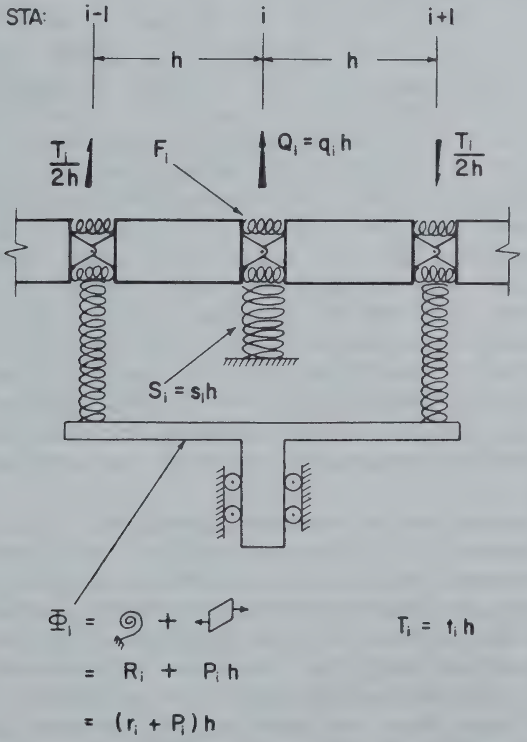

Fig. 3 — Mechanical finite-element beam model for simulating beam-column behavior.

Fig. 3 — Modelo de um elemento mecánico finito de la viga, para simular el comportamiento de la viga-columna.

quantities either may represent concentrated effects directly or may be used as approximations of distributed effects per increment length h.

If input-data quantities are considered to be concentrated at the increment points, the beam-element model in Fig. 3 represents an exact mechanical model of Eq. 5. The figure shows all quantities related to a single typical point, Station i. The bending stiffness F_i is represented as concentrated at the increment point in the form of a spring-restrained hinge between tyo rigid segments. All load and support values are ultimately felt by the beam as transverse forces applied at increment points. This is obviously true for the lateral load Q_i and for the couple created by forces $T_i/2h$. It is also true for the reaction from the spring S as well as for two equal but opposite reactions from the angular restraint Φ which serves to express the combined effect of a rotational spring R and the axial load P.

It is possible to solve the system of $m + 3$ difference equations by a direct procedure in which unknowns are eliminated progressively. The process is particularly convenient for machine computations since it can be summarized in the form of a set of recursion equations which are solved in succession at station after station along the beam. Figure 4 illustrates the sequence of computations and summarizes all the equations that are needed. The derivation of Eqs. 6 and 7 proceeds from Eq. 5 in a relatively simple manner. First it is assumed that an equation exists which is of the form given as Eq. 7 in Fig. 4. In this equation the deflection y_i at any station is expressed in terms of three previously computed continuity coefficients A_i, B_i, and C_i plus two previously computed deflections at the two adjacent upstream stations. In the process of verifying the existence of Eq. 7, the expressions in Eq. 6 are more or less automatically developed.

The procedure for solving a problem is quite simple and straight-forward. (1) The continuity coefficients A_i, B_i, C_i, are computed starting at a fictitious station past the left end of the beam and proceeding through a second fictitious station at the right end. (2) Equation 7 is then applied in reverse direction along the beam and the solution of the set of $m + 3$ simultaneous equations is completed. The various derivatives are then computed to obtain such items as the bending moment and the net reactions at each station. Modern high-speed computers such as the Control Data Corporation 1604 can perform these computations for 100-increment problems in a total time of the order of one second. Furthermore, the amount of computational effort increases in pro-

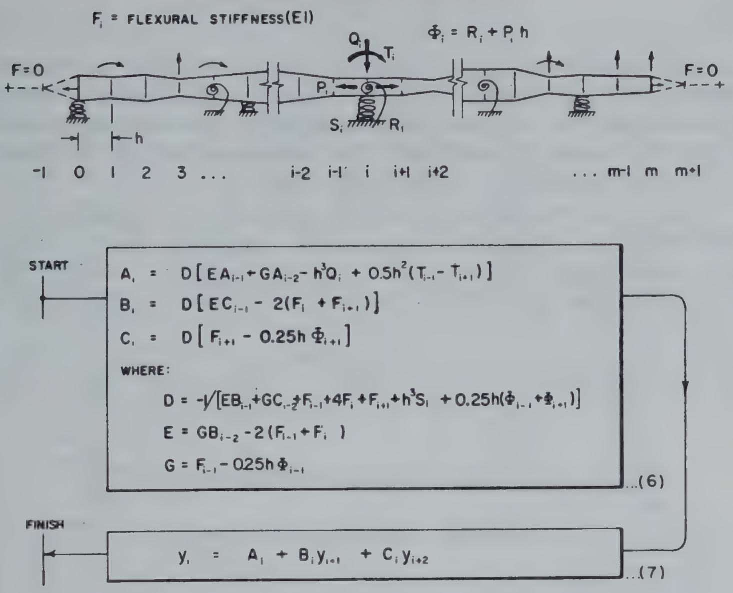
F_i = FLEXURAL STIFFNESS(EI)
Φ_i = R_i + P_i h
Q_i
T_i
F=0
F=0
P_i
S_i
R_i
h
-1 0 1 2 3 ... i-2 i-1 i i+1 i+2 ... m-1 m m+1
START
FINISH

$$A_i = D[EA_{i-1} + GA_{i-2} - h^3Q_i + 0.5h^2(T_{i-1} - T_{i+1})]$$

$$B_i = D[EC_{i-1} - 2(F_i + F_{i+1})]$$

$$C_i = D[F_{i+1} - 0.25h\Phi_{i+1}]$$

WHERE:

$$D = -1/[EB_{i-1} + GC_{i-2} + F_{i-1} + 4F_i + F_{i+1} + h^3S_i + 0.25h(\Phi_{i-1} + \Phi_{i+1})]$$

$$E = GB_{i-2} - 2(F_{i-1} + F_i)$$

$$G = F_{i-1} - 0.25h\Phi_{i-1} \quad \ldots(6)$$

$$y_i = A_i + B_iy_{i+1} + C_iy_{i+2} \quad \ldots(7)$$

Fig. 4 — Format for direct once-through solution of the system of m + 3 simultaneous equations.

Fig. 4 — Formato para resolver directamente y de una vez, el sistema de m + 3 ecuaciones simultáneas.

portion to only the first power of the number of increments whereas in other methods of solution of simultaneous equations the amount of arithmetic may increase in proportion to the second or higher power of the number of increments.

Some degree of approximation is inherent in all finite-difference expressions of continuous functions. The errors in the present method are indicated by the mechanical model of Fig. 3. The model represents a finite, lumped-value approximation of the real beam-column. No further error is introduced in the solution since the equations are exact representations of the finite-element model. Errors may be minimized by increasing the number of increments into which the member is divided. As an example, the maximum deflection of a simply supported beam with constant cross-section and a concentrated load at the center can be computed to an accuracy of 2.0 percent with 10 increments and 0.1 percent with 50 increments. For practical problems the errors in the method are seldom troublesome.

Five different problems and their solutions have been selected to illustrate applications of the general method.

CONTINUOUS FOOTING

The problem described in Fig. 5a is that of a continuous concrete footing which supports equal loads from 6 columns. It is desired to determine the deflection curve and the corresponding bending moments for computation of stresses and for proportioning of reinforcing steel.

The model which is used to simulate the footing for the beam-column solution is shown in Fig 5b. Each of the 5 bays is divided into thirty 10-inch increments. With the 20-inch extension past the center line of the column at each

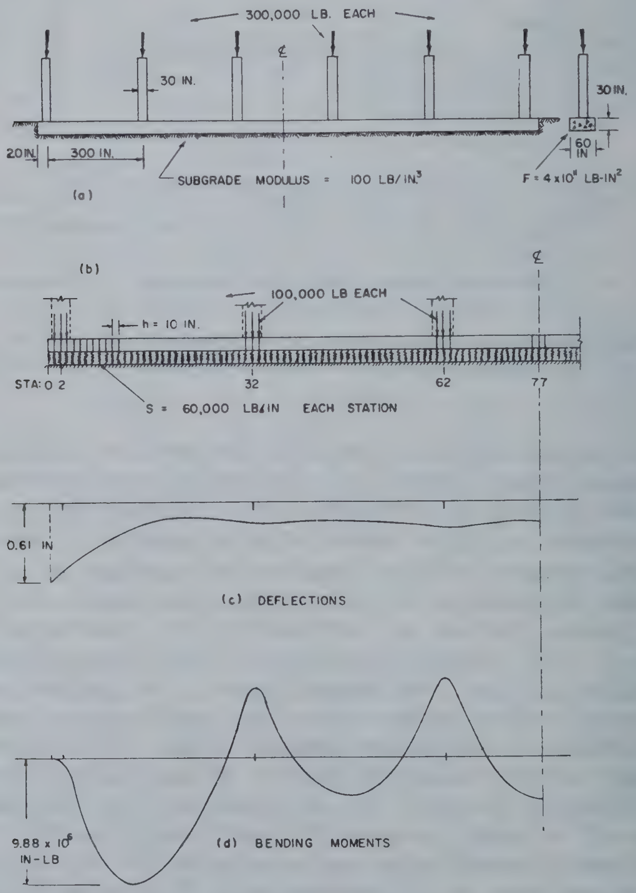
300,000 LB. EACH
℄
30 IN.
30 IN.
20 IN.
300 IN.
60 IN
SUBGRADE MODULUS = 100 LB/IN.^{3}
F = 4 x 10^{11} LB-IN^2
(a)
(b)
℄
100,000 LB EACH
h = 10 IN.
STA: 0 2
32
62
77
S = 60,000 LB/IN EACH STATION
0.61 IN
(c) DEFLECTIONS
9.88 x 10^6 IN-LB
(d) BENDING MOMENTS

Fig. 5 — Solution of a continuous footing by computer simulation with a finite-element model.

Fig. 5 — Solución de una fundación continua por simulación de computador con un modelo de elemento finito.

end, the total number of stations is 155 and the total length is 1540 inches. The soil is assumed to act as a series of independent, linear springs. The value of the spring constant S at each station is computed as the product of the width of the footing, the 10-inch increment length, and the assumed subgrade modulus. One-half of the regular value is put at each end station to account for the half-increment effect.

The main part of the computer program performs the calculations described in Fig. 4. Convenient arrangements are provided to minimize the number of input-data. After the deflections are computed, they are differentiated to obtain the slope, the bending moment, and the derivatives of the bending moment at each station. The computed deflections for the continuous footing are shown in Fig. 5c and the bending moments are given in Fig. 5d.

MULTI-SPAN BRIDGE

Figure 6a illustrates a problem in which settlements of piers influence the bending and deflection of a bridge girder. Such a problem is in the class of those considered by Chamecki in studying the influence of structural rigidity on footing settlements (Ref. 4) except that in the present example the soil behavior is represented by simple, independent, linear springs, at least temporarily. Repeated solutions, with intermediate adjustments of the spring stiffness, can be applied to solve for nonlinear soil response or for the effects of the interaction of pressure bulbs on the settlements of adjacent footings.

The 10 spans are assumed to be supported near the ends by a rock foundation and in the middle by a compressible soil. Two hinges are shown and haunches are used across the supports to represent cover plates on the girder. It is desired to (1) determine the effect of dead load on the settlement of supports and on the bending moments throughout the structure and (2) to observe the total effects of the dead load plus a short-time live load.

The structure, as modeled in the beam-column solution, is shown in Fig. 6b. It has been divided into 100 increments, each 8 ft. in length. In the middle zone the linear spring at each column represents the soil support and the angular restraint provided by the rigidly connected columns is indicated by a spiral spring. The flexural stiffness variations are shown; also, the two hinges are modeled by simply setting the flexural stiffness equal to zero at the proper stations.

The zero deflections at the outer supports can be enforced in either of two ways. (1) An extremely large spring stiffness S may be placed at each support point so as to limit the deflection to a negligible value. Furthermore, it is possible to produce any desired deflection at any station simply by applying an extremely large force Q together with a correspondingly large spring constant S in such magnitude and in such ratio as to override any other data at that location. (2) The same end result can be accomplished by setting the continuity coefficient A_i in Eq. 7 equal to the desired deflection and B_i and C_i equal to zero.

The solid curve in Fig 6c shows the resulting deflected shape of the structure and the settlement at each central

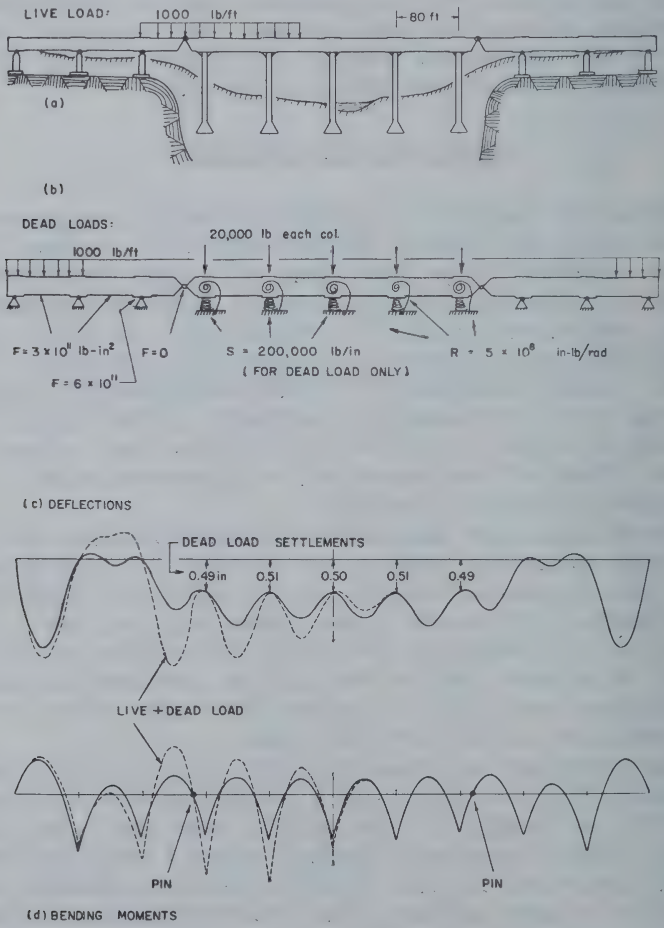
LIVE LOAD:
1000 lb/ft
80 ft
(a)
(b)
DEAD LOADS:
1000 lb/ft
20,000 lb each col.
F = 3 × 10¹¹ lb-in²
F = 0
S = 200,000 lb/in
(FOR DEAD LOAD ONLY)
R = 5 × 10⁸ in-lb/rad
F = 6 × 10¹¹
(c) DEFLECTIONS
DEAD LOAD SETTLEMENTS
0.49 in
0.51
0.50
0.51
0.49
LIVE + DEAD LOAD
PIN
PIN
(d) BENDING MOMENTS

Fig. 6 — Solution of girder-type bridge considering both dead-load and live-load effects.

Fig. 6 — Solución del puente de viguetas considerando tanto los efectos de la carga viva como de la carga muerta.

support caused by the dead load. No deflections occurred at the locations founded on rock. Settlements of aproximately 0.5 inch occurred at each of the five central columns.

The solid curve in Fig. 6d shows the bending moments resulting from the dead load of the structure. The maximum negative moment occurred at the first interior support and a moment of zero occurred at each of the two hinges.

To study the effects of a temporary live load, the five central supports were locked at the deflections previously found by the dead-load solution and then the live load shown in Fig. 6a was added to the dead-load values. The resulting deflection and bending moment curves are given as dashed lines in Fig. 6. It would be relatively easy to move the live load and repeat the solution until the most critical position is found.

ANCHORED BULKHEAD

An example of a flexible bulkhead has been selected which is almost the same as a problem previously solved by Richart (Ref. 5) by a process of superposition. The bulkhead is embedded in sand and has a sand backfill. Figure 7a describes the general problem and Fig. 7b is the corresponding representation for the beam-column solution.

All values for the solution are given in terms of a beam one foot wide. The loads consist of the ultimate active earth pressure above the dredge line, and the difference between the front and rear at-rest earth pressures below the dredge line. A modulus of subgrade reaction of 240 lb/in^3 is assumed at the bottom of the bulkhead and has been converted to an equivalent concentrated spring on the beam. The springs are shown to vary linearly from zero stiffness at the dredge line to the maximum at the bottom of the bulkhead. Whereas Richart assumed zero deflection at the anchor rod, in the present solution the anchor rod is conveniently simulated by the spring at the 12-ft depth.

The resulting deflections and bending moments are shown in Figs. 7c and 7d. The elongation of the anchor rod is 1.12 inches. Except that the anchor rod deflection has some effect on deflections and bending moments, the present solution is in good agreement with that obtained by Richart.

Solutions for a similar bulkhead have been obtained for cases where non-linear behavior of the soil is considered (Refs. 6 and 7). The method is readily applicable to many forms of flexible bulkheads or excavation bracing.

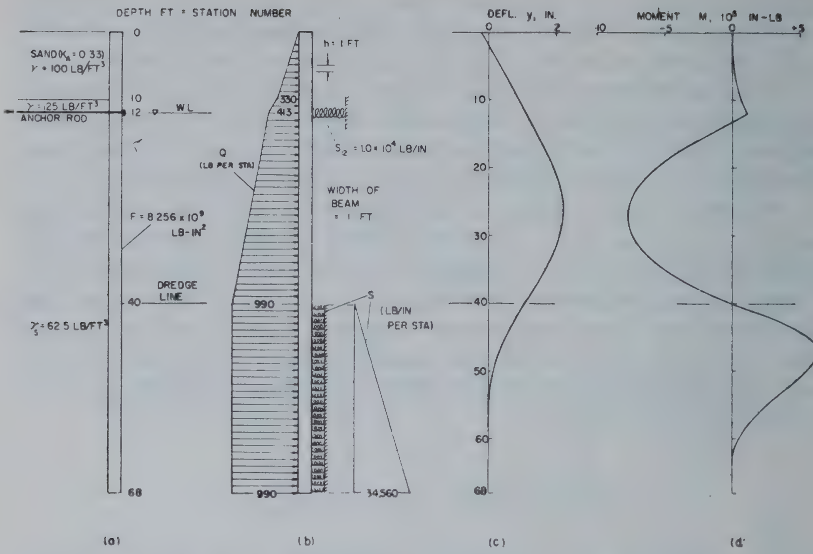
DEPTH FT = STATION NUMBER
0
SAND(K_A = 0 33)
γ = 100 LB/FT^3
10
γ = 125 LB/FT^3
12
WL
ANCHOR ROD
F = 8 256 x 10^9 LB-IN^2
DREDGE LINE
40
γ_s = 62 5 LB/FT^3
68
h = 1 FT
330
413
S_{12} = 1.0 x 10^4 LB/IN
Q (LB PER STA)
WIDTH OF BEAM = 1 FT
990
S (LB/IN PER STA)
990
34,560
DEFL. y, IN.
0
2
10
20
30
40
50
60
68
MOMENT M, 10^5 IN-LB
-10
-5
0
+5
(a)
(b)
(c)
(d)

Fig. 7 — Direct solution of an anchored bulkhead.

Fig. 7 — Solución directa del muro de contención anclado.

OFFSHORE FOUNDATION AND STRUCTURAL ANALYSIS

To achieve a rational solution for a laterally loaded pile, a deflected shape must be computed for the pile which is compatible with the characteristics of the superstructure and with the force-deformation characteristics predicted for the soil (Ref. 8). Figure 8a illustrates a jacket-leg-and-pile combination from an offshore structure and Fig. 8b indicates how this complete member can be represented in the beam-column solution. The translation and tilt indicated in Fig 8b either may be the finally determined position of the structure or may represent a trial position used during reaching the ultimate solution. The wave forces produces bending between the support points, and the rotational restraints from connecting membres of the structure at the support points are also introduced. An axial load is included and the soil characteristics are described in this example by a series of linear springs which increase in stiffness in proportion to depth. Changes in bending stiffness are also indicated at several points along the leg-and-pile combination. The resulting deflection curve is shown in Fig 8c and the corresponding bending moments are given in Fig. 8d.

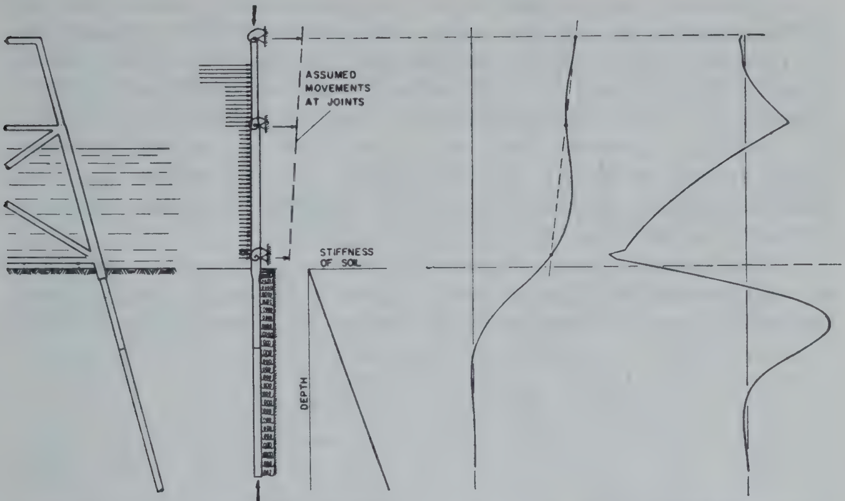

(a) STRUCTURE (b) BEAM-COLUMN REPRESENTATION (c) DEFLECTION CURVE (d) BENDING MOMENT DIAGRAM

Fig. 8 — Analysis of the pile-supported leg of an offshore drilling structure.

Fig. 8 — Análisis de la pata soportada por pilotes de una estructura de perforación de plataforma submarina.

This example illustrates how a complete solution may be made directly for bending in the main members in a structure by the reduced-frame approach. It also appears feasible to use the general beam-column representation as an element in the solution of complex frames.

BUCKLING OF A LONG PILE

To illustrate the ability to use the general beam-column procedure to solve elastic buckling problems by incremental variation of axial load, the problem in Fig. 9 has been selected. The case is similar to one considered by Hromadik (Ref. 9, p. 76). Previous methods for determining the effective length of a column partially embedded in soil have involved various methods of approximation. Because the degree of end restraint is a critical factor in determining buckling loads, such approximations may lead to considerable error.

The structure selected is shown in Fig. 9a and the corresponding model used in the beam-column solution is in Fig. 9b. The spiral spring at the top represents the angular restraint furnished by the connecting members and a knife-edge support is shown to indicate complete lateral restraint.

The soil characteristics are represented by the series of linear springs in Fig. 9b. For this example they are assumed constant with depth, but in general they may be varied in any way to suit an estimate of the soil behavior. Some eccentricity or a small horizontal load is required to initiate the buckling process just as is required by a real column. Such a load is shown in the figure. It influences the rate of development of deflection with increase in axial load but does not affect the critical buckling load.

Figure 9c shows a series of deflection curves obtained by the process of incremental increase of axial load. When the axial load is increased to values near the critical buck-

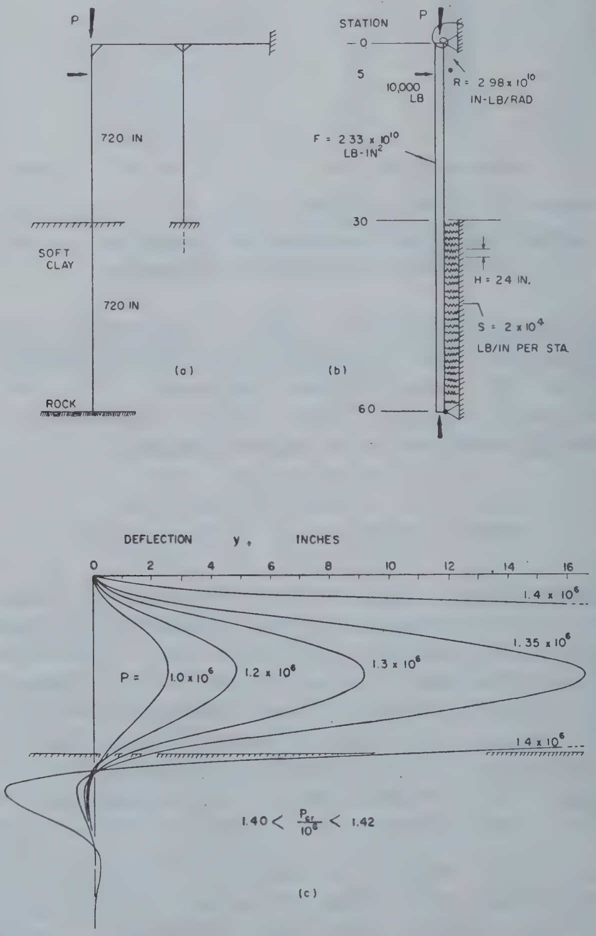
P
720 IN
SOFT CLAY
720 IN
ROCK
(a)
STATION
P
0
5
10,000 LB
R = 2.98 x 10^10 IN-LB/RAD
F = 2.33 x 10^10 LB-IN^2
30
H = 24 IN.
S = 2 x 10^4 LB/IN PER STA.
(b)
60
DEFLECTION y, INCHES
0
2
4
6
8
10
12
14
16
1.4 x 10^6
1.35 x 10^6
P =
1.0 x 10^6
1.2 x 10^6
1.3 x 10^6
1.4 x 10^6
1.40 < Pcr/10^6 < 1.42
(c)

Fig. 9 — Buckling of a long partially embedded pile.

Fig. 9 — Pandeo de un pilote largo y parcialmente empotrado.

ling load, the deflections increase more and more rapidly. On passing the critical load the solution is discontinuous and the sign of deflections reverses suddenly as the region of unstable equilibrium is entered. For the problem considered, the critical load was found to lie between values of 1.40 and 1.42 million pounds.

The advantages of this procedure are that the complete structure is modeled and solved at one time, no equivalent pinned-end length or point of fixity assumptions are necessary, and the estimate of soil behavior may be varied from problem to problem. For this particular problem only 9 input-data cards were required for the first load, and for subsequent loads only one data value was changed. Each solution was performed in 5 seconds, including input operations and a printout of the deflection, slope, moment, shear, and reaction at each of 60 stations. Thus the cost and effort of computation is entirely negligible and more of the attention of the engineer may be directed toward formulating the appropriate model of the real problem.

APPLICATION OF THE METHOD

The developed expressions yield a direct, one-pass solution for a beam-column on a linearly elastic foundation. The approach provides a simple, direct method for the simulation of otherwise complex or insolvable problems in bending and buckling of soil-supported structures. It has been shown that cumbersome methods and sometimes unjustified assumptions may be by-passed in favor of a solution that involves a simple finite-element model of the real problem.

The basic method may be used with repeated trial and correction procedures to achieve compatibility even when more complex behavior of the soil is considered. The transverse loads Q and springs S may be used as convenient devices which are adjusted to express the effects of nonlinearity and time-dependent behavior. Furthermore, adjustments can be made, if they can be rationally supported, to account for continuity within the soil mass itself.

The application of engineering judgment, decision and endeavor is not by-passed by the method described; only the tedious calculations have been avoided. The primary effort of the soils engineer may be directed toward development of improved descriptions of soil behavior. Many problems in foundation engineering cannot be solved satisfactorily when consideration is limited to conventional ultimate strength characteristics and a much broader understanding of the mechanical and rheological response of soil masses is needed.

REFERENCES

1. Gleser, Sol M. — "Lateral Load Tests on Vertical Fixed-head and Free-head Piles". *Symposium on Lateral Load Tests on Piles,* American Society for Testing Materials, Special Publication No. 154, 1953, pp. 75-101.

2. Focht, John A., Jr. and Bramlette McClelland — "Analysis of Laterally-Loaded Piles by Difference Equation Solution", *The Texas Engineer,* Texas Section, American Society of Civil Engineers, 1955.

3. Reese, Lymon and Hudson Matlock — "Numerical Analysis of Laterally Loaded Piles", *Proceedings,* Second Structural Division Conference on Electronic Computation, American Society of Civil Engineers, Pittsburgh, 1960, pp. 657-668.

4. Chamecki, Samuel — "Structural Rigidity in Calculating Settlements", *Proceedings,* American Society of Civil Engineers, Journal of the Soil Mechanics and Foundations Division, Vol. 82, No. SM1, Paper 865, January, 1956.

5. Richart, F. E., Jr. — "Analysis for Sheet Pile Retaining Walls", *Proceedings,* American Society of Civil Engineers, Journal of the Engineering Mechanics Division, Vol. 81, Paper 694, May, 1955.

6. Lytton, Robert L. — "A General Numerical Solution for the Mechanics of Beams", unpublished Master's thesis, The University of Texas, Austin, Texas, August, 1961.

7. Ingram, Wayne B. — "Solution of Generalized Beam-Columns on Non-linear Foundations", unpublished Master's thesis, The University of Texas, Austin, Texas, August, 1962.

8. Matlock, Hudson and Lymon C. Reese — "Foundation Analysis of Offshore Pile-Supported Structures", *Proceedings,* Fifth International Conference, International Society of Soil Mechanics and Foundation Engineering, 3B/14, Paris, July, 1961.

9. Hromadik, J. J. — "Column Strength of Long Piles", Technical Report 133, U.S. Naval Civil Engineering Laboratory, Port Hueneme, California, May, 1961.

DIVISÃO III — *Obras de Terra e Rocha*

DIVISIÓN III — *Obras de Tierra y Roca*

DIVISION III — *Earth and Rock Structures*

IIIa. *Barragens de terra e de enrocamento*

Presas de tierra y de enrocamiento

Earth and rockfill dams

IIIb. *Obras de terra e rocha diversas de barragens. Geologia Aplicada*

Obras de tierra y roca diferentes de presas. Geología Aplicada

Earth and rock structures other than dams. Engineering Geology

THOUGHTS CONCERNING THE MECHANICS OF SLOPE STABILITY ANALYSIS

ROBERT V. WHITMAN

Associate Professor of Civil Engineering, Massachusetts Institute of Technology, Cambridge, Massachusetts, U.S.A.

PETER J. MOORE

Research Assistant, Department of Civil Engineering, Massachusetts Institute of Technology, Cambridge, Massachusetts, U.S.A.

SUMMARY

Some of the factors relating to the mechanics of slope stability analysis are studied, using particularly the Fellenius method (ordinary method of slices), the Bishop simplified method and the friction circle method. Arguments are presented to support the contention that the erroneous Fellenius method should no longer be used in practice. These arguments are illustrated by means of six examples, for which the factors of safety by various methods of slope stability analysis are compared.

RESUMEN

Algunos de los factores relacionados al análisis de estabilidad de pendientes son estudiados, usando en particular, el método de Fellenius (método ordinario de tajadas), el método simplificado de Bishop y el método del círculo de fricción. Se presentan argumentos indicando que el método erróneo de Fellenius no debería usarse en la práctica. Estos argumentos están ilustrados mediante seis ejemplos para los cuales los factores de seguridad se comparan mediante varios métodos de análisis de estabilidad de pendientes.

INTRODUCTION

Many obstacles confront the engineer who wishes to make an accurate assessment concerning the stability of an existing or proposed slope. Undoubtedly the most difficult problem is selection of appropriate shear strength parameters or shear strength values. It is of course necessary to know the geometry of the slope, and in general it is also necessary to establish the present and/or future pattern of pore water pressures within the slope. Once all of this information is assembled, the available shear resistance and the shear resistance required for equilibrium must then be related by an exercise in mechanics. If use of a detailed mechanics procedure is justified in any particular design problem, it is essential to minimize and evaluate any errors introduced by this part of the whole analysis.

Over the years, many formalized procedures have been developed for the last of these steps. Whenever formalized methods are used repeatedly, it is easy to lose sight of the errors that are inherent in the procedure. For example, the ordinary method of slices (also called the Fellenius method or Swedish circle method) can lead to a serious underestimate of the safety of a slope. This method, as with many other methods, assumes a circular failure surface and thereby introduces some error, but the real difficulty with the Fellenius method lies in its failure to satisfy the requirement of static equilibrium.

The papers and discussions presented at the European Conference on the Stability of Earth Slopes (see Geotechnique, 1955) placed the shortcomings of the Fellenius method in clear focus, and a simple and more satisfactory alternative was proposed. The shortcomings of this method had been studied at an even earlier date in the United States of America (see Taylor, 1949). Yet, a review of the recent literature would indicate that the Fellenius method is still used widely in the U.S.A. and elsewhere.

This paper presents a number of examples which compare the results obtained using several of the available procedures, and the theory underlying these procedures is analyzed critically.

THEORY OF CIRCULAR ARC METHOD OF ANALYSIS

This section will describe and discuss a number of procedures that have been developed to analyze the stability of the earth mass lying above an assumed failure surface. Since these procedures are described in detail elsewhere, only their salient features will be presented here. To simplify this discussion of the basic theory, it will be assumed that the pertinent soil properties are constant throughout the mass of soil in question. The example shown in Figure 1 will be used to illustrate the presentation.

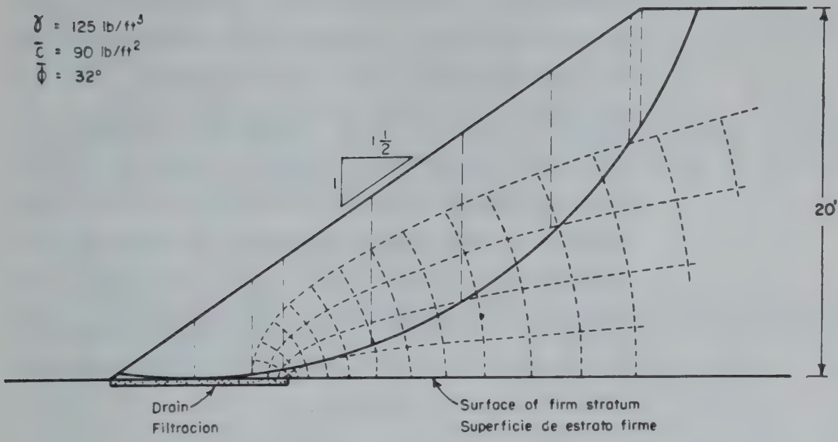

Fig. 1 — Example 1 — Steady seepage.

Fig. 1 — Ejemplo 1 — Filtración uniforme.

GENERAL LOOK AT EQUILIBRIUM OF THE SOIL MASS

To lay the basis for a critical examination of the stability analysis procedures, it is worthwhile to examine the equilibrium of the soil mass in general terms. The following presentation is taken from the works of Taylor (1937) and Fröhlich (1955).

The free body cut from the slope by an assumed circle of failure is acted upon by; (1) the pull of gravity upon the mass of soil in the free body, (2) a pore water pressure distributed along all or a portion of the boundaries of the free body, (3) a normal effective stress distributed along the assumed failure surface, and (4) a shear stress distributed along the assumed failure surface. Let us consider that the weight of the soil and the magnitude of the boundary pore water pressures are known, and that the resultant force vectors W and U can thus be evaluated: see Figure 2(a).

Now let us make the following two assumptions: (I) the soil strength is represented by $s = \bar{c} + \bar{\sigma} \tan\bar{\Phi}$; (II) at each point of the assumed failure surface, the mobilized shear resistance is $s_m = (\bar{c}/F) + \bar{\sigma} (\tan \bar{\Phi}/F)$, where F is a constant and is known as the safety factor. These are the standard assumptions commonly made in most methods of slope stability analysis. With these assumptions, the stresses distributed along the assumed failure surface can be replaced by the following three resultant forces, as shown in Figure 2(b):

(a) Resultant of cohesion R_c. The line of action of this resultant is completely determined by the assumptions, and the magnitude can be expressed in terms of $\bar{c}$ and the unknown F.

(b) Resultant of normal effective stress $\bar{N}$. Both the magnitude and line of action of $\bar{N}$ are unknown at this stage, although $\bar{N}$ must by definition be normal to the assumed failure arc.

(c) Resultant of friction R_Φ . R_Φ must be normal to $\bar{N}$, and $R_\Phi = \bar{N} \tan \bar{\Phi}/F$. However, the line of R_Φ is unknown.

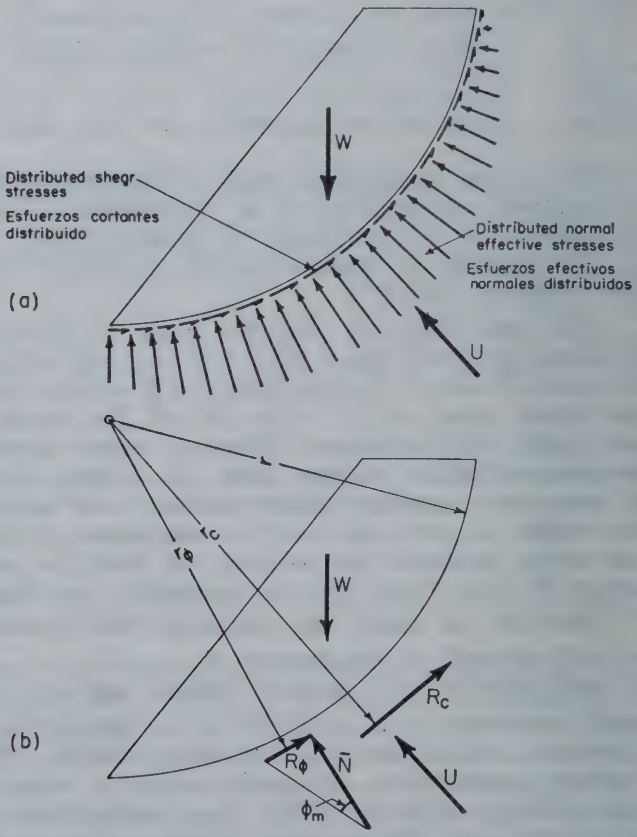
W
Distributed shear stresses
Esfuerzos cortantes distribuido
Distributed normal effective stresses
Esfuerzos efectivos normales distribuidos
(a)
U
r_c
r_ϕ
W
R_c
(b)
R_ϕ
$\bar{N}$
U
ϕ_m

Fig. 2 — Forces acting on free body.
Fig. 2 — Fuerzas que actuan sobre un cuerpo libre.

Thus there are four unknown quantities: F, the magnitude of $\overline{N}$, β (an angle describing the line of direction of $\overline{N}$), and r_Φ (a distance describing the line of action of R_Φ).

Since there are four unknowns and only three equations of static equilibrium, the problem is indeterminate, and an exact solution is impossible without consideration of the deformation characteristics of the soil.

FRICTION CIRCLE METHOD

If the pattern of distribution of normal effective stresses is assumed as known, the r_Φ can be calculated and the remaining unknowns can then be found from statics. The procedure used to complete the analysis is known as the "friction circle method", since the resultant of $\overline{N}$ and R_Φ must pass tangent to a circle, centered upon the assumed failure circle, of radius $r \sin \Phi_m$ where $\Phi_m = \arctan [(\tan \overline{\Phi})/F]$ (see Taylor, 1937).

One possible, although somewhat ridiculous, assumption is that all of the normal stress is concentrated at a single point along the failure arc. In such a case, r_Φ is equal to the radius of the failure arc. This assumption thus gives the smallest possible value for the ratio r_Φ/r. It can be shown that, all other factors remaining equal, an increase in r_Φ/r means an increase in the safety factor F. Thus this "ordinary friction circle method" establishes a *lower bound* for F. Any method of analysis which satisfies statics (and which is based upon the two fundamental assumptions of I and II) must give a safety factor at least as large as the value computed by the ordinary friction circle method.

The combined efforts of Fröhlich and of Jacobsen have provided a method for computing an *upper bound* for the safety factor (see Geotechnique, Vol. V, 1955, pp. 48-49, 50-51). This upper limit would be realized if the normal effective stress were concentrated entirely at the two end points of the assumed failure arc.

Taylor (1937) has computed the ratio r_Φ/r for the cases of normal effective stress distributed uniformly or as a half-sine curve. Intuitively, this latter case should provide a quite realistic value for the safety factor.

For the example shown in Figure 1, the upper and lower bounds for the safety factor are 1.60 and 1.27 respectively. Assuming that the normal effective stresses are distributed as a half sine curve, the safety factor would be 1.34. The critical failure circle pertinent to the assumed stress distribution was located for the lower bound case, and this circle was used for the other cases.

FELLENIUS METHOD

The basic steps of the ordinary method of slices are outlined in Figure 3. The forces N_i and T_i are set equal to the normal and tangential components of the weight W_i of the slice in question. The summation of T_i over all slices provides a measure of the "driving moment". Pore water forces across the base of the slices are subtracted from N_i to give the normal effective forces $\overline{N}_i$. The summation of $\overline{N}_i$ is taken as a measure of the frictional component of the "resisting" moment. The safety factor is computed from the equation for moment equilibrium about the center of the assumed failure circle.

The basic shortcoming of the procedure is illustrated well by an example in pp. 433-438 of Taylor (1948). From the N_i determined for each slice, the mobilized shear resistance at that slice may be computed. This mobilized shear force will not in general be equal to the T_i for that slice. The summation of the T_i does provide a reasonable measure of the driving moment, but the individual T_i do not represent the shear forces actually present at the bottoms of the several slices. Hence, by following the Fellenius procedure the individual slices are placed in force equilibrium in a direction normal to the arc at the base of the slice, but not in a direc-

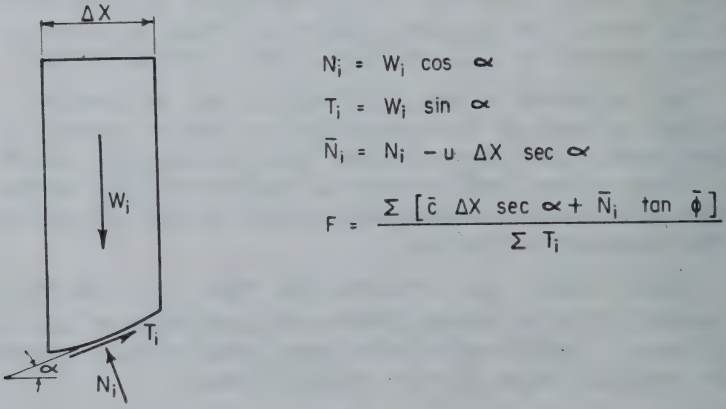
ΔX
W_i
T_i
α
N_i
$N_i = W_i \cos \alpha$
$T_i = W_i \sin \alpha$
$\overline{N}_i = N_i - u\ \Delta X \sec \alpha$
$F = \dfrac{\Sigma\,[\bar{c}\ \Delta X \sec \alpha + \overline{N}_i \tan \bar{\phi}]}{\Sigma\ T_i}$

Fig. 3 — Ordinary method.

Fig. 3 — Método ordinario.

TABLE I — Factors of safety by various methods

Method	Example 1	Example 2	Example 3	Example 4	Example 5	Example 6
Fellenius	1.19	1.43	1.08	1.38	1.05	1.57
Lower bound	1.27	1.59	1.15	1.43		
Simplified Bishop	1.31	1.62	1.16	1.54	1.86	1.77
Friction circle (half sine dist.)	1.34	1.69	1.17	1.49		
Including side forces				1.52		1.88
Upper bound	1.60	2.24	1.23	1.74		
Ratio Fellenius/Bishop	0.91	0.88	0.93	0.90	0.57	0.89

tion tangent to this arc. The method in effect assumes that the magnitude of both $\overline{N}$ and r_{ϕ} can be computed from the given data. This assumption leaves but two unknowns to be solved by three equations of equilibrium. The solution obtained on the basis of this assumption cannot in general satisfy force equilibrium of the whole free body even though moment equilibrium is satisfied.

It is difficult to make an a priori estimate as to the error introduced by this assumption. However, numerous examples have shown that the safety factor obtained by the Fellenius solution usually falls *below the lower bound* of solutions which satisfy statics (see examples in Table I). For the example shown in Figure 1, the Fellenius method yields a safety factor of 1.19.

There is still another reason why the ordinary method of slices gives only an approximate answer: summation of forces computed for slices of finite width is a potentially inexact integration procedure. However, the basic fault of the method remains even though a more accurate integration scheme is used. Utilizing a large number of slices or a graphical procedure (see, for example, the paper by May, 1936) does not remove the inherent source of error.

TABLE II — Stability analysis — Bishop method — Example 1

	(1)	(2)	(3)	(4)	(5)	(6)	(7)		(8)	
Slice No.	Width of slice ΔX - (ft)	$\sin \alpha$	Weight of slice kips	Pore pressure U - kips/ ft^2	$W \sin \alpha$	$c . \Delta X + (W - U\Delta X) \tan \bar{\phi}$	M_α		$\frac{\text{col. (6)}}{\text{col. (7)}}$	
							F = 1.25	F = 1.35	F = 1.25	F = 1.35
1	4.5	-.050	0.9	—	-0.04	0.96	.97	.97	.99	.99
2	3.2	+.053	1.7	—	0.09	1.35	1.02	1.02	1.32	1.32
2A	1.8	.137	1.3	.025	0.18	0.97	1.06	1.05	.92	.92
3	5.0	.250	4.6	.206	1.15	2.70	1.09	1.08	2.48	2.50
4	5.0	.416	5.6	.287	2.32	3.01	1.12	1.10	2.69	2.74
5	5.0	.583	5.8	.249	3.38	3.14	1.10	1.08	2.86	2.90
6	4.4	.740	4.6	.106	3.41	3.03	1.05	1.02	2.89	2.97
6A	0.6	.823	0.5	—	0.41	0.36	.98	.95	.37	.38
7	3.2	.870	1.5	—	1.31	1.23	.93	.92	1.32	1.34
				Sum =	12.21			Sum =	15.84	16.06

$$M_\alpha = \cos \alpha \left[1 + \frac{\tan \alpha \tan \bar{\phi}}{F} \right]$$

$$F_{①} = \frac{15.84}{12.21} = 1.30$$

$$F_{②} = \frac{16.06}{12.21} = 1.31 \qquad \therefore \underline{\underline{F = 1.31}}$$

BISHOP METHOD OF SLICES

Bishop (1955) has proposed an alternative method* which, like the Fellenius method, ignores the possible influence of the forces acting on the sides of each slice. This simple procedure is mentioned at the end of a paper which also discusses a more complex procedure. The Norwegian Geotechnical Institute has developed a graph and a tabulation scheme whereby the simple Bishop procedure may readily be used in practical work: see Table II and Figure 4. A set of stability charts based upon the Bishop procedure have been prepared and may be used to obtain quick, preliminary answers to many problems (Bishop and Morgenstern, 1960).

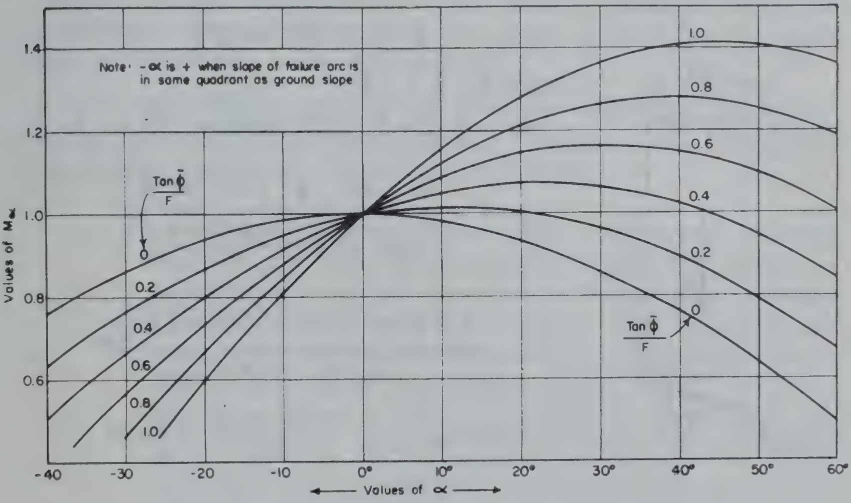

Fig. 4 — Graph for determination of M_α.

Fig. 4 — Gráfico para determinar M_α.

The basic step in the Bishop approach is shown in Figure 5. Forces T_i are found as with the Fellenius method, and are likewise summed to give a measure of the driving moment. However, the forces N_i are found by applying a different rule. This rule provides for force equilibrium in the *vertical* direction, while ignoring the requirement of force equilibrium in the horizontal direction.

---

* The Bishop method referred to in this paper is the simplified method unless otherwise mentioned.

It is not immediately apparent that it is any batter to insist upon equilibrium in the vertical direction than in the direction normal to the arc of each slice. Yet numerous examples have shown that the Bishop assumption is superior. For the slope of Figure 1, the simple Bishop approach gives a safety factor of 1.31. This result is greater than the lower bound, and approaches the answer obtained by a friction circle solution with a half sine wave distribution of stress. The simplified Bishop method assumes, in effect, that the forces on the sides of any slice have no net component in the vertical direction. Apparently this assumption is more realistic than the assumption that these side forces have no net component in a direction normal to the arc of each slice.

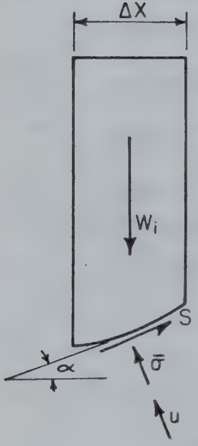

$$S = \frac{1}{F}(\bar{c} + \bar{\sigma}' \tan\bar{\phi})$$

To find $\bar{\sigma}$, $\Sigma V = 0$

$$W_i - \frac{1}{F}(\bar{c} + \bar{\sigma} \tan\bar{\phi})\,\Delta X \tan\alpha - (\bar{\sigma} + u)\,\Delta X = 0$$

$$\therefore\ \bar{\sigma} = \frac{W_i - u\Delta X - \frac{1}{F}\bar{c}\,\Delta X \tan\alpha}{\Delta X\left(1 + \frac{\tan\bar{\phi}\ \tan\alpha}{F}\right)}$$

$$F = \frac{\Sigma\left[\bar{c}\,\Delta X + (W_i - u\Delta X)\tan\bar{\phi}\right]\frac{1}{M_\alpha}}{\Sigma\, W_i \sin\alpha}$$

where $M_\alpha = \left(1 + \frac{\tan\alpha\ \tan\bar{\phi}}{F}\right)\cos\alpha$

Fig. 5 — Bishop Method.

Fig. 5 — Método de Bishop.

OTHER METHODS

A number of procedures have been developed in which the forces acting upon the sides of slices are included. One such procedure is outlined in pp. 437-438 of Taylor (1948), and an example of the use of this procedure appears in the paper by Lowe and Karafiath (1960). Bishop (1955) has presented a procedure which does not involve graphical construction.

Because of their complexity, these methods will not be described and analyzed in this paper. Generally these methods fail in some minor way to satisfy all of the requirements of static equilibrium, but the resultant errors are of minor consequence.

THE MOST CORRECT SOLUTION

Since the force condition for the free body is statically indeterminate, it is impossible to determine "the correct solution" solely from equilibrium conditions. In general, the problem remains indeterminate even when it is specified that the Coulomb failure condition may not be exceeded on any vertical surface through the free body. Until a complete stress-strain law is formulated for soils, it will not be possible to find "the correct solution".

By analyzing a number of problems wherein the forces on the sides of slices were included, Bishop (1952) suggests a principle which can be stated as follows:

> The values of safety factor computed by any method for any given problem will fall within a very narrow range, provided that the computation procedure (1) satisfies statics, (2) assumes an intuitively reasonable distribution of normal effective stress along the failure circle, and (3) does not cause shear stresses in excess of shear strength along vertical lines trough the free body. Since this range of uncertainty is far less than the other remaining uncertainties as regards the proper shear strength, etc., any one of these values can be selected as the "most correct" solution.

Naturally this range of "most correct" solutions must fall between the upper and lower bound as found by the friction circle approach.

The results found for the slope of Figure 1 have been listed in Table I, under the heading of Example 1. A distribution of normal effective stresses according to a half sine wave comes close to being intuitively reasonable, although this solution has not been checked with regard to stresses along vertical cuts. Perhaps this modified friction circle solution is close to being a "most correct" solution.

EXAMPLES

In each of the following examples, some but not all of the computational procedures have been applied. The various results are listed in Table I. The circle which would be "critical" for the method in use was not always located.

EXAMPLE 2 *

The section with the grid of centers for slip circles is shown in Figure 6. Preliminary analyses showed that the critical circle for both the ordinary method of slices and for Bishop's method would be tangent to the foundation line. Analyses by the ordinary method were continued until the center of the circle with the minimum factor of safety was located. The contours of the factors of safety are shown in Figure 7. The minimum safety factor is about 1.43 and applies for a circle with a center somewhere near line C5-D6.

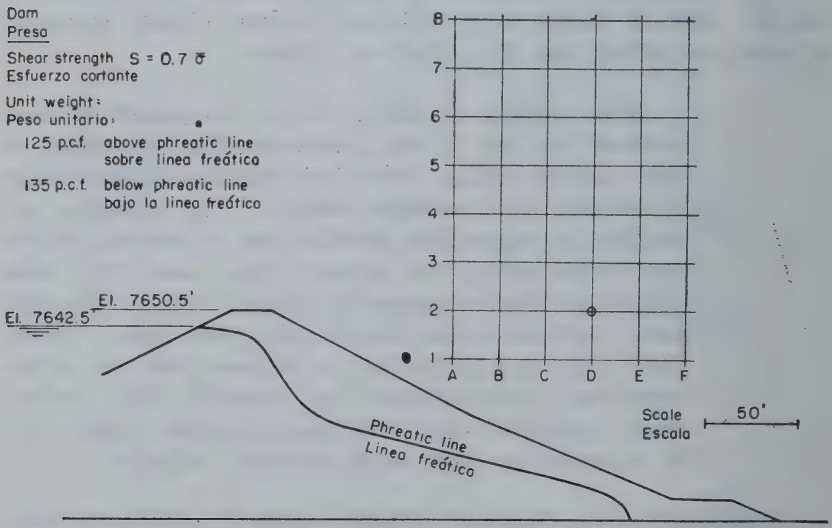
Dam
Presa
Shear strength S = 0.7 $\bar{\sigma}$
Esfuerzo cortante
Unit weight:
Peso unitario:
125 p.c.f. above phreatic line
sobre linea freática
135 p.c.f. below phreatic line
bajo la linea freática
El. 7650.5'
El. 7642.5'
8
7
6
5
4
3
2
1
A
B
C
D
E
F
Scale
Escala
50'
Phreatic line
Linea freática

Fig. 6 — Example 2 — Steady seepage.

Fig. 6 — Ejemplo 2 — Filtración uniforme.

Using selected centers and tangent circles, the Bishop method was used to locate the center of the circle with the minimum factor of safety. These results are shown in Figure

---

* This cross-section is typical for the downstream slope of Vermilion Dam (Terzaghi and Leps, 1960) with an assumed steady seepage condition.

8. It is of interest to note that the location of the center for the minimum factor of safety of 1.62 by the Bishop method corresponds generally with that of the minimum factor of safety of 1.43 by the ordinary method.

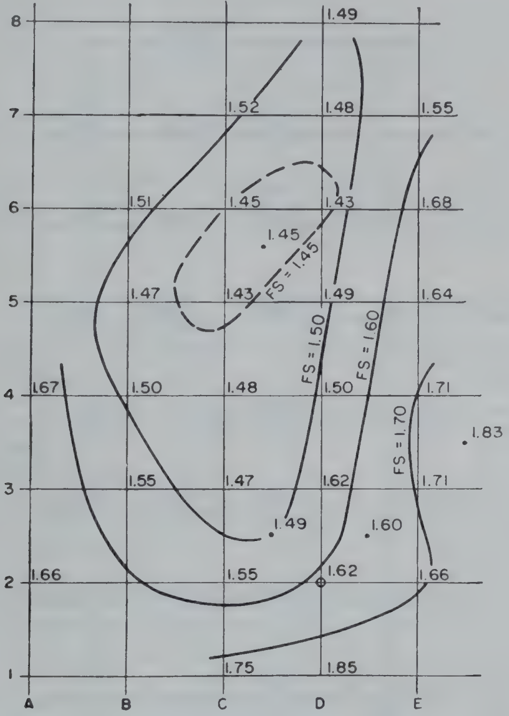

Fig. 7 — Factors of safety for tangent slip circles Ordinary Method — Example 2.

Fig. 7 — Factores de seguridad para círculos de resbalamiento tangencial — Método ordinario — Ejemplo 2.

The friction circle, upper and lower bound values of safety factor were also determined for this critical circle and these results are summarized in Table I.

EXAMPLE 3

A comparison has been made between the results of safety factor determined by the various methods of calculation for a particular arc. The section analyzed is shown in Figure 9 and represents the seepage in the upstream slope of an earth dam following drawdown. The factor of safety by the ordinary method came to 1.08, and by the Bishop method the value was 1.16. A summary of safety factors by all methods treated is presented in Table I.

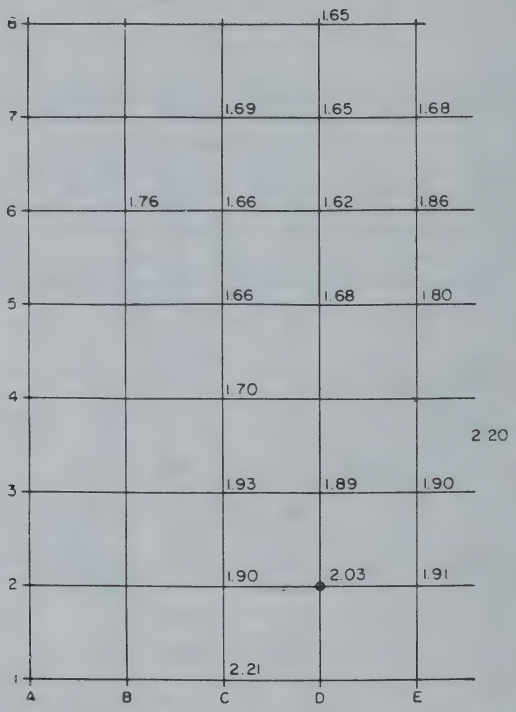

Fig. 8 — Factors of safety for tangent slip circles Bishop Method — Example 2.

Fig. 8 — Factores de seguridad para círculos de resbalamiento tangencial — Método de Bishop — Ejemplo 2.

EXAMPLE 4

A number of methods of analyzing the stability of slopes was examined by Sutherland (1951). He examined a section, which is shown in Figure 10, by the ordinary method of slices and found the location of the critical arc, shown also in that figure. Using this same arc Sutherland calculated factors of safety making a variety of assumptions with regard to the forces acting on the sides of the slices. These factors of safety are listed in Table III.

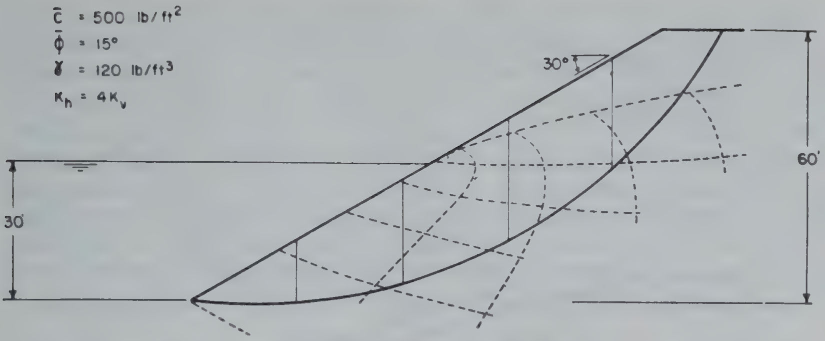

Fig. 9 — Example 3 — Seepage following drawdown.
Fig. 9 — Ejemplo 3 — Filtración luego de bajar el nivel del embalse.

TABLE III — Factors of safety for stability of slope in example 4

Description	Factor of Safety
(a) Ordinary method of slices	1.38
(b) Same as (a) with inclusion of horizontal pore pressures on sides of slices	1.39
(c) For the assumption that the combination of intergranular and pore pressures on the sides of the slices, are parallel for all slices	1.53
(d) For the assumption that the intergranular pressures on the sides of the slices are parallel for all slices, and using actual pore pressures on the sides of the slices	1.53
(e) For the assumption that the combination of intergranular and pore pressures on the sides of the slices act parallel to the arc in each slice	1.38
(f) Using a mathematical approach to determine actual line of action of combination of intergranular and pore pressures on sides of the slices	1.52

Recalculating the factor of safety for this arc using the Bishop method a value of 1.54 was obtained. Factors of safety by friction circle methods were also determined and these are summarized in Table I.

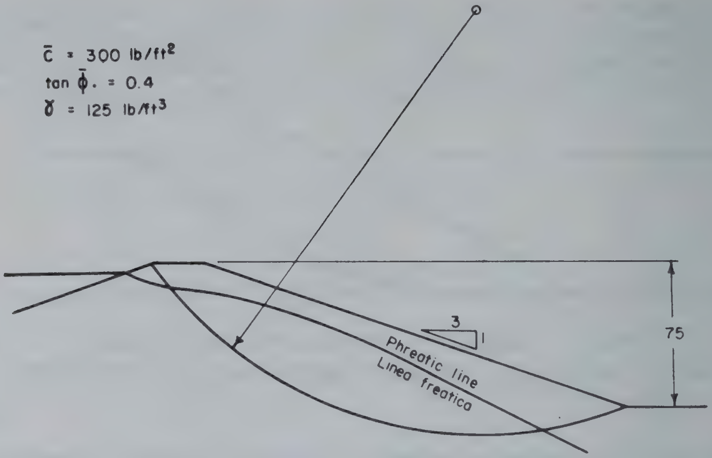

Fig. 10 — Example 4 — Steady seepage.

Fig. 10 — Ejemplo 4 — Filtración uniforme.

EXAMPLE 5

A comparison of the ordinary method of slices and the Bishop method for several potential slip circles was made for a sloping core rockfill dam in West Virginia. The situation which was examined was the upstream slope with full reservoir and steady state seepage, the section being shown in Figure 11. The five potential slip circles shown in this figure were carefully selected to pass through the minimum quantity of rockfill with as much of the arc as possible in the high pore pressure portion of the impervious core. The

Table IV — Factors of safety for stability of slope in example 5

Circle No.	Ordinary Method	Bishop Method
Circle I	2.54	3.00
Circle II	2.02	2.70
Circle III	1.66	2.45
Circle IV	1.13	1.90
Circle V	1.36	2.44

comparison of factors of safety by the two methods is shown in Tables I and IV. By plotting the factor of safety as a function of the distance between the dam center line and the point where the arc intersects the upstream slope, the relationship in Figure 12 is obtained. It is to be noted that both methods indicate a minimum factor of safety at about the same point. Also of interest is the observation that the difference in factors of safety by both methods increases with distance of the slip circle from the centerline of the dam. Both Bishop (1955) and Taylor (1948) have shown that this is to be expected because of the increase in the central angle.

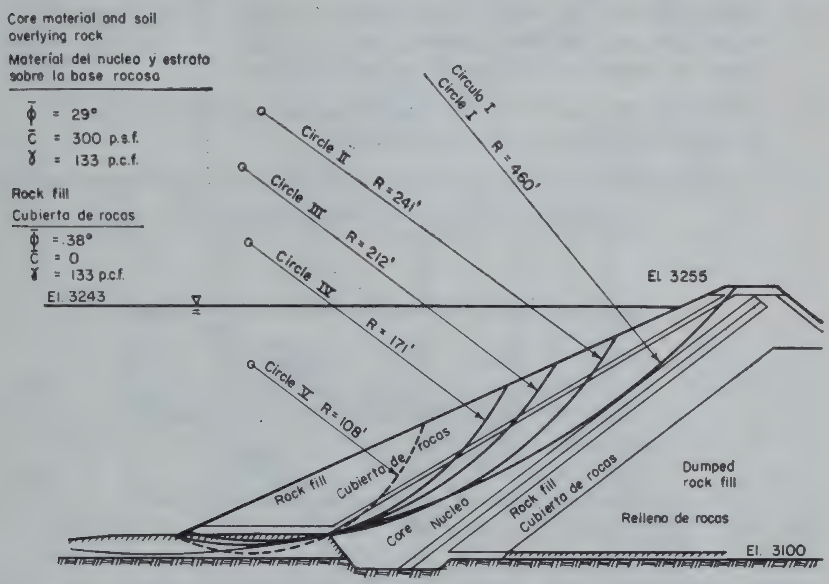
Core material and soil overlying rock
Material del nucleo y estrato sobre la base rocosa
$\bar{\phi}$ = 29°
$\bar{c}$ = 300 p.s.f.
γ = 133 p.c.f.
Rock fill
Cubierta de rocas
$\bar{\phi}$ = 38°
$\bar{c}$ = 0
γ = 133 p.c.f.
El. 3243
Circulo I
Circle I
R = 460'
Circle II
R = 241'
Circle III
R = 212'
Circle IV
R = 171'
Circle V
R = 108'
El 3255
Rock fill
Cubierta de rocas
Core
Nucleo
Rock fill
Cubierta de rocas
Dumped rock fill
Relleno de rocas
El. 3100

Fig. 11 — Example 5 — Steady seepage.

Fig. 11 — Ejemplo 5 — Filtración uniforme.

EXAMPLE 6 *

A comparison between the ordinary method of slices and Bishops method was carried out by LaCasta (1959) for the upstream slope following rapid drawdown of the section in Figure 13 which is shown with details of material properties. For the assumed failure surface shown in the figure, the ordinary method and Bishop's method yielded safety factors of 1.57 and 1.77 respectively. Some determinations were

---

* This cross-section is typical for the upstream slope of Hirfanli Dam in Turkey (Lowe and Karafiath, 1960).

also carried out by allowing for the forces on the sides of the slices in some reasonable manner. These results are summarized in Table V.

TABLE V — Factors of safety for stability of slope in example 6

Description	Factor of Safety
(a) Fellenius method	1.57
(b) Bishop method	1.77
(c) Considering that the forces on the sides of slices are applied in a direction bisecting the angle between the slope and the tangent to the slip circle	1.91
(d) Considering the forces on the sides of slices are parallel at an angle of 20° to horizontal	1.88

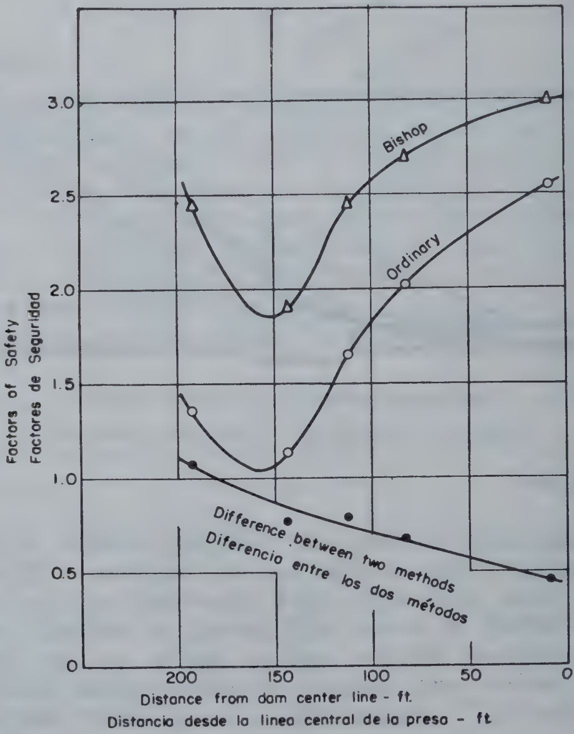

Fig. 12 — Variations in factors of safety — Example 5.
Fig. 12 — Variación en los factores de seguridad — Ejemplo 5.

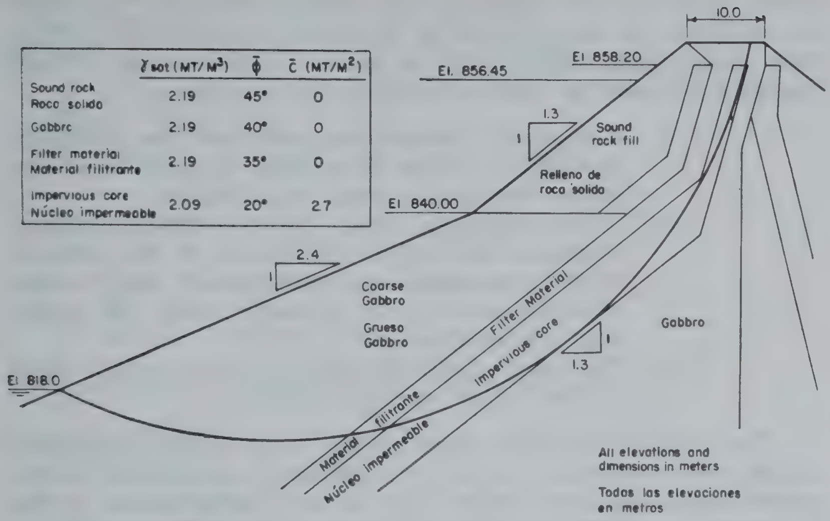

	γ_{sat} (MT/M^3)	$\bar{\phi}$	$\bar{c}$ (MT/M^2)
Sound rock Roca solida	2.19	45°	0
Gabbro	2.19	40°	0
Filter material Material filitrante	2.19	35°	0
Impervious core Núcleo impermeable	2.09	20°	2.7

10.0
El 858.20
El. 856.45
1.3
1
Sound rock fill
Relleno de roca solido
El 840.00
2.4
1
Coarse Gabbro
Grueso Gabbro
Filter Material
Impervious core
1
1.3
Gabbro
El 818.0
Material filitrante
Núcleo impermeable
All elevations and dimensions in meters
Todos los elevaciones en metros

Fig. 13 — Example 6 — Rapid drawdown.

Fig. 13 — Ejemplo 6 — Descenso rápido del nivel del embalse.

CLOSING COMMENTS

The ideas set forth in this paper of course apply only when use of a detailed mechanics procedure is justified by the circumstances of the slope stability problem. A detailed procedure is generally needed only when the stability of the slope is to be analyzed in terms of effective stress. In many problems, the shear resistance of the soil is not known well enough to warrant a detailed analysis. Even when a detailed mechanics procedure is justified, there are of course a number of practical problems which must be considered before selecting a method of analysis. One group of problems has to do with the ease of carrying out the calculations. Most engineers find that the numerical procedures of the slices methods are more convenient than the graphical friction circle approach. The simple Bishop method of slices does require one extra trial-and-error procedure. Another problem arises from the matter of selecting a suitable safety factor. Present practice with regard to minimum required safety factors is obviously tied in to the type of analysis that has been used in past practice. If the less conservative Bishop method were to be adopted, perhaps the minimum required safety factors should be increased.

These arguments must be set against the benefits of employing a sound method of analysis. For only one of the examples in this paper is there much more than a 10% difference between the Fellenius and Bishop solutions; however, the examples of Bishop and of Kjaernsli and Simons (1962) show much larger differences in some circumstances. These examples all lead to three important conclusions:

(a) The safety factor computed by the ordinary method of slices invariably is less than the lower bound for static equilibrium.
(b) The percentage error in the ordinary method increases as the central angle of the critical circle increases, and is especially large when stronger material is present along the upper portions of the arc.
(c) The simple Bishop method gives a result close to the "most correct solution".

The second of these conclusions is a telling argument against the continued use of the ordinary method of slices. Arguments based upon practicality become insignificant if the "practical" method is not only in error but the magnitude of the error varies greatly with the problem. The slight extra work involved in the Bishop method is trivial considering the size of the errors that can be avoided. Certainly, as the use of time-saving computers grows, it would be unfortunate to prepare programs based upon an erroneous procedure.

REFERENCES

Bishop, A. W. — "The Use of the Slip Circle in the Stability Analysis of Slopes", Geotechnique, Vol. V, 1955.

Bishop, A. W. and Morgenstern, N. — "Stability Coefficients for Earth Slopes", Geotechnique, Dec. 1960.

Bishop, A. W. — "The Stability of Earth Dams", Ph.D. Thesis, University of London, 1952.

Fellenius, W. — "Calculation of the Stability of Earth Dams", Trans. 2nd Congress on Large Dams, Vol. 4, Washington, D.C., 1936.

Fröhlich, O. K. — "General Theory of Stability of Slopes", Geotechnique, 1955.

Kjaernsli, B. and Simons, N. — "Stability Investigations of the North Bank of the Drammen River", Geotechnique, June 1962.

LaCasta-Sanchez, S. — "A Comparison of the Existing Methods of Studying the Stability of Earth Slopes", M.S. Thesis, Mass. Inst. of Tech., 1959.

Lowe, J. and Karafiath, L. — "Stability of Earth Dams upon Drawdown", Proc. 1st Pan American Conf. on Soil Mech. & Found. Eng., México, 1960.

May, D. R. — Part I, "Proposed Methods of Calculating the Stability of Earth Slopes", Question VII, Proc. 2nd Int. Conf. on Large Dams, Vol. IV, 1936.

Sutherland, W. R. — "Development of Improved Methods for Analyzing the Stability of Earth Slopes", M.S. Thesis, Mass. Inst. of Tech., 1951.

Taylor, D. W. — "Stability of Earth Slopes", Jr. of Boston Soc. of Civil Engrs., Vol. XXIV, No. 3, July 1937.
Taylor, D. W. — "Fundamentals of Soil Mechanics", 1948.
Taylor, D. W. — "Notes on the Slices Method", prepared as Jan. 1949 Report of the ASCE Subcommittee on Design of Earth Dams and Their Foundations.
Terzaghi, K. and Leps, T. — "Design and Performance of Vermilion Dam", Trans. ASCE, Vol. 125, Part I, 1960.

APPENDIX

LIST OF SYMBOLS

W = resultant of weight of free body

U = resultant of boundary pore water pressures

s_m = mobilized shear stress

s = available shear resistance

$\bar{c}$ = cohesion intercept in terms of effective stress

$\bar{\sigma}$ = normal effective stress

$\bar{\Phi}$ = angle of shearing resistance in terms of effective stress

F = safety factor

R_c = resultant of mobilized "cohesive" shear stress along failure arc

$\bar{N}$ = resultant of normal effective stresses along failure arc

$R\Phi$ = resultant of mobilized "frictional" shear stress along failure arc

r_c = radius to R_c

$r\Phi$ = radius to R_Φ

β = direction of R_Φ

r = radius of assumed failuure surface

Δ_x = width of slice

α = the angle between the vertical and the normal to the assumed failure arc for any slice

Φ_m = mobilized angle of shearing resistance in terms of effective stress

γ = unit weight of soil

N_i = normal force on arc for any slice

T_i = tangential force on arc for any slice

PIEZÔMETROS EM TRÊS MARIAS

OCTÁVIO M. ARÊAS

Engenheiro, Centrais Elétricas de Minas Gerais, S.A., Belo Horizonte, MG, Brasil.

SUMÁRIO

Neste trabalho são apresentados dados referentes a instalação, operação e manutenção dos piezômetros colocados na Barragem de Três Marias.

Uma interpretação parcial das pressões neutras indicadas por êsses piezômetros é tentativamente feita comparando-as com as pressões neutras teóricas calculadas segundo processo de Hilf [3].

Pelo fato, talvez sem precedentes na história da construção de barragem de terra, do emprêgo simultâneo de diversos tipos de piezômetros, de diferentes procedências, reputamos de grande utilidade, para o meio técnico em geral, a difusão da experiência adquirida e os resultados obtidos neste particular.

SUMMARY

Data related to the installation, operation and maintenance of the piezometers installed in the Três Marias Dam is presented herein.

A partial interpretation of the observed pore pressures is tentatively made by comparing them with estimated pore pressures determined by following Hilf's method of pore pressure computation.

In the Três Marias Dam several types of piezometers of different makes were used, a fact perhaps unprecedented in the history of earth dam construction control.

We deem it, therefore, worthy to set forth the results obtained and the experience gained in handling such an installation.

INTRODUÇÃO

O Aproveitamento de Três Marias (Fig. 1), situado no rio São Francisco, no Estado de Minas Gerais, Brasil, foi construído com as múltiplas finalidades de contrôle de enchentes, navegação, irrigação e energia elétrica, interessando a vasta região que é aquela banhada pelo grande rio.

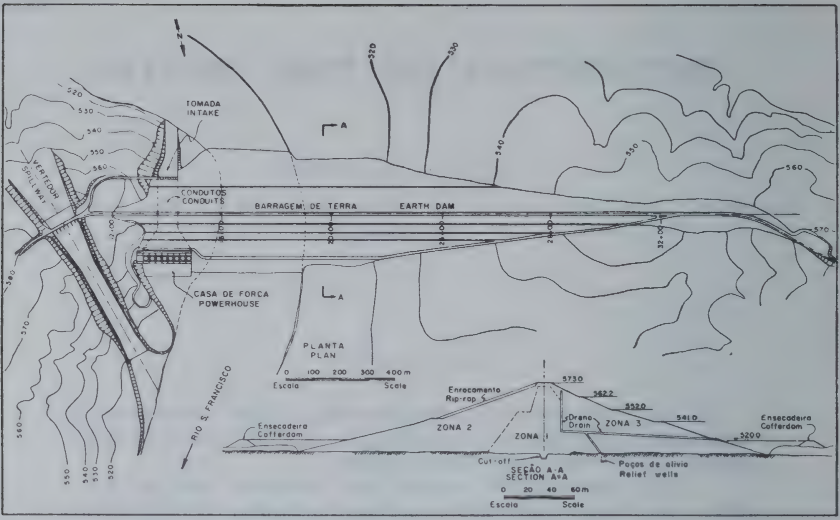
N
TOMADA
INTAKE
VERTEDOR
SPILLWAY
CONDUTOS
CONDUITS
BARRAGEM DE TERRA
EARTH DAM
CASA DE FORCA
POWERHOUSE
PLANTA
PLAN
0 100 200 300 400 m
Escala Scale
RIO S. FRANCISCO
A
A
520
530
540
550
560
570
580
320
330
340
350
360
370
12+00
16+00
20+00
24+00
28+00
32+00
5730
5622
5520
5410
5200
Enrocamento
Rip-rap
Ensecadeira
Cofferdam
ZONA 2
ZONA 1
Dreno
Drain
ZONA 3
Ensecadeira
Cofferdam
Cut-off
Poços de alívio
Relief wells
SEÇÃO A-A
SECTION A-A
0 20 40 60 m
Escala Scale

Fig. 1 — Aproveitamento de Três Marias — Planta Geral e Seção da Barragem de Terra.

Fig. 1 — Três Marias Project — General Plan and Earth Dam Section.

Para a sua realização, que se enquadra no plano geral de valorização do vale, a Comissão do Vale do São Francisco fêz um convênio com a Centrais Elétricas de Minas Gerais S.A. (CEMIG), segundo o qual esta emprêsa de capital misto foi encarregada como empreiteira geral para projeto e construção da Barragem, cabendo-lhe ainda o projeto e a construção, por conta própria, da Usina Elétrica de 520.000 kW localizada no pé da Barragem.

A obra foi iniciada em junho de 1957 com a construção do acampamento e ensecadeiras. Em março de 1958 começou-se a construção do atêrro sôbre parte do leito do rio prèviamente preparada. Em setembro de 1961 foi colocado o último metro cúbico de terra, sendo que, entretanto, o enchimento do reservatório já começara em janeiro de 1961 e atingira a cota 559.7, máxima daquele ano, em março.

A Barragem de Terra tem um comprimento de 2.700 m e se estende por tôda a seção, de ombreira a ombreira. A altura máxima é de 65 m e se verifica no trecho do rio.

Para um aproveitamento mais racional dos materiais disponíveis nas áreas de empréstimo investigadas, foi estabelecido um certo zoneamento na seção transversal do atêrro, segundo o qual os materiais mais argilosos, com LL igual ou superior a 40%, foram colocados na parte central, denominada Zona 1, e os menos argilosos foram colocados nos flancos, denominados Zona 2, a montante, e Zona 3, a jusante.

Duas principais áreas de empréstimo forneceram o material colocado no atêrro no período em que os piezômetros foram instalados. Da denominada Área de Empréstimo Sul, 90% das amostras ensaiadas possuem limites de liquidez entre 31% e 56%, com média igual a 42.3%, sendo que os valores se dispõem paralelamente e logo acima da linha "A" do diagrama de plasticidade do Prof. A. Casagrande; os limites de plasticidade têm valor médio de 23.7%. Da denominada Área de Empréstimo Norte, 90% dos valores do limite de liquidez se situam entre 27.5% e 49%, com média de 37.3%, e se situam também paralelamente e logo acima da linha "A" do diagrama de plasticidade; os limites de plasticidade têm para média o valor de 21.3%.

As áreas de empréstimo citadas eram constituídas principalmente de solo aluvionar fino, que se encontrava geralmente sobreposto a camadas contendo areia e pedregulhos, seguindo-se material residual decorrente da alteração de siltitos e arenitos da série Bambuí (siluriano).

A extração dos materiais dos empréstimos foi realizada com carregadeiras mecânicas ("loader"), deslocando-se aproximadamente segundo as curvas de nível. Isto fêz com que pouco ou nenhum misturamento se verificasse em profundidade e ocorresse carregamentos homogêneos numa mesma época, porém um tanto heterogêneos quando comparados os de épocas distantes.

A prévia investigação detalhada dos empréstimos e o contrôle efetivo da sua exploração, aliados ao rigoroso contrôle do lançamento e compactação no atêrro, permitiram, entretanto, a fiel observação das especificações no tocante à seleção dos materiais, grau de compactação e desvio da umidade.

A Zona 1, além de receber material mais argiloso, tinha, pelas especificações, uma faixa de umidade de compactação em tôrno da umidade ótima dada pelo ensaio de Proctor Normal, com a finalidade de tornar mais plástico o material e, assim, melhor se acomodar aos recalques diferenciais, ocasionados por variações relativamente bruscas de altura de barragem ou proximidade de fundações de compressibilidades diferentes.

Nas Zonas 2 e 3 o material foi compactado, em média, abaixo da umidade ótima.

Quando da instalação da maior parte dos piezômetros, as especificações em vigor limitavam a umidade para a Zona 1 entre 1% acima e 1% abaixo da umidade ótima; para as Zonas 2 e 3 a faixa de umidade se situava entre o ótimo e 3% abaixo. Nas estações chuvosas as faixas de umidade eram ampliadas de 1% em ambos os lados, com a finalidade de permitir o prosseguimento dos trabalhos naquele período, observadas, entretanto, certas restrições referentes ao número de camadas colocadas nestas condições.

Os coeficientes de permeabilidade do material compactado variam entre valores da ordem de 10^{-6} e 10^{-8} cm/seg.

PIEZÔMETROS EMPREGADOS EM TRÊS MARIAS — JUSTIFICATIVA, LOCALIZAÇÃO, INSTALAÇÃO E OPERAÇÃO

Sendo a Barragem pràticamente homogênea, constituída de materiais argilosos e siltosos de baixa permeabilidade, sujeita a um ritmo intenso de construção, mesmo nas estações chuvosas, presumiu-se que pressões neutras elevadas iriam se desenvolver no atêrro compactado, com poucas probabilidades de dissipação imediata.

Considerando que os processos de previsão de pressão neutra existentes não ofereciam ainda resultados seguros, nas primeiras análises de estabilidade procedidas para o talude de jusante, relativas às condições de fim de construção, empregaram-se os parâmetros de resistência dados pelos ensaios triaxiais rápidos em amostras indeformadas do atêrro experimental, realizado em Três Marias, conjugados com tensões totais.

Posteriormente, à luz dos primeiros ensaios de compactação, dos resultados dos ensaios de compressão triaxial em amostras indeformadas do atêrro da Barragem e, finalmente, das primeiras indicações dos piezômetros já instalados, a estabilidade dos taludes foi reexaminada para as mesmas condições de fim de construção.

Êsse reexame mostrou, com base nos resultados dos ensaios triaxiais lentos, que o fator de segurança seria inferior a um quando a pressão neutra ultrapassasse 36% da sobrecarga, admitida a coesão igual a zero.

Dessas considerações e da comparação com valores de pressão neutra observados em outras barragens homogêneas, estabeleceu-se, para Três Marias, que o valor máximo admissível para o coeficiente $\overline{B} = u/\sigma$ seria de 40%.

Assim pôsto, o emprêgo de piezômetros se fêz necessário para o contrôle efetivo das pressões neutras durante a construção.

E para maior confiança nos resultados gerais, decidiu-se utilizar diferentes tipos de piezômetro, de diferentes procedências, procurando-se destarte compensar os êrros sistemáticos e, ao mesmo tempo, estudar comparativamente o comportamento de cada tipo de aparelho sob diversos aspectos e condições.

Foram instalados na Barragem 104 piezômetros distribuídos em 4 seções transversais. Nas seções da Est. 18 + 00, Est. 20 + 00 e Est. 23 + 27 os piezômetros foram instalados aos pares, isto é, dois piezômetros em cada posição, afastados de aproximadamente 30 m no sentido longitudinal; na Est. 23 + 27 os piezômetros estão localizados na fundação, para efeito de observação e estudos da argila porosa situada naquela área; e na Est. 16 + 50 os diferentes tipos de piezômetros foram agrupados em três posições na seção transversal para comparação dos seus comportamentos sob as mesmas condições, sendo que em cada posição há um piezômetro de cada tipo. A Fig. 2 mostra a localização dos piezômetros em cada uma das seções onde êles foram instalados.

Dos quatro tipos de piezômetros empregados em Três Marias, três são hidráulicos e um é elétrico. Dos hidráulicos, um forma um sistema aberto e os outros dois formam um sistema fechado, saturado. A Fig. 3 mostra, esquemàticamente, os principais componentes dos piezômetros instalados em Três Marias.

O piezômetro elétrico é de fabricação alemã, da H. Maihak A.G., de Hamburgo, e compõe-se de um elemento transmissor, ou célula, constituído por um cilindro metálico encerrando o diafragma e as conexões elétricas, e na extremidade do qual é atarrachada a ponta porosa quando da instalação. A célula é ligada por meio de um cabo isolado a um receptor para doze elementos munido de um osciloscópio.

Funciona pelo princípio da corda vibrante: uma corda vibrante dentro da célula é ligada a um diafragma em contacto com a água intersticial através da ponta porosa; um simples impulso elétrico faz vibrar a corda, cuja freqüência depende da pressão sôbre o diafragma; esta vibração, transmitida ao receptor através do cabo elétrico, é comparada com a vibração de uma corda de freqüência variável instalada no receptor; da sintonização resulta um valor, lido no dial do receptor, que aplicado numa fórmula juntamente com a constante da célula permite determinar a pressão neutra.

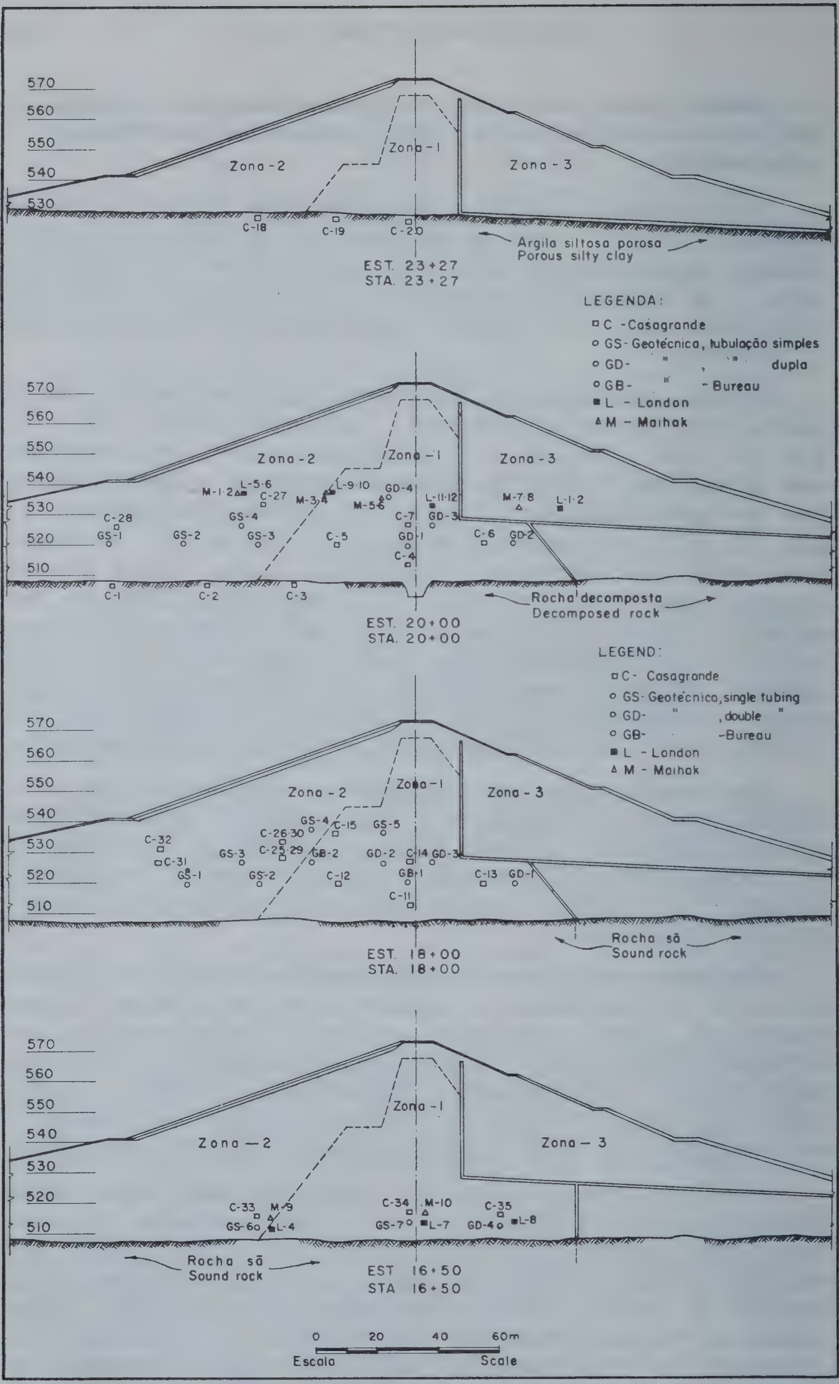
570
560
550
540
530
520
510
Zona - 1
Zona - 2
Zona - 3
C-18
C-19
C-20
Argila siltosa porosa
Porous silty clay
EST. 23+27
STA. 23+27
LEGENDA:
C - Casagrande
GS - Geotécnica, tubulação simples
GD - " , " dupla
GB - " - Bureau
L - London
M - Maihak
L-5·6
M-1·2
C-27
M-3·4
L-9·10
GD-4
M-5·6
L-11·12
M-7·8
L-1·2
C-28
GS-1
GS-2
GS-4
GS-3
C-5
C-7
GD-3
GD-1
C-6
GD-2
C-4
C-1
C-2
C-3
Rocha decomposta
Decomposed rock
EST. 20+00
STA. 20+00
LEGEND:
C - Casagrande
GS - Geotécnico, single tubing
GD - " , double "
GB - " -Bureau
L - London
M - Maihak
GS-4
C-15
GS-5
C-26·30
C-32
C-25·29
GS-3
GB-2
GD-2
C-14
GD-3
C-31
GS-1
GS-2
C-12
GB-1
C-13
GD-1
C-11
Rocha sã
Sound rock
EST. 18+00
STA. 18+00
C-33
M-9
C-34
M-10
C-35
GS-60
L-4
GS-7
L-7
GD-4
L-8
Rocha sã
Sound rock
EST 16+50
STA 16+50
0
20
40
60m
Escala
Scale

Fig. 2 — Localização dos Piezômetros nas Seções da Barragem.

Fig. 2 — Location of the Piezometers in the Dam Sections.

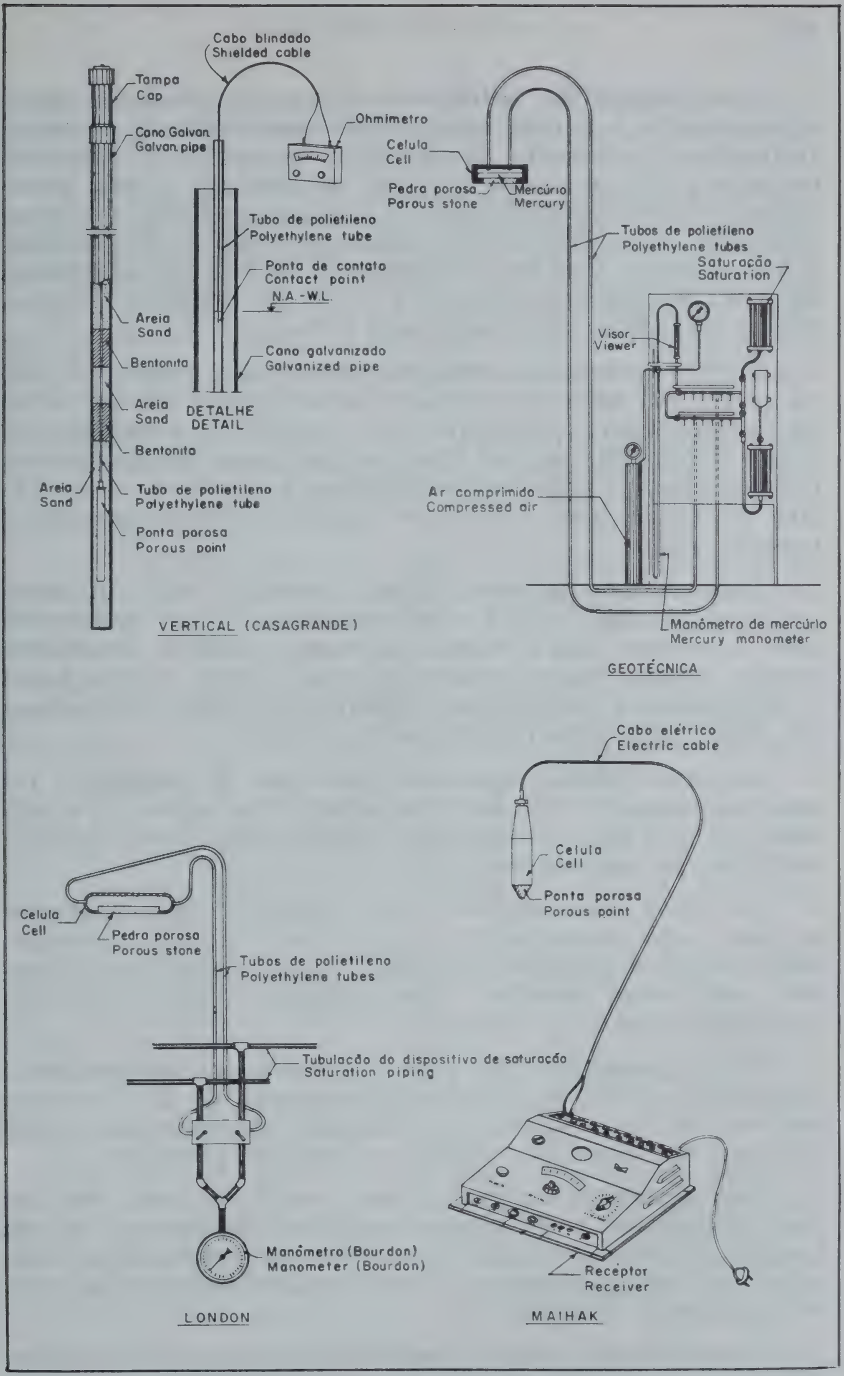
Tampa
Cap
Cano Galvan.
Galvan. pipe
Areia
Sand
Bentonita
Areia
Sand
Bentonita
Areia
Sand
Tubo de polietileno
Polyethylene tube
Ponta porosa
Porous point
Cabo blindado
Shielded cable
Ohmimetro
Tubo de polietileno
Polyethylene tube
Ponta de contato
Contact point
N.A.-W.L.
Cano galvanizado
Galvanized pipe
DETALHE
DETAIL
VERTICAL (CASAGRANDE)
Celula
Cell
Pedra porosa
Porous stone
Mercúrio
Mercury
Tubos de polietileno
Polyethylene tubes
Saturação
Saturation
Visor
Viewer
Ar comprimido
Compressed air
Manômetro de mercúrio
Mercury manometer
GEOTÉCNICA
Celula
Cell
Pedra porosa
Porous stone
Tubos de polietileno
Polyethylene tubes
Tubulacão do dispositivo de saturacão
Saturation piping
Manômetro (Bourdon)
Manometer (Bourdon)
LONDON
Cabo elétrico
Electric cable
Celula
Cell
Ponta porosa
Porous point
Receptor
Receiver
MAIHAK

Fig. 3 — Vista esquemática de cada tipo de piezômetro usado em Três Marias.

Fig. 3 — Schematic View of each Type of Piezometer Used in Três Marias.

Dos piezômetros hidráulicos, o tipo em sistema aberto (Casagrande) é o mais simples em constituição e operação, tratando-se meramente de um tubo piezométrico, composto de uma ponta porosa e um tubo de plástico. Como ponta porosa foi empregada uma vela comum de filtro doméstico com cêrca de 0,20 m de comprimento e 0,025 m de diâmetro, à qual é ligada uma das extremidades do tubo de polietileno, de 3/8" de diâmetro interno e 1/2" de diâmetro externo, que se estende verticalmente pelo atêrro.

Com o desenvolvimento da pressão nos vazios do solo na região em tôrno da célula, a água emigra do atêrro ou da fundação para dentro do tubo através da ponta porosa, e sobe dentro dêle até um nível tal que iguale aquela pressão. Conhecendo-se a cota da ponta porosa e a cota do nível d'água alcançado dentro do tubo tem-se automàticamente a pressão neutra.

Para medida do nível d'água dentro do tubo, utiliza-se um cabo blindado n.º 18 AWG conectado a um ohmímetro com capacidade até 1 milhão de ohms. Caso se desenvolva pressão neutra muito elevada, tal que o nível d'água tenda a ultrapassar a extremidade superior do tubo, utilizar-se-á um manômetro ligado diretamente ao tubo.

As extremidades superiores dos tubos de polietileno foram mantidas a 0,50 e até 3,50 m acima do atêrro, e, à medida que êste subia, iam sendo acrescentadas seções de tubo de 3,0 m de comprimento.

Os tubos piezométricos ficam dentro de revestimentos de cano galvanizado de 2" de diâmetro. Quando aconteceu serem os tubos dobrados e levados a posições mais convenientes, onde foram reunidos numa prumada única, utilizou-se revestimento de 4" de diâmetro.

Para a instalação das pontas porosas nas posições mais profundas recorreu-se à sonda à percussão de 2½" para a abertura do furo; quando da instalação em cotas mais altas, próximas da superfície, utilizou-se trado-cavadeira de 4".

Dos piezômetros hidrálicos em circuito fechado, um dos tipos empregados é de fabricação da Soil Mechanics Ltd., de Londres. Para referência a êste tipo de piezômetro, doravante, no texto e desenhos, êle será denominado simplesmente de piezômetro "London".

Consta de um estôjo de polietileno com a pedra porosa, através da qual é transmitida a pressão neutra, e no qual se liga uma tubulação dupla de polietileno que se estende até o painel de medição, onde cada ramo dessa tubulação é ligado a um manômetro por meio de um "Y" de latão provido de torneiras que permitem se faça a leitura separadamente em cada ramo.

A tubulação com dois ramos facilita a saturação do sistema quando da instalação das células, utilizando-se para isto de um painel apropriado fornecido pelo fabricante. Para essa saturação do sistema usa-se água desaerada, que pode ser água destilada, fervida ou água comum submetida a vácuo no próprio painel de saturação. Esta providência tem por finalidade evitar o aparecimento de bolhas de ar por efeito de variações de temperatura e/ou pressão.

Quando das leituras, os dois ramos deverão indicar valores proximamente iguais; quando tal não acontece, o sistema deve ser verificado, pois provàvelmente há vazamentos ou presença de ar no sistema.

Para a instalação das células e tubulações abriram-se valetas de 0,80 × 0,80 m estendendo-se das guaritas dos painéis até os locais das células; estas foram colocadas tendo a face com a pedra porosa voltada para baixo.

Tanto os piezômetros London quanto os Maihak chegaram na Obra com grande atraso devido a dificuldades de importação, razão porque só foi possível sua instalação acima da cota 533.0 nas Zonas 1 e 2 e, na Zona 3, acima da cota 531.0, mantido neste último caso um afastamento mínimo de 3,0 m do dreno horizontal de areia. Na Est. 16 + 50, seção do fechamento da Barragem, foi possível a instalação em cotas mais baixas porque esta parte da Barragem foi construída mais tarde.

O outro tipo de piezômetros hidráulicos compreende aquêles fabricados pela Geotécnica S.A., de São Paulo. Foram empregados em Três Marias os modelos de tubulação simples e de tubulação dupla, sendo que êstes compreendem o modêlo com célula semelhante aquela empregada pelo Bureau of Reclamation, dos Estados Unidos, e o modêlo Geotécnica pròpriamente dito.

Com exceção do modêlo "Bureau", os demais possuem na célula uma espécie de "tampa" de mercúrio que, situada sôbre a pedra porosa, impede a migração de água da tubulação para o atêrro ou fundação, e com isso se procura evitar a saturação prematura da região em tôrno de célula com água oriunda do piezômetro.

Para a instalação das células foram abertos poços de mais ou menos 1,40 m × 1,40 m nos locais escolhidos prèviamente. Uma sapata cortante especial abria uma cavidade circular no fundo do poço com diâmetro aproximadamente igual ao da célula; com um soquete especial comprimia-se ligeiramente o fundo da cavidade, colocando-se em seguida a célula com a face porosa voltada para baixo.

A tubulação de polietileno que liga a célula ao painel de leitura foi estendida dentro de uma valeta, como se pode ver na Fig. 4, em muitos casos juntamente com as tubulações dos piezômetros London e com os cabos dos Maihak.

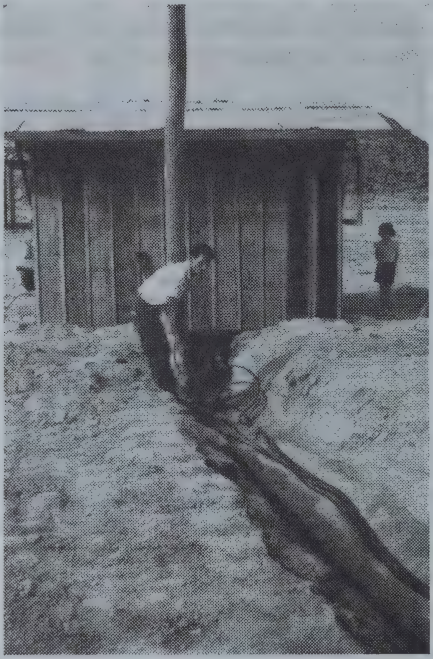

Fig. 4 — Guarita provisória dos painéis de leitura dos piezômetros. Aspecto dos tubos nas valetas.

Fig. 4 — Temporary Shack for Sheltering Reading Panels. Piezometer Tubes Laid in the Trench.

Um único manômetro de mercúrio, situado no painel de leitura, serve para a leitura de todos os piezômetros através de suas torneiras individuais, que, abertas, põem os piezômetros em ligação com o circuito de medição. A pressão transmitida pelo piezômetro é equilibrada por ar comprimido manobrado através de uma torneira especial e controlada num visor de vidro, estando o ar comprimido em contacto, na outra extremidade, com a coluna de mercúrio.

Os piezômetros de tubulação dupla têm uma torneira em cada ramo, para que sejam feitas separadamente as leituras.

Um conjunto especial colocado no mesmo painel serve para a saturação do sistema. Como acontece com os piezômetros London, aqui também se emprega água desaerada, e pelos mesmos motivos.

As leituras em todos os piezômetros instalados na Barragem foram feitas semanalmente durante a construção; após o término desta, foram feitas quinzenalmente. Os resultados das medidas foram anotados em fôlhas especiais. Além disso, foram também os resultados transferidos para um gráfico onde o tempo figura no eixo das abscissas e no eixo das ordenadas figuram a sobrecarga, a pressão neutra e a relação $\overline{B}$ entre a pressão neutra e a sobrecarga.

Os painéis de leitura dos piezômetros Geotécnica e London e os terminais dos Maihak foram instalados em duas guaritas situadas no pé do atêrro, a jusante, uma na Est. 18 + 00 e a outra na Est. 20 + 00, sendo que as tubulações e cabos elétricos foram reunidos em um número mínimo possível de valetas, colocados não totalmente esticados mas com certa ondulação, de modo a terem folga no comprimento com que possam se adaptar aos recalques do atêrro e da fundação. Estas valetas, depois de lançados os cabos e tubos, foram cuidadosamente reenchidas e compactadas manualmente.

Em resumo foram instalados na Barragem 43 piezômetros do tipo Casagrande, 39 do tipo Geotécnica, 12 do tipo London e 10 do tipo Maihak.

DIFICULDADES DE INSTALAÇÃO, OPERAÇÃO E MANUTENÇÃO DOS PIEZÔMETROS

As observações que se seguem têm caráter estritamente informativo e objetivam orientar aquêles que vierem a empregar piezômetros em suas obras.

Comecemos pelos piezômetros verticais. Êstes piezômetros, de instalação e operação fáceis, apresentam sérios problemas de manutenção, pois expostas que ficam as extremidades dos tubos acima da superfície do atêrro, estão elas sujeitas a freqüentes danificações pelo equipamento de terraplenagem, mormente em obra construída em ritmo intenso como no caso de Três Marias.

Apesar da sinalização e de recomendações freqüentes aos operadores de equipamento, foram comuns os acidentes com êsses instrumentos. Êsses abalroamentos não só causavam prejuízo pela destruição de revestimentos e tubos, como exigiam trabalhos, às vêzes demorados, de reparo, e podem ser apontados como a causa principal das obstruções que muitos piezômetros apresentaram à passagem do cabo elétrico utilizado nas leituras, tais obstruções sendo atribuíveis, nestes casos, a torrões de argila ou mesmo pedregulhos que teriam entrado no tubo de polietileno quando do acidente.

Essas obstruções, que se verificaram numa freqüência um tanto elevada, são atribuídas também ao dobramento e ao encaracolamento do tubo no revestimento por ação de seu pêso próprio: apesar de leves e de certa rigidez que possuem devido à sua parede relativamente espêssa, é possível que lentamente e plàsticamente êles se deformem por flambagem ou se enrolem segundo uma espiral dentro do revestimento.

Inicialmente, colocava-se areia para encher o vazio entre o tubo e o revestimento, porém tinha o inconveniente de transformar o tubo e o revestimento num conjunto rígido, ocorrendo fatalmente a ruptura do tubo quando dos abalroamentos.

Outro fato importante, e que só se tornou evidente mais tarde, é a alteração do polietileno quando exposto prolongadamente ao tempo sêco, que em Três Marias ocorre no inverno quando as chuvas estão completamente ausentes, o céu é freqüentemente claro e a umidade relativa do ar atinge a média de 45%. Esta ação dos agentes climáticos sôbre o polietileno sòmente foi percebida quando os tubos de três piezômetros se romperam à profundidade durante as operações de leitura. Verificou-se que nos locais de ruptura os tubos se apresentavam amarelecidos, mais rígidos e quebradiços. Medindo-se a parte que se desprendeu, constatou-se que as tubulações romperam-se entre as cotas 541,0 e 543,0; esta coincidência aliada ao fato de ter ficado o atêrro, além da Est. 17 + 00, paralisado na cota 540,0 a 541,0 durante 9 meses, enquanto se concentrava tôda a atividade no desvio do rio para dentro dos condutos e na construção da seção de fechamento, mostra claramente que os tubos se romperam justamente naquele trecho que ficou por muito tempo exposto, fora dos revestimentos.

A Fig. 5 mostra a foto da seção de um dos tubos que se partiram, podendo-se ver a diferença de côr entre os tubos nôvo e velho e o caráter quebradiço do tubo mais antigo.

Os piezômetros Maihak requerem alguns cuidados especiais na instalação, mormente quando da colocação da ponta porosa na célula, pois, depois de atarrachada no cilindro metálico, ficará a uma distância de sòmente 0,05 mm do diafragma, exigindo por isso a montagem em lugar limpo, isento de poeira.

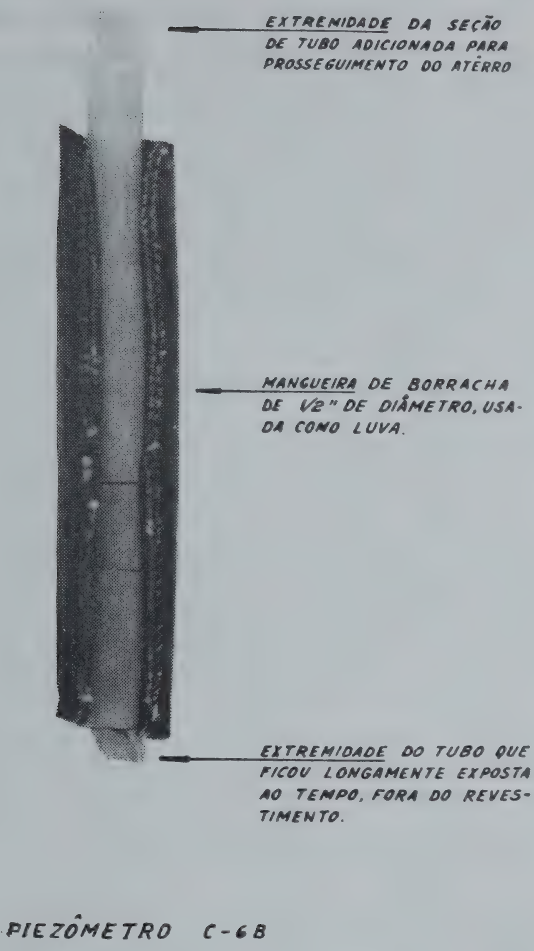
EXTREMIDADE DA SEÇÃO DE TUBO ADICIONADA PARA PROSSEGUIMENTO DO ATÊRRO
MANGUEIRA DE BORRACHA DE 1/2" DE DIÂMETRO, USADA COMO LUVA.
EXTREMIDADE DO TUBO QUE FICOU LONGAMENTE EXPOSTA AO TEMPO, FORA DO REVESTIMENTO.
PIEZÔMETRO C-6B

Fig. 5 — Tubo rompido devido à alteração do polietileno.

Fig. 5 — Piezometer Tube that Broke Due to Weathering of the Polyethylene.

Os cabos elétricos devem ser encomendados em comprimentos prèviamente estabelecidos, evitando-se a sua emenda no campo, para a qual é exigido um conector especial fornecido pela Maihak A.G.

Além disso, as medidas podem estar sujeitas a interferências por variações de voltagem e ciclagem em locais onde não haja bom suprimento de energia elétrica; entretanto, de acôrdo com informações do fabricante, são permissíveis variações na voltagem até ±10% e na freqüência até ±20%.

Outro ponto que merece atenção é a capacidade de cada transmissor (célula), pois sendo a medida do valor da pressão neutra função da constante do transmissor é necessário certo planejamento na distribuição das células no atêrro ou na fundação, escolhendo-se para os pontos onde são esperadas maiores pressões aquelas células que têm maior constante, sem o que corre-se o risco de ficar impossibilitado de medir além de um determinado valor, a não ser que se mude o "zero" do receptor, o que pode ser feito de acôrdo com instruções especiais do fabricante e dentro de certos limites.

Os piezômetros Geotécnica e London, semelhantes na estrutura geral, não apresentam maiores problemas de instalação, a não ser a abertura das valetas para as tubulações e os poços para as células, que causam alterações no tráfego do equipamento de terraplenagem, tendo-se, em Três Marias, deixado êsse trabalho para ser feito nos domingos ou feriados.

As tubulações devem ter o mínimo de emendas, pois trabalhando permanentemente sob pressão, devem estar livres de qualquer possibilidade de vazamento. A propósito, quando do lançamento das tubulações, devem as valetas ter profundidade tal que ponha os tubos a salvo de serem atingidos por caçambas de escavadeiras, escarificadores, etc.

Os painéis de leitura, devido ao grande número de torneiras e conexões, devem merecer verificação freqüente, providenciando-se a mudança imediata das peças defeituosas, principalmente aquelas que parecem apresentar desgaste prematuro ou possuem deficiência de ajustagem.

De um modo geral, pode-se admitir que quanto mais simples os piezômetros em construção, instalação e operação melhores resultados serão obtidos, pois eliminando-se ao máximo as possibilidades de mascaramento das medidas de pressão neutra, poder-se-á pesquisar, sem outras preocupações, as razões de ordem eminentemente científica que expliquem as discrepâncias entre as pressões neutras realmente desenvolvidas e as previstas.

INTERPRETAÇÃO PRELIMINAR DAS PRESSÕES NEUTRAS REGISTRADAS

Os piezômetros indicaram, de um modo geral, valôres de pressão neutra que, à primeira vista, pareceram um tanto incoerentes entre si, em alguns casos desviados daquilo que era de se esperar com base nas previsões iniciais e nos valores registrados em outras barragens.

Numa tentativa preliminar de se procurar explicações para os valores observados, foi feita inicialmente uma seleção dos piezômetros com base no histórico de cada um desde a sua instalação, levando-se em conta as interrupções por acidente, vazamentos, perdas repentinas de pressão, etc.; em seguida, foi feita para cada piezômetro ou grupo de piezômetros localizados relativamente próximos, dentre os selecionados, uma estimativa do desenvolvimento da pressão neutra em função da sobrecarga direta e das condições de colocação do atêrro, valendo-se para isso dos dados de campo obtidos no contrôle da compactação, isto é, dos valores de densidade e umidade de campo, e das características de compressibilidade do material, evidenciadas nos ensaios de adensamento realizados em corpos de prova de amostras indeformadas do atêrro compactado.

Em Três Marias foi empregado o Método Rápido, de Hilf, no contrôle da compactação. Êste método, dada a brevidade com que se conseguem os desvios da umidade e o grau de compactação sem determinação da umidade, permitiu uma freqüência média razoàvelmente grande das determinações de campo, da ordem de uma determinação para cada 500 a 600 metros cúbicos de material compactado, e desta forma, reunir elementos suficientes para calcular as condições médias de colocação do atêrro em tôrno da célula.

O método de Hilf possibilita ainda um contrôle mais rigoroso das condições de compactação do atêrro, pela diminuição da dispersão em relação às condições ótimas, do que os métodos de contrôle clàssicamente usados, desde o método de inspeção visual e táctil até o da família de curvas[6]. Porém, embora podendo-se manter os desvios de umidade dentro de uma faixa estreita, a Fig. 6 mostra que o grau de saturação nas condições ótimas varia de 82% a 91%.

Sendo a pressão neutra função do grau de saturação, conclui-se que, apesar do contrôle rigoroso, sua estimativa é difícil, pois podendo-se admitir homogeneidade no material em tôrno da célula num mesmo plano, haverá, no entanto, heterogeneidade no sentido vertical, isto é, as camadas abaixo e acima do plano da célula poderão ser constituídas de materiais em condições diferentes, correspondentes a diferentes zonas do empréstimo, e portanto, podendo apresentar heterogeneidade nos graus de saturação embora possam apresentar homogeneidade nos desvios da umidade em relação ao ótimo.

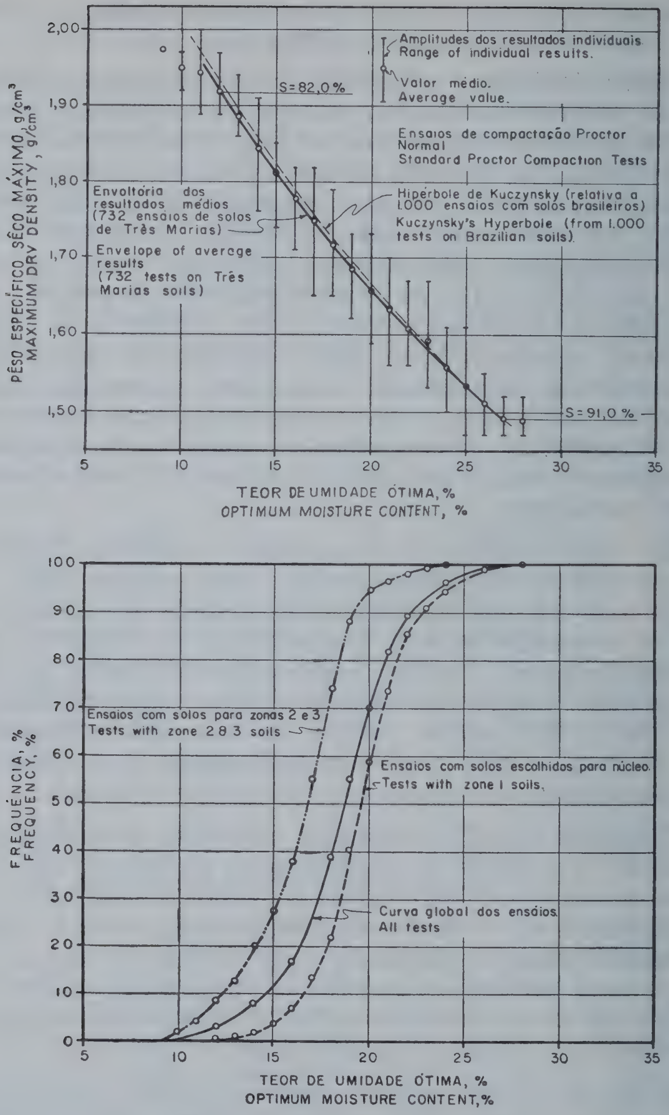

Fig. 6 — Materiais do Empréstimo Sul — Resultados globais dos ensaios de compactação de laboratório [7].

Fig. 6 — South Borrow Pit — Overall Results of Laboratory Compaction Tests [7].

Além disso, a Fig. 6 mostra também que, mesmo nas condições ótimas, há uma grande dispersão em tôrno dos valores médios das densidades sêcas. Desta forma, é de se esperar que as pressões neutras realmente desenvolvidas não sigam muito de perto as previsões e apresentem diferenças sensíveis entre pontos do atêrro relativamente proximos entre si.

Outrossim, as simplificações necessàriamente introduzidas no cálculo das pressões neutras previstas também concorrem para o afastamento entre pressões neutras teóricas e reais.

As curvas teóricas de pressão neutra a se desenvolverem durante a construção foram calculadas segundo os processos desenvolvidos por Brahtz e Hilf com referência ao adensamento de solos insaturados e relações ar-água nos vazios do solo [2, 3].

Alguns dos conceitos físicos introduzidos por Terzaghi na teoria clássica do adensamento são admitidos na aplicação dos processos de Brahtz e Hilf [2, 3].

A equação desenvolvida por Hilf e utilizada nesse cálculo dá a pressão neutra em função das condições iniciais do material (logo após a compactação) e das características de compressibilidade dêsse mesmo material:

$$u = \frac{P_a \triangle}{V_a + h V_w - \triangle}$$

onde:

P_a — é a pressão atmosférica, corrigida para a altitude do lugar; para Três Marias tomou-se uma cota média de 525 m acima do nível do mar, resultando $P_a = 0{,}976$ kg/cm^2;

$\triangle$ — é a deformação vertical do solo, expressa em percentagem;

V_a — é o volume inicial de ar livre nos vazios, expresso em percentagem do volume total inicial do solo do atêrro;

V_w — é o volume d'água no solo, em percentagem do volume total inicial do solo;

h — é a constante de solubilidade do ar na água, que para as condições de temperatura e pressão abrangidas por êste estudo pode ser tomada igual a 0,02.

A fórmula acima é aplicável até o ponto em que a compressão do solo iguale o volume inicial de ar livre; neste ponto $\triangle = V_a$ e o solo se encontra completamente saturado, de modo que daí em diante todo aumento de sobrecarga provoca um aumento igual da pressão neutra, admitido que não haja drenagem. A pressão neutra neste ponto em que a saturação é atingida é:

$$u_s = \frac{P_a V_a}{h V_w}$$

Considerando que a Barragem de Terra de Três Marias é homogênea, constituída de materiais de baixa permeabilidade, é de se esperar que pouca ou nenhuma dissipação de pressão se dará por drenagem da água intersticial durante o relativamente curto período de construção, a não ser nas vizinhanças do dreno de areia. Assim, neste caso, a suposição de não haver drenagem durante o crescimento da sobrecarga, admitida na dedução da pressão neutra, parece não ter contra-indicação.

A suposição de adensamento unidimensional, isto é, deformação por ação da sobrecarga sòmente no sentido vertical, admitido perfeito confinamento lateral, parece não introduzir êrros significativos, mormente para as zonas centrais da barragem [2].

Com exceção dos verticais, que não estão capacitados para tal, os piezômetros de um modo geral acusaram pressões negativas para sobrecargas pequenas. Essa pressão negativa inicial é atribuível à tensão capilar que se desenvolveria nos vazios microscópicos do solo pela tensão superficial da água nêles existente.

Isto importa em admitir que a superfície de contacto entre o ar e água dos vazios não é uma superfície plana, mas uma superfície curva caracterizada pelo menisco típico dos fenômenos capilares, e que, devido à tensão superficial, a água estará sob uma pressão menor do que a do ar, sendo a diferença igual a tensão desenvolvida pelo menisco, isto é:

$$u_c = \frac{2\,T_s}{r}$$

sendo:

T_s = tensão superficial da água = 0,073 g/cm a 20°C;

r = raio de curvatura do menisco.

Considerando-se que os solos usados na Zona 1 têm 20% a 40% de argila e os das Zonas 2 e 3 têm de 0% a 30% de argila, admitiu-se que as dimensões iniciais dos vazios sejam da ordem de 0,005 mm. Tomando-se êste valor para diâmetro do menisco, teremos que a pressão capilar inicial é da ordem de —0,6 kg/cm^2.

Foi observado[3], entretanto, que a pressão capilar cresce, em valor relativo, com a compressão do solo e o aumento da saturação, de modo que as curvas teóricas, a convencional (calculada segundo a fórmula apresentada) e a corrigida da pressão capilar, tenderão a se aproximar à medida que cresce a sobrecarga e o grau de saturação.

Para efeito de comparação com as pressões observadas, no presente trabalho as curvas teóricas de pressão neutra versus pressão total foram corrigidas do valor da capilaridade, admitindo igual a —0,6 kg/cm^2 para pressão efetiva igual a zero e crescendo até zero quando a compressão atinge o valor correspondente a completa saturação do solo.

De acôrdo com essas considerações foi feito o cálculo das pressões neutras teóricas, a partir da deformação específica $\triangle$ do solo e aplicando-se a fórmula mencionada linhas atrás. Os valores calculados foram marcados contra valores correspondentes da tensão total σ, calculada a partir do mesmo $\triangle$ e com ajuda das curvas de adensamento do material compactado.

Do total de 104 piezômetros instalados na Barragem de Três Marias, 74 foram selecionados para esta comparação entre as pressões neutras realmente desenvolvidas e as previstas, levando-se em conta para esta seleção o histórico do piezômetro, como já mencionado linhas atrás.

Dos piezômetros mencionados, 30 indicaram valores da pressão neutra que se colocam pràticamente ao longo da curva teórica de u versus σ ou se colocam razoàvelmente próximos dela. Os demais, ou estavam suficientemente próximos do dreno de areia, e neste caso a pressão neutra logo se dissipava, como aconteceu com os piezômetros L-1, L-2, M-7 e M-8 (Est. 20 + 00) e GD-1 (Est. 18 + 00), ou indicaram pressões neutras que se colocam numa curva mais baixa, como é o caso dos piezômetros GS-3, C-25 e C-29 (Est. 18 + 00) situados mais exteriormente na Zona 2, parecendo mostrar que a pressão neutra nessa região da Barragem não é função da sobrecarga direta, ou, finalmente, não reagiram ao aumento da sobrecarga, como é o caso dos piezômetros M-1, M-2, M-3, M-4, L-5, L-6, L-9 e L-10.

A Fig. 7 mostra os valores registrados por alguns dêstes piezômetros.

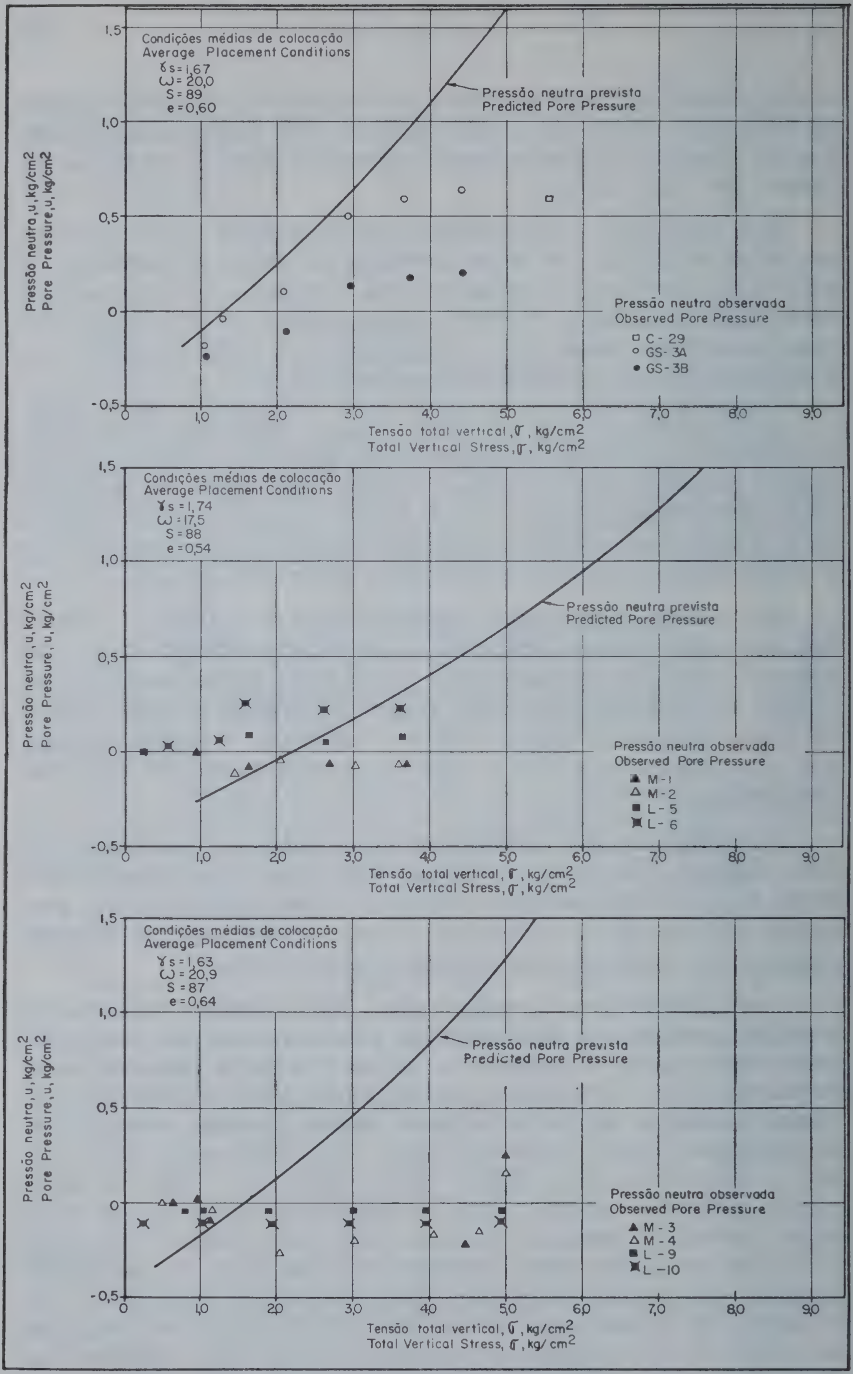

Fig. 7 — Comparação entre pressões neutras previstas e observadas — Piezômetros laterais.

Fig. 7 — Comparison of Predicted and Observed Pore Pressures — Piezometers in the Outer Upstream Portion of Dam Section.

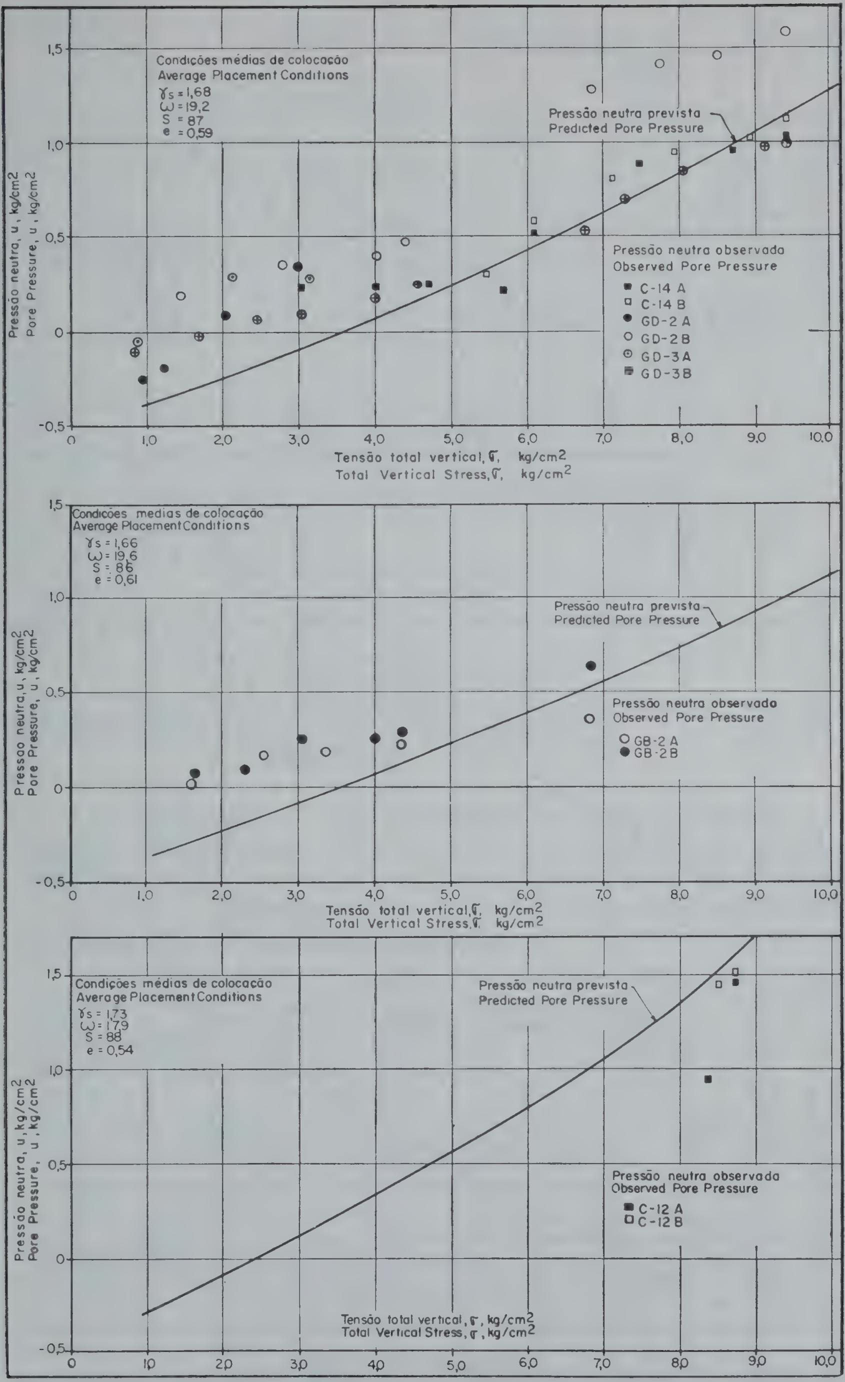

Fig. 8 — Comparação entre pressões neutras previstas e observadas — Piezômetros centrais, Est. 18 + 00.

Fig. 8 — Comparison of Predicted and Observed Pore Pressures — Piezometers in the Central Zone, Est. 18 + 00.

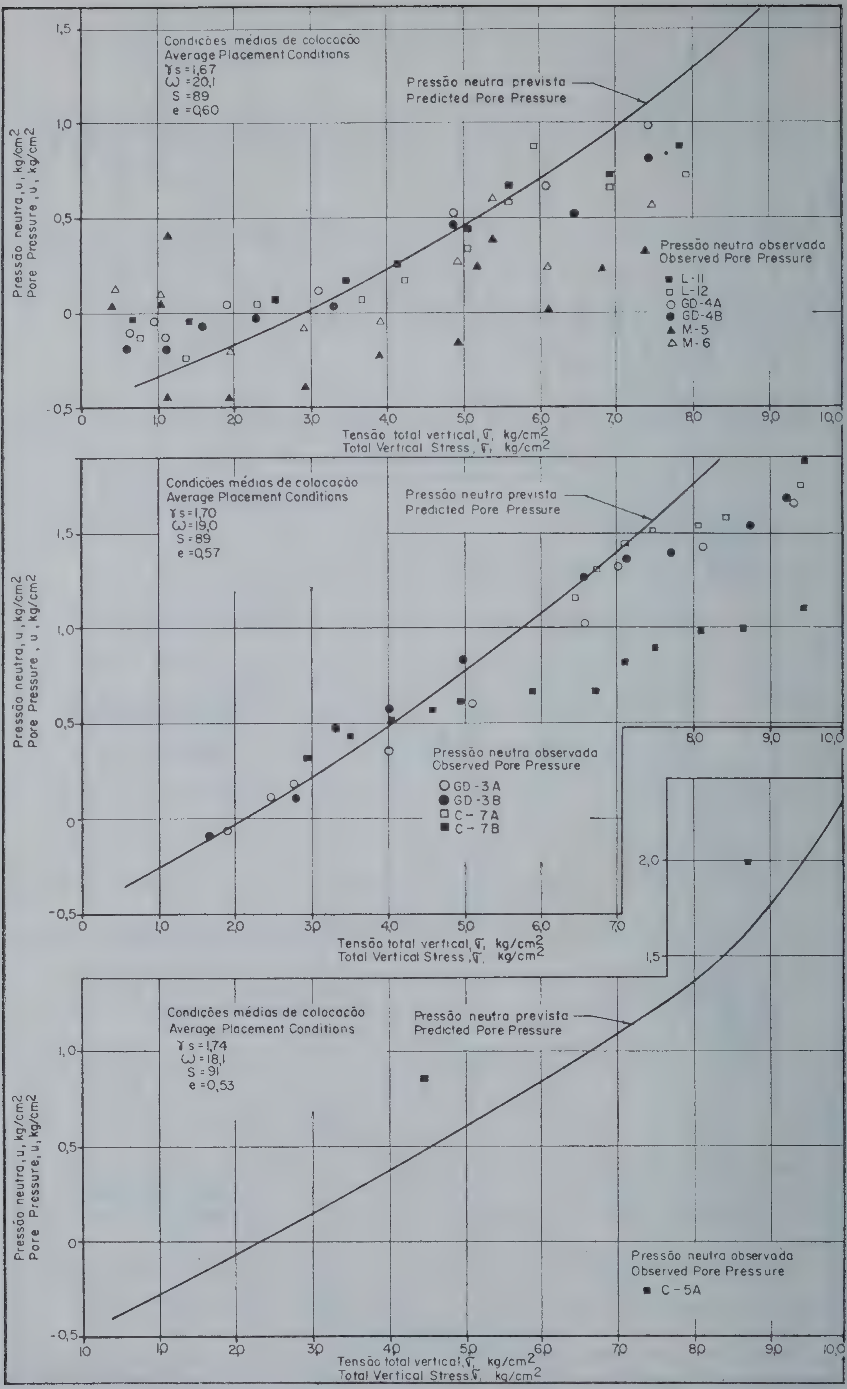

Fig. 9 — Comparação entre pressões neutras previstas e observadas — Piezômetros centrais, Est. 20 + 00.

Fig. 9 — Comparison of Predicted and Observed Pore Pressures — Piezometers in the Central Zone, Est. 20 + 00.

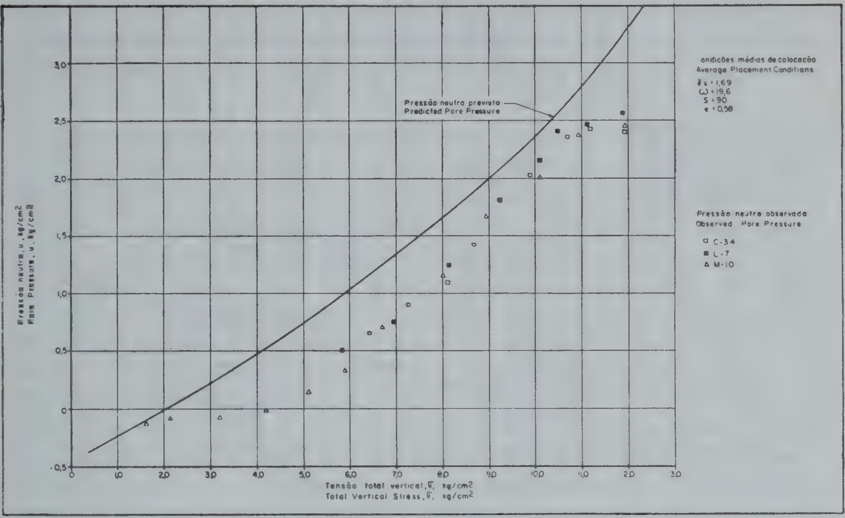

Fig. 10 — Comparação entre pressões neutras previstas e observadas — Piezômetros centrais, Est. 16 + 50.

Fig. 10 — Comparison of Predicted and Observed Pore Pressures — Piezometers in the Central Zone, Est. 16 + 50.

Os piezômetros cujas indicações de pressão neutra melhor se identificaram com as curvas teóricas foram aquêles situados na parte central do atêrro, como mostram as Figs. 8, 9, 10 e 11, podendo-se observar que os desvios dos valores medidos em relação à curva teórica são pouco significativos.

A influência das condições médias de colocação do material no atêrro é ressaltada quando se comparam os valores dos piezômetros GB-1 e C-11 (Est. 18 + 00), Fig. 11. Inicialmente fôra calculada uma única curva teórica para êstes piezômetros, por economia de tempo e trabalho, e admitindo-se que naquela região da Barragem pouca variação houvera nas condições de colocação do atêrro. Em vista das distintas tendências mostradas pelos valores medidos de um e outro piezômetro, resolveu-se calcular separadamente para cada posição, quando, então, tornou-se evidente a diferença sensível entre as umidades médias de colocação e, em conseqüência, nos graus de saturação com reflexos acentuados no desenvolvimento das pressões neutras.

Era de se esperar que situação semelhante ocorresse entre os piezômetros GD-1 e C-4 que ocupam posições análogas na Est. 20 + 00. Calculada, porém, a curva teórica inicialmente para as condições médias globais, os valores medidos

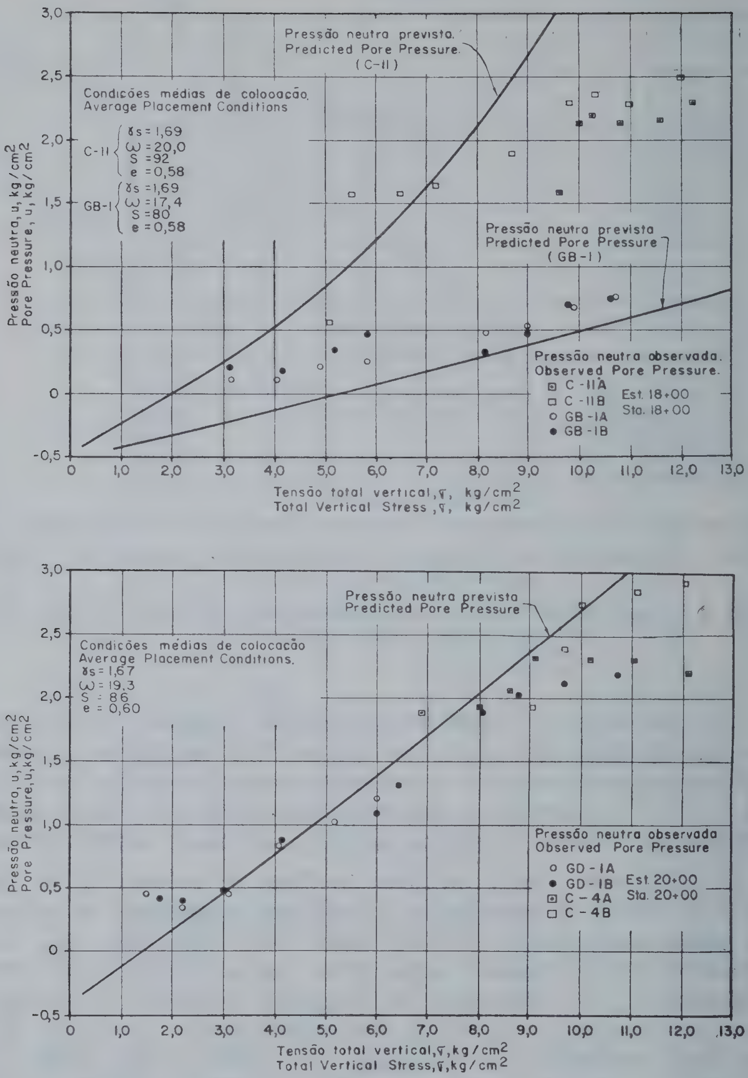

Fig. 11 — Comparação entre pressões neutras previstas e observadas — Influência das condições de colocação do atêrro.

Fig. 11 — Comparison of Predicted and Observed Pore Pressures — Influence of Fill Placement Conditions.

da pressão neutra em ambos os piezômetros se situavam próximos uns dos outros e seguindo de perto a curva teórica. Na hipótese de indicações erradas em um dêsses piezômetros, determinou-se, separadamente, para cada piezômetro em questão, as condições médias do atêrro em tôrno da célula. Resultaram valores médios do grau de saturação de 87% e 90%, respectivamente para os piezômetros GD-1, A e B e C-4, A e B.

A aparente incoerência dêsses valores com aquêles dos piezômetros correlatos da Est. 18 + 00 explica-se pelo fato de ter havido no atêrro, por motivos vários, uma ligeira inclinação no sentido longitudinal além daquela normalmente feita no sentido transversal com o propósito de drenagem em caso de chuva. Revendo-se os dados do contrôle da compactação, verificou-se que em julho de 1958 o atêrro tinha na Est. 18 +00, a superfície na cota 513,0, e na Est. 20 + 00, na cota 509,6; em setembro do mesmo ano a situação era, respectivamente, 520,0 e 519.4. Dessa forma, embora as células dos piezômetros em pauta se localizassem, duas a duas, na mesma cota, o material do atêrro que as circundava, havia sido lançado e compactado em épocas diferentes, e, portanto, sob condições suficientemente diferentes para influírem de maneira significativa nas pressões neutras.

Apesar de alguns piezômetros tipo Geotécnica acusarem acentuada dissipação de pressão durante o tempo em que a construção do atêrro estêve paralisada a oeste da Est. 17 + 00 e se concentravam tôdas as operações na construção do atêrro no trecho por onde o rio estêve desviado, não foi necessário proceder-se à correção das curvas teóricas de u versus σ devida à dissipação de pressão neutra em função do tempo e da sobrecarga.

Tudo leva a crer que, considerando a baixa permeabilidade do material compactado, a dissipação observada se deveu a gradientes hidráulicos locais acentuados, isto é, o fenômeno foi governado por condições reinantes num pequeno raio em volta da célula piezométrica ainda no estágio de pequenas sobrecargas. Com o crescimento da sobrecarga e o passar do tempo, os gradientes hidráulicos locais se dissiparam pela homogeneização das condições e a dissipação da pressão neutra se tornou mais difícil, principalmente na zona central da Barragem.

A Fig. 12 mostra o crescimento do atêrro, portanto, da sobrecarga, com o tempo em cada seção onde se localizam os piezômetros.

CONCLUSÕES

Fatôres diversos, e algumas vêzes de difícil determinação, influem sobremaneira no desenvolvimento das pressões

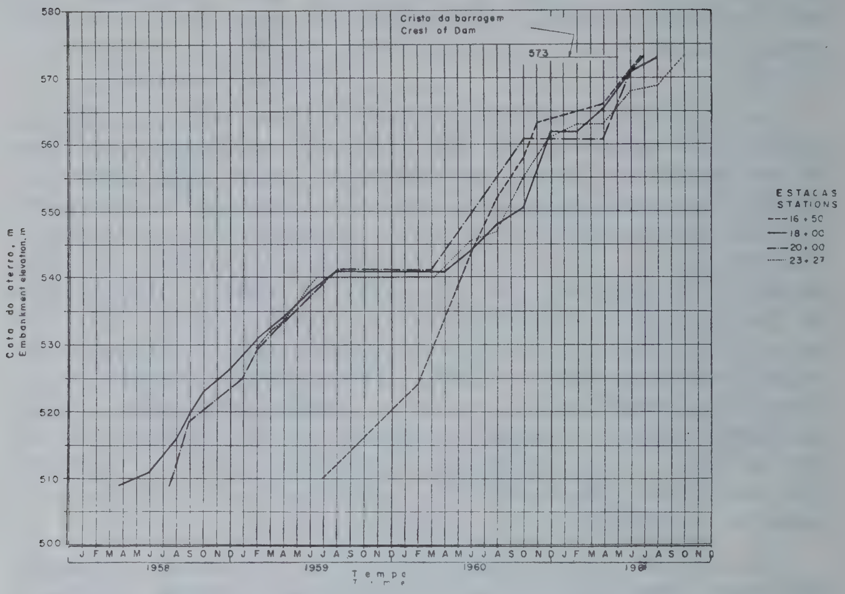

Fig. 12 — Ritmo de construção do atêrro da Barragem.

Fig. 12 — Rate of Construction of the Dam Embankment.

neutras. Os processos disponíveis para o cálculo teórico dessas pressões não permitem ainda resultados com o grau de precisão desejado, desde que várias hipóteses simplificadoras se fazem necessárias no estabelecimento da teoria e na dedução das equações, ficando muito da sua aplicação dependente da experiência e julgamento de quem os utiliza.

O emprêgo de piezômetros se torna, então, uma necessidade sempre que as condições de projeto e construção indiquem que pressões neutras poderão influir de modo acentuado na estabilidade da estrutura e medidas adequadas devam ser tomadas quando seus valores ultrapassam aquêles admissíveis, conforme estabelecido no projeto.

Os tipos de piezômetros presentemente conhecidos não são ainda de todo completos, suas indicações estando ainda sujeitas a interferências várias, algumas inerentes ao princípio de funcionamento, outras inerentes aos materiais de que são feitos, e outros, ainda, de ordem externa.

Conseqüentemente, o emprêgo de mais de um tipo de piezômetro para observação e contrôle das pressões neutras é medida de boa técnica e, antes de tudo, de segurança, malgrado as inconveniências que trazem a aquisição, operação e manutenção de aparelhos de diferentes marcas e princípios de funcionamento.

Em Três Marias, muito empenho e trabalho foi necessário para a aquisição e instalação dos piezômetros, e embora a sua operação não requeresse muito trabalho, a sua manutenção foi relativamente dispendiosa. O custo de aquisição de todos os piezômetros foi de, aproximadamente, Cr$...... 2.850.000,00 que, ao câmbio da época, dá aproximadamente US$ 15,000.00. Malgrado o colapso de alguns piezômetros e o mau funcionamento e indicações estranhas de outros, de um modo geral os esforços dispendidos nesse empreendimento foram satisfatòriamente compensadores.

Graças aos piezômetros, zonas críticas do atêrro no que se refere a umidade de compactação — aquelas construídas nos períodos chuvosos, principalmente — puderam ser controladas; faixas de umidade de compactação prèviamente estabelecidas nas especificações puderam ser reexaminadas e novos limites, que atendessem a conveniências técnicas e construtivas, puderam ser fixados; e, inegàvelmente, a experiência foi ampliada, alguns conceitos novos puderam ser ventilados e outros já estabelecidos foram verificados ou mereceram reexame.

A comparação das pressões neutras observadas com as pressões neutras estimadas segundo processo de Hilf, em função da sobrecarga direta, mostrou uma considerável identidade de resultados no que se refere aos piezômetros localizados na parte central da Barragem, o mesmo não se verificando para os piezômetros situados mais lateralmente.

Isto parece indicar que nestas posições a pressão neutra ou não é função da sobrecarga direta ou existem condições propícias para sua rápida dissipação.

A correção devida à tensão capilar parece válida, visto que muitos piezômetros assinalaram pressões negativas para pequenas sobrecargas e as pressões observadas se situariam abaixo da curva teórica, não corrigida, de u versus σ.

Correções devidas à dissipação da pressão neutra com o tempo e a variação da sobrecarga não foram feitas, visto que, à exceção de um pequeno número de casos, não houve evidência de tal fenômeno na maioria dos piezômetros instalados em Três Marias.

A dissipação registrada em alguns piezômetros ocorreu no período em que a construção do atêrro a oeste da Est. 17 + 00 estêve longamente paralisada enquanto se concentravam as operações noutro local.

Outras pequenas interrupções de construção em certos trechos da Barragem ocorreram posteriormente e, no entanto, não se notou qualquer dissipação. Tudo parece indicar que as dissipações ocorridas inicialmente se deveram a gradientes hidráulicos locais acentuados. Com o passar do tempo, foi havendo progressiva homogeneização de condições, tornando-se, então, mais difícil a dissipação da pressão neutra.

Os piezômetros de Três Marias continuaram em observação depois do término da construção da Barragem de Terra. Novos dados se somaram e se somarão àqueles que serviram à elaboração dêste trabalho. Novas análises e melhores conclusões poderão ser experimentadas no futuro, inclusive sob outros aspectos.

RECONHECIMENTO

O autor expressa aqui o seu agradecimento à Diretoria da Centrais Elétricas de Minas Gerais S.A. pela oportunidade da apresentação dêste trabalho, especialmente ao Diretor Eng. João Camilo Penna pelo interêsse demonstrado e pelas sugestões feitas para seu aprimoramento.

REFERÊNCIA BIBLIOGRÁFICA

1. Casagrande, A. — Barragem de Três Marias, Relatórios Técnicos, não publicados, 1957-1960.

2. Gould, James P. — "Construction Pore Pressures Observed in Rolled Earth Dams", Technical Memorandum 650, U.S. Bureau of Reclamation, April 1959.

3. Hilf, Jack W. — "An Investigation of Pore-water Pressure in Compacted Cohesive Soils", Technical Memorandum 654, U.S. Bureau of Reclamation, October 1956.

4. Hilf, Jack W. — "A Rapid Method of Construction Control for Embankments of Cohesive Soil", Engineering Monographs No. 26, U.S. Bureau of Reclamation, October 1959.

5. Lambe, T. William — "Pore Pressures in a Foundation Clay", Journal of the Soil Mechanics and Foundations Division, ASCE, Vol. 88, No. SM2, April 1962.

6. De Mello, Victor F. B.; Silveira, Araken; Silveira, Evelyna B. — "La Experiencia de la Geotécnica en el Control de Compactación de Presas de Tierra", Anais do Primer Congreso Panamericano de Mecanica de Suelos y Cimentaciones, México, 1959.

7. Queiroz, Lincoln A. — "Barragem de Três Marias. Investigações das Áreas de Empréstimo para o Maciço". Relatório, não publicado, agôsto 1961.

ROCKFILL COMPACTION BY VIBRATORY ROLLERS

GEORGE E. BERTRAM

Chief, Soil Mechanics Branch; Office, Chief of Engineers; Washington 25, D.C.

SYNOPSIS

The results of compaction by vibratory rollers of rockfill materials at the sites of three earth and rockfill dams are described. The tests were conducted to evaluate the effectiveness of vibratory rolling on layered quarry-run rockfill which is to form the outer zones of three dams. Two vibratory rollers of approximately 5-ton and 10-ton static weight, respectively, were used for the investigations. Test results are compared with those obtained by a 50-ton rubber-tired roller which has also been specified for rockfill compaction. The results of vibratory test rolling at two large earth and rockfill dam projects in Europe are also discussed.

SINOPSIS

Los resultados de la compactación mediante rodillos vibradores sobre materiales rocosos están descritos para tres obras de presas de tierra y roca. Los ensayos han sido llevados a cabo en forma de apreciar la eficiencia de los rodillos vibradores en relleno de piedra cargada en cantera sin seleccionar y colocadas por capas, según está previsto sean formadas las zonas exteriores de las tres presas. Se han empleado para la investigación dos rodillos vibradores de aproximadamente 5 y 10 toneladas de peso estático respectivamente. Los resultados han sido comparados con los obtenidos con un rodillo neumático de 50 toneladas que también ha sido empleado para compactación de relleno de roca. Los resultados de compactación vibratoria en dos grandes proyectos de presas de tierra y enrocamiento en Europa se discuten también.

INTRODUCTION

This paper presents the results of the first experiments conducted in the United States for compacting rockfill for earth and rockfill dams by vibratory rolling. Compaction of layered rockfill zones is generally accomplished by the manipulation of the bulldozer in spreading and leveling the dumped material into the specified lift thickness supplemented by the random movement of hauling equipment as successive layers of the fill are placed. Because of the size of the quarry-run rock used in these zones, it is not practical to exercise compaction control by in-place density measurements, as is done for impervious or random fill zones. Accordingly, the effectiveness of the compaction of rockfill is usually determined only by settlement observations on the completed structure. On dams of low to moderate height with large central earth cores in which the rock acts principally to provide stability in the outer shells, the absence of specific compaction procedures is not detrimental to the structure. Acceptable values of unit weight are obtained and deformations are of minor consequence to the safety of the embankment. However, deformation of rockfill assumes major significance in earth and rockfill dams in which a thin earth core in either a central or an inclined position is supported between rockfill zones having steep outer slopes. Since this type of cross-section usually proves to be economical for very high dams, measures to reduce rockfill deformation are essential to prevent cracking of the earth core due to differential settlement between the core and the rockfill. An effective method for accomplishing this purpose is to specify a zone of small sized rock placed in thin layers adjacent to the core. Because of the cost of such a procedure, particularly if processing is involved, it would be desirable to substitute thicker lifts of quarry-run rock compacted sufficiently to achieve equally small deformations in the zone adjacent to the earth core. The reported success of vibratory rollers in compacting a variety of granular and rockfill materials in Europe led to the decision to conduct a series of compaction tests on rockfill at the sites of three dams under construction by the Corps of Engineers in the United States. Since a vibratory roller weighing 17,500 lbs. was used on several European projects, an attempt was made to obtain equally heavy equipment. When the tests were started, only a 9,950 lb. roller was available. Later, another roller was obtained having a static weight of 18,900 lbs. For convenience, these rollers were designated as 5 ton and 10-ton rollers during the test program. Both rollers were used in compacting quarry-run rock in layers ranging from 45 to 90 cm. in thickness. In this paper, the results of these investigations will be discussed as well as results obtained from test fills compacted by vibratory rolling at two European earth and rockfill dam projects.

LAYOUT OF THE TEST FILLS

Because of the difficulties involved in measuring volume changes resulting from the compaction of rockfill materials, it was decided to use vertical settlement as a measure of relative compactive effort. To ensure that the measurements obtained would be truly representative averages, it was important that the test fills have sufficient surface area so that a large number of separate readings could be made. Accordingly, the test fills measured between 35 and 50 feet in width, and from 80 to 125 feet in length. Ramps having a slope of approximately 1 vertical to 5 horizontal were provided at each end of the fills for access. The rollers were towed over the sections in alternate directions, and turn-around areas for the equipment were provided beyond the limits of the test sections. In general, placement procedures duplicated those in use in the normal routine of dam construction. Each truckload of rock was dumped approximately in place and was spread into a uniform layer by a D-8 Caterpillar bulldozer having a total weight of tractor and dozer blade of 55,000 lbs. Usually, the trucks backed over the layer being placed to dump successive loads. The initial settlement due to the traffic of the loaded trucks and the movement of the bulldozer in spreading the layer could not be included in the measurements. After each lift was spread to a uniform thickness, a grid system was laid out on the fill from reference markers located beyond the test fill limits. Each of the points established on the rockfill was marked by a splash of spray paint so that it could be readily identified for subsequent measurements. Elevations were taken on these points prior to rolling and after the completion of a selected number of passes of the roller. In order that the measurements reflect an average elevation at each point, level readings were taken on a raised button in the center of a steel plate, 30 cm. square and 3 cm. thick, placed on the fill. For the convenience of the rodman, a handle made from 6 cm. diameter steel rod was welded to one corner of the plate so that the plate could be moved about slightly to obtain a firm seating of the plate on the rock. Between successive lifts, the surface of the completed layer was painted with spray paint or spread with lime to identify the top surface for later observations. At the conclusion of the construction, trenches or cuts were excavated into the fills in order that an exposed cross-section might be examined to observe the uniformity of the compaction and the extent of bond between the layers. The settlement records and other observations at each location are discussed under the subsequent headings.

INITIAL TESTS AT COUGAR DAM

Cougar dam is a 135 m. high earth and rockfill dam under construction on the McKenzie River in Oregon. A steeply inclined earth core rests against an inner rockfill zone immediately downstream which is composed of small rock having a maximum size of 30 cm. placed in layers 45 cm. in thickness. Zones of larger rock in 90 cm thick layers form the outer shells. The rock for all zones is obtained from spillway excavation on the right abutment and is a black, glassy, porphyritic basalt. The close, blocky, or small columnar, jointing produces the required sizes for the several zones by selective loading from normal quarry operations. The specifications under which construction was initiated required compaction of the inner rockfill zone by two passes of a 50-ton rubber-tired roller. During the first season's construction, observation disclosed that rolling of the fill with the rubber-tired roller was not producing a noticeable improvement in the appearance of the layer over that obtained by the hauling and spreading equipment. It was decided, therefore, to substitute a vibrating steel-wheeled roller for the rubber-tired roller. A Bros Vibra-pactor, Model VP-9D, with a static weight of 9,950 lbs. was obtained. This roller was used until Bros Incorporated completed development of their Model VP-20D Vibra-pactor weighing 18,900 lbs. At this time comparative tests of the two rollers were considered to be advisable to determine whether further changes in construction procedure should be made at Cougar dam. Figure 1 shows the two rollers on the downstream rockfill zone of the dam.

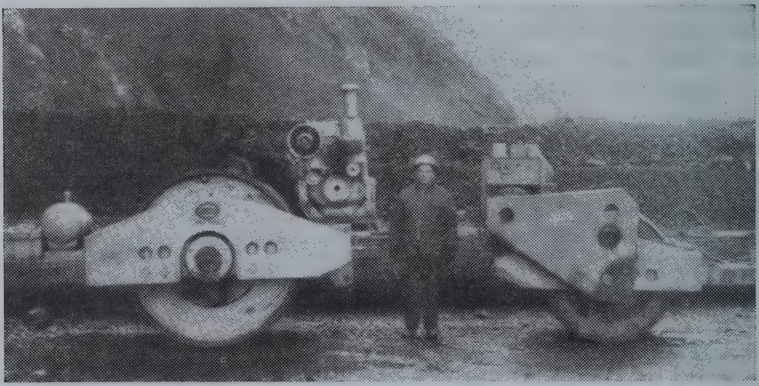

Fig. 1 — Vibratory Rollers at Cougar Dam.

Fig. 1 — Rodillos Vibratorios en la Presa Cougar.

Since the lift thicknesses for the various rockfill zones in the dam vary from 45 cm. for the zone immediately downstream of the core to 90 cm. for the outer shells, the first test fills were constructed within these limits of layer thickness. The test sections were located on the outer downstream shell of the dam, and fills of three different layer thicknesses were placed: 45 cm., 60 cm., and 90 cm. The rollers were towed over the test fills at speeds between 1.5 and 2 miles per hour by a rubber-tired Euclid truck tractor weighing 30,000 lbs. The frequency of each of the rollers was approximately 1,400 vibrations per minute. Settlement was measured after 2, 4, and 6 passes of the rollers. The best interpretation of the data which could be obtained by plotting the actual settlement measurements directly against layer thickness was a series of straight lines having a slight upward slope in the direction of increasing layer thickness. This appeared to be of little significance. It seems logical that the energy exerted by each pass of a vibrating roller as it moves over a layer of rock of any thickness at a uniform forward rate of travel is a constant. Therefore, it was decided that the test results could best be illustrated by a plot of the cumulative percent of settlement against layer thickness. The test data plotted in this manner result in a series of smooth curves sloping downward in the direction of increasing layer thickness, as shown in Figure 2.

The group of curves obtained from the use of the 10-ton roller shows its obvious advantage over that of the 5-ton roller in achieving compaction of the rockfill. The flat slope of all three curves for the 5-ton compacted layers was unexpected but the data were too consistent to be ascribed to errors in measurement. It is most probable that the shape of the curves was caused by a change in gradation of the rock from the quarry during the fill placement. For both the 5-ton and 10-ton rollers, the curves indicate that the major settlement is achieved by the first four roller passes. This may also be demonstrated by plotting the settlement for a given layer thickness versus the number of passes. If passes of the roller are plotted as the abscissa on such a diagram, the curve obtained will be concave in a downward direction indicating that the maximum settlement is being approached. The tests were not continued to such a point for it was considered that 6 roller passes were an economic limit beyond which rolling would delay other operations during dam construction.

Because the 5-ton roller was being used on the construction of the dam, it was decided to determine the effect of superimposing rolling with the 10-ton roller on a fill previ-

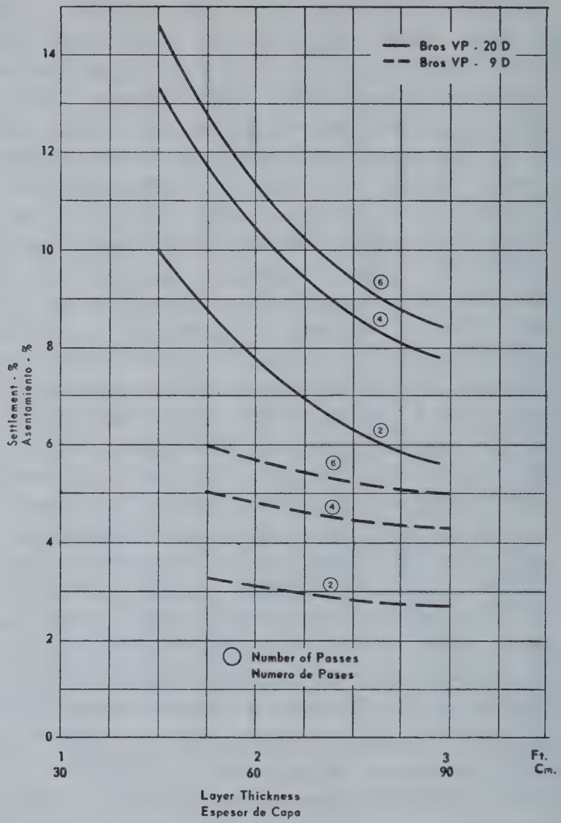

Fig. 2 — Initial Test Results from Cougar Dam.

Fig. 2 — Resultados Iniciales de las Pruebas en la Presa Cougar.

ously compacted with a 5-ton roller. After 6 passes of the 5-ton roller had been made on each of the three sections, additional settlement was measured for compaction by the 10-ton roller. It is interesting to note that the effectiveness of the 10-ton roller used in this manner is considerably less than that of the 10-ton roller used alone. The additional cumulative settlement was relatively independent of layer thickness, and averaged only 1.5 percent for 2 passes of the roller, 2.5 percent for 4 passes of the roller, and 3.6 percent for 6 passes of the roller. The lack of effectiveness of superimposed rolling is believed to be due to the "plastic zone" which builds up ahead of a vibratory roller as it is towed over the fill. In this plastic zone the rock is very noticeably in motion. Apparently the lighter roller causes an interlocking of the individual stones which the heavier roller cannot release when it is used over previously compacted fill.

INVESTIGATIONS AT CARTERS DAM SITE

As part of the field investigations for the design of a 140 m. high earth and rockfill dam at the Carters site in northwestern Georgia, test fills were constructed to provide a basis for the selection of rock for the outer zones of the embankment. Available materials at this location are all metamorphosed sediments consisting mainly of micaceous quartzite, phyllite, and argillite. The quartzite is a hard, dense, medium to coarse-grained rock with scattered conglomeratic areas. The phyllite is composed of clay-sized particles of sericite and has a wavy irregular foliation. It is not as hard as the other rocks and tends to break in a semi-schistose manner. The argillite is fine-grained and because of its bedding breaks into elongated but not slabby pieces. The quartzite was investigated in one series of test fills, a combination or argillite and phyllite in another series. Since the 10-ton vibrating roller was not available when the test program was established, the test fills were compacted with a Ferguson Model 65 vibrating roller having a static weight of 10,250 lbs.

Rock was obtained from test quarry blasts on the left abutment. Two lift thicknesses, 45 and 75 cm., were selected for the fills for both types of rock. The roller was towed by a D-8 Caterpillar crawler tractor at a rate of approximately 1.5 miles per hour. Settlements were measured after 2, 4, and 8 passes of the roller. Actual settlement measurements plotted against layer thickness resulted in a series of nearly horizontal straight lines, and the relation between cumulative percent of settlement and lift thickness was used in the same manner as for the Cougar data. The group of curves obtained is shown in Figure 3-A. Only a single group of curves is shown, as the data from the two series of tests were so similar that a separate plotting of the results was not justified. This was not expected, for the quartzite was considered to be harder and less liable to breakdown under roller action than the other rocks tested. It is possible that the similarity of test results can be attributed to the relatively light weight of the 5-ton roller and that a greater difference in results would have been obtained had a 10-ton roller been used. In the figure, a curve for 6 roller passes is interpolated to emphasize the equal degree of compaction obtained by all passes succeeding the first two. This effect is considered to be the result of a gradual breakdown of the rock under the action of the vibratory roller.

It should be noted that the slope of these curves is steeper than that of the 5-ton curves from Cougar dam and thus shows better agreement with the slope of the 10-ton Cougar curves. This may be considered as substantiation of the comment that the flap slope of the 5-ton Cougar curves can be attributed to a change in rock gradation rather than to the light weight of the roller. Regardless of the lack of correlation in slopes of the curves resulting from 5-ton roller compaction at the two test sites, the range of settlements obtained was sufficiently close to warrant the assumption

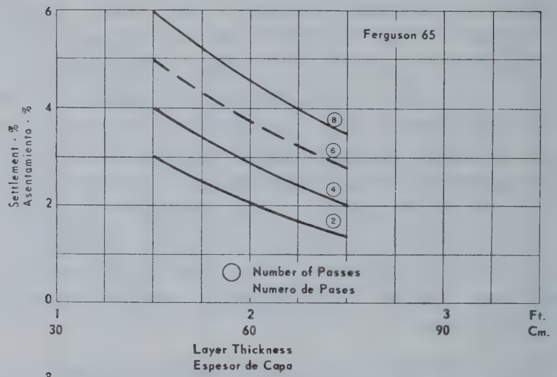

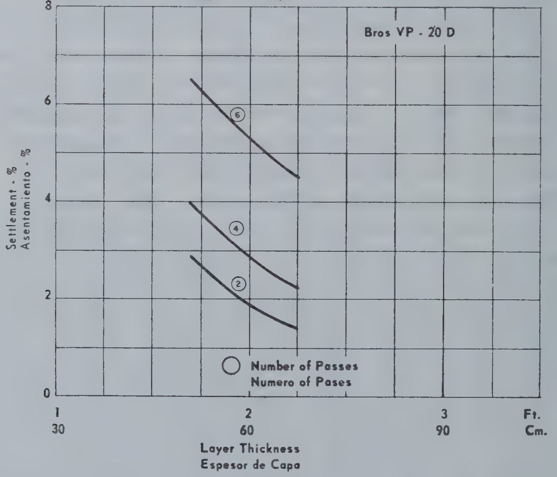

Fig. 3-A — Results of Tests at Carters Dam Site.
Fig. 3-B — New Hogan Test Results.

Fig. 3-A — Resultado de Pruebas en el Sitio de la Presa Carters.
Fig. 3-B — Resultados de Pruebas em New Hogan.

that a substantial increase in compaction can be achieved at Carters dam site by a 10-ton vibratory roller. Accordingly, a series of 10-ton roller tests is planned for the Carters site early in 1963.

TESTS AT NEW HOGAN DAM

Planning for New Hogan dam, a 61 m. high earth and rockfill dam on the Calaveras River in California, was undertaken shortly after the design of Cougar dam was completed. The specifications for the placement of material in the rockfill zones required that the rock be spread in 60 cm. thick layers and be compacted either by two passes of a 50-ton pneumatic roller or by two complete coverages of a D-9 Caterpillar tractor. When the contractor opened the rock quarry and began placement of the rockfill, it was discovered that the percentage of plastic fines from weathered zones in the quarry was so great that a pervious rockfill in accordance with the intent of the specifications could not be obtained. Construction was halted until a grizzly could be installed to remove the objectionable material. The spacing of the bars on the vibrating screen varied from 7.5 to 15 cm., resulting in a processed rock that was completely free of small fines.

The rock from the quarry is a dense, hard, greenish-gray metamorphic rock retaining most of the grain-size relationships of the volcanic tuff and volcanic agglomerate from which it was formed. Because of the processing operation the rock was much coarser than either the Cougar or the Carters material, although it was generally well graded. Since the specifications required the entire rockfill to be placed in 60 cm. layers, the test fills were constructed to this nominal thickness. Also because of the specification requirements, a 50-ton rubber-tired roller was used on one test fill for comparison with the 10-ton vibratory roller. The Bros Model VP-20D vibratory roller which was used at Cougar dam was shipped to New Hogan for the tests. A Ferguson Model T-100 S rubber-tired roller towed by a DW-21 power unit was used for the pneumatic compaction. The test fills for each type of roller were constructed side by side, and 2, 4, and 6 passes of each type of roller were made on each layer of the respective fills. Settlements were measured in the same manner as for the tests conducted at the other sites.

Although all layer thicknesses were nominally 60 cm., it was possible to obtain a relationship between the cumulative percent of settlement and layer thickness, similar to that previously used for Cougar and Carters data, by plotting average measurements for the individual layers. The curves shown in Figure 3-B were prepared on this basis for comparative purposes. It will be noted that there is a pronounced increase in settlement as the number of passes is increased from four to six due to a breakdown of the rock. When the excavation was made through the vibratory roller fill upon completion of the testing program, it was found that the voids between the larger rocks for the full depth of the layer were well filled with fragments grading in size from 1 inch down to very fine particles. Inasmuch as the rock was processed before being placed, the fine material was produced by the actions of the bulldozer in spreading and the vibrating roller in compacting the fill. Observation suggests that the principal breakage was caused by the roller, for as the roller was being towed over the fill, shattering of the surface rock was very noticeable.

The pneumatic compacted fill had much larger open voids than the vibratory fill and bore out the observations made during the early stage of construction at Cougar dam that this type of compaction is generally ineffective on quarry-run rockfill. Less than 0.5 percent of settlement was produced by 6 passes of the pneumatic roller. A further 2.5 percent of settlement was obtained by 4 passes of the vibratory roller over the pneumatic compacted fill after 6 passes of the pneumatic roller had been completed.

ADITIONAL TESTS AT COUGAR DAM

A second series of tests was made at Cougar dam following completion of the New Hogan test fills. Again the Bros Model VP-20D roller was used. The purpose of these tests was to obtain a more accurate definition of the relationship between actual settlement and layer thickness for rockfill having a definite maximum size. It was believed that variations in the test results which might be traceable to random large rocks in the separate layers would thereby be eliminated. Sound well-graded hard basalt similar to that used in the initial tests was dumped over horizontal splitter bars to remove the oversize rock above 30 cm. in diameter. The processed material was uniformly graded between a maximum size of 30 cm. and a minimum size of 1 cm. with only 2 percent of quarry fines less than the No. 4 mesh sieve. Fills having nominal layer thicknesses of 45, 60, 75, and 90 cm. were constructed of this rock. After being spread into uniform layers by the bulldozer, the actual thicknesses were 54, 63, 81, and 99 cm. As in the first tests, 2, 4, and 6 passes of the roller were made. Settlement measurements were recorded, and the curves for actual settlement plotted against layer thickness (shown by the solid lines in Figure 4) were obtained.

It will be noted that these curves clearly indicate a peak value of settlement for a layer thickness of 81 cm. The reason for the shape of the curves cannot be deduced from a single test fill, but it seems possible that a resonant frequency is obtained for a given roller which is a function of both the rock size distribution in the fill and the thickness of the layer. If the relationship is a function of the maximum size of rock used, it will be noted that the layer thickness for the maximum settlement is slightly more than two and a half times the maximum rock size of 30 cm. The percent-of-settlement curve for 6 passes of the roller, similar to the curves plotted for the results of the other tests, is shown by the dashed line in Figure 4. On this curve there is a pronounced change in slope corresponding to the peak of the actual settlement curve. Furthermore, if maximum

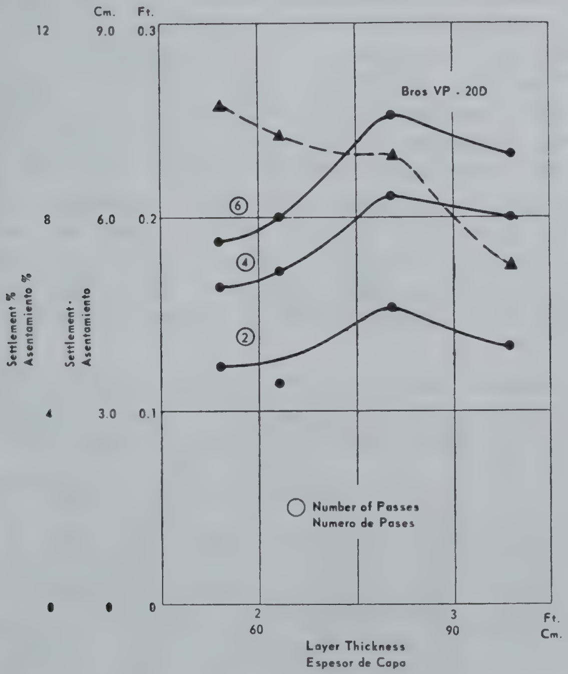

Fig. 4 — Additional Test Results from Cougar Dam.

Fig. 4 — Resultados Adicionales de Pruebas en la Presa Cougar.

rock size in the gradation of material exerts an influence, the initial Cougar tests were not made on sufficiently thick layers to develop the pronounced change in slope because the maximum layer thickness of 88 cm. was only one and a half times the maximum rock size of 60 cm. The percent-of-settlement curves for Carters and Hew Hogan were developed for comparison with the initial Cougar curves and the data on layer thickness from these projects are too limited to permit speculation regarding the influence of any factors other than those show in Figures 3-A and 3-B.

RESULTS OF EUROPEAN TESTS

In 1961, Electricité de France constructed a large test fill to determine the compaction requirements for the rockfill zones of Mont Cenis dam. This earth and rockfill dam will rise to a height of 109 m. in the Alps in the Department of Savoy. An ABG Model SAW vibrating roller weighing 17,500 lbs. with a frequency of vibration of approximatey 1500 vibrations per minute towed by a D-8 Caterpillar tractor was used to compact the fill. In the initial studies, 3 passes of the roller were made on a layer thickness of 1 m. The rock used was calc schist produced from a test quarry near the site. The rock tended to break in long flat pieces, and quarry fines amounted to as much as 10 percent by weight below 25 mm. in size. The settlement obtained from the test fill averaged 3 percent of the lift thickness. The rock at Mont Cenis is most similar to the rock at the Carters dam site, but no comparisons can be made because of the differences in both roller weights and lift thicknesses. Further tests are being made at Mont Cenis for a 2 m. layer thickness.

In the same year, test fills were constructed by the Tyrolean Hydroelectric Company at the site of Gepatsch dam in the Austrian Alps. The test program included an ABG roller drawn by a D-8 Caterpillar tractor. Gepatsch dam will be a 150 m. high earth and rockfill dam comparable, on the whole, to the Cougar project. The rock at the site is an augen gneiss of generally angular shape similar to the basalt at Cougar dam. The program included rock placement by dumping and sluicing in 6 m. lifts, compaction by a Keller vertical vibrator suspended from a crane on 4 m. lifts, and compaction by a vibrating roller on layered fill. The layer thicknesses for the vibrating roller test fills varied from 0.87 m. to 1.86 m., and measurements were made after 2, 4, and 6 passes on some test fills and 4 and 8 passes on others. The vibrating roller proved to be the most effective method for compacting rock at this location. A plot was made of the data from the three test fills compacted by the vibrating roller to determine whether a relationship similar to that developed for the additional tests at Cougar dam could be found. The actual settlement curves sloped upward but did not reach a peak value. The rock was well graded but the maximum layer thickness was only twice the maximum rock size of 1 m. It should be noted that as the result of the test-fill program, the rockfill zones for the dam are being compacted in 2 m. layers.

CONCLUSIONS

In general, the test programs that have been described demonstrate the effectiveness of vibratory rolling in achieving substantial compaction on a variety of quarry-run rockfill materials. Observations of the cross-sections of the compacted fills, particularly at New Hogan dam, showed a marked uniformity to appearance throughout the entire depths of the fills. There was no plane of demarkation at the layer boundaries, and the rock was well interlocked. Fines were well distributed in the voids, and the movement of this fraction into the interstices is considered to be superior to the effect which can be obtained by sluicing the surface of a traffic-compacted layer with a water jet.

The superiority of the 10-ton vibratory roller over the 5-ton roller was demonstrated in the initial tests at Cougar dam. The large size of the individual pieces in a rockfill requires a roller with sufficient weight to actually cause vibration of the materials in the "plastic zone" just ahead of the roller as it moves over the fill. The 10-ton roller achieves this effect for the layer thicknesses tested.

On the basis of the tests made to date, a 10-ton roller has been substituted for the 5-ton roller for the remainder of the construction on Cougar dam. The layer thickness in the zone downstream of the core has been increased from 45 to 60 cm. in accordance with the test results for rock with a maximum size of 30 cm. Further testing needs to be conducted on thicker lifts with rock of a definite maximum size before relationships based on grading and layer thickness can be established. However, it has been demonstrated that on layers of 95 cm. thickness, compaction by the 10-ton roller provides a definite advantage in the ease of movement of hauling equipment over the fill during construction. The economic benefit of this procedure cannot as yet be fully evaluated.

A further important result of the investigations had been the development of a tentative specification for vibratory rollers for use on earth and rockfill dam construction. This specification is worded as follows:

> *Vibratory rollers* — Vibratory rollers shall have a total static weight of not less than 20,000 lbs., with at least 90 percent of the weight transmitted to the ground through a single smooth drum when the roller is standing in a level position hitched to the towing vehicle. The diameter of the drum shall be between 150 and 165 cm. and the width between 180 and 200 cm. The unsprung weight of drum, shaft, and internal mechanism shall not be less than 12,000 lbs. The frequency of vibration during operation shall be between 1,100 and 1,500 fpm, and the dynamic force shall be not less than 40,000 lbs. at 1,400 fpm. The roller shall be towed at speeds not to exceed 1.5 miles per hour by a crawler tractor with a minimum drawbar rating of 50 horsepower. The equipment manufacturer shall furnish sufficient data, drawings, and computations for verification of the above specifications, and the character and efficiency of this equipment shall be subject to the approval of the Contracting Officer.

Future testing will be directed toward verification of the shape of the actual settlement curves for varying layer thicknesses, and an attempt will be made to evaluate the effect of grading, shape, and maximum size of rock on the compaction characteristics of layered rockfills. It is suggested that layer thickness for rock placement be based on field tests at each dam site. Both the actual settlement and the percent of settlement plotted against layer thickness should be used as guides in selecting the optimum layer thickness for the various rockfill zones. In summary, the basic criterion for the extent of compaction given to the rock shells of an earth and rockfill dam should be the influence of rockfill density on possible cracking of the earth core.

ACKNOWLEDGMENTS

The tests at Cougar dam were conducted under the direction of Mr. D. H. Basgen, Resident Engineer, U.S. Army

Engineer District, Portland, Oregon. Mr. F. A. Robeson, Chief, Foundations and Materials Branch, U.S. Army Engineer District, Mobile, Alabama, supervised the investigations at the Carters dam site. The test program at New Hogan dam was in charge of Mr. D. H. Doble, Chief, Soils Branch, U.S. Army Engineer District, Sacramento California. The assistance of these gentlemen in furnishing test data for use in this paper is gratefully acknowledged.

ASPECTOS DO CONTRÔLE DE CONSTRUÇÃO DA BARRAGEM DE FURNAS

LINCOLN A. QUEIROZ

Engenheiro, M. Sc., Central Elétrica de Furnas — Brasil

SUMÁRIO

O presente artigo relata experiência obtida com a utilização de materiais residuais no núcleo e zonas de transição da barragem de enrocamento de Furnas, com apresentação dos resultados finais do contrôle de compactação.

São focalizados aspectos particulares relativos aos resultados do contrôle de compactação do núcleo, indicando-se diferenças de importância encontradas em métodos de ensaios.

Breve descrição das condições geológicas do local da barragem recém-completada é incluída.

São também apresentados resultados de recentes nivelamentos, os quais evidenciam mínimos assentamentos verticais e deslocamentos horizontais de marcos colocados na crista e taludes, após o término da barragem e início do represamento.

SUMMARY

This article reports experience obtained during the construction of Furnas rockfill dam with residual type of materials, residual clay and weathered quartzitic rock.

Special attention is given to the differences of results found in compaction control tests for the clay core.

Besides brief description of geologic features, results of recent surveyings are included showing the vertical and horizontal movements which were recorded since the completion of the dam and start of reservoir filling on January 9, 1963.

INTRODUÇÃO

A barragem de Furnas com 125 metros sôbre o ponto mais baixo da fundação e 9.450.000 m^3 de maciço compactado, é atualmente a mais alta na América do Sul, constituindo parte integrante do aproveitamento hidrelétrico cujo potencial após total instalação atingirá 1.200.000 KW.

É barragem do tipo enrocamento com núcleo de argila, flanqueado por zonas de transição e enrocamentos de rocha branda pouco alterada (random rock) e rocha sã (rockshell zone), conforme indicado na figura 1.

GEOLOGIA LOCAL

A barragem de Furnas se situa na parte jusante de um "canyon" que o rio Grande erodiu nos quartzitos e xistos da série de Minas e Itacolomi.

As formações rochosas do Estado de Minas Gerais pertencem essencialmente a estas duas séries.

De acôrdo com o consenso geral geológico, constituíam inicialmente sedimentos (argilas, siltes e areias finas e grossas) depositados em extenso geosinclinal em um mar interior, o de Minas, de época pré-cambriana. Êstes sedimentos, estendendo-se em espessura a milhares de metros, foram em época posterior submetidos a soerguimento e dobramentos de grande vulto, durante orogênese assinalada ao fim do período Proterozóico.

Pressões tectônicas que causaram dobras e desnivelamentos deram lugar a altas temperaturas com conseqüente metamorfismo das rochas, resultando a formação dos quartzitos e xistos respectivamente a partir dos sedimentos arenosos e siltosos.

As características geomorfológicas na área da barragem estão diretamente relacionadas com a estrutura rochosa predominante. Nas vizinhanças do local, quartzitos de granulação fina e muito resistentes, formam espigões típicos ou monoclinais de mergulho suave na encosta de um flanco e escarpa íngreme no flanco oposto.

Locais de afloramentos de xistos, intercalando-se aos quartzitos, tornaram-se vales abertos, resultantes da erosão mais fácil daquelas rochas.

Escarpas verticais denotam geralmente escarpas de falha. A maior falha atravessa diagonalmente o local da barragem, com direção N55°W. Esta falha foi injetada por dique de diabásio, provàvelmente no período triássico e possìvelmente como parte do vulcanismo intenso que naquele período se registrou no Sudoeste do Brasil, caracterizado por inúmeras intrusões magmáticas.

A região onde a barragem se localiza é caracterizada topogràficamente por consideráveis diferenças de nível. O leito do rio, exceto no local da falha mencionada, apresen-

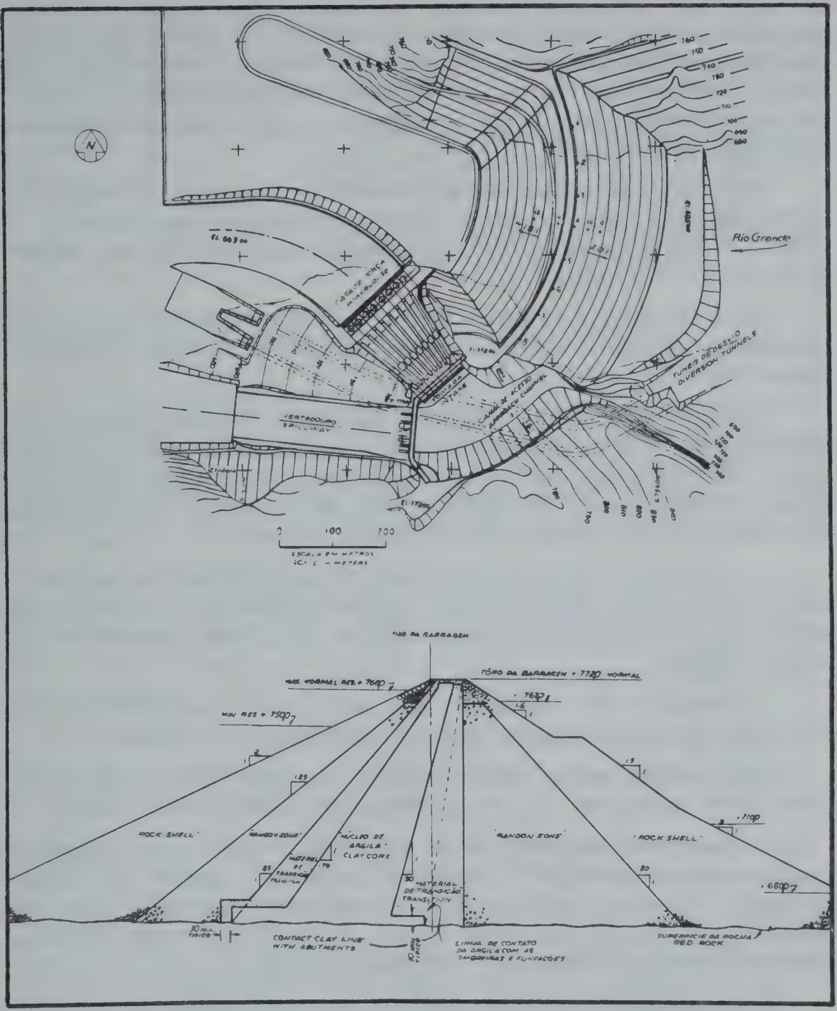
Rio Grande
TUNEIS DE DESVIO
DIVERSION TUNNELS
CASA DE FORÇA
TOMADA
INTAKE
CANAL DE ACESSO
APPROACH CHANNEL
VERTEDOURO
SPILLWAY
EL 663.00
EL 772.00
0
100
200
ESCALA EM METROS
SCALE IN METERS
760
750
740
730
720
710
700
690
680
EIXO DA BARRAGEM
NÍVEL NORMAL RES. + 766.0
TÔPO DA BARRAGEM + 772.0 NORMAL
MIN RES + 750.0
+ 762.0
+ 710.0
+ 680.0
ROCK SHELL
RANDOM ZONE
NÚCLEO DE ARGILA
CLAY CORE
MATERIAL DE TRANSIÇÃO
TRANSITION
CONTACT CLAY LINE WITH ABUTMENTS
LINHA DE CONTATO DA ARGILA COM AS OMBREIRAS E FUNDAÇÕES
SUPERFÍCIE DA ROCHA
BED ROCK
30 MIN. TÍPICO
2
1.85
1.6
1.5
.85
.70
.30
.80

Fig. 1 — Aproveitamento hidrelétrico de Furnas — Planta geral e seção transversal típica da barragem.

Fig. 1 — Furnas hydroelectric project — General plan and typical cross section of the dam.

ta-se em tôda a largura do vale, na cota 670 aproximadamente. A partir desta cota, alteiam-se as margens tanto direita e esquerda até cota 870.

No contato e ombreira esquerda da barragem assinala-se a ocorrência principal de quartzito são, duro, silícico e de granulação fina. Apresenta-se êste medianamente a muito estratificado, fragmentando-se ao longo dos planos de acamamento e diaclases. Devido aos esforços tectônicos sofridos durante dobramentos, o quartzito friável converteu-se em massa formada de blocos interligados, cujas diaclases e planos de acamamento não se colmatizaram quer por cristalização quer por cementação.

Êste tipo de rocha sã foi escavado na margem esquerda para abertura do canal de acesso, estrutura da Tomada e Casa de Fôrça e constitui o material compactado na barragem como "rockshell".

No leito do rio, alternam-se quartzitos e xistos sãos, com mergulho de 15 a 30°SW, para jusante e direção predominante N25°W.

Na falha geológica, situada no meio do rio, o dique de diabásio foi provàvelmente erodido pelas águas até cota máxima 647, atingida após escavação de preparo da fundação. Quartzito fraturado foi encontrado lateralmente ao diabásio, estando êste em estado de reduzida alteração.

A ombreira direita compõe-se de quartzitos muito laminados e já bastante alterados, entremeados por camadas de xistos micáceos também alterados e atingindo espessura de vários metros.

A condição de alteração não se limita à superfície mas continua horizontalmente até às distâncias sondadas.

São encontrados nesta ombreira: quartzitos alterados, quartzitos micáceos, xistos quartzíticos e xistos sericíticos.

O quartzito micáceo é de côr cinza-claro, com delgadas laminações de sericita e mica ao longo dos planos de estratificação. Quando intensamente laminado (camadas com espessura da ordem de milímetros), e rico em teor micáceo, torna-se flexível formando um itacolomito.

O xisto quartzítico é similar em côr e em textura ao quartzito micáceo quando são, diferindo por apresentar teor de mica sericita muito maior e xistosidade bem acentuada, paralela aos planos originais de estratificação. É mais silícico e conseqüentemente mais friável que o quartzito micáceo, sendo geralmente branco ou amarelo-claro quando mais alterado.

Xisto sericítico côr cinza-prateado a cinza-esverdeado, contém essencialmente mica sericita com lentes ocasionais de quartzo.

Os quartzitos alterados e os quartzitos micáceos e pouco xistosos constituíram os materiais utilizados na construção dos zoneamentos de transição e "random" da barragem. São materiais bastante friáveis, fragmentando-se fàcilmente sob ação dinâmica de compactação.

Na margem direita, ainda se localiza a mais possante jazida de material argiloso para núcleo, situada no entôrno da cota 840 e a 2 km a noroeste da barragem.

É constituída de argila pouco siltosa, sendo solo residual resultante da alteração in-situ de xistos decompostos.

CONSTRUÇÃO E CONTRÔLE DO NÚCLEO DE ARGILA

Na construção do núcleo impermeável foi compactada argila inorgânica pouco siltosa, de côr vermelha laterítica, encontrada na jazida da margem direita. Granulomètricamente, apresenta-se com 30 a 50% de fração de argila (diâmetro menor que 2 μ) e de 60 a 80%, passando na peneira 200 "mesh".

Ensaios de Atterberg definem êste solo como argila de média a alta plasticidade (símbolo CH), situando-se os pontos representativos ligeiramente acima da linha A entre os valores 40 e 60%, com linha média pràticamente coincidente com a linha A.

A figura 2 apresenta dados típicos dos ensaios de Atterberg e de compactação do laboratório obtidos para furo representativo da jazida de argila.

O ensaio de compactação é o Proctor normal, executado de acôrdo com as normas brasileiras (MB 33), as quais es-

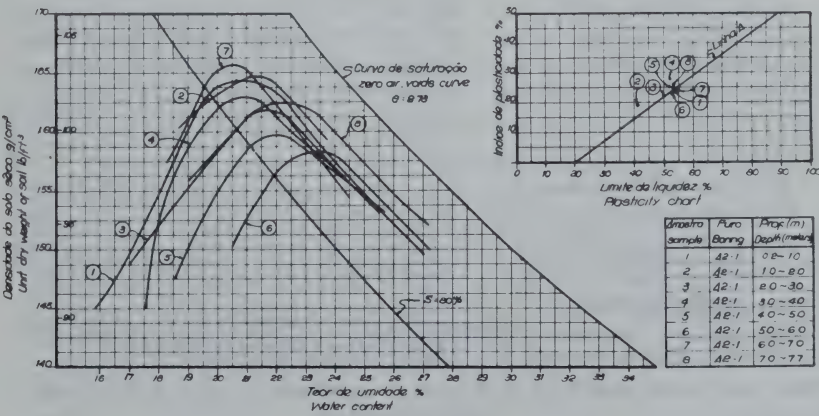

Amostra sample	Furo Boring	Prof. (m) Depth (meters)
1	42·1	02–10
2	42·1	10–20
3	42·1	20–30
4	42·1	30–40
5	42·1	40–50
6	42·1	50–60
7	42·1	60–70
8	42·1	70–77

Fig. 2 — Ensaios de compactação (tipo SR) e de Atterberg — Empréstimo nº 1.

Fig. 2 — Atterberg and compaction tests (SR type) — Borrow Pit No. 1.

pecificam a reutilização do solo durante o ensaio, após compactação do primeiro ponto para o traçado da curva.

Os solos da jazida se apresentam, apesar da elevada situação em cota, com teor de umidade muito alto, excedendo mesmo o valor ótimo a partir do primeiro metro de escavação. Lençol freático bastante próximo à superfície, especialmente nas estações chuvosas, determina aquela condição.

Do ponto de vista da construção do núcleo, esta circunstância foi, porém, muito favorável. Permitiu, com escavação superficial feita com "scrapers", a compactação de materiais com umidade geralmente igual ao valor ótimo ou acima, com benéficos resultados quanto à desejada plasticidade e homogeneidade do núcleo. Além disto, representou econômicamente uma ótima solução, pois não se tornaram necessários métodos especiais para umedecimento dos materiais quer na jazida quer na área de compactação, circunstância normal no país, em projetos desta magnitude. Como conseqüência, adotou-se a compactação das camadas lançadas no núcleo com rôlo compactador de pneumático, com resultados muito bons.

Êstes resultados estão apresentados na figura 3 na forma usual de distribuição estatística para os valôres do chamado desvio da umidade ótima ou diferença entre umidade ótima e umidade do atêrro e da percentagem de compactação. Assinala-se:

— A média global dos desvios foi de 0,18% acima do valor ótimo do ensaio adotado para contrôle, no caso "Proctor

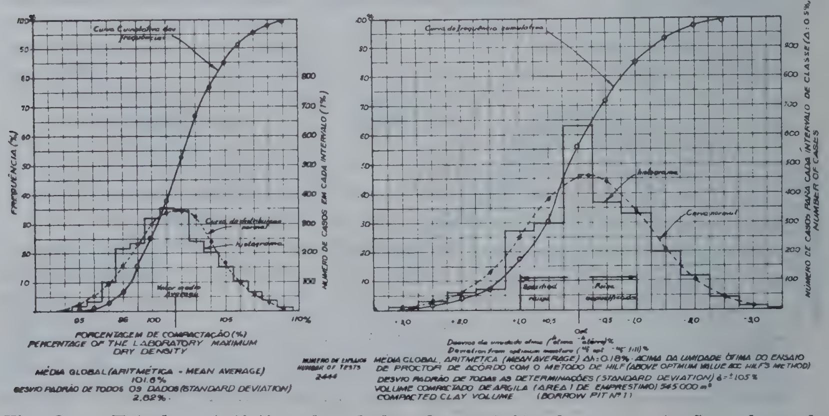

Fig. 3 — Estudo estatístico dos dados de contrôle de compactação. Área de empréstimo nº 1.

Fig. 3 — Statistical analysis of all data from compaction control. Borrow Pit No. 1.

Standard", executado de acôrdo com o método desenvolvido por J. Hilf no Bureau of Reclamation.

— Um total de 68% de valores ficaram compreendidos na faixa especificada de +1 a —1% do valor ótimo, sendo de 93% o total compreendido entre +2 e —2% dêste valor.

— Valor do desvio padrão global foi de apenas 1,05% do valor médio, indicando condições altamente satisfatórias quanto à homogeneidade das umidades.

— A distribuição dos valores determinados no campo foi aproximadamente normal, tendo sido modal o valor ótimo.

— O valor médio da percentagem de compactação resultou igual a 101,6%, bem superior à média especificada de 98%.

Evidencia-se alta eficiência da compactação executada com rôlo pneumático de 50 toneladas, aplicando 4 passadas em camada compactada de 15 centímetros.

— Desvio padrão global de 2,8% pode também ser considerado muito satisfatório. Evidência da alta eficiência alcançada na compactação é dada também pela curva de compactação de campo, apresentada na figura 4.

Verifica-se que, para a faixa especificada de umidades de —1 a +1% do ótimo, obtêm-se em média valôres da percentagem de compactação bem acima dos 100%. Esta percentagem não decresce inclusive na compactação de materiais com umidade fora da faixa especificada.

A curva tracejada do mesmo desenho que delimita inferiormente 5% de todos os resultados indica que para os materiais com umidade dentro dos limites da faixa especificada, não haverá pràticamente valores inferiores a 95%.

No segundo gráfico da figura 4 estão apresentados os resultados das determinações de campo do teor de umidade e densidade sêca do solo. Observa-se a tendência dos pontos mais úmidos se disporem mais próximos à linha de saturação, característica de compactação com rolos pneumáticos.

Os excelentes resultados poderiam justificar redução da energia de compactação no campo, quer com a redução do número de passadas do equipamento, quer pelo aumento da espessura da camada compactada. Entretanto, a compactação pròpriamente dita da argila, não representou em época alguma ponto crítico da construção. Ao mesmo tempo, maior espessura de camada resultaria certamente em diferenças sensíveis do grau de compactação dentro da própria camada devido ao fato conhecido dos rolos pneumáticos não conseguirem compactar eficientemente o solo a profundidades maiores.

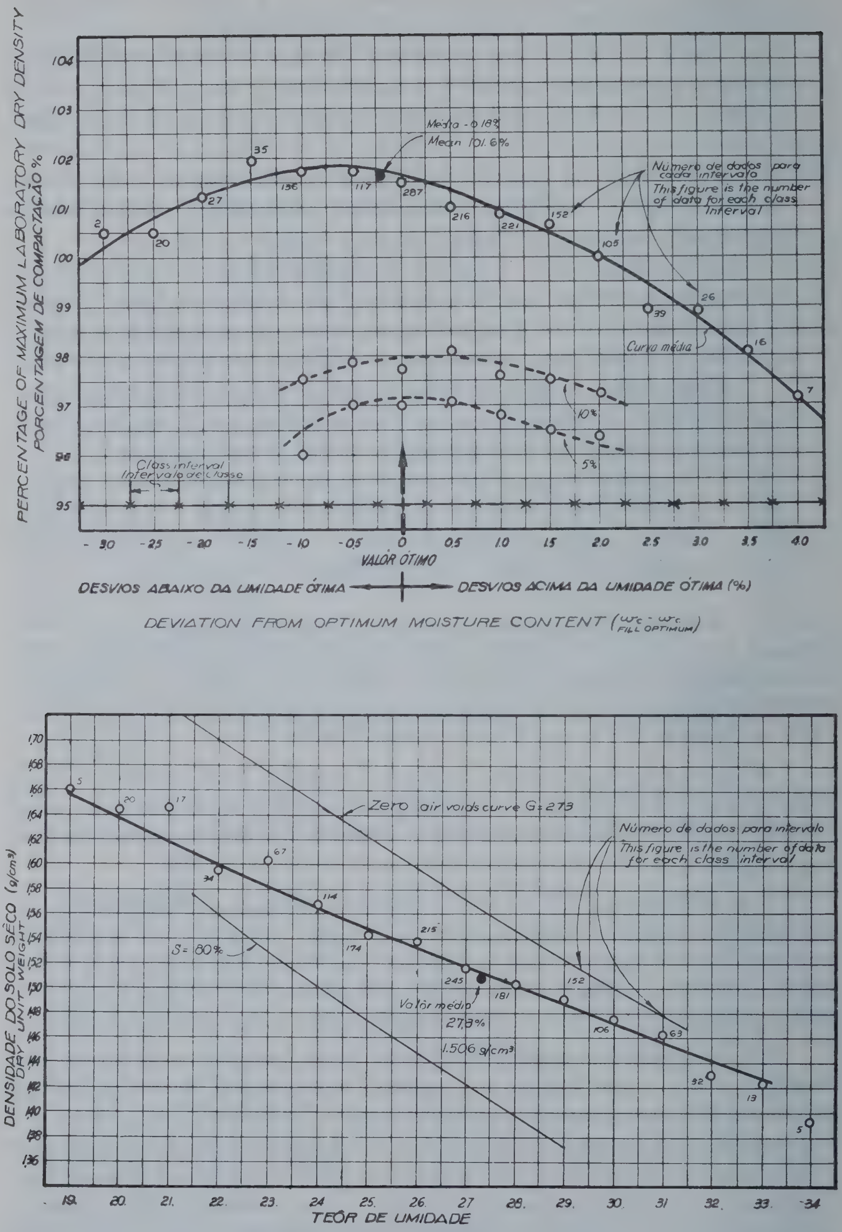

Fig. 4 — Curva de compactação de campo e curva dos valores densidade vs. umidade do solo compactado.

Fig. 4 — Field compaction curve and dry density vs. moisture content curve for field values.

O traçado da curva média indica que as condições máxima e ótima seriam obtidas para compactação de materiais com teores de umidade da ordem de 0.5 a 1.0% abaixo do valor ótimo do ensaio adotado. Tal fato é aparentemente contraditório em se tratando de compactação com rolos pneumáticos, os quais são mais eficientes na compactação de materiais quando na umidade ótima do ensaio Proctor normal ou ligeiramente acima desta.

Esta aparente contradição tem sua origem na diferença encontrada para as curvas de compactação obtidas para o ensaio de compactação tipo Proctor normal com reutilização e sem reutilização do solo compactado após o primeiro ponto da curva, conforme evidenciado pela figura 5.

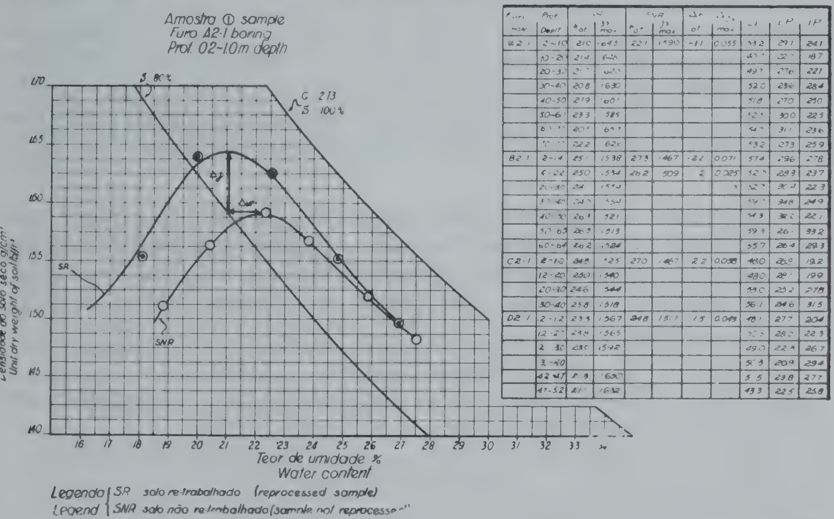

Furo	Prof	[illegible]		SNR		Δh	Δγs	LL	LP	IP
hole	Depth	h ot	γs max	h ot	γs max	ot	max			
A2 1	2~10	210	·645	221	1590	-11	0.055	532	291	241
	10-20	214	[illegible]					[illegible]	[illegible]	187
	20-30	[illegible]	[illegible]					497	270	221
	30-40	208	1630					520	236	284
	40-50	219	1601					518	270	250
	50-60	233	585					[illegible]	300	225
	[illegible]	[illegible]	[illegible]					[illegible]	311	236
	[illegible]	222	[illegible]					[illegible]	273	259
B2 1	2-14	251	1538	273	1467	·22	0.071	574	296	278
	[illegible]	250	·534	262	509	2	0.025	[illegible]	283	237
	[illegible]	24	[illegible]					[illegible]	[illegible]	223
	[illegible]	[illegible]	[illegible]					[illegible]	348	249
	[illegible]	[illegible]	521					543	[illegible]	221
	[illegible]	263	·513					593	[illegible]	332
	60-64	262	·524					557	264	293
C2·1	2-10	248	[illegible]	270	[illegible]	22	0.058	480	269	192
	12-20	250	·540					480	[illegible]	199
	20-30	246	544					530	252	278
	30-40	258	·518					561	246	315
D2 1	2-12	233	·567	248	[illegible]	15	0.049	481	277	204
	[illegible]	238	·565					[illegible]	282	223
	[illegible]	230	·542					490	[illegible]	267
	[illegible]							503	209	294
	[illegible]	[illegible]	·650					[illegible]	238	277
	47-52	[illegible]	·632					433	225	258

Fig. 5 — Ensaios de compactação de laboratório com solo retrabalhado e não retrabalhado.

Fig. 5 — Laboratory compaction tests with reprocessed and not reprocessed soil.

Observa-se a diferença sensível encontrada quanto à umidade ótima, no caso igual 22.1 — 21.0 = 1.1%.

A diferença entre densidade do solo sêco nos pontos máximos é relativamente menor 1.645 — 1.590 = 0.055 g/cm³, ou seja 3.7% do maior valor. Entretanto, também pode ser considerada como importante.

O método rápido do contrôle de compactação, idealizado pelo Dr. J. Hilf, do Bureau of Reclamation, utiliza a mesma energia de compactação do Proctor normal, porém, parte da compactação de três porções distintas da mesma amostra às quais é adicionada quantidade específica de água. Trata-se, portanto, de ensaio sem reutilização ou sem reprocessamento do material. É aliás o método de ensaio mais condizente com a compactação de campo. Durante a construção do núcleo em Furnas apenas se condicionou água ou se deixou secar o solo ligeiramente para ajuste às condições ótimas.

Ainda na figura 5 é apresentada tabela relacionando dados de 25 amostras de furos feitos na jazida. Constata-se a homogeneidade bastante grande dos materiais encontrados naquela área, o que permite sem dúvida extrapolar-se as conclusões iniciais obtidas.

Com base na média dos ensaios comparativos realizados, verifica-se um deslocamento considerável do valor da umidade ótima igual a 1.53% acima do valor ótimo do ensaio de laboratório. O deslocamento do valor máximo da densidade do solo sêco é em média 1.548 — 1.450 = 0.048 g/cm³ (3.1% do maior valor). Deslocamentos verificados para 18 das amostras ensaiadas estão apresentados gràficamente na figura 6.

O estudo estatístico dos pontos de "máxima" indica que os solos não retrabalhados durante o ensaio apresentam linha de máximos sensìvelmente diferente da curva média de máximos, estabelecida para 1000 solos brasileiros, indicada também na figura 6.

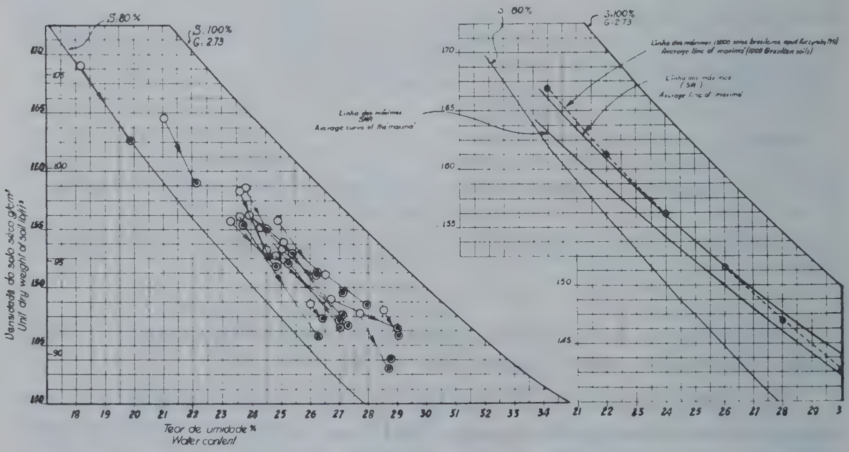

Fig. 6 — Relação entre os pontos máximos dos ensaios tipo SR (solo retrabalhado, pontos marcados por círculos brancos) e SNR (solo não retrabalhado, pontos marcados por círculos brancos e prêtos).

Fig. 6 — Correlation between the peak points of compaction tests with reprocessed soil (SR, points marked as white circles) and not-reprocessed soil (SNR, points marked as black and white circles).

Já a linha dos máximos dos solos retrabalhados durante o ensaio, pràticamente coincide com aquela curva média.

Investigações das causas prováveis dêstes deslocamentos dos pontos máximos indicaram influência marcante de partículas de argila aglutinadas pelo secamento ao ar e que não se dissociam imediatamente com adição de água para a compactação do laboratório. Assinale-se que na execução do ensaio com solo não reprocessado as porções das amostras foram deixadas absorver água durante 24 horas antes de serem compactadas. Quebramento de partículas durante a compactação é igualmente possível. Não se acumulou, entretanto, evidência suficiente para apontar qual a causa fundamental daquelas variações.

Considerando-se a nova posição dos pontos de máximo, constata-se que a argila do núcleo foi compactada com umidade mais próxima à do limite plástico. Embora não tenha sido ultrapassado êste valor, é uma diferença sensível, que para barragem de terra com seção homogênea pode explicar desenvolvimento de pressões neutras de valor superior às previsões.

No caso da barragem de Furnas, constatou-se que, apesar desta circunstância, a resistência ao cisalhamento do material compactado excedeu as hipóteses de cálculo do projeto.

Ensaios triaxiais do tipo lento (S) e adensado-rápido com medida de pressão neutra ($\bar{R}$) forneceram ângulos de atrito cujos menores valôres foram de 33°.

Ensaios do tipo rápido (Q) apresentaram intersepto de 1,5 kg/cm^2 e ângulo de resistência ao cisalhamento de 18° até valores da tensão normal correspondente à pressão de pré-adensamento quando o ramo da envoltória torna-se horizontal para valôres da tensão de cisalhamento de 3,2 kg/cm^2 independente da tensão normal.

Além disto, o desenvolvimento normal dos assentamentos da barragem como observado na figura 8 faz supor que as características de compressibilidade de todo o maciço são também muito satisfatórias. As amostras ensaiadas em laboratório apresentaram índice de compressão variando de 0,17 a 0,20 e pressão de pré-adensamento compreendida entre prováveis valôres 5,5 e 2,4 kg/cm^2.

CONTRÔLE DE COMPACTAÇÃO DAS ZONAS DE TRANSIÇÃO E ENROCAMENTO

Transição colocada adjacente ao núcleo de argila consiste de material resultante da desagregação ou alteração dos quartzitos locais. Essencialmente, é areia grossa e fina com quantidade considerável de fragmentos de maior diâmetro, forma lamelar, muito friáveis.

Tal material apresenta granulometria contínua, com aparente falta de partículas de diâmetro compreendido entre peneiras de n.º 40 (0,42 mm de abertura) e 4 (4,8 mm de abertura). Entretanto, tal circunstância é apenas devida à forma lamelar dos fragmentos de rocha e os quais se apresentam com a foliação própria do quartzito alterado. O traçado da curva média de 162 ensaios executados, conforme indicado na figura 7 evidencia percentagem elevada (14%) de material passando na peneira de 200 "mesh", sem entretanto apresentar partículas de diâmetro inferior a 0,05 mm ou fração silte. Não só a linha média como também as duas curvas que limitam 90% de todos os ensaios executados permitem generalizar esta característica, a qual representa ótimas condições granulométricas para o material de transição, no caso perfeitamente enquadrado na faixa usualmente recomendável de materiais drenantes.

Com a compactação de materiais brandos e friáveis, dotados igualmente de considerável parte fina, e adjacentes às zonas de transição pode-se concluir haver segurança plena contra quaisquer assentamentos diferenciais do núcleo mesmo que êstes atingissem valores excessivos.

A compatação dos materiais de transição, efetuada também para os materiais tipo "random" e "rockshell", foi feita

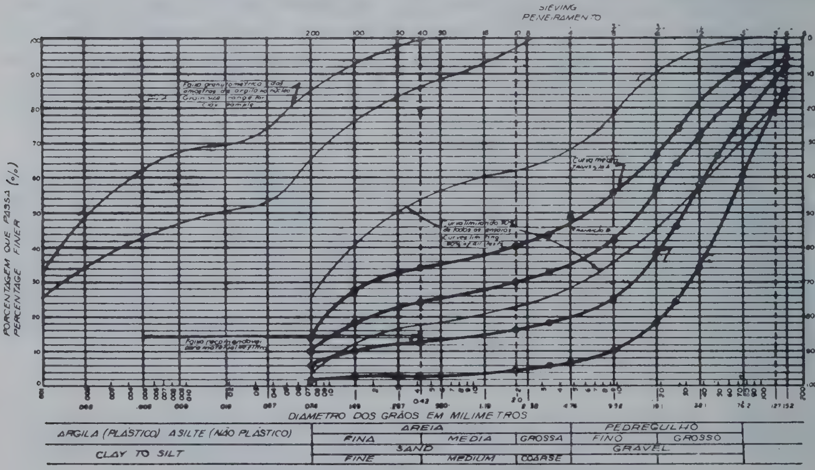

Fig. 7 — Curvas granulométricas dos materiais compactados na barragem.

Fig. 7 — Grain size curves of materials compacted in the dam.

com trator de esteira D-8, aplicando-se no mínimo duas passadas após espalhamento das camadas cuja espessura variou de 0,30 m na zona de transição a 0,70 m nos enrocamentos, após compactação.

A granulometria contínua dos materiais favoreceu sobremaneira a obtenção de altas densidades, dispensando inclusive a necessidade de qualquer umedecimento ou mesmo encharcamento dos materiais.

As determinações de densidade dêstes materiais no campo foram feitas escavando-se poços na superfície compactada, após cuidadoso nivelamento no tôpo da camada. Retirou-se quantidade de material da ordem de 200 kg para cada ensaio, tomando-se cuidado de não se alterar o estado de compacidade das paredes do poço.

Um lençol de plástico bastante fino e aderente revestindo as paredes do poço permite determinar o volume do mesmo pela quantidade de água necessária para enchê-lo até a borda.

Os seguintes resultados foram obtidos dos ensaios de densidade:

	Densidade aparente sêca t/m³	Teor de umidade de compactação (%)	Número de ensaios
Transição A	1.89	4.2	162
Transição B	1.97	4.0	54
"Random"	1.98	2.5	141
"Rockshell"	1.85	1.5	111

Dois tipos de transição A e B são mencionados. A distinção está na proporção ligeiramente maior de fragmentos de dimensões maiores que 2 mm encontráveis na transição B, a qual foi colocada à jusante da transição mais fina (tipo A) e também à montante do núcleo, nas cotas mais inferiores da barragem não atingidas inclusive pelo nível mínimo de depleção do reservatório.

Análises granulométricas foram igualmente feitas para materiais tipo "random" e "rockshell" compactados nos demais enrocamentos.

As respectivas curvas médias também apresentadas na figura 7 confirmam a observação visual de quebramento considerável dêstes materiais verificado durante espalhamento e compactação com trator.

Não sòmente o quartzito alterado ou brando como também o quartzito duro e são se fragmentam com muita facilidade, ao longo dos planos de estratificação, embora não sòmente ao longo dêstes planos.

Ensaios comparativos de granulometria executados com quartzito são, na área de escavação e após compactação na barragem, indicaram que a percentagem de "finos" (diâmetro menor que 1 polegada) aumentou de 5 para 22% em pêso total das amostras ensaiadas. A percentagem de material de diâmetro menor que 6 polegadas passou de 50 a 84%.

Devido a tão intensivo quebramento, mínimos assentamentos são previstos, muito embora o efeito de encharcamento possa resultar em algum assentamento adicional no enrocamento de montante.

Com efeito, resultados de ensaios de compressão simples com atuação da carga normalmente aos planos de estratificação e executados no Instituto de Pesquisas Tecnológicas em São Paulo evidenciam para a rocha considerada sã ou ligeiramente alterada e em estado sêco, resistência média igual a 1.720 kg/cm^2 (24.460 p.s.i.). Após encharcamento durante 48 horas, a resistência média de corpos de prova das mesmas amostras foi de 901 kg/cm^2 (12.820 p.s.i.). A relação entre resistência após encharcamento e resistência em estado sêco seria o "fator de abrandamento" da rocha sob ação da água. Seu valor seria 52% para os quartzitos de Furnas.

Apesar da perda sensível de resistência, seu valor após encharcamento ainda pode ser considerado elevado. Por conseguinte, embora previsíveis, tais assentamentos adicionais não serão de vulto.

Os resultados dos ensaios poderiam talvez apontar como recomendável, a operação de encharcamento ("sluicing") além da compactação de camadas, de modo a reduzir ao mínimo tais assentamentos.

Ensaios triaxiais com pressão de confinamento máximo de 10 atmosferas em amostras de material que posteriormente foi utilizado na barragem foram executados pelo Bureau of Reclamation (U.S.A.) e forneceram ângulos de atrito variando de 33 a 38° com média provável de 36°.

Êstes ensaios revelaram, a par de ângulo de atrito relativamente baixo, deformações específicas elevadas atingindo até 20% na ruptura e nos ensaios de maiores pressões de confinamento. Intenso quebramento dos fragmentos se verificou durante o ensaio.

É possível que, dado o quebramento que se obteve no ato de compactação no campo, as deformações do maciço da barragem sejam de muito reduzidas.

Ensaios adicionais com amostras extraídas do enrocamento compactado estão sendo executados pelo Corps of Engineers (U.S.A.) e fornecerão provàvelmente informações mais conclusivas.

COMPORTAMENTO DO MACIÇO

Após término da barragem em dezembro de 62 e prèviamente ao fechamento das comportas dos túneis de desvio para início de represamento, foram instalados marcos na crista e talude da barragem para medida dos assentamentos verticais e deslocamentos horizontais.

A barragem foi projetada em arco com raio de 450 metros; melhorando as condições dos contatos com as ombreiras, esta disposição tem como finalidade principal anular a possibilidade de trincamento no núcleo devido a recalques diferenciais próximos aos contatos e devido às deflexões horizontais para jusante, observadas em tôdas as barragens desta magnitude.

a. *Deslocamentos horizontais* — A figura 8 apresenta os resultados das medições dos deslocamentos horizontais dos monumentos de concreto colocados na crista e talude. Verifica-se que, exceto para os marcos mais próximos da margem esquerda para os quais não está ainda perfeitamente definida, está-se processando efetivamente a ação de arco da barragem com transmissão de empuxos para as ombreiras.

Os movimentos iniciais foram assinalados sòmente três semanas após o fechamento dos túneis e após o reservatório ter subido 59 metros. Êstes movimentos iniciais foram em sua maioria para montante, refletindo influência do encharcamento do maciço de enrocamento de montante.

Movimentos adicionais estão nìtidamente orientados para jusante, tendo sido registrado o máximo acumulado de 5,2 cm referente ao marco n.º 11.

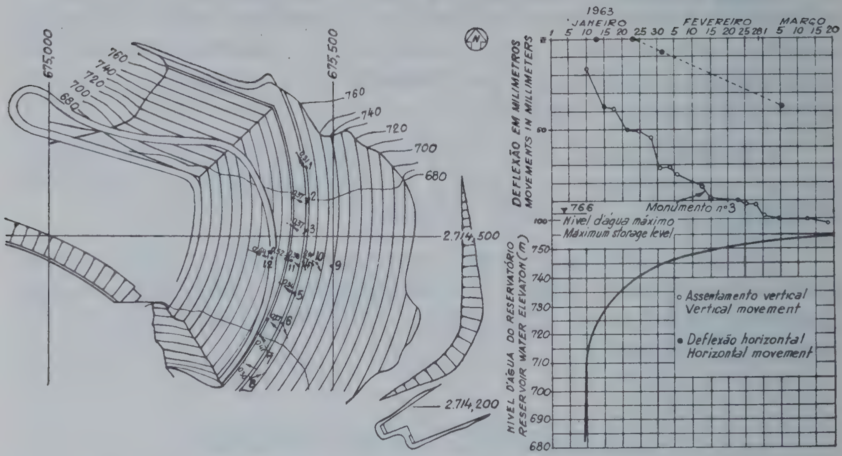

Fig. 8 — Deflexões horizontais e assentamento do maciço.

Fig. 8 — Vertical and horizontal movements.

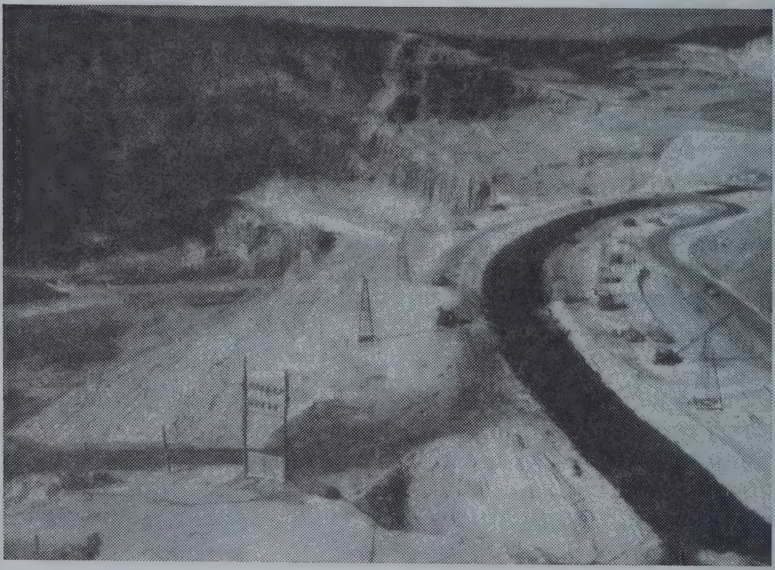

Fig. 9 — Aspecto da construção em agôsto de 1962.

Fig. 9 — View from right bank in August 1962.

b. *Assentamentos verticais* — Na figura 8 está apresentado o gráfico correspondente ao máximo assentamento vertical, medido para o marco de n.º 3 até à data.

Conforme se pode verificar, o assentamento atinge total de 10 cm apenas e seu desenvolvimento se processa com absoluta regularidade.

Considerando-se os reduzidos valores dêste assentamento assim como os da deflexão horizontal medida com reservatório a 90% de sua altura d'água final, já se pode antecipar condições altamente satisfatórias de comportamento do maciço.

NOTA FINAL

O aproveitamento hidrelétrico de Furnas é obra a cargo da Central Elétrica de Furnas S.A., entidade brasileira de economia mista.

A barragem foi recém-completada pelo Consórcio Anglo-Brasileiro formado pelas firmas George Wimpey (Londres) e Companhia Construtora Nacional S.A.

O projeto foi executado pela Companhia Internacional de Engenharia e Construções, sendo consultor do projeto o Prof. Arthur Casagrande.

CÁLCULO DE ESTABILIDADE DE BARRAGENS DE TERRA PELO COMPUTADOR ELETRÔNICO UNIVAC-1105 (*)

OTTO PFAFSTETTER

Diretor da Divisão de Projetos Estruturais do Departamento Nacional de Obras de Saneamento do Ministério da Viação e Obras Públicas
Rio de Janeiro — Brasil

SINOPSE

A verificação gráfica da estabilidade de taludes de barragens de terra pelo método sueco ou dos círculos de escorregamento é muito laboriosa. Para facilitar êstes cálculos de estabilidade, várias soluções têm sido propostas para efetuá-los com auxílio de computadores eletrônicos dígitos (ver referências 1 a 4). No presente trabalho será discutido um programa para o computador UNIVAC-1105 (**).

Na verificação da estabilidade, adotou-se o método sueco de círculos de escorregamento descrito em literatura do assunto. Quando o círculo de escorregamento encontra a base de rocha, admitiu-se que a superfície de escorregamento desvia da forma circular na parte inferior, acompanhando o contôrno desta camada mais resistente.

A estabilidade do talude de jusante e de montante são investigados separadamente. Para cada talude o programa instrui a verificação da estabilidade em duas etapas sucessivas: Primeiro são examinadas as condições com as poropressões desenvolvidas logo após a construção. Depois são examinadas as condições com as pressões intersticiais da água que percola através da barragem.

Para o talude de jusante é considerada a rêde de percolação permanente com reservatório cheio, enquanto para o talude de montante prevalece a rêde de percolação para esvaziamento brusco do reservatório, por ser mais desfavorável à estabilidade.

(*) Condensação de um estudo mais completo publicado por ocasião dêste Congresso pelo Departamento Nacional de Obras de Saneamento — M.V.O.P.

(**) No Brasil existe um computador UNIVAC-1105 no Centro de Processamento de Dados do Serviço Nacional de Recenseamento do Instituto Brasileiro de Geografia e Estatística à Av. Pasteur nº 404 — Rio de Janeiro.

Para cada posição do centro do círculo de escorregamento são examinados vários círculos com diferentes raios. O menor coeficiente de segurança encontrado para os diversos círculos de um mesmo centro é fornecido como resultado externo, datilografado pela máquina ao lado da indicação da ordem do raio correspondente. Com êstes resultados pode-se traçar as linhas de igual coeficiente de segurança, que permitem localizar o círculo de menor estabilidade.

Na última parte do trabalho será discutido um programa para o cálculo dos potenciais na rêde de percolação com o computador UNIVAC-1105. Êstes potenciais são utilizados na verificação da estabilidade da barragem, podendo também ser obtidos por processos gráficos ou em modelos hidráulicos e de analogia elétrica. O computador calcula os potenciais pelo método das relaxações, partindo de uma rêde de percolação aproximada, cujos potenciais são definidos pelo programa. São calculados sucessivamente os potenciais para o escoamento permanente com o reservatório cheio e para esvaziamento brusco do mesmo.

Para ilustrar a aplicação dêstes programas, será apresentado como exemplo a verificação da estabilidade e o cálculo da rêde de percolação na Barragem de Chapéu d'Uvas (*).

SYNOPSIS

The graphical stability computation of earth dam slopes with the Swedish slip circle method is very tedious. In order to improve these stability computations, considerable effort has been spent to give a solution with electronic computers (see references 1 through 4). This article discusses a program for stability computations with the UNIVAC-1105 electronic digital computer.

The proposed solution endeavors to cover all practical cases, from the simplest homogeneous sections to the most complicate zoned embankments on heterogeneous foundations. The pore pressures developed in the impervious zones during construction, as well as the effect of percolating water for steady flow or draw-down conditions may be considered in this computation.

The stability of the upstream and the downstream slopes are investigated separately. The program instructs the stability computation for each slope in two successive steps. First are investigated the conditions right after construction and subsequently the conditions after the establishment of a flow net.

For each position of the slip circle center, several circles with different radii are investigated. As external

---

(*) A barragem de Chapéu d'Uvas, no município de Juiz de Fora, Minas Gerais, foi projetada e está sendo construída pelo Departamento Nacional de Obras de Saneamento, Ministério da Viação e Obras Públicas para o refôrço do abastecimento de água e energia elétrica de Juiz de Fora.

result, the computer types the smallest safety factor found for each center and the order number of the corresponding radius. With these results, lines of equal safety factor may be drawn and the slip circle of least stability located.

The last part of the article shows how to get the flow net potentials with the UNIVAC-1105 computer. It serves as a complement to the stability computation of dams. The potentials are obtained by the relaxation method, starting with an approximate flow net.

The flow net and stability computation of Chapéu d'Uvas Dam illustrates the application of the program for a very general case of zoned embankments.

CÁLCULO DA ESTABILIDADE DOS TALUDES

Os contornos dos diferentes materiais que compõem a barragem e sua fundação são definidos por linhas poligonais. Admite-se que a estrutura se compõe de no máximo dez materiais com características físicas diferentes e que as superfícies de separação entre os mesmos possam ser definidas por linhas poligonais tendo cada uma no máximo dez vértices. Basta assim fornecer ao computador as coordenadas dos cem (100) vértices das poligonais de contôrno das diferentes camadas para definir a forma de estruturas relativamente complexas.

As características físicas dos materiais que definem seu comportamento mecânico compreendem o pêso específico, a coesão e o ângulo de atrito interno. Os ângulos de atrito interno dos materiais argilosos devem ser determinados em ensaios de cisalhamento triaxiais com medidas de poropressões. Pode-se assim considerar no cálculo o efeito dêstes coeficientes de atrito em conjunto com as poropressões previstas para a estrutura.

Para o cálculo da estabilidade logo após a construção, a relação entre as poropressões e as pressões totais nos materiais impermeáveis pode ser determinada a partir de ensaios de adensamento em amostras compactadas, com drenagem livre, conforme foi descrito na referência 5.

Para cada material impermeável são fornecidos ao computador as coordenadas de oito pontos da curva que define a relação entre as poropressões e as pressões totais.

Para os materiais permeáveis é fornecido um valor que os distingue dos impermeáveis, outro que indica se o mesmo está ou não saturado e finalmente o nível livre da água contida nos seus poros, quando a mesma estiver sob pressão.

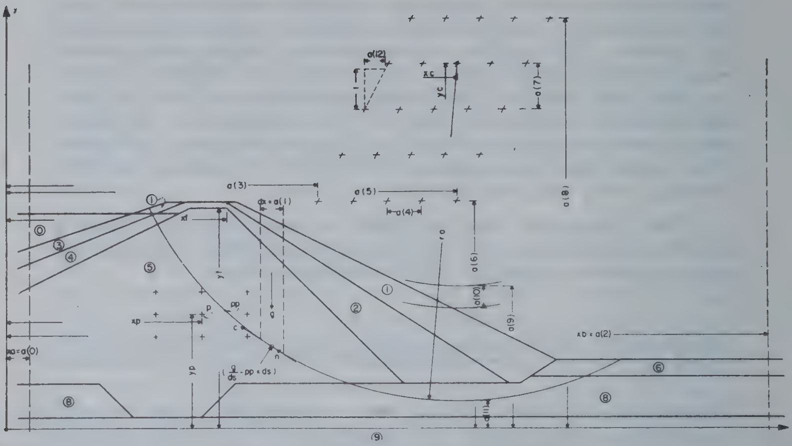

Fig. 1 — Definição das variáveis.

Fig. 1 — Definition of the variables.

O computador calcula com êstes dados as pressões intersticiais desenvolvidas nos materiais permeáveis e impermeáveis logo após a construção.

Para o cálculo da estabilidade com a rêde de percolação, define-se os potenciais nos nós de uma rêde ortogonal, cujas abscissas e ordenadas são respectivamente xp e yp (ver fig. 1). Dando assim, os potenciais em *192* pontos, o computador calcula por interpolação linear a pressão intersticial em qualquer parte da estrutura ao longo do círculo de escorregamento.

O cálculo da estabilidade consiste na determinação do coeficiente de segurança à rotura, definido pela relação entre os momentos das fôrças estabilizantes e as de derrubamento. Êstes momentos, obtidos para cada faixa vertical de largura dx, são integrados ao longo do círculo de escorregamento (ver fig. 1). Os centros dêstes círculos de escorregamento são dispostos segundo os nós de uma rêde oblíqua de abscissas xc e ordenadas yc. A rêde oblíqua acompanha a conformação das linhas de igual coeficiente de segurança, permitindo uma melhor definição das mesmas com o mínimo de centros.

Para cada centro são examinados vários círculos de escorregamento com raios diferentes, fazendo o computador a seleção do círculo que corresponde ao menor coeficiente de segurança. É fornecido como resultado externo sòmente o coeficiente de segurança mínimo para cada centro e a ordem do raio correspondente. Economiza-se assim tempo na utilização do computador, porque a datilografia dos resultados, por ser uma operação mecânica, é mais demorada que o processamento dos cálculos eletrônicos correspondentes. Todos os cálculos referentes a um círculo de escorregamento são efetuados pelo computador em aproximadamente um (1) segundo, enquanto a datilografia de um coeficiente de segurança como resultado externo dura cêrca de três (3) segundos.

A figura 2 mostra os resultados do cálculo da estabilidade do talude de jusante da Barragem de Chapéu d'Uvas.

A zona impermeável desta barragem será executada com material residual escavado na ombreira direita, onde o desmonte do contraforte ali existente, permitirá a implantação de um amplo sangradouro auxiliar. Êste material residual possui aproximadamente 53% de areia, 39% de silte e 8% de argila (*). O limite de liquidez é de 38,6% e o índice de plasticidade 15,3%. O coeficiente de permeabilidade vertical médio é de $1{,}1 \times 10^{-6}$ cm/s. Os valores da umidade ótima e pêso específico máximo relativos à compactação Proctor Standard são respectivamente 17,8% e 1,710 g/cm^3.

Os ensaios de cisalhamento triaxial com medidas de poropressões forneceram na média uma coesão de 0,10 kg/cm^2 e um ângulo de atrito interno de 34°.

Os ensaios de cisalhamento triaxial com medidas de poram calcular a relação entre poropressões e pressões totais a esperar na obra, caso não ocorra drenagem do fluido intersticial, conforme a referência 5. Resultaram poropressões entre 15% e 20% das pressões totais, dentro dos limites de solicitações que vão ocorrer na obra.

A capa superior da jazida de material impermeável com cêrca de 3 m de espessura apresenta uma alteração mais acentuada, sendo mais argilosa e mais impermeável, possuindo um ângulo de atrito interno menor e compressibilidade maior. Sendo êste material menos favorável à estabilidade, pretende-se usá-lo sòmente numa estreita faixa central da barragem, melhorando as condições de impermeabilidade sem influir pràticamente na resistência mecânica.

A zona permeável externa do talude de jusante será formada de areia extraída do leito do rio. Esta zona, além de melhorar as condições de estabilidade por eliminar as poropressões na região que ocupa na seção da barragem, ainda permite coletar as águas que percolam através da zona im-

---

(*) Os ensaios de caracterização, compactação, adensamento e cisalhamento triaxial com medidas de poropressões foram efetuados no laboratório de RODIO S/A.

permeável até uma altura em que outro tipo de filtro difìcilmente seria eficiente. A zona permeável é protegida contra a erosão superficial por uma camada de enrocamento.

Na figura 2 estão indicadas as posições dos centros dos círculos de escorregamento examinados, alinhando-se segundo os nós de uma rêde oblíqua. Para cada um dêstes centros foram examinados dez círculos de escorregamento tendo raios variando em intervalos de 3 m. Os raios mínimos correspondem aos círculos, cuja tangente horizontal inferior passa a 42 m do eixo das abscissas. Os raios máximos correspondem aos círculos, cuja tangente horizontal inferior passa a 15 m do eixo das abscissas. A ordem dos raios para cada centro cresce assim de 0 a 9, conforme se passa do valor mínimo ao máximo com acréscimos de 3 m.

Ao lado e abaixo de cada centro figura o coeficiente de segurança mínimo encontrado e acima do mesmo o número de ordem do raio do círculo de escorregamento que lhe corresponde.

Com êstes valores traçou-se as curvas de igual coeficiente de segurança que permitiram localizar o círculo de escorregamento de menor estabilidade. Êste círculo para o caso logo após a construção foi traçado na figura 2, sendo o coeficiente de segurança correspondente convenientemente realçado. Como os coeficientes de segurança achados se referem a círculos de escorregamento com raios diferentes, a forma das linhas de igual coeficiente de segurança é um pouco irregular.

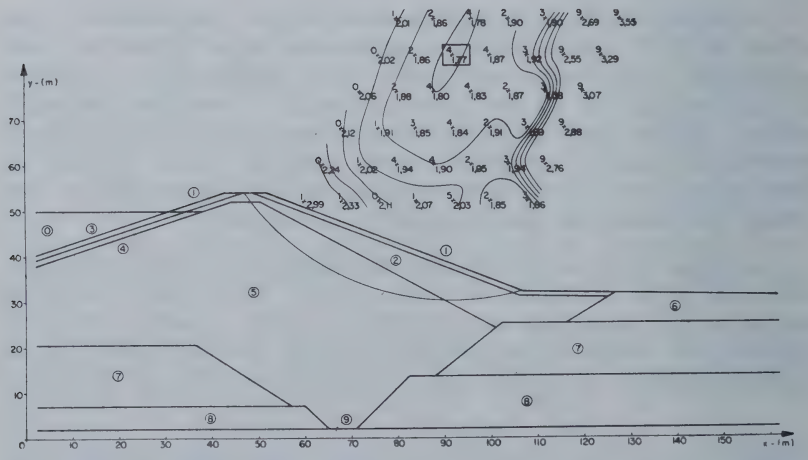

y-(m)
70
60
50
40
30
20
10
0
10
20
30
40
50
60
70
80
90
100
110
120
130
140
150
x-(m)
1 2,01
2 1,86
4 1,78
2 1,90
3 1,90
9 2,69
9 3,55
0 2,02
2 1,86
4 1,77
4 1,87
3 1,92
9 2,55
9 3,29
0 2,05
2 1,88
4 1,80
4 1,83
2 1,87
3 1,98
9 3,07
0 2,12
1 1,91
3 1,85
4 1,84
2 1,91
3 1,89
9 2,88
0 2,24
1 2,02
4 1,94
4 1,90
2 1,86
3 1,94
9 2,76
1 2,99
1 2,33
0 2,11
1 2,07
5 2,03
2 1,85
3 1,86
①
⓪
③
④
①
②
⑤
⑥
⑦
⑦
⑧
⑧
⑨

Fig. 2 — Estabilidade do talude de jusante logo após a construção.

Fig. 2 — Stability of the downstream slope right after construction.

Nesta apresentação sumária não figuram os resultados do cálculo de estabilidade do talude de jusante com a rêde de percolação, nem a verificação da estabilidade do talude de montante.

CÁLCULO DA RÊDE DE PERCOLAÇÃO

O processo de relaxações usado para calcular os potenciais numa rêde de percolação consiste em determinar o potencial num ponto a partir dos potenciais em pontos vizinhos, segundo relações que traduzem a lei de escoamento em meios porosos. Efetuando êste cálculo para todos os pontos dispostos segundo os nós de uma rêde ortogonal que cobre a estrutura em estudo e repetindo esta operação numerosas vêzes para todo o campo, aproxima-se progressivamente do resultado procurado.

Aplicando o princípio da continuidade e a lei de escoamento em meios porosos de Darcy, obtém-se uma expressão que dá o potencial num nó da rêde referida, em função dos potenciais nos quatro nós vizinhos. Escolheu-se para relação entre a dimensão horizontal e vertical das malhas em cujos nós se determina os potenciais, um valor igual à raiz quadrada da relação entre coeficientes de permeabilidade nestas duas direções. Assim a expressão antes referida se simplifica, sendo o potencial num ponto dado pelo média aritmética dos potenciais em pontos vizinhos.

O cálculo das relaxações deve partir de valores aproximados, estimados para os os potenciais nos diversos pontos da rêde ortogonal. Para um certo número de relaxações, obtém-se um resultado tanto mais próximo da solução exata quanto melhor forem estimados os potenciais iniciais.

A distribuição dos potenciais iniciais na região da zona impermeável foi definida por leis de variação linear. Fora da zona impermeável os potenciais definem as condições limites, sendo iguais ao nível da água no reservatório na parte de montante e iguais ao nível livre da água intersticial nos materiais permeáveis a jusante. Na região em que se encontra ar, ou materiais permeáveis não saturados, os potenciais são iguais à cota do ponto considerado. Ao longo da superfície da rocha na base da trincheira de impermeabilização, introduziu-se a condição de não escoamento, igualando em cada relaxação os potenciais na rocha aos dos pontos vizinhos na zona impermeável.

Introduziu-se no programa do cálculo dos potenciais, a pesquisa automática da forma da linha freática. Sua posi-

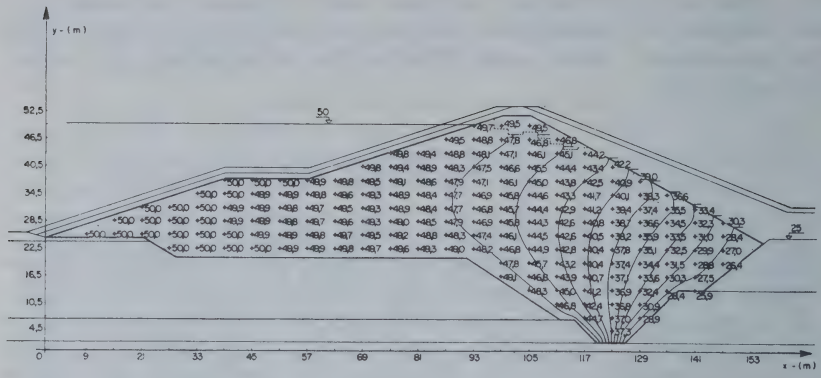

Fig. 3 — Potenciais para escoamento permanente.

Fig. 3 — Steady flow potentials.

ção ficou definida pela condição dos potenciais nos pontos imediatamente abaixo dela terem valores maiores, porém mais próximos possíveis ao de suas cotas.

O resultado do cálculo da rêde de percolação com regime permanente e reservatório cheio para a Barragem de Chapéu d'Uvas se encontra na figura 3. Em 15 minutos de operação do computador efetuaram-se 200 relaxações em 724 pontos de rêde ortogonal que se encontravam dentro da zona impermeável. Para reduzir os resultados de saída da máquina, esta forneceu sòmente os potenciais em pontos alternados tanto no sentido horizontal como no vertical. Êstes potenciais na quarta parte dos pontos da rêde ortogonal estão indicados na figura 2. Traçou-se as linhas equipotenciais por interpolação entre êstes potenciais fornecidos pelo computador. Êstes valores dos potenciais na rêde ortogonal foram usados no cálculo da estabilidade descrito no capítulo anterior.

Aparece também na figura 2 em tracejado a linha freática determinada pelo computador. Esta linha tem forma denteada devido às sucessivas tentativas da máquina para mantê-la junto aos pontos, cujos potenciais se aproximam de suas cotas.

Nesta apresentação resumida não figuram os resultados obtidos para a rêde de percolação com abaixamento rápido do reservatório que serviram para o cálculo da estabilidade do talude de montante.

BIBLIOGRAFIA

1. The Use of an Electronic Computer for Slope Stability Analysis, by A. L. Little and V. E. Price. Géotechnique — Volume 8 — 1958 — London.

2. Über die Verwendung von Elektronenrechenmaschinen beim Entwurf von Erddämen, von Dipl. — Ing. Klaus John. Die Bautechnik — 7/1961 — Berlin.

3. Computer Analysis of Slope Stability, by John A. Horn. Paper 2501, Volume 86, No. SM3 — June 1960 — Part 1. Journal of the Soil Mechanics and Foundations Division. Proceedings of the American Society of Civil Engineers.

4. Computation of the Stability of Slopes, by Otto H. Meyer, Paper 1824, Volume 84, No. SM4, October 1958, Part 1. Journal of the Soil Mechanics and Foundations Division, Proceedings of the American Society of Civil Engineers.

5. Estimating Construction Pore Pressure in Rolled Earth Dams, by J. W. Hilf — Vol. III — 1948. Proceedings of the Second International Conference on Soil Mechanics and Foundation Engineering.

THE EFFECT OF UNDERDRAIN CARPET ON SEEPAGE QUANTITIES THROUGH EARTH DAMS

A. R. JUMIKIS

Dr. Eng. Sc., Professor of Soil Mechanics and Foundation Engineering, Rutgers The State University, New Brunswick, New Jersey, U.S.A.

W. J. WEBER, Jr.

Assistant Instructor in Civil Engineering, Rutgers — The State University, New Brunswick, New Jersey. Fall, 1962 doctoral candidate in Sanitary Engineering, Harvard University, Cambridge, Massachusetts.

SUMMARY

This paper describes the results obtained in the laboratory from small-scale experiments on the effect of the width of an underdrain carpet on the amount of gravitational seepage flowing through earth dam models made of five different types of soils. Based on these experimental results, this effect could be expressed for the experimental limits by an exponential function, the exponent depending upon the soil type used (viz., the system's permeability) and the width ratios of the carpet to the length of the horizontal projection of the downstream slope. The experiment permits to determine the system's permeability.

This paper may also serve as a comparative guide to those who may themselves wish to perform similar studies as described in this paper.

SUMARIO

Esta obra detalla los resultados obtenidos en el laboratorio a base de experimentos escalados, tratandose del efecto de la anchura de la carpeta de desague inferior en la magnitud de la filtración de agua a través de diques de tierra. Cinco series de experimentos fueron cumplidos, la composición del dique variando en cada serie. Basandos en los resultados de estos experimentos, este efecto puede ser expresado, entre limites experimentales, por medio de una función exponencial, en cual el expoente depende en el tipo de suelo utilizado (viz., la permeabilidad del sistema) y la relación de anchura de carpeta a la proyección horizontal del faldón (río abajo). Este ensayo puede servir también como un guia para otros investigadores interesados en aspectos similares del problema.

INTRODUCTION

General Notes — It is a universally established practice to use toe drains, filter galleries, underdrain carpets and other kinds of drainage facilities built into the body of an earth dam to intercept water seeping from upper levels and thus to provide for stability of the downstream slope and the dam itself. It is also well known that the greater the ratio of underdrain width to the length of horizontal projection of the downstream slope, the better is the stability of that slope. Under many conditions authorities on earth dam design [1] favor the use of a filter carpet set back under the dam a distance of 30% to 50% of the distance from the center line of the dam to the downstream toe. This, of course, neglects the importance of the amount of seepage flow, although these authorities on earth dam design say that often the increase of seepage because of the underdrainage facilities is not enough to be of economic importance.

In several instances, however, the consideration of seepage discharge is of relatively great importance. The relative importance of the seepage discharge depends primarily upon the uses to which the reservoir, impounding water, is assigned. For instance, the seepage trough an earth dam from a water supply reservoir should be maintained at a minimum, whereas seepage through a dam which is to be used for flood control purposes is not a major factor.

Although increased seepage through an earth dam brought about by an underdrain carpet may not contribute effectively to flood control, the underdrain carpet would contribute considerably to the stability of the dam regardless of whether the dam is used for impounding water, or for flood control.

Definition — By an underdrain carpet is here understood a horizontal drainage facility placed at the base of the dam and built back from the toe in the cross section of the dam (Fig. 1). Such an underdrain facility of a certain thickness and width extends continuously in the direction of the length of the dam; hence the term underdrain carpet in contradistinction to drainage galleries, which have a certain thickness, width and length, and may be spaced at the base of the dam at certain intervals.

Object of Study — A direct calculation on the effest of the width of an underdrain carpet on the amount of seepage encounters some mathematical difficulties, which may be

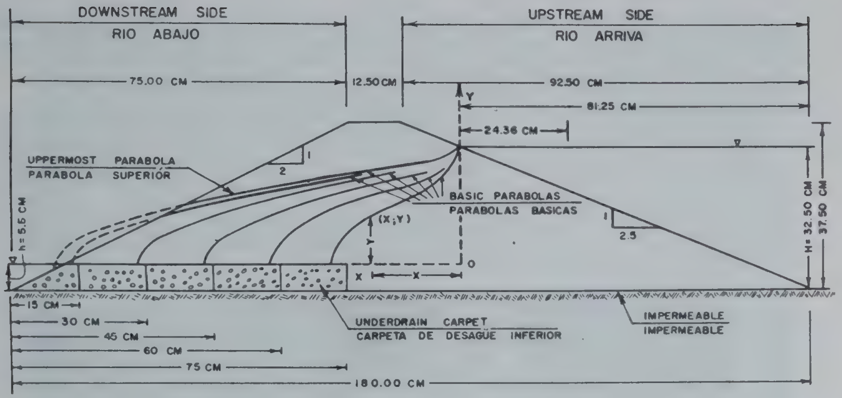
DOWNSTREAM SIDE
RIO ABAJO
UPSTREAM SIDE
RIO ARRIVA
75.00 CM
12.50 CM
92.50 CM
81.25 CM
24.36 CM
Y
UPPERMOST PARABOLA
PARABOLA SUPERIOR
1
2
BASIC PARABOLAS
PARABOLAS BASICAS
(X;Y)
Y
O
X
X
1
2.5
h=5.5 CM
H=32.50 CM
37.50 CM
15 CM
30 CM
45 CM
60 CM
75 CM
180.00 CM
UNDERDRAIN CARPET
CARPETA DE DESAGÜE INFERIOR
IMPERMEABLE
IMPERMEABLE

Fig. 1 — Experimental system.

Fig. 1 — Sistema experimental.

considered as the explanation why so little published information is available on this subject.

To obtain at least some insight into this problem, the study of the effect of width of an underdrain carpet on gravitational seepage quantities through earth dams was performed to a small scale experimentally. No capillary effects were considered. The experiments were performed at the Soil and Foundation Engineering Laboratory of the Department of Civil Engineering at Rutgers — The State University, New Brunswick, New Jersey.

Seepage Tank — The seepage tank, the inside dimensions of which are 74 in long × 25 in high × 6 in wide (188 cm long × 83 cm high × 15 cm wide), is a partly welded lightweight structural alumininum frame. Bolts are provided to tighten the unit to prevent leakage. The front and rear sides are covered with ½ in (12.7 mm) thick clear, translucent plastic sheets (Fig. 2). To prevent them from buckling out horizontally when filled with soil and water, three clamps are provided across the width of the tank at its top. From the front such a seepage tank affords an unobstructed visibility of the flow lines through the dam.

Overflow for maintaining constant heads of water at the upstream and downstream sides is provided by brass pipes installed vertically through the bottom of the tank. These overflow pipes are movable vertically. Leakage is prevented by water-tight graphite packings.

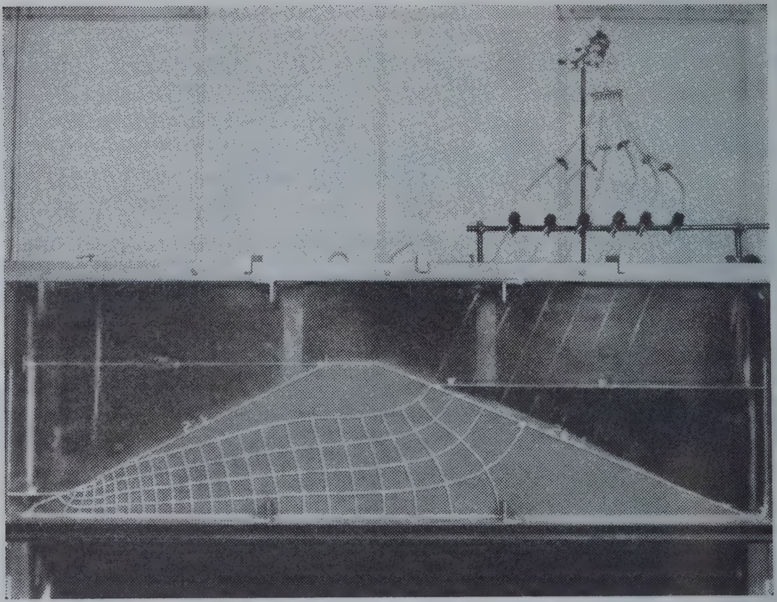

Fig. 2 — Seepage tank.

Fig. 2 — Tanque de filtración.

Water Suppy — The water supply to the upstream side of the dam is provided by means of a hose from tapwater.

Water temperatures before and after each seepage experiment were measured, and all seepage data in this paper are converted and reported at a standard temperature of +20°C [2].

Earth Dam Model — The dam model was constructed to the dimensions indicated in Fig. 1. The dam model simulates to scale its prototype built on an impervious foundation. Five types of soil were used to construct the dam models. The soil types are listed in Table 1. The dams were placed and compacted in layers 5 cm thick. For each layer the compacted density was determined, and the dry densities of the dam calculated.

The profile of the experimental dam is shown in Figs. 1 and 2. The slopes of the dam were kept always the same.

Soils Used in Experiment — Five different soil types were submitted to a series of experimental seepage determinations with and without the use of underdrain carpets. These soil types were found in Middlesex County, New Jersey [3, 4]. Some of their physical properties are compiled in Table 1.

The dry weights of compacted dry densities are tabulated in column 5, Table 1. The critical hydraulic gradient, i_c, of these soils relative to a quick condition is calculated by the following equation:

$$i_c = \frac{G-1}{1+e} \tag{1}$$

The particle size accumulation curves of these soils are shown in Fig. 3.

The material used in the underdrain carpet was the same in all cases. Its particle size accumulation curve is also shown in Fig. 3.

Underdrain Carpet — When needed, a horizontal drainage carpet, or porous underdrain, at the toe and back in the cross-section of the dam was constructed of washed, clean medium and fine gravel (see Figs. 1 and 2). Its permeability property, K_c, should be considerably greater than the per-

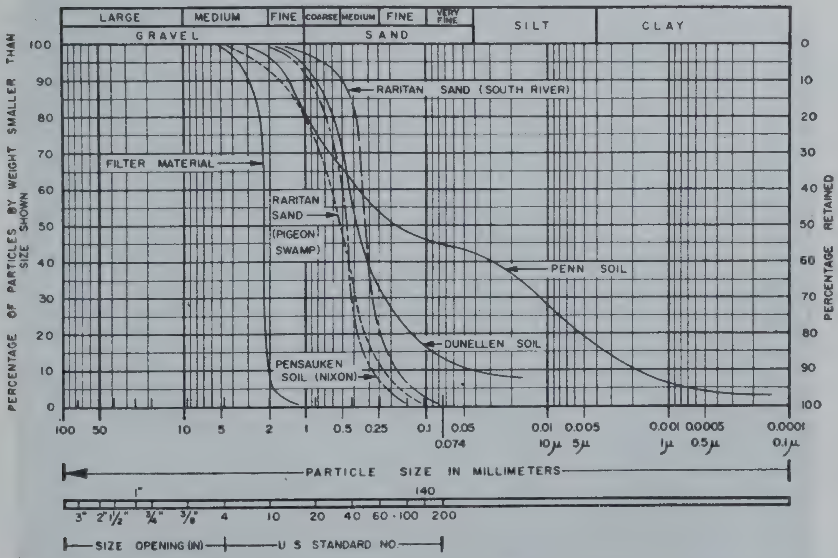

Fig. 3 — Soil particle size accumulation curves (U.S.D.A., Bureau of Soil Classification).

Fig. 3 — Curvas de acumulación de partículas de suelo (U.S.D.A., Bureau of Soil Classification).

meability, K_d, of the soil material of which the body of the earth dam is made. In the experiments the size of the underdrain carpet was 15.0 cm wide and 5.5 cm thick. Its length was varied in 15.0 cm increments, from 15.0 cm to 75 cm. The thickness, 5.5 cm, of the underdrain carpet was also the depth of the tailwater.

To prevent the underdrain carpet from clogging up at its top and entrance end of seepage water by fines which might be washed into the carpet from the body of the dam above the carpet a thin layer, about 1 cm thick, of fine gravel and coarse sand was placed on and at the entrance end of the carpet. The grading of this intermediate material was such that no clogging of the coarse underdrain carpet occurred.

The dye was carried along by the flowing water particles, visible by the green trail of the dye, (Fig. 5). The flowing dye was traced with a white china marker on the outside of the front sheet of plastic, by following the forward-most tip of the translocating green dye filaments. This tracing procedure resulted then in a flow line.

The equipotential lines are most readily sketched in to complete the flow net.

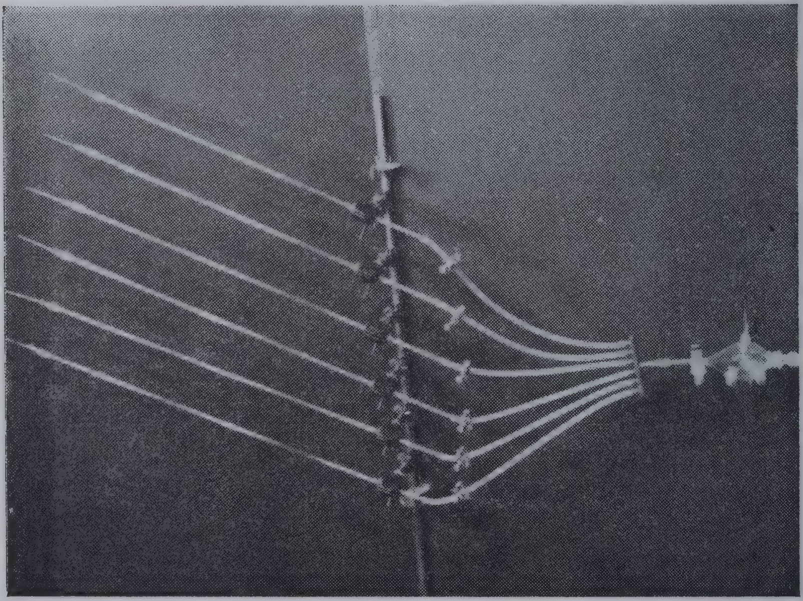

Fig. 4 — Dye injection device.

Fig. 4 — Aparato para la inyección del tinte.

TABLE 1 — Some Physical Properties of Soils Used in the Experimental Studies

Soil			Specific Gravity G	Dry Unit Weight γ g/cm	Void Ratio e	Consistency Limits		Critical Gradient i_{cr}	Homogeneous System's Permeability K cm/sec
No.	Type	Description				Liquid Limit LL %	Plasticity Index PI %		
1	2	3	4	5	6	7	8	9	10
1	Sand, white	Angularly grained quartzic material from the Raritan formation, South River, N.J.	2.65	1.58	0.676	N. L.	N. P.	0.985	9.20×10^{-2}
2	Sand, brownish-yellow (Nixon soil)	Angular, quartzic material of the Pennsauken formation, Edison Township, N.J.	2.66	1.72	0.545	N. L.	N. P.	1.075	4.44×10^{-2}
3	Sand, yellowish-white	Raritan formation (Pigeon Swamp sand), South Brunswick, N.J.	2.66	1.67	0.591	N. L.	N. P.	1.043	1.88×10^{-2}
4	Dunellen soil	Reddish-brow glacial outwash, a clayey, silty sand, Dunellen, N.J.	2.67	1.62	0.642	16	N. P.	1.015	3.36×10^{-3}
5	Penn soil	Triassic shale derivative, red, silty clay, University Heights, N.J.	2.64	1.40	0.892	30	8	0.866	4.72×10^{-4}

Dye Injection Device — The dye injection device consists of a dye container and a manifold to which 6 glass tubings are connected. The end of each tubing is provided with a hypodermic needle (Fig. 4). The injection device is rigged up as shown in Fig. 2. Fluorescein was used as the flowing tracing dye.

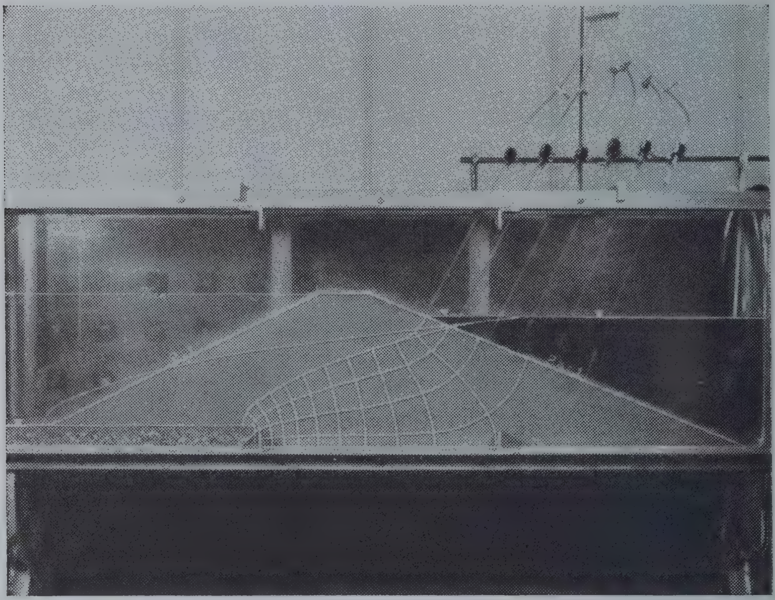

Fig. 5 — Experimental flow lines.

Fig. 5 — Lineas experimentales de filtración.

EXPERIMENTAL SYSTEM

System — The experimental system used in the experiments for all five types of soil is a homogenous dam resting on a horizontal, impervious foundation (Fig. 1), and five compound cross-section dams having an underdrain carpet of a certain width (Fig. 1).

Methodology — The amount of seepage was determined by blocking the discharge quantities through the dams having various widths of underdrain carpets. The seepage waters were collected in a covered container to minimize the loss of the collected water by evaporation.

These seepage quantities were also compared with those obtained from the flow net (using the experimentally determined system's permeability, K), and with those calculated analytically using the experimental K-values.

The amount of the system's seepage, Q, of the earth dam is characterized by the position of the seepage line in the cross-section of the dam.

With the dimensions and slopes of the dam shown in Fig. 1, the outcrop of the seepage line of a homogenous dam was always some distance above the base of the dam for all five types of soil used. It was interesting to observe that soon after the dam became saturated and the seepage established the failure of the homogeneous dam started at the toe of the downstream slope. As undercutting or sloughing of the slope progressed, small slides of soil developed and eventually a major slide resulted. This failure points to the need either for additional weight on the downstream slope or an underdrain carpet to assist in carrying the seepage water away from the toe, without erosion of soil and hence without failure. The underdrain carpet, placed underneath a part of the dam on the downstream side a certain distance back of the toe, receives weight from the dam from above, and thus keeps the seepage line within the cross-section of the dam, preventing erosion and loss of stability.

The study of the effect of the width of the underdrain carpet on the amount of seepage discharge through the earth dam was made with the following widths of carpets:

1) dam with no underdrain carpet $L = 0$ cm

2) same dam, length of underdrain carpet $L = 15$ cm

3) same dam, length of underdrain carpet $L = 15$ cm

3) same dam, length of underdrain carpet $L = 30$ cm

4) same dam, length of underdrain carpet $L = 45$ cm

5) same dam, length of underdrain carpet $L = 60$ cm

6) same dam, length of underdrain carpet $L = 75$ cm

Because the capillary phenomenon affects the position of the uppermost flow line, the system's permeability, K cm/sec, was also obtained analytically from the following differential equation[5] expressing discharge, Q, through an earth dam:

$$Q = v \, . \, A = v \, . \, y \, . \, 1 = - K \, . \, y \, . \frac{dy}{dx} \qquad (2a)$$

where Q = experimentally measured seepage quantity, in cm^3/sec per 1 cm of shoreline of dam;

v = velocity of seepage flow, cm/sec;

A = y . 1 = cross-sectional area at any point x, in cm^2;

y = general ordinate of the uppermost flow line, in cm (Fig. 1);

K = coefficient of system's permeability, in cm/sec, and

$- \dfrac{dy}{dx}$ = hydraulic gradient (with increasing x as the y-ordinate decreases).

From the integral of Eq. (2a), the K-value is expressed as:

$$K = \frac{2 \, . \, Q \, . \, x}{H^2 - h^2} \ [cm/sec] \qquad (2)$$

where H = head of the supstream water, in cm, and

h = head of the downstream water level.

The position of the uppermost flow line was also checked by plotting the basic parabola as suggested by A. Casagrande[6]. Within the limits of the experimental range and methodology used, it was found that the experimentally obtained values are always smaller than those obtained from using the basic parabola.

The K-values were also calculated, using the experimental Q's, by the following equation:

$$K = \frac{Q}{H - h} \, . \, \frac{N_e}{N_f} \ [cm/sec], \qquad (3)$$

where

H — h = total head, in cm, and (H — h) (1.00), in cm^2;

N_e = number of equipotential spaces in one flow-strip between two adjacent flow lines, and

N_f = number of flow strips.

The experimental flow-line method was successful with the sandy soils, Nos. 1, 2 and 3 (see Table 1), the K-values of the system's permeabilities of which were in the order of magnitude of 10^{-2} cm/sec. It was less successful with the glacial outwash soil (Dunellen soil), at K-values of 10^{-3} cm/sec, and was unsuccessful with the shale derivative (clayey Penn soil), with K-values of 10^{-4} cm/sec.

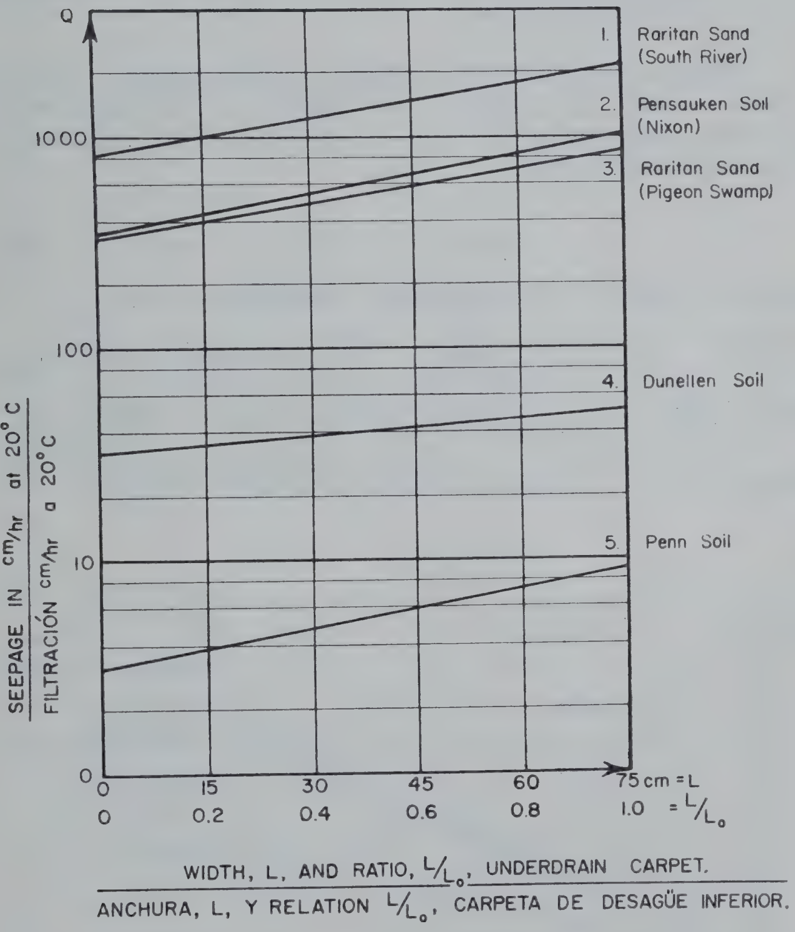

Fig. 6 — Seepage as a function of width of underdrain carpet, Q=f (L).

Fig. 6 — Filtración como función de anchura de carpeta de desagüe inferior, Q=f (L).

OBSERVATIONS AND CONCLUSIONS

Experimental Data — The experimental data, the amount of seepage quantity as a function of the width, L, of the underdrain carpet, are plotted in Fig. 6.

In Fig. 7 are plotted the experimental data in dimensionless ratios, namely, Q/Q_0 as functions of L/L_0, where Q/Q_0 is the ratio of seepage through the dam with an underdrain carpet of width L to seepage through a homogeneous dam (with no carpet), and L_0 is the horizontal projection of the downstream slope.

Equations of Seepage Ratios — The general equation of the seepage ratio, Q/Q_0, as a function of the carpet length to slope projection ratio, L/L_0, is of the general, exponential type of function of:

$$Q/Q_0 = c_1 \cdot e^{C_2 \cdot L/L_0} \tag{4}$$

where c_1 and c_2 = experimental coefficients, and

$e = 2.71828$ = base of natural logarithms.

When $L/L_0 = 0$, then $Q/Q_0 = 1.00$ ($c_1 = 1.000$).

When $L/L_0 = 1$, then e^{C_2} gives the Q/Q_0 — value.

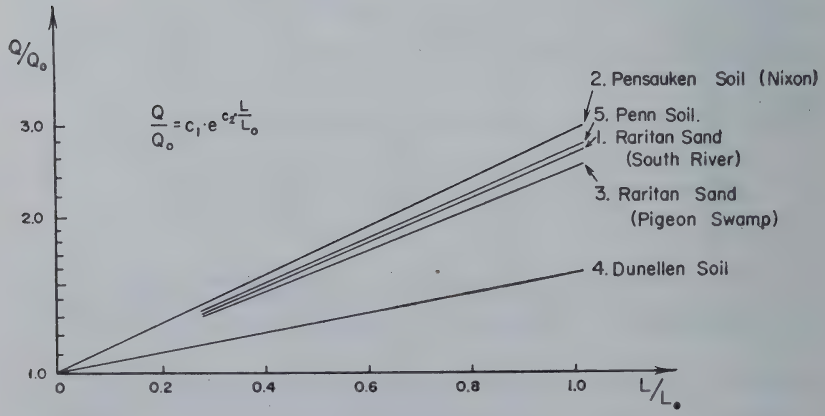

Fig. 7 — $Q/Q_0 = f\ (L/L_0)$

The c_1 and c_2 coefficients were determined analytically. They are tabulated in Table 2.

TABLE 2 — c_1 and c_2 constants

No.	Soil Types	c_1	c_2
1	2	3	4
1	Raritan Sand	1.000	0.978
2	Pennsauken (Nixon) Sand	1.000	1.060
3	Pigeon Swamp Sand	1.000	0.896
4	Dunellen Soil	1.000	0.452
5	Penn Soil	1.000	0.997

The c_1 constants are the cut-offs on the Q/Q_o axis when $L/L_o = 0$ (Fig. 7). The c_2 constants are the slopes of the curves (Fig. 7). The c_2 constants are to be determined for any particular soil type used in the experiment. The Q/Q_o equations are compiled in Table 3.

TABLE 3 — Q/Q-Equations

No.	Soil Type	Equation	Equation No.
1	2	3	4
1	Raritan Sand (South River)	$Q/Q_o = e^{(0.978)\ (L/L_o)}$	(5)
2	Pennsauken (Nixon) Soil	$Q/Q_o = e^{(1.060)\ (L/L_o)}$	(6)
3	Pigeon Swamp Sand	$Q/Q_o = e^{(0.896)\ (L/L_o)}$	(7)
4	Dunellen Soil	$Q/Q_o = e^{(0.452)\ (L/L_o)}$	(8)
5	Penn Soil	$Q/Q_o = e^{(0.997)\ (L/L_o)}$	(9)

TABLE 4 — Discharge quantities, Q, as a function of L

$$Q = Q_o \cdot e^{c_2 (L/L_o)}$$

No.	Width of Underdrain Carpet L in cm	Q	Soil Types				
			Raritan Sand (South River)	Pennsauken Soil (Nixon)	Raritan Sand (Pigeon Swamp)	Dunellen Soil	Penn Soil
1	2	3	4	5	6	7	8
1	$L_o = 0$	$Q_o =$	(1.00) . Q_o	(1.00) . Q_o	(1.00) . Q_o	(1.00) . Q_o	(1.00) . Q_o
2	$L_1 = 15$	$Q_1 =$	(1.22) . Q_o	(1.24) . Q_o	(1.20) . Q_o	(1.11) . Q_o	(1.22) . Q_o
3	$L_2 = 30$	$Q_2 =$	(1.48) . Q_o	(1.53) . Q_o	(1.43) . Q_o	(1.20) . Q_o	(1.49) . Q_o
4	$L_3 = 45$	$Q_3 =$	(1.80) . Q_o	(1.89) . Q_o	(1.71) . Q_o	(1.31) . Q_o	(1.81) . Q_o
5	$L_4 = 60$	$Q_4 =$	(2.18) . Q_o	(2.33) . Q_o	(2.05) . Q_o	(1.44) . Q_o	(2.21) . Q_o
6	$L_5 = 75$	$Q_5 =$	(2.66) . Q_o	(2.89) . Q_o	(2.45) . Q_o	(1.57) . Q_o	(2.71) . Q_o

The seepage discharge, Q, increases curvilinearly as the width of the carpet, L, increases according to the following general equation (Fig. 7):

$$Q = Q_0 \, . \, e^{c_2 \, . \, L/L_0} \qquad (10)$$

The seepage quantity, Q, increases for various widths, L, of underdrain carpets, as tabulated in Table 4.

ACKNOWLEDGMENT

The authors acknowledge the material aid received for the performance of the experiments and the issuance of this paper from Dr. M. L. Granstrom, Chairman of the Department of Civil Engineering, from Professor J. J. Slade, Jr., Research Director of the Bureau of Engineering Research, and from Dr. E. C. Easton, Dean of the College of Engineering, all of Rutgers — The State University, New Brunswick, New Jersey. Mrs. Ruth Ahrens edited the typescript.

REFERENCES

1. W. P. Creager, J. D. Justin and J. Hinds — *Engineering for Dams,* Vol. III, John Wiley & Sons, Inc., New York, 1945, p. 693.

2. A. R. Jumikis — "Dynamic Viscosity Correction Factor Tables for Water (η_T / η_{20})", Soil Mechanics, D. Van Nostrand Co., Inc., Princeton, New Jersey, 1962.

3. W. W. Holman and A. R. Jumikis — Engineering Soil Survey of New Jersey, *Middlesex County,* Engineering Research Bulletin No. 24, College of Engineering, Rutgers — The State University, New Brunswick, New Jersey, November, 1953.

4. J. H. C. Martens — *Industrial Sands of New Jersey,* Bulletin No. 6, Bureau of Mineral Research, Rutgers — The State University, Rutgers University Press, New Brunswick, New Jersey, 1956.

5. Ph. Forchheimer — *Hydraulik,* B. G. Teubner, Leipzig, 1914.

6. A. Casagrande — "Seepage Through Earth Dams", *Journal of the New England Water Works Association,* Vol. 51, No. 2, June, 1937.

A ANISOTROPIA DE MACIÇOS ROCHOSOS E A CONCENTRAÇÃO DE TENSÕES EM TÔRNO DE OBRAS SUBTERRÂNEAS

MURILLO DONDICI RUIZ

Responsável pela Secção de Geologia Aplicada do Instituto de Pesquisas Tecnológicas, São Paulo. Assistente da Cadeira de Mineralogia, Petrografia e Geologia Aplicada da Escola Politécnica da Universidade de São Paulo, Brasil.

SUMÁRIO

O presente trabalho realça alguns aspectos da anisotropia de maciços rochosos, indicando a conveniência, quando possível, da separação da anisotropia da rocha pròpriamente dita e da anisotropia causada por defeitos mecânicos do maciço. Apresenta, como exemplo, os resultados obtidos em ensaios em galerias submetidas a pressões hidrostáticas, na Barragem de Graminha, São Paulo (Brasil). Considerações sôbre a influência das características anisotrópicas de meios que envolvem orifícios nos fatôres de concentração de tensões indicam as dificuldades relacionadas com estudos de determinação de tensões agentes em paredes de obras subterrâneas e suas interpretações, principalmente no que toca à tentativa de determinação quantitativa de esforços de origem tectônica, pela separação da parcela correspondente ao pêso próprio do maciço suprajacente.

SUMMARY

This paper contains a discussion about the anisotropy of rock masses and the convenience of subdividing it into anisotropy of the rock itself and anisotropy of the mechanical defects of the rock mass. The role of the anisotropy of rock masses on the stress concentration factor around holes is discussed in the paper. The difficulties with the determination of stresses on the wall of underground is mentioned. Other difficulties arise on the interpretation of test results mainly in the quantitative determination of tectonic forces considering the parcel due to the own weight of overlying rock masses.

INTRODUÇÃO

O simples fato de se realizar escavação no interior de um maciço rochoso determina uma redistribuição das tensões anteriormente agentes nesse maciço. Essa redistribuição de tensões é função de diversos fatôres; entretanto, entre êles se destacam a forma da secção e as características mecânicas do maciço rochoso.

Muitas vêzes tem surgido o interêsse do estudo, tanto para a Geologia, como para a Engenharia Civil ou de Minas, das tensões existentes em tôrno de obras subterrâneas, bem como da determinação das tensões que agiam no maciço antes da abertura da escavação. A medida dessas tensões, a separação da parcela corresponde ao pêso próprio do maciço e a análise da presença de possíveis fôrças de origem tectônica têm sido realizadas usando-se esquemas teóricos onde não é considerada a anisotropia do maciço rochoso, o que pode conduzir a conclusões que se desviam demasiado da realidade.

A influência da forma da secção na concentração de tensões em tôrno de orifícios tem sido objeto de investigação por parte de estudiosos, sendo vasta a bibliografia sôbre o assunto. Êsses estudos têm sido conduzidos tanto pela análise matemática, como por fotoelasticidade e modelos reduzidos e os resultados obtidos, por êsses diferentes meios, concordam satisfatòriamente entre si [1]. Apesar de se considerar meios isotrópicos, elásticos e homogêneos, é possível avaliar-se a influência da forma da secção da obra subterrânea na concentração de tensões em suas proximidades. Nos casos de obras subterrâneas para aproveitamentos hidrelétricos, a forma da secção afasta-se freqüentemente de formas geométricas simples e que importa em uma maior aplicação de processos fotoelásticos.

ANISOTROPIA DE MACIÇOS ROCHOSOS

As características mecânicas de maciços rochosos são decisivas sôbre a concentração de tensões em tôrno de obras subterrâneas e em seu estudo e aplicação residem as dificuldades de interpretação de resultados obtidos através da medida direta ou indireta das tensões atuantes em tôrno dessas obras.

A anisotropia dos maciços rochosos é fixada, predominantemente, por fatôres *petrográficos* (constituição mineralógica, textura, xistosidade, micro-fissuras) e fatôres *geológicos* (diáclases, fendas, falhas e dobras), cuja interação resulta num corpo complexo e heterogêneo. É conveniente, sempre que possível, considerarmos êsses fatôres separadamente. Assim, da anisotropia total do maciço podemos distinguir duas parcelas: *anisotropia intrínseca* e *anisotropia adquirida.*

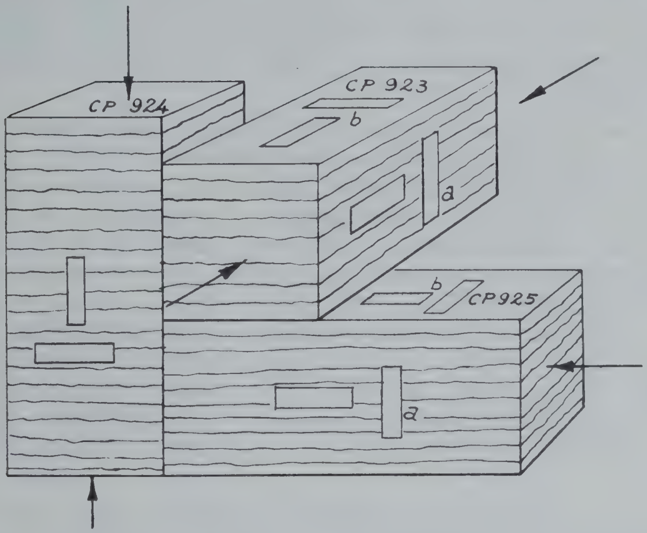

		Corpo de prova CP 923	Corpo de prova CP 924		Corpo de prova CP 925
Módulo de elasticidade (kg/cm^2)		840 000	780 000		810 000
Coeficiente de Poisson λ	face a	0,28	0,38	face a	0,23
	face b	0,23		face b	0,20

Fig. 1 — Anisotropia de amostra de gnaisse xistoso da Barragem de Graminha (São Paulo — Brasil).

Fig. 1 — Anisotropy of a schistose gneiss from Graminha Dam (São Paulo — Brazil).

A anisotropia intrínseca é a anisotropia da rocha pròpriamente dita e é resultante de fatôres petrográficos, ou seja, de uma certa constituição mineralógica, um certo arranjo e orientação dos minerais e de micro-fissuras. Pode ser medida em laboratório através de ensaios de corpos de prova obtidos a partir de amostras do maciço. Por suas reduzidas dimensões êsses corpos de prova são isentos da ação dos fatôres geológicos. A *anisotropia adquirida* é aquela resultante de fatôres geológicos, ou seja, da presença de um ou mais sistemas de diáclases, fraturas, falhas ou dobras, acrescidos de efeitos de dinamitagem e descompressão resultante da escavação. A anisotropia total do maciço rochoso sofrerá variações locais segundo as variações dos fatôres petrográficos e geológicos.

A anisotropia intrínseca pode manifestar-se tanto no módulo de elasticidade como no coeficiente de Poisson. A fig. 1 indica resultados obtidos por Ruiz[2] em ensaios de determinação de módulo de elasticidade e coeficiente de Poisson, dentro do regime elástico, em três corpos de prova obtidos por serragem de um bloco de gnaisse proveniente da Barragem de Graminha, Rio Pardo, São Paulo. Êsses corpos de prova, de eixos ortogonais entre si, foram submetidos à compressão axial simples. O contrôle das deformações longitudinais e transversais foi efetuado com estensômetros elétricos de resistência (strain gauges) e os resultados, ali indicados, representam a média de valores obtidos em faces opostas.

Como é possível constatar, as maiores deformações longitudinais (menor módulo de elasticidade) deram-se segundo a direção perpendicular à xistosidade da rocha (CP 924); entretanto, a anisotropia é mais acentuada no que respeita aos coeficientes de Poisson.

A anisotropia total do maciço rochoso pode ser diminuída pela eliminação parcial ou total da anisotropia adquirida, através de tratamentos por injeções. A anisotropia intrínseca não pode ser modificada.

Daí o interêsse de analisarmos essas duas parcelas na anisotropia total, determinando a possível eficiência de tratamentos por injeções. Geralmente essa análise é de fácil execução. A figura 2 mostra os resultados obtidos por Ruiz[3] em ensaio de medida de deformações diametrais em galeria de 2,0 metros de diâmetro, submetida a pressões hidrostáticas. A galeria foi escavada no mesmo gnaisse xistoso inalterado, da Barragem de Graminha, a 100 metros de profundidade, e os ensaios foram conduzidos para fins de cálculo de revestimento de túneis sob pressão hidrostática. Os resultados da figura 2 referem-se a ensaios da rocha "in natura". O sistema de medida de deformações diametrais foi disposto de maneira tal que o dispositivo de n.º 2 era perpendicular à xistosidade da rocha. Os demais dispositivos de n.os 1 a 3 formavam ângulo de 60° com o de n.° 2. Essa disposição fêz com que o medidor 3 estivesse quase perpendicularmente disposto em relação a um pequeno sistema de diáclases presente no maciço, como pode ser observado pela figura 4.

As deformações diametrais foram registradas em ciclos de carga e descarga. A pressão hidrostática crescia lentamente até atingir a pressão máxima de cada ciclo e aí era mantida até estabilização das deformações. Neste caso particular essa estabilização sempre se estabelecia em tempos inferiores a 3 minutos.

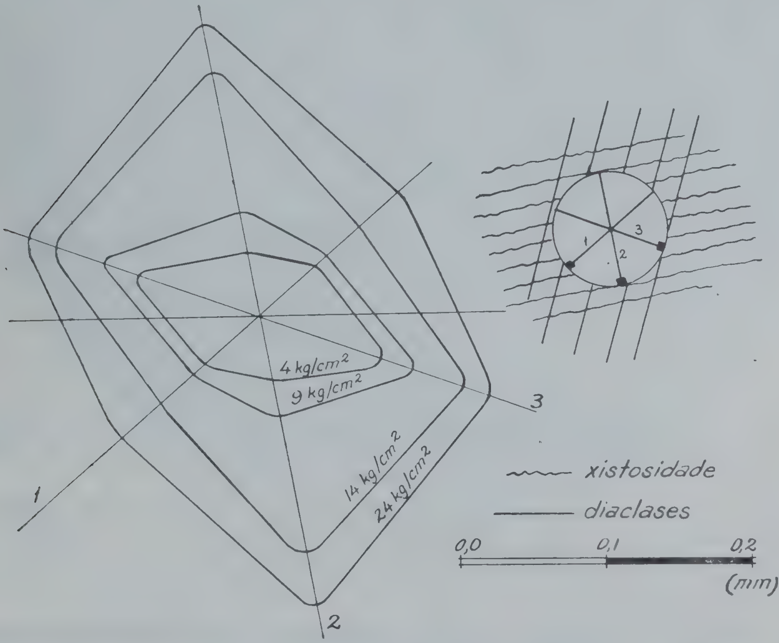

Fig. 2 — Diagrama de deformações diametrais obtidas por Ruiz em gnaisse xistoso da Barragem de Graminha (São Paulo — Brasil) em galeria submetida a pressões hidrostáticas. Rocha "in natura".

Fig. 2 — Diagram of diametral deformation obtained by Ruiz in the schistose gneiss of Graminha Dam (São Paulo — Brazil) in a gallery subjected to hydrostatic pressure. Natural rock.

A figura 3 apresenta deformações diametrais, obtidas no mesmo local e usando-se os mesmos processos, após injeção do maciço com calda de cimento à baixa pressão, sem revestimento da galeria.

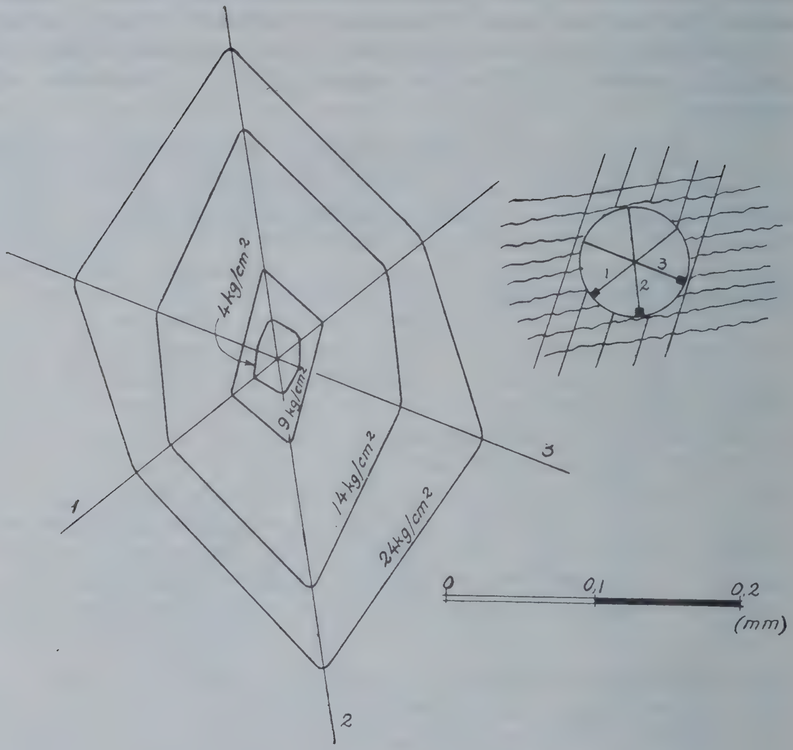

Fig. 3 — Diagrama de deformações diametrais obtidas por Ruiz em gnaisse xistoso da Barragem de Graminha (São Paulo — Brasil), em galeria submetida a pressões hidrostáticas. Rocha injetada.

Fig. 3 — Diagram of diametral deformation obtained by Ruiz in the schistose gneiss of Graminha Dam (São Paulo — Brazil), in a gallery subjected to hydrostatic pressure. Grouted rock.

Tanto a figura 2 como a figura 3 indicam anisotropia do maciço rochoso. Para rocha "in natura" e para as pressões máximas de 4 e 9 kg/cm^2 a anisotropia adquirida, pela presença de pequeno sistema de diáclases ali existente, predomina sôbre a anisotropia intrínseca da rocha, resultando maiores deformações segundo a direção 3, perpendicular a êsse sistema de diáclases. Ainda para rocha "in natura", mas agora para as pressões máximas de 14 e 24 kg/cm^2, verifica-se o fechamento dessas pequenas diáclases, pelo deslocamento do maciço rochoso circundante, surgindo as maiores deformações segundo o eixo 2, perpendicular à xistosidade, predominando, nestes ciclos, a anisotropia intrínseca. O exposto é confirmado plenamente pela análise da figura 2.

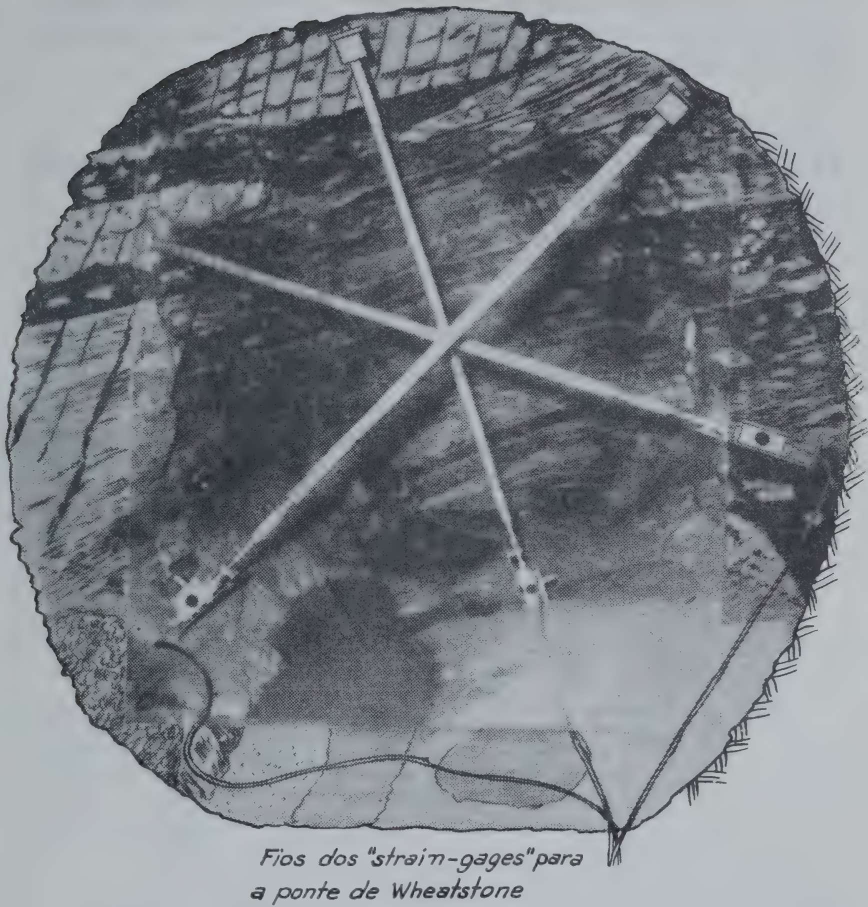

Fig. 4 — Vista da galeria escavada na rocha e posição dos sistemas de medidas de deformações diametrais em relação à xistosidade e diáclases.

Fig. 4 — Internal view of the gallery and relative position of diametral deformation gages, schistosity and diaclasis.

Para a rocha injetada verifica-se o fechamento prévio das diáclases referidas. Para as pressões máximas de 4, 9, 14 e 24 kg/cm^2, predomina a anisotropia intrínseca do maciço rochoso, dando-se as maiores deformações segundo o diâmetro 2, como pode ser notado na figura 3.

Conclui-se, pois, que a anisotropia total do maciço "in natura" pode depender das tensões solicitantes e que essa anisotropia pode apresentar-se não homogêneamente distribuída, pela rotação dos eixos de maior e menor deformações. Isto conduz-nos à presença de corpos complexos e heterogêneos, de difícil tratamento teórico.

EFEITO DA ANISOTROPIA SÔBRE A DISTRIBUIÇÃO DE TENSÕES EM TÔRNO DE ORIFÍCIOS

Savin [4] determinou, teòricamente, a distribuição de tensões em tôrno de orifícios em meios indefinidos, anisotrópicos, elásticos e homogêneos. Como aplicação prática êste autor apresenta a distribuição de tensões em tôrno de orifícios elípticos de relações (a/b) = 1/3 e (a/b) = 3, em meios indefinidos com as características elásticas das madeiras carvalho, pinho e bétula e compara essas distribuições de tensão com o caso equivalente em meio isotrópico.

TABELA I

Posição da tensão P e constantes elásticas Orientação das elipses segundo a tensão P	Tensão P agente segundo o eixo x	Tensão (P) agente na mesma direção do maior módulo de elasticidade			Tensão (P) agente na mesma direção do menor módulo de elasticidade		
	MEIO I	MEIO II	MEIO III	MEIO IV	MEIO II	MEIO III	MEIO IV
	Isotrópico	$E_x = 58\,200 kg/cm^2$ $E_y = 21\,900 kg/cm^2$ $\nu_x = 0,32$ $(E_x/E_y) \cong 2,6$	$E_x = 167000 kg/cm^2$ $E_y = 11\,300 kg/cm^2$ $\nu_x = 0,49$ $(E_x/E_y) \cong 15$	$E_x = 170\,000 kg/cm^2$ $E_y = 8\,300 kg/cm^2$ $\nu_x = 0,37$ $(E_x/E_y) \cong 20$	$E_y = 58\,200 kg/cm^2$ $E_x = 21\,900 kg/cm^2$ $\nu_y = 0,32$ $E_x/E_y \cong 0,4$	$E_y = 167\,000 kg/cm^2$ $E_x = 11\,300 kg/cm^2$ $\nu_y = 0,49$ $E_x/E_y \cong 0,07$	$E_y = 170\,000 kg/cm^2$ $E_x = 8\,300 kg/cm^2$ $\nu_y = 0,37$ $E_x/E_y \cong 0,05$
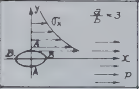	$\left(\frac{\sigma_x}{p}\right)_A = 1,65$	1,883	2,514	2,969	1,542	1,394	1,435
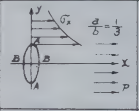	$\left(\frac{\sigma_x}{p}\right)_A = 7,00$	8,951	14,626	18,718	5,875	4,546	4,916
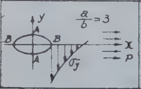	$\left(\frac{\sigma_x}{p}\right)_B = -1,0$	−0,61	−0,26	−0,22	−0,6	−0,3	−0,2

A tabela I apresenta os resultados obtidos por êsse autor para os casos em que a tensão p, agente em pontos infinitamente afastados do orifício, ora coincide com o eixo de maior módulo de elasticidade, ora com o de menor módulo de elasticidade. Constam dessa tabela:

a) as relações (a/b) das elipses;

b) as constantes elásticas dos diversos meios anisotrópicos (II, III e IV) e relações (Ex/Ey);

c) "stress concentration factor" (s.c.f.), ou seja, as relações $\frac{\sigma_y}{p}$ ou $\frac{\sigma_x}{p}$ para os pontos A e B das elipses.

Comparando os diversos s.c.f. dos meios anisotrópicos (II, III e IV) com o do meio isotrópico (I), podemos verificar que o efeito da anisotropia sôbre a concentração de tensões em tôrno do orifício pode causar tanto uma maior como uma menor concentração dessas tensões em função da posição do eixo de maior e de menor módulo de elasticidade e, ainda, que essa concentração pode desviar-se bastante do caso isotrópico.

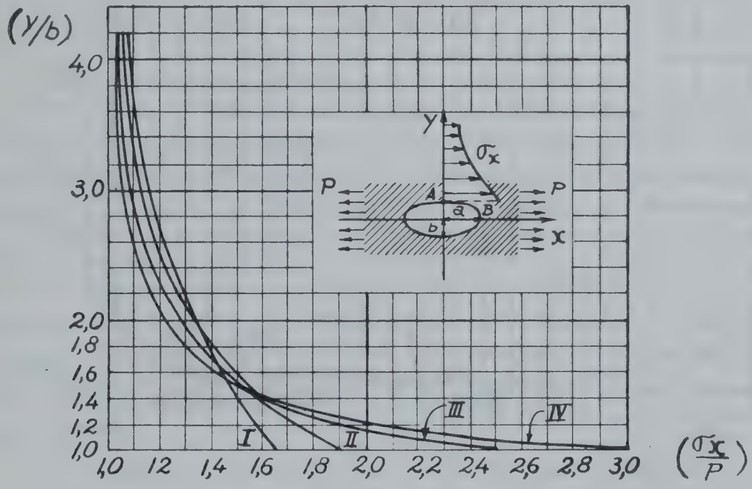

Fig. 5 — Variação de $\frac{\sigma_x}{p}$ em tôrno de cavidade elíptica de razão a/b=3, para a seção x=0, em meios anisotrópicos (II, III e IV) e isotrópico (I). Tensão agente na mesma direção do maior módulo de elasticidade (Savin).

Fig. 5 — Function $\frac{\sigma x}{p} = f\left(\frac{y}{b}\right)$ around elliptical hole with $\frac{a}{b} = 3$, section x=0, in anisotropic (II, III, IV) and isotropic media (I). The stress has the same direction of the largest modulus of elasticity (Savin).

As figuras 5, 6 e 7 indicam as variações dos diversos fatôres de concentração de tensões em função da distância às paredes de orifício, para os meios anisotrópicos considerados (II, III e IV) e isotrópicos (I), ainda para secções elípticas de relações (a/b) = 3 e (a/b) = 1/3.

De uma maneira geral verifica-se um contínuo abrandamento das tensões, à medida em que nos afastamos das paredes do orifício. Êsse abrandamento é acentuado a partir, pràticamente, de uma distância igual a duas vêzes a menor dimensão do orifício elíptico.

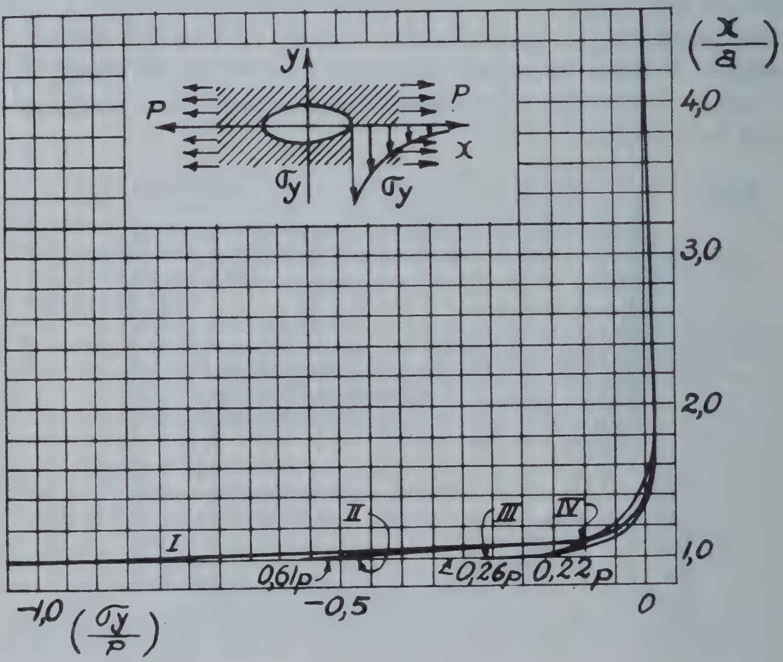

Fig. 6 — Variação de $\frac{\sigma_y}{p}$ em tôrno de cavidade elíptica de razão a/b=3, para a seção y=0, em meios anisotrópicos (II, III, IV) e isotrópico (I). Tensão p agente na mesma direção do maior módulo de elasticidade (Savin).

Fig. 6 — Function $\frac{\sigma_y}{p}$ around elliptical hole with $\frac{a}{b} = 3$, section y=0, in anisotropic (II, III e IV) and isotropic (I) media. The stress p has the same direction of the largest modulus of elasticity (Savin).

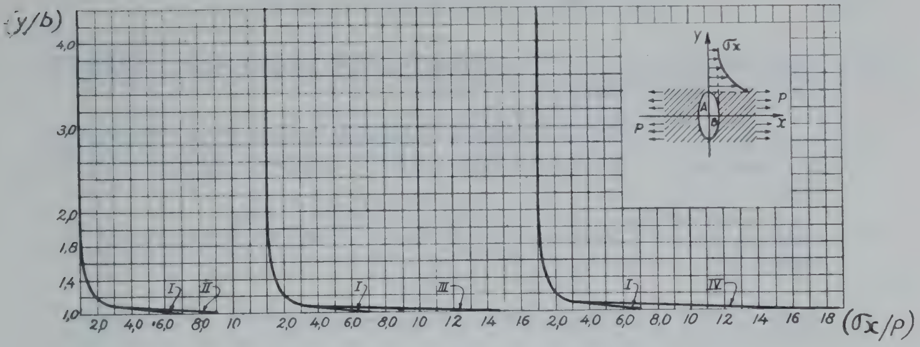

Fig. 7 — Variação de $\frac{\sigma_x}{p}$ em tôrno de cavidade elíptica de razão (a/b) = = 1/3 para seção x = 0, em meios anisotrópicos (II, III e IV) e isotrópico (I). Tensão p agente na mesma direção do maior módulo de elasticidade (Savin).

Fig. 7 — Function $\frac{\sigma_x}{p}$ around elliptical hole with a/b = 1/3, section x = 0, in anisotropic (II, III, IV) and isotropic (I) media. The stress p has the same direction of the largest modulus of elasticity (Savin).

Êste fato coloca em vantagem o método adotado por Nils Hast[5] para a determinação de tensões em volta de obras subterrâneas, sôbre os métodos de determinação dessas tensões nas paredes das escavações, não se podendo, entretanto, deixar de considerar que o método adotado por Hast introduz um nôvo orifício no maciço rochoso, que por sua vez também está sujeito à influência da anisotropia do meio e portanto com deformações diametrais que se afastam daquelas obtidas para a calibração do aparêlho de medida, em laboratório[6, 7].

Os elementos apresentados indicam ainda os cuidados que devem ser adotados na interpretação dos resultados obtidos em medidas de tensões em tôrno de obras subterrâneas, principalmente em algumas tentativas que têm sido realizadas para a determinação quantitativa de esforços tectônicos em determinados locais, através da separação da parcela de tensão correspondente ao pêso próprio do maciço rochoso[8] da tensão total medida em paredes de obras subterrâneas, pelo método de alívio de tensões.

REFERÊNCIAS BIBLIOGRÁFICAS

1. Heywood, R. B. — "Designing by photoelasticity". Chapman Hall — London, 1952.

2. Ruiz, M. D. — "Características elásticas de túnel da Barragem de Graminha — Rio Pardo, São Paulo". Relatório 3.216 do I.P.T., 1961.

3. Ruiz, M. D. — "Tecnologia de rochas". Pesquisa n.º 51 do I.P.T., 1963.

4. Savin, G. N. — "Stress concentration around holes". Aeronautical Series, 1961.

5. Hast, N. — "The measuring of rock pressure in mines". Sveriges Geologiska Undersokning, Stockholm, 1958.

6. Terzaghi, K. — "Measurement of Stresses in Rock". Géotechnique, Vol. XII, n.º 2.

7. Coates, D. F. — Correspondence to Secretary. Géotechnique, Vol. II, n.º 4, pág. 352.

8. Serafim, J. L. — "Internal stresses in galleries". VII Congresso Internacional de Grandes Barragens, 1961.

MERITS AND MISTAKES OF GEOPHYSICS IN CIVIL ENGINEERING

H. Q. GOLDER and L. G. SODERMAN
Canada

SUMMARY

The paper indicates the value of the resistivity and seismic refraction methods of geophysical exploration in civil engineering problems and warns against the unduly optimistic claims made by some for what can be done by these methods. Seven examples are given of actual case records from the authors' experience. In some of these the methods were successful and in others they were not.

SUMARIO

La publicación indica el valor de la resistividad y métodos de refracción sismica de la exploración geofisica en los problemas de la ingeniería civil y advierte contra las indebidas y optimistas reclamaciones hechas por algunos para lo que puede ser hecho por estos métodos. Son expuestos siete ejemplos de casos actuales extraidos del registro de la experiencia de los autores. En algunos de los mismos los métodos tuvieron éxito y en otros no.

INTRODUCTION

In one way a civil engineer is very like a plumber — he has a bag of tools. Just as the traditional comic figure of the plumber who has left his bag of tools behind him has been replaced nowadays by a highly competent technician moving round in a motor van which is a mobile and efficient workshop containing tools of which the plumber of a generation or two ago would never have heard, so the civil engineer of today has in his "bag of tools" items which are too specialized and complicated for him to operate himself but which he must nevertheless use in order to solve his problems in the most efficient way.

These new tools include such things as electronic computers, tellurometers, geodimeters and echo sounders, radioactive tracers and meters, strain gauges, pressure cells and slope indicators, carbon dating, aerial photography and helicopters, and a group of geophysical methods of exploration of subsurface conditions.

When using these tools the engineer is at the mercy of the expert unless he (the engineer) knows something of what the tool can and cannot do, even though he does not expect to be able to operate it himself.

The purpose of this paper is to give the soil engineer an idea of those problems in which geophysical methods of ground exploration can help him and, even more important, to state some of the limitations of these methods. Examples are given from the authors' experience of cases of both successful and unsuccessful geophysical work in civil engineering problems. In those cases which were unsuccessful, it was without exception the interpretation of the data which was at fault.

THE GEOPHYSICAL METHODS OF EXPLORATION USED IN CIVIL ENGINEERING

Geophysical methods of subsurface exploration were originally developed for use in oil and mining problems. Many different methods now exist, and although it would be too sweeping to say that some of these are of no use in civil engineering problems, it is a fact that two methods are better suited than the others to the scale of these problems. These methods are the resistivity method and the seismic refraction method.

New methods are continually being developed and several akin to echo sounding but using a source of greater energy are now available for work through water and, in suitable conditions can give some indication of the structure of the material below a river, lake or sea bottom.

One important characteristic which all geophysical methods have in common is that they are indirect methods. Every method measures some property of the soil and by the interpretation of changes and variations in this property purports to give a picture of the subsurface conditions. Direct methods of exploration, on the other hand, are those which allow samples of the soil to be seen, handled, and tested, and include borings, test pits, trial shafts and adits and the like.

The best simple statement of the principles of the resistivity and seismic refraction methods and their application to civil engineering problems of which the authors are aware, is the paper by Robertshaw and Brown given in the list of references.

THE RESISTIVITY METHOD

In this method the electrical resistivity of the soil is the property measured. Although there can be many variations in detail, in general a slowly alternating square wave form current is fed into the ground through steel probe electrodes and this current is measured. The drop in electrical potential is measured between other electrodes stuck into the ground between the current electrodes. From these two measurements the apparent resistivity of the ground can be calculated. By moving the electrodes laterally or by expanding the electrode spacing, variations in the apparent resistivity position or depth can be measured. In very general terms the apparent resistivity of soils is lower the higher the water content, thus a clay would show a low resistivity compared to a saturated sand and gravel which in turn would be lower than the same soil in a drained condition. In rocks the constituent minerals play a large part in controlling the resistivity, rocks containing minerals such as pyrite or magnetite naturally having a lower resistivity than rocks without such minerals.

THE SEISMIC REFRACTION METHOD

In this method the velocity of a vibration passing through the ground is measured. The velocity in soils such as sands or clays is low (less than 5,000 ft/sec. (1,500 m/sec.) while in rocks it is 10,000 ft/sec. (3,000 m/sec.) and upwards. In general the velocity increases with the modulus of elasticity of the rock reaching values over 20,000 ft/sec. (6,000 m/sec.) for hard igneous rocks. Thus the property measured is related to the engineering properties of the rocks which is claimed by some to be an advantage. However, the measured velocities are used in general simply to calculate the depth to the rock surface.

In a seismic refraction survey, the shock which causes the ground waves is generally the explosion of a small charge of explosive, although in some very lightweight modern instruments of limited scope, it is a blow of a heavy hammer on a steel plate placed on the ground. The shock is picked up by a series of geophones (usually 12 or 24) laid out on the ground some distance from the source of the shock. The time intervals between the shock and the arrival of the ground wave at the geophones are recorded electrically. From the records the depth to rock can be calculated directly for simple cases. Where the conditions are more complicated, direct velocity measurements in rock and overburden may have to be made, and borings are necessary to calibrate the results. Many variations of technique, such as fan shooting, exist for different purposes, but they will not be discussed here. For a very useful paper on the seismic method see Domzalski (1956).

THE SPARKER METHODS

These methods have been developed in the last few years for work over water. In principle they resemble an echo sounder which is used to determine the depth of water under a boat by emitting an impulse which travels down in the water to the bottom, where it is reflected up again to the surface. The time required for the pulse to travel down and up again is measured, and since the velocity of sound in water is known the depth of water can be calculated. Thus the Sparker Methods can be classed as modified seismic reflection methods.

In the Sparker Methods (of which there are more than one under different names) the impulse has a much greater energy than in the echo sounder and so penetrates some distance into the bottom material. Reflections from other surfaces than simply the sea or river bottom can be obtained and these are shown on a chart. To interpret the chart some assumption must be made about the velocity of wave transmission in the bottom material, since time only is measured.

EXAMPLES OF THE USE OF GEOPHYSICAL METHODS OF EXPLORATION IN CIVIL ENGINEERING PROBLEMS

The examples below, which are taken from the authors' experience (except Example I), illustrate the use of the methods described above. In some cases the methods were successful and in some they were not. In the first example, geophysical methods were not used, as they were not available at the time, but the example is given as it is a well known case in which their use would assuredly have been of the greatest value.

Three of the examples refer to the resistivity method, which was correctly interpreted in only one of the cases. Three refer to the seismic method which was wrong as often as it was right, and one of these cases also refers to the Sparker Method which was quite wrongly interpreted.

EXAMPLE I — SILENT VALLEY RESERVOIR (NORTHERN IRELAND)

This work was carried out before the development of geophysical methods, or at least before their application to civil engineering problems. It provides an extremely good example of a case in which either the resistivity or the seismic refraction method, if they had been used, would certainly have indicated an anomaly which did not agree with the results of the boreholes.

The reservoir is in a valley in the Mountains of Mourne in North Ireland. The area is mountainous, uninhabited, largely rocky and devoid of trees, being covered with heather, gorse and bracken, and granite rock and boulders. Borings across the valley of the Kilkeel River at the site chosen for the dam had stopped on granite rock at a maximum depth of about 65 feet (20 m.) after passing through sand, gravel and silt. The earth dam was to have a maximum height of 88 feet (27 m.) above river bed level, was to be 1580 feet (480 m.) long and there was to be a concrete filled cutoff trench to rock.

The trench on both sides of the valley was completed without difficulty over a length of 720 feet (220 m.) but great difficulties were encountered in the central section 860 feet (260 m.). Further borings were put down in this section and these showed that the depth to rock was 196 feet (60 m.) i.e., over three times that originally expected. It later became evident when the trench was excavated, that the original borings had mistaken granite boulders for bedrock (see figure 1). The late Mr. W. J. E. Binnie, who was called in to advise on the measures to be taken to complete the job after this error had been discovered, said in the discussion of the paper (see McIldowie): "The silt contained very large boulders indeed, and the original boreholes, on reaching them, had been assumed to have found the surface of the rock. As one of the boulders subsequently found was as big as a cottage, it was not surprising that wrong conclusions had been drawn". Later, Mr. Binnie comments that some of the boulders "were not of local origin; most of them came from Scandinavia". (Ice transported). This fact was not lost on at least one geologist who had previously said that the borings were not on bedrock, an example of the aid which can be given by geology to the civil engineer. However, a resistivity or seismic refraction survey across the dam site would have shown quite conclusively that there was something wrong either with the borings or with the geophysical survey since they would not have agreed, and this anomalous result should have led to further investigation which would have revealed the facts before construction commenced. Unfortunately these methods were not available at the time (1923-6).

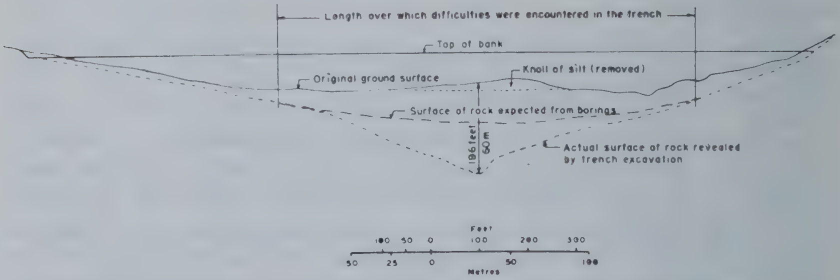
Length over which difficulties were encountered in the trench
Top of bank
Original ground surface
Knoll of silt (removed)
Surface of rock expected from borings
196 feet
60 m
Actual surface of rock revealed by trench excavation
Feet
100 50 0 100 200 300
50 25 0 50 100
Metres

Fig. 1 — Example I — Cross section of Silent Valley, North Ireland.

Fig. 1 — Ejemplo I — Corte transversal de Silent Valley, Irlanda del Norte.

EXAMPLE II — VOLTA RIVER (WEST AFRICA)

An interesting and amusing example, in which a mistake of interpretation had no serious consequences, is afforded by a resistivity survey carried out across the Volta River some few years ago.

The purpose of the survey was to determine whether or not a buried channel existed in the rock below the soft river deposits at the site of a proposed dam. The engineer decided quite properly to treat the problem as a three layer problem, using the water of the river as the first layer and floating the electrodes on the surface. The depth of the river was known at all points and the velocity of flow was not great. The electrodes were moved across the river with a fixed spacing, and the curve of resistivity showed a dip at one point, which was interpreted by the engineer as the buried channel for which he was looking (figure 2).

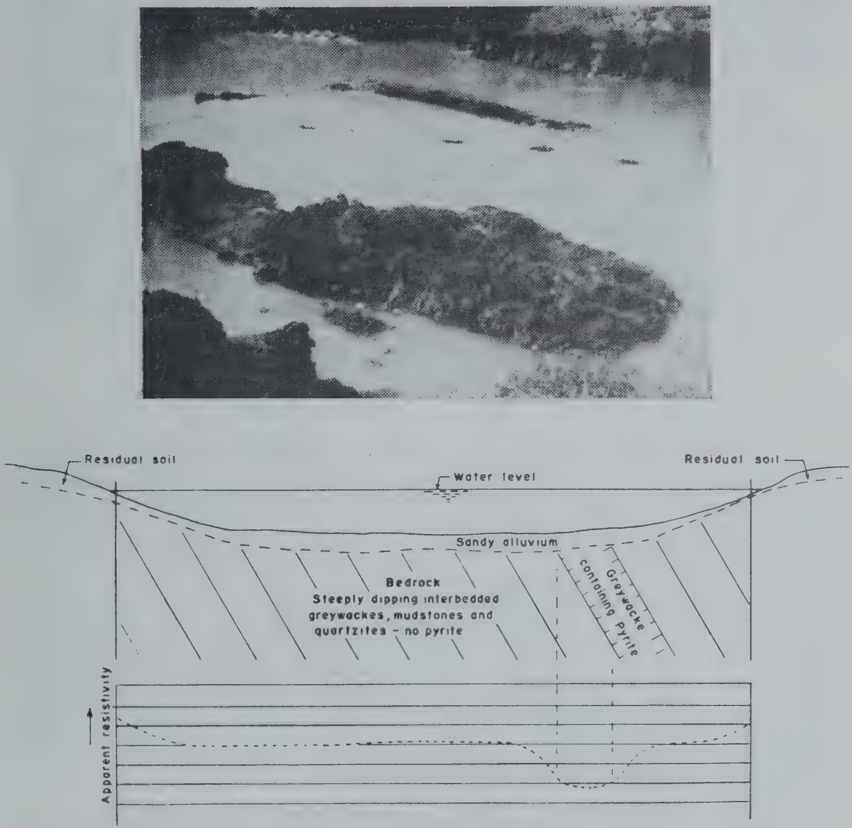
Residual soil
Water level
Residual soil
Sandy alluvium
Bedrock
Steeply dipping interbedded greywackes, mudstones and quartzites – no pyrite
Greywacke containing Pyrite
Apparent resistivity

Fig. 2 — Example II — View of work in progress and cross section of Volta River, West Africa.

Fig. 2 — Ejemplo II — Vista de los trabajos en progreso y corte transversal del Rio Volta, Africa Occidental.

A drill was placed at the position of the buried channel, but produced good rock core at a depth consistent with the general rock level. There was in fact no buried channel.

The rocks on the site were steeply dipping interbedded greywackes, mudstones and quartzites and they were overlain by sandy alluvium. Thin sections were prepared of the greywacke taken from the borehole at the resistivity anomaly. These sections contained an appreciable amount of pyrite with a continuous intergranular distribution. Little or no pyrite was found in the cores from boreholes away from the anomaly. Laboratory tests were made on the cores, and it was found that the presence of the pyrite in the greywacke increased the conductivity by five times, and made the resistivity very similar to that of the overlying sandy alluvium. Thus the resistivity record was very similar to that which would have been obtained from a buried channel.

This example demonstrates perfectly a truth which must never be forgotten when using geophysical methods, namely, that indirect methods indicate only anomalies. These must be investigated by direct methods before they can safely be labelled as anything but anomalies. In this case the correct procedure, which is to investigate an anomaly by a boring, was followed. As it happens the cause of the anomaly posed no engineering difficulties, but this is not usually the case.

EXAMPLE III — SPANISH RIVER (ONTARIO)

This example is interesting psychologically as well as technically. An investigation was planned to decide on the best site for a road crossing for the Trans-Canada Highway over the Spanish River near the town of Massey in Ontario (see figure 3).

It was known from the general geology of the area that the bedrock consisted of Precambrian diorite or diabase of intrusive origin, and that the preglacial valleys and depressions between the steep sided igneous rock outcrops were filled with post glacial lacustrine and fluvial sediments. The Spanish River follows a southwesterly course towards Lake Huron through such a preglacial valley.

Resistivity surveys were carried out at four sites (numbered 1 to 4 in figure 3) and at least one sampled boring was made at each site. Depth to bedrock varied from zero in the south bank of the river to 170 feet (62 m.) along the north river bank. The borings showed a shallow (less than 15 feet [5 m.]) stratum of clayey silt, underlain by a deposit of soft varved clay varying in thickness from 6 to 20 feet (2 to 6 m.). The varved clay was underlain by a deep deposit of fine to medium sand which extended to bedrock. This soil stratigraphy was consistent at each of the four sites and there was good agreement between the borings and the resistivity surveys.

Site 5 was the last location to be investigated, and because of the apparently good correlation between the resistivity readings and the borehole data obtained at sites 1 to 4, the decision was made that boring at site 5 would not be necessary. Resistivity depth determinations were made and the inferred bedrock profile is shown in figure 3.

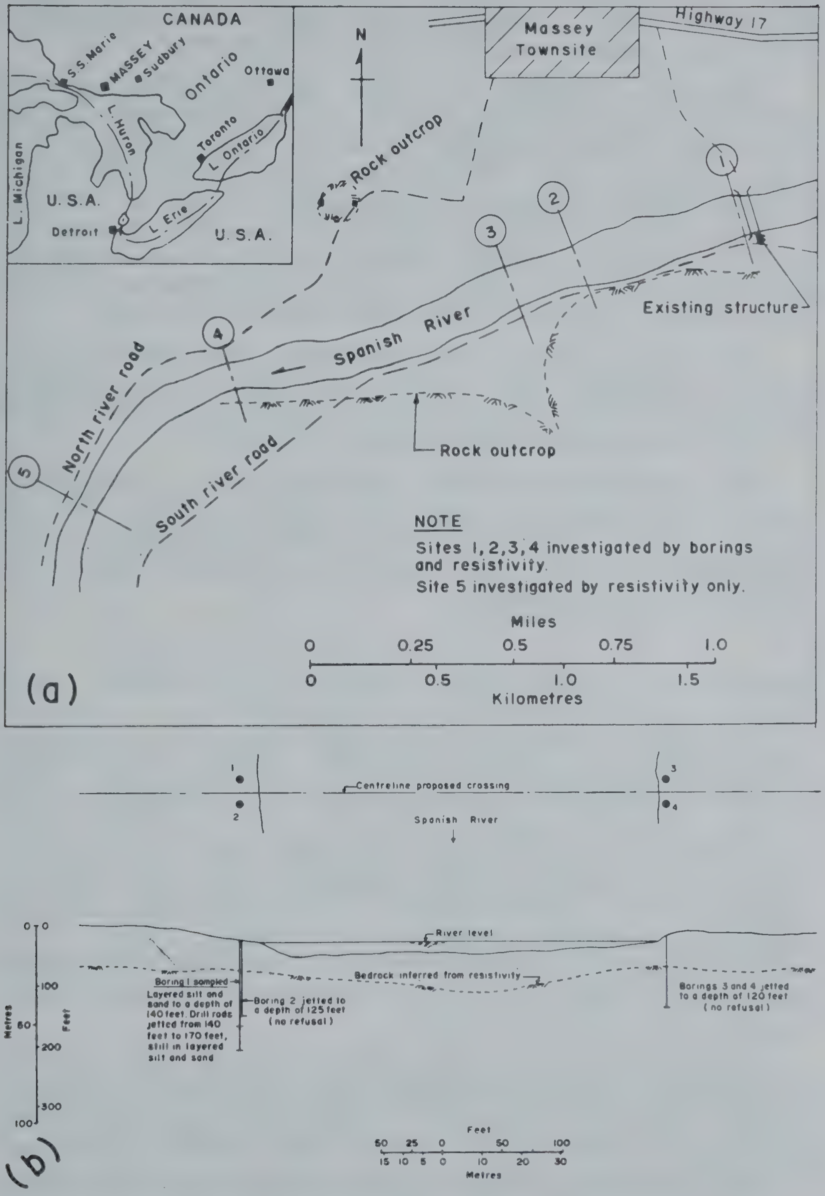
CANADA
S.S. Marie
MASSEY
Sudbury
Ontario
Ottawa
L. Huron
Toronto
L. Ontario
L. Michigan
U. S. A.
Detroit
L. Erie
U. S. A.
N
Massey Townsite
Highway 17
Rock outcrop
1
2
3
4
5
Existing structure
Spanish River
North river road
South river road
Rock outcrop
NOTE
Sites 1, 2, 3, 4 investigated by borings and resistivity.
Site 5 investigated by resistivity only.
Miles
0 0.25 0.5 0.75 1.0
0 0.5 1.0 1.5
Kilometres
(a)
1
2
3
4
Centreline proposed crossing
Spanish River
0 0
100
50
200
300
100
Metres
Feet
River level
Bedrock inferred from resistivity
Boring 1 sampled
Layered silt and sand to a depth of 140 feet. Drill rods jetted from 140 feet to 170 feet, still in layered silt and sand
Boring 2 jetted to a depth of 125 feet (no refusal)
Borings 3 and 4 jetted to a depth of 120 feet (no refusal)
Feet
50 25 0 50 100
15 10 5 0 10 20 30
Metres
(b)

Fig. 3 — Example III — Spanish River, Ontario — plan and section.

Fig. 3 — Ejemplo III — Spanish River, Ontario — plano y corte.

Site 5 was chosen as the most suitable location for the structure, presumably because of the relatively shallow (50-60 feet) (15-18 m.) and consistent depth to bedrock, and a preliminary design was made for the structure.

Prior to completing the final structural drawings the designers were advised to confirm the bedrock depth at the pier and abutment locations in order to negotiate a firm piling contract price. Borings were made rather reluctantly and the results are shown on the profile for site 5 in figure 3. Instead of 60 feet to bedrock as indicated by the resistivity results, the borings showed bedrock to be at a depth greater than 174 feet (53 m.) on the north side and greater than 120 feet (36 m.) on the south side of the river.

As a result site 5 was abandoned, and based on additional exploration the structure was relocated immediately downstream of the existing bridge where the maximum depth to rock was approximately 100 feet (30 m.).

This interesting example indicates that it is possible to become an enthusiast after only four successes. It also teaches us how dangerous unwarranted enthusiasm can be. Geophysical methods are indirect and should always be checked by direct methods.

EXAMPLE IV — PORT PERRY CAUSEWAY (ONTARIO)

A resistivity survey to determine the soil stratigraphy along a proposed causeway alignment crossing Lake Scugog in Ontario (see figure 4) was carried out during the winter of 1959. Prior to starting the survey it was known from a geological reconnaissance of the area that the soil profile consisted of relatively shallow strata of peat and soft clay overlying dense glacial clay till. It was reasoned that the conditions of marked variations in moisture content of the strata, non-salinity of the pore water and relatively shallow depth to the dense till stratum would be well suited for a satisfactory resistivity survey.

The expanding electrode survey method was used and two borings were made during the survey for correlation. A total length of two miles (3 km.) was investigated in a period of one week during severe winter weather conditions.

On completion of the survey and preparation of stratigraphic sections nine check borings were made. A typical section showing the strata type and horizon boundaries determined from the resistivity survey and check borings is shown on figure 4.

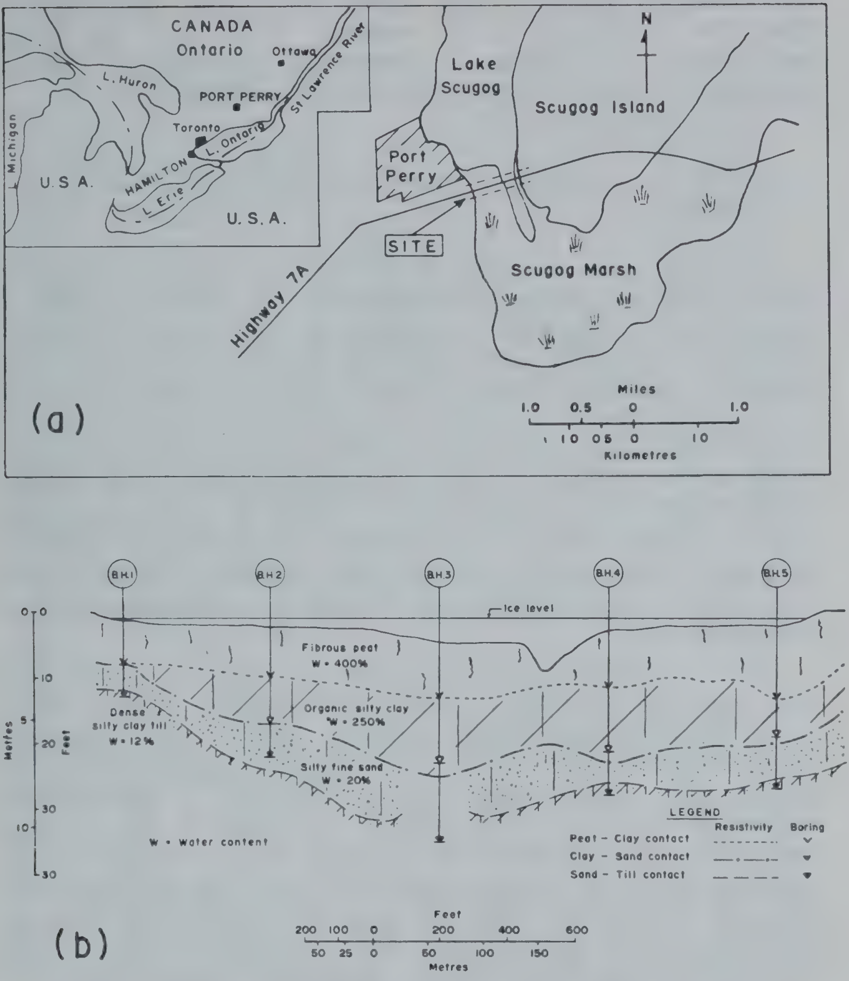
CANADA
Ontario
Ottawa
L. Huron
PORT PERRY
St Lawrence River
Toronto
L. Ontario
L. Michigan
U.S.A.
HAMILTON
L. Erie
U.S.A.
Lake Scugog
N
Scugog Island
Port Perry
SITE
Highway 7A
Scugog Marsh
Miles
1.0 0.5 0 1.0
1.0 0.5 0 1.0
Kilometres
(a)
B.H.1
B.H.2
B.H.3
B.H.4
B.H.5
Ice level
Fibrous peat
W = 400%
Organic silty clay
W = 250%
Dense silty clay till
W = 12%
Silty fine sand
W = 20%
W = Water content
Metres
Feet
0 5 10
0 10 20 30 30
LEGEND
Resistivity
Boring
Peat – Clay contact
Clay – Sand contact
Sand – Till contact
Feet
200 100 0 200 400 600
50 25 0 50 100 150
Metres
(b)

Fig. 4 — Example IV — Port Perry Causeway, Ontario — plan and section.

Fig. 4 — Ejemplo IV — Port Perry Causeway, Ontario — plano y corte.

The accuracy of the resistivity survey was further confirmed during construction of the causeway. The displacement method of fill construction was used and quantities calculated on the basis of the resistivity profile agreed with quantities actually placed.

This example is the sort that geophysical salesmen dream about. All the pamphlets are full of examples like this. But the examples given in this paper are a fair cross-section from the experience of the authors. Note that the client here made nine borings to check the geophysical results, exhibiting a caution which the authors applaud.

EXAMPLE V — CHEDOKE EXPRESSWAY (HAMILTON, ONTARIO)

A very good example of the consequence of accepting seismic bedrock profiles without proof by sampled boring is afforded by the authors' experience on the Chedoke Expressway (see figure 5). The western section of the four lane divided expressway follows a route along the scarp slope of the Niagara Escarpment and it was in connection with choosing the alignment along this portion that a seismic survey to determine overburden depth was carried out. The escarpment proper is an erosion feature cut into the shales, sandstones, and limestones of the Silurian and Ordovician periods. The scarp face investigated is about 300 feet (90 m.) high, has average slope of some 35° and is to be negotiated by a 3% grade line.

It was originally thought that the slope consisted of a thin covering of talus material (fragmented angular limestone, sandstone and shale) overlying bedrock, the interstices being filled or partly filled by downwash material from the glacial drift which caps the escarpment. A preliminary survey of the slope was carried out using a one channel refraction seismograph of the hammer type to determine the bedrock profile at sections every 100 feet (30 m.) along the proposed road center line. At each 100 foot station four set ups were used to give bedrock depth determinations at centre line and 150 feet (45 m.) right and left of centre line.

Velocities of 900 to 1,100 ft/sec. (270 to 330 m/sec.) were measured for the overburden and 10,000 to 15,000 ft/sec. (3,000 to 4,500 m/sec.) for the bedrock. From this bedrock contact was inferred to be at 5 to 12 feet deep (1.5 to 4 m.). Shallow pits were put down to check these depths, but when no bedrock was found at a depth of 15 feet (4.5 m.) work was halted and some borings were put down. From the borings it was difficult to define the bedrock surface since the blocks of broken rock (talus material) were of the same rock as the bedrock. However, a definition was made based on continuous core recovery and this gave depths to bedrock of 30-50 feet (9 to 15 m.).

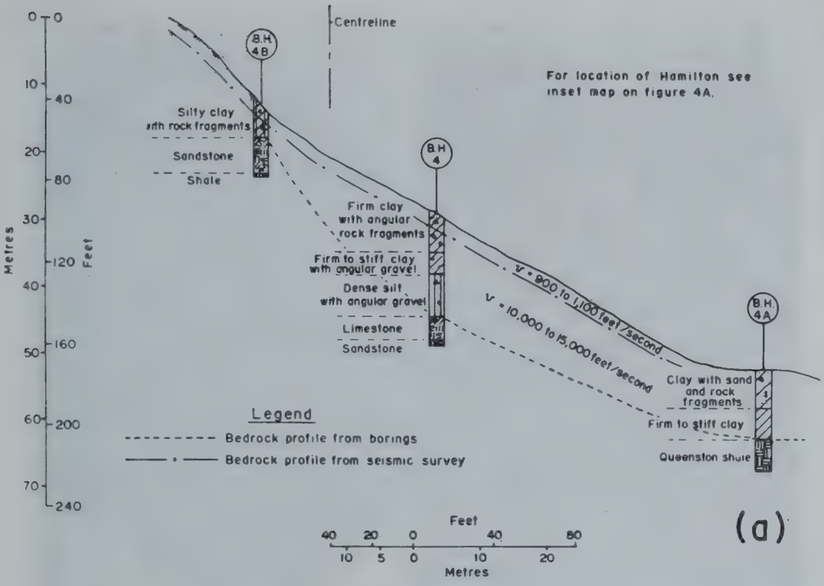
Centreline
B.H. 4B
B.H. 4
B.H. 4A
For location of Hamilton see inset map on figure 4A.
Silty clay with rock fragments
Sandstone
Shale
Firm clay with angular rock fragments
Firm to stiff clay with angular gravel
Dense silt with angular gravel
Limestone
Sandstone
V = 900 to 1,100 feet/second
V = 10,000 to 15,000 feet/second
Clay with sand and rock fragments
Firm to stiff clay
Queenston shale
Legend
Bedrock profile from borings
Bedrock profile from seismic survey
Metres
Feet
0 10 20 30 40 50 60 70
0 40 80 120 160 200 240
Feet
40 20 0 40 80
10 5 0 10 20
Metres
(a)

LOG OF TRIAL SHAFT 'B'

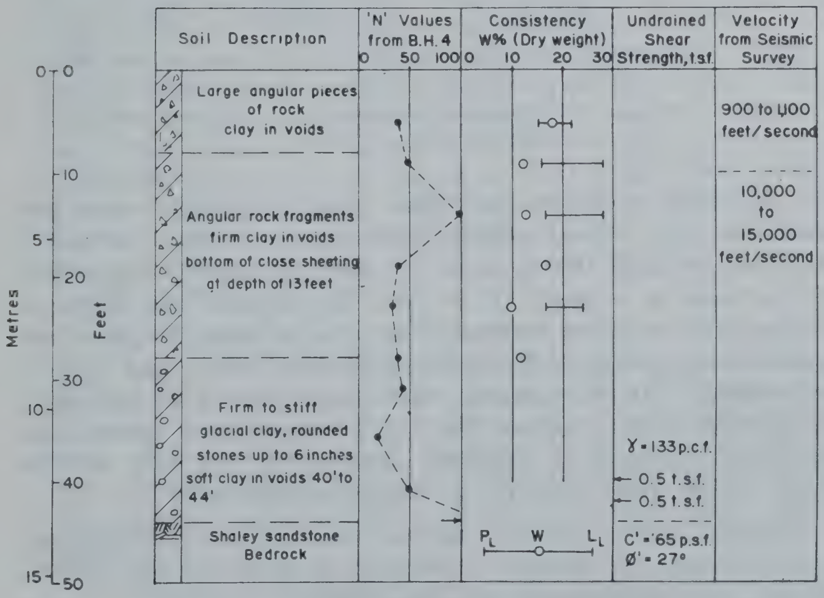

Fig. 5 — Example V — Chedoke Expressway, Ontario — section and log of trial shaft.

Fig. 5 — Ejemplo V — Chedoke Expressway, Ontario — corte y perfil de pozo de prueba.

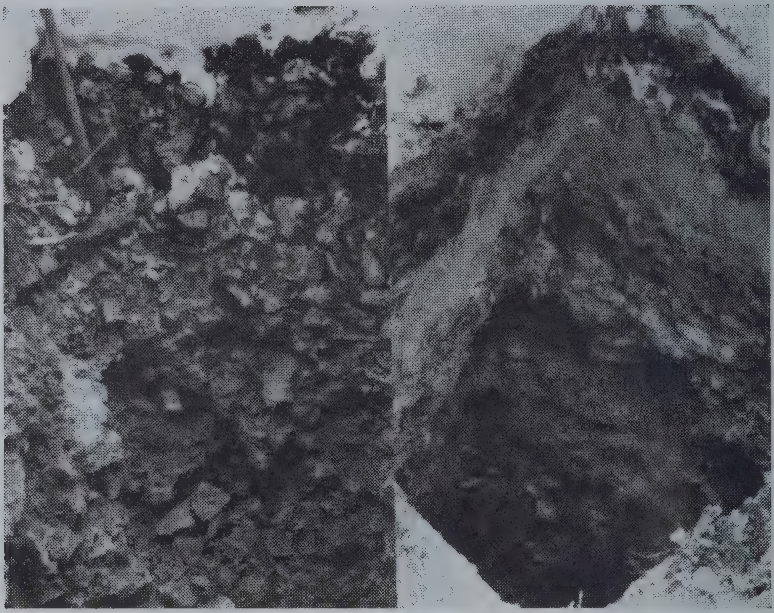

loose rock — roca suelta   dense overburden — capa densa

Fig. 6 — Example V — Chedoke Expressway — test pits in loose and dense material.

Fig. 6 — Ejemplo V — Chedoke Expressway — pozos de prueba en material suelto y denso.

To check these findings two large test shafts were put down to rock. These shafts were 6 foot × 6 foot (2 m. × 2 m.) and enabled the rock to be seen in place. One shaft hit bedrock at a depth of 30 feet (9 m.) and the other at 44 feet (13 m.), the bedrock from the borings at these two points being given as 30 feet and 50 feet (9 m. and 15 m.) respectively. In the second shaft there was a 4 foot drop in bedrock surface across the shaft. The shafts served the additional purpose of allowing samples of the clay in the voids of the loose rock to be taken for testing.

Figure 5 shows a section through the hillside at the second shaft showing the depths to bedrock as given by the seismic survey, the borings and the trial shaft.

Had this seismic work not been checked by direct methods, the results would have been extremely serious since it was proposed to build here an embankment some 70 feet

(21 m.) high, and the clay was found to be too weak for this to be a sound design.

It is of interest to note that this conclusion that a bank of 70 feet high should not be attempted at this site could not have been reached without the use of a trial shaft. The steps taken in the investigation, namely, seismic survey, shallow test pits, borings, and deep trial shafts form a good example of the logical way in which a site investigation should be carried out. In many cases it is not feasible to plan the whole investigation at the start, but a step by step development is the more correct approach.

EXAMPLE VI — SITE IN WESTERN CANADA

In connection with the design of a dam in Western Canada a certain amount of geophysical work was carried out only some of which was successful.

A survey was made along the river using a waterborne continuous underwater profiler of the Sparker type. The purpose of this was to find the depth to bedrock, and a supposed bedrock profile was prepared by the survey crew showing depths to bedrock of about 100 feet (30 m.). Later borings showed this profile to be completely in error. Above and at the depths at which bedrock was shown, sand and gravel existed and continued downwards for several hundred feet (over 100 m.). What the horizon was which the instrument had picked up was not evident from the borings. One suggestion was that a change in density might have occurred at the indicated depth, possibly coincident with the scour depth in past heavy floods, but there was no direct evidence to support this suggestion. The important point is that the profile read "bedrock".

At a later stage some seismic refraction work was carried out. First of all a rapid survey was made along the river valley using a modified fan shooting technique to see if there was any place at which an undiscovered ledge of rock existed which might be suitable for the foundation of the concrete flood discharge section of the proposed dam. This survey was successful in that one such ledge was discovered.

This ledge and another one which was previously known, were then surveyed in detail by line shooting, the lines being 100 feet apart. The interpretation of this work left much to be desired.

At site A, the depth to rock was known by borings at nine points before the survey was made. It was later possible to check the interpretation at the positions of five further boreholes. The actual depths to rock ranged from 59 to 205 feet (18 to 63 m.). The errors in the depths to rock given by the seismic survey were from 20 to 91 feet (6 to 27 m.). In one case the seismic survey showed the rock deeper than it was and in four cases shallower. The percentage errors ranged from 21 to 138 with an average value of 58%.

At site B, the depth to rock was not known before the survey was made and interpreted. It was later possible to check the depths given, by boreholes at five points. The depths to rock varied from 34 to 60 feet (10 to 18 m.). The depths given by the seismic survey were from 68 to 255 feet (21 to 78 m.). In every case the seismic work showed the rock to be deeper than it really was. The errors ranged from 33 to 205 feet (10 to 62 m.), the average percentage error being 240%.

These results were naturally referred back to the geophysicist who made the interpretation. His explanation, that there was a gradual change in average overburden velocity, was unconvincing, although probably correct.

A similar effect was noted some eight years ago on a site in Northern Ireland. The soil conditions were boulder clay overlying basalt, with a mantle of peat in places. The boulder clay consisted of basalt boulders in a matrix of sand, clay and silt. The initial seismic work indicated a mean wave velocity of 2,300 ft/sec. (700 m/sec.) in the overburden and 12,000 ft/sec. (3,600 m/sec.) in the basalt. These values gave depths to bedrock which were too small compared with the boreholes. A more careful study was made of the overburden velocity by reducing the spacing of the geophones near the shot point. This indicated two overburden velocities of 1,500 ft/sec. (400 m/sec.) in the peaty mantle and 5,000 ft/sec. (1,500 m/sec.) in the boulder clay. Using these velocities the interpreted rock profile was in close agreement with the borehole data. Needless to say on all subsequent surveys the geophysicists concerned used low velocity spreads to determine accurately the velocities in the overburden.

It is realized that the Canadian case was a difficult site. There was the possibility of refractions or reflections from the steep rock walls of the valley. It was known that some of the overburden was probably lacustrine, some fluvial and some slumped material which had fallen from a higher level in a frozen condition. But the most difficult correlation on this site was between the confident claims of the geophysicists before the start of the job and the gap existing between real and predicted rock levels at the end of the job. Maybe this was another case of a competent oil exploration geophysicist being unable to adjust himself to the scale of a civil engineering problem. In problems of this sort, as in all work with soils, attention to detail is a prime requisite.

EXAMPLE VII — SITE IN SCOTLAND

During an investigation for a proposed high pressure tunnel in Scotland four boreholes were drilled in line and about 1,000 feet (300 m.) apart from each other. The first boring hit rock at 14 feet (4 m.) and went 60 feet (18 m.) into it. The other three boreholes encountered what was assumed to be rock at depths varying from 10 to 30 feet (3 to 9 m.). The rock was drilled to a depth of 20 feet (6 m.) and some blasting was done.

The engineers although naturally delighted that the rock was so shallow, wisely decided that further information was desirable and asked for a seismic refraction survey across the valley.

A seismic traverse was then shot, but the original spread, which was calculated for a medium depth, proved to be insufficient, and two further spreads were used with increased distances between geophones, covering a total distance of 1,200 feet (370 m.). The calculated depth was over 300 feet (100 m.) at the borehole where the engineers had assumed 20 feet (6 m.) depth.

Further drilling was then commenced and the driller soon began to get good cores of rock, first 10 feet (3 m.) then 20 feet (6 m.). The geophysicist stuck to his assertion that this also must be a boulder, although a very large one. Amid increasing scepticism on the part of the drillers, the geophysicist continued to maintain that rock was 300 feet (100 m.) down even when 25 feet (8 m.) of rock core had been obtained. After drilling just under 30 feet (10 m.) and obtaining about 100% core recovery, the driller came out below the boulder into sand and gravel again and continued drilling in this to a depth which was within 15% of that predicted from the seismic survey.

This exercise demonstrated great courage on the part of the geophysicist, Dr. W. Domzalski.

DISCUSSION

It is not the purpose of this paper to discredit the use of geophysical methods in civil engineering. The examples given above indicate that when properly used the methods can be of great help to the engineer. They also indicate that where they have failed the fault is usually in the interpretation of the results.

In some cases there are limitations inherent in the physics of the methods which mean that they cannot produce a true answer, for instance, the seismic method cannot indicate the depth of a deep narrow valley in rock filled with soft material when the valley is so deep that the time path through the rock of the valley walls is longer than that through the lower velocity material which fills the valley. In cold climates frozen ground introduces a complicating factor which must be considered in interpretation.

On the other hand, sometimes the geophysical method has the advantage over borings, for instance, in basalt regions it is sometimes extremely difficult to decide whether a core is from bedrock or a basalt boulder, and a geophysical survey may help by indicating a resistivity or seismic anomaly.

In one case, to the authors' knowledge, a resistivity survey for a bridge site was condemned because the results were found to be in error when the bridge foundations were constructed. In fact the site had been moved 100 yards (30 m.) upstream after the survey was made and in this distance there was a change in rock level of 60-80 feet (18 to 24 m.) due to a buried erosion feature in the rock. This is another example of the psychological problem with which engineers are sometimes faced.

There are so many uncertainties in these indirect methods that dogmatic statements such as "rock is at elevation X" should be avoided. In general the methods reveal anomalies which should be checked by borings or excavations. Overconfidence and overselling are grievous errors which have already led many engineers to distrust the use of geophysical methods. In many cases these faults are because the operators and interpreters are trained in oil and mining work and do not realize the great difference in scale involved in civil engineering work, nor the differences in technique thereby demanded. In an otherwise admirable presentation of the value of a sparker survey in a current project the authors of a recent paper say: "The sparker records later *proved* that this hole did not reach bedrock but had encountered boulders. . . ." and "The bedrock could be *seen* on the records 50 feet (15 m.) below the river bottom". (our italics). A sparker survey *proves* nothing, and all that can be *seen* on the record is a wavy line. Whether or not the *interpretation* was correct in the above case is beside the point. The statements are not true, the authors are unconsciously overselling the method.

Perhaps the best summing up of the value of geophysical methods in civil engineering was given by H. J. B. Harding when discussing the paper by Robertshaw and Brown. He said: "It should be remembered that a geophysical survey proved nothing, but it indicated closely if carried out by men of experience, what was probably there. The only way to prove what was underground was to go there, either by digging a hole or borehole, or after the excavation had been done".

In claims for the results which can be obtained by geophysical methods in civil engineering problems, the dictum of St. Paul should guide us: "Let your moderation be known unto all men!"

ACKNOWLEDGEMENTS

The examples from Ontario are given by permission of the Chief Engineer of the Department of Highways Ontario.

The first author is grateful to Mr. J. Robertshaw for refreshing his memory on the details of Example II and of the work in Ireland mentioned in Example VI, and to Dr. W. Domzalski who served a like purpose in Example VII. The title of the paper was suggested by Dr. Domzalski, as an improvement on an originally more pessimistic approach by the authors. The authors had hoped that Dr. Domzalski might have been a joint author of the paper in which case its merit would have been greatly enhanced, but for reasons of timing this unfortunately proved impossible.

REFERENCES

Domzalski, W. (1956) — "Some Problems of Shallow Refraction Investigations". Geophysical Prospecting, Vol. IV, No. 2, June.

McIldowie, G. (1934-5) — "The Construction of the Silent Valley Reservoir, Belfast Water Supply". Proc. I.C.E. Vol. 239.

Robertshaw, J. and Brown, P. D. (1955) — "Geophysical Methods of Exploration and their Application to Civil Engineering Problems". Proc. I.C.E. Part I, September.

MECANISMO DE DESAGREGAÇÃO DE ROCHAS BASÁLTICAS SEMI-ALTERADAS

MURILLO DONDICI RUIZ

Engenheiro Responsável pela Secção de Geologia Aplicada do Instituto de Pesquisas Tecnológicas, São Paulo. Assistente da Cadeira de Mineralogia, Petrografia e Geologia Aplicada da Escola Politécnica da Universidade de São Paulo, Brasil.

SUMÁRIO

Tem-se constatado que rochas basálticas semi-alteradas possuem pequena resistência à variação de umidade. Dada a importância que essas rochas assumem no Estado de São Paulo, como materiais de construção, fundação de grandes barragens e outras importantes estruturas, julgou-se de primordial importância o estudo do mecanismo das desagregações que essas rochas apresentam após alguns ciclos de variações de umidade. Êste trabalho apresenta um resumo de alguns estudos mineralógicos efetuados, de método de ensaio para determinação de características expansivas de argilo-minerais que ocorrem em rochas basálticas semi-alteradas e os resultados obtidos.

SUMMARY

Basaltic semi-weathered rocks disrupt when subjected to moisture content variation. This paper deals with the mineralogic constitution of semi-weathered basalts and expansive properties of the clay-mineral nontronite present in most basaltic rocks from São Paulo (Brazil). Expansion pressures as high as 200 kg/cm^2 *were found in the tests described in this paper.*

GENERALIDADES

Durante o desenvolvimento de inúmeros ensaios para determinação das características tecnológicas de rochas basálticas do Estado de São Paulo[1], notou-se que essas rochas quando atingem determinado estágio de alteração mineralógica possuem pequena resistência à variação de umidade. Essa pequena resistência à variação de umidade traduz-se por uma desintegração total da rocha a tal ponto que blocos de dimensões da ordem de 0,5 m^3 reduzem-se a pó após alguns ciclos de secagem e umidecimento. Êste fenômeno tem sido observado também em vários locais onde atualmente se constroem barragens. Na Barragem de Jupiá (Urubupungá) foram utilizados blocos de rocha basáltica para proteção do talude de montante das ensecadeiras de terra compactada, aparentemente resistentes no momento da extração de pedreira existente na margem direita do Rio Paraná. Após algumas semanas, a maior parte dêsses blocos apresentou um sistema de fraturas que aumentava progressivamente, por simples exposição a sol e chuva, até que os fragmentos do antigo bloco de rocha fôssem reduzidos a pequenas dimensões. A figura 1 apresenta o aspecto de blocos de rocha basáltica, em início de desagregação, no enrocamento da margem direita da Barragem de Jupiá.

Idêntico fato tem-se constatado no lastro da Estrada de Ferro Noroeste do Brasil, empregado no trecho Andradina (SP)-Três Lagoas (MT) e nas Barragens de Barra Bonita e Bariri, ambas no Rio Tietê (SP).

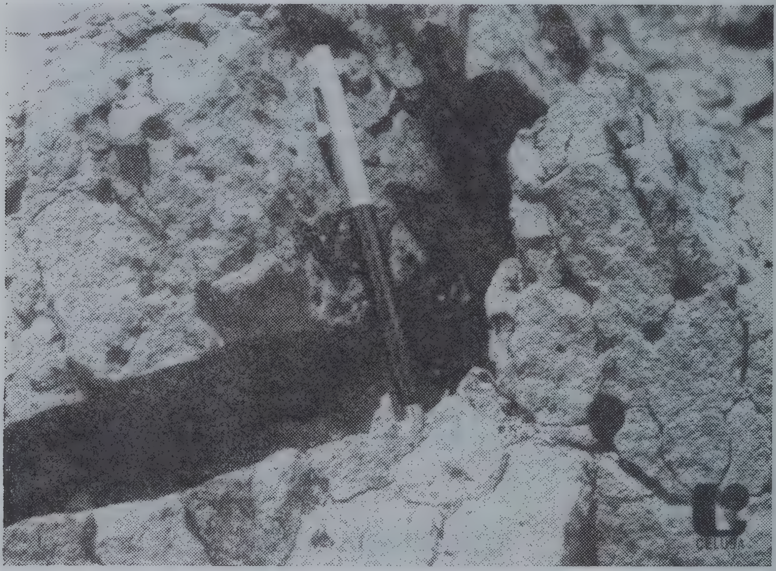

Fig. 1 — Aspectos de blocos de basalto vesicular em início de desagregação.

Fig. 1 — Vesicular basalt stones during the desaggregation process.

Em todos os casos foi possível a verificação de fator comum a tôdas essas desagregações: apesar dos graus de alterações mineralógicas variarem, o fenômeno ocorria sempre na presença de um material de côr verde-garrafa, disseminado no seio da rocha ou preenchendo fraturas e vesículas. Êste trabalho apresenta um resumo de suas características mineralógicas e de seu comportamento ante variações de umidade, para melhor caracterização do mecanismo de desagregação dessas rochas basálticas.

CARACTERIZAÇÃO MINERALÓGICA

Santos e Ruiz[2, 3] através de ensaios compreendendo análise em microscópio petrográfico, análise térmica diferencial, capacidade de troca de cátions, análise química, difração de raios X e microscopia eletrônica, caracterizaram materiais semelhantes provenientes das barragens de Barra Bonita e Bariri. As principais conclusões foram:

1) Na Barragem de Barra Bonita constatou-se a presença de nontronita e plagioclásios não decompostos em fragmentos de basaltos em decomposição. Foram também constatadas as presenças de montmorilonita côr rosa e caulita, preenchendo diáclases do maciço rochoso, na margem esquerda do Rio Tietê.

2) Na Barragem de Bariri os materiais de preenchimento de diáclases e vesículas, de côr verde, são constituídos por mineral montmorilonítico, provàvelmente tratando-se de nontronita ou membro da série nontronita-badeleíta, por mineral do grupo das micas hidratadas, por plagioclásio e por calcedônia. Não foram encontradas nem clorita nem vermiculita em quantidades detectáveis pela difração de raios X.

A presença dêsses minerais montmoriloníticos nessas rochas basálticas semi-alteradas pode explicar o seu mecanismo de desagregação por variações de umidade. De fato, sendo os argilo-minerais montmoriloníticos materiais suscetíveis de absorverem água em proporção elevada em relação ao seu próprio pêso, apresentam-se sensíveis a variações de umidade, com aumento ou diminuição de volume. Os aumentos de volume ocorrem com o desenvolvimento de pressões que êsses minerais podem exercer contra paredes de materiais que porventura os envolvam. Essas pressões exercidas durante a expansão são as responsáveis pelas desagregações observadas.

MATERIAIS E MÉTODO DE ENSAIO

Para o estudo das características expansivas dêsses minerais foram colhidos materiais da Barragem de Bariri. Nesse local, preenchendo diáclases e fraturas da rocha basáltica, ocorre grande quantidade do material, cuja constituição mineralógica foi descrita acima. Trata-se, portanto, de uma mistura de minerais e os resultados obtidos devem considerar êste fato. Entretanto, sòmente os minerais montmoriloníticos, presentes em grande proporção, são suscetíveis de absorverem água em grandes quantidades e acusarem expansão.

No local, o material de preenchimento de diáclases constitui um aglomerado dos minerais mencionados, que para facilidade de redação chamaremos simplesmente de *nontronita,* por tratar-se da parcela mais importante. Êste aglomerado, preenchendo fissuras, fraturas e vesículas da rocha, apresenta-se com a forma dêsses vazios. Por exemplo, a nontronita proveniente das diáclases apresenta-se com a forma de placas, de dimensões variáveis desde 5,0 cm em sua maior dimensão e 0,2 cm de espessura até a fração argila.

Ao dinamitarmos o maciço rochoso para implantação da casa de máquinas, essas placas de nontronita destacavam-se parcialmente dos blocos de rocha basáltica, acumulando-se aos pés das escavações. Essas acumulações apresentavam uma certa distribuição granulométrica, com tendência a apresentar, progressivamente, maior percentagem de finos ao ser submetida a variação de umidade. A figura 2 apresenta essa tendência. A curva I representa a distribuição granulométrica de uma amostra de nontronita agregada, acumulada aos pés das escavações, e a curva II representa a nova distribuição granulométrica, da mesma amostra após dezesseis ciclos de secagem e umidecimento.

O método de ensaio utilizado para determinação das características de expansão da nontronita proveniente da Barragem de Bariri, consiste na medida da expansão volumétrica dêsse material prèviamente comprimido em anéis metálicos de área S, com pressões estáticas P_m, ao ser submetida a imersão em água e confinada com pressões P_o. As expansões davam-se, pois, contra as pressões de confinamento P_o e eram medidas através do contrôle das alturas iniciais H_i e finais teóricas H_f, da nontronita, antes e após imersão e estabilização.

A aparelhagem utilizada é a mesma que se emprega para a determinação de adensamento de solos, agora, inversamente, utilizada para medida de expansão da nontronita. O esquema de montagem para ensaio pode ser observado na figura 3. Em cada ensaio têm-se as seguintes variáveis:

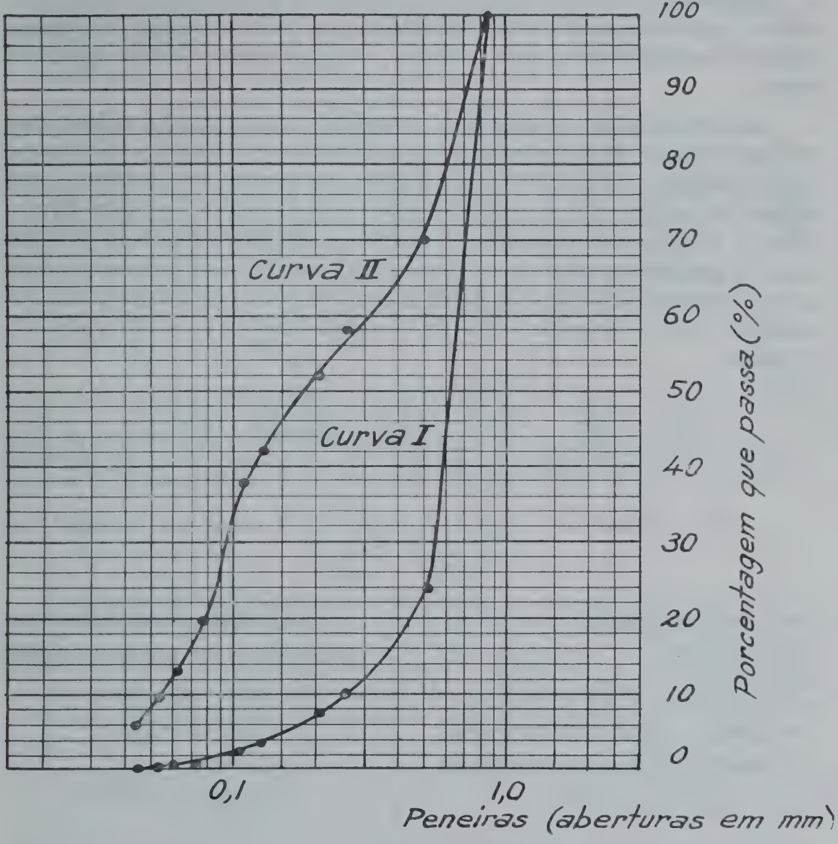

Fig. 2 — Variação granulométrica da nontronita ao ser submetida a ciclos de secagem e saturação d'água.

Fig. 2 — Granulometric change of nontronite subjected to wetting and drying.

1) Quantidade de nontronita a ser ensaiada (M)

2) Granulometria da nontronita (G)

3) Área do anel ou seja área do corpo de prova (S)

4) Umidade inicial da nontronita (H)

5) Temperatura de secagem, para T $\geq$ 105°C

6) Pressão de moldagem do corpo de prova (P_m)

7) Pressão de confinamento, durante a imersão (P_o)

Outras variáveis tais como cátions presentes na nontronita e outros líquidos de imersão que não a água destilada foram considerados, mas fogem ao interêsse desta apresentação.

As expansões eram, pois, medidas com os contrôles das variações das alturas do corpo de prova em função do tempo após imersão. As curvas altura do corpo de prova-tempo são idênticas às obtidas para adensamento de solos, porém invertidas. Assim foi adotado o mesmo critério de Casagrande para a determinação da altura final teórica de adensamento, agora empregado para determinação da altura teórica de expansão. As expansões foram calculadas pela aplicação da fórmula:

$$E = \frac{H_f - H_i}{H_i} \,.\, 100(\%)$$

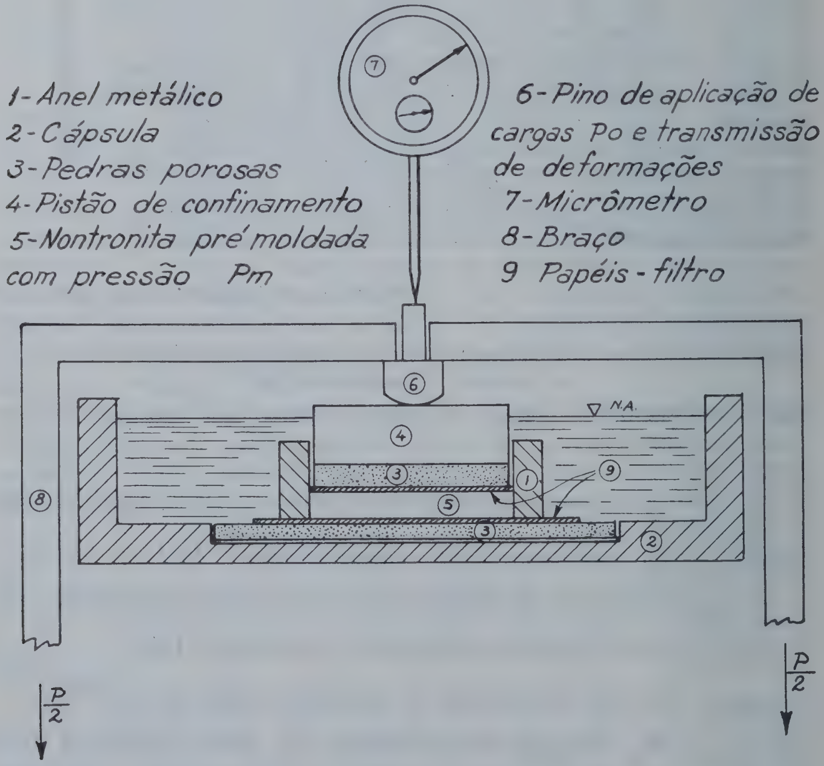
1- Anel metálico
2- Cápsula
3- Pedras porosas
4- Pistão de confinamento
5- Nontronita pré moldada com pressão Pm
6- Pino de aplicação de cargas Po e transmissão de deformações
7- Micrômetro
8- Braço
9 Papéis - filtro
7
6
4
3
1
9
5
3
2
8
N.A.
P/2
P/2

Fig. 3 — Esquema de montagem para ensaio.

Fig. 3 — Sketch of test assembly.

Definimos como *pressão de expansão,* para dadas condições de ensaio, à pressão de confinamento P_o que causa expansão nula.

RESULTADOS EXPERIMENTAIS

Das sete variáveis consideradas em cada ensaio (M, S, H, G, T, P_m e P_o) serão consideradas, neste trabalho sòmente as influências de H, G, P_m e P_o sôbre as expansões. Inúmeros ensaios demonstraram que as variáveis M e S não influenciam nos valores obtidos nos testes de expansão se:

a) M (em gramas)/S (em cm^2) $=$ 1,5

b) S $\geq$ 5 cm^2

Essas duas condições foram mantidas em todos os ensaios cujos resultados são aqui apresentados. As variações da expansão acusada pela nontronita, com aquecimento prévio a altas temperaturas (T), fogem ao interêsse dêste trabalho.

1) EXPANSÃO EM FUNÇÃO DA GRANULOMETRIA DA NONTRONITA

Como já foi dito, a nontronita proveniente das fendas e diáclases das rochas basálticas da Barragem de Bariri apresenta-se como um agregado com uma certa granulometria. É possível, pois, por peneiramento, separar parcelas que ficam retidas entre a série normal de peneiras. Essas frações granulométricas foram ensaiadas separadamente a fim de se determinar a influência da granulometria da agregação de nontronita nas expansões por adsorção de água. Os dados de ensaio e os resultados experimentais obtidos estão representados na figura 4.

Foi ainda levado a ensaio um corpo de prova constituído por uma única placa de nontronita, com as dimensões de 5,0 cm de diâmetro e 0,3 cm de espessura, prèviamente sêco em estufa a 105°C. Após 36 horas de imersão êste corpo de prova não acusou expansão ou qualquer outra alteração.

2) EXPANSÃO EM FUNÇÃO DA UMIDADE INICIAL

A umidade inicial da nontronita antes da moldagem dos corpos de prova nos anéis metálicos, começa a interferir nas expansões por adsorção de água a partir de certos valores. Na figura 5 vemos, por exemplo, que para umidades iniciais entre 0% e 12% as variações obtidas para as expansões, para as condições de ensaio ali indicadas, foram pràticamente desprezíveis. Para maiores umidades iniciais da nontronita obtêm-se índices de vazios menores; nos corpos de prova, entretanto, as expansões são inferiores.

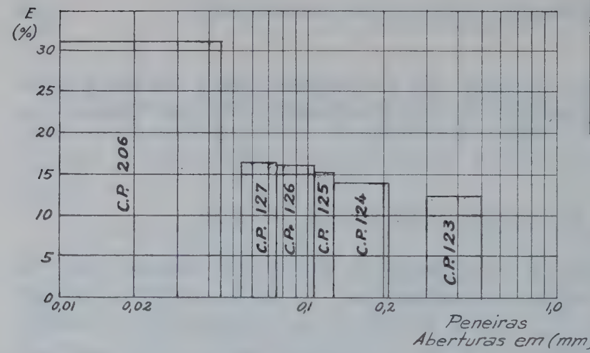

Corpo de Prova nº	Peneiras (mm) Passa	Peneiras (mm) Retido
123	0,500	0,297
124	0,210	0,125
125	0,125	0,105
126	0,105	0,074
127	0,074	0,053
206	0,044	–

Corpos de prova

$S = 10\ cm^2$
$M = 15\ g$
$T = 105\ °C$
$Pm = 1000\ kg/cm^2$
$Po = 1\ kg/cm^2$

Fig. 4 — Variação da expansão em função da granulometria da nontronita.

Fig. 4 — Expansion in terms of grain size distribution of nontronite samples.

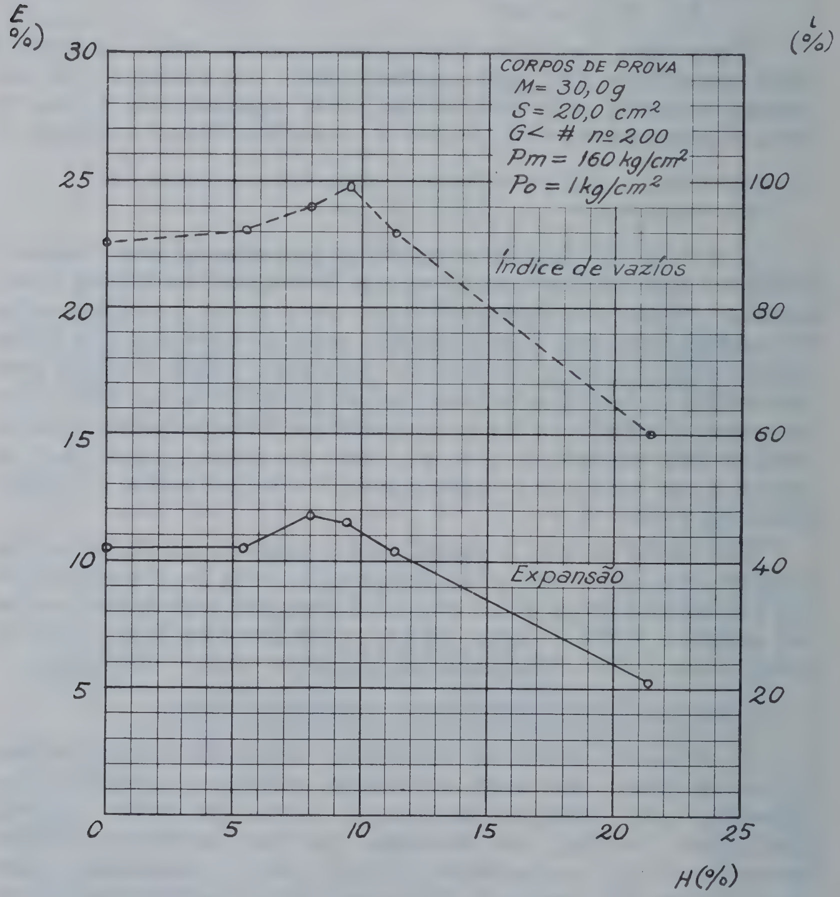

Fig. 5 — Variação do índice de vazios e expansão em função da umidade inicial da nontronita.

Fig. 5 — Void ratio and expansion in terms of initial moisture content of nontronite.

3) EXPANSÃO EM FUNÇÃO DAS PRESSÕES DE MOLDAGEM (P_m) E CONFINAMENTO (P_o)

A figura 6 indica, simultâneamente, as variações das expansões em função de P_m e de P_o. Verifica-se, por exemplo, que para corpos de prova moldados com pressões 1000 kg/cm² obteve-se a pressão de expansão de 100 kg/cm². Os demais dados de ensaio acham-se indicados nessa figura.

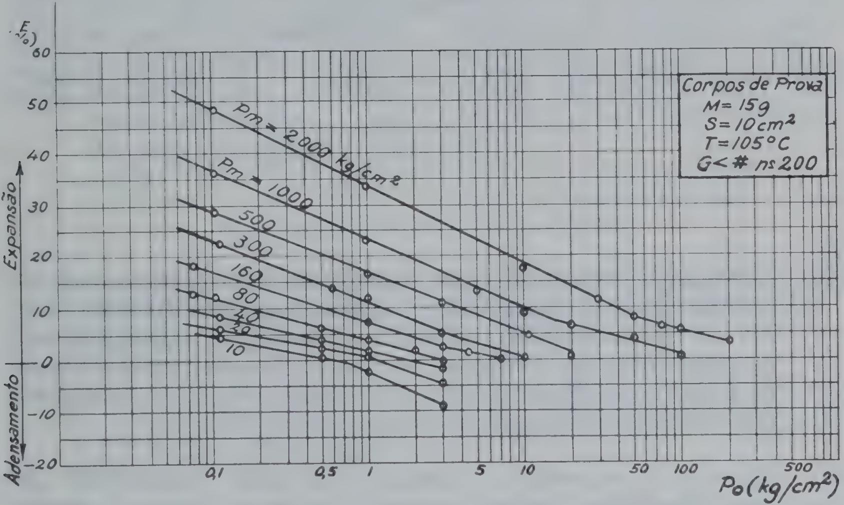

Fig. 6 — Curvas E = f (P_m, P_o).

Fig. 6 — Curves E = f (P_m, P_o).

A figura 7 indica os mesmos resultados, porém, substituindo-se as expansões E pelos valores das alturas iniciais e finais teóricas dos corpos de prova. A curva I representa a função $H_i = f(P_m)$. As curvas II representam as funções $H_f = f(P_o, P_m)$. A análise das curvas II mostra que para $P_m \geq 1000$ kg/cm², $H_f = f(P_o)$ e independente de P_m.

RESUMO E DISCUSSÃO DOS RESULTADOS

1) Rochas basálticas semi-alteradas podem apresentar desagregação parcial ou completa ao serem submetidas a variações de umidade. Como tem sido constatada a presença de argilo-minerais montmoriloníticos em determinada fase de suas alterações mineralógicas, principalmente nontronita, o mecanismo dessas desagregações pode ser explicado pela capacidade de adsorção de água dêsses minerais.

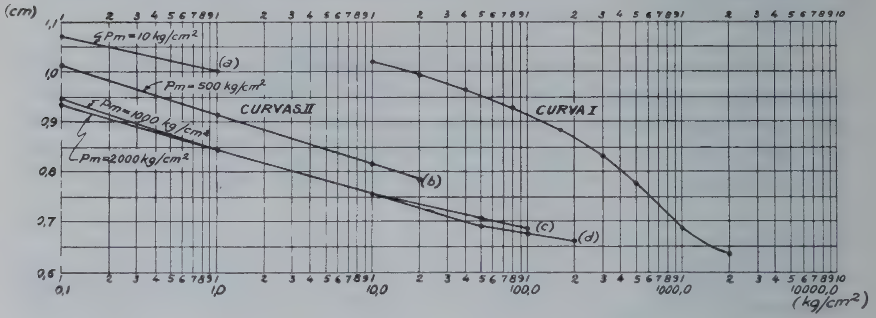

Fig. 7 — Curva I: $H_i = f(P_m)$. Curva II: $H_f = f(P_m, P_o)$.

Fig. 7 — Curve I: $H_i = f(P_m)$. Curve II: $H_f = f(P_m, P_o)$.

2) Agregados minerais dêsses argilo-minerais fragmentam-se sucessivamente ao sofrerem variações de umidade (fig. 2). A fragmentação sucessiva aumenta a superfície específica total do conjunto, aumentando concomitantemente a sua capacidade de adsorver água. Tal fato traduz-se por expansões volumétricas crescentes (fig. 4).

3) Durante a expansão, a nontronita pode, dependendo de suas condições iniciais, exercer pressões elevadas contra as paredes de rocha, que porventura a envolva. Essas pressões medidas em laboratório, sob condições especiais, chegaram a 200 kg/cm², entretanto, por extrapolação de valores obtidos, essas pressões chegam a 450 kg/cm² para pressões de moldagem correspondente a 2.000 kg/cm² (fig. 6).

4) A análise da figura 6 indica que as expansões processam-se segundo lei logarítmica. Essa lei logarítmica, entretanto, apresenta mudança em seus coeficientes, pois obtêm-se, para determinado valor de P_m, dois segmentos retilíneos bem definidos na função $E = f(P_o)$. Êsses segmentos retilíneos mostram que a partir de uma determinada distância $2d_o$ entre partículas de nontronita ou deixam de agir fôrças de atração ou começam a agir fôrças de repulsão entre essas mesmas partículas.

5) A análise da figura 7 mostra que

a) para $P_m \leq 500$ kg/cm²

$H_f = f(P_o, P_m)$

b) Para $P_m \geq 1000$ kg/cm^2
$H_f = f\ (P_o)$

O fato de que H_f independe de P_m, quando $P_m \geq 1000$ kg/cm^2 é particularmente interessante. Isto pode significar que acima dêsses valores corpos de prova moldados com P_m diferentes entre si possuem índices de vazios diferentes (H_i diferentes entre si), entretanto devem possuir, estatìsticamente, idêntica orientação das partículas de nontronita. Êste fato é ainda comprovado pela observação ao microscópio dos corpos de prova moldados com pressões elevadas, que se apresentavam como filitos, isto é, com partículas orientadas adquirindo uma xistosidade acentuada.

REFERÊNCIAS BIBLIOGRÁFICAS

1. Ruiz, M. D. — "Contribuição ao estudo tecnológico de algumas rochas basálticas do Estado de São Paulo". Tese de Doutoramento em Geologia Aplicada pela Escola Politécnica da U.S.P. Fevereiro 1962.

2. Santos, P. S.; Ruiz, M. D. — "Composição mineralógica de um material em forma de placas, de côr verde, de enchimento de diáclases de rochas basálticas da Barragem de Bariri (SP)". Pesquisa n.º 78 do IPT, 1962.

3. Santos, P. S.; Ruiz, M. D. — "Caracterização mineralógica de alguns materiais argilosos que ocorrem em formações basálticas da Barragem de Barra Bonita, Rio Tietê, São Paulo". Pesquisa n.º 64, IPT — 1961.

DIVISÃO IV — *Mecânica dos Solos para Estradas e Aeroportos*

DIVISIÓN IV — *Mecánica de Suelos para Carreteras y Aeropuertos*

DIVISION IV — *Soil Mechanics for Roads and Airports*

IV/1

EFFECTS OF CHEMICAL ADDITIVES ON THE STRENGTH OF SOIL-CEMENT MIXTURES

MANUEL MATEOS, ROBERT H. TAWES
and DONALD T. DAVIDSON

Respectively Research Associate, Captain, Corps of Engineers and Late Professor of Civil Engineering. Iowa State University, Ames, Iowa.

ABSTRACT

Three chemical additives were used with Portland cement to stabilize sandy, silty and clayey soils.

The results of a study made to determine the effect of the chemical additives on the unconfined compressive strength of the stabilized soils are presented. The chemicals, used were sodium silicate, sodium hydroxide and sodium carbonate. A cost analysis of soil-cement with and without chemical additive and a modified version of the British standard freeze-thaw test are also included.

The use of selected chemical additives in small amounts with soil-cement mixtures results in significant strength increases over soil-cement with equal Portland cement content but no chemical additive. Nevertheless the use of chemical additives in soil-cement may not be economical under normal conditions.

SUMARIO

Se presentan los resultados de un estudio hecho para determinar los efectos de la adición de pequeñas cantidades de silicato sódico, hidróxido sódico y carbonato sódico en tres suelos estabilizados con cemento. Los suelos usados fueron uno arenoso, otro limoso y otro arcilloso. La evaluación se hizo comparando las resistencias a la compresión sin confinar de probetas compactadas a la máxima densidad Proctor. Se incluyen estudios de hielo y deshielo asi como un análisis económico sobre el uso de suelo-cemento con o sin aditivos.

El empleo de ciertos aditivos con mezclas de suelo-cemento puede causar un aumento en las resistencias del suelo-cemento. Sin embargo el uso de aditivos químicos en el suelo-cemento parece ser que no es económico en condiciones de trabajo normales.

INTRODUCTION

The role of soil-cement in today's roads and airfields has been proven through many years of satisfactory service. From an unobstrusive beginning in 1917, when Dr. J. H. Amies took out a patent on soil and cement mixtures, which he labeled "Soilamines", this new structural material has grown in importance until today over 10,000 miles (16,090 km) of soil-cement pavement are in use.

As in other structural materials, a constant effort is being made to improve soil-cement. In 1935 the Portland Cement Association started an extensive investigation to develop a series of standard tests for the evaluation of soil-cement. From this work evolved the moisture-density, wet-dry and freeze-thaw tests. These tests permit the correlation of field performance with laboratory results. Another valuable function of these tests is the comparison of specimens in the laboratory. By laboratory comparisons, using standardized tests, the best methods and materials may be selected for further investigation.

Improvements in soil-cement may be brought about either by decreasing costs or by increasing strengths. The inflationary spiral of construction costs makes it desirable to find a means of making the use of soil-cement more economical. Today's heavier axle loads and higher traffic volumes make greater strength a necessity. It remains for the engineer-scientist to find a reasonable solution for these divergent trends.

This report presents a comparison of the effects of three chemical additives on cement-stabilized sandy, silty, and clayey soils. The investigation consists of three studies, which are:

1. Preliminary. Moisture content-density-strength relationships are determined.

2. Strength. Unconfined compressive strengths of specimens with varying chemical additive and Portland cement contents are compared.

3. Freeze-thaw. An analysis of freeze-thaw resistance using a modified version of the British standard test is made.

PRIOR WORK ON CHEMICAL TREATMENT OF SOIL-CEMENT

Research at Iowa State University

Investigation on the use of chemical additives to soil-cement mixtures started at Iowa State University in 1950. In the early work several organic and inorganic compounds were tried; vinsol resin and calcium chloride were found to be most promising[1]. Strength of soil-cement specimens was found to increase upon immersion in a solution of sodium hydroxide[2]. Soil-cement specimens were increased in strength by sprinkling them with a solution of sodium silicate or sodium hydroxide[3]; sodium silicate was effective with a sand-loess soil and sodium hydroxide was best with a friable loess soil. The addition of sodium carbonate to soil-cement-fly ash mixtures increased their early strength[4].

Chemical additives have also been tried with soil-lime-fly ash[5, 6, 7, 8, 9, 10] and soil-lime mixture[11, 12]. In these studies, sodium carbonate, sodium hydroxide and sodium silicate were the most promising additives. The cementitious compounds formed in soil-lime-fly ash and in soil-lime mixtures might be similar to those formed in soil-cement mixtures. Sodium carbonate, sodium hydroxide and sodium silicate were therefore studied in this investigations.

Other Research

Studies of mixing chemical with soil-cement have been made at the Massachusetts Institute of Technology[13, 14, 15]. From this research it was concluded that the best additives were sodium metasilicate for clean sands, sodium sulfate and sodium aluminate for silts, sodium hydroxide for heavy clays, and sodium sulfate for organic sands. It was also found that sodium additives increase the resistance of all types of soil-cement to sulfate attack[15].

Some work has been done in India to determine the detrimental effects on soil-cement of sodium sulfate, sodium carbonate, or magnesium sulfate that might be already present in soils[16, 17, 18]. Excess amounts of these constituents proved detrimental to soil-cement, but the deleterious effects could be overcome by an increase in the cement content.

LABORATORY INVESTIGATION

Methods

MOLDING

Tests were performed with 2 inch (5,08 cm) diameter by approximately 2 inch high test specimens compacted to near standard Proctor density. These specimens were made with the Iowa State Compaction Apparatus using the 5 pound (2.268 kg) hammer dropped from a height of 12 inches (30.40 cm) and giving 5 blows to each side of the specimen [19].

CURING

After being molded, specimens were wrapped in wax paper and sealed with cellophane tape.

They were then placed in a high humidity room kept at 72 ± 4°F (22.2 ± 2.2°C) and stored there for the specified time.

TESTING

After being cured, specimens were immersed for 24 hours in water kept at room temperature. They were then tested in unconfined compression at a rate of 0.05 inch (0.127 cm) per minute. The highest load obtained in compression was the value used. All strength determinations were run in triplicate; the average value is reported.

FREEZE-THAW TEST

The freeze-thaw test used to evaluate the durability of soil-cement-chemical mixtures is a modification of the British Standard Test B. S. 1924-1927 [20]. The modifications are as follow: use 2 inch (5.08 cm) by 2 inch instead of 2 inch by 4 (10.16 cm) inch test specimens, use waxed paper sealed with cellophane tape instead of paraffin to reduce moisture evaporation during curing, and use a resin-base paint instead of tar as the seal coat on the top of specimens.

Two identical specimens were molded for each mixture. One specimen was designated the control specimen and the other the freeze-thaw specimen. After moist curing for 7 days the flat top surface of each specimen was sprayed with the resin-base paint to a thickness of approximately 1 mm.

Then the control specimen was immersed for 15 days in distilled water at a temperature of 77 ± 4°F (25 ± 2.2°C); the freeze-thaw specimen was immersed for one day, then it was exposed alternately to temperatures of 23 ± 2°F (—5 ± ± 1.1°C) for 16 hours and 77 ± 4°F (25 ± 2.2°C) for 8 hours during 14 cycles, each cycle lasting 24 hours. A vacuum flask specimen container was used to cause freezing from the top down; the water inside the vacuum flask was at 46°F (7.77°C) at the start of each freeze cycle. The unconfined compressive strength of the control specimen (p_c) and the freeze-thaw specimen (p_f) were then determined. The index of resistance to the effect of freezing (R_f) was calculated from the formula:

$$R_f = \frac{100\, p_f}{p_c} \text{ (percent)}$$

SOILS

Information concerning sampling locations and properties of the sandy, silty, and clayey soils used is given in Table 1. All three soils are representative of widespread and easily available materials for stabilized road construction in Iowa and adjacent Midwest states.

PORTLAND CEMENT

The cement used was Type I and its properties are given in Table 2.

CHEMICALS

The three chemical additives used were analytical grade reagents: sodium metasilicate ($Na_2SiO_3.9H_2O$), sodium hydroxide ($NaOH$), and sodium carbonate (Na_2CO_3).

Procedure

The laboratory investigation was divided into three studies: preliminary, strength and freeze-thaw. In all studies the amount of additive used, both cement and chemical, is expressed as a percentage of the dry weight of the soil. The Portland cement and the sodium carbonate were added as dry powder; the sodium hydroxide and sodium metasilicate were dissolved in the mix water.

TABLE 1 — Properties of Soils

Property	Sand-loess	Friable loess	Kansan till
Geological description:	Mix of approximately 82% sand and 18% Wisconsin-age loess, oxidized, calcareous, medium plastic	Wisconsin-age loess, oxidized, calcareous, friable	Kansan-age glacial till, oxidized, calcareous, plastic
Location:	Jasper County, Iowa	Harrison County, Iowa	Ringgold County, Iowa
Horizon:	Loess: C	C	C
Textural composition, %:			
Gravel (>2 mm)	0.0	0.0	0.0
Sand (2.0-0.074 mm)	70.7	0.4	31.5
Silt (0.074-0.005 mm)	22.3	80.0	30.0
Clay (<0.005 mm)	7.0	19.6	38.5
Colloids (<0.001 mm)	6.0	14.5	31.0
Predominant Clay minerals:	Montmorillonite, vermiculite	Montmorillonite, illite	Montmorillonite, illite
Chemical properties:			
Cation exchange cap.* (m.e./100 gm)	11.0	13.4	29.4
Carbonates, %	11.6	10.2	4.9
pH **	8.0	8.7	8.2
Organic matter, %	0.2	0.2	0.2

---

* For fraction passing No. 40 sieve.

** For fraction passing No. 10 sieve.

TABLE 1 (continued)

Property	Sand-loess	Friable loess	Kansan till
Physical properties:			
Liquid limit, %	19	31	42
Plastic limit, %	16	25	20
Plasticity index	3	6	22
Classification:			
Textural ***	Sandy loam	Silty loam	Clay
Engineering (AASHO)	A-2-4	A-7-6(12)	A-7-6(12)

*** Textural classification is from the triangular chart developed by the U.S. Bureau of Public Roads. Sand and silt sizes are separated on No. 200 sieve (0.074 mm).

PRELIMINARY STUDY

In this study the moisture content, dry density and strength relationships were determined. The Iowa State Compaction Apparatus was used in molding soil-cement specimens with both one and two percent of each chemical additive; the percentage of cement was kept constant for each soil. The specimens molded for the determination of the moisture-density relationships were cured for seven days, then immersed in water for 24 hours, and tested in unconfined compression. Using these strengths, the moisture-strength relationships were determined.

STRENGTH STUDY

Specimens were molded with moisture content for optimum strength as determined in the preliminary study. The percentage of chemical additive was varied and the percentage of cement was kept constant. For percentages of additive not used in the preliminary study, moisture content values were interpolated from the available data.

After obtaining the test results from varying the chemical additive, the data were plotted and a smooth curve was drawn. Using the optimum percentage of chemical additive for maximum strength, another series of specimens was molded holding the percentage of chemical additive constant and varying the amount of cement. This experiment was performed only with the chemical additive determined best for each soil. It is recognized that the optimum percentage of additive determined by the curve is an assumption, but it is the most valid one that may be made other than by connecting the points with straight lines. The use of straight lines was not considered suitable, since the optimum percentage of additive then would have to be at a plotted point. The possibility of this is remote. Two other assumptions made are that the optimum percentage of chemical additive and the moisture content for optimum strength do not vary with the cement content.

FREEZE-THAW STUDY

To obtain a correlation between the Portland Cement Association's freeze- thaw test (A.S.T.M. Specification D 560-44; A.A.S.H.O. Specification T 136-45) and the modified British standard test, the estimated required strengths necessary to pass the Portland Cement Association test were obtained for the three soils from the Soil-Cement Bureau of

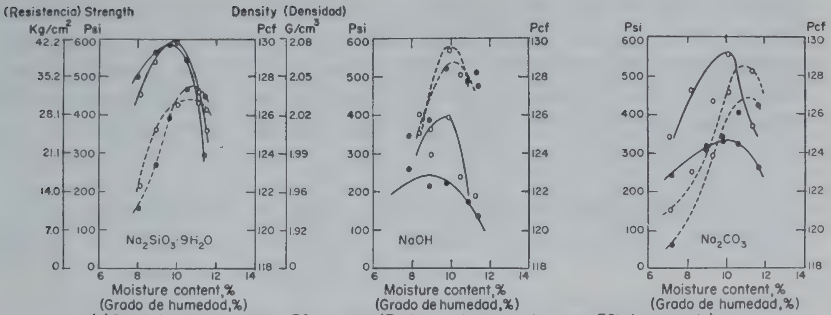

(a) Sand-loess specimens, 5% cement (Probetas de arena-loes con 5% de cemento)

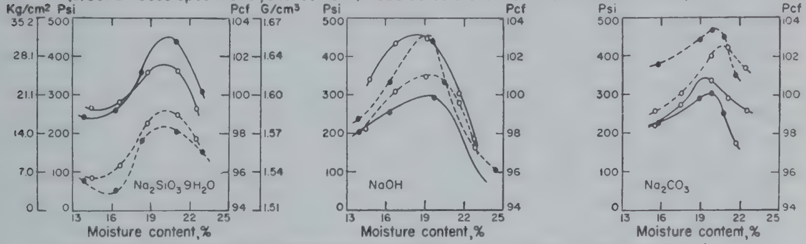

(b) Friable-loess specimens, 5% cement (Probetas de loes friable con 5% de cemento)

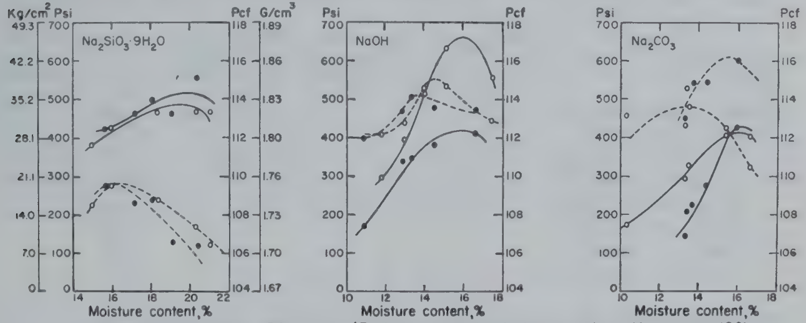

(c) Kansan till specimens, 10% cement (Probetas de suelo glacial del perio do Kansan con 10% de cemento)

Legend: —— Strength: – – – Dry density. ● 2% Additive: ○ 1% Additive
(Legenda: —— Resistencia: – – – Densidad seca: ● 2% Aditivo: ○ 1% Aditivo)

Fig. 1 — Moisture-density-strength relationships.

Fig. 1 — Relaciones de humedad-densidad y humedad-resistencia.

the Association*. These strengths were 290 psi (20.4 kg/cm^2) for the sandloess, 275 psi (19.3 kg/cm^2) for the friable loes, and 250 psi (17.5 kg/cm^2) for the Kansan till. Freeze-thaw specimens were then molded with the cement content necessary to obtain these strengths, using plain soil-cement and soil-cement plus additive. Additional specimens for each soil were molded with and without chemical additive using both higher and lower cement contents than required to meet the freeze-thaw requirements. This experiment was designed to determine the results of the modified British standard test over a range of soil-cement strengths.

---

* J. A. Leadabrand; Portland Cement Association; Chicago, Illinois; Information on required compressive strengths; Private communication; 1958.

PRESENTATION AND DISCUSSION OF RESULTS

Preliminary Study

The relationships of 7 day unconfined compressive strengths and densities to molding moisture content are shown in Figure 1. The general characteristics of the curves for mixtures containing chemical additives are the same as those obtained with plain soil and soil-cement. It may be seen that the same moisture content does not necessarily prevail for both maximum density and maximum strength. This indicates an intimate relationship between the amount of water consumed in the lubrification of soil particles, hydration of the cement, and adsorption by the soil particles.

TABLE 2 — Properties of Type I Portland cement

Chemical composition, % by wt:	21.42
Silicon dioxide	5.72
Aluminum dioxide	2.90
Calcium oxide	63.71
Magnesium oxide	3.43
Sulphur trioxide	1.73
Loss on ignition	0.64
Insoluble residue	0.19
Physical properties:	
Specific surface (Wagner), sq. cm./gm.	1744
Air Permeability (Blaine)	3025
Setting time (Gillmore test)	
Initial, hr.	2.84
Final, hr.	5.00
Autoclave expansion, %	0.160
Compressive strength (1:2.75 (G.O.S.)	
At 3 days, psi	1882 (132 kg/cm^2)
At 7 days, psi	3133 (220 kg/cm^2)
At 28 days, psi	5121 (360 kg/cm^2)

Each chemical has its own characteristic effect on the optimum moisture contents for strength and density. The moisture contents for maximum strength generally are on the dry side of those for maximum density of sand-loess and on the wet side for clayey Kansan till. The moisture contents for maximum density with silty friable loess are about the same as those for maximum strength.

These variations between the optimum moisture contents for maximum strength and for maximum density possibly may be related to the particle size of the soil. One explanation could be that the larger the soil particles, the smaller the surface area in a given volume of soil. This change in surface area with particle size is partially reflected in the change of moisture content required for proper lubrication for maximum density.

The surface area in sands is relatively small, and most of the lubrication water is available also for hydration of the cement. When less water is added, the proper hydration of the cement increases the overall strength of the soil-cement, even though the dry density is slightly less than maximum. The surface area in clays is so great that most of the mix water is adsorbed by the soil particles, and insufficient water is then available for hydration of the cement. This requires the addition of more water to obtain proper hydration, raising the moisture content for maximum strength above that required for maximum density. Silts have soil particles sizes between those of sands and clays; therefore the moisture contents for maximum strength and maximum density are approximately the same. This explanation of moisture variation in sands, clays and silts is purely conjecture and has no experimental verification other than that the moisture contents for maximum density and maximum strength do not always coincide and seem to be related to soil texture.

Strength Study

EFFECT OF VARYING CHEMICAL ADDITIVE CONTENT

The changes in unconfined compressive strength caused by varying the amount of each chemical additive while holding the Portland cement content constant are shown in Figure 2. In general, the strengths of the specimens were increased as the percentage of each additive was increased. This continued until an optimum percentage of chemical additive was reached. After that the addition of more chemical caused a decrease in strength. The deleterious effects of the higher percentages of the additives were still evident after 28 day curing; it is possible that they might disappear or even increase after long periods. The strength curves resulting from different chemical treatments often are similar, indicating perhaps the same general mechanism of strength improvement.

Sodium metasilicate was definitely the best of the three additives with sand-loess-cement and with friable loess-cement, and contributed some strength improvements at very low percentages in Kansan till-cement. Sodium carbonate provided some strength improvement in sand-loess-cement and in friable loess-cement, but at all percentages it had a definitely deleterious effect in Kansan till-cement. Sodium hydroxide was moderately effective in sand-loess-cement and in friable loess-cement, and was the best additive for Kansan till-cement.

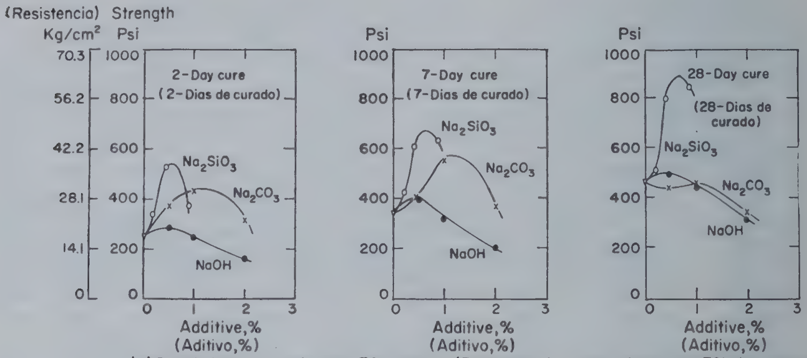

(a) Sand-loess specimens, 5% cement (Probetas de arena-loes con 5% de cemento)

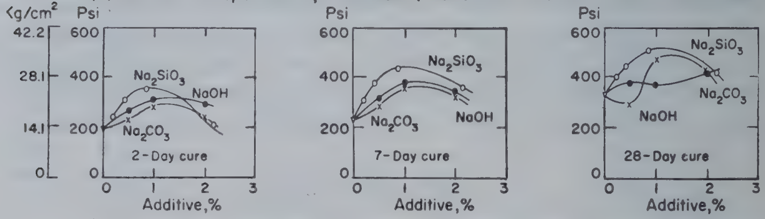

(b) Friable loess specimens, 5% cement (Probetas de loes friable con 5% de cemento)

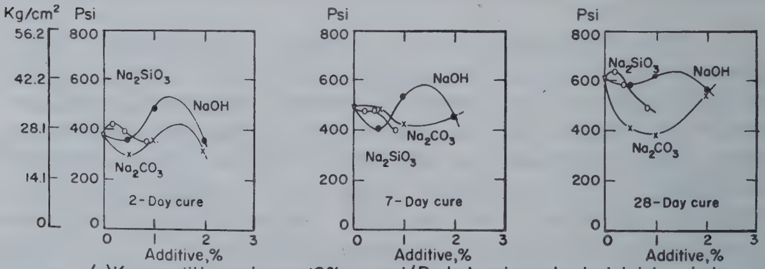

(c) Kansan till specimens, 10% cement (Probetas de suelo glacial del periodo Kansan con 10% de cemento)

Fig. 2 — Effect of varying chemical additive content with Portland cement content held constant.

Fig. 2 — Efectos obtenidos variando la cantidad de aditivos químicos y manteniendo constante el contenido de cemento.

EFFECT OF VARYING THE PORTLAND CEMENT CONTENT

The effects of varying the Portland cement content while holding the amount of chemical additive constant at its optimum percentage are shown in Figure 3. The increase in strength obtained through the use of additives is still present after 28 days curing. This indicates that the strength increases may be of a permanent nature and that additives do not act solely as accelerators; nevertheless, this should be verified for longer curing periods.

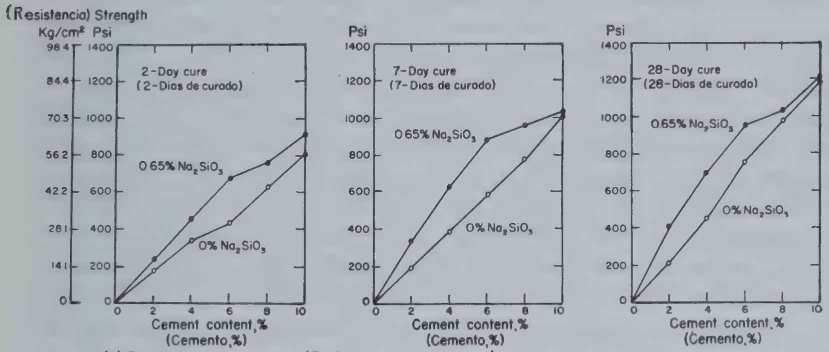

(a) Sand-loess specimens (Probetas de arena-loes)

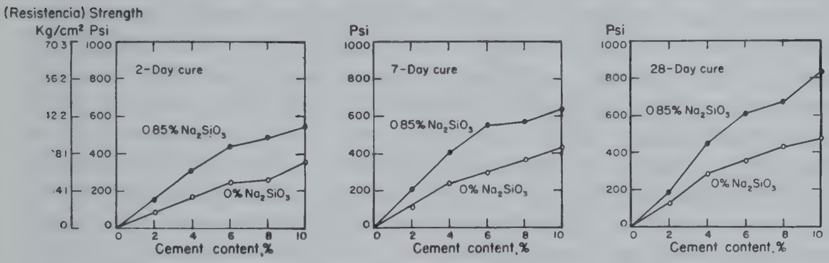

(b) Friable loess specimens (Probetas de loes friable)

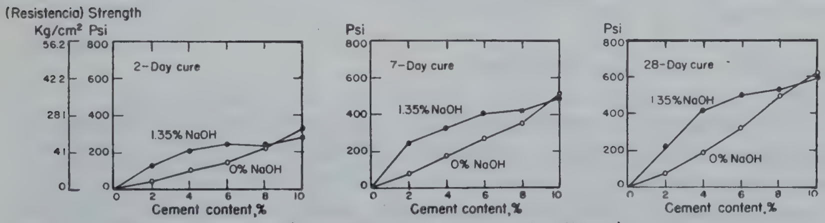

(c) Kansan till specimens (Probetas de suelo glacial del periodo Kansan)

Fig. 3 — Effect of varying Portland cement content with chemical additive held constant.

Fig. 3 — Efectos obtenidos variando la cantidad de cemento y manteniendo constante el contenido de aditivos químicos.

The chemical additive held constant in this phase of the investigation was chosen on the basis of the test results from varying the chemical additive content, the best additive for each soil being used with that particular soil. Sodium metasilicate was chosen for both the sand-loess and the friable loess; sodium hydroxide was used with the Kansan till.

At all three curing times in all three soils, the strength curve changes slope with increasing cement content when a chemical additive is used. This may indicate that a chemical additive is effective only up to a certain cement content, and above this content any additional strength increase is due primarily to the higher cement content and not from any reaction of the additive with the soil particles. This also would support the concept that the amount of additive required depends on the amount of silica surface area present, and that strength increases, due to the additive, only until the amount of lime furnished by the cement is adequate to satisfy this same amount of additive. After this condition is reached, any excess lime does not have silica surfaces with which to react, and further strength increases are due solely to the cementitious material provided by the Portland cement.

Another factor relative to the change of slope of the strength curve when sodium metasilicate is used as the chemical additive must be considered. Sodium metasilicate furnished silica, which reacts directly with the lime from the cement and forms calcium silicate and, possibly, sodium hydroxide. The sodium hydroxide is then free to react with the silica surface of the soil particles. It releases more silica and, as a result, creates more calcium silicate. This means that the Portland cement must furnish sufficient lime to react with both the silica from the soil particles and the silica from the sodium metasilicate. The cement content where the desire of the silica for lime is satisfied is the point where the change of slope occurs.

VALIDITY OF ASSUMPTIONS

It was first assumed that an optimum percentage of chemical additive for maximum strength could be obtained by determining the strengths of specimens molded at different chemical additive contents with a constant Portland cement content. The results obtained using sodium metasilicate in sand-loess-cement and friable loess-cement specimens substantiate this assumption. Strengths obtained with the chemical additive in both were greater than those obtained without the additive, provided the cement contents were equal. However, when sodium hydroxide was used with Kansan till-cement, the strength values of specimens with ten percent cement were practically the same as for specimens without the hydroxide. This suggests that future investigation using this soil might determine a better relationship between chemical additive content and strength. Another guide to this would be the high percentage of sodium hydroxide indicated by the curves in Figure 2 for Kansan till (1.35%) as compared with the amount of sodium metasilicate required in the other two soils (0.65%, 0.85%). The strength increases gained through using the hydroxide at lower cement contents do show that the beneficial use of additives in clay is feasible.

The other assumptions made were that the optimum chemical additive content and the moisture content for maximum strength do not vary with the percentage of Portland cement. The relatively straight lines obtained in Figure 3 for strength versus cement content without chemical additive would seem to indicate that the moisture content for maximum strength is not seriously affected by changing the cement content. The fairly consistent strength increases gained from the use of the metasilicate with both sand-loess and friable loess supports the assumption that the optimum chemical additive content is not greatly changed by varying the cement content. According to the mechanism theory presented herein, the chemical additive content should depend for the most part on the amount of reactive silica surface area present. As mentioned earlier, sodium metasilicate furnished silica directly. However, this is not the basic purpose of the chemical additive and any added cementation from the silica furnished by the sodium metasilicate must be considered a beneficial by-product.

Freeze-Thaw Phase

RESULTS

All estabilized specimens except sand-loess specimens gained strength during the freeze-thaw cycles (Table 3). This increase in strength may be explained by the findings that soil-cement will harden in cold weather as long as the temperature is above 0°C [22]. In the modified British test, the temperature of the water in the vacuum flask, with which the bottom of the specimen is in contact, is always above freezing. Thermal conductivity may explain why sand-loess specimens lost strength. Freezing is only from the

TABLE 3 — Results of modified British standard freeze-thaw test *

Soil	Cement content, %	Additive content, % **	Normal cure ***		Soaking ****		Freeze-thaw *****		Ratio: freeze-thaw/soaking
			Dry density, pcf (g/cm^3)	Strength psi (kg/cm^2)	Dry density, pcf (g/cm^3)	Strength psi (kg/cm^2)	Dry density, pcf (g/cm^3)	Strength psi (kg/cm^2)	
Sand-loess	2.0	0.0	128.8 (2.06)	225 (15.8)	128.9 (2.06)	250 (17.6)	128.9 (2.06)	189 (13.3)	75.6
	3.0	0.0	129.4 (2.07)	303 (21.3)	129.5 (2.07)	307 (21.6)	129.8 (2.08)	286 (20.1)	93.2
	4.0	0.0	129.8 (2.08)	421 (29.6)	129.7 (2.08)	454 (31.9)	129.9 (2.08)	375 (26.4)	83.0
	1.0	0.65	127.9 (2.05)	146 (10.3)	127.4 (2.04)	161 (11.3)	127.8 (2.05)	82 (5.8)	50.9
	2.0	0.65	126.6 (2.03)	239 (16.8)	126.7 (2.03)	293 (20.6)	126.6 (2.03)	207 (14.6)	71.0
	3.0	0.65	127.4 (2.04)	368 (25.9)	127.3 (2.04)	493 (34.6)	127.2 (2.04)	364 (25.6)	73.9

* Percentages of anhydrous chemical additive and portland cement are based on the dry weight of soil.

** Sodium metasilicate used in sand-loess and friable loess, sodium hydroxide in clay.

*** Normal cure consists of 7 day moist cure plus 24 hours immersion in water. Not a part of British standard test.

**** Soaking consists of 7 day moist cure plus 24 hours immersion in water, followed by an additional 14 days immersion in water.

***** Freeze-thaw consists of 7 day moist cure plus 24 hours immersion in water, followed by 14 cycles of freeze-thaw in accordance with British method.

TABLE 3 (continued)

Soil	Cement content, %	Additive content, % **	Normal cure ***		Soaking ****		Freeze-thaw		Ratio: freeze-thaw/soaking
			Dry density, pcf (g/cm³)	Strength psi (kg/cm²)	Dry density, pcf (g/cm³)	Strength psi (kg/cm²)	Dry density, pcf (g/cm³)	Strength psi (kg/cm²)	
Friable loess	4.0	0.0	102.5 (1.64)	261 (18.3)	103.1 (1.65)	336 (23.6)	103.2 (1.65)	282 (19.8)	83.9
	6.0	0.0	103.1 (1.65)	371 (25.1)	103.3 (1.65)	464 (32.6)	103.5 (1.66)	422 (29.7)	90.8
	8.0	0.0	102.9 (1.65)	454 (31.9)	103.1 (1.65)	557 (39.1)	103.2 (1.65)	529 (37.2)	94.9
	2.0	0.85	101.1 (1.62)	168 (11.8)	100.8 (1.61)	175 (12.3)	101.5 (1.63)	125 (8.9)	71.4
	3.0	0.85	101.5 (1.63)	343 (24.1)	101.2 (1.62)	589 (27.3)	101.5 (1.63)	368 (25.9)	94.6
	4.0	0.85	101.2 (1.62)	411 (28.9)	101.2 (1.62)	500 (35.2)	101.6 (1.63)	493 (34.7)	98.6
Kansan till	4.0	0.0	111.0 (1.78)	168 (11.8)	112.1 (1.79)	257 (18.1)	112.2 (1.80)	236 (16.6)	91.8
	6.0	0.0	111.9 (1.79)	329 (23.1)	112.4 (1.80)	436 (30.7)	113.1 (1.81)	429 (30.2)	98.2
	8.0	0.0	111.7 (1.79)	425 (29.9)	112.3 (1.80)	565 (39.7)	113.6 (1.82)	547 (38.5)	96.8
	2.0	1.35	112.8 (1.81)	218 (15.3)	113.5 (1.82)	297 (20.9)	113.0 (1.81)	272 (19.1)	91.6
	3.0	1.35	113.5 (1.82)	304 (21.4)	113.2 (1.81)	343 (24.1)	113.6 (1.82)	318 (22.4)	92.8
	4.0	1.35	113.7 (1.82)	372 (26.2)	114.3 (1.83)	490 (34.4)	114.2 (1.83)	400 (28.1)	81.6

surface, and the depth of frost penetration is much greater in sand-loess than in friable loess and Kansan till. Calculations using the modified Berggren formula show that under the freezing conditions imposed in the modified British test frost penetration in the sand-loess is 2.9 inches (7.37 cm) while it is only 1.8 inches (4.57 cm) in the friable loess and 1.9 inches (4.83 cm) in the Kansan till[23].

In general the results of the modified British tests were comparable with those expected from the Portland Cement Association's test. Using a ratio of 80% as the criterion of being sufficiently resistant to frost damage, all stabilized sand-loess specimens, except one, with a 7 day strength (7 days moist cure + 1 day immersion) greater than 290 psi (20.4 kg/cm^2) passed the test; the one exception was the specimen with 3% cement and 0.65% sodium metasilicate. No sand-loess specimen with a 7 day strength less than 290 psi (20.4 kg/cm^2) passed the test. Friable loess specimens had a similar record; one exception was one with 4% cement without additive, where the 7 day strength was just under 275 psi (19.3 kg/cm^2) and the ratio was slightly over 80%. Kansan till specimens were resistant to the British test, with all specimens giving a ratio greater than 80%.

The results show that the modified British test is practical, and that further investigation concerning standards and procedures for more rigorous climates is warranted. The specimen strengths obtained with cement plus chemical additives appear to indicate as high a resistance to freeze-thaw as those obtained with plain Portland cement, with the possible exception of sand-loess specimens. Here, in the specimen with 3% cement plus 0.65% sodium metasilicate, even though the 7 day strength was high, the ratio was low. However it appears that the immersion of the specimen had a tendency to accelerate the reaction of the additive. The strength increases, during 14 days immersion, of sand-loess specimens with cement plus chemical additive were considerably greater than the strength increases of cement stabilized specimens without chemical additive.

Further study should be made to determine whether or not the stabilized Kansan till specimens are as resistant to freeze-thaw as is indicated by the modified British test. As has been said, frost penetration is approximately the same in both the friable loess and the Kansan till under the freezing conditions imposed by the modified British test, but the textural characteristics of the two soils are quite different. The better gradation and higher clay content of the Kansan till lowers the permeability to such an extent that water can not enter at a rate which would cause great frost damage. The low clay content and the higher percentage of uniformly graded silt particles in the friable loess result in a higher permeability which causes greater damage by frost action. The damage, however, in both cases is a retarding of strength increase rather than a reduction in strength. The effects of the differences in permeability also were shown by the increases in strength during soaking, where the infiltration of water into the friable loess specimens hindered their strength increase somewhat.

In calculating the depth of frost penetration it was assumed that the soil moisture freezes at 32°F (0°C). Actually, the moisture contained in the Kansan till probably freezes at a temperature slightly below that contained in the friable loess, which would also help explain why the Kansan till specimens are more resistant to frost damage than friable loess specimens.

Experiments have shown that considerable strength increases may be obtained using additives, and we may assume that even greater strengths may be obtained as soon as better methods of preparing and mixing the soil are found. This main reason for the lack of economy in using sodium metasilicate and sodium hydroxide, the additives found most beneficial, is their high cost as compared with that of Portland cement. However, as the market for a product increases, the greater production lowers the unit cost. This may happen to chemical additives for soil-cement. Other less costly grades and types of chemicals may be found satisfactory. Sodium metasilicate was used in this study. If sodium silicate (water glass) can be substituted, its lower cost will result in savings. Sodium carbonate gave fairly good strength gains with the friable loess, and possibly future investigation using this additive will show that it may be used economically, though it does not produce as great strengths as sodium metasilicate.

Analytical grade reagents of high purity were used in this investigation. This naturally raises the question of whether technical grade reagents, which must be used in actual field work, would produce comparable strengths. Specimens were molded using analytical grade sodium metasilicate, 3 percent Portland cement, and friable loess. At the same time, identical specimens with technical grade sodium metasilicate were molded. The analytical grade specimens were tested at 317 psi (22.3 kg/cm^2) after 7 day curing and one day immersion; the technical grade gave 293 psi (20.6

kg/cm²), a difference of only 7.6 percent in favor of the analytical grade. This difference in strength is not significant. Technical grade reagents will give results in the field that will compare favorably with those obtained with analytical grade reagents.

The economic value of the additives has been determined on the basis of the normal uses of soil-cement. It is possible that the quantity of stabilizing material must be held to a minimum, then chemical additives may prove to be practical. One example would be in military operations, where supply lines are always taxed to capacity and loads must be as small and light as possible. Other examples would be construction in remote, inaccessible areas where normal supply is difficult.

RELATIVE COSTS

To determine the relationship between the cost of soil-cement with and without chemical additives, curves comparing relative cost with strength were drawn (Figure 4). To obtain the points for these curves, the percentages of cement required to obtain certain designated strengths at 7 day cure were determined from Figure 3. These percentages were multiplied by the cost of cement for each of the mixtures. The relative cost of chemical additives in cents per pound was then added to the relative cost of cement to obtain the

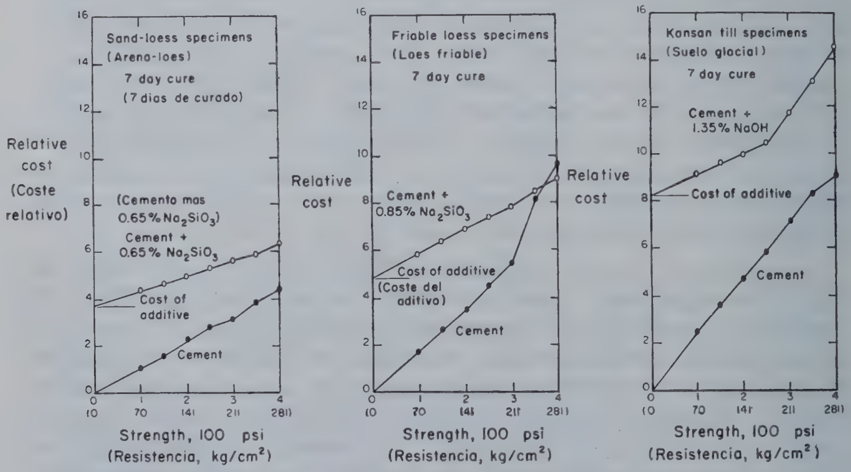

Fig. 4 — Comparison of relative cost.

Fig. 4 — Comparación del coste relativo.

total relative cost for each of the mixtures. Relative costs of soil-cement and of soil-cement plus additive were then plotted against strength for each of the three soils. Prices used for the Portland cement and the three chemical additives are given in Table 4.

TABLE 4 — Current chemical prices

Chemical	Price * \$/lb (\$/kg)	Source of Price
Portland cement, Type I	0.0106 (0.0233)	Iowa State Highway Commission, Ames, Iowa
Sodium carbonate, bulk	0.0155 (0.0341)	Chemical and Engineering News[21]
Sodium hydroxide, flak, ground, or powdered	0.0618 (0.136)	Chemical and Engineering News[21]
Sodium metasilicate, anhydrous	0.0570 (0.125)	Chemical and Engineering News[21]

* Prices based on car load lots without cost of freight to work site. When applicable, prices given to referenced material were adjusted to allow for one pound of pure anhydrous chemical.

At the present time, the use of additives is economical only in the friable loess when a strength greater than 350 psi (24.6 kg/cm^2) is desired (Figure 2). The desired strength in the other two soils may be obtained more economically through the use of additional cement. This does not agree with the findings of others that definite savings may be effected through the use of chemical additives[13, 14].

CONCLUSIONS

The following conclusions, applicable only to the three soils used, are a result of the investigation.

1. The optimum moisture contents for maximum strength and for maximum density are not necessarily the same for soil-cement and for soil-cement plus chemical additive.

2. The use of selected chemical additives in small amounts with soil-cement results in significant strength increases over soil-cement with equal Portland cement content but no chemical additive.

3. The type and exact percentage of chemical additive are unique for each soil. Sodium metasilicate in the amount of 0.65% of the dry weight of soil is the best of the three chemical additives used in this investigation for sand-loess-cement. It is also the best additive for silty friable loess-cement in the amount of 0.85%. Sodium hydroxide in the amount of about 1.35% is the best additive for clayey Kansan till-cement.

4. The use of chemical additives in soil-cement may not be economical under normal conditions, since any strength increases resulting from the use of chemical additives can usually be obtained more economically by an increase in cement content. Under certain conditions where the volume and weight of stabilizing material must be held to a minimum, the use of chemical additives may be feasible, since the volume and weight are much less than those of Portland cement for an equivalent strength increase.

5. The use of chemical additives does not have any deleterious effect on freeze-thaw resistance. Strengths obtained using chemical additives with soil-cement indicate as great a resistance to frost damage as to equal strengths of soil-cement obtained without chemical additive.

6. The modified British standard freeze-thaw test is a practical and reasonable guide in the design of frost resistance soil-cement.

ACKNOWLEDGEMENTS

This work was done at the Iowa Engineering Experiment Station under Project HR-83 of the Iowa Highway Research Board of the Iowa State Highway Commission.

REFERENCES

1. Robert L. Nichols — "Preliminary Investigation for the Chemical Stabilization of Loess in Southwestern Iowa"; M.S. Thesis; Iowa State University Library, Ames, Iowa; 1952.
2. Richard L. Handy — "Cementation of Soil Minerals with Portland Cement or Alkalies"; Highway Research Board Bulletin 198: 55-64; 1958.
3. Richard L. Handy, Joseph L. Jordan, Louis E. Manfre and D. T. Davidson — "Chemical Treatments for Surface Hardening of Soil-Cement and Soil-Lime-Fly Ash"; Highway Research Board Bulletin 241:49-66; 1959.

4. Coleman A. O'Flaherty, Manuel Mateos and Donald T. Davidson — "Fly Ash and Sodium Carbonate as Addtives to Soil-Cement Mixtures"; Highway Research Board Bulletin 353; 1962.

5. Donald T. Davidson, Manuel Mateos and Ramanah K. Katti — "Activation of the Lime-Fly Ash Reaction by Trace Chemical"; Highway Research Board Bulletin 231:67-81; 1959.

6. Manuel Mateos and Donal T. Davidson — "Further Evaluation of Promising Chemical Additives for Accelerating Hardening of Soil-Lime-Fly Ash Mixtures"; Highway Research Board Bulletin 304:33-50; 1961.

7. Manuel Mateos and Donald T. Davidson — "Effect of Chemical Additives on Strength of Sand-Lime-Fly Ash Mixtures Cured at Low Temperatures"; Mimeo Report; Iowa Engineering Experiment Station; 1961.

8. Manuel Mateos and Donald T. Davidson — "Stabilization of Alaska Silty Soils with Inorganic Additives"; Mimeo Report; Iowa Engineering Experiment Station; 1961. To be presented at the 9th Panamerican Highway Congress.

9. Manuel Mateos and Donald T. Davidson — "Gypsum as an Additive in Stabilized Soils"; Presented at the First International Symposium on Public Works on Gypseous Grounds, Madrid, Spain; October 1962.

10. Manuel Mateos and Donald T. Davidson — "Physical and Mineralogical Factors in the Stabilization of Iowa Soils with Lime and Fly Ash"; Iowa Engineering Experiment Station Bulletin 196:175-272; 1962.

11. Donald T. Davidson, Manuel Mateos and Harold F. Barnes — "Improvement of Lime Stabilization of Montmorillonitic Clay Soils with Chemical Additives"; Highway Research Board Bulletin 262:33-50; 1960.

12. Clarence R. Ruff and Donald T. Davidson — "Lime and Sodium Silicate Stabilization of Montmorillonite Clay Soil"; Highway Research Board Bulletin 304:76-92; 1961.

13. T. W. Lambe and Z. C. Moh — "Improvement of Strength of Soil-Cement with Additives"; Highway Research Board Bulletin 183:38-47; 1957.

14. T. W. Lambe, A. S. Michaels and Z. C. Moh — "Improvement of Soil-Cement with Alkali Metal Compounds"; Highway Research Board Bulletin 241:67-108; 1959.

15. Z. C. Moh, T. W. Lambe and Alan S. Michaels — "Improvement of Soil-Cement with Chemical Additives"; Highway Research Board Bulletin 309:57-76; 1962.

16. S. R. Mehra, L. R. Chadda and R. N. Kapur — "Role of Detrimental Salts in Soil Stabilization With and Without Cement: 1 — The Effect of Sodium Sulfate"; Indian Concrete Journal 29(10):336-337; 1955.

17. L. R. Chadda and H. Raj — "The Role of Detrimental Salts in Soil Stabilization With and Without Cement: 2 — The Effect of Sodium Carbonate"; Indian Concrete Journal 29(12):401-402; 1955.

18. A. S. Uppal and B. P. Kapur — "The Role of Detrimental Salts in Soil Stabilization With and Without Cement: 3 — The Effect of Magnesium Sulfate"; Indian Concrete Journal 31(7):228-231; 1957.

19. Coleman A. O'Flaherty, C. E. Edgar and Donald T. Davidson — "The Iowa State Compaction Apparatus"; Presented at the 42nd Annual Meeting of the Highway Research Board, Washington, D.C.; January 1963.

20. British Standards Institution; 1958 Yearbook; London, England; 1958.

21. "Quarterly Report on Current Prices"; Chemical and Engineering News 36:47-70; June 1958.

22. K. E. Clare and A. E. Pollard — "The Effect of Curing Temperature on the Compressive Strength of Soil-Cement Mixtures"; Géotechnique 4:97-107; 1954.

23. D. T. Davidson and B. W. Bruns — "Comparison of Type I and Type III Portland Cements for Soil Stabilization"; Highway Research Board Bulletin 267:28-45; 1960.

TIPOGRAFIA EDANEE S. A.
IMPRIMIU — SÃO PAULO

UNIVERSITY OF ILLINOIS-URBANA

3 0112 005566531